An investigation into the regulatory mechanisms of neutrophil migration into lymphatic vessels *in vivo*.

A thesis submitted in partial fulfilment of the requirements of the Degree of Doctor of Philosophy

By

Samantha Arokiasamy

Centre for Microvascular Research

William Harvey Research Institute

Barts & The London School of Medicine and Dentistry

Queen Mary University of London

Charterhouse Square

London EC1M 6BQ

UK

Acknowledgements

I would firstly like to express my utmost thanks and gratitude to my supervisors, Dr Mathieu-Benoit Voisin, Prof Wen Wang and Prof Sussan Nourshargh, for all the support, guidance, and encouragement throughout the past 3 years of my PhD. Special mention goes to my primary supervisor, Mathieu. My PhD has been an amazing experience and I thank him wholeheartedly, not only for his tremendous academic support, but also for his dedication to this project and for enabling me to grow as a research scientist. I must also thank my supervisors for giving me the opportunity to undertake this project within the Centre for Microvascular Research, and both the Institute of Bioengineering at Queen Mary University of London (QMUL) and Arthritis Research UK (ARUK) for providing the funds to support this work.

I wish to thank all my colleagues, both past and present, at the Centre for Microvascular Research, for their support, advice, expertise and friendships over the last 3 years. On that note, I would like to express my thanks to Rob Beal, with whom I have shared this rollercoaster journey with, for all the laughs and good times despite being a right pain at times! My thanks also go to all the other PhD students for being constant sources of support. My sincere thanks also goes to Dr James Whiteford, for proof-reading this thesis and for being such an understanding boss over the last couple of months.

A special thank you goes to James Almond, not only for being my rock these past few years, but for loving and believing in me. This would have been a struggle without his constant support, motivation and encouragement. Without doubt, experiencing the trials and tribulations of a PhD together has made this journey far less of a battle.

Finally, I am eternally grateful to my family for the love and unbelievable support they have given me despite being thousands of miles away, not just in the last 3 years. To my parents, Alice Goh Lee Kheng and Kilbert Joseph Arokiasamy, for raising me with a love of science, and for sacrificing so much in order to support me in all my pursuits. To my brother, Clarence, for always being a listening ear. Thank you. They are the most important people in my world and to them, I dedicate this thesis.

Statement of originality

I, Samantha Arokiasamy, confirm that the research included within this thesis is my own work or that where it has been carried out in collaboration with, or supported by others, that this is duly acknowledged below and my contribution indicated. Previously published material is also acknowledged below.

I attest that I have exercised reasonable care to ensure that the work is original, and does not to the best of my knowledge break any UK law, infringe any third party's copyright or other Intellectual Property Right, or contain any confidential material.

I accept that the College has the right to use plagiarism detection software to check the electronic version of the thesis.

I confirm that this thesis has not been previously submitted for the award of a degree by this or any other university.

Signature:

Date: 10th March 2017

List of presentations and prizes awarded at scientific meetings

Oral presentations

- **22nd CLSS-UK Annual Conference**, London, September 2016;
- **WHRI New Year Celebration**, London, January 2016;
- **27th UK Cell Adhesion Meeting**, Birmingham, September 2015.

Poster presentations

- **28th UK Cell Adhesion Meeting**, London, September 2016;
- **Neutrophil 2016**, Verona, September 2016;
- **WHRI 30th Anniversary Celebration**, London, October 2016;
- **Institute of Bioengineering Launch Event**, QMUL, London, October 2015;
- **26th UK Cell Adhesion Meeting**, London, October 2014;
- **William Harvey Annual Review**, London, July 2014;
- **WHRI New Year Celebration**, London, January 2014

Prizes

- **Best Talk** at the **22nd CLSS-UK Annual Conference**, London, September 2016;
- **Best Talk** at the **27th UK Cell Adhesion Meeting**, Birmingham, London, September 2015.

Abstract

Neutrophils are recognised to play a pivotal role at the interface between the innate and adaptive immune responses following their rapid recruitment to inflamed tissues and lymphoid organs. Whilst neutrophil trafficking through blood vessels has been extensively studied, the molecular mechanisms regulating their migration into the lymphatic system are still poorly understood. This thesis therefore aimed to investigate the mechanisms involved in neutrophil migration across the lymphatic endothelium during TNF- or Complete Freund's Adjuvant + antigen (CFA+Ag)-induced inflammation of cremaster muscles *in vivo*.

This work revealed that TNF- or CFA+Ag-stimulation induces a rapid but transient entry of tissue-infiltrated neutrophils into lymphatic vessels, a response associated with the regulation and redistribution of the lymphatic endothelial cell glycocalyx. Interestingly, antigen sensitisation resulted in the production of endogenous TNF within cremaster muscles. Using anti-TNF blocking antibodies and mice deficient in both TNF receptors (p55 and p75), endogenous TNF was demonstrated for the first time to be involved in priming and triggering the migration of neutrophils into tissue-associated lymphatic vessels upon antigen challenge. Additionally, the use of chimeric mice exhibiting neutrophils deficient in both TNFRs demonstrated that TNF directly acts on leukocytes to induce neutrophil migration into lymphatic vessels. Furthermore, the results show that TNF-induced migration of neutrophils into the lymphatic system occurs in a strictly CCR7-dependent manner; blocking CXCR4 or CXCL1 signalling does not affect this response. Finally, both TNF- or CFA+AG-stimulation induced ICAM-1 up-regulation on lymphatic vessels, allowing neutrophils to crawl along the lumen; a response that was demonstrated to be TNF-dependent.

These results have provided new insights into the mechanisms that mediate neutrophil migration into lymphatic vessels and their subsequent crawling within these vessels during inflammation. In particular, a new role for TNF as a key regulator of these processes has been demonstrated. Taken together, this work has highlighted potential and effective targets to manipulate the role of neutrophils in adaptive immune responses *in vivo*.

Publications arising from this work

Samantha Arokiasamy, Christian Zakian, Jessica Dilliway, Wen Wang, Sussan Nourshargh and Mathieu-Benoit Voisin (2017). **Endogenous TNF orchestrates the trafficking of neutrophils into and within lymphatic vessels during acute inflammation.** *Nature Scientific Reports.*

Table of Contents

List of Tables

List of Figures

List of acronyms and abbreviations

Ab	Antibody
ACK	Ammonium-Chloride-Potassium
Ag	Antigen
ANCA	Antineutrophil cytoplasm autoantibodies
ANOVA	Analysis of variance
APCs	Antigen presenting cells
APRIL	A proliferation-inducing ligand
$\alpha_L\beta_2$	Alpha L Beta 2 integrin
$\alpha_4\beta_1$	Alpha 4 Beta 1 integrin
α-SMA	Alpha-smooth muscle actin
BAFF	B cell activating factor
BCA	Bicinchoninic Acid
BCG	*Mycobacterium bovis* bacille Calmette-Guérin
BECs	Blood endothelial cells
BM	Bone marrow
b.p	Base pair
BSA	Bovine serum albumin
Cat. #	Catalogue number
CAM	Cell adhesion molecule
C5a	Complement component C5a
C5aR	Complement component C5a receptor
CCL	Chemokine (C-C motif) ligand
CCR	Chemokine (C-C motif) receptor
CCR7KO	Chemokine (C-C motif) receptor 7 knockout
CD	Cluster of differentiation
CFA	Complete Freund's adjuvant
CHS	Contact hypersensitivity
Conc	Concentration

CS	Chondroitin sulfate
CTL	Control
CXCL	Chemokine (C-X-C) ligand
CXCR	Chemokine (C-X-C) receptor
DAPI	4’,6-diamidino-2-phenylindole dihydrochloride
DAMPs	Danger-associated molecular pattern
DCs	Dendritic cells
dLNs	Draining lymph nodes
DNA	Deoxyribonucleic acid
DNase I	Deoxyribonuclease I
dNTPs	Deoxynucleotide triphosphates
DMSO	Dimethyl sulfoxide
ECs	Endothelial cells
EDTA	Ethylenediaminetetraacetic acid
eGFP	Enhanced green fluorescent protein
ECM	Extracellular matrix
ELISA	Enzyme-linked immunosorbent assay
ESAM	Endothelial-cell selective adhesion molecule
FACS	Fluorescence-activated cell sorting
FBS	Fetal bovine serum
FITC	Fluorescein isothiocyanate
fMLP	N-formyl-methionyl-leucyl-phenylalanine
FPR1	Formyl peptide receptor-1
FSC	Forward scatter
GAG	Glycosaminoglycan
G-CSF	Granulocyte-colony stimulating factor
G-CSFR	Granulocyte-colony stimulating factor receptor
GM-CSF	Granulocyte-macrophage colony-stimulating factor
GPCR	G-protein coupled receptor
h	Hours

HA	Hyaluronan
HDLECs	Human dermal lymphatic endothelial cells
HEVs	High endothelial venules
HRP	Horseradish peroxidase
HSPG	Heparan sulfate proteoglycan
HUVECs	Human umbilical vein endothelial cells
HS	Heparan sulfate
IB4	Griffonia (Bandeirafa) Simplicifolia Lectin I Isolectin B4
ICAM-1	Intercellular cell adhesion molecule-1
ICAM-2	Intercellular cell adhesion molecule-1
Iso	Isotype
IFNα	Interferon alpha
IFNγ	Interferon gamma
IFZ	Interfollicular zone
Ig	Immunoglobulin
IL	Interleukin
IL-1β	Interleukin-1 beta
i.p.	Intraperitoneal
I/R	Ischemia/reperfusion
i.s.	Intrascrotal
IVM	Intravital microscopy
JAM	Junctional adhesion molecule
KC	Keratinocyte-derived chemokine
kg	Kilogram
KO	Knockout
LECs	Lymphatic endothelial cells
LEL	Lycopersicon Esculentum (tomato) Lectin
LFA-1	Lymphocyte function-associated antigen-1
LNs	Lymph nodes
LPS	Lipopolysaccharide

LTB_4	Leukotriene B_4
LysM	Lysozyme M
LYVE-1	Lymphatic vessel endothelial receptor-1
mAb	Monoclonal antibody
MAC-1	Macrophage-1 antigen
MAL-1	Maackia Amurensis Lectin -1
MFI	Mean fluorescence intensity
µg	Microgram
mg	Milligram
$MgCl_2$	Magnesium chloride
MHC	Major histocompatibility complex
MHC-I	Major histocompatibility complex Class I
MHC-II	Major histocompatibility complex Class II
MIP-2	Macrophage inflammatory protein-2
min	minutes
MI	Myocardial infarction
µl	Microlitre
ml	Millilitre
MOF	Multiple organ failure
mM	Micromolar
MMP	Matrix metalloproteinase
MRP14	Myeloid-related protein-14
NA	Numerical aperture
NADPH	Nicotinamide adenine dinucleotide phosphate
NETs	Neutrophil extracellular traps
NF-κB	Nuclear factor- kappa B
ng	Nanogram
NGS	Normal goat serum
NH_4	Ammonium
NO	Nitric oxide

NSAIDs	nonsteroidal anti-inflammatory drugs
OVA	Ovalbumin
PAF	Platelet-activating factor
PAFR	Platelet-activating factor receptor
PAMPs	Pathogen-associated molecular patterns
PBS	Phosphate buffered saline
PCR	Polymerase chain reaction
PECAM-1	Platelet endothelial cell adhesion molecule-1
PFA	Paraformaldehyde
Plt	Paucity of lymph node T cells
PMN	Polymorphonuclear leukocytes
Prox1	Prospero-related homeobox gene 1
PSGL1	P-selectin glycoprotein ligand 1
RA	Rheumatoid arthritis
RF	Rheumatoid factor
RFI	Relative fluorescence intensity
ROCK	Rho-associated protein kinase
ROS	Reactive oxygen species
RT	Room temperature
S1P	Sphingosine-1-phosphate
SA	Sialic acids
SDF-1α	Stromal-derived factor 1 alpha
SEM	Standard error of mean
SF	Synovial fluid
sIRNA	Small interfering RNA
SLE	Systemic lupus erythematosus
SNA	Sambucus Nigra (Elderberry) Bark Lectin
SSC	Side scatter
SVV	Small vessel vasculitis
TAE	Tris-Acetate-EDTA

TEM	Transendothelial migration
TPA	12-O-tetradecanoylphorbol 13-acetate
TLRs	Toll-like receptors
TMB	3,3',5,5'-Tetramethylbenzidine
TNF	Tumour necrosis factor (formerly known as tumour necrosis factor alpha)
TNFRdbKO	Tumour necrosis factor receptors double knockout
TNFRI	Tumour necrosis factor receptor type I (p55)
TNFRII	Tumour necrosis factor receptor type II (p75)
V	Volts
VCAM-1	Vascular endothelial cell adhesion molecule-1
VE-cadherin	Vascular endothelial cadherin
VEGF	Vascular endothelial growth factor
VEGFR	Vascular endothelial growth factor receptor
VLA-4	Very late antigen-4
v/v	Volume per volume
WT	Wild type
w/v	Weight per volume

1 : General Introduction

1.1 Neutrophils in innate and adaptive immunity

Inflammation is a physiological process crucial for the body's immune response to harmful stimuli, such as viruses, bacteria, fungi or parasites and/or cell damage. The immune system of all mammals can be divided into two interdependent branches: innate and adaptive immune responses. The innate immune system comprises of cells and mechanisms that provides the host with general protection against all foreign antigens, whilst adaptive immunity occurs within lymphoid organs and results in an antigen-specific response to each pathogen. Amongst all leukocytes, neutrophils are the first cells to arrive at sites of inflammation where they play a crucial role in the clearance of pathogens. Although neutrophils are indisputably major effectors of acute inflammation, increasing evidence has shown an emerging role for them in shaping adaptive immune responses.

1.1.1 Neutrophils

Neutrophils are the most abundant type of white blood cells in humans, and are well recognised as one of the key players during acute inflammation (Amulic et al., 2012; Ley et al., 2007; Phillipson and Kubes, 2011). They are typically the first cells to arrive at sites of inflammation and are capable of eliminating pathogens by multiple mechanisms (see section 1.1.2.1); thus, providing a critical first line of defence in the immune response against invading pathogens. These immune cells are continuously generated in the bone marrow (BM) from myeloid precursors, with their daily production reaching up to 2 x 10^{11} cells in humans (Borregaard, 2010). In humans, neutrophils make up 50-70% of circulating leukocytes, whereas in mice, 10-25% of neutrophils are present within the circulation under physiological conditions (Mestas and Hughes, 2004). Mature neutrophils are polymorphonuclear (PMN) leukocytes, and possess a distinctive multi-lobed nucleus; they are distinguishable by their expression of Ly6G (recognised by the antibody, GR1) in the murine system (Fleming et al., 1993). In humans, CD66, CD16b, CD15 and myeloid peroxidase (MPO) have been used to identify neutrophils (Dransfield et al., 1994; Watt et al., 1991). In the circulation, these immune cells have an average

diameter of 7-10 μm and have a cytoplasm enriched with pre-formed granules and secretory vesicles (Borregaard, 2010). The lifespan of a circulating neutrophil is debated within the scientific community but has been reported to be between 1.5 and 12.5 hours in mice (Kolaczkowska and Kubes, 2013) and an unprecedented 5.4 days in humans (Pillay et al., 2010). Given their destructive potential, neutrophil extravasation into inflamed tissues has to be tightly regulated to avoid damage to the host. Numbers of circulating neutrophils are therefore controlled through rate of neutrophil precursor proliferation in the BM, egress of mature neutrophils from the BM into the circulation, and their clearance in the spleen, liver and BM (see section 1.1.2.3) (Sadik et al., 2011).

1.1.2 Neutrophils in innate immunity

1.1.2.1 Roles in innate immune responses

The innate immune system is the first line of host defence against invading pathogens and neutrophils are indispensable to this response. This involves a series of cellular and molecular mechanisms that protect the host from infection and limits the expansion and dissemination of bacterial and viral infections, without relying on the second arm of the immune response - adaptive immunity (acquired immunity). Neutrophils are recruited to sites of inflammation by chemoattractants (see section 1.1.2.2), which provide a chemical gradient for them to migrate along; the highest concentration of chemoattractants are normally found at the site of infection in order to attract neutrophils for them to carry out their functions and resolve inflammation.

During the innate immune response, neutrophils exert their functions in 3 ways: phagocytosis, degranulation and the newly discovered release of neutrophil extracellular traps (NETs). Neutrophils can engulf pathogens they encounter in a process called phagocytosis (**Figure 1.1**), whereby bacteria or cell debris are rapidly ingested, removing them from the body and thus limiting further damage (Phillipson and Kubes, 2011). Mature neutrophils possess three main types of granules (primary, secondary and tertiary) in the cellular cytoplasm containing a variety of proteases and antimicrobial peptides (Faurschou and Borregaard, 2003). Secretory vesicles containing membrane proteins (e.g. β2 integrins) are also present within the cytoplasm, which can be rapidly mobilised to the cell surface upon activation (Hager et al., 2010). Upon engulfment of a pathogen, the contents of the resulting phagosomes are degraded by reactive oxygen species (ROS)

and lytic enzymes using granule stores of NADPH oxidase, or antibacterial proteins (cathepsins, defensins, lactoferrin and lysozyme), respectively (Borregaard, 2010; Hager et al., 2010). These antibacterial proteins can also be released by neutrophils into the extracellular milieu through a process called degranulation (**Figure 1.1**), thus promoting the killing of pathogens present in the tissue. Finally, highly activated neutrophils can eliminate extracellular microorganisms through the expulsion of NETs (**Figure 1.1**), which are composed of core DNA elements to histones, proteins and degrading enzymes (i.e. neutrophil elastase and MPO). This immobilises pathogens to prevent their dissemination and facilitates their subsequent phagocytosis (Brinkmann et al., 2004). However, in order for any of these killing mechanisms to occur, circulating neutrophils have to undergo a process known as "priming", whereby cytokines such as tumour necrosis factor (TNF, formerly known as TNFα) or leukotriene B_4 (LTB_4), or contact with activated vascular endothelium, results in a markedly augmented responsiveness to activating stimulus, such as bacteria or sterile injury (Wright et al., 2010).

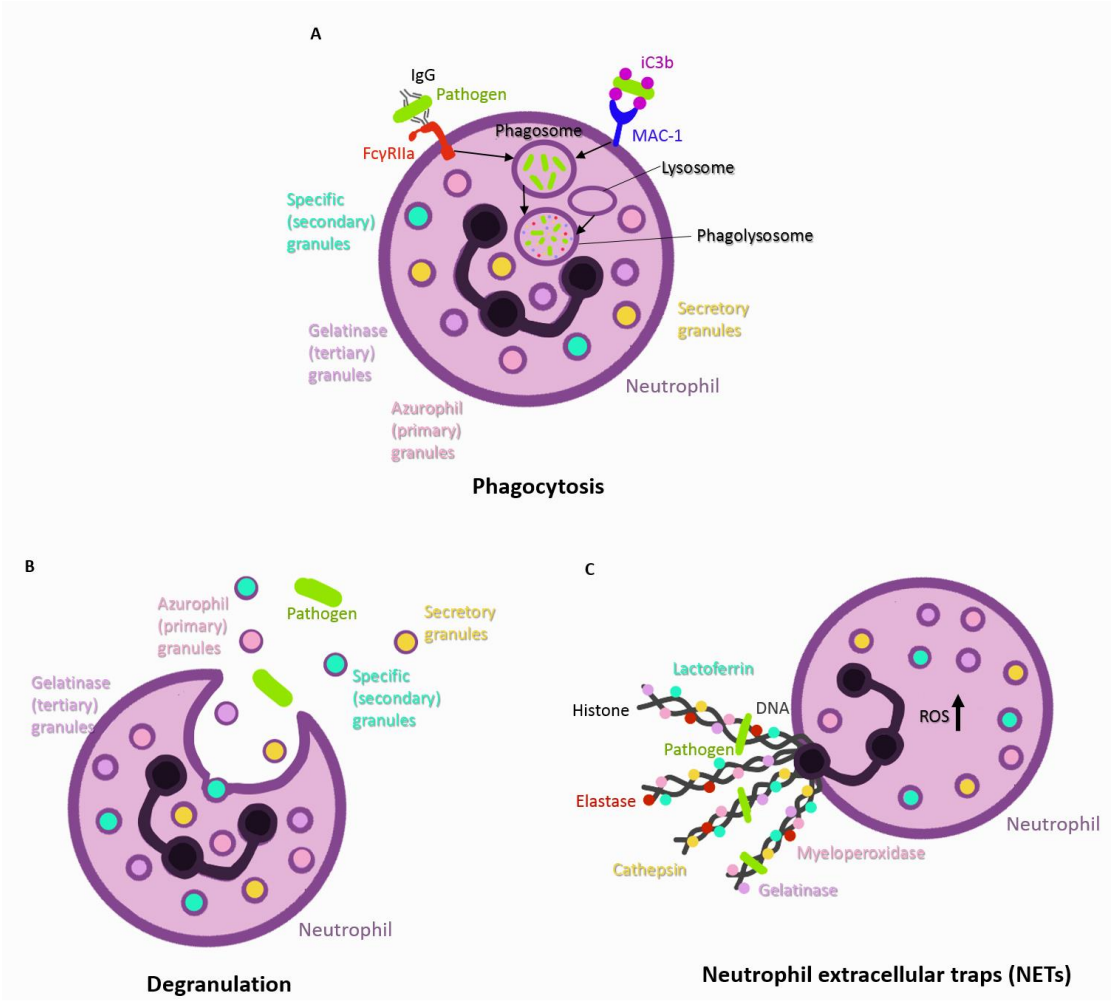

Figure 1.1: Neutrophil killing mechanisms. This occurs through (A) phagocytosis, (B) degranulation and (C) the release of neutrophil extracellular traps (NETs). (A) Neutrophils recognise opsonised pathogens through Fc receptors (FcγRIIa) or complement receptors (MAC-1) on their surface membrane via antibody molecules (e.g. IgG) or iC3B – a proteolytically inactive product of the complement cleavage fragment C3b. The pathogen is internalised into a nascent phagosome, which then matures by fusing with lysosomes forming a phagolysosome. (B) Granules (primary, secondary, tertiary and secretory vesicles) situated within neutrophils have complex immunomodulatory and anti-microbial effects, and are released by activated neutrophils during degranulation at inflammatory sites leading to the killing of pathogens. (C) NETs are formed when neutrophils release decondensed chromatin decorated with proteins possessing antimicrobial properties into the extracellular space to trap pathogens. This immobilises them and not only prevents their dissemination but also facilitates their subsequent phagocytosis. Once phagocytosed, neutrophils kill pathogens using NADPH oxygenase-dependent mechanisms (ROS) or anti-microbial proteins. NETS are also thought to directly kill pathogens through the release of anti-microbial histones and proteases. Anti-microbial proteins include myeloperoxidase (primary granules), lactoferrin (secondary granules), gelatinase (tertiary granules), cathepsin (secretory vesicles). Enzymes such as neutrophil elastase are also released from primary granules upon activation to aid the formation of NETs. ROS, reactive oxygen species.

1.1.2.2 Chemoattractants and their receptors involved in neutrophil recruitment and activation

In order for neutrophils to be recruited from the circulation to sites of inflammation, they need to be mobilised from the BM into the bloodstream before transmigrating (extravasating) across blood vascular endothelial cells (ECs) into the inflamed tissue. The process by which inflammatory cells are recruited to the tissue involves cellular activation and subsequent secretion of cytokines, which in turn provides a gradient for leukocytes to follow towards sites of pathogen challenge. In mammals, this gradient is achieved by chemoattractant molecules, such as chemokines, which are small-secreted proteins (Mantovani et al., 2006). Chemokines form the largest family of cytokines, with approximately 50 endogenous chemokine ligands present in humans and mice (Griffith et al., 2014). Chemokines are subdivided into families based on the number and location of cysteine residues at the amino terminus: C, CC, CXC, CXXXC and CX_3, whereby a succeeding 'L' indicates a ligand, 'X' represents an amino acid, and 'R' indicates a receptor (Luster, 1998; Charo and Ransohoff, 2006). The major chemokines involved in neutrophil recruitment from postcapillary venules to sites of inflammation are listed (**Table 1.1**). Following their secretion, chemokines bind to glycosaminoglycans (GAGs) on the luminal side of ECs, thus forming a chemotactic gradient and preventing their removal from the blood stream (Mantovani et al., 2006). On the leukocytes, chemokines bind to their cognate chemokine receptors, which are G-protein coupled receptors (GPCRs) that are differentially expressed amongst leukocyte subsets. Binding results in the activation of complex signalling cascades that trigger cellular activation, thereby orchestrating the inflammatory response to recruit specific leukocyte subsets to the site of infection.

In addition to chemokines, other chemoattractants, such as the lipid mediator LTB4, complement component C5a (C5a), N-formyl-methionyl-leucyl-phenylalanine (fMLP), and platelet-activating factor (PAF) are also potent leukocyte chemoattractants (**Table 1.2**). Atypical chemokine receptors (ACKRs), such as ACKR1 (DARC), expressed by blood vascular ECs also play a role in regulating the bioavailability of circulating chemokines by binding them with high affinity (Bonecchi and Graham, 2016). DARC is able to induce transcytosis of chemokines, thus facilitating the presentation of inflammatory chemokines on the luminal side of blood vascular ECs (Pruenster et al., 2009) (**Table 1.2**).

Classification			Receptors		Source	Reference
Systemic	**Murine**	**Human**	**Murine**	**Human**		
CXCL1	KC	GROα	CXCR2	CXCR2	Macrophages	(Bozic et al., 1995)
CXCL2	MIP-2	GROβ	CXCR2	CXCR2	Macrophages	(Wuyts et al., 1998)
CXCL5	LIX	ENA-78	CXCR2	CXCR2	Macrophages, eosinophils, epithelial cells	(Soehnlein and Lindbom, 2010)
CXCL7	NAP-2	NAP-2	CXCR2	CXCR1/CXCR2	Platelets	(Schenk et al., 2002)
CXCL8	n/a	IL-8	CXCR2	CXCR1/CXCR2	Macrophages, neutrophils	(Baggiolini et al., 1989)
CXCL12	SDF-1α	SDF-1α	CXCR4	CXCR4	Stromal cells (BM)	(Martin et al., 2003)

Table 1.1: Major chemokines involved in murine neutrophil migration and their human orthologues/analogue.

Chemoattractants	Receptors	Source	Reference
Murine/Human	**Murine/Human**		
LTB_4	**BLT1**	Macrophages	(Casale et al., 1992; Haribabu et al., 2000)
C5a	**C5A receptor (C5aR)**	Macrophages	(Hetland et al., 1986; Monari et al., 2002; Ooi et al., 1980)
PAF	**PAF Receptor (PAFR)**	Platelets, ECs, neutrophils, monocytes, macrophages	(Casale et al., 1992; Wardlaw et al., 1986)
fMLP	**Formyl peptide receptor-1 (FPR1)**	Tissue bacteria	(Casale et al., 1992; Marasco et al., 1984)
Atypical chemokine receptors (ACKRs)	**Ligands**		**Reference**
ACKR1 (DARC)	CCL2, 5 7, 11, 13, 13, 17; CXCL1, 5, 6, 8, 11		(Bonecchi and Graham, 2016)

Table 1.2: Other chemoattractants and ACKRs involved in neutrophil chemotaxis.

1.1.2.3 Neutrophil mobilisation from bone marrow

Before extravasating into interstitial tissue during inflammation, neutrophils need to be mobilised from the BM. The BM is both a large storage pool for immune cells and the site of neutrophil production; in mice, neutrophil reserves are estimated to be 120 million cells (Furze and Rankin, 2008). Leukocytes are continually being released into the circulation and upon inflammatory insult, the BM reserve is rapidly mobilised, thus amplifying neutrophil release. The molecular mechanism of sequestration and release is thought to be mediated by the co-ordinated actions of cytokines and chemokines. Interactions of the chemokine, CXCL12, with its chemokine receptor, CXCR4, are essential for normal BM development of multiple immune cell lineages, including B cells, monocytes, macrophages, neutrophils, natural killer (NK) cells and dendritic cells (DCs) (Mercier et al., 2012); this interaction also promotes the retention of both developing and mature neutrophils within the BM (Furze and Rankin, 2008; Ma et al., 1999). The blockade of CXCR4 by a specific antagonist, AMD3100, or repopulation of irradiated WT mice with CXCR4-deficient BM cells, resulted in a rapid increase in circulating neutrophils as a result of egress from the BM (Liu et al., 2014; Ma et al., 1999; Martin et al., 2003). This led to the conclusion that CXCR4 negatively regulates the egress of neutrophils from BM stores. In support of this, neutrophils' expression of CXCR4 was also found to progressively decrease as they mature, thus permitting their release from the BM into the circulation (Eash et al., 2010). These observations along with constitutive expression of the CXCR4 ligand, CXCL12, by BM stromal cells suggests that the CXCL12:CXCR4 chemokine axis provides a key retention signal for neutrophils in the BM (Martin et al., 2003). Whilst CXCR4 blockade leads to the release of neutrophils into the circulation, the mechanism by which this occurs has been reported to be via CXCR2 signalling (Eash et al., 2010). The CXCR2 ligands, CXCL1 (also known as KC or GROα) and CXCL2 (also known as MIP-2 or Groβ), are chemokines that are produced both remotely and constitutively expressed in BM ECs which act on neutrophil-expressed CXCR2 to promote their mobilisation (Eash et al., 2009). Thus, whilst the CXCL12:CXCR4 chemokine axis acts as a retention pathway for BM neutrophils, the CXCL1/2:CXCR2 axis acts antagonistically to promote neutrophil release (Eash et al., 2010). Nevertheless, the CXCL12:CXCR4 chemokine axis plays a dominant role in neutrophil trafficking as neutrophils doubly deficient in both CXCR2 and CXCR4 exhibited constitutive mobilisation of neutrophils similar to CXCR4-deficient cells (Eash et al., 2010). Interestingly, it has been reported that mice genetically deficient in either

the cytokine, granulocyte colony-stimulating factor (G-CSF), or the G-CSF receptor (G-CSFR) had very few neutrophils within the circulation and BM, with evidence suggesting that G-CSF reduces the production of CXCL12 by BM stromal cells and down-regulates the expression of CXCR4 on neutrophils (Semerad et al., 2002; Sierra et al., 2007). Thus, G-CSF is believed to disrupt the retention signal delivered by CXCL12 in the BM and thereby facilitates the migration of neutrophils across the BM sinusoidal endothelium in response to the chemotactic gradients created by the blood-borne chemokines, CXCL1 and CXCL2, leading to the mobilisation of neutrophils into the circulation (**Figure 1.2**).

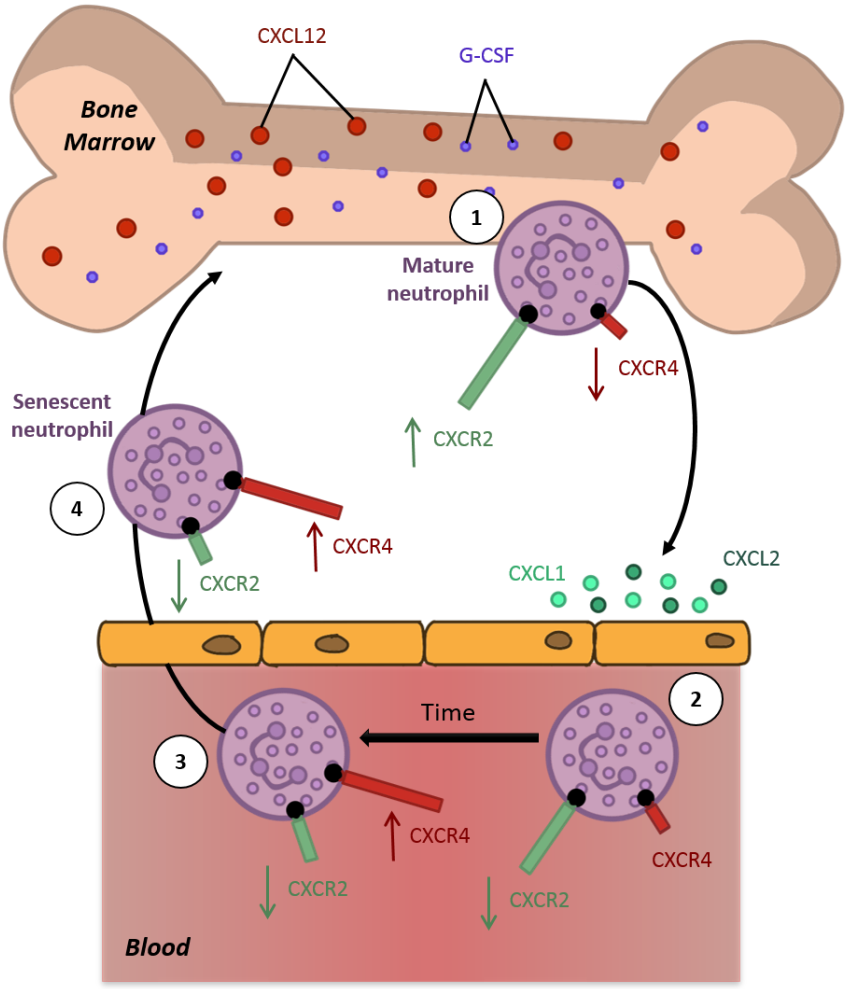

Figure 1.2: Alterations in neutrophil chemokine receptors following inflammation. (1) Neutrophils are generated and stored in the bone marrow (BM) via CXCL12:CXCR4 interactions. BM neutrophils progressively down-regulate CXCR4 and up-regulate CXCR2, which allows them to be mobilised in response to CXCL1 and CXCL2 produced following inflammation. Inflammation also results in the production of G-CSF, which aids this process via inhibition of the CXCL12:CXCR4 chemokine axis. (2) Neutrophils expressing high levels of CXCR2 gain entry into the circulation from the BM during inflammation. (3) Senescent neutrophils progressively down-regulate CXCR2 and up-regulate CXCR4. (4) High levels of CXCR4 expression lead to the homing of senescent neutrophils back to the BM via the CXCL12 chemotactic gradient.

1.1.2.4 Recruitment to sites of inflammation

During the initiation of an innate immune response, neutrophils extravasate out of blood vessels into interstitial tissue to get to the sites of inflammation; this takes place mainly in small blood vessels called postcapillary venules (PCVs) *in vivo*. This response occurs as neutrophils are guided by a plethora of chemotactic agents, acting on only a handful of cell surface receptors (**Table 1.1** & **Table 1.2**). In response to infection or injury, sentinel cell-derived inflammatory mediators such as interleukin-1β (IL-1β) and TNF, activate nearby vascular ECs, thus inducing increased expression of adhesion molecules and vascular permeability (Nourshargh et al., 2010; Soehnlein and Lindbom, 2010). This promotes the adhesion and transmigration of neutrophils across the vascular endothelium, respectively. The CXCR2 ligands, CXCL1, CXCL2 and CXCL5, are imperative for neutrophil chemotaxis and activation (Bozic et al., 1995; Soehnlein and Lindbom, 2010; Wuyts et al., 1998). *In vivo* immunoneutralisation of CXCL1 and CXCL2 resulted in an 85% abrogation of neutrophil migration into the glomeruli in a model of toxin-induced renal injury (Roche et al., 2007). Similarly, neutralisation of both these chemokines resulted in an 84% decrease in neutrophil mobilisation in a model of peritonitis (Wengner et al., 2008). The potency of these chemokines in aiding neutrophil chemotaxis can be further increased through enzymatic cleavage by the metalloproteinases (MMPs), MMP9 and MMP8, both of which are proteases released by neutrophils, macrophages and ECs (Soehnlein and Lindbom, 2010). In addition to this, it is reported that macrophage-specific, MMP12, inactivates both chemokines through their cleavage, a vital step for the orchestration and regulation of neutrophil influx (Dean et al., 2008). In humans, the chemokine, CXCL8 (or IL-8), is analogous to the murine CXCR2 ligands; this acts via CXCR2 in the same way as CXCL1/2 to induce the same potent recruitment of neutrophils to sites of infection (Baggiolini et al., 1989).

In addition to recruitment of neutrophils within the circulation, chemokines also promote mobilisation of the BM store as previously discussed (see section 1.1.2.3), to ensure adequate supplies of circulating neutrophils. Furthermore, chemokines critically activate integrins during the multi-step leukocyte adhesion cascade (see section 1.1.2.4.1). On the whole, these mechanisms ensure influx of neutrophils to sites of infection or injury to rapidly eliminate any pathogens or damaged tissue by phagocytosis, ROS and protease production. However, it is worth mentioning that many neutrophil functions can be potentially harmful to the host and thus may have causative roles in many diseases (refer to section 1.2).

1.1.2.4.1 The multi-step adhesion cascade

During inflammation, leukocytes have to cross the blood vessel wall; a process involving the penetration of multiple barriers including vascular ECs, pericytes and a basement membrane that is generated by both of these cell types (Nourshargh et al., 2010; Voisin and Nourshargh, 2013). This process requires the induction of cellular machinery to physically aid the process of extravasation. In addition to leukocyte-targeted chemokines, activated tissue resident macrophages also release inflammatory mediators (such as, TNF and IL-1β) that activate and alter the phenotype of the vascular endothelium (Nourshargh et al., 2010). The cellular mechanisms that support the efficient extravasation of inflammatory cells from the circulation, through the blood vessel wall, and into the interstitial tissue is a well-characterised phenomenon that involves 5 main stages: thethering/rolling, firm adhesion, luminal crawling, transendothelial migration (TEM), and abluminal crawling/interactions with pericytes and basement membrane penetration (**Figure 1.3**); collectively, this process is termed the 'multi-step leukocyte adhesion cascade' (Ley et al., 2007).

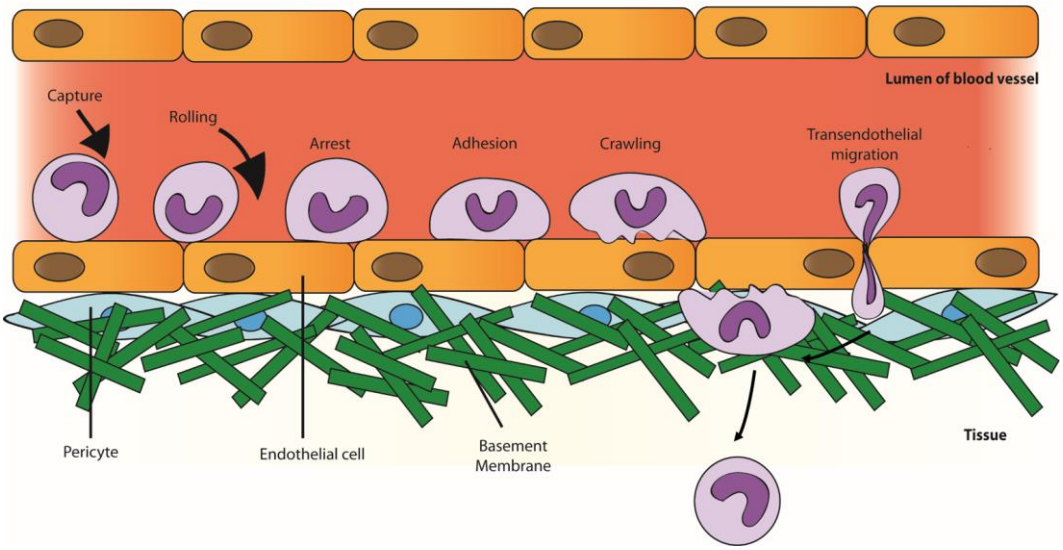

Figure 1.3: The multi-step leukocyte adhesion cascade. Following inflammatory insult, circulating leukocytes migrate into peripheral tissues in response to secretion of cytokines and chemokines by resident immune cells. Leukocytes are first captured on the vascular endothelium before beginning the rolling process, which is mediated by selectins. Chemokines drive activation of rolling and leukocyte activation, which enables arrest and firm adhesion to the endothelium followed by subsequent crawling. The leukocyte eventually transmigrates by either the transcellular or paracellular route (depicted). This is followed by abluminal crawling/interactions with pericytes and basement membrane penetration before it detaches from the blood vascular endothelium and goes into the interstial tissue. Figure adapted from (Nourshargh et al., 2010).

Circulating leukocytes, including neutrophils, are captured and begin rolling along the venular wall by interaction of leukocyte-expressed L-selectin and activated endothelium-expressed E- and P-selectin, with both endothelium and leukocyte-expressed P-selectin glycoprotein ligand 1 (PSGL1) (McEver and Cummings, 1997). Leukocyte integrins also take part in rolling and play a pivotal role in the subsequent arrest of leukocytes and their firm adhesion to the endothelium. Chemokines are essential for the activation of these integrins leading to inside-out signalling, which results in conformational changes in the functionally inactive integrin to an active adhesive configuration (Abram and Lowell, 2009). This causes an increase in ligand binding affinity and clustering of integrins in the cell membrane, which allows cell attachment (Abram and Lowell, 2009).

The recruitment of leukocytes into tissue is regulated by a sequence of interactions between the circulating leukocytes and the endothelial cells. In the case of neutrophils, this occurs via the leukocyte-expressed β_2-integrins, namely, lymphocyte function-associated antigen 1 (LFA-1, $\alpha_L\beta_2$-integrin) and macrophage-1 antigen (MAC-1, $\alpha_M\beta_2$-integrin), interactions with the endothelial intracellular adhesion molecule 1 (ICAM-1) (Ley et al., 2007). In the case of monocytes and lymphocytes, this occurs via the β_1-integrin, very late antigen 4 (VLA-4, $\alpha_4\beta_1$-integrin) interactions with vascular cell-adhesion molecule 1 (VCAM-1) (Ley et al., 2007). These integrins support intraluminal crawling of firmly adhered leukocytes; a process involving the formation of membrane protrusions and microvilli that interact with adhesion molecules expressed on the inflamed vascular endothelium (Kansas, 1996). In neutrophils, LFA-1 has been shown to be more important for adhesion, whilst MAC-1 has been shown to be key for intraluminal crawling; both integrins interact with ICAM-1 and this ultimately leads to efficient emigration out of the vasculature (Phillipson et al., 2006). ICAM-2 also plays a role in facilitating luminal interactions between neutrophils and ECs (Halai et al., 2014). Chemokines expressed on the luminal side of the endothelium activate leukocytes through GPCR signalling, thus inducing conformational changes of leukocyte integrins that allow adhesion whilst chemotactic gradients along the endothelium provide directional cues for leukocyte crawling and TEM. This involves other endothelial-expressed adhesion molecules, including platelet/endothelial cell adhesion molecule 1 (PECAM-1), junctional adhesion molecules (JAMs), ICAM-1, ICAM-2, CD99, CD99L2 and endothelial cell-selective adhesion molecule (ESAM) (Bixel et al., 2007; Huang et al., 2006; Muller, 2003; Thompson et al., 2001; Wegmann et al., 2006; Woodfin et al., 2007). TEM occurs either by the paracellular route (between ECs) or the transcellular

route (through individual cells), thus allowing extravasated leukocytes to contribute to the immune response within inflamed tissues (Kolaczkowska and Kubes, 2013). Paracellular TEM is considered to be the most prevalent in the peripheral circulation (Schulte et al., 2011; Woodfin et al., 2011). The blood EC layer is surrounded by pericytes, which are embedded within the vascular basement membrane (Diazflores et al., 1991; Shimada et al., 1992; Voisin et al., 2010), thus forming an additional barrier for transmigrating leukocytes. Once through the endothelium, abluminal crawling of neutrophils along the pericyte layer occurs (through MAC-1/LFA-1 interactions with ICAM-1). At this step, neutrophils also interact with the basement membrane, presumably via integrin-mediated mechanisms (VLA-3/6 interactions with laminin), before breaching the pericyte layer by migrating through gaps between adjacent cells, and regions of low matrix protein deposition (LERs) in the basement membrane (Voisin and Nourshargh, 2013). Finally, neutrophils detach from the vessel through the formation of an elongated uropod that must be disengaged before they can initiate their movement towards the site of inflammation (Hyun et al., 2012).

1.1.2.5 Neutrophil fate

During inflammation, neutrophils become activated resulting in increased viability and survival within the tissue; this ensures the presence of primed neutrophils at the inflammatory foci before they undergo cell death (Colotta et al., 1992; Summers et al., 2010). Daily, more than 10^{11} neutrophils undergo cell death in humans (Athens et al., 1961). It is generally agreed upon that the physiological form of cell death in neutrophils is apoptosis. Under homeostatic conditions, neutrophils are thought to be cleared from the circulation in the liver, spleen and BM; increased CXCR4 expression is seen in senescent neutrophils, which presumably aids in directing them back to the BM for their elimination (Furze and Rankin, 2008). For the resolution of inflammation, the control of neutrophil cell death and their subsequent clearance is crucial. Neutrophils undergo programmed cell death by apoptosis at inflamed sites and in addition, they are also killed at these sites by death receptor-induced apoptosis (Rae and MacEwan, 2004; Renshaw et al., 2000). Infiltrating macrophages have been shown to release death receptor ligands, such as TNF and Fas-ligand, which triggers neutrophil apoptosis (Renshaw et al., 2000). Additionally, phagocytosis of certain bacteria by neutrophils has been shown to augment their apoptosis at sites of infection (DeLeo, 2004). Finally, a new mode of neutrophil death via the prolonged expulsion of NETs has been discovered; the remnants of such

neutrophils and NETs themselves are cleared by macrophages along with extracellular DNase I degradation (Colotta et al., 1992; Farrera and Fadeel, 2013; Fuchs et al., 2007). Neutrophil cell death and their subsequent clearance is a crucial process that not only contributes to the maintenance of homeostatic cell numbers, but also ensures the safe disposal of phagocytosed bacteria and resolution of inflammation (DeLeo, 2004). It also drives the production of anti-inflammatory cytokines through clearance by resident or infiltrating macrophages (Hellberg et al., 2011). The interplay of all of these mechanisms ultimately promotes the resolution of inflammation.

1.1.3 Neutrophils in adaptive immunity

1.1.3.1 The adaptive immune response

Adaptive - or acquired - immunity is the second defence strategy found within all vertebrates (the other being innate immunity) (Boehm, 2012). The primary functions of adaptive immune responses are to recognise specific "non-self" antigens in the presence of "self antigens", generate immunity against pathogen-specific antigens (e.g. bacterial, viral, toxins) to eliminate them as well as infected cells, and develop immunologic memory for rapid elimination of a specific pathogen should subsequent infections occur (Bonilla and Oettgen, 2010; Warrington et al., 2011). Cells of the adaptive immune system include T cells, which are activated through the presentation of antigens to them by APCs (e.g. DCs, macrophages, monocytes, neutrophils) (Ni and ONeill, 1997; Radsak et al., 2000), and B cells within secondary lymphoid tissues. Adaptive immune responses are subdivided into two branches: cell-mediated and antibody-mediated immunity. Cell-mediated immunity is governed mainly by effector T cells and is directed primarily at pathogens that survive in phagocytes as well as those that infect other cells. This response specifically targets virus-infected cells, fungi, protozoa and intracellular bacteria, but can also participate in eliminating cancer cells (Warrington et al., 2011). Antibody-mediated immunity is mainly facilitated by B cell antibody production, which binds to antigens on the surface of pathogens, thus flagging them for destruction through classical complement activation and/or opsonisation supporting phagocytosis (Bonilla and Oettgen, 2010). During the initiation of adaptive immunity, naïve T cells are activated within lymphoid organs when they encounter an APC that has processed an antigen, which then displays it on cell-surface proteins known as the major histocompatibility complex (MHCs)

(Janeway, 1999). Interactions between naïve T cells (CD8+ and CD4+) and APCs displaying antigens on MHC-I and -II, respectively, stimulates the former to differentiate into mature cytotoxic T cells (CD8+ cells) or T-helper cells and regulatory T cells (CD4+ cells), respectively. The main function of cytotoxic T cells are to destroy cells infected by foreign agents. Clonal expansion of these cells results in the effector T cells, which release enzymes, such as perforin and granzyme (induces lysis of target cells), and granulysin (induces apoptosis of target cells) (Janeway, 1999). Following the clearance of infection, most effector T cells die and are removed by macrophages (Krammer et al., 2007). The few remaining cells develop into memory T cells, which will quickly differentiate into effector T cells that are able to rapidly respond upon subsequent encounters with the same antigen (Warrington et al., 2011). On the other hand, T-helper cells have no cytotoxic or phagocytic activity, and are therefore unable to directly destroy infected cells or pathogens. However, they mediate the immune response by directing other immune cells within the body to perform these tasks. They are known to produce various pro-inflammatory cytokines (e.g. IFNγ, TNF, IL-1β, IL-2, 4, 5, 6 and 17) that activate many cell types, including APCs, to indirectly assist the destruction of invading microbes (Janeway, 2005). In particular, the cytokines (IL-4, 5, 6) they produce stimulate activated B cells, which allows them to undergo proliferation and maturation into short-lived antibody-secreting plasma cells or memory B cells (Warrington et al., 2011). Memory B cells express antigen-binding receptors, and like memory T cells can rapidly respond and eliminate specific antigens upon re-exposure. Finally, another subclass of T lymphocytes, called regulatory T cells, exert their functions to maintain tolerance to self-antigens, and thus the prevention of autoimmune diseases. Overall, these processes take place over several weeks, ultimately resulting in the development of antigen-specific T and B cell clones, and the formation of a pool of effector and memory lymphocytes, which are indispensable for the elimination of invading pathogens, foreign agents and tumour cells (Alberts, 2002).

1.1.3.2 Role of neutrophils in shaping adaptive immune responses

Neutrophils have always been classically thought of as being cells pivotal for the first line of defence against invading pathogens. However, recent evidence has mounted suggesting their importance in the orchestration of adaptive immunity. During the early phase of infection, a characteristic influx of neutrophils and monocytes precedes the establishment of adaptive immune response. During this phase, small numbers of tissue-

resident effector memory T cells are also recruited to the site of infection, some of which can be activated and proliferate "*in situ*" in response to antigen presentation by DCs (McGill and Legge, 2009). Additionally, inflammatory cytokines produced by activated macrophages cause the proliferation and activation of non-specific T cells in a process called "bystander response"; one that was first observed in viral infections (Tough et al., 1996). It is thought that a large and uncontrolled bystander response might influence auto-immunity and self-reactivity through the activation and proliferation of self-reactive T cells (Burroughs et al., 2011). Thus, there is a possibility that neutrophils are involved to limit and control this response as the timing of *en masse* neutrophil recruitment into inflamed tissues and the bystander response coincide (**Figure 1.4**).

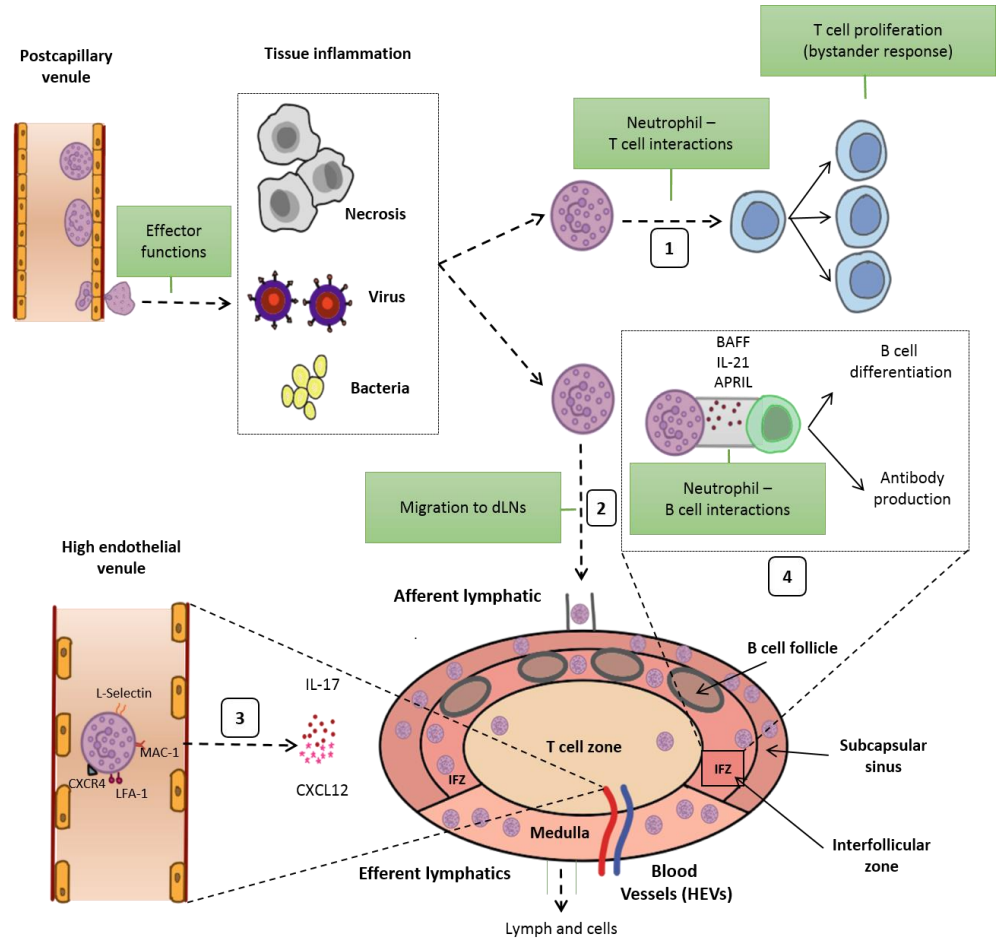

Figure 1.4: Invasion of pathogens (e.g. viruses and bacteria) or inflammation due to necrosis and cancer leads to extravasation of neutrophils across postcapillary venules. (1) Interaction of neutrophils with T cells within the inflamed tissue leading to the bystander response. (2) Migration of neutrophils to draining lymph nodes (dLNs) via afferent lymphatics during inflammation (mechanisms discussed in section 1.6. (3) IL-17 and CXCL12-mediated migration of neutrophils via HEVs to the LN that requires MAC-1, LFA-1, L-selectin and CXCR4. (4) Activation of humoral responses by neutrophils in the IFZ and medullary region through the secretion of APRIL, BAFF and IL-21. HEV, high endothelial venule; IFZ, interfollicular zone; APRIL, a proliferation-inducing ligand; BAFF, B cell activating factors.

Contrary to previous generally held views that neutrophils die within peripheral tissues following their recruitment to inflamed sites, it has since been shown that infection-induced inflammation results in neutrophils being the first lymph-born antigen-carrying cell type found within draining lymph nodes (dLNs) (Abadie et al., 2005; Chtanova et al., 2008; Hampton et al., 2015; Mocsai, 2013). To date, most studies investigating the cellular transport of antigens to LNs for the initiation of adaptive immune responses have focused on the ability of DCs to exert this function, which will be discussed in section 1.5. DC mobilisation to dLNs is a slow process that typically only peaks a couple of days after activation of the inflammatory response. In contrast, neutrophils have been found within dLNs as early as 4-6 h following inflammatory insult, suggesting that this early neutrophil influx may influence the developing immune response (Beauvillain et al., 2011; Hampton et al., 2015; Yang and Unanue, 2013). Neutrophils have been shown to migrate to dLNs in response to tissue inflammation in various murine models, such as following injection of bacteria such as *Staphylococcus aureus* (Hampton et al., 2015; Kamenyeva et al., 2015), *Listeria monocytogenes* (Chtanova et al., 2008), *Pseudomonas aeruginosa* (Lammermann et al., 2013), *Yersinia pestis* (St John et al., 2014) or BCG (Abadie et al., 2005). Neutrophils have also been found within dLNs following infections with the protozoan parasites *Toxoplasma gondii* (Chtanova et al., 2008) and *Leishmania major* (Tacchini-Cottier et al., 2000), as well as after intradermal administration of viruses like modified vaccinia virus Ankara (Abadie et al., 2009; Sagoo et al., 2016). Neutrophils have also been demonstrated to play roles in many models of vaccination and allergy, which are mainly used to study the development of adaptive immune responses (Leliefeld et al., 2015). These cells are able to effectively cross-prime CD8+ T cells in a MHC-I-dependent manner (Beauvillain et al., 2007), function as APCs (Abi Abdallah et al., 2011; Maletto et al., 2006), or influence the capacity of other APCs to present antigens (Schuster et al., 2013). For example, DCs have been shown to uptake antigens from phagocytosed apoptotic neutrophils (Schuster et al., 2013).

The localisation of different immune cells within LNs is strongly linked to their particular functions. Therefore, the localisation of neutrophils within LNs will determine which cells they encounter and may elucidate LN-specific neutrophil functions (**Figure 1.4**). Afferent lymphatic vessels drain lymph into the subcapsular sinus of dLNs. This region is located between the capsule and cortex, and has been shown to be the site of entry for pathogens and innate immune cells, including neutrophils (Chtanova et al., 2008; Kastenmuller et al., 2012; Yang et al., 2010). Neutrophils have also been observed in the

interfollicular zone (IFZ) of the LN following bacterial-induced infections; the IFZ is the region located directly below the subcapsular sinus (Cheminay et al., 2004; Kamenyeva et al., 2015; Kastenmuller et al., 2012). In this region, neutrophils are located in close proximity to T and B cells, as well as innate-like lymphocytes such as γδ T, NK and NKT cells, and they have been found to amplify the anti-pathogenic activities of these lymphocytes by enhancing their IFN-γ production (Kastenmuller et al., 2012; Kamenyeva et al., 2015). Within this region, they also exhibit short- and long-term interactions with B cells, thus inhibiting the production of antibodies and subsequently the humoral immune response (Kamenyeva et al., 2015). Conversely, neutrophils have been observed to contribute to antibody production as well as activating B cells through the production of B cell activating factors (BAFF), a proliferation-inducing ligand (APRIL) and the cytokine, IL-21 (**Figure 1.4**) (Puga et al., 2014). A small number of neutrophils have also been detected in the T cell zone following bacterial infection (Abadie et al., 2005; Kamenyeva et al., 2015) (**Figure 1.4**). Here, neutrophils have been shown to present antigens to T cells *in vitro*; whether or not this occurs *in vivo* is currently unknown (Takashima and Yao, 2015). Finally, neutrophils have also been detected within the medullary regions of lymph nodes following bacterial-induced infections (Kamenyeva et al., 2015; Kastenmuller et al., 2012). Little is known about their precise role in this location, but it is thought they are localised within this region to prevent pathogen dissemination via the efferent lymphatic vessels. Collectively, all of these results provide evidence that alongside their roles in innate immunity within inflamed tissue, neutrophils may also play roles in regulating adaptive immune responses (**Figure 1.4**). Thus, further investigations into the mechanisms of neutrophil migration (also known as intravasation) into the lymphatic system are key in increasing our understanding and potentially allow us to manipulate adaptive immune responses.

1.2 Neutrophils in disease

Leukocyte recruitment to sites of infection or injury is an essential response for the clearance of pathogens and cell debris, leading to the subsequent restoration of tissue homeostasis. Immune cells involved in the inflammatory response clearly have powerful functions, which have to be tightly regulated in order to not cause any damage to the host. Whilst the pathogenesis of many diseases is highly complex and thus poorly understood, increasing evidence has pointed to the dysregulation of immune cell infiltration, particularly in the context of neutrophils, as the underlying cause of many diseases. Therefore, understanding the exact context of dangers to the host versus the importance of leukocyte infiltration could provide potential new targets for the treatment of inflammatory conditions.

1.2.1 Sepsis

Sepsis is a rare but life-threatening condition that arises when the body's responses to infection results in injury to its own tissues and organs. The pathogenesis of sepsis is unclear, although most cases are initiated by gram-negative bacterial infection of the blood, abdomen, lungs or urinary tract (Cohen, 2002). Activation of leukocytes and the vascular endothelium by bacteria results in the activation of complement, imbalance of coagulation pathways, and the production of cytokines and subsequent oxygen and lipid intermediates. The result is a combination of vascular instability triggered by an uncontrolled and systemic inflammatory response responsible for the classical signs of septic shock (fever, vasodilation, increased vascular permeability), characterised by multiple organ failure (MOF) and profound immune suppression (Angus and van der Poll, 2013).

The recruitment and migration of neutrophils to sites of infection is significantly reduced during sepsis, thus resulting in the loss of a crucial arm of the innate immune response to infection (Benjamim et al., 2000). Several mechanisms responsible for this impairment in the directed migration of neutrophils include cytoskeletal changes, disruption of leukocyte–EC interactions, and alterations in GPCR expression or signalling, as well as nitric oxide (NO)-mediated alterations in neutrophil chemotaxis (Fialkow et al., 2007; Freitas et al., 2006; Yoshida et al., 2006). Moreover, the function of neutrophils are affected during sepsis via toll-like receptors (TLRs) and GPCR signalling, as well as

NETs formation, all of which lead to overexpression or enhanced activity of pro-inflammatory mediators resulting in tissue damage and MOF (Clark et al., 2007; Hakkim et al., 2010). TLRs are expressed by immune cells and recognise self and non-self structures, such as pathogen-associated molecular patterns (PAMPs) derived from microbes, and danger-associated molecular patterns (DAMPs) released during tissue injury. It is therefore clear that the dysregulation of neutrophil function results in sepsis. However, exactly how this response becomes both aberrant and systemic to culminate in sepsis is considered a complex web of events that are not entirely clear.

1.2.2 Ischaemia reperfusion injury

Ischaemia reperfusion (I/R) injury is another example of neutrophil recruitment having a causative role in tissue damage. Ischemia occurs during myocardial infarction (MI), stroke, or organ transplantation, followed by the essential reperfusion phase, whereby oxygen is reintroduced to the tissue (Eltzschig and Eckle, 2011). Absence of the reperfusion phase would result in tissue death due to the lack of oxygenation. Restoration of blood flow in the reperfusion phase is accompanied by the release of cytokines and chemokines, activation of vascular ECs, up-regulation of adhesion molecules and activated neutrophil accumulation within the reperfused area (Eltzschig and Eckle, 2011; Vinten-Johansen, 2004). Recruitment and activation of neutrophils results in ROS generation and subsequent imbalances of superoxide (O_2-) and NO; these imbalances promote the accumulation of highly toxic oxygen products, such as peroxynitrite (OONO-), hypochlorous acid (HOCI) and hydrogen peroxide (H_2O_2), all of which have the capacity to oxidise DNA, proteins and lipids, thus resulting in cell destruction and ultimately tissue damage (Thannickal and Fanburg, 2000). The release of inflammatory mediators and activated leukocytes into the circulation during the reperfusion phase therefore results in remote organ damage, and is a severe problem following ischaemic events as it could potentially result in MOF (Pierro and Eaton, 2004; Woodfin et al., 2011). The role of neutrophil infiltration in enhancing the progression of disease has been demonstrated in neutrophil depletion experiments that resulted in suppression of neutrophil toxic activities in models of myocardial (Kohtani et al., 2002), kidney (Klausner et al., 1989), liver (Jaeschke et al., 1990) and brain (Matsuo et al., 1995) I/R.

1.2.3 Rheumatoid arthritis and other neutrophil-related autoimmune diseases

Rheumatoid arthritis (RA) is an autoimmune disease that causes inflammation in the affected joints. Amongst all the cells implicated in the pathology of RA, neutrophils are the ones that retain the greatest cytotoxic potential, due to their capacity to release degradative enzymes and ROS (Wright et al., 2014). During the acute phase of the disease in RA patients, neutrophils are the most abundant immune cells found within the synovial fluid (SF) of the affected joints; they have also been found at the pannus/cartilage boundary in synovial tissue, where active destruction of cartilage and bone occurs (Mohr, 2003). Following their migration into RA joints, activated neutrophils encounter complexes of immunoglobulins, such as rheumatoid factor (RF), within the SF and on the surface of the joint. These immune complexes bind to Fcγ receptors expressed by neutrophils and results in their degranulation and production of ROS, either into the SF or directly onto the joint surface in a process called 'frustrated phagocytosis' (Kraan et al., 2000). Oxidative stress resulting from the inappropriate release of ROS by activated neutrophils is implicated in the pathology of RA, and neutrophils isolated from SF of RA patients have shown evidence of initiated ROS production *in vivo* (Elferink et al., 1997). These oxygen radicals result in DNA damage, oxidation of lipids, proteins and lipoproteins, and have potentially been implicated in causing immunoglobulin mutations that lead to the formation of RF (Akahoshi et al., 1997; Wandall, 1991). Degranulation has also been demonstrated to contribute to host tissue damage, particularly in the destruction of the collagen matrix within cartilage (Hoenderdos et al., 2016). Emerging evidence suggests that neutrophil release of NETs, which is a killing mechanism for extracellular microorganisms, also provide a source of autoantigens, such as citrullinated proteins (Romero et al., 2013). In fact, citrullinated proteins have been detected within SF before the onset of symptoms in RA patients, and can be predictive of erosive disease (Romero et al., 2013). Furthermore, neutrophils isolated from patients with RA have been found to have an increased tendency to form NETs containing citrullinated proteins, in addition to autoantibodies recognising these proteins being present in the sera of these patients (Pratesi et al., 2014). Thus, this suggests that neutrophils may be a source of the autoantigens that drive the autoimmune processes underlying RA. In line with this, one of the crucial pathogenetic features of another autoimmune disorder, systemic lupus erythematosus (SLE), is the presence of DNA-containing immune complexes, which triggers interferon-α (IFNα) production by plasmocytoid DCs (Ronnblom and Pascual,

2008). The source of this extracellular DNA has been shown to originate from NETs, thus implicating neutrophils in this disease (Garcia-Romo et al., 2011; Lande et al., 2011).

In small vessel vasculitis (SVV), a chronic autoinflammatory condition linked to antineutrophil cytoplasm autoantibodies (ANCA), ANCA-stimulated neutrophils release NETs which contain autoantigens and MPO (Kessenbrock et al., 2009). The deposition of these NETs in inflamed kidneys and circulating MPO-DNA complexes indicates that NET formation triggers vasculitis and thus results in the autoimmune response against neutrophil components in SVV patients (Kessenbrock et al., 2009).

The introduction of TNF inhibitors, or anti-TNF therapies, has majorly improved the treatment of RA, providing a mechanism to treat even patients severely affected by the disease. TNF is a pro-inflammatory cytokine that influences many elements of immune dysregulation that contributes to disease, such as cellular infiltration into RA-affected joints, cytokine synthesis and the production of autoantibodies. TNF has been shown to prime neutrophil respiratory bursts, up-regulate the expression of adhesion molecules, cytokines and chemokines, as well as stimulate ROS production when present locally at high concentrations (Cross et al., 2008; Dewas et al., 2003; Fujishima et al., 1993; Ginis and Tauber, 1990). Anti-TNF therapy is able to successfully block cytokine and chemokine synthesis in synovial tissue, lower concentrations of MMPs, reduce the influx of immune cells (neutrophils in particular) to synovial joints by down-regulating the expression of adhesion molecules, induce the apoptosis of monocytes and macrophages, as well as restore regulatory T cell function, which is important in maintaining tolerance to self-antigens and in the prevention of autoimmune diseases (Feldmann et al., 2010). Anti-TNF therapy also results in the down-regulation of neutrophil activation through decreasing cytokine production and (nuclear factor- kappa B) NF-κB expression, all of which are associated with improvements in disease activity (Wright et al., 2011). Treatment for SVV incorporates cytotoxic drugs and glucocorticoids (Molloy and Langford, 2006). However, these are associated with significant risks of relapse and treatment-related toxicity (Molloy and Langford, 2006). Existing treatment for SLE include nonsteroidal anti-inflammatory drugs (NSAIDs) and immunosuppresants (Haubitz, 2010). However, the first ever targeted drug, Belimumab, for the treatments of these patients has been approved by the Food and Drug Administration (FDA), and results have been positive (Dubey et al., 2011). Belimumab works by decreasing B cell survival and the production of autoantibodies (Halpern et al., 2006).

RA, sepsis and I/R injuries are 3 diverse examples of inflammatory conditions, where neutrophil infiltration along with their associated functions no longer result in helpful responses, but instead result in host attack. These conditions are a result of dysfunctional regulation and therefore demonstrate the importance of understanding mechanisms of leukocyte recruitment both into peripheral tissues and the lymphatic system, in the clearance of infection and tissue damage along with the restoration of normal tissue homeostasis.

1.3 The lymphatic system

The lymphatic vascular system is the second circulatory system within the human body that is crucial for tissue homeostasis and a vital part of the immune system. It is composed of a unidirectional system of conduits interrupted by LNs that run in parallel to the blood vascular system (**Figure 1.5**) (Teijeira et al., 2013). The lymphatic system works in conjunction with the blood vascular system and plays an important role in the regulation of tissue fluid resorption, facilitating interstitial protein transport, and immune surveillance through the initiation of adaptive immunity (Pepper and Skobe, 2003). It is the afferent lymphatics that control the trafficking of antigen-presenting leukocytes into LNs, where initiation of the adaptive immune response takes place. Lymphatic vessels carry a clear fluid called lymph, which comprises of lymphocytes, APCs, lipids, waste

products and cellular debris (pathogens and proteins), directionally towards the heart

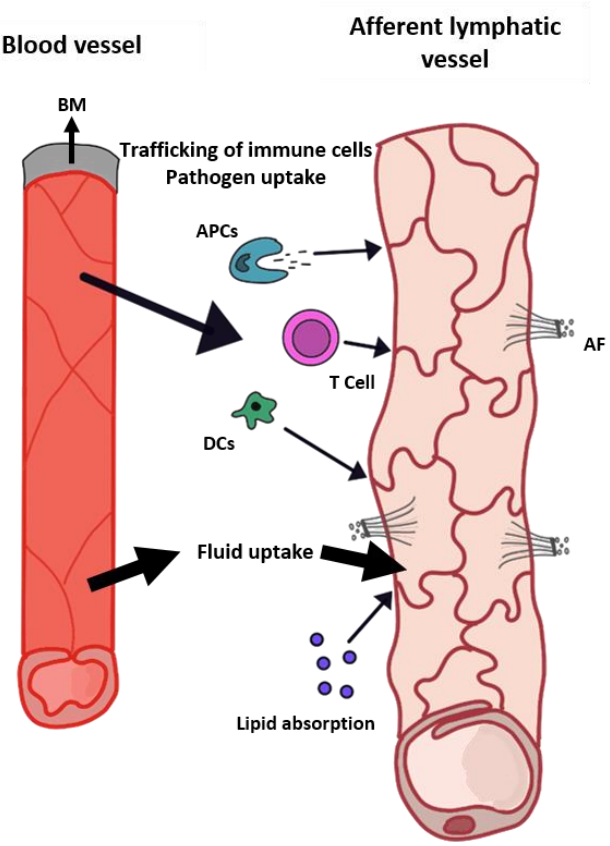

(**Figure 1.6 &**

Figure 1.5).

Lymph is formed when constituents of the blood exit blood vessels and enter initial lymphatic vessels along with interstitial fluid and its constituents (**Figure 1.5**). The lymph is then transported along the lymphatic vessel network through either intrinsic contractions of the vessels themselves or through extrinsic compression of the vessels via external tissue forces, such as skeletal muscle contractions, respiratory movement and contraction of smooth muscle cells in walls of collecting lymphatic vessels (Cueni and Detmar, 2008). The function of initial lymphatics is heavily dependent on its connections with the extracellular matrix (ECM); anchoring filaments attach lymphatic endothelial cells (LECs) to interstitial collagen, which provides structural integrity and prevents the collapse of these vessels when interstitial pressure rises (**Figure 1.5**) (Gerli et al., 1990; Leak and Burke, 1966). Eventually, the lymph is returned to the blood circulation through drainage into thoracic or lymphatic ducts, which join up to one of the two subclavian veins (**Figure 1.6**) (Choi et al., 2012).

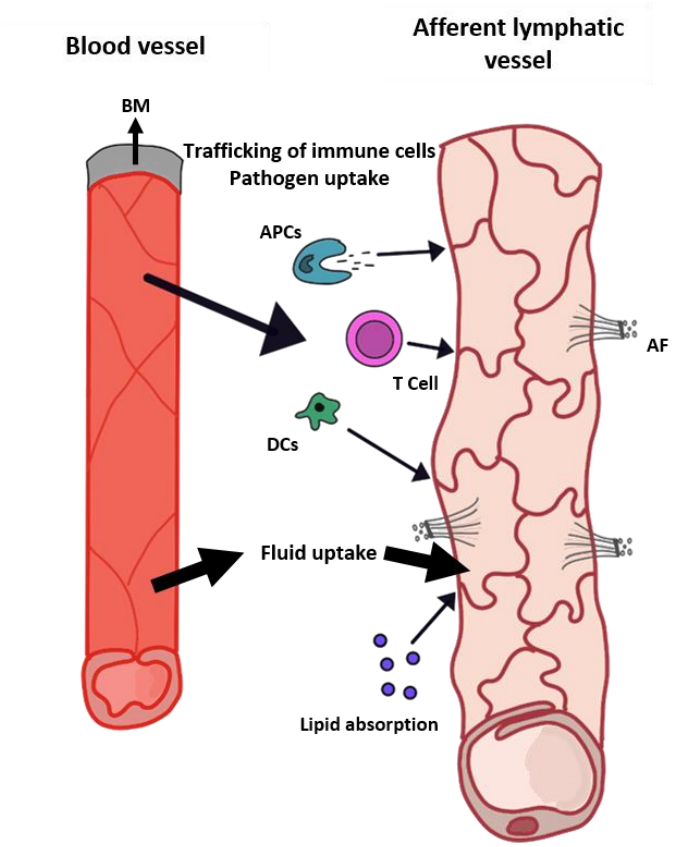

Figure 1.5: Fluid exchange between blood vessels and lymphatics. Initial lymphatics are uniquely adapted for the uptake of fluid, lipids, macromolecules, cellular debris and cells from the interstitial tissue. In contrast to blood vessels, afferent lymphatic vessels have a relatively undeveloped basal lamina (BM) and lack pericytes (P). LECs are connected directly to the interstitial collagen via anchoring filaments (AF). BM, bone marrow; DC, dendritic cell; APC, antigen-presenting cell.

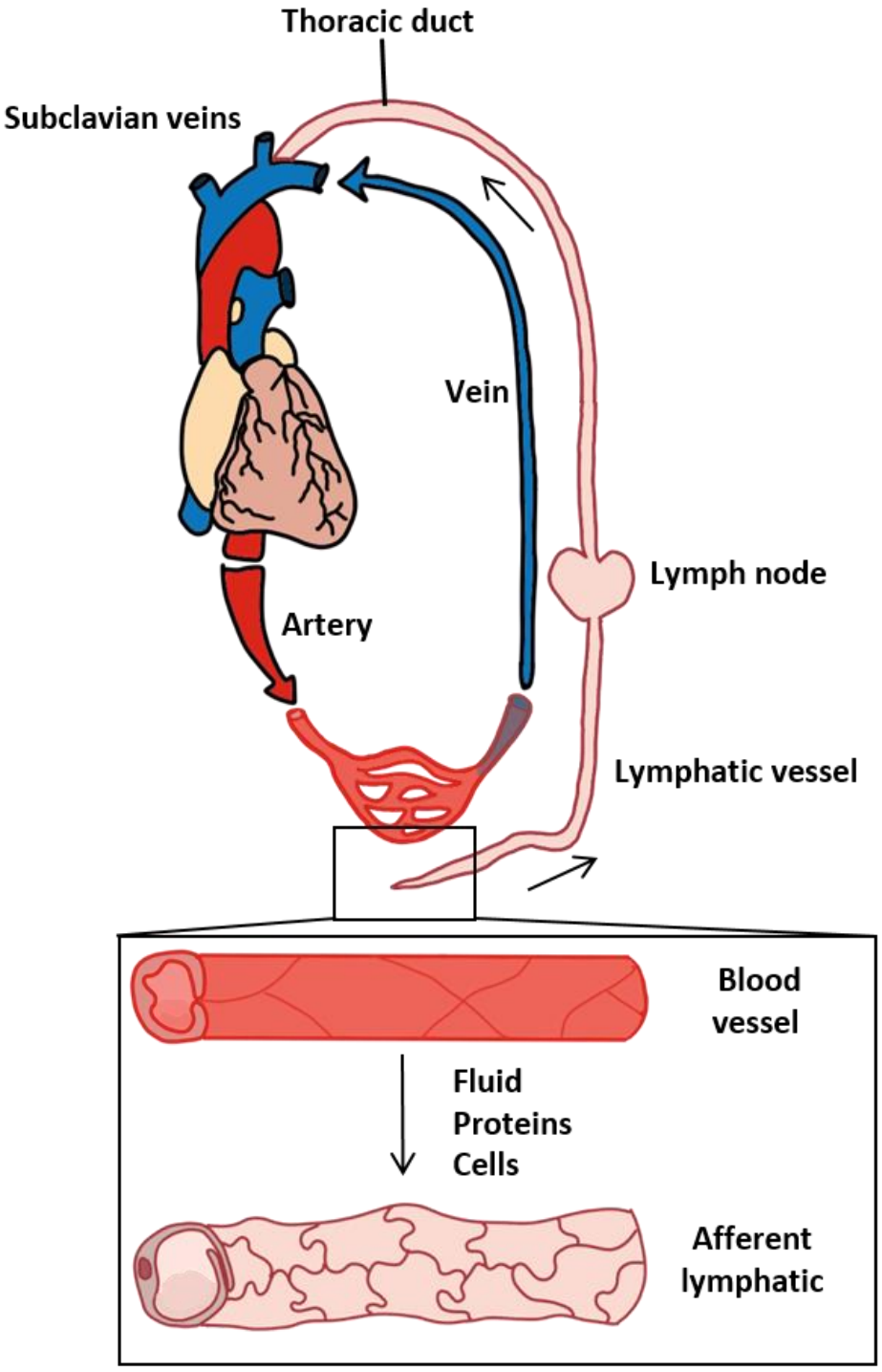

Figure 1.6: The circulatory system. The lymphatic vasculature collects fluid from the interstitial space that has exited the blood vessels, and transports it towards the heart via the filtering mechanism of the LNs into collecting vessels that connect through the thoracic ducts into the subclavian veins.

1.3.1 Structural organisation of the lymphatic endothelium

Despite many advances in the investigation towards understanding lymphatic function, the cellular features responsible for entry of fluid and cells into the lymphatic system are still not completely understood (Oliver and Alitalo, 2005). It has since been reported that the unique junctional organisation of the lymphatic endothelium plays an important role in the recirculation of fluid and cells in normal tissue homeostasis, inflammatory diseases and cancer (Baluk et al., 2007; Dejana et al., 2009). Initial lymphatic vessels express the lymphatic vessel endothelial receptor-1 (LYVE-1) and Prox-1 (prospero-related homeobox gene 1) (Baluk et al., 2007). Initial lymphatic vessels are characterised by round blinded-ends and have been found to exhibit overlapping flaps at borders of oakleaf-shaped LECs, which lack junctions at the tips but are anchored on the sides by discontinuous button-like junctions (buttons); this is in contrast to collecting lymphatic vessels and blood vessels, which exhibit continuous, zipper-like junctions (zippers) (**Figure 1.7**) (Baluk et al., 2007; Dejana et al., 2009). Buttons are found at the perimeter of LYVE-1–positive LECs. Both buttons and zippers are composed of vascular endothelial cadherin (VE-cadherin) and tight junction-associated proteins including claudin-5, occludin, occludens-1, junctional adhesion molecule-A (JAM-A), and ESAM (Baluk et al., 2007). Additionally, PECAM-1 and LYVE-1 partially co-localise at flaps on the borders of oak leaf–shaped LECs of initial lymphatics, and at zippers of collecting lymphatics (Baluk et al., 2007).

In initial lymphatics, the free overlapping cell edges form ‘flap valves’ through which fluid flows unidirectionally along pressure gradients from the interstitium into the initial lymphatic lumen. Whole mount experiments have also revealed that these loose flaps are about 2–3 μm in diameter, through which leukocytes (DCs and T cells) are thought to migrate into the lymphatic vessel lumen; they have been shown to do this by squeezing through and subsequently displacing the flap valves towards the lumen of the lymphatic vessel (Baluk et al., 2007; Pflicke and Sixt, 2009). It has been described that actively sprouting lymphatics have zippers rather than buttons, which suggests that these button-

like junctions are a specialised characteristic of quiescent and functionally active initial lymphatics (Baluk et al., 2007).

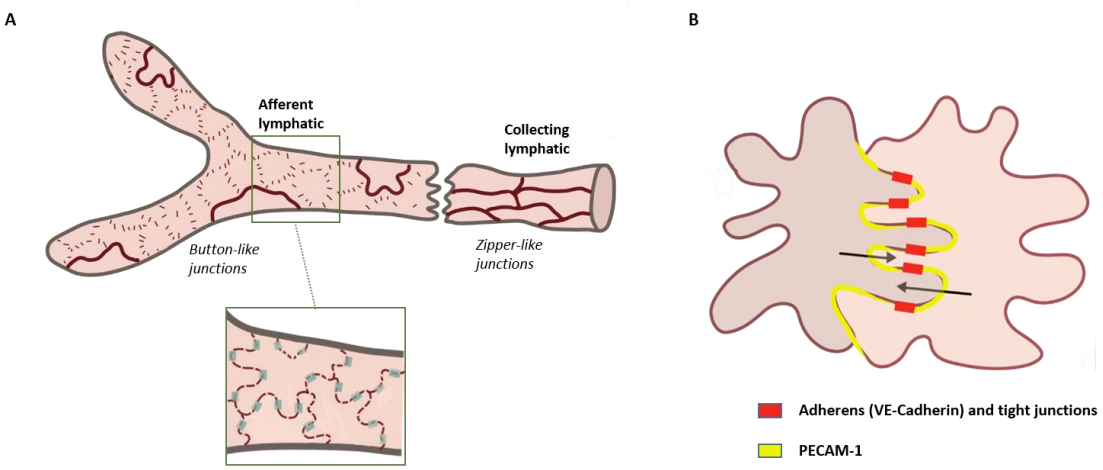

Figure 1.7: Button-like junctions in initial lymphatics border sites of fluid entry. (**A**) Schematic diagram showing distinctive, discontinuous buttons in endothelium of initial lymphatics and continuous zippers in collecting lymphatics. The magnified insert (green box) shows a more detailed view of oakleaf-shaped LECs with button-like junctions. Buttons (green) appear to be perpendicular to cell borders but are actually parallel to the sides of flaps. (**B**) Enlarged view of oakleaf-shaped LECs showing that flaps of adjacent LECs have complementary shapes with overlapping edges. Adherens and tight junctions parallel to flaps direct fluid entry (black arrows) to the junction-free region without disruption and reformation of junctions.

1.3.2 Lymphatic and vascular endothelial cell glycocalyx

Amongst the few universal biological findings, it has been established that all mammalian cells are covered with a dense coating of glycans (Varki and Varki, 2007). This layer, known as the glycocalyx, spans between several hundred nanometres to a few micrometres; and lines the surface of cells (Reitsma et al., 2007). In particular, blood vascular endothelial cells (BECs) cover the entire luminal surface of the vascular system, where the glycocalyx forms a barrier between circulating blood and the venular wall (Haldenby et al., 1994; Wang, 2007). It is worth pointing out that a considerable lack of literature is available regarding the composition of the glycocalyx on lymphatic vasculatures, with the presence of a glycocalyx on LECs being largely unknown. However, it has recently been reported that the LEC glycocalyx exists on the LEC membrane of rat mesenteric collecting lymphatic vessels, with an indication that it is highly likely that the composition of the LEC glycocalyx is similar to that of the glycocalyx found on blood vessels (Zolla et al., 2015). This suggests that the LEC glycocalyx may play similar roles to the BEC glycocalyx.

The majority of studies investigating the glycocalyx involves the blood vasculatures, therefore the role of the LEC glycocalyx could potentially be inferred from them (Kolarova et al., 2014; Reitsma et al., 2007; Tarbell et al., 2005; Van Teeffelen et al., 2007; Wang, 2007). Studies have indicated that the BEC glycocalyx plays an important role in numerous physiological processes, including regulation of vascular permeability, regulation of leukocyte adhesion during TEM, mechanotransduction of shear stress and the modulation of inflammatory processes (Kolarova et al., 2014; Reitsma et al., 2007; Tarbell et al., 2005; Wang, 2007). A number of studies have shown that perturbation of the glycocalyx structure in response to inflammatory mediators, such as cytokines and chemoattractants, promote inflammatory processes in vessels and contribute to the development of vascular diseases, such as atherosclerosis (Nieuwdorp et al., 2007; van den Berg et al., 2006; Vink et al., 2000).

Theoretical models and experimental research over the years have shown that the glycocalyx is a complex carbohydrate layer comprised of membrane-bound macromolecules from plasma proteins and the glycoproteins (e.g. adhesion molecules, selectins and integrins) to the sulfated proteoglycans (e.g. syndecans, glypicans, mimecans, biglycan) along with their associated glycosaminoglycan (GAG) side chains

(**Figure 1.8**) (Kolarova et al., 2014). These molecules have also been recently reported to be found on the LEC glycocalyx (Zolla et al., 2015).

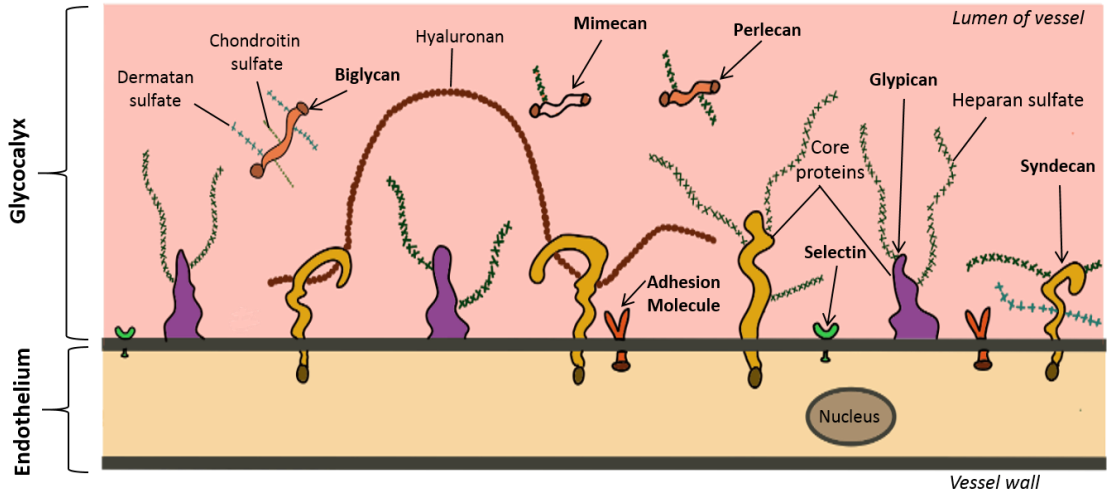

Figure 1.8: Schematic of the vascular EC glycocalyx. Situated within the luminal side of the vessel wall, the EC glycocalyx consists of glycoproteins (adhesion molecules, selectins and integrins), membrane-bound proteoglycans (syndecans and glypicans), as well as secreted proteoglycans (mimecans, biglycans, perlecans). All proteoglycans are attached to GAG chains, made up of HS, HA, DS and CS. HS occurs as a proteoglycan (HSPG)

GAGs are linear polymers of repeating disaccharides that are composed of D-glucoronic acid, L-iduronic acid, or D-galactose linked to either D-N-acetylglucosamine or D-N-acetylgalactosamine (Kolarova et al., 2014). Specific combinations of these sugar residues give rise to different GAG families, such as heparan sulfate (HS), chondroitin sulfate (CS), and hyaluronan (HA), with HS being the most abundant in the BEC glycocalyx (Oohira et al., 1983). These GAGs interact with a variety of proteins and are involved in the mediation of numerous physiological and pathological functions, including inflammation.

Glycoproteins are small transmembrane molecules bound to the glycocalyx bearing acidic oligosaccharides and terminal sialic acids (SAs) (Van Teeffelen et al., 2007). Established oligosaccharides of glycoproteins include a variety of saccharide motives, including galactosyl residues, as well as N-acetyl-glucosamine and N-acetylgalactosamine (Pries et al., 2000; Weinbaum et al., 2007). Key glycoprotein players known to play significant roles in leukocyte TEM during an inflammatory response include the adhesion molecules such as intercellular adhesion molecules -1 and -2 (ICAM-1 and -2), platelet endothelial cell adhesion molecule-1 (PECAM-1), vascular cell adhesion molecule-1 (VCAM-1) and junctional adhesion molecule (JAM) family members (Muller, 2009).

As a whole, the BEC glycocalyx is involved in the regulation of leukocyte transmigration following inflammatory stimuli. The GAG, HS, is involved in the initial adhesion of leukocytes to the endothelium following inflammation by interacting with cytokines/chemokines and participating in leukocyte-selectin binding during TEM (Reitsma et al., 2007). Additionally, degradation of the glycocalyx has been shown to stimulate immobilisation of leukocytes at the endothelial surface prior to TEM (Constantinescu et al., 2003). A recent study also found that sepsis-associated acute lung injury was initiated by degradation of the pulmonary endothelial glycocalyx, leading to neutrophil adherence and inflammation (Schmidt et al., 2012). In lymphatic vessels, a recent report has shown that a decrease in the thickness of the LEC glycocalyx and its associated molecules is observed in aging lymphatic vessels; this is linked to enhanced permeability that results in increased extravasation of bacteria and fungi into peripheral tissues (Zolla et al., 2015). This decrease in the ability to transport bacteria to the dLNs, where adaptive immune responses are initiated, likely contributes to the reduced ability of the immune system to clear pathogens in the elderly. Furthermore, a reduction in the LEC glycocalyx and its associated molecules has been implicated in senescence-associated lymphatic vessel hyperpermeability leading to impaired fluid homeostasis (Zolla et al., 2015). This could also affect the transport of large molecules, lipids, proteins and products of tissue metabolism/catabolism, all of which are important for normal tissue homeostasis (Ahn and Simpson, 2007; Clement et al., 2011; Kolarova et al., 2014).

1.3.3 Development and phenotypic characteristics of lymphatic vessels

In the early twentieth century, Florence Sabin proposed the most widely accepted view of lymphatic development. Following ink injection experiments, she proposed that the peripheral lymphatic system originated by the sprouting of ECs from embryonic veins, leading to the formation of primitive lymph sacs from which LECs then sprout into surrounding tissues and organs to form mature lymphatic networks; a process known as lymphangiogenesis (Sabin, 1902, 1904). An alternative model has also been suggested where these primary lymph sacs arise in the mesenchyme independently from veins and secondarily established venous connections (Huntington and McClure, 1910). Following these pioneering studies, the field of lymphatic research remained neglected up till the discovery of new markers for LECs and identification of lymphatic growth factors, which has allowed the molecular mechanisms that control lymphatic development to be investigated (Oliver and Detmar, 2002). Importantly, these studies have generally

provided evidence to support Sabin's original hypotheses regarding lymphatic development within the mammalian system (**Figure 1.9**).

Prospero-related homeobox gene 1 (*Prox1*) was the first gene demonstrated to be essential for early lymphatic development. From embryonic day (E) 9.5 of murine development, Prox1 starts being specifically expressed in a sub-population of ECs located on one side of the anterior cardinal vein (Wigle et al., 1999). At this stage, the vascular endothelium also expresses the hyaluronan receptor, LYVE-1, which is a CD44 homologue (Banerji et al., 1999). The vascular EC growth factor receptor 3 (VEGFR-3), which is a receptor for the lymphangiogenesis factors, vascular endothelial growth factor (VEGF)-C and VEGF-D, is also expressed at this point (Alitalo and Carmeliet, 2002). The expression of both receptors, LYVE-1 and VEGFR-3 (now well-known LEC markers), becomes specific to the lymphatic endothelium during the later stages of development along with Prox1 (Kaipainen et al., 1995). Subsequently, polarised budding and migration of progenitor Prox1+ LECs leads to a gradual down-regulation of the blood vascular genes, such as CD34, CD31 and laminin, and increased expression of the lymphatic markers, VEGFR-3 and the lymphoid chemokine CCL21 (Wigle et al., 2002; Wigle and Oliver, 1999). Studies have revealed that mice express two functional isoforms of CCL21: $CCL21^{Ser}$, which is found in both lymphatics and LNs, and $CCL21^{Leu}$, which is only found within tissue-associated LECs (Nakano and Gunn, 2001; Vassileva et al., 1999).

The budding and sprouting of LECs from the veins of *Prox1* knockout (KO) mice is halted at around E11.5-E12.0; these mice have been observed to lack lymph sacs and lymphatic vessels, in conjunction with low survival rates due to multiple developmental defects (Wigle and Oliver, 1999). Additionally, EC-specific KO of *Prox1* has been shown to result in lymphatic vasculature defects, as well as postnatal lethality (Harvey et al., 2005). Nonetheless, the exact mechanisms of action of *Prox1* during and after switching over to the lymphatic from the blood vascular phenotype remain unknown. The only existing evidence is that overexpression of *Prox1* leads vascular ECs towards a LEC fate both *in vitro* (Hong et al., 2002) and *in vivo* (Kim et al., 2010). Collectively, these results identify *Prox1* as a master regulator gene in the programme specifying LEC fate (**Figure 1.9**) (Hong et al., 2002; Sleeman et al., 2001).

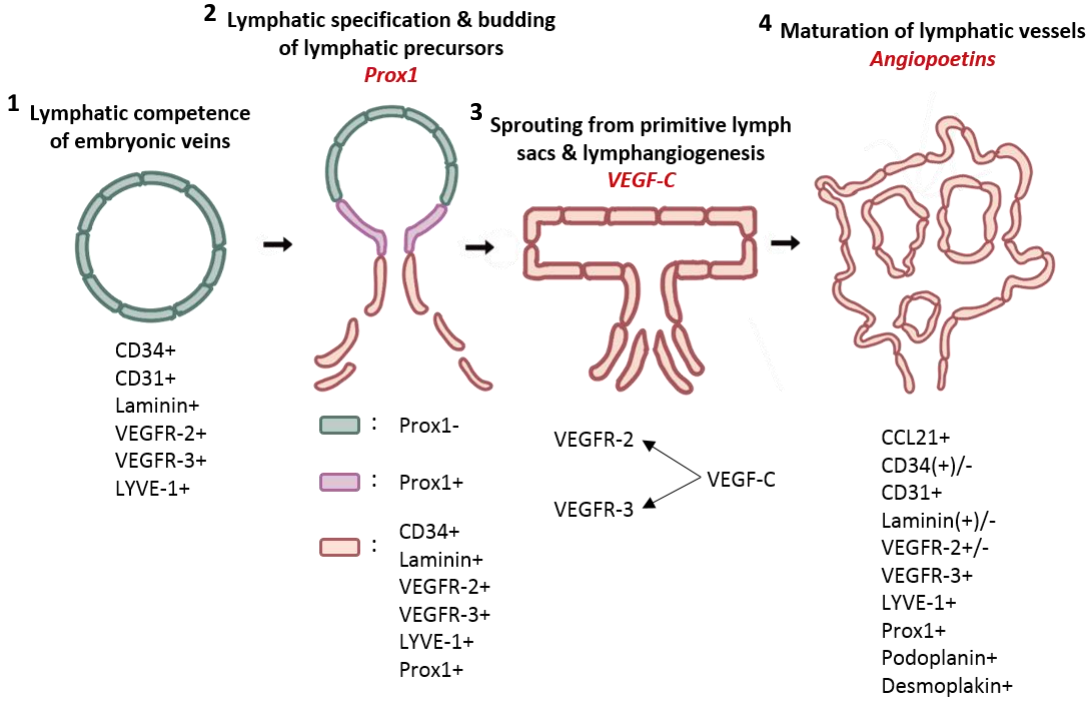

Figure 1.9: Hypothetical model of the distinct steps involved in the embryonic development of the mammalian lymphatic vasculature. (1) Embryonic veins are the origin of both the vein and lymph plexus. Lymphatic endothelial cell competence is the autonomous ability of venous ECs to respond to a specific, inductive signal. This stage is characterised by the appearance or disappearance of a receptor or by different expression levels of certain transcription factors. Specifically, two receptors are expressed on the surfaces of embroyonic cardinal veins: LYVE-1 and VEGFR-3. At this stage, it is not possible to determine whether lymphatic or venous vessels are involved, although both receptors characterise lymphatic vessels in adults. (2) An inductive signal, the origin of which is still unknown, triggers the expression of the homeobox gene *Prox1*. Prox1 starts being specifically expressed in a sub-population of ECs located on one side of the anterior cardinal vein. This results in LEC specification and the budding of lymphatic precursors signalling the first step towards the differentiation of embryonic cardinal ECs into LECs. (3) Specified LECs sprout towards VEGF-C producing mesodermal cells and aggregate to form lymph sacs. (4) Subsequently, polarised budding and migration of progenitor Prox1+ LECs leads to a gradual down-regulation of the blood vascular genes, such as CD34, CD31 and laminin, and increased expression of the lymphatic markers, VEGFR-3 and the lymphoid chemokine CCL21. The density of the VEGFR-3 receptors increases, and angiopoetins together with their Tie-2 receptors are produced, both of which are responsible for the further maturation of the newly formed lymphatic vessels. Figure adapted from Detmar and Hirakawa, 2002.

During the final developmental steps of the mature lymphatic network and their patterning, studies in angiopoietin-2 KO mice have suggested crucial roles of angiopoietins and their receptor, Tie2 (**Figure 1.9**) (Gale et al., 2002). However, the mechanisms controlling the sprouting of LECs from primitive lymph sacs followed by their migration into adjacent organs and tissues during lymphangiogenesis is still unclear. VEGF-C has been demonstrated to be a potent inducer of lymphatic sprouting and in addition to VEGFR-3, its interaction with its other known receptor, VEGFR-2, is also likely to be required for this process (Saaristo et al., 2002). Continual investigations into the development of lymphatic vessels, as well as the molecular cues governing their formation and morphogenesis are still missing, as further understanding of these processes may provide us with essential knowledge that might improve our ability to treat lymphatic-related diseases.

1.3.3.1 Neo-lymphangiogenesis

Once adulthood is reached, lymphangiogenesis primarily occurs during tissue regeneration, tumour growth, as well as during acute and chronic inflammation (Jones and Min, 2011). During inflammation, macrophages have been extensively shown to produce VEGF-C and VEGF-D, which leads to lymphangiogenesis (Cursiefen et al., 2004). In a murine model of *Mycoplasma pulmonis* infection, TNF signalling has been demonstrated to be involved in neo-lymphangiogenesis, but its effects on driving this process requires inflammatory mediators produced by recruited leukocytes (Baluk et al., 2009). Inflammation creates a hostile microenvironment, from which antigens, toxins and debris have to be immunologically removed. In parallel, excess interstitial fluid and oedema has to be drained, thus lymphangiogenesis occurs for efficient lymphatic draining and clearance of pathogens, as well as enhanced antigen presentation within dLNs to initiate an adaptive immune response (Kim et al., 2012). Indeed, the activation of lymphangiogenesis by overexpression of VEGFR-3-specific ligands has been demonstrated to result in the inhibition of acute and chronic inflammation (Huggenberger et al., 2011; Huggenberger et al., 2010). Nevertheless, neo-lymphangiogenesis can also result in adverse effects within the human body (see section 1.4.2), thus proper regulation of this process is key.

1.4 Lymphatic vessels in the pathology of diseases

Lymphatic vessels have unique roles in regulating fluid homeostasis, assisting in immune surveillance, as well as transporting dietary lipids. However, dysfunctional lymphatic vessels can result in severe pathologies, whilst normal lymphatic functions can also contribute to the exacerbation of diseases.

1.4.1 Lymphoedema

Infections, surgery, radiotherapy or genetic defects can result in the absence or dysfunction of lymphatic vessels, which leads to a set of pathological conditions called lymphoedema (Rockson, 2016). Lymphoedema is characterised by chronic accumulation of protein-rich fluid in tissues that results in swelling (oedema), usually of extremities. There are two classifications of lymphoedema: primary and secondary lymphedema. Primary lymphoedema has a genetic aetiology that results in the lymphatics being unable to drain fluid away from parts of the body; this can present at birth or arise later in life (Jones and Min, 2011). Milroy's disease is an example, which results in congenital lymphoedema that has been linked with a mutation in the tyrosine kinase domain of the VEGFR-3 gene (Ferrell et al., 1998; Evans et al., 2003)

Secondary lymphoedema is the most common cause of oedema. In industrialised countries, this is caused by damage or obstruction to normal lymphatic vessels, stemming from surgery, radiotherapy and infections (Rockson, 2016). In tropical and subtropical countries, pathogenic filarial parasites are the main cause of lymphoedema, which often leads to a disease known as elephantiasis that is characterised by severe swelling of the extremities (Pfarr et al., 2009). These mosquito-borne parasites reside in and cause damage to the lymphatic vessels, leading to an inhibition of lymphatic function. No cure currently exists for lymphoedema but therapies including compression bandages, exercises, and manual lymphatic draining massages exist. Therefore further research into lymphatic vessels has to be carried out for the identification of potential therapeutic targets to cure this condition.

1.4.2 Chronic inflammation and cancer

Several reports have demonstrated that the generation of new lymphatic vessels during inflammation are not beneficial to the host (Jeon et al., 2008; Wu et al., 2006). In a murine model of ovarian cancer, significant generation of lymphatic vessels occurred; these vessels, however, were found to be non-functional (Jeon et al., 2008). Similarly, lymphatic contractile activity was found to be compromised in a model of intestinal inflammation (Ileitis) (Wu et al., 2006); this could be linked to the autoimmune inflammatory bowel disease, Crohn's disease, which is often associated with a dysfunction in lymphatic vessels (von der Weid et al., 2011). Cytokines, such as IL-1β and IFNγ, normally generated during inflammation have negative effects on LEC growth, activation and barrier function, thus may affect lymphatic clearance and increase tissue oedema (Chaitanya et al., 2010).

Lymphatic vessels have also been implicated in the metastasis of primary tumour cells to dLNs and distant organs; tumour cells have been widely shown to disseminate in the body through pre-existing lymphatic vessels (Karaman and Detmar, 2014). Additionally, tumours have been shown to release the growth factors, VEGF-A, VEGF-C and VEGF-D, which induces lymphangiogenesis in primary tumours and sentinel dLNs, thereby promoting LN metastasis to distant organs (Schoppmann et al., 2002). Specifically, tumour-derived VEGF-C upregulates CCL21 production by the lymphatic endothelium, thus promoting the entry of CCR7-expressing tumour cells into those vessels (Issa et al., 2009). VEGF-C overexpression in human melanomas transplanted onto nude mice resulted in the formation of intratumoral lymphatics and enlargement of these vessels (Skobe et al., 2001). Additionally, mice bearing VEGF-D overexpressing xenographs resulted in a higher rate of LN metastasis and greater tumour volume (Du et al., 2014). This therefore sheds light on why a high level of VEGF-C and VEGF-D is associated with increased metastasis and poor prognosis in cancer patients (Tobler and Detmar, 2006). The blockade of lymphangiogenesis as an independent therapeutic concept does not exist, although therapies with anti-VEGF-C antibodies (Abs) have been tested in preclinical studies (Visuri et al., 2015). However, no positive results in human tumour studies have been published in the peer-reviewed literature.

Collectively, all of these studies demonstrate that further characterisation of the underlying molecular mechanisms of lymphangiogenesis is required, in order to identify therapeutic avenues for the selective inhibition of lymphatic vessels in diseases, such as

cancer. In addition, identifying components of lymphatic vessels that could be targeted to prevent the metastasis of cancers via this route is also important.

1.4.3 Pathogen dissemination

Similar to the metastasis of tumour cells, pathogens are also known to invade the host via the lymphatic system. There has been increasing evidence showing that infection results in neutrophils being the first lymph-born antigen-carrying cell type found within dLNs, indicating that pathogens use neutrophils as shuttles in order to disseminate (Abadie et al., 2005; Chtanova et al., 2008; Hampton et al., 2015; Lynskey et al., 2015; Mocsai, 2013). For example, following *S. aureus* infection, neutrophils within lymphatic vessels and dLNs were observed to carry *S. aureus* bioparticles, which had been fluorescently labelled (Hampton et al., 2015). Similarly, vaccination with *mycobacterium bovis* BCG resulted in BCG-infected neutrophils being observed within the lumen of lymphatic vessels, as well as accumulating within the subcapsular sinuses of dLNs (Abadie et al., 2005).

Furthermore, there has been clear clinical evidence that pathogens using lymphatic vessels as their dissemination route, for instance Group A streptococcus, can induce pathology within the lymphatic system. This includes lymphangitis (inflammation of lymphatic vessel walls) and lymphadenitis (infection of the LNs) (Bisno and Stevens, 1996; Vindenes and McQuillen, 2015). It has recently been demonstrated that the hyaluronan capsule secreted by group A streptococcus is imperative for bacterial dissemination to dLNs; this occurs through specific interactions with the hyaluronan receptor, LYVE-1 (Lynskey et al., 2015). Additionally, injections of an obligatory intracellular pathogen, live *Toxoplasma gondii*, into the earflaps of mice resulted in the parasites being found within the subcapsular sinus of dLNs in association with LYVE1+ lymphatic vessels, thus indicating they had arrived from afferent lymphatics (Chtanova et al., 2008).The recognition that the lymphatic system plays such an important role in the dissemination of pathogens has brought the field to the forefront in immunology and cell biology. Therefore, research is ongoing in a race to find therapeutic targets within the lymphatic system to prevent the spread of pathogens within the human body.

1.5 Leukocyte recruitment into the lymphatic system

Of the immune cells that migrate into sites of inflammation, only certain types of leukocytes are able to exit peripheral tissues and migrate towards LNs through lymphatic vessels. DCs, macrophages, tissue-resident (memory) T cells, and more recently neutrophils have been shown to partake on a journey through the afferent lymphatic vessel towards dLNs (Abadie et al., 2005; Harmsen et al., 1985; Mackay et al., 1990; Maletto et al., 2006; Randolph et al., 2005). HEVs are also another route of entry into the lymphatic system (Hampton and Chtanova, 2016). In the following sections, the mechanisms of leukocyte trafficking into the lymphatic system will be discussed. In particular, mechanisms of DC and T cell migration across the lymphatic endothelium will be covered as literature on this subject is most abundant due to the intrinsic nature of adaptive immune responses. Neutrophil trafficking into the lymphatic system is sparse but studies that exist are heavily influenced by mechanisms used by other leukocytes. The currently known mechanisms for neutrophil migration into the lymphatic system will be covered separately in section 1.6.

1.5.1 Leukocyte trafficking to lymphatics during innate and adaptive immunity

The adaptive immune response is initiated within the LNs, where naïve T and B cells encounter APCs, and results in lymphocyte activation and clonal expansion. Naïve T cells migrate from the blood circulation across the LN postcapillary venules (HEVs) to enter the paracortical regions of these organs. Unlike activated effector or memory T cells which can be found within peripheral tissues, naïve T cells are generally unable to enter the interstitium and thus mainly rely on DCs to deliver antigens from these tissues to them within the LN; DCs do this by "picking up" antigens from inflamed tissues and migrating to LNs via afferent lymphatics (Austyn, 1989). They are also required to process antigens for presentation to the T lymphocytes (Blum et al., 2013). Whilst other immune cells, such as monocytes, macrophages, and B cells can act as APCs to activate memory T cells, DCs are the main class of APCs that are able to activate naïve T cells, leading to the stimulation of clonal expansion and initiation of the adaptive immune response (Randolph, 2001). Immature DCs are resident within epithelial and connective tissues, where they acquire foreign antigens from pathogens during any potential infection of peripheral tissue. It was widely thought that the entry of leukocytes into the afferent

lymphatics is a passive process. However, the discovery of chemokines promoting the migration of DCs into lymphatic vessels and their subsequent trafficking to LNs has provided compelling evidence that this migration is a highly regulated process (Merad and Manz, 2009; Randolph, 2001).

1.5.2 Chemokine:chemokine receptor axes involved in lymphatic trafficking of leukocytes

In steady state, immature and semi-mature DCs migrate constitutively from inflamed peripheral tissues into LNs via afferent lymphatic vessels, allowing both normal immune surveillance and the induction of peripheral tolerance (Huang et al., 2000; Johnson and Jackson, 2014). Following infection or inflammation, the number of migrating DCs rapidly increases as a result of their inflammation-induced maturation that promotes increased DC motility and responsiveness to LN chemoattractants. These maturation events result in the conversion of DCs from phagocytes to professional APCs (Steinman et al., 2003). There are a large number of factors that induce maturation of DCs, including components of microbial cell wall, such as bacterial lipopolysaccharides (LPS), and the classical inflammatory cytokines, such as IL-1β and TNF (Steinman et al., 2003). DC maturation results in several phenotypic changes that enhance antigen uptake and presentation by the MHCs, and expression of co-stimulatory molecules, such as CD83 and CD86, for T cell activation. Mature DCs have also been shown to down-regulate their expression of pro-inflammatory chemokine receptors CCR1, CCR2, CCR5, and CXCR1, all of which are required for chemotaxis within peripheral tissues; they have also been shown to up-regulate chemokine receptors required for efficient migration from the skin to dLNs (Ardeshna et al., 2002; Foti et al., 1999) - detailed in the following sections.

1.5.2.1 CCL21/CCL19:CCR7 chemokine axis

There has been compelling evidence showing that CCR7 is a key regulator of DC migration into the lymphatic system. Seminal studies involving the chemokine receptor, CCR7, and its major ligands, CCL21 and CCL19, have implicated the CCL21/CCL19:CCR7 chemokine axis in DC migration into the lymphatic system through the development of a unique mouse strain exhibiting genetic deficiency for CCR7 (CCR7KO mice) (Forster et al., 1999). Currently, the accepted paradigm is that CCR7 governs the two distinct migratory paths of DCs and T cells, which converge in the T cell

zones of secondary lymphoid organs (Sanchez-Sanchez et al., 2006). CCR7 plays a critical role in the homing and positioning of naïve T cells and DCs within secondary lymphoid organs, and the resulting effects on the immune response is demonstrated by the profoundly disrupted cellular architecture of the LNs in CCR7KO mice (Forster et al., 1999; Schneider et al., 2007). As a consequence, CCR7KO mice have a reduced ability to mount primary immune responses (Forster et al., 1999). It has been shown that these mice lack contact sensitivity and delayed hypersensitivity responses, resulting in failure to mobilise epidermal DCs to dLNs as assessed by Fluorescein isothiocyanate (FITC) skin painting (technique to induce DC maturation and mobilisation) (Hill et al., 1990). However, recent evidence has emerged demonstrating that whilst CCR7 can be bypassed for the induction of immunity, its expression by T regulatory cells is required for their migration into LNs and contributes to their suppressive function *in vivo* (Schneider et al., 2007). Schneider *et al*. used CHS reactions in CCR7KO mice to show that T cell-mediated immunity to contact antigens develops in the absence of CCR7 (Schneider et al., 2007). Furthermore, they showed that these responses are exacerbated in CCR7KO mice as compared to WT BALB/c mice, and that these responses are ameliorated by the transfer of WT regulatory T cells. Thus, this suggests that T regulatory cells require CCR7 for their *in vivo* suppressive activity. On the basis of this, CCR7 plays a role in balancing immunity and its regulation. The absence of this chemokine receptor in CCR7KO mice has also been shown to result in DC retention within the dermis and loss of their accumulation within dermal lymphatics, under both inflammatory and steady state conditions (Ohl et al., 2004). Other studies have used a naturally occurring mutant mouse strain, *plt* (paucity of lymph node T cells) mice, which exhibit defects in the production of CCL19 and $CCL21^{Ser}$ but retain the expression of $CCL21^{Leu}$ in peripheral lymphatics (Gunn et al., 1999; Vassileva et al., 1999). As the *plt* mutation disrupts the expression of CCL21 specifically in lymphoid tissue, it is logically assumed that $CCL21^{Ser}$ regulates homing within LNs and $CCL21^{Leu}$ regulates DC entry to afferent lymphatics (Nakano and Gunn, 2001). Consequently, DCs in *plt* mice are still able to migrate into dermal afferent lymphatics, but their infiltration into the dLNs is impaired (Gunn et al., 1999; Luther et al., 2000). The involvement of LECs in generating CCL21 for transmigration across the lymphatic endothelium was proposed from studies that visualised skin-derived DCs migrating into CCL21+ lymphatic vessels, where the use of anti-CCL21 Abs resulted in the inhibition of DC migration to the dLNs (Saeki et al., 1999). Other studies have since directly visualised CCL21 production in the lymphatic endothelium through the use of immunohistochemistry studies, *in situ* RNA hybridisation and confocal microscopy

(Johnson and Jackson, 2010; Martin-Fontecha et al., 2003). LECs constitutively express CCL21, but this expression has been demonstrated to increase in response to the pro-inflammatory cytokines, TNF and IL-1α, which promote DC migration into the lymphatic system *in vivo* (Johnson and Jackson, 2010; Martin-Fontecha et al., 2003). This suggests that increased availability of CCL21 could contribute to the enhancement of DC migration into the lymphatic system, which is typically found during inflammation *in vivo* (Martin-Fontecha et al., 2003; Vigl et al., 2011). Several additional studies using *in vitro* cultured primary dermal LECs since confirmed the production of CCL21, but not CCL19, by the lymphatic endothelium (Johnson and Jackson, 2010; Kriehuber et al., 2001; Wick et al., 2007). More recently, extracellular staining of CCL21 showed that a gradient of CCL21 forms around dermal lymphatic vessels, whereby the chemokine is immobilised in the interstitium on heparan sulfates (HS); CCL19 was also found to be dispensable during DC migration into afferent lymphatic vessels (Britschgi et al., 2010; Weber et al., 2013). Taken together, these results suggests that the CCL21:CCR7 chemokine axis appears to be indispensable during DC migration across the lymphatic endothelium.

The CCL21/CCL19:CCR7 chemokine axis has also been shown to be key for the regulation of T cell trafficking into the lymphatic system. The sole function of CCR7 was previously thought to be in stimulating motility of naïve and central memory T cells, which recirculate between the blood and LNs (via HEVs) (Worbs et al., 2007). However, CCR7 has been shown to be expressed by a subset of T cells found within the interstitium that resemble central memory T cells, but are able to further exit peripheral tissues through afferent lymphatic vessels (Bromley et al., 2005; Debes et al., 2005). Effector memory T cells are negative for CCR7 and instead express receptors (e.g. CCR1, CCR3, CCR5) for inflammatory cytokines used for migration to inflamed tissues to display immediate effector function (Sallusto et al., 1999). Thus CCR7 seems to be important in regulating central memory T cells to LNs via both the blood and lymphatic routes.

1.5.2.2 CXCL12:CXCR4 chemokine axis

Genetic deletion of neither CCR7 (CCR7KO mice) nor its ligands, CCL19 and CCL21 (*plt* mice), results in full impairment of DC migration to LNs, suggesting that the process is far more complex and that additional chemokine:chemokine receptor axes are likely to be involved. The chemokine, CXCL12, is a potential candidate as it has been demonstrated to be expressed by murine dermal lymphatics and its receptor, CXCR4, has

been shown to be expressed by dermal DCs both *in vivo* and *in vitro* (Kabashima et al., 2007; Vigl et al., 2011). During tissue inflammation, LECs up-regulate the expression of CXCL12, which was demonstrated to enhance the migration of CXCR4-expressing dermal DCs to dLNs (Kabashima et al., 2007; Vigl et al., 2011). Moreover, pharmacological blockade with the CXCR4 antagonist, 4F-benzoyl-TN14003, resulted in a 50% reduction of the migration of skin DCs into LNs during the sensitisation phase of contact hypersensitivity (CHS) in mice (Kabashima et al., 2007). Interestingly, the chemotactic effects of CXCL12 and CCL21 were reported to be non-additive (Kabashima et al., 2007), suggesting that these chemokine:chemokine receptor pairs may either have sequential modes of action or may function independently of one another.

1.5.2.3 CX_3CL1:CX_3CR1 chemokine axis

In addition to the CCL21:CCR7 and CXCL12:CXCR4 chemokine axes, one other chemokine axis, CX_3CL1:CX_3CR1, was recently discovered to play a role in DC migration into the lymphatic system (Johnson and Jackson, 2013). Membrane-bound CX_3CL1 found on activated ECs promote strong adhesion of those leukocytes thus aiding in their transmigration across the blood vascular endothelium (Bazan et al., 1997). The soluble isoform of CX_3CL1 has been shown to have strong chemoattractant activity for monocytes, NK cells and T cells (Bazan et al., 1997). In the case of lymphatics, CX_3CL1 was found to promote basolateral-to-luminal migration of DCs across monolayers of human dermal lymphatic endothelial cells (HDLECs) *in vitro* (Johnson and Jackson, 2013). Furthermore, neutralisation of CX_3CL1 in mice resulted in reduced allergen-induced trafficking of dermal DCs to dLNs as assessed by FITC skin painting. Finally, mice with DCs lacking CX_3CR1 exhibited significant delays in cell trafficking into lymphatics *in vivo* and impaired DC migration across LECs *in vitro*. Collectively, these results have established a previously unrecognised role of the CX_3CL1:CX_3CR1 chemokine axis in regulating DC trafficking into the lymphatic system.

1.5.2.4 Other chemokines and chemokine receptors involved in leukocyte trafficking into the lymphatic system

Besides CCL21, CXCL12 and CX_3CL1, a number of lymphocyte, and neutrophil chemokines, such as CCL1, CCL2, CCL5, CCL20, CXCL2, CXCL5, CXCL9, CXCL10, CXCL13, and XCL1 may potentially regulate the migration of DCs or other leukocytes

into the lymphatic system (Johnson and Jackson, 2010; Mancardi et al., 2003). This is on the basis of their transcriptional upregulation in primary HDLECs in response to TNF or their expression in LECs derived from adjuvant-induced murine lymphangiomas (Johnson and Jackson, 2010; Mancardi et al., 2003). Monocyte-derived DCs have been shown to use CCR8, the chemokine receptor for CCL1, in addition to CCR7, during migration from the peripheral tissues to dLNs (Qu et al., 2004).

Lastly, the atypical chemokine-scavenging receptor D6, which binds to inflammatory CC (β) chemokines but not homeostatic chemokines, such as CCL21, has been shown to be expressed by the lymphatic endothelium in various different tissues (McKimmie et al., 2013; Nibbs et al., 2001). Unlike the other chemokine receptors described in the previous sections, D6 does not signal via G-proteins or chemotaxis following ligand binding. Instead, it acts as an endocytic receptor that efficiently internalises and degrades inflammatory chemokines during the resolution of inflammation (Fra et al., 2003; Weber et al., 2004). D6 ensures that the only chemokines presented on the lymphatic endothelium are those for CCR7, which could contribute to the selective presentation of CCR7 ligands, such as CCL21, on afferent lymphatic vessels during inflammation (McKimmie et al., 2013). Mice genetically deficient in D6 have been shown to display impairments in their ability to initiate adaptive immune responses; this is associated with aberrant leukocyte adhesion to afferent lymphatic vessels and accumulation of inflammatory leukocytes within dLNs (Lee et al., 2011). A summary of the chemokine:chemokine receptors involved in leukocyte trafficking via afferent lymphatics can be found in the table below (**Table 1.3**).

LEC Receptor /ligand	Leukocyte receptor/ ligand	Experimental model	Key observations	Reference
CCL21	CCR7	DC and T cell adoptive transfer of CCR7KO cells LN analysis on CCR7KO mice IVM of footpad	DC, lymphocytes and neutrophils fail to migrate via lymphatic vessels to LNs both under steady-state and inflammatory conditions.	(Bromley et al., 2005; Debes et al., 2005; Martin-Fontecha et al., 2003; Ohl et al., 2004; Tal et al., 2011; Weber et al., 2013)
CXCL12	CXCR4	FITC painting in the presence of a chemical inhibitor (4-F-Benzoyl-TN14003) *In vitro* transwell assays *In vivo* inflammatory models	Impaired DC migration to LN following treatment with inhibitor. CXCL12 stimulation induces transmigration across LEC in *in vitro* transwell assays. Impaired CHS response when axes is inhibited *in vivo.*	(Kabashima et al., 2007; Torzicky, 2012)
CX_3CL1	CX_3CR1	FITC painting in CHS pre-inflamed skin in the presence of CX_3CL1 Abs Adoptive transfer of CX_3CL1 KO BMDCs *In vitro* transwell assays	DC migration to LN is delayed. Impaired *in vitro* migration when the chemokine or its secretion is blocked. Effects only observed under inflammation.	(Johnson and Jackson, 2013)
D6	Inflammatory chemokines	Immunofluoresce-nce of skin lymphatics and LNs and study of LN DC populations after TPA induced inflammation in D6KO mice	Accumulated inflammatory cells blocking lymphatic vessel function and other DC migration in D6 KO mice	(Lee et al., 2011)

Table 1.3: Chemokines and chemokine receptors involved in leukocyte trafficking through lymphatic vessels.

1.5.2.5 Other chemoattractants/molecules involved in leukocyte trafficking into the lymphatic system – S1P and Galectins

Sphingosine 1-phosphate (S1P) is indispensable for T cell egress from LNs into efferent lymphatics, and has also been implicated in the regulation of T cell entry into afferent lymphatics, where increased levels of S1P in inflamed tissue potentially resulted in T cell retention within peripheral tissues and inhibition of T cell entry into lymphatic vessels (Cyster and Schwab, 2012; Ledgerwood et al., 2008). Thus, whilst the CCL21:CCR7 chemokine axis (discussed previously in section 1.5.2.1) promotes constitutive T cell migration into afferent lymphatic vessels, S1P acts as an antagonist during immunisation challenge to retain T cells within inflamed tissues until the inflammation resolves.

A role for galectins in leukocyte migration across the lymphatic endothelium has also been reported in two fairly recent studies (Fulcher et al., 2009; Hsu et al., 2009). Galectins are a family of carbohydrate-binding proteins (lectins) that are expressed by both vascular and lymphatic ECs, and have been shown to regulate immune cell migration during inflammation (Fulcher et al., 2009; Hsu et al., 2009; Rabinovich et al., 2007; Thijssen et al., 2008). Fifteen galectins have been identified to date and they share the carbohydrate recognition domain (CRD) responsible for β-galactoside binding, such as N-acetyllactosamine (Barondes et al., 1994). In particular, galectin-1 and galectin-3 have been demonstrated to be involved in the exit of tissue-resident DCs into the afferent lymphatics and thus their subsequent migration to the dLNs (Fulcher et al., 2009; Hsu et al., 2009). Galectin-1 has been shown to activate monocyte-derived DCs and specifically increase the expression of genes related to DC cell motility and migration within the ECM (Fulcher et al., 2006). Mice with defects in skin-derived DCs to dLNs were found to exhibit an increase in migration to dLNs *in vivo* following intradermal injection of galectin-1 (Fulcher et al., 2009). Galectin-3 has been shown to be expressed on DCs and macrophages during their activation and maturation (Liu, 2005). It is involved in a number of different intracellular and extracellular functions, including regulation of cell apoptosis, cell activation, as well as cell aggregation and adhesion to the substratum within the ECM (Hughes, 2001; Liu, 2005; Nakahara et al., 2005). Experiments using galectin-3 KO mice have demonstrated that galectin-3-deficient DCs exhibit signalling defects in response to chemokines *in vitro* and impaired cell migration to dLNs via lymphatic vessels *in vivo* (Hsu et al., 2009). These results collectively suggest that galectin-1 and galectin-3 play important roles during DC migration into the lymphatic system.

1.5.3 Leukocyte-endothelial cell adhesion molecules (CAMs) involved in leukocyte adhesion to and transmigration across lymphatic endothelium

Since the exit of DCs from peripheral tissues into lymphatic vessels involves basolateral to luminal migration, some studies have tried to mimic this process by growing LECs on the bottom of transwell inserts before the addition of exogenous DCs to investigate their migration responses (Johnson et al., 2006; Johnson and Jackson, 2010; Miteva et al., 2010). It is worth mentioning that a potential limitation of these *in vitro* experiments is the fact that LECs grown in monolayers form continuous zipper-like junctions (Dunworth et al., 2008; Kriehuber et al., 2001), resembling the architecture of collecting lymphatic vessels rather than the button-like junctions found on initial lymphatic vessels, which are thought to be the site of leukocyte entry. Despite this, *in vitro* transmigration assays have provided evidence that the same adhesion molecules that mediate leukocyte migration across the blood vascular endothelium, also mediate key events in this process. Some of the key adhesion molecules expressed by LECs that are also involved in *in vitro* DC migration across the lymphatic endothelium as demonstrated with the use of blocking mAbs include PECAM-1 (Torzicky, 2012), CD99 (Torzicky, 2012), VCAM-1 (Johnson et al., 2006), ICAM-1 (Johnson et al., 2006), L1CAM (Maddaluno et al., 2009), CD137 (Teijeira et al., 2012) (**Table 1.4**). Most of these adhesion molecules were also confirmed to affect DC migration *in vivo* (Johnson et al., 2006; Maddaluno et al., 2009). Notably, transmural lymph flow was shown to augment DC transmigration, likely through inducing the upregulation of CCL21 and ICAM-1 expression by LECs (Miteva et al., 2010).

In particular, the LEC-expressed adhesion molecule that has been identified as being fundamental in the process of DC migration is ICAM-1. FITC skin painting and adoptive transfer experiments have shown that in ICAM-1 KO mice, DC migration from skin to dLNs was significantly reduced, demonstrating a critical role for ICAM-1 in this process (Sligh et al., 1993; Xu et al., 2001). It has also been reported that ICAM-1 and ICAM-2, but not VCAM-1 are expressed at low levels in murine dermal LECs (Johnson et al., 2006). However, both ICAM-1 and VCAM-1 were massively upregulated (40- to 80-fold increase) on LECs in response to TNF-induced inflammation, which is similar to previously published findings in BECs (Johnson et al., 2006).

LEC Receptor/ ligand	Leukocyte receptor/ ligand	Experimental model	Key observations	Reference
ICAM-1	CD11a,b (β2 integrins)	FITC painting in the presence of blocking Abs or in ICAM-1 KO mice, BMDC adoptive transfer in the presence of blocking Abs or from CD18KO mice, whole mount immunofluorescence of ears after DC injection, *in vitro* transwell assays	In inflammatory and high flow conditions. blockade of ICAM-1 and blockade of β2 integrins inhibit TEM and DC migration to LNs.	(Johnson et al., 2006; Ma et al., 1994; Miteva et al., 2010; Teijeira et al., 2013; Xu et al., 2001)
VCAM-1	VLA-4	BMDC adoptive transfer in the presence of blocking Abs, *in vitro* transwell assays	LN impaired DC migration under inflammation and impaired in vitro trans-endothelial migration.	(Johnson et al., 2006)
PECAM-1	PECAM-1	*In vitro* transwell assays, *ex vivo* human skin culture in the presence of blocking Ab, immunofluorescence, and DC count inside LVs	Impaired trans-endothelial migration and intravasation in human skin explants, evidence provided only in humans.	(Torzicky, 2012)
L1CAM	L1CAM	FITC painting assays in mice deficient in L1CAM under Tie 2 promoter, transwell, and adhesion assays	Impaired adhesion, transmigration in human and mice (BMDC), impaired migration to LN.	(Maddaluno et al., 2009)
CD99	PILR	*In vitro* transwell assays, *ex vivo* human skin culture in the presence of blocking Ab, immunofluorescence, and DC count inside LVs	Impaired trans-endothelial migration and intravasation in human skin explants, evidence provided only in humans.	(Torzicky, 2012)
CD137	CD137L	CD137 cross-linking with agonistic or natural ligand (CD137L), *in vitro* transwell assays, *ex vivo* human explants treated with CD137 blocking Ab	Cross-linking with agonistic mAb or CD137L leads to increase in CCL21 production and enhanced CCR7-dependent migration across LECs *in vitro*. Blocking Ab induces CCL21 expression and DC accumulation close to lymphatic vessels *ex vivo*.	(Teijeira et al., 2012)
JAM-A	JAM-A	CHS response and FITC painting in JAM-A KO mice and adoptive transfer of JAM-A deficient BM DCs, *in vitro* transwell assays	JAM-A deficiency increases DC migration to LN and CHS responses *in vivo* as well as *in vitro* TEM.	(Cera et al., 2004)

Table 1.4: Adhesion molecules involved in leukocyte trafficking through lymphatic vessels.

Additionally, monoclonal blocking antibodies (mAbs) for ICAM-1 and VCAM-1, which blocked their binding to their corresponding integrin ligands, LFA-1/MAC-1 ($\alpha_L\beta_2$) and VLA-4 ($\alpha_4\beta_1$), respectively, were found to inhibit adhesion of DCs to TNF-stimulated LECs, as well as block DC transmigration across the cultured lymphatic endothelium (Johnson et al., 2006). These molecules were also shown to be involved in DC migration to dLNs *in vivo* (Johnson et al., 2006). In support of this, blockade of DC-expressed LFA-1 has been shown to reduce DC migration to dLNs from inflamed skin *in vivo* (Teijeira et al., 2013). Thus, ICAM-1 and VCAM-1 mediate leukocyte adhesion steps that are required for inflammation-induced DC transmigration, similar to the adhesion molecule-mediated firm adhesion that occurs before leukocyte transmigration across the vascular endothelium in the leukocyte adhesion cascade (Ley et al., 2007). Interestingly, DCs have been found to express JAM-A, a junctional molecule also expressed on the blood and lymphatic vascular endothelium (Cera et al., 2004; Del Maschio et al., 1999). The use of JAM-A KO mice along with adoptive transfer experiments showed that whilst JAM-A-deficient DCs exhibited enhanced migration across the lymphatic endothelium both *in vivo* and *in vitro* in FITC painting and transwell experiments; this was not observed in JAM-A-deficient LECs (Cera et al., 2004). An accumulation of DCs within dLNs was also found in mice with JAM-A deficient DCs but not with JAM-A-deficient LECs (Cera et al., 2004). Despite this, the mechanism involved in LEC-independent promotion of DC trafficking to lymph nodes in JAM-A KO mice remains to be fully elucidated.

Collectively, the results show that DC-expressed JAM-A, CX_3CR1, CCR7, MAC-1 and LFA-1, along with LEC-expressed D6, CX_3CL1, CCL21, ICAM-1 and VCAM-1, are involved in the mechanisms of DC entry into lymphatic vessels (**Figure 1.10**), and are key in regulating DC migration across the lymphatic endothelium during inflammation and immunity.

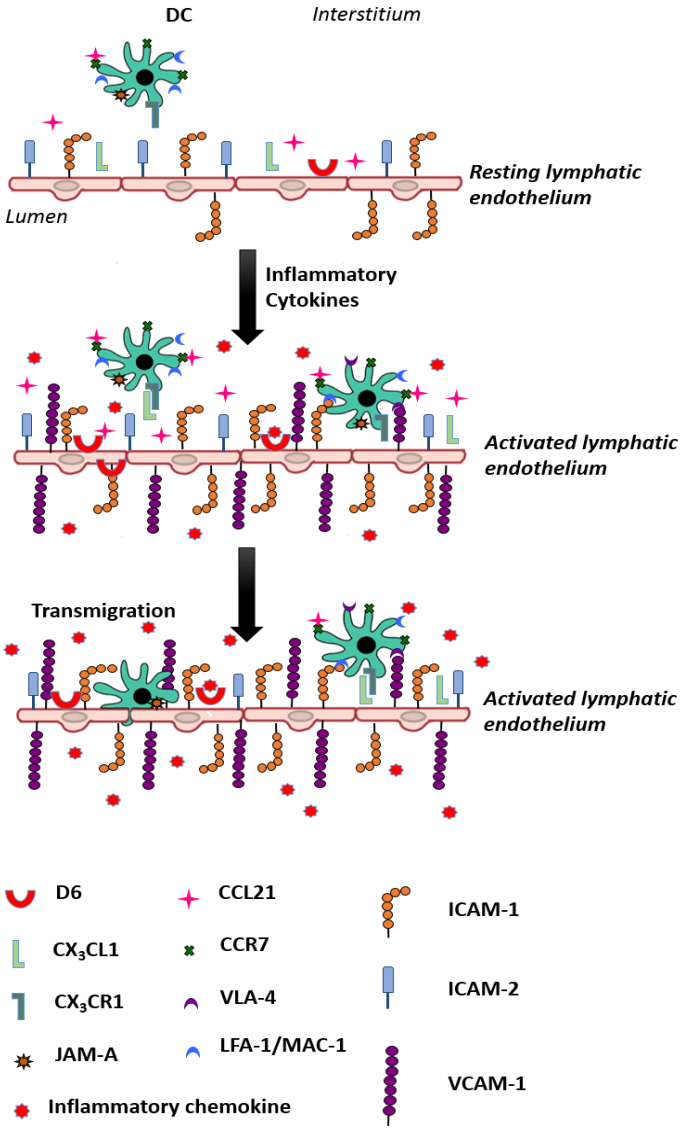

Figure 1.10: Key molecules involved in DC adhesion and transmigration across the lymphatic endothelium. At resting state, the lymphatic endothelium constitutively expresses the adhesion molecules ICAM-1 and ICAM-2, the ACKR D6, and the lymphatic chemokine CCL21 – all of which play important roles in DC migration across the lymphatic endothelium. The presence of pro-inflammatory cytokines results in the upregulation of ICAM-1, ICAM-2 and VCAM-1 on the lymphatic endothelium. DCs express LFA-1/MAC-1 and VLA-4, which are corresponding integrin ligands to ICAM-1 and ICAM-2, and VCAM-1, respectively. The binding of these integrins with their corresponding receptors is important in DC migration across the lymphatic endothelium during inflammation. Additionally, the expression of the chemokines CCL21 and CX_3CL1 are also upregulated by the activated lymphatic endothelium. The corresponding chemokine receptors CCR7 and CX_3CR1 are expressed by DCs and their binding to CCL21 and CX_3CL1, respectively, is required for DC migration across the activated lymphatic endothelium. Furthermore, LEC-expressed D6 scavanges pro-inflammatory chemokines within the tissue, and it is likely that this process plays a role in the trafficking of DCs across the activated lymphatic endothelium. Finally, inflammatory and DC-expressed JAM A are required for DC migration across the activated lymphatic endothelium although the mechanisms behind this process remains to be elucidated.

1.5.4 Molecules involved in intraluminal crawling of leukocytes within initial lymphatic vessels

The crawling of DC and other leukocytes within the lumen of lymphatic vessels towards dLNs, following their transmigration across the lymphatic endothelium, has generally been thought of as a passive transport process owing to lymph flow (Alvarez et al., 2008; Randolph et al., 2005). This hypothesis was supported by intravital microscopy (IVM) experiments observing collecting lymphatic vessels within the rat mesentery, where free flowing lymphocytes were shown to rapidly disseminate in a pulsatile fashion (Dixon et al., 2005; Galanzha et al., 2005). Interestingly, the peak velocities of lymph flow within collecting vessels were found to be comparable to blood flow velocities, whereas lymph flow velocities within initial vessels were found to be much lower in comparison (Akl et al., 2011; Dixon et al., 2006; Dixon et al., 2005). Thus, doubts were raised with regards as to whether the hydrodynamic forces found within initial lymphatic vessels are adequate to support the passive transport of flowing leukocytes. Indeed, other IVM experiments have since shown that most DCs actively migrate within initial lymphatics and appear to only be passively transported by lymph once reaching collecting vessels (**Figure 1.11**) (Nitschke et al., 2012; Sen et al., 2010; Tal et al., 2011).

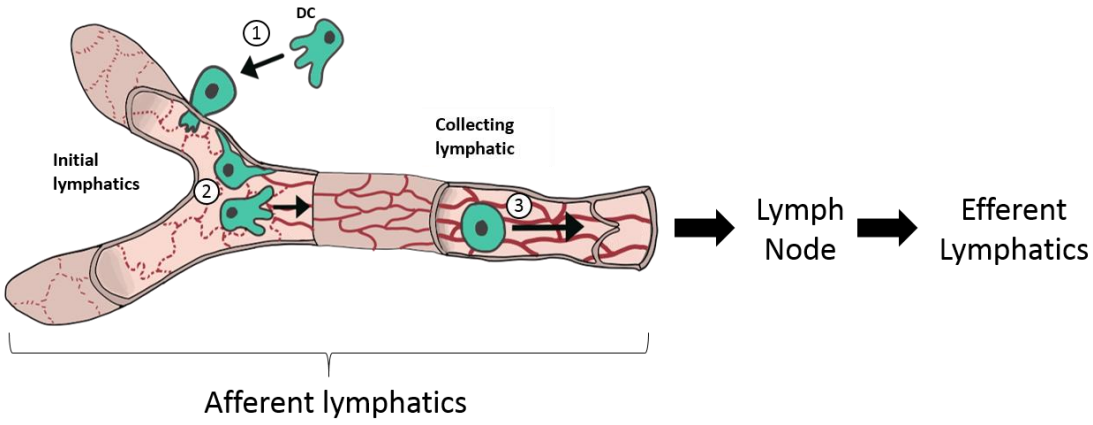

Figure 1.11: DC crawling and transport within lymphatic vessels. (1) Initial lymphatics exhibit adjacent oakleaf-shaped LECs, which partially overlap, thus creating open flaps (red dotted lines) where DCs are thought to migrate through. (2) DC crawling occurs within initial lymphatics. (3) DCs are transported by flow of lymph once reaching collecting lymphatics, eventually reaching dLNs where they present antigens to B and T cells. DCs are not found within efferent lymph and therefore must accumulate and die in the lymph node. FAS/FAS-ligand mediated DC apoptosis is a likely mechanism which has been shown in rodent and human DCs (Ingulli et al., 1997).

The first candidate signalling molecule identified as being involved in intralymphatic DC migration was the Rho-associated protein kinase (ROCK) (Nitschke et al., 2012). This molecule is required for actomyosin-mediated cellular contraction when leukocytes migrate through narrow pores, such as through the interstitial space or across the vascular endothelium (Nourshargh et al., 2010; Vicente-Manzanares et al., 2009). Additionally, ROCK was shown to aid leukocyte migration by mediating cellular de-adhesion of leukocyte-expressed integrins, LFA-1 and MAC-1, at the cellular rear from the endothelial-expressed integrin ligand, ICAM-1, during their crawling on vascular ECs (Smith et al., 2003; Vicente-Manzanares et al., 2009). It has been reported that pharmacological blockade of ROCK had little to no effect on reducing intralymphatic crawling at steady state. However, following CHS-induced inflammation, blockade of ROCK resulted in a considerable reduction in the velocity of DC crawling within lymphatic capillaries; this is likely due to ROCK inhibiting de-adhesion from inflammation-induced expression of ICAM-1 (Nitschke et al., 2012). To date, no other molecules have been shown to be involved in intralymphatic DC crawling. However, it is highly possible that molecules previously shown to be critical for DC migration across the lymphatic endothelium could also support DC crawling within initial lymphatics, thus further experiments will have to be carried out to provide evidence for this.

1.6 Identified mechanisms of neutrophil migration into the lymphatic system

Two possible routes of neutrophil entry into dLNs exist – via specialised blood vessels known as high endothelial venules (HEVs) or via afferent lymphatics.

1.6.1 Neutrophil migration via HEVs

The first route involves neutrophils exiting the circulation via high HEVs; this however remains controversial, as human neutrophils apart from those that have infiltrated tumours seem to lack surface expression of CCR7 (Beauvillain et al., 2011; Eruslanov et al., 2014), a receptor for the chemokine, CCL21, which is required for lymphocyte migration across HEVs (Forster et al., 2008). Nevertheless, in mice, a sub-population of neutrophils have been found to express CCR7 on the cell surface following stimulation, suggesting the

existence of a preformed stock that can be rapidly mobilised at the cell membrane in response to an inflammatory stimulus (Beauvillain et al., 2011). It has also been shown in a murine model of Complete Freund's Adjuvant (CFA) and ovalbumin (OVA)-induced inflammation that neutrophil homing to dLNs via HEVs occurs and requires the neutrophil-expressed β2 integrins, MAC-1 and LFA-1, and chemokine receptor, CXCR4, as well as the EC-expressed adhesion molecules, L- and P-selectin (refer back to **Figure 1.4**) (Gorlino et al., 2014). CFA is able to stimulate responses associated with adaptive immunity, and consists of a mixture of paraffin oil and surfactant with heat-killed *Mycobacterium tuberculosis* in which an aqueous antigen solution is emulsified (Coffman et al., 2010).

The CXCR4 ligand, CXCL12, has also been shown to be expressed by cells in the medulla of LNs (Hargreaves et al., 2001); therefore, it is possible that this chemokine plays a role in neutrophil homing to these tissues. Additional chemokines and cytokines secreted by activated tissue-resident macrophages are likely to play roles in orchestrating the attraction of neutrophils into dLNs via HEVs; this has been shown to be the case in tumour-dLNs, where tumours subjected to photodynamic therapy to induce additional sterile inflammation, led to neutrophil recruitment to tumour-dLNs via HEVs in an IL 17-dependent manner (Brackett et al., 2013). Similarly, macrophage-derived IL-1β and TNF were found to be required for neutrophil entry into dLNs following injections of bacteria and viruses (Kastenmuller et al., 2012; Sagoo et al., 2016). Collectively, this suggests that at least some of the molecules responsible for neutrophil homing to inflamed tissues also play roles in regulating neutrophil recruitment to LNs.

1.6.2 Migration via afferent lymphatics

The second route of neutrophil migration to LNs involves their migration (a.k.a intravasation) into afferent lymphatics, presumably via initial lymphatics, where they are eventually carried to dLNs. Neutrophil migration into the lymphatic system and their influence on the orchestration of the adaptive immune response was discussed in section 1.1.3.2. Here, presently known potential mechanisms of neutrophil migration across the lymphatic endothelium, an essential part of their journey towards the dLNs where adaptive immune responses are initiated are discussed.

In steady state, DCs constitutively migrate to dLNs via afferent lymphatic vessels. Neutrophils, however, have only been observed to migrate via afferent lymphatics in the

context of acute inflammation or infection (Abadie et al., 2005; Beauvillain et al., 2011; Chtanova et al., 2008; Hampton et al., 2015). Following CFA+Ag-induced inflammation, OVA+ neutrophils were found to not only appear at the injection site, but they also represented the main OVA+ cells present within dLNs (Gorlino et al., 2014). These OVA+ neutrophils were found to localise in the subcapsular sinuses of dLNs, thus indicating that these neutrophils had reached the LNs via afferent lymphatics (Gorlino et al., 2014). It has been reported only neutrophils primed with certain cytokines (i.e. GM-CSF and IL-17), or microbial moieties (LPS) can migrate toward lymphatic chemokines (i.e. CCL19 and CCL21) *in vitro* (Beauvillain et al., 2011). Furthermore, activation of cultured LEC monolayers with inflammatory cytokines lead to the up-regulation of ICAM-1 and VCAM-1, as well as chemokines that are compulsory for an efficient migration of the neutrophils across these cell monolayers *in vitro* (Aebischer et al., 2014). Indeed, blockade of ICAM-1, VCAM-1 and their integrin-binding partners (β2 or α4 integrins) resulted in reduced neutrophil migration across the lymphatic endothelium (Rigby et al., 2015). The involvement of the neutrophil-expressed β2 integrin subunit, CD11b (MAC-1), and its LEC-expressed ligand, ICAM-1, in neutrophil migration to the dLNs was also confirmed *in vivo* (Rigby et al., 2015). Other studies have also provided evidence to support the involvement of CD11b as blocking of this integrin subunit *in vivo* resulted in a reduction in the numbers of neutrophils infiltrating dLNs (Gorlino et al., 2014; Hampton et al., 2015). However, the ligand or combination of ligands required for CD11b-dependent migration of neutrophils from inflamed tissues into LNs is still not known as CD11b has well over 40 known ligands (Podolnikova et al., 2015).

DC migration via the afferent lymphatics route requires the chemokine receptors, CCR7 and/or CXCR4 (Kabashima et al., 2007; Ohl et al., 2004). However, the role of CCR7 during migration of neutrophils into the LNs is highly controversial. CCR7 was shown to be required for LN recruitment of neutrophils in response to adjuvant challenge (Beauvillain et al., 2011), but this was proved to not be the case following *S. aureus* challenge (Hampton et al., 2015). Thus, CCR7 seems to be dispensable for some modes of neutrophil recruitment to LNs. This could possibly be due to the theory that different waves of neutrophil recruitment are governed by diverse mechanisms since the downstream Gαi signalling of many chemokine receptors is not required for neutrophil migration into dLNs immediately after immunisation, but yet is essential for neutrophil recruitment into dLNs after 72 h (Yang and Unanue, 2013). On the other hand, the CXCL12:CXCR4 chemokine axis, as well as S1P have recently been implicated in

neutrophil migration across the lymphatic endothelium *in vivo* (**Figure 1.12**) (Gorlino et al., 2014; Hampton et al., 2015). In the context of infection-induced inflammation with *S. aureus*, neutrophils within the dLNs were found to express elevated levels of the chemokine CXCR4 (Hampton et al., 2015). Consequently, CXCR4 blockade with CXCR4-specific inhibitor, AMD3100, resulted in a significant reduction in the number of neutrophils found within dLNs (Gorlino et al., 2014; Hampton et al., 2015). More recently, LEC-expressed CXCL8, a ligand of the chemokine receptors CXCR1 and CXCR2, was found to be one of the main chemoattractants in driving human neutrophil transmigration across a cultured lymphatic endothelium *in vitro*. It is unclear if this response is valid *in vivo* too and the role of murine CXCL8 analogous proteins need to be tested (**Table 1.1**). However, *in vivo* neutralisation of CXCR2 demonstrated that this chemokine receptor is not required for neutrophil migration into the lymphatic system (Hampton et al., 2015).

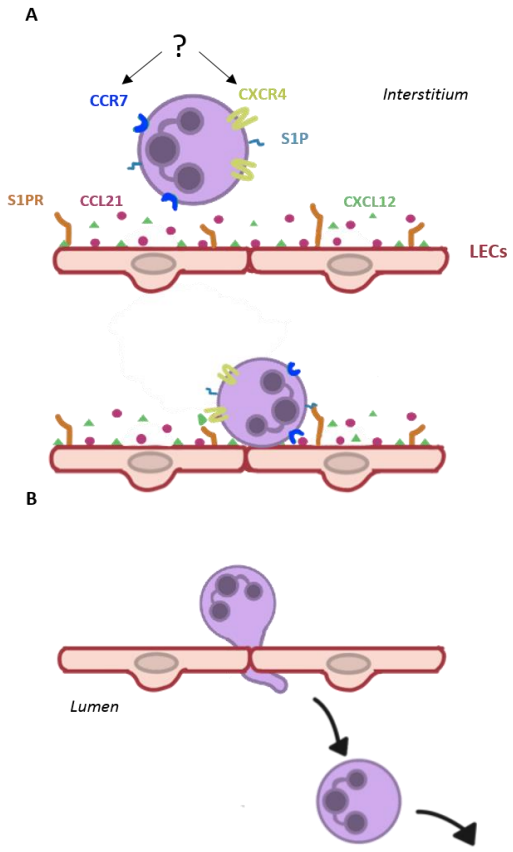

Figure 1.12: Chemokine:chemokine receptor axes potentially involved in neutrophil transmigration across lymphatic endothelium *in vivo*. Following inflammation, (A) chemotaxis of neutrophils towards inflamed LECs secreting CCL21 and CXCL12 is triggered, leading to CCL21:CCR7 and CXCL12:CXCR4 interactions. (B) Neutrophil migration across the inflamed endothelium occurs as a result of these chemokine:chemokine receptor interactions. S1P and S1PR interactions are also potentially important in this process. Neutrophils are depicted in purple; LECs in red/pink.

It is clear that DCs and neutrophils have differential requirements for chemokines and integrins during migration into the lymphatic system (Gorlino et al., 2014; Hampton et al., 2015). DC migration is highly CCR7-dependent and only becomes integrin-dependent following inflammation; DCs are also able to migrate to dLNs in a completely integrin-independent manner, which could explain why DCs are capable of constitutively migrating across the lymphatic endothelium at resting state despite low levels of integrin ligands being present (Teijeira et al., 2014). It has recently been reported that upon CXCL8-dependent chemotaxis and integrin-mediated adhesion to LECs *in vitro*, neutrophils are able to induce the enzymatic degradation of LEC junctions, as well as LEC retraction, thereby creating large portals that enable rapid migration of neutrophils across the lymphatic endothelium (**Figure 1.13**) (Rigby et al., 2015). Strikingly, neutrophil migration across the lymphatic endothelium *in vitro* resulted in an increase in LEC monolayer permeability, as subsequent applications of neutrophils resulted in a much more accelerated rate of migration across the LECs, thus implying that these preformed gaps had served as hotspots for successive neutrophils (Rigby et al., 2015). The induction of retraction of LEC-LEC junctions and gap formation by neutrophils was shown to be associated with their secretion of MMP8 and MMP9, as well as lipoxygenase products, in particular, the arachidonic acid-derived chemorepellent, 12(S)-HETE (**Figure 1.13**).

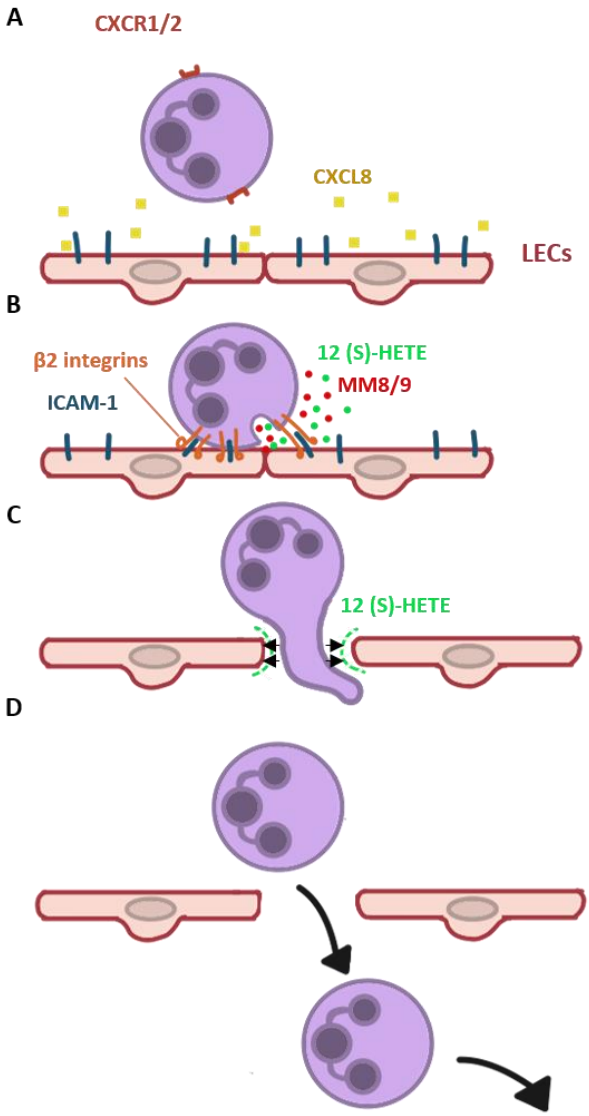

Figure 1.13: Proposed model of neutrophil transmigration across lymphatic endothelium *in vitro*. (A) Neutrophil chemotaxis towards inflamed LECs secreting CXCL8 leads to binding of CXCR1/2 to the chemokine. (B) β2 integrin-mediated neutrophil adhesion to LECs and focal secretion of MMP8, 9 and 12(S)-HETE. (C) Proteolytic activity of MMPs and LEC retraction leads to disruption of LEC-LEC junctions, which is mediated by 12(S)-HETE-induced chemorepulsion. (D) Resulting gap in lymphatic endothelium acts as a hotspot for apical to basolateral neutrophil transmigration.

This is in contrast to neutrophil migration across the blood vascular endothelium during the inflammatory response, where EC junctions reportedly remain intact in vitro (Burns et al., 2000). Additionally, DC migration across the lymphatic endothelium has also been shown to not harm the integrity of LEC monolayers in vitro (Rigby et al., 2015). In vivo studies have shown that the perilymphatic basement membrane of initial lymphatic vessels is discontinuous, thus the presence of preformed portals facilitates the entry of DCs into these vessels (Pflicke and Sixt, 2009). All of these results suggest that this neutrophil-specific mechanism of generating openings within the lymphatic endothelium might be an explanation as to why neutrophils have the capacity to cross LEC barriers so rapidly. However, as these experiments were primarily done in vitro, more studies have to be carried out to validate these results in vivo. This is especially important since initial lymphatics are organised in a highly specialised manner, with button-like junctions present that are considered to be the main site of leukocyte entry into lymphatic vessels (discussed in section 1.3.1). These junctions are not present in vitro, which makes it difficult to assess whether this unique neutrophil migration process is indeed what occurs at the level of the lymphatic endothelium in vivo.

It is worth mentioning that the handful of studies that investigated the mechanisms of neutrophil migration in vivo made use of very different inflammatory models, ranging from inflammation induced by injection of inactivated pathogens, pathogenic constituents, parasites, to live bacilli (Abadie et al., 2005; Chtanova et al., 2008; Gorlino et al., 2014; Hampton et al., 2015; Rigby et al., 2015). Therefore, it is possible that the molecular mechanisms involved may vary depending on the type of inflammatory stimuli or infectious challenge used; this is supported by a plethora of studies showing that the upregulation of these molecules on LECs is highly stimulus specific (Aebischer et al., 2014).

1.7 Aims of this study

Recently, neutrophils have also been found to play a role in regulating the adaptive immunity *in vitro* following their rapid migration to LNs (Abi Abdallah et al., 2011). Several studies have indeed shown their early presence in LNs of infected or immunised animals *in vivo* (Abadie et al., 2005; Gorlino et al., 2014; Hampton et al., 2015). However, their unique recruitment into the lymphatic structures has not been extensively studied so far, but evidence suggests their arrival into LNs from afferent lymphatics like DCs (Beauvillain et al., 2011; Gorlino et al., 2014; Maletto et al., 2006). Thus, it was hypothesised that neutrophils gain entry into lymphatic vessels to shape adaptive immune responses. The overall aim of this study was to investigate some of these regulatory mechanisms *in vivo* using a murine model of antigen challenge in the cremaster muscle by addressing the following key objectives:

1.7.1 Investigate the dynamics of neutrophil migration from the blood circulation into the lymphatic system during inflammation and the potential role of TNF in driving these responses *in vivo*

To elucidate the mechanisms of neutrophil migration into lymphatic vessels, a model of antigen sensitisation of the mouse cremaster muscles will be established. Experiments will include:

- Characterising neutrophil migration responses across blood vasculatures and into lymphatic vasculatures following TNF and CFA+Ag-induced inflammation at different time periods *in vivo*.
- The use of mice genetically deficient in both TNF receptors (TNFRI and II) to investigate the importance of TNF signalling in mediating neutrophil migration into lymphatic vessels.
- The use of chimeric mice to elucidate if TNF-induced migration is due to a direct effect of TNF signalling on the neutrophils.

1.7.2 Investigate potential chemokines and receptors involved in neutrophil migration into initial lymphatics *in vivo*

The potential involvement of several chemokine:chemokine receptor axes, namely, CXCL1:CXCR1/2, CXCL12:CXCR4, and CCL21:CCR7, will be investigated following TNF- or CFA+Ag-induced inflammation *in vivo*. Experiments will include:

- The use of blocking mAbs to CXCL1, a specific inhibitor of CXCR4, or mice genetically deficient in CCR7, followed by immunostaining and confocal microscopy analysis.

1.7.3 Examine the regulation and distribution of the LEC glycocalyx and chemokines during inflammation *in vivo*

As the modulation of the BEC glycocalyx plays a role in neutrophil extravasation across the blood vessel wall, the regulation and redistribution of components of the LEC glycocalyx from cremaster lymphatic vessels upon inflammation will be investigated. Experiments will include:

- Analysing changes in sugar residues on lymphatic vessels using lectin-binding
- Analysing changes in HS and CCL21 (prototypical LEC chemokine) expression using fluorescent staining and confocal microscopy analysis.

1.7.4 Analyse interactions between neutrophils and the lymphatic endothelium post-migration into the vessels *in vivo*

The interactions – and associated mechanisms- between neutrophils and the lymphatic endothelium following their entry into lymphatic vessels will be further investigated. Experiments will include:

- The use of confocal IVM to visualise and quantify the intraluminal crawling of neutrophils in inflamed cremaster muscles of LysM-eGPF animals.
- The use of blocking mAbs to study the role of TNF and adhesion molecules in driving this response.

2 : Materials and methods

2.1 Animals

All animal studies were performed according to the guidelines of the United Kingdom Home Office Animals (Scientific Procedures) Act (1986).

2.1.1 Strains

All animals used weighed an average of 28 g and were between 8-12 weeks old. Where required, age-matched control mice were litter mates or commercially purchased C57BL/6 mice.

C57BL/6 mice Male wild-type (WT) between the ages of 8-12 weeks were routinely used and purchased from Charles River Laboratories (Margate, UK).

CCR7 knockout (CCR7KO) mice

These are mutant mice lacking the gene for the chemokine receptor CCR7, *Ccr7*^{tm1Rfor} (Forster et al., 1999). They were generated by the insertion of a neomycin resistance cassette with a targeting vector designed to replace a fragment of the third exon of the targeted gene. Homozygous mice are viable and fertile and show delayed primary B or T cell immune responses. These mice are backcrossed 8 generations on a WT C57BL/6 background and breeders were purchased from The Jackson Laboratory (stock number: 006621).

CCR7KO LysM-eGFP mice

These are mutant mice lacking the gene for the chemokine receptor CCR7, *Ccr7*^{tm1Rfor}, as well as expressing eGFP-labelled myelomonocytic cells with especially high fluorescence intensity in mature neutrophil granulocytes. CCR7KO mice were crossed with LysM-eGFP mice (Faust et al., 2000) to generate CCR7KO mice expressing Lysozyme M promoter-driven expression of enhanced green fluorescent protein in myelomonocytic cells

LysM-eGFP mice These mice exhibit eGFP-labelled myelomonocytic cells and especially high fluorescence intensity is observed in mature neutrophil granulocytes. This mouse strain was generated as described by Faust et al. in 2000 and contains the mutated murine lysozyme M (*lys*) locus into which the coding sequence for eGFP (enhanced Green Fluorescent Protein) has been inserted (Faust et al., 2000). Homozygous mice are viable and fertile and show normal development. This strain was generated in a C57BL/6 background and was obtained as a gift from Prof. Markus Sperandio (Walter Brendel Centre of Experimental Medicine, Ludwig-Maximillians-Universität, Munich, Germany). Heterozygous mice were used in all experiments.

Tumour necrosis factor receptor double knockout (TNFRdbKO) mice

These are double mutant mice lacking the genes for both TNF receptors, *Tnfrsf1a* (p55) and *Tnfrsf1b* (p75) (Peschon et al., 1998). They were generated by intercrossing singly deficient mice whereupon the *Tnfrsf1b* mutation was transferred into the *Tnfrsf1a* background (C57BL/6). All mice are viable and fertile and were purchased from The Jackson Laboratory.

2.1.2 Generation of chimeric mice

To further investigate the mechanisms of neutrophil migration into lymphatic vessels in response to CFA+Ag-induced inflammation, chimeric mice were generated. Briefly, WT recipient mice were given acidified water (pH 2.6) for 1 week before bone marrow transfer. Bone marrow was isolated from the tibias of WT, TNFRdbKO and CCR7KO x LysM-eGFP mice under sterile conditions and suspended in sterile PBS at $5x10^6$ cells/ml. WT recipient mice were irradiated with two doses of 5 Gy, 4 hours (h) apart using a RadSource-2000 irradiator. After the second irradiation, mice were given an intravenous (i.v.) injection of $1x10^6$ bone marrow cells in 200 µl PBS. After irradiation and bone marrow transfer, animals were maintained in individually ventilated cages and given acidified (pH 2.6) water and Baytril for 4-6 weeks before use.

Verification of chimera reconstitution by flow cytometry was carried out at the end of each experiment and is described further on in section 2.14.

CCR7KO LysM-eGFP chimeric mice

These are C57BL/6 WT mice reconstituted with bone marrow from CCR7KO LysM-eGFP mice to generate WT mice with neutrophils lacking in the chemokine receptor CCR7.

TNFRdbKO chimeric mice

These are C57BL/6 WT mice reconstituted with bone marrow from TNFRdbKO knockout mice to generate WT mice with neutrophils lacking in both TNF receptors, p55 and p75.

2.1.3 Genotyping and phenotyping

2.1.3.1 Phenotyping of LysM-eGFP mice

LysM-eGFP mice were phenotyped by fluorescence microscopy. For this purpose, mice were tail-bled before the whole blood was placed on glass slides for fluorescence microscopy to look for the presence of GFP positive leukocytes. Flow cytometry was also used to confirm GFP positive neutrophils were present.

2.1.3.2 Genotyping of TNFR double knockout mice

TNFRdbKO mice were genotyped by polymerase chain reaction (PCR), which were performed by the laboratory manager, Dr Matthew Golding.

2.1.3.3 Genotyping of CCR7 knockout mice

CCR7KO mice were genotyped by PCR. For this purpose, ear notch samples were taken, placed into a 1 ml eppendorf tube before digested in 500 µl lysis buffer containing 100 µg/ml proteinase K overnight at 55 °C. The following day, tubes containing the digested samples were lightly vortexed and cooled to room temperature (RT) prior to DNA purification using isopropanol/ethanol precipitation. To precipitate the DNA, 500 µl isopropanol was added to each tube before they were inverted to mix. The mixtures were then centrifuged for 5 min at 20,000 g at RT and the resulting supernatents were discarded. The remaining pellets were washed with 1 ml of 70 % (v/v) ethanol before being centrifuged again for 5 min at 20,000 g at RT and the resulting supernatents discarded. All remaining traces of ethanol were carefully removed with a pipette and the pellets were air dried for approximately 10 min. The DNA was resuspended in 50 µl molecular biology grade water and stored at 4 °C or 20 °C for short- and long-term storage, respectively. 1 µl of purified DNA was used for each PCR reaction.

Detection of CCR7 (Ccr7^{tm1Rfor}) knockout

CCR7 knockout (CCR7KO) was detected using the protocol from Jackson Laboratory. Three primers were used to amplify both the WT and knockout allele at the same time (**Table 2.1**). PCR master mixes were prepared (**Table 2.2**), distributed into PCR tubes and 1 µl of purified DNA was added. Subsequently, DNA fragments were amplified in a PCR block (PTC-200 thermal cycler, MJ Research,) using the CCR7KO program (**Table 2.3**).

Primer	Primer Sequence	Melting temperature	Primer type
oIMR7074	5'-TAA GGG CAT CTT TGG CAT CT-3'	94 °C	Common
oIMR7075	5'-GCA TAC AAG AAA GGG TTG ACG-3'	50 °C	WT reverse
oIMR8162	5'-TGG ATG TGG AAT GTG TGC GAG-3'	72 °C	Mutant reverse

Table 2.1: Primers used to amplify the CCR7 WT or mutant (knockout) allele.

Reagent	Stock concentration	Volume per sample	Final concentration
Primer 1: oIMR7074	100 mM	0.125 µl	0.5 uM
Primer 2: oIMR7075	100 mM	0.125 µl	0.5 uM
Primer 3: oIMR8162	100 mM	0.125 µl	0.5 uM
dNTPs	10 mM	0.5 µl	0.2 mM
$MgCl_2$	50 mM	1 µl	2 mM
NH_4^+ buffer	10 x	2.5 ul	1 x
TAQ polymerase	5 U/µl	0.1 µl	0.05 U/µl
DNA/RNA free water (molecular biology grade)	N/A	20.525 µl	N/A
Total		25 µl	

Table 2.2: PCR mastermix to amplify the CCR7 WT and mutant (knockout) allele.

Step	Temperature and time	No. of cycles
Initial denaturation	94 for 2 min	1
Denaturation	94 for 20 sec	Repeat denaturation and annealing step for 10 cycles
Annealing	65 for 15 sec (-1.5 per cycle) 68 for 10 sec	
Elongation of primer 1: oIMR7074	94 for 15 sec	Repeat elongation steps for 28 cycles
Elongation of primer 2: oIMR7075	50 for 15 sec	
Elongation of primer 3: oIMR8162	72 for 10 sec	
Final elongation	72 for 2 min	1

Table 2.3: PCR program for CCR7KO.

Following amplification, 1 µl of 6 x agarose gel blue loading dye was added to 5 µl of each sample and 5 µl were run on a 2 % (w/v) agarose gel (in TAE buffer) with the addition of 0.5 µl/ml of GelRed^{TM}. A 100 b.p DNA ladder was used as a marker. Gels were left running in an electrophoresis chamber (Mupid®-One) for approximately 35 min at 135 V. Pictures of gels were then taken under ultraviolet light on a UV White Darkroom BioImaging System (UVP, Cambridge, UK). 594 b.p PCR products corresponded to WT alleles, 200 b.p PCR products corresponded to knockout alleles and the presence of both corresponded to heterozygous alleles (**Figure 2.1**).

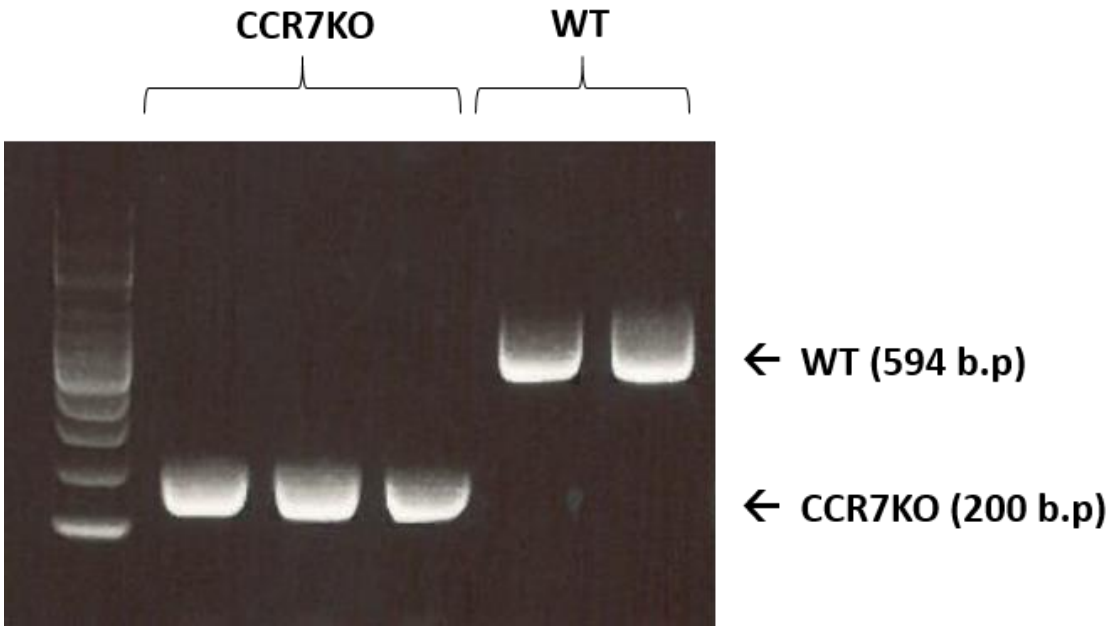

Figure 2.1: Example gel of expected bands for WT and CCR7KO samples.

2.1.3.4 Genotyping of CCR7 LysM-eGFP mice

CCR7KO LysM-eGFP mice were genotyped by PCR to confirm CCR7 knockout as described in section 2.1.3.3. They were also phenotyped by fluorescent microscopy to confirm the presence of GFP positive leukocytes as described in section 2.1.3.1.

2.2 Reagents

2.2.1 Anaesthetics

Isoflurane IsoFlo®, Zoetis, Zaventem, Belgium;

Ketamine Ketaset Injection, conc. = 100 mg/ml, Cat. #SH4405D, Pfizer Ltd, Kent, UK;

Xylazine Rompun 2%, conc. = 20 mg/ml, Cat. #8109987, Bayer Plc., Newbury, UK.

2.2.2 Antibodies

2.2.2.1 Primary antibodies

αSMA Purified monoclonal mouse anti-mouse α-smooth muscle actin, clone 1A4, conc. = 1.3 mg/ml, used at 2.5 µg/ml Cat. #A2547, Sigma-Aldrich, Saint Louis, USA. This antibody was directly conjugated to Alexa-488 using an Alexa® 488 antibody labelling kit (Invitrogen, Cat. #A-20181, Paisley, UK) according to the manufacturer's protocol;

CCL21 Purified polyclonal rabbit anti-mouse Exodus-2, conc. = 1 mg/ml, used at 7.5 µg/ml, Cat. #500-P114, Peprotech, London, UK;

CCR7 Biotin conjugated rat anti-mouse CD197 (CCR7), clone 4B12, conc. = 0.5 mg/ml, used at 10 µg/ml, eBioscience, Hatfield, UK;

CD45.2 PE-Cy7 conjugated anti-mouse CD45.2, clone 104, conc. = 0.2 mg/ml, used at 0.2 µg/ml, Cat. #14-5931-81, BioLegend, London, UK;

CD3ε	APC conjugated anti-mouse CD3ε, clone 145-2C11, conc. = 0.2 mg/ml, used at 0.2 µg/ml, Cat. #17-0031-81, eBioscience, Hatfield, UK;
CD11c	PE-Cy5 conjugated hamster anti-mouse CD11c, clone N418, conc. = 0.2 mg/ml, used at 0.2 µg/ml, Cat. #117316, BioLegend, London, UK;
CXCR4	PE conjugated anti-mouse clone 2B11, conc. = 0.2 mg/ml, used at 0.5 µg/ml, at Cat. #146505, eBioscience, Hatfield, UK;
Fc Block™	Purified monoclonal rat anti-mouse CD16/CD32 (FCγIII/II receptor), clone 2.4G2, conc. = 0.5 mg/ml, used at 5 µg/ml, Cat #553141, BD Biosciences, Oxford, UK;
ICAM-1	Alexa Fluor® 488 conjugated rat anti-mouse CD54, clone YN1/1.7.4, conc. = 0.2 mg/ml, used at 16.7 µg/ml, at Cat. #116111, BioLegend, London, UK;
LYVE-1	Purified monoclonal rat anti-mouse LYVE-1, clone ALY7, conc. = 0.5 mg/ml, used at 2.5 µg/ml for *ex vivo*-fixed staining and 10 µg/ml for *in vivo*-live staining, Cat. #14-0443, eBioscience, Hatfield, UK. This antibody was directly conjugated to Alexa-488, Alexa-532, and Alexa-555 using Alexa® 488, 532 or 555 antibody labelling kits (Invitrogen, Cat. #A-20181; A-20182; A20187, Paisley, UK) according to the manufacturer's protocol;
Ly6G	Alexa Fluor® 647 conjugated anti-mouse Ly-6G, clone 1A8, conc. =0.2 mg/ml, used at 0.2 µg/ml, Cat. #127609, BioLegend, London, UK;
PECAM-1	Purified monoclonal rat anti-mouse CD31, clone 390, conc. = 1 mg/ml, used at 2.5 µg/ml, eBioscience, Hatfield, UK. This antibody was directly conjugated to Alexa-488, Alexa-555 and Alexa-647 using the Alexa® 488, 555 or 647 antibody labelling kit (Invitrogen, Cat. #A-20181; A20187;

A-20186, Paisley, UK) according to the manufacturer's protocol;

Heparan Sulfate (HS) Mouse anti-heparan sulfate (10E4 epitope), clone F58-10E4, conc. = 1 mg/ml, used at 70µg/ml. Cat. #370255-S, Amsbio, Abingdon, UK;

MRP14 Purified monoclonal rat anti-mouse MRP14, clone 2B10, conc. = 1.4 mg/ml, used at 2.5 µg/ml, received as a gift from Prof. Nancy Hogg (Cancer Research, UK). This antibody was directly conjugated to Alexa-488 and Alexa-555 using the Alexa® 647 antibody labelling kit (Invitrogen, Cat. #A-20186, Paisley, UK) according to the manufacturer's protocol. MRP14 is an intracellular marker for neutrophils (Hobbs et al., 2003).

MECA-79 Alexa Fluor® 488 conjugated rat anti-mouse/human High Endothelial Venule (HEV) mAb, clone MECA-79, conc. = 0.5 mg/ml, used at 2.5 µg/ml, Cat. #AF-425-SP, eBioscience, Hatfield, UK;

TNFRI (p55) Purified goat anti-mouse CD120a (TNFR Type I/p55) Ab, conc. = 0.5 mg/ml, used at 2 µg/ml, Cat. #113001, R&D Systems, Abingdon, UK;

TNFRII (p75) Purified goat anti-mouse CD120b (TNFR Type II/p75) Ab, conc. = 0.5 mg/ml, used at 2 µg/ml, Cat. #AF-426-SP, R&D Systems, Abingdon, UK.

VE-Cadherin Purified rat anti-mouse CD144 mAb, clone eBioBV13 (BV13), conc. = 1 mg/ml, used at 2.5 µg/ml, eBioscience, Hatfield, UK. This antibody was directly conjugated to Alexa-555 using the Alexa® 555 antibody labelling kit (Invitrogen, Cat. #A20187, Paisley, UK) according to the manufacturer's protocol;

2.2.2.2 Secondary antibodies

Anti-hamster-A488 Alexa Fluor® 488 goat anti-Hamster IgG (H+L) Cross-Adsorbed Secondary Ab, conc. = 2 mg/ml, used at 5 µg/ml, Cat. #R37118, Invitrogen, Paisley, UK;

Anti-rabbit-A488 Alexa Fluor® 488 conjugated donkey anti-rabbit IgG secondary Ab, conc. = 2 mg/ml, used at 5 µg/ml, Cat. #R37118, Invitrogen, Paisley, UK;

Anti-mouse-A488 Purified Alexa Fluor® 488 conjugated goat anti-mouse IgG (H+L) secondary Ab, conc. = 2 mg/ml, used at 3.3 µg/ml, Cat.#A-11001, Invitrogen, Paisley, UK;

Streptavidin-A488 Alexa Fluor® 488 conjugate, conc. = 2 mg/ml, used at 3.3 µg/ml, Cat. #S11223, Invitrogen, Paisley, UK.

2.2.2.3 Blocking antibodies

Anti-CXCL1 mAb Purified rat anti-mouse CXCL1/GROα/KC/CINC-1 mAb, used at 30 µg/mouse, Cat. #MAB453, R&D Systems, Abingdon, UK;

Anti-ICAM-1 mAb Purified rat anti-mouse ICAM-1 mAb, clone YN1/1.4.7, conc. = 0.5 mg/ml, used 10 µg/mouse, eBioscience, Hatfield, UK;

Anti-MAC-1 mAb Purified rat anti–mouse MAC-1 mAb, clone M1/70, conc. = 0.5 mg/ml, used at 10 µg/mouse, Cat. #101202, BioLegend, London, UK;

Anti-TNF mAb LEAF™ Purified anti-mouse TNF Antibody, clone MP6-XT22, conc. = 1 mg/ml, used 50 µg/mouse, Cat. #506310, BioLegend, London, UK.

2.2.2.4 Isotype controls

for CCL21 Purified normal goat IgG control antibody, conc. = 1 mg/ml, used at 7.5 µg/ml. Cat. #AB-108-C, R&D Systems, Abingdon, UK;

for CCR7 Biotin conjugated rat IgG2a, κ isotype control, eBR2a, conc. = 0.5 mg/ml, used at 10 µg/ml, Cat. #13-4321-82, eBioscience, Hatfield, UK;

for CD45.2 PE-Cy7 conjugated rat anti-mouse IgG2a, κ isotype control antibody, conc. = 0.5 mg/ml, used at 0.2 µg/ml, clone MOPC-173, Cat. #400231, BioLegend, London, UK;

for CD3ε APC conjugated Armenian hamster anti-mouse IgG isotype control antibody, conc. = 0.5 mg/ml, used at 0.2 µg/ml, clone eBio299Arm, Cat. #17-4888-81, eBioscience, Hatfield, UK;

for CD11c PE-Cy5 conjugated hamster IgG2 isotype control antibody, conc. = 0.2 mg/ml, used at 0.2 µg/ml, clone HTK888, Cat. #400909, BioLegend, London, UK;

for CXCR4 PE conjugated rat IgG2B, κ isotype control, clone RTK2758, conc. = 0.2 mg/ml, used at 0.5 µg/ml, Cat. #17-4321, eBioscience, Hatfield, UK;

for ICAM-1 Alexa Fluor® 488 conjugated rat IgG2b, κ isotype control antibody, clone RTK4530, conc. = 0.2 mg/ml, used at 16.7 µg/ml, Cat. #400625, BioLegend, London, UK;

for Ly6G Alexa Fluor® 647 conjugated rat IgG2a, κ isotype control, clone eBR2a, conc. = 0.2 mg/ml, used at 0.2 µg/ml, Cat. #400526, BioLegend, London, UK;

for HS LEAF™ purified mouse IgM, κ isotype control antibody, conc. = 1 mg/ml, used at 70 µg/ml, Cat. #401604, BioLegend, London, UK;

for TNFRI (p55) and TNFRII (p75)

Purified normal goat IgG control, conc. = 1 mg/ml, Cat. #AB-108-C, R&D Systems, Abingdon, UK;

for anti-CXCL1 Purified monoclonal rat IgG2a, κ, clone eBR2a, conc. = 0.5 mg/ml, used at 30 µg/ml. Cat. #53-4321, eBioscience, Hatfield, UK;

for anti-ICAM-1/MAC-1 mAb

LEAF™ purified rat IgG2b, κ isotype control antibody, conc. = 1 mg/ml, used 10 µg/mouse, Cat. #400622, BioLegend, London, UK;

for anti-TNF mAb LEAF™ purified rat IgG1, κ isotype control antibody, conc. = 1 mg/ml, used 50 µg/mouse, Cat. #400414, BioLegend, London, UK.

2.2.3 Chemokine receptor antagonists

AMD3100 octahydrochloride hydrate (CXCR4 antagonist)

1,1′-[1,4-Phenylenebis(methylene)]bis-1,4,8,11-tetraazacyclotetradecane octahydrochloride, 5mg, used at 10 mg/kg, Cat # A5602. Sigma-Aldrich, Saint Louis, USA.

2.2.4 Fluorescent nuclei marker (viability)

DAPI 4’,6-Diamidino-2-phenylindole dihydrochloride, 1 mg, Cat. #D9542, Sigma-Aldrich, Saint Louis, USA.

2.2.5 Lectins and inhibitory sugars

Lectins

All lectins were directly conjugated in-house to Alexa-647 using the Alexa® 647 antibody labelling kit (Invitrogen, Cat. # A-20186, Paisley, UK) according to the manufacturer's protocol.

Griffonia (Bandeirafa) Simplicifolia Lectin I Isolectin B4 (IB4)

IB4, conc. = 1 mg/ml, Cat. #L-1104, Vector Laboratories, California, U.S.A;

Lycopersicon Esculentum (Tomato) Lectin (LEL)

LEL, conc. = 1 mg/ml, Cat. #L-1170, , Vector Laboratories, California, U.S.A;

Maackia Amurensis Lectin (MAL-1)

MAL-1, conc. = 1 mg/ml, Cat. #L-1310, Vector Laboratories, California, U.S.A;

Sambucus Nigra (Elderberry) Bark Lectin (SNA)

SNA, conc. = 1 mg/ml, Cat. #L-1300, Vector Laboratories, California, U.S.A.

Inhibitory sugars

of IB4 Galactose, conc. = 100 mg/ml, Cat. #S-9003, Vector Laboratories, California, U.S.A;

of LEL Chitin hydrolysate, 100 mg/ml, Cat. #0090, Vector Laboratories, California, U.S.A;

of MAL-1 and SNB Lactose. Conc. 1.4 mg/ml. Cat. #S-9004, Vector Laboratories, California, U.S.A.

2.2.6 Enzymes

DNase I Deoxyribonuclease I from bovine pancreas, conc. = 5 mg/ml, used at 50 µg/ml. Activity less than 2000 Kunitz units/mg, Cat. # D5025, Sigma-Aldrich, Saint Louis, USA.

Liberase™ TL Research Grade

Conc. = 2.5 mg/ml, Activity = 13 Wünsch/ml, used at 200 µg/ml, Cat. #05401020001, Sigma-Aldrich, Saint Louis, USA;

Proteinase K Conc. = 10 mg/ml, used at 100 µg/ml, Cat. #BIO-37037, Activity = bigger than sign 400 units/ml, Bioline, London, UK.

2.2.7 Inflammatory stimuli

Complete Freund's Adjuvant (CFA)

Conc. = 20 mg/ml, used 200 µg/mouse, Cat. #7024, Amsbio, Abingdon, UK;

Ovalbumin (OVA) Albumin from chicken egg white, 250 mg, reconstituted in PBS to 1 mg/ml, used 200 µg/mouse, Cat. #A2512, Sigma-Aldrich, Saint Louis, USA;

Tumour necrosis factor alpha (TNF)

Recombinant Mouse TNF, Cat. #410-MT-050/CF, R&D Systems, Abingdon, UK;

2.2.8 Buffers

ACK lysis buffer	150mM NH4Cl, 10mM KHCO3, 0.1mM EDTA, pH 7.3 in H_20;
FACS buffer	1 x PBS supplemented with 1% heat-inactivated fetal bovine serum;
Cremaster homogenising buffer	1 x PBS supplemented with 1% Triton X-100 and 1% protease inhibitor cocktail;
TAE buffer	UltraPureTM 10x TAE buffer, Cat. No. 15558-026, Invitrogen, Paisley, UK.

2.2.9 Other miscellaneous reagents and solutions

DNA ladder	SmartLadder SF (100 – 1,000 bp), Cat. No. MW-1800-04, Eurogentec, Southampton, UK;
DNA gel loading dye (6X)	Cat. #R0611, ThemoFisher Scientific, Paisley, UK;
DMSO	Dimethyl sulfoxide, Cat. # W387520, Sigma-Aldrich, Saint Louis, USA;
EDTA	Ethylenediaminetetraaceticacid disodium salt dehydrate, Cat #E5134, Sigma-Aldrich, Saint Louis, USA;
Fetal bovine serum (FBS)	Cat. #10270-106, Gibco, Paisley, UK;
GelRed	Cat. No. 41003, Biotium, via Cambridge BioScience, Cambridge, UK;

Halt™ Protease Inhibitor Cocktail (100X)

Cat. #87786, ThemoFisher Scientific, Paisley, UK;

Heparin Heparin sodium salt from porcine intestinal mucosa, ≥ 180 USP units/mg, Cat #H3149, Sigma-Aldrich, Saint Louis, USA;

Molecular biology grade water UltraPureTM DNase/RNase-free distilled water, Cat. No. 10977-049, Invitrogen, Paisley, UK;

Normal goat serum (NGS) Goat serum, Cat #G6767, Sigma-Aldrich, Saint Louis, USA;

Nystatin Nystatin powder reconstituted in DMSO, 1 mg/ml, used at 50 μM, Cat. # N6261, Sigma-Aldrich, Saint Louis, USA;

Halt™ Protease Inhibitor Cocktail (100X)

Halt protease and phosphatase inhibitor cocktail, Cat. #87786, ThemoFisher Scientific, Paisley, UK;

Incomplete Freund's Adjuvant (IFA)

Liquid Freund's Adjuvant, Incomplete, Cat. # F5506, Sigma-Aldrich, Saint Louis, USA;

4% Paraformaldehyde (PFA)

Paraformaldehyde powder reconstituted in dH2O, Cat #158127, Sigma-Aldrich, Saint Louis, USA;

Phosphate buffered saline (PBS)

Dulbecco's 1 x PBS, pH 7.2, Cat. #D8662, Sigma-Aldrich, Dorset, UK;

Triton™ X-100	Laboratory grade, Cat. #X100, Sigma-Aldrich, Saint Louis, USA.
Tyrode's salt solution	Cat. No. 127K8303, Sigma-Aldrich, Poole, Dorset, UK;

2.2.10 Kits

Fixation/Permeabilisation Solution Kit

BD Cytofix/Cytoperm™, Cat. #554714, BD Biosciences, Oxford, UK;

Mouse CXCL12/SDF-1α Quantikine ELISA kit

Cat. #MCX120, R&D Systems, Abingdon, UK;

Mouse TNF ELISA Ready-SET-Go!®

Cat. #88-7324-22, eBioscience, Hatfield, UK;

Mouse GM-CSF ELISA Ready-SET-Go!®

Cat. #88-7334-22, eBioscience, Hatfield, UK;

Mouse IL-17A (homodimer) ELISA Ready-SET-Go!®

Cat. #88-7371-22, eBioscience, Hatfield, UK;

Pierce™ BCA Protein Assay Kit

Cat. #23225, ThermoFisher Scientific, Paisley, UK.

2.3 Preparation of Complete Freund's Adjuvant (CFA) emulsion for inducing inflammation in the cremaster muscle

To induce inflammation in the cremaster muscle with CFA, an emulsion of CFA and antigen (CFA+Ag) containing equal volumes of CFA/incomplete Freund's adjuvant (IFA) and antigen/PBS was prepared. 300 µl of this emulsion was injected into each mouse to induce an inflammatory response. To make the emulsion, the antigen ovalbumin (OVA, 200 µg) was first diluted in sterile PBS. The required amount of CFA (200 µg/mouse) was then pipetted into a 1.5 ml screw-top tube and topped up with the required amount of IFA. An equal volume of antigen/PBS was then added to the tube before being placed in a high-throughput tissues homogeniser, Precellys® 24 (Precellys, Derbyshire, UK), for 1 cycle of 45 s homogenisation at 6500 r.p.m to combine the adjuvant and antigen and form an emulsion. A 1 ml silliconised syringe (Plastipak Luer Lock, BD, Oxford, UK) was used to draw up the emulsion before a 23 gauge needle was attached.

2.4 Inducing inflammation in murine tissues and analysis by immunofluorescence labelling and confocal microscopy

All i.s. injections of TNF/lectins/antibodies were given in a total volume of 400 µl made up with PBS. All i.s. injections of CFA+Ag were given in a total volume of 300 µl made up with CFA and OVA (see section 2.3).

2.4.1 Inducing inflammatory reactions of murine cremaster muscles *in vivo*

8-12 week old male mice (strain used dependent on experiments) were sedated using an isoflurane machine (IsoFlo®, Zoetis, Belgium) before their cremaster muscles were stimulated via intrascrotal (i.s) injection of TNF (300 ng/400 µl PBS) or CFA (200 µg/mouse) alongside OVA (200 µg/mouse), hereafter known as CFA+Ag. Control mice received 400 µl of PBS via i.s. injection. Several time-points following TNF/CFA+Ag

stimulation were investigated over the course of 48 h. At the end of each time point, mice were sacrificed and their cremaster muscles and cremaster dLNs (Inguinal) were dissected away and fixed at 4 °C for 1 h and overnight, respectively. Tissues were then permeabilised for 4 h at room temperature, followed by immunofluorescence labelling and confocal microscopy analysis as described in the sections below.

2.4.2 Immunofluorescence labelling of whole-mounted murine cremaster muscles and cremaster draining lymph nodes

To investigate neutrophil migration responses across post-capillary venules and intravasation into initial lymphatic vessels and into the dLNs, whole-mounted murine tissues such as the cremaster muscle and dLNs (namely inguinal) had to be immunostained with fluorescent conjugated antibodies following fixation/permeabilisation for confocal microscopy analysis.

Mice were sacrificed via cervical dislocation before cremaster muscles and cremaster draining LNs (inguinal and lumbar) were dissected away. These tissues (unstimulated, respective controls or stimulated with inflammatory mediators described above in section 2.4.1) were then subjected to a modified version of the immunostaining protocol previously described (Wang et al., 2005). Briefly, cremaster tissues were fixed in 4% PFA in PBS for 1 hour at 4 °C and dLNs were fixed overnight at 4 °C. LNs were cut in half longitudinally with a scalpel following fixation. Fixed tissues were blocked and permeabilised in PBS (containing 12.5% goat serum, 12.5% fetal bovine serum [FBS] and 0.5% Triton X-100) for 4 h at room temperature. Tissues were then immunofluorescently stained for ECs (0.25 µg/100 µl, anti-PECAM-1 mAb) and LECs (0.25 µg/100 µl, anti-LYVE-1 mAb), and/or for neutrophils (0.25 µg/100 µl anti-MRP14 mAb), in PBS (with 10% FBS) overnight at 4°C. Draining LNs were immunostained for high endothelial venules (HEVs) instead of BECs with an anti-MECA-79 mAb (0.25 µg/100 µl) in PBS (with 10% FBS) overnight at 4°C. Following a 3 h wash, the tissues were imaged with a Leica SP5 or SP8 confocal microscope (Leica Microsystems, Milton Keynes, UK) as described in the following sections (section 2.4.3 and 2.4.4) for cremasters and dLNs, respectively.

2.4.3 Confocal analysis of neutrophil migration responses in immunostained whole-mounted murine cremaster muscles

Following immunostaining, all cremaster muscles were imaged with a Leica SP8 confocal microscope at 20 to 24°C with the use of a 20× water-dipping objective (numerical aperture [NA]: 1.0). Images of postcapillary venules and lymphatic vessels (at least 6 vessels per tissue) were acquired with the use of sequential scanning of different channels at every 0.52 μm of tissue depth at a resolution of 1024 × 470 and 1024 x 800 pixels in the x × y plane, corresponding to a voxel size of 0.24 × 0.24 × 0.5 μm in x × y × z planes. Postcapillary venules and lymphatic vessels were imaged at a zoom factor of ×1.9 and ×1.2, respectively. Quantification of neutrophil transmigration and intravasation into lymphatic vessels were analysed with the 3D-reconstructing image processing software IMARIS (Bitplane, Switzerland). Transmigrated neutrophils were defined as the number of neutrophils present in the extravascular tissue across a 300 μm blood vessel segment and within 50 μm from each side of the venule of interest. Data was expressed as the number of neutrophils per volume of tissue. Intravasated neutrophils were defined as the number of neutrophils present inside the lymphatic vessels and data was expressed as the number of neutrophils per given volume of vessel. To get the volume of lymphatic vessels, an isosurface was created using the channel showing immunofluorescence labelling of LYVE-1 as a source to represent the lymphatic endothelium (**Figure 2.2**). IMARIS then uses this information to give the volume of this isosurface (i.e. lymphatic vessels).

A

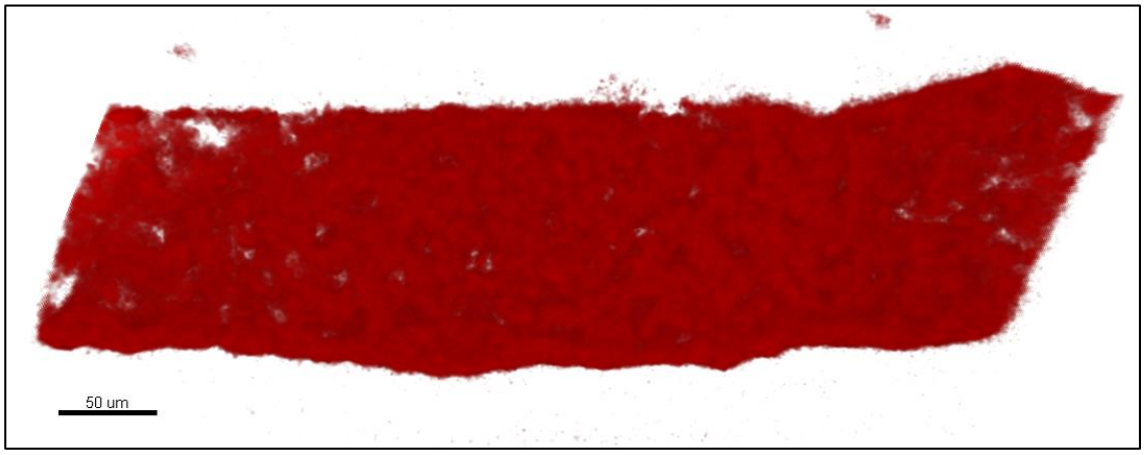

B

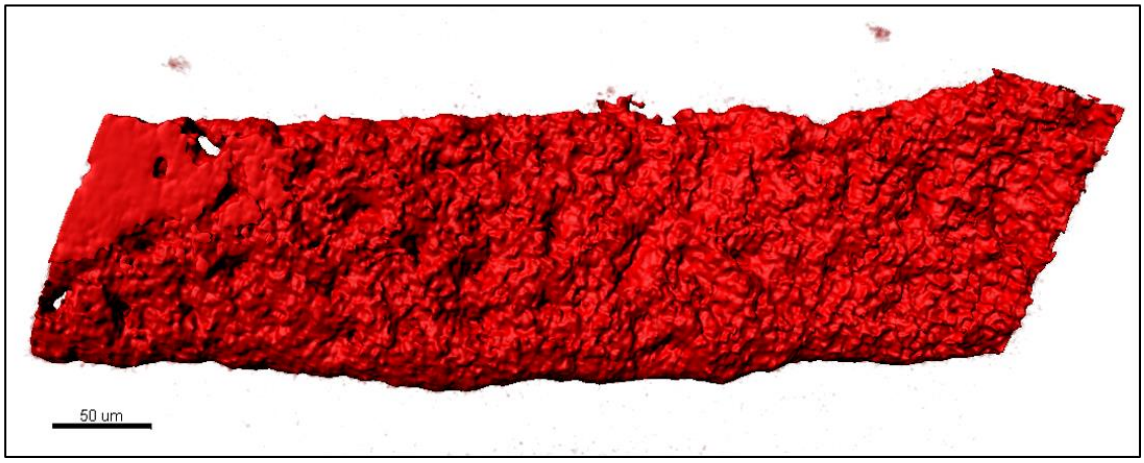

Figure 2.2: Creating isosurface of lymphatic vessels using IMARIS software. A representative isosurface showing the lymphatic endothelium (B) is illustrated, which has been generated using immunofluorescence labelling of LYVE-1 (A) as a source. Bars: 50 µm.

2.4.4 Quantification of neutrophil recruitment in immunostained cremaster draining LNs via confocal microscopy

Following immunostaining, the LNs were imaged with a Leica SP8 confocal microscope at 20 to 24°C with the use of a 10× water-dipping objective (NA: 0.25). Images (12 in total from each pair of LNs/mouse) were obtained with the use of sequential scanning of different channels at every 5.8 µm of tissue depth at a resolution of 1024 × 1024 pixels in the x × y plane, corresponding to a voxel size of 0.91 × 0.91 × 5.8 µm in x × y × z planes. Quantification of neutrophil recruitment into the inguinal and lumbar LNs were analysed with the 3D-reconstructing image processing software IMARIS (Bitplane, Switzerland). Recruited neutrophils were defined as the number of neutrophils present per volume of tissue, excluding (unless specified) the blood circulating neutrophils present in HEVs.

2.5 Characterising the LEC glycocalyx of murine cremaster muscles

2.5.1 Visualising sugar residues on lymphatic vessels

In order to visualise carbohydrates of LEC glycocalyx in tissues, two methods of glycocalyx staining using lectins were tested. The first involved *ex vivo*-fixed staining as previously described (Section 2.4.2), whereas the second staining method involved *in vivo*-live (intrascrotal [i.s. injection]) staining. Both methods are described below. Different techniques were tested as fixation could impact the binding capacity of the lectins and possibly affect analysis, thus live labelling was also carried out. *In vivo*-live staining is rapid but potential phagocytosis of fluorescent lectins can lead to non-specific signals. In *ex vivo*-fixed staining, sugar epitopes are present intracellularly in tissues (as opposed to *in vivo*-live staining, where sugar epitopes are on the surface of cells). Therefore, this could be used as an indication as to whether lectin staining is intracellular.

All commercially available lectins, namely IB4, MAL-1, LEL and SNA with specific sugar residue binding properties were labelled in-house with an Alexa Flour® 647 protein labelling kit (Invitrogen).

2.5.2 *Ex vivo*-fixed staining

Cremaster muscles were harvested from WT mice and immunostained for the lectins (0.25 µg/ 100 µl, Alexa 647-conjugated), BECs (0.25 µg/100 µl, anti-PECAM-1 mAb, Alexa 488-conjugated) and LECs (0.25 µg/100 µl, anti-LYVE-1 mAb, Alexa 555-conjugated) as described in section 2.4.2. In some experiments, cremaster muscles of mice were subjected to TNF- or CFA+Ag-stimulation before tissues were harvested. Neutrophils (0.25 µg/100 µl, anti-MRP14 mAb, Alexa 488-conjugated) were also labelled in some experiments.

2.5.3 *In vivo*-live staining

Sugars (lectin), BECs (PECAM-1) and LECs (LYVE-1) labelling was achieved by i.s. injection of the fluorescent-conjugated lectin/antibodies (1 µg/100 µl). After 2 hours, mice were sacrificed and the cremaster muscles were dissected away and whole-mounted for fixation in 4% PFA in PBS followed by imaging with a Leica SP8 confocal microscope. In some experiments, cremaster muscles of mice were subjected to TNF- or CFA+Ag-stimulation before tissues were harvested.

2.5.4 Analysis of sugar residues on lymphatic vessels and blood vessels

Expression of sugars to which the lectins bind to on the surface of lymphatic vessels and blood vessels was assessed by determining the mean fluorescence intensity (MFI) of tissue vessel structures stained with the lectins using IMARIS software. To do this, an isosurface was created using the channel showing immunofluorescence labelling of LYVE-1/PECAM-1 as a source to represent the lymphatic endothelium/blood vascular endothelium. This parameter depicts the limitation of the volume of interest in which IMARIS determines the MFI of the channel showing fluorescent labelling of the lectins.

2.6 Investigating heparan sulfate and chemokine expression by lymphatic vessels

2.6.1 CCL21 immunostaining of TNF- or CFA+Ag-stimulated murine cremaster muscles

Expression of the prototypical lymphatic chemokine, CCL21, on the lymphatic vasculatures was investigated by immunostaining of the lymphatic endothelium via *in vivo*-live staining (i.e. both surface and intracellular expression). For *in vivo*-live staining, C57BL/6 WT mice were i.s. injected with TNF or an emulsion of CFA+Ag and the inflammatory response was allowed to develop for 16 h. Two hours before the end of the inflammation period, mice received an i.s. injection of anti-LYVE-1 mAb (1 μg/100 μl), anti-CCL21 mAb/rabbit IgG isotype control Ab (0.75 μg/100 μl) to label lymphatic vasculatures and CCL21, respectively. Intrascrotal injections were carried out using an isoflurane anaesthetic machine. At the end of the inflammation period, cremaster muscles were dissected away and immediately visualised using a Leica SP5 or SP8 confocal microscope.

2.6.2 Heparan sulfate immunostaining of TNF-stimulated murine cremaster muscles

Expression of the GAG, heparan sulfate (HS), by lymphatic vessels was investigated by immunostaining of the lymphatic endothelium via *ex vivo*-fixed staining. For *ex vivo*-fixed staining, C57BL/6 WT mice were i.s. injected with TNF (300 ng/mouse) and the inflammatory response was allowed to develop for 16 h. Following dissection of the cremaster muscles, tissues were whole-mounted and fixed in 4% PFA for 1 h before being blocked and permeabilised in PBS (containing 12.5% goat serum, 12.5% fetal bovine serum (FBS) and 0.5% Triton X-100) for 3 h at room temperature. Tissues were then immunostained with an anti-HS Ab or mouse IgM isotype control Ab (7 μg/100 μl, purified) and anti-LYVE-1 mAb (0.25 μg/100 μl PBS) to label HS and lymphatic vasculatures, respectively, in PBS (with 10% FBS) overnight at 4°C. The following day, tissues were washed for 3 h before being immunostained with an anti-mouse IgM

secondary Ab (0.5 µg/100 µl, Alexa 488-conjugated) in PBS (with 10% FBS) for 2 h at RT. Following a 3 h wash, the tissues were imaged with a Leica SP8 confocal microscope.

2.7 Investigating neutrophil migration responses following chemokine/chemokine receptor blockade

To investigate the CXCL1:CXCR1/2 chemokine axis, C57BL/6 WT male mice (8-12 weeks) received i.s. injection of CFA+Ag (200 µg/mouse) as per section 2.4.1. Unstimulated control mice received 400 µl of PBS via i.s. injection. 4 h post-i.s. injection, mice received i.s. injections of either an anti-CXCL1 or rat IgG2a isotype control Ab (30 µg/mouse). Eight hours post-i.s. injection, mice were sacrificed and their cremaster muscles and cremaster dLNs were dissected away and whole-mounted for fixation in 4% PFA in PBS for 1 h followed by immunofluorescence labelling (as carried out in section 2.4.2), confocal microscopy and IMARIS analysis (as carried out in sections 2.4.3 and 2.4.4 for the cremaster muscles and dLNs, respectively).

To investigate the CXCL12:CXCR4 chemokine axis, C57BL/6 WT male mice (8-12 weeks) received i.s. injection of TNF (300 ng/mouse) or CFA+Ag (200 µg/mouse) as per section 2.4.1. Unstimulated control mice received 400 µl of PBS via i.s. injection. 4 h post-i.s. injection, mice received i.s. injections of either AMD3100 (10 mg/kg) (Liu et al., 2014) or vehicle control (PBS). Sixteen hours post-i.s. injection, mice were sacrificed and their cremaster muscles and cremaster dLNs were dissected away and whole-mounted for fixation in 4% PFA in PBS for 1 h followed by immunofluorescence labelling (as carried out in section 2.4.2), confocal microscopy and IMARIS analysis (as carried out in sections 2.4.3 and 2.4.4 for the cremaster muscles and dLNs, respectively).

To investigate the CCL21/CCR7 chemokine axis, CCR7KO male mice (8-12 weeks) received i.s. injection of TNF (300 ng/mouse) or CFA+Ag (200 µg/mouse) as per section 2.4.1. Control mice received 400 µl of PBS via i.s. injection. Different time-points such as 8 h and 16 h were investigated following which the mice were sacrificed and their cremaster muscles and cremaster dLNs were dissected away and whole-mounted for fixation in 4% PFA in PBS for 1 h followed by immunofluorescence labelling (as carried out in section 2.4.2), confocal microscopy and IMARIS analysis (as carried out in sections 2.4.3 and 2.4.4 for the cremaster muscles and dLNs, respectively). In some experiments,

chimeric mice exhibiting CCR7KO neutrophils in a WT environment were used. In other experiments, CCR7KO mice were given i.s. injections of the CXCR4-specific inhibitor, AMD3100, 4 h post-i.s. injection. At the end of the inflammatory period, cremaster muscles were dissected away and subjected to the same staining protocol as above, before being analysed by confocal microscopy and IMARIS software.

2.7.1 Analysis of heparan sulfate and chemokine staining on lymphatic vessels

Expression of HS and CCL21 by lymphatic vessels was assessed by determining the mean fluorescence intensity (MFI) of tissue vessel structures stained with HS and CCL21 using IMARIS software. To do this, an isosurface was created using the channel showing immunofluorescence labelling of LYVE-1 as a source to represent the lymphatic endothelium. This parameter depicts the limitation of the volume of interest in which IMARIS determines the MFI of the channel showing fluorescent labelling of HS and CCL21. Intensity profiles for CCL21 expression along a certain distance (10 μm away from lymphatic vessels) were performed using Image J.

2.8 Investigating the role of TNF in neutrophil migration responses during antigen sensitisation

To investigate the role of TNF signalling in neutrophil migration into lymphatic vessels, TNFRdbKO male mice (8-12 weeks) were given i.s. injection of CFA+Ag (200 μg/mouse) as per section 2.4.1. Control mice received 400 μl of PBS via i.s. injection. Different time-points such as 8 h and 16 h were investigated following which the mice were sacrificed and their cremaster muscles and cremaster dLNs were dissected away and whole-mounted for fixation in 4% PFA in PBS for 1 h followed by immunofluorescence labelling (as carried out in section 2.4.2), confocal microscopy and IMARIS analysis (as carried out in sections 2.4.3 and 2.4.4 for the cremaster muscles and dLNs, respectively). In some experiments, chimeric mice exhibiting TNFRdbKO neutrophils in a WT environment were used.

2.9 ICAM-1 expression on lymphatic vasculatures

2.9.1 ICAM-1 immunostaining in TNF- or CFA+Ag-stimulated murine cremaster muscles with/without TNF signalling blockade

Expression of the adhesion molecule, ICAM-1, on the lymphatic vasculatures was investigated by immunostaining of the lymphatic endothelium. Male WT mice were i.s. injected with TNF (300 ng/mouse) or CFA+Ag (200 μg/mouse) as per section 2.4.1 and the inflammatory response was allowed to develop for 8 h. In some experiments, CFA+Ag-stimulated animals were pre-treated with a local (i.s.) injection of the blocking anti-TNF or rat IgG1κ isotype control mAbs (50 μg/mouse). Two hours before mice were sacrificed and the cremaster tissues dissected away, non-blocking doses of an anti-LYVE-1 mAb (1 μg/100 μl, Alexa 555-conjugated) and an anti-PECAM-1 mAb (1 μg/100 μl, Alexa 647-conjugated) was injected i.s. to immunolabel LECs and EC junctions to aid with visualisation of the lymphatic endothelium and endothelial cell layer, respectively. For i.s. injections, an isoflurane anaesthesia machine was used. Following dissection of the cremaster muscles, tissues were whole-mounted and fixed in 4% PFA for 1 h before being blocked and permeabilised in PBS (containing 12.5% goat serum, 12.5% fetal bovine serum (FBS) and 0.5% Triton X-100) for 3 h at room temperature. Tissues were then immunofluorescently stained with an anti-ICAM-1 mAb or the rat IgG2b,κ isotype control (2 μg/100 μl, Alexa 488-conjugated) in PBS (with 10% FBS) overnight at 4°C. Following a 3 h wash, the tissues were imaged with a Leica SP8 confocal microscope.

2.9.2 Analysis of ICAM-1 staining on lymphatic vessels

Expression of ICAM-1 on lymphatic vessels was assessed by determining the MFI of tissue vessel structures labelled with ICAM-1 using IMARIS software. To do this, an isosurface was created using the channel showing immunofluorescence labelling of LYVE-1 as a source to represent the lymphatic endothelium. This parameter depicts the limitation of the volume of interest in which IMARIS determines the MFI of the channel showing fluorescent labelling of ICAM-1.

2.10 Confocal Intravital Microscopy

Confocal intravital microscopy (IVM) was used to observe neutrophil responses within lymphatic vessels of the cremaster muscle upon TNF- or CFA+Ag-stimulation with or without TNF/ICAM-1/MAC-1-blockade in real-time in 4D. Appropriate techniques were adapted from confocal IVM of postcapillary venules carried out by previous members of the group (Woodfin et al., 2011), and developed to investigate neutrophil interactions with LECs *in vivo* (Arokiasamy et al., 2017), as described in the following sections.

2.10.1 Investigation of neutrophil migration responses in TNF- or CFA+Ag-stimulated murine cremaster muscles

To investigate neutrophil migration across lymphatic vessels during inflammation *in vivo*, the cremaster muscles of male LysM-eGFP mice were stimulated by i.s. injection of TNF (300 ng/ml) or CFA+Ag (200 µg/mouse) and the inflammatory response was allowed to develop for 4 (TNF) to 6 h (CFA+Ag) before visualisation of the response by IVM. Two hours before surgery, non-blocking doses of an anti-LYVE-1 mAb (2.5 µg in 250 µl, Alexa 555-conjugated) and an anti-PECAM-1 mAb (2.5 µg in 250 µl, Alexa 647-conjugated) was injected i.s. to immunolabel LECs and EC junctions to aid with visualisation of the lymphatic endothelium and endothelial cell layer, respectively. For i.s. injections, an isoflurane anaesthesia machine was used. Thirty minutes before surgery, mice were anaesthetised by i.p. injection of ketamine (100 mg/kg) and xylazine (10 mg/kg) and maintained at 37 °C in an incubator (MediHeat^{TM}, Ascon Tecnologic, Pavia, Italy). Surgery to exteriorise the cremaster muscle was carried out on a custom-built heated microscope stage, where the tissue was pinned out flat over the optical window of the stage and superfused with Tyrode's solution (**Figure 2.3A-B**). Z-stack images of a lymphatic vessel were captured every 1 min for 90 min using a Leica SP5 confocal microscope. Z-stacks were captured at every 0.7 µm of tissue depth at a resolution of 1045 × 600 in the x × y plane. 4D confocal image sequences acquired were then analysed using IMARIS software, enabling the dynamic interaction of neutrophils with lymphatic vessels to be observed, tracked and quantified as previously described for blood vessels (Woodfin et al., 2011; Proebstl et al., 2012).

A

B

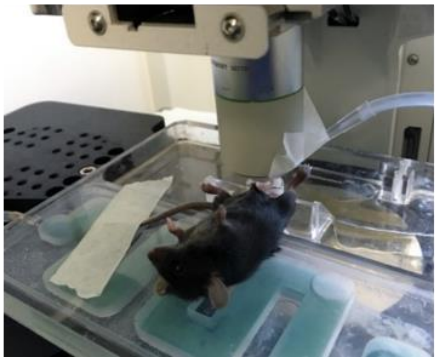

Figure 2.3: Surgical exteriorisation and preparation of the cremaster muscle for confocal intravital microscopy. (A) The cremaster muscle of a mouse was exteriorised before being pinned out flat over the optical window of a heated microscope stage. (B) Following this, it was positioned under the microscope and superfused with Tyrode's solution before being imaged.

2.10.2 Investigation of neutrophil migration and intraluminal crawling responses with TNF and ICAM-1/MAC-1 blockade

To investigate neutrophil migration across lymphatic vessels and changes in intraluminal crawling within the lymphatic endothelium during inflammation *in vivo*, the cremaster muscles of male WT mice were stimulated by i.s. injection of CFA+Ag (200 μg/mouse) and the inflammatory response was allowed to develop for 6 h (CFA+Ag) before visualisation of the response by IVM. Mice were pre-treated with a local (i.s.) injection of the following blocking antibodies 90 to 120 min before surgery: anti-TNF or rat IgG1κ

isotype control mAbs (50μg/mouse), anti-ICAM-1/anti-MAC-1 mAbs or rat IgG2b isotype control mAbs (10μg/mouse) along with non-blocking doses of anti-LYVE-1 mAb (2.5 μg in 250 μl, Alexa 555-conjugated) and an anti-PECAM-1 mAb (2.5 μg in 250 μl, Alexa 647-conjugated) to immunolabel LECs and EC junctions to aid with visualisation of the lymphatic endothelium and endothelial cell layer, respectively. For i.s. injections, an isoflurane anaesthesia was used. Thirty minutes before surgery, mice were anaesthetised by i.p. injection of ketamine (100 mg/kg) and xylazine (10 mg/kg) and maintained at 37 °C in an incubator (MediHeat^{TM}, Ascon Tecnologic, Pavia, Italy). Surgery to exteriorise the cremaster muscle was carried out on a custom-built heated microscope stage, where the tissue was pinned out flat over the optical window of the stage and superfused with Tyrode's solution (**Figure 2.3B**). Z-stack images of a lymphatic vessel were captured every 1 min for 90 min using a Leica SP5 confocal microscope. Z-stacks were captured at every 0.7 μm of tissue depth at a resolution of 1045 × 600 in the x × y plane. 4D confocal image sequences acquired were analysed using IMARIS software.

2.11 Investigating cytokine expression profile of cremaster muscles following inflammation

To determine whether the cytokines TNF, GM-CSF and IL-17A were produced following CFA+Ag-induced inflammation in the cremaster muscle, ELISAs were carried out to quantify cytokine release using supernatents obtained from homogenisation of inflamed cremaster tissues. BCA protein assays were carried out on the same samples in order to normalise the ELISA measurements by total protein concentration.

2.11.1 Inducing inflammation in the cremaster and tissue preparation

Inflammation was induced in the cremaster muscles of WT C57BL/6 with CFA+Ag (as per section 2.4.1). After 16 h of CFA+Ag stimulation, mice were sacrificed and their cremaster muscles were dissected away, placed in 1.5 ml eppendorf tubes before being immediately snap-frozen in liquid nitrogen. Tissues were transferred into screw-top tubes containing homogenising beads along with 500 μl homogenising buffer (1% Triton™ X-100, 1% protease inhibitor, PBS) prior to being placed in a high-throughput tissue

homogeniser, Precellys® 24 (Precellys, Derbyshire, UK), for 3 cycles of 20 s homogenisation at 6500 r.p.m with 40 s rest between each cycle. Homogenised samples were then frozen at -80 °C for 1 h before being thawed and centrifuged for 5 min at 10 000 g using a tabletop centrifuge. The supernatent was taken and used to quantify the release of the cytokines TNF, GM-CSF and IL-17A, and total protein concentration by Enzyme-Linked Immunosorbent Assay (ELISA) and Bicinchoninic Acid (BCA) protein assay, respectively.

2.11.2 ELISAs

The production of the cytokines TNF, GM-CSF, IL-17A and the chemokine CXCL12 following stimulation with CFA+Ag were investigated. For this purpose, different kits were used and brief descriptions of the methods used for the ELISAs are detailed in the sections below.

2.11.2.1 Cytokine ELISAs

To determine the expression of the cytokines TNF, GM-CSF and IL-17A in the cremaster muscle following inflammation, ELISAs were carried out. Before doing this, animals were subjected to CFA+Ag-induced inflammation of the cremaster muscles. Control mice received an injection of PBS (300 µl). Tissues were prepared (as described above in section 2.11.1). Mouse ELISA Ready-SET-Go® kits (eBioscience, Hatfield, UK) for all 3 cytokines were used according to the manufacturer's protocol. Briefly, flat-bottom 96 well ELISA plates (NUNC MaxiSorp®, eBioscience, Hatfield, UK) were coated with 100 µl/well of capture antibody (pre-titrated, 48 µl diluted in 12 ml 1× coating buffer), sealed and incubated at 4 °C overnight. The next day, wells were aspirated and washed 3 times with 250 µl/well of wash buffer (1× PBS and 0.05% Tween-20). Following this, 200 µl/well of 1× ELISA diluent was used to block the wells at room temperature for 1 h after which wells were aspirated and washed at least once with wash buffer. Standards were then diluted with 1× ELISA diluent according to the manufacturer's instructions to prepare the top concentration of the standard. 100 µl of the top standard concentration was added to the appropriate wells in duplicates and 2-fold serial dilutions were performed to make the standard curve for a total of 8 points. 100 µl/well of homogenised tissue samples was added to the appropriate wells in triplicates before the plate was sealed and incubated at room temperature for 2 h. Wells were aspirated and washed for a total

of 5 washes before 100 µl/well of detection antibody (pre-titrated, 48 µl diluted in 12 ml 1× ELISA diluent) was added to the plate and incubated for 1 h after being sealed. Wells were aspirated and washed again for a total of 5 washes. 100 µl/well of Avidin-HRP (pre-titrated, 48 µl diluted in 12 ml 1× ELISA diluent) was added to the plate before it was sealed and incubated at room temperature for 30 min. Wells were aspirated and washed as before with the addition of soaking wells in wash buffer for 1 to 2 min prior to aspiration between each wash. 100 µl/well of 1× 3,3',5,5'-Tetramethylbenzidine (TMB) solution diluted in 1× ELISA diluent was added to the plate and incubated at room temperature for 15 min after being sealed. Wells were aspirated and washed again for a total of 5 washes. 50 µl/well of stop solution (2mM sulfuric acid [H_2SO_4]) was added to the plate before it was read on a plate reader (Spectra MR, Dynex Technologies Ltd, West Sussex, UK) at a wavelength of 450nm. Sample concentrations were calculated using the standard curve. A BCA protein assay was carried out (as per section 2.11.3) on the same samples in order to normalise the ELISA measurements by total protein concentration (ng/ml).

2.11.2.2 Chemokine ELISA

To assess differences in the levels of the chemokine CXCL12 in the cremaster draining LNs of WT and CCR7KO mice, ELISAs were carried out to quantify CXCL12 levels using supernatents obtained from homogenisation of dLNs from unstimulated mice. Tissues were prepared as described in section 2.11.1. A mouse CXCL12/SDF-1α Quantikine ELISA kit (R&D Systems, Abingdon, UK) was used according to the manufacturer's protocol. Briefly, reagents were reconstituted and standards were diluted with Calibrator Diluent RD6Q according to the manufacturer’s instructions. As the plate comes pre-coated with the CXCL12 capture antibody, 50 µl of Assay Diluent RD1-55 was directly added to each well along with 50 µl of Standard, Control or sample (1:2 dilution) per well. The plate was sealed with the adhesive strip provided and incubated for 2 h at RT on a horizontal plate shaker (LSE™ Vortex Mixer, Corning, UK) at a low speed setting. Wells were aspirated and washed for a total of 5 washes before 100 µl/well of Mouse SDF-1α Conjugate was added to the plate and incubated for 2 h at RT on a shaker after being sealed. Wells were aspirated and washed again for a total of 5 washes. 200 µl/well of Substrate Solution was added to the plate and incubated for 30 mins at RT, protected from light. Following this, 50 µl of Stop Solution was added to each well before the plate was read on a microplate reader at a wavelength of 450nm and the sample

concentrations were calculated from the standard curve. A BCA protein assay was carried out (as per section 2.11.3) on the same samples in order to normalise the ELISA measurements by total protein concentration (ng/ml).

2.11.3 BCA Protein Assay

To determine the total protein concentration of each inflamed cremaster muscle in order to normalise the ELISA measurements by total protein concentration, BCA protein assays were carried out. Before doing this, animals were subjected to inflammation of the cremaster muscle and tissue samples were prepared (as described above in 2.11.1). Following this, a Pierce™ BCA Protein Assay Kit (ThermoFisher Scientific, Paisley, UK) was used according to the manufacturer's protocol. The assay was performed in a 96-well plate. Briefly, diluted protein standards were prepared using 1× PBS and the contents of one bovine serum albumin (BSA) ampule provided in the kit. Next, 25 µl of each standard or unknown sample was incubated with 200 µl of BCA working reagent (50:1, Reagent A:B). The plate was incubated at 37 °C for 30 mins and after leaving to cool to RT, the absorbance was measured at 570 nm on a plate reader (Spectra MR, Dynex Technologies Ltd, West Sussex, UK). The protein concentration in each sample was calculated using the BSA standard curve.

2.12 Investigating the expression of CXCL12 by cremaster draining lymph nodes

To assess differences in the levels of the chemokine CXCL12 in the cremaster draining LNs of WT and CCR7KO mice, ELISAs were carried out (as per section 2.11.2) to quantify CXCL12 levels using supernatents obtained from homogenisation of dLNs from unstimulated mice. Tissues were prepared as described in section 2.11.1. A mouse CXCL12/SDF-1α Quantikine ELISA kit (R&D Systems, Abingdon, UK) was used according to the manufacturer's protocol. Briefly, reagents were reconstituted and standards were diluted with Calibrator Diluent RD6Q according to the manufacturer's instructions. As the plate comes pre-coated with the CXCL12 capture antibody, 50 µl of Assay Diluent RD1-55 was directly added to each well along with 50 µl of Standard, Control or sample (1:2 dilution) per well. The plate was sealed with the adhesive strip

provided and incubated for 2 h at RT on a horizontal plate shaker (LSE™ Vortex Mixer, Corning, UK) at a low speed setting. Wells were aspirated and washed for a total of 5 washes before 100 µl/well of Mouse SDF-1α Conjugate was added to the plate and incubated for 2 h at RT on a shaker after being sealed. Wells were aspirated and washed again for a total of 5 washes. 200 µl/well of Substrate Solution was added to the plate and incubated for 30 mins at RT, protected from light. Following this, 50 µl of Stop Solution was added to each well before the plate was read on a microplate reader at a wavelength of 450nm and the sample concentrations were calculated from the standard curve. A BCA protein assay was carried out (as per section 2.11.3) on the same samples in order to normalise the ELISA measurements by total protein concentration.

2.13 Investigating neutrophil expression of chemokine receptors following TNF stimulation

2.13.1 Isolation and TNF stimulation of leukocytes

To examine the expression of the chemokine receptors: CCR7 and CXCR4 on neutrophils in naïve and inflamed conditions, flow cytometry was used as a tool. Certain experiments investigating intracellular and extracellular expression of CCR7 by neutrophils from digested cremaster muscles and dLNs were previously done by Dr. Christian Zakian and will be specified in the results section where appropriate.

For experiments looking at extracellular expression of CCR7 and CXCR4 on neutrophils, whole blood was recovered from WT and CCR7KO mice by cardiac puncture using a 27 gauge needle and 1 ml syringe filled with 20 µl heparin sodium. 0.5 – 1 ml of blood was obtained per mouse. Circulating cells were lysed with ACK lysis buffer as required (150mM NH_4Cl, 1mM $KHCO_3$, 0.1mM EDTA) before being passed through a 40 µm cell strainer for a single-cell suspension. Blood samples were then centrifuged at 300 g for 5 mins at 4 °C and serum supernatant discarded. All samples were then washed twice with FACS buffer (1× PBS supplemented with 10% FBS) by centrifugation before being resuspended in the same buffer.

Following isolation of leukocytes as above, TNF (1, 10 or 100 ng/ml) or PBS was added to stimulated or unstimulated groups, respectively, and left in an incubator (10% $C0_2$) at

37 °C in RPMI (supplemented with 10% FBS and 2mM of L-Glutamin) for 4 h before being fluorescently labelled for flow cytometry as detailed in section 2.13.3.

2.13.2 Inhibiting caveolae-dependent endocytic pathways

In some experiments investigating CCR7 extracellular expression on neutrophils, the caveolae-dependent inhibitor, nystatin (50 μM), was used. Inhibitors were either added alongside TNF and used throughout the rest of the experiment or added 30 min prior to immunofluorescence staining with conjugated antibodies against CCR7 or the appropriate isotype control antibodies (0.2–2 μg/ml, various fluorochromes) and DAPI (for viability).

2.13.3 Immunofluorescence labelling of leukocytes and flow cytometry

Cells were fluorescently labelled with mAbs against CD45.2, Ly6G, CD3ε, CD11c, CCR7, CXCR4 or the appropriate isotype control Abs (0.2–2 μg/ml, various fluorochromes) and DAPI (for viability) for at least 1 h at 4 °C along with 0.5 μg FcγIII/II receptor blocking antibody (Fc-block™) to prevent unspecific Fc-receptor binding. CCR7-intracellular expression was performed using the Cytofix/Cytoperm kit (BD Biosciences) according to the manufacturer's recommendations.

Antibody-labelled cells were washed twice with FACS buffer by centrifugation at 300 g for 5 mins at 4 °C before being resuspended in 200 μl cold FACS buffer to achieve a single cell suspension. Following this, all samples were kept on ice. DAPI (1 μg/ml), a fluorescent dead cell nuclear marker, was added prior to analysis by flow cytometry. Samples were run on a BD LSR-Fortessa flow cytometer (BD Biosciences) using FACSDIVA software. Multi-colour fluorescence overlap was compensated for by using single-stained cells. At least 20,000 events were acquired per sample.

Leukocytes were identified by FSC and SSC characteristics, CD45.2 positive staining and DAPI negative staining. Neutrophils were identified based on Ly6G high staining. T cells were identified based on CD3ε-high staining (**Figure 2.4**). The chemokine receptor CXCR4 was identified by CXCR4-high staining. CCR7 was labelled with a biotin-conjugated Ab followed by streptavidin A488-conjugated secondary Ab and positive neutrophils were gated after determining the level of background fluorescence in the

CCR7KO or isotype control stained samples using 495/519 nm excitation/emission. Data were analysed with FlowJo analysis software (Treestar).

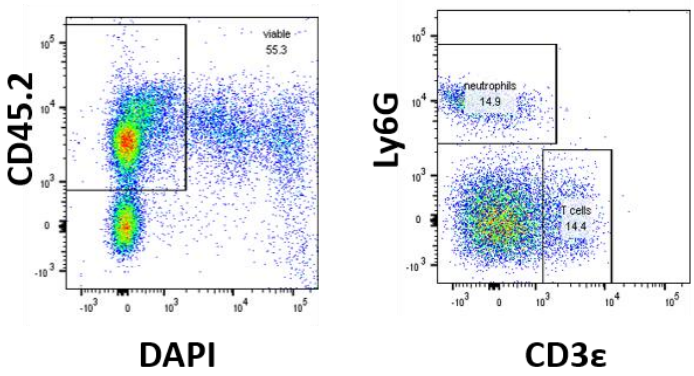

Figure 2.4: Leukocyte subset gating strategies for cells of interest.

2.14 Verification of chimera reconstitution

Alongside each experiment, whole blood was taken from each mouse via cardiac puncture and processed as described in section 2.13.1, to check reconstitution levels of chimerism by flow cytometry analysis.

2.14.1 CCR7KO LysM-eGFP/TNFRdbKO chimera verification

Blood leukocytes from LysM-eGFP/TNRdbKO or chimeric animals were immunostained for neutrophil specific markers, CD45.2 and Ly6G, and TNFRs (p55 and p75). Neutrophil expression of GFP/TNFRs were analysed by flow cytometry to determine levels of chimerism.

2.15 Statistical Analysis

Analysis of data was carried out using GraphPad Prism 6 software (San Diego, CA). Significant differences between groups were assessed by one-way analysis of variance (ANOVA) followed by Newman-Keuls multiple comparison test or unpaired two-tailed Student's T-test. Data is expressed as means ± standard error of mean (SEM). In all cases, a P value ≤ 0.05 was considered significant.

3 : Investigating the dynamics of neutrophil migration during inflammation and the importance of TNF in driving these responses *in vivo*

3.1 Introduction

The lymphatic system is composed of a hierarchical network of two basic vessels: lymphatic capillaries (or initial lymphatics) and collecting vessels, both of which have specific features serving their unique functions. Blind-ended initial lymphatics are comprised of oak-leaf shaped LECs with specialised flaps and buttons that regulate the drainage of interstitial fluid and the formation of lymph (Baluk et al., 2007). Once the lymph is formed, it is transported through a network of collecting lymphatic vessels back into the circulatory system (Bazigou et al., 2014). Although the structure of lymphatic vessels have been well-characterised in other tissues, those in the cremaster muscle have yet to be characterised.

To date, neutrophil migration into the lymphatic system has been poorly studied. This process has been described in several models of infections and immunisation sensitisation (Abadie et al., 2005; Beauvillain et al., 2011; Chtanova et al., 2009; Maletto et al., 2006). However, the majority of these earlier studies did not study the cellular mechanisms regulating neutrophil entry into lymphatic vessels but were mostly looking at the regulation of downstream entry into the lymph nodes.

In this chapter, the dynamics of neutrophil migration into the lymphatic vessels within cremaster muscles following inflammatory insult was investigated to further develop our understanding in order to progress towards the main goal of elucidating the mechanisms of neutrophil migration into lymphatic system. The murine cremaster muscle was chosen because it is a gold standard for both *in vivo*- and *ex vivo*-fluorescence staining for confocal microscopy analysis. The pro-inflammatory cytokine, TNF, and an emulsion of an antigen in CFA (CFA+Ag) were used as inflammatory mediators. TNF was chosen for its potency in mediating inflammation as well as its ability to prime neutrophils and trigger their mobilisation to sites of infection or inflammation (Hallett and Lloyds, 1995). CFA+Ag is able to stimulate responses associated with adaptive immunity and consists

of a mixture of paraffin oil and surfactant with heat-killed *Mycobacterium tuberculosis* in which an aqueous antigen solution, in the case of this study ovalbumin (OVA), is emulsified (Coffman et al., 2010). Recent evidence suggests neutrophils not only play roles in resolving acute inflammation but are also involved in shaping adaptive immune responses through their migration into lymphatic vessels and into lymph nodes (LNs) where adaptive responses take place (Hampton et al., 2015; Teijeira et al., 2013). Using an emulsion of CFA+Ag is a way for us to model antigen sensitisation that is achieved using the classical immunisation protocol to mimic the initiation of an adaptive immune response.

Despite the role of TNF in priming neutrophils for numerous immune functions, such as triggering the production of microbicides and oxidants to fight invading pathogens (Kowanko et al., 1996; She et al., 1989), its role in the process of neutrophil migration into lymphatic vessels *in vivo* remains unknown. This chapter therefore aimed to further explore this avenue.

3.2 Aims

The structure of lymphatic vessels has previously been reported in the mouse trachea and various other organs (Baluk et al., 2007), but not in the cremaster muscle. Thus, it is important to first characterise these in the current model used in this study. Furthermore, despite previous investigations into the effect of TNF and CFA+Ag on the inflammatory response in the lymphatic system, many if not all have focused on neutrophil trafficking into lymph node (LNs) and not on the mechanisms of their entry via lymphatic vessels (Abadie et al., 2005; Beauvillain et al., 2011; Hampton et al., 2015; Maletto et al., 2006). Therefore, further investigations into the migratory responses of leukocytes, specifically neutrophils, into lymphatic vessels are required to understand this phenomenon. This chapter therefore aimed to characterise the structure of lymphatic vessels found in the cremaster muscle and to investigate the effects of the inflammatory mediators, TNF and CFA+Ag, on neutrophil migration into lymphatic vessels *in vivo* using a mouse model of cremaster muscle inflammation. The effects of TNF and CFA+Ag were characterised over time in the cremaster muscle to explore the dynamics of neutrophil migration into the lymphatic system as observed by immunostaining and confocal microscopy. Furthermore, neutrophil-lymphatic vessel interactions following TNF-stimulation and

antigen sensitisation through the use of an emulsion of CFA+Ag were observed in real-time via intravital confocal microscopy (IVM), allowing the direct visualisation of cell-cell interactions in high-resolution. IVM is a powerful technique for real-time *in vivo* investigation of leukocyte/vessel wall interactions in inflammatory reactions and our group has developed immunofluorescence *in vivo* labelling to be able to visualise different components of the vessel wall for confocal IVM.

Subsequently, the effect of endogenous TNF release during antigen sensitisation (CFA+Ag) was investigated *ex vivo* by carrying out ELISAs on tissue homogenates, and *in vivo* through the use of transgenic mice, immunostaining and confocal microscopy.

The specific aims were to:

- Investigate the structure of lymphatic vessels in the cremaster muscles of mice.
- Investigate the effects of the pro-inflammatory cytokine TNF and antigen sensitisation with the use of an emulsion of an antigen in CFA (CFA+Ag) on neutrophil migration into lymphatic vessels through the use of *ex vivo* immunofluorescence staining and confocal microscopy analysis.
- Use neutrophil reporter LysM-eGFP mice to track GFP^{high} neutrophils at the site of inflammation using IVM to observe TNF- or CFA+Ag-induced migration into lymphatic vessels *in vivo*.
- Investigate TNF release in the cremaster muscle following antigen sensitisation by carrying out ELISAs.
- Investigate the role of TNF in neutrophil migration into lymphatic vessels by using TNFRdbKO mice as a means of abolishing TNF signalling.

3.3 *Results*

3.3.1 Structure of lymphatic vasculature in the murine cremaster muscle

To determine the structure of lymphatic vessels in the cremaster muscle of mice, whole-mount cremaster tissues of naïve WT C57BL/6 mice were immunostained for LYVE-1 and PECAM-1/VE-Cadherin. This showed the presence of a unidirectional network of lymphatic vessels (LYVE-1, red channel) with characteristic blind-ended lymphatic capillaries (orange arrows) (**Figure 3.1A**). LYVE-1 was also found to be expressed all over these lymphatic vessels (**Figure 3.1A**). Further analysis of the expression of the adhesion molecules, PECAM-1 and VE-Cadherin, on initial lymphatic vessels showed the presence of VE-Cadherin-rich buttons (red channel) and PECAM-1-rich flaps (blue channel). Lymphatic endothelial cells (LECs) also exhibited an oak-leaf shaped morphology (**Figure 3.1B**).

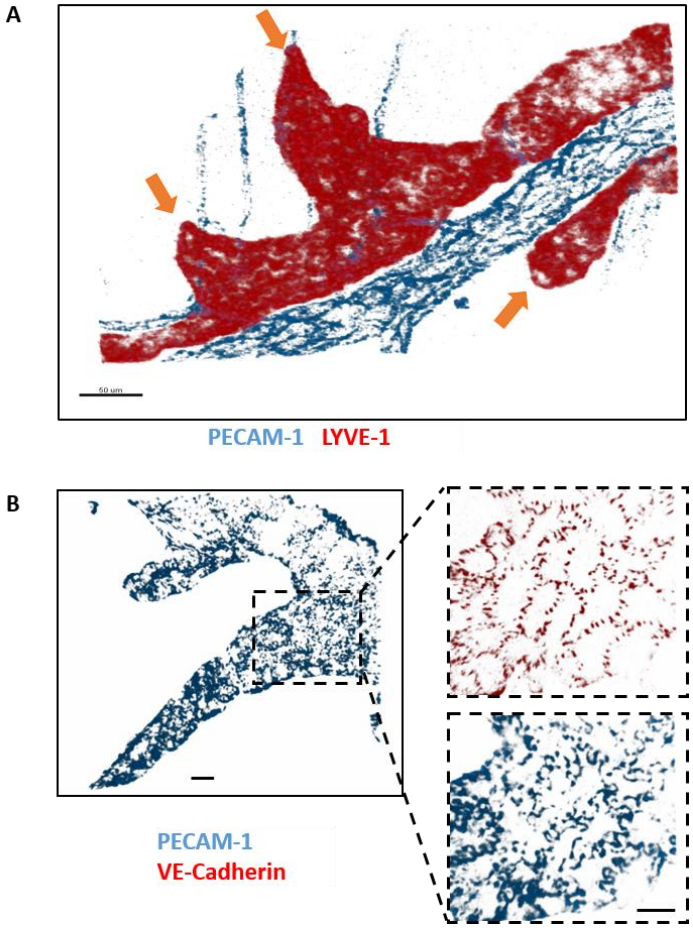

Figure 3.1: Lymphatic architecture of the murine cremaster muscle.

(A) Representative 3D confocal image of a whole-mount fixed cremaster muscle of a WT mouse, immunostained with an antibody against LYVE-1 (red, Alexa555-conjugated) and PECAM-1 (blue, Alexa647-conjugated) to visualise lymphatic and blood vasculatures, respectively. Orange arrows indicate the blind-ended capillaries of the initial lymphatic vessels. Bar: 50 μm. (B) Representative confocal image (kindly provided by Dr Mathieu-Benoit Voisin) of a fixed cremasteric lymphatic vessel immunostained for VE-Cadherin (Alexa555-conjugated, red) and PECAM-1 (Alexa647-conjugated, blue). The inserts on the right area show a magnified view of the heterogeneous distribution of the adhesion molecules (with VE-cadherin-rich buttons and PECAM-1-rich flaps) expressed by the endothelial cells of the cremasteric lymphatic vessels and exhibiting an oak-leaf shape morphology. Bar: 20 μm.

3.3.2 Time-course of TNF- or CFA+Ag-induced neutrophil migration across postcapillary venules and their migration into the lymphatic vessels and dLNs in the murine cremaster muscle

In order to characterise the effects of TNF and CFA+Ag in the cremaster muscle on neutrophil trafficking from blood vessels into the lymphatic system, time-courses of the responses elicited by these inflammatory mediators were investigated. The dose employed for both TNF and CFA+Ag were those known to elicit significant leukocyte transmigration in this model based on previous findings from our group (Woodfin et al., 2009). For this purpose, WT mice were given intrascrotal (i.s.) injections of either 300ng TNF (in 400 μl PBS) or CFA+Ag (200 μg of each in 300 μl total volume) and their cremaster muscles and draining lymph nodes (dLNs) were dissected away at different time-points, fixed and used whole-mounted for immunofluorescence staining and confocal analysis. The cremaster muscles were immunostained with anti-PECAM-1, anti-LYVE-1 and anti-MRP14 mAbs to label the blood vasculatures, lymphatic vasculatures and neutrophils, respectively. The dLNs were immunostained with anti-HEV, anti-LYVE-1 and anti-MRP14 mAbs to label blood vasculatures, lymphatic vasculatures and neutrophils, respectively. The timecourse for CFA+Ag-induced inflammation was carried out in collaboration with a previous member of the group, Dr Christian Zakian, and neutrophil migration responses into the draining LNs were analysed via flow cytometry. Draining LNs (dLNs) of the cremaster muscle were previously determined by Dr Mathieu-Benoit Voisin with the use of i.s. injections of Evans blue.

Following TNF stimulation, 3D-reconstructed confocal images showed that a significantly higher number of neutrophils were present within the interstitial tissue

surrounding postcapillary venules (PCVs) at the 16 h time-point (**Figure 3.2A, right**) as compared to the unstimulated controls (**Figure 3.2A, left**). Quantification of these images using IMARIS software showed that neutrophil migration across PCVs into the inflamed interstitial tissue upon local injection of exogenous TNF occurred in a time-dependent manner (**Error! Reference source not found.C**). After 2 h TNF stimulation, neutrophil ransmigration could be detected and this was further increased at the 4–8 h timepoint before peaking at the 16 h time point and returning to basal levels after 48 h. This extravasation response observed in PCVs was associated with neutrophil migration into lymphatic vessels. 3D-reconstructed confocal images showed that a higher number of neutrophils were seen within lymphatic vessels at the 8h time point (**Figure 3.2B, right**) as compared to the unstimulated controls (**Figure 3.2B, left**). Quantification of these images using IMARIS software revealed a rapid but transient migration of neutrophils into lymphatic vessels at 8 h post-i.s. injection before returning to basal levels at the 48 h time point (**Figure 3.2D**).

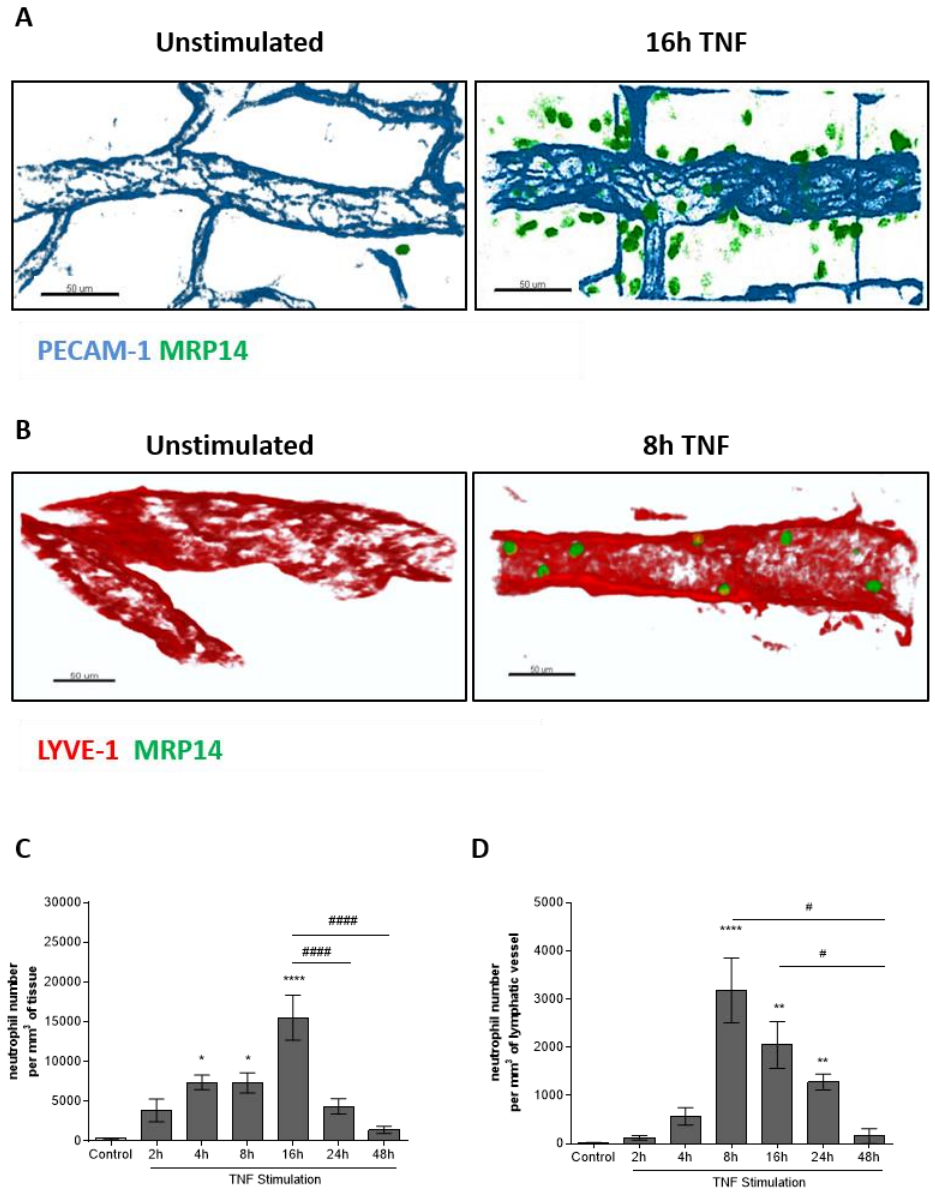

Figure 3.2: Neutrophil transmigration across postcapillary venules and into lymphatic vessels following TNF-induced inflammation in the cremaster muscle. TNF was injected i.s. into WT C57BL/6 mice and cremaster muscles were dissected at different time-points after stimulation, fixed, immunostained for PECAM-1 (blue), LYVE-1 (red) and MRP14 (green) and analysed by confocal microscopy and IMARIS software. (A) Representative 3D reconstructed confocal images from unstimulated (left) and TNF- stimulated (right) postcapillary venules illustrating neutrophil transmigration responses obtained at the 16 h time point. Bar: 50 µm. (B) Representative 3D reconstructed confocal transverse-section images of a unstimulated (left) and TNF- stimulated (right) lymphatic vessels at 8 h showing selected neutrophils within the lumen of the vessel. Bar: 50 µm. (C) Time course of transmigrated neutrophils per mm^3 of tissue. (D) Time course of neutrophil migration into lymphatic vessels per mm^3 of vessel. Data are expressed as mean ± SEM from at least 8-10 vessels/animals, with 5-12 animals per group (at least 5 independent experiments). Statistically significant differences between stimulated and unstimulated treatment groups are indicated by asterisks: *, $P < 0.05$; **, $P < 0.01$; ***, $P < 0.001$; ****, $P < 0.0001$. Significant differences between responses at different time points are indicated by hash symbols: #, $P < 0.05$; ####, $P < 0.0001$. Statistical significance was determined using one-way ANOVA.

3D-reconstructed confocal images also showed that considerably more neutrophils can be seen within the dLNs (inguinal) at 24 h post-i.s. injection (**Figure 3.3A, right**) as compared to unstimulated controls (**Figure 3.3A, left**). Quantification of these images indicated the same time-dependent neutrophil response was occuring in cremaster muscle dLNs (inguinal) (**Figure 3.3B**), with neutrophil infiltration peaking at a delayed time-point of 24 h before returning to basal levels after 48 h.

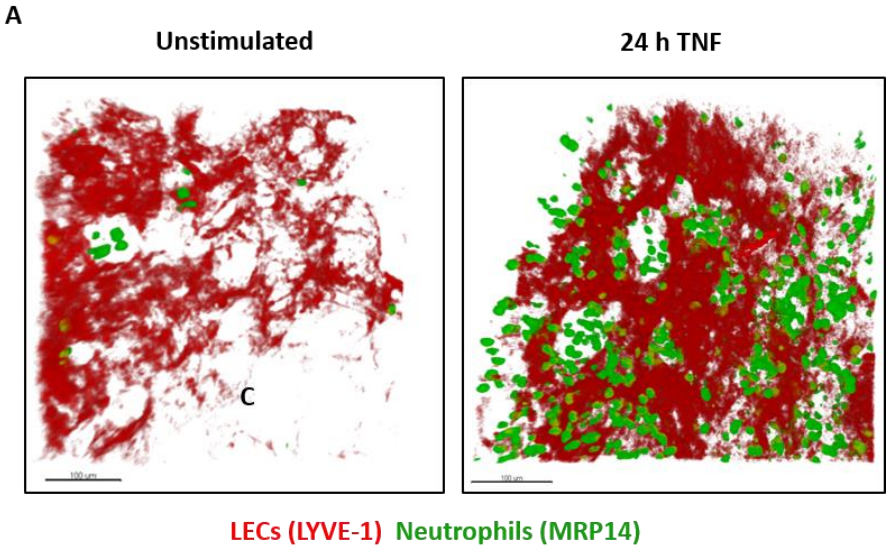

Figure 3.3: Neutrophil migration into dLNs following TNF-induced inflammation of the cremaster muscle. PBS (unstimulated control) or TNF was injected i.s. into WT C57BL/6 mice and inguinal dLNs were dissected away 24 h after stimulation, fixed, immunostained for LYVE-1 (red), MRP14 (green) and analysed by confocal microscopy. Representative images from unstimulated (left) and TNF-stimulated (right) dLNs illustrating neutrophil infiltration responses obtained at the 24 h time point. Bars: 100 µm. (B) Time course of the total neutrophil infiltration per mm^3 of dLNs. Data are expressed as mean ± SEM from at least 8-10 vessels/animals, with 5-12 animals per group (at least 5 independent experiments). Statistically significant differences between stimulated and unstimulated treatment groups are indicated by asterisks: *, $P < 0.05$; **, $P < 0.01$; ***, $P < 0.001$; ****, $P < 0.0001$. Significant differences between responses at different time points are indicated by hash symbols: #, $P < 0.05$; ####, $P < 0.0001$. Statistical significance was determined using one-way ANOVA.

Next, the inflammatory responses elicited by i.s. injection of an emulsion of CFA+Ag was looked at. 3D-reconstructed confocal images showed that at 8 h post-i.s. injection, neutrophils could still be seen in the process of migrating into lymphatic vessels (**Figure 3.4, top and middle**) but most were within lymphatic vessels by 8 h post-i.s. injection (**Figure 3.4, bottom**). Quantification of these images also showed that CFA+Ag-induced transmigration through PCVs and into lymphatic vasculatures exhibited a time-dependent increase in the number of neutrophils, with detection of neutrophils within the inflamed tissues at 2 h post-i.s. injection and migration across PCVs peaking at 16 h post-i.s. injection (**Figure 3.5A**). Neutrophil migration into lymphatic vessels peaked at 8 h (**Figure 3.5B**) post-i.s. injection.

The responses seen in the cremaster muscle were associated with an increase in neutrophil infiltration of the tissue dLNs (inguinal) but not in non-dLNs (axillary) as quantified by flow cytometry (**Figure 3.5C**). This response peaked at 8 h post-i.s. injection before gradually returning to basal levels after 24 h. Confocal microscopy analysis also confirmed this response and a significantly higher number of neutrophils was observed within the dLNs at 8 h post-i.s. injection (**Figure 3.6, right**) as compared to the unstimulated controls (**Figure 3.6, left**).

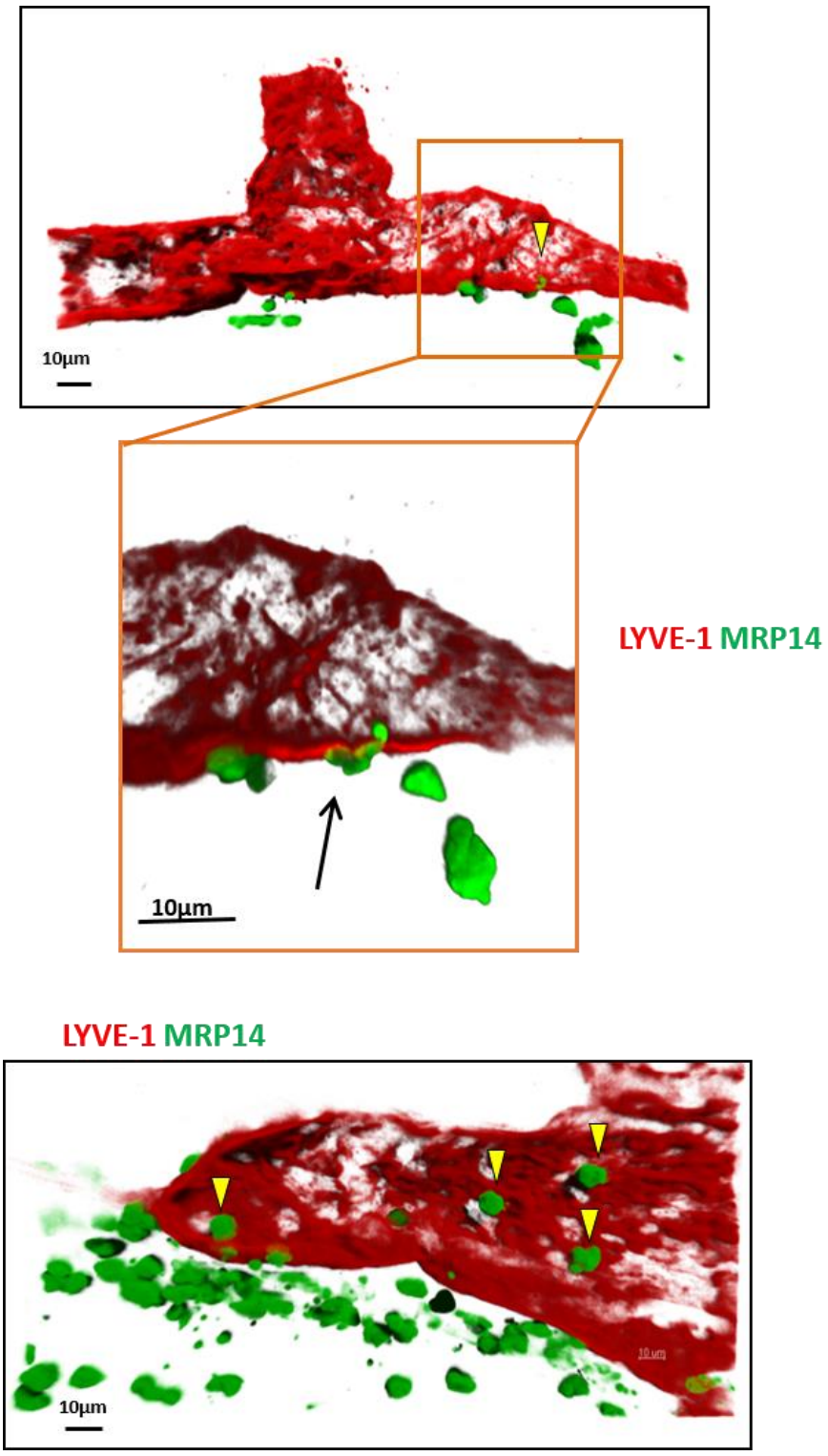

Figure 3.4: CFA+Ag-induced migration of neutrophils into lymphatic vessels. These are 3D-reconstructed confocal images showing neutrophils labelled with an anti-MRP-14 mAb within the lumen of a lymphatic vessel labelled with an anti-LYVE-1 mAb (as indicated by yellow arrows in top and bottom images). The top image depicts a lymphatic vessel surrounded by neutrophils. The middle image (insert from top image in orange box) shows a neutrophil mid-migration at 8 h post-i.s. injection with CFA+Ag. The bottom image is a transverse section of another lymphatic vessel showing neutrophils within the lumen (yellow arrows) at 8 h post-i.s. injection with CFA+Ag. Bars: 10 µm. Images kindly provided by Dr Mathieu-Benoit Voisin.

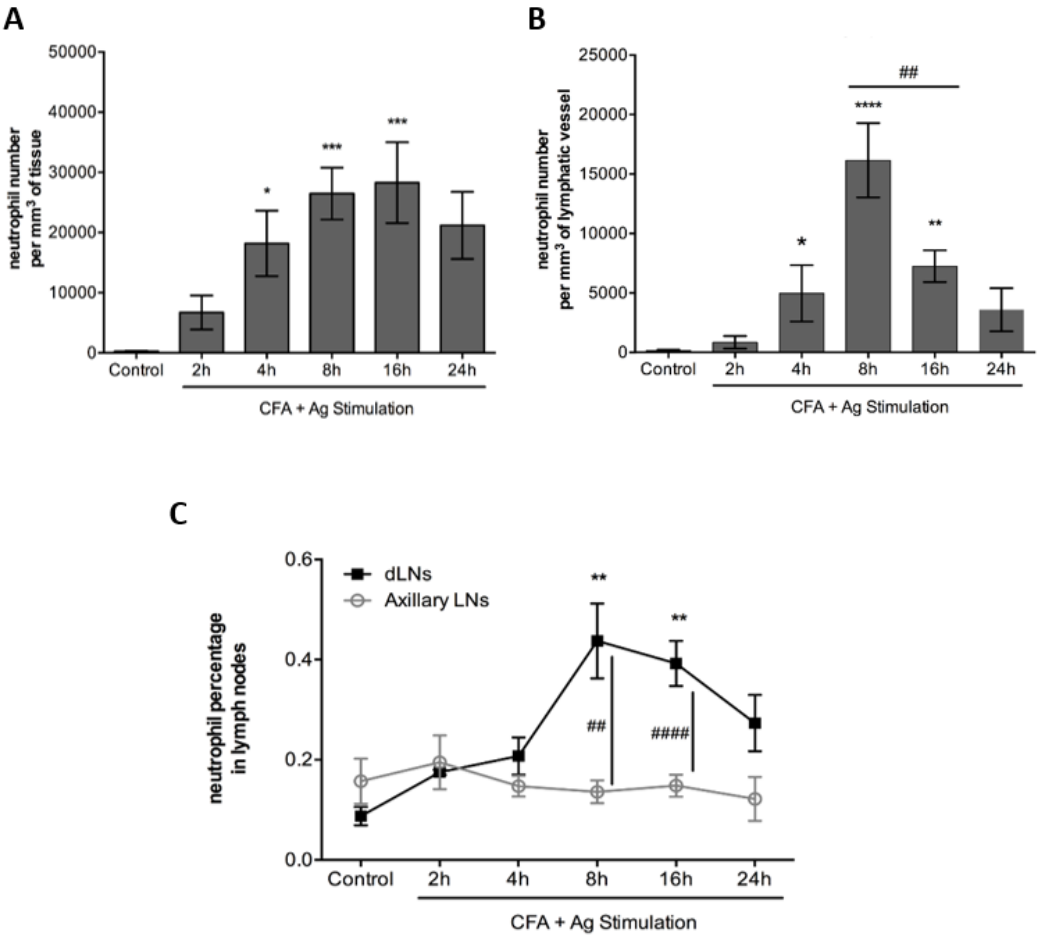

Figure 3.5: Time course of neutrophil migration into the lymphatic system following CFA+Ag-induced inflammation in the murine cremaster muscle. WT C57BL/6 mice received i.s. injections of CFA+Ag (200 µg of each in 300 µl total volume) and were left for several in vivo test periods. Control mice received i.s. of PBS (300 µl). Neutrophil migration into the lymphatic system of WT C57BL/6 mice cremaster muscles was visualised by confocal microscope following dissection, fixation and permeabilisation of the tissues at the end of each time point. (A) Time course of transmigrated neutrophils per mm^3 of tissue. (B) Time course of neutrophil migration into lymphatic vessels per mm^3 of vessel. (C) Time course of neutrophil migration into draining LNs (inguinal) or non-draining LNs (axillary) of mice injected intradermally with CFA+Ag and as analysed by flow cytometry. Data was obtained with Dr Mathieu-Benoit Voisin and Dr Christian Zakian. Data are expressed as mean ± SEM from at least 8-10 vessels/animal (for confococal microscopy), with 5-12 animals per group (at least 5 independent experiments). Statistically significant differences between stimulated and unstimulated treatment groups are indicated by asterisks: *, $P < 0.05$; **, $P < 0.01$; ***, $P < 0.001$; ****, $P < 0.0001$. Significant differences between responses at different time-points are indicated by hash symbols: ##, $P < 0.01$; ####, $P < 0.0001$. Statistical significance was determined using one-way ANOVA

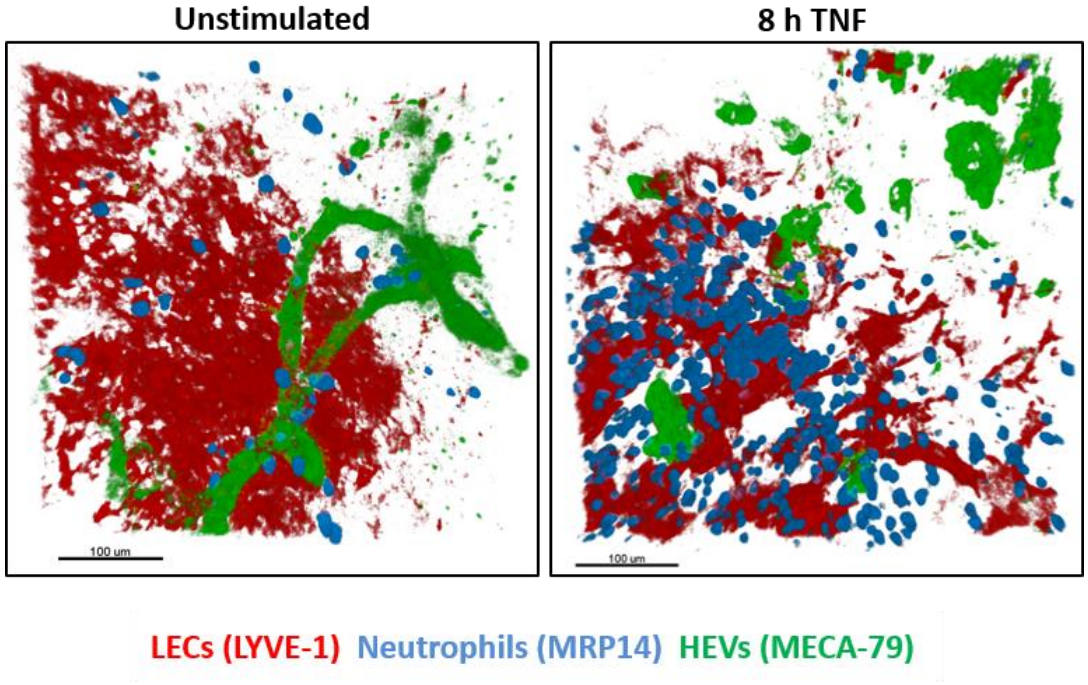

Figure 3.6: Neutrophil migration into dLNs following CFA+Ag-induced inflammation of the cremaster muscle. PBS (unstimulated control) or CFA+Ag was injected i.s. into WT C57BL/6 mice and inguinal dLNs were dissected away at 8 h post-i.s. injection, fixed, immunostained for HEVs (green), LYVE-1 (red), MRP14 (blue) and analysed by confocal microscopy. Representative images from unstimulated (left) and CFA+Ag-stimulated (right) dLNs illustrating neutrophil infiltration responses obtained at the 8 h time point. Bars: 100 µm.

Due to the low incidence of neutrophils present in the dLNs (less than 1% of total LN-infiltrated leukocytes as observed by flow cytometry) and to exclude the increase of circulating neutrophils due to CFA+Ag-induced neutrophilia (as observed by previous group members) from the current data analyses, a detailed investigation of whole-mount dLNs immunostained for HEVs (blood vasculatures), LYVE-1 (lymphatic vasculatures) and MRP14 (neutrophils) was carried out by confocal microscopy (**Figure 3.7A-D**). This showed that out of the total number of neutrophils (655 ± 180) in the dLNs of unstimulated mice (**Figure 3.7A**), 125 ± 32, 231 ± 57, 746 ± 228 neutrophils were within the HEVs, lymphatics and stroma, respectively (**Figure 3.7B-D**). At 8 h post-i.s. injection, the highest number of neutrophils (5684 ± 1236) were found within the lymphatic vessels, representing the majority of neutrophils of the total number found within dLNs at this time-point (9984 ± 2050). At 16 h post-i.s. injection, out of 4085 ± 920 neutrophils, only 1173 ± 222 neutrophils were within lymphatic vessels, whilst 2002 ± 460 neutrophils were found in the LN stroma. This indicated that at 8 h post-i.s. injection, neutrophils were mainly within lymphatic vessels but by the 16 h timepoint,

they had moved on into the stroma. Overall, only a minority of the neutrophils were found within the HEVs at these time-points.

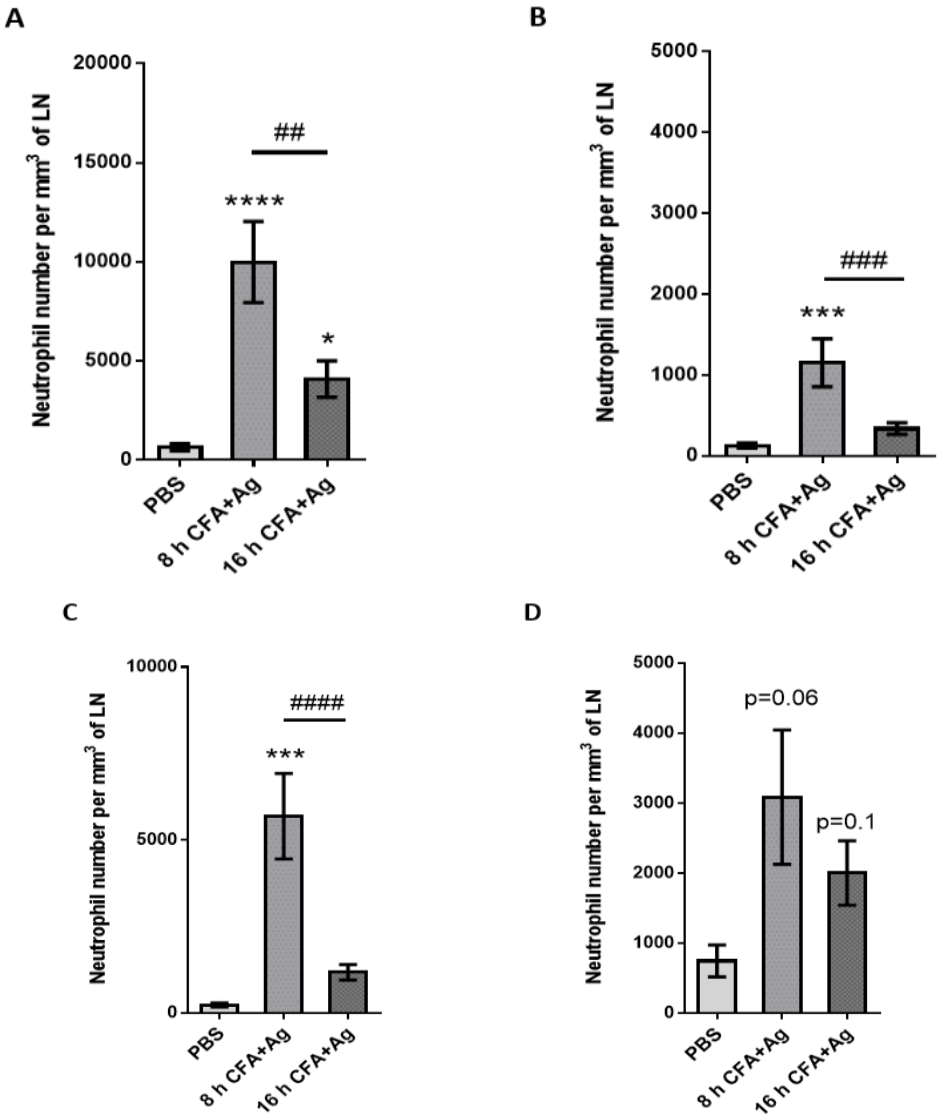

Figure 3.7: Number of neutrophils within the stroma, HEVs and lymphatics of the cremaster dLNs. Neutrophil migration into the lymphatic system was induced in WT animals following antigen sensitisation with complete Freund's adjuvant (CFA+Ag). (A) Quantification of total neutrophil numbers in the dLNs of mice stimulated with CFA+Ag (8 or 16 h) or with PBS (control). (B) Quantification of neutrophil localisation within HEVs in the dLNs of mice stimulated with CFA+Ag (8 or 16 h) or with PBS (control). (C) Quantification of neutrophil localisation within lymphatic vessels in the dLNs of mice stimulated with CFA+Ag (8 or 16 h) or with PBS (control). (D) Quantification of neutrophil localisation within the stroma in the dLNs of mice stimulated with CFA+Ag (8 or 16 h) or with PBS (control). Data are represented as absolute numbers of neutrophils present in the HEV, LYVE-1+ vessels and in the stroma of the LNs as analysed by confocal microscopy. Data are expressed as mean±SEM of N = 5-12 animals (~10 images per pair of dLNs for confocal microscopy) per group from at least 5-10 independent experiments. Statistically significant differences between unstimulated and stimulated mice are indicated by asterisks: ***, $P < 0.001$; ****, $P < 0.0001$. Significant differences between responses in CFA+Ag stimulated groups are indicated by hash signs: ##, $P < 0.01$; ###, $P < 0.001$; ####, $P < 0.0001$. Statistical significance was determined using one-way ANOVA

3.3.3 Confocal intravital microscopy to observe TNF- or CFA+Ag-induced migration of neutrophils into lymphatic vasculatures in real-time *in vivo*

As a next step, the dynamics of neutrophil-lymphatic vessel interactions *in vivo* was analysed in real-time in the cremaster muscle of neutrophil reporter LysM-eGFP mice upon TNF or CFA+Ag-stimulation. For this purpose, LysM-eGFP mice were given i.s. injections of either 300ng TNF (in 400 µl PBS) or CFA+Ag (200 µg of each in 300 µl total volume) for 4 h and 6 h, respectively. Following this, *in vivo* fluorescent-immunostaining with a non-inhibitory dose of anti-LYVE-1 mAbs was applied to the tissues to visualise lymphatic vessels to allow the tracking of GFP^{high} neutrophil migration responses into and within the lymphatic vasculature by confocal IVM. LysM-eGFP mice are currently the most widely used mouse line for intravital neutrophil imaging, in which neutrophils are very bright (GFP^{high}) and reasonably well differentiated from other less bright (GFP^{low}) myeloid cells (Bruns et al., 2010; Faust et al., 2000; Proebstl et al., 2012; Woodfin et al., 2011). Mice were anaesthetised and cremaster muscles were exteriorised and pinned out flat over the optical window of a heated microscope stage. Z-stack images of a lymphatic vessel were captured every 1 min for 90 mins in order to capture neutrophils migrating across the lymphatic endothelium between the time frames of 4–5.5 h (for TNF stimulation) or 6–7.5 h (for CFA+Ag-stimulation). These time frames were chosen in order to allow enough time for neutrophils to transmigrate into the interstitial tissue and allow migrating neutrophils to be tracked and captured before the peak of neutrophil migration into lymphatic vessels, which occurs at 8 h for both inflammatory mediators. Tyrode's salt solution was used to constantly superfuse cremaster muscles during all experiments.

Following stimulation with TNF, neutrophils were observed to migrate rapidly through LECs into the lumen of lymphatic vessels (**Figure 3.9A & Video 1**). The actual transmigration process of neutrophils from the abluminal side of the LECs into the lumen of lymphatic vessels took on average 4.5 ± 0.58 min (**Figure 3.9B**).

Surprisingly, neutrophil migration into lymphatic vessels following CFA+Ag-induced inflammation at the time-points chosen was not able to be observed as the majority of neutrophils were already within the lumen of the lymphatic vessel during the timeframe that was investigated (6–7.5 h).

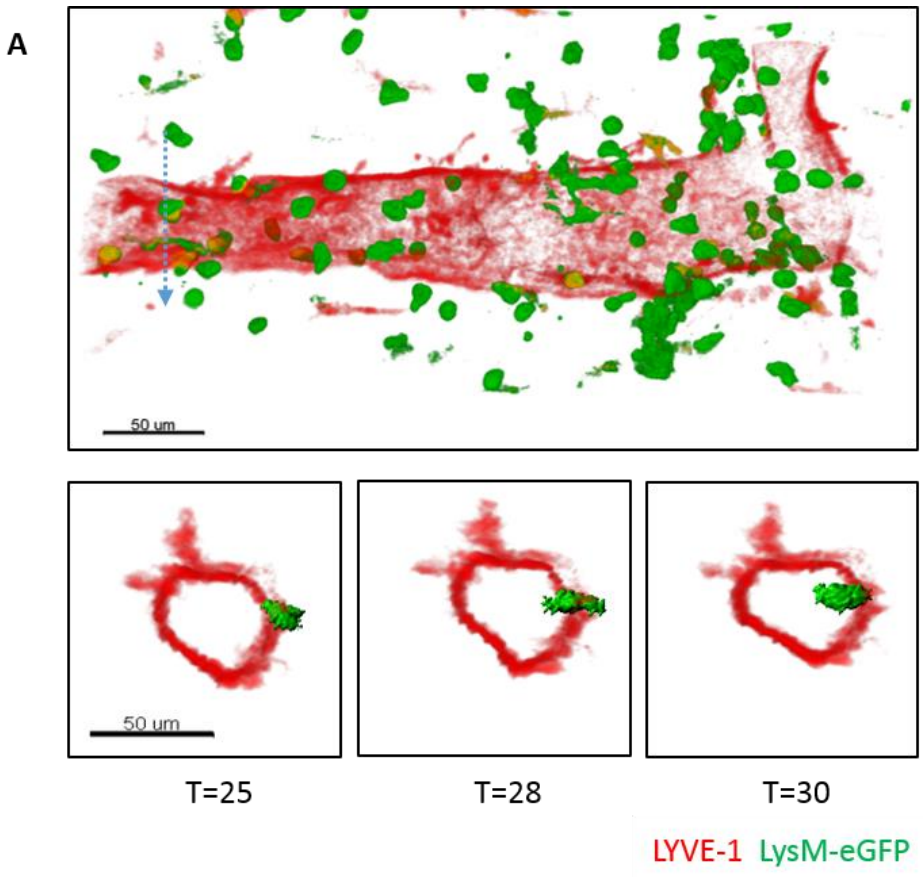

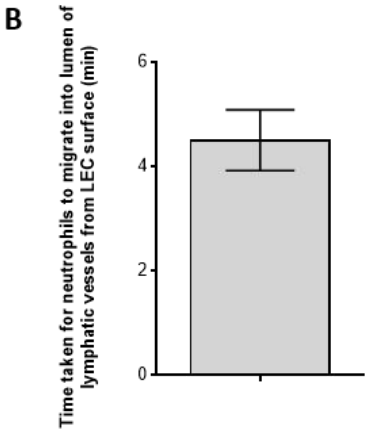

Figure 3.8: Neutrophil breaching lymphatic endothelium during IVM of a TNF-stimulated cremaster muscle. Mice were subjected to TNF-induced inflammation of the cremaster muscle and the dynamics of neutrophil migration into the tissue and lymphatic vessels was analysed by intravital confocal microscopy. (A) Representative 3D-reconstructed still image of a live recording of a cremaster region including a lymphatic vessel of a LysM-eGFP mouse and immunostained *in vivo* with anti-LYVE-1 mAb (red, conjugated to Alexa555). The bottom panel images illustrate a time-lapse series of 2µm-thick cross-sections along the z-plane (dotted blue arrow) and shows the migration of a neutrophil into the lymphatic vessel. Bars: 50 µm. (B) Time taken for neutrophils to migrate into the lumen of lymphatic vessels from the LEC surface. Results are from analysis of 10 cells from n=8 mice, each mouse representing one independent experiment. T, time.

3.3.4 The effect of TNF signalling on neutrophil migration into lymphatic vessels following CFA+Ag-induced inflammation

To investigate the effect of endogenous TNF release during CFA+Ag-induced inflammation, ELISAs were carried out to determine the amount of TNF released following antigen sensitisation in WT mice. For this purpose, WT mice were given i.s. injections of CFA+Ag as before and their cremaster muscles were dissected away following different *in vivo* test periods, snap-frozen and homogenised for analysis by ELISA. Interestingly, stimulation of WT cremaster muscles with CFA+Ag induced a modest but rapid release of TNF in the tissue between 4-8 h with the maximal release (17.5 ± 4.4 pg/ml) occurring at 16 h post-i.s. injection (**Figure 3.9**).

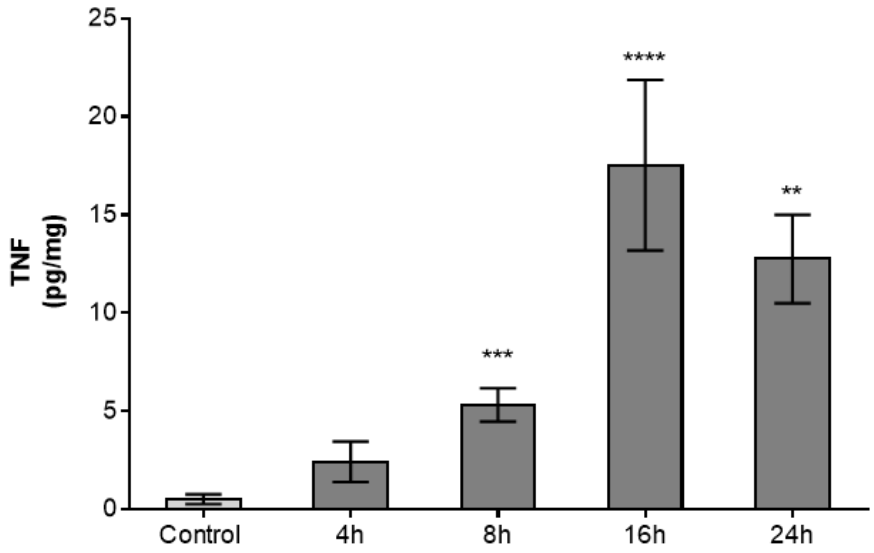

Figure 3.9: TNF release in murine cremaster muscles following antigen sensitisation (CFA+Ag) *in vivo*. Time course of TNF release in the cremaster muscles of WT C57BL/6 mice following intra-scrotal injection of CFA+Ag and as quantified by ELISA. Mice were stimulated intrascrotally with CFA+Ag for different in vivo test periods before being sacrificed by cervical dislocation and their cremaster muscles isolated, snap-frozen and homogenised for use in ELISAs. Data are expressed as mean±SEM of N = 6-21 animals per group from 7 independent experiments. Statistically significant differences between unstimulated and stimulated mice are indicated by asterisks: **, $P < 0.01$; ***, $P < 0.001$; ****, $P < 0.0001$. Statistical significance was determined using one-way ANOVA.

Next, the significance of TNF signalling during the migration of neutrophils into lymphatic vessels was investigated. In order to block TNF signalling, global knockout mice lacking both TNF receptors (p55 and p75) were used. Neutrophil migration responses at 16 h post-i.s. injection (this being the peak of TNF release) in these TNF receptor double knockout (TNFRdbkO) mice and WT mice were studied and compared by confocal microscopy following antigen sensitisation. For this purpose, WT and TNFRdbkO mice were given i.s. injections of CFA+Ag as before. Control mice were given i.s. injections of PBS (300 µl). Cremaster muscles were then dissected away 16 h post-i.s. injection, fixed and immunostained with anti-PECAM-1, anti-LYVE-1 and anti-MRP14 mAbs to label the blood vasculatures, lymphatic vasculatures and neutrophils, respectively. Cremaster dLNs were also harvested for flow cytometry analysis. Cells from digested LNs were immunostained with anti-CD45.2 and anti-Ly6G Abs in order to gate for leukocytes and neutrophils.

Quantification of confocal microscopy images demonstrated that neutrophil transmigration across PCVs of WT and TNFRdbKO mice were similar at 16 h post-i.s. injection (**Figure 3.10A**). Interestingly, neutrophil migration into lymphatic vessels showed approximately 75% reduction in KO animals as compared to WT animals (**Figure 3.10B**). This response was also associated with a reduction of approximately 64% in the number of neutrophils that had infiltrated the dLNs of KO animals in comparison to WT animals (**Figure 3.10C).** This is presumably because neutrophils are unable to migrate downstream into dLNs due to their entry into initial lymphatic vessels being blocked.

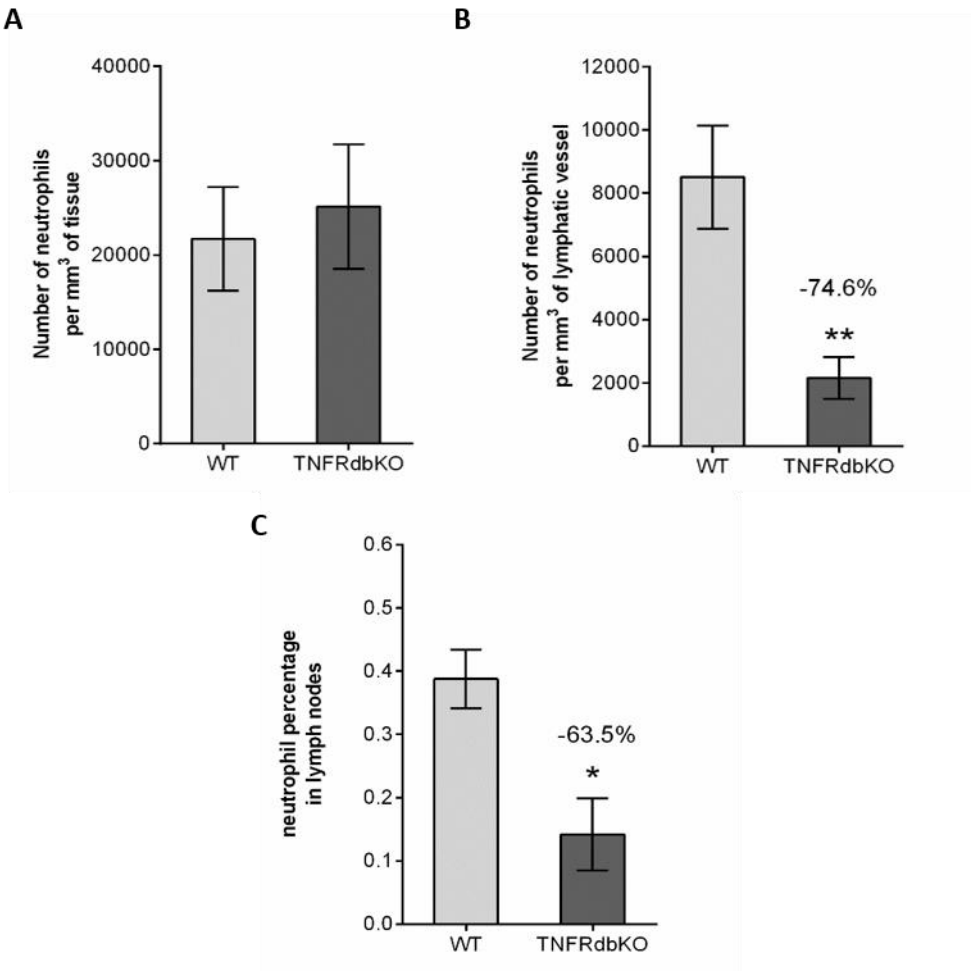

Figure 3.10: Neutrophil migration responses of WT and TNFRdbKO mice following CFA+Ag-induced inflammation in the cremaster muscle. Neutrophil migration into the lymphatic system of the cremaster muscle following antigen sensitisation with complete Freund's adjuvant (CFA+Ag) was induced in WT and TNFRdbKO mice. (A) Number of extravasated neutrophils in cremaster muscles of WT and TNFRdbKO mice at 16 h post-CFA+Ag-stimulation as quantified by confocal microscopy. (B) Number of neutrophils within cremaster lymphatic vessels of WT and TNFRdbKO mice at 16 h post-CFA+Ag-stimulation as quantified by confocal microscopy. (C) Percentage of neutrophils in dLNs of WT and TNFRdbKO mice at 16 h post-CFA+Ag-stimulation as quantified by flow cytometry. Data are expressed as mean±SEM of N = 5-12 animals (~10 images per cremasters for confocal microscopy) per group from at least 5-10 experiments. Statistically significant differences between WT and TNFRdbKO mice are indicated by asterisks: *, $P < 0.05$; **, $P < 0.01$. Statistical significance was determined using one-way ANOVA.

TNFRdbKO chimeric mice

In order to address whether neutrophils respond directly or indirectly to endogenous TNF released during inflammation, chimeric animals exhibiting either WT or TNFR-deficient neutrophils were generated. For this purpose, lethally irradiated WT mice were reconstituted with bone marrow hematopoietic cells from either WT or TNFRdbKO animals before being subjected to antigen sensitisation.

Chimerism of reconstituted mice were also verified at the end of the inflammatory period for each experiment. Briefly, whole blood was taken from TNFRdbKO or chimeric animals via cardiac puncture before being lysed in preparation for immunostaining. Blood leukocytes were then immunostained for neutrophil specific markers (CD45+ Ly6G+) and their surface expression of TNFR p55 and p75 before being analysed by flow cytometry.

Phenotypic analysis by flow cytometry confirmed that all chimeras were fully reconstituted with the intended bone marrow hematopoietic cells (**Figure 3.11A**). Leukocytes from WT mice reconstituted with cells from TNFRdbKO mice showed no changes in fluorescence intensity for the TNFRs, p55 and p75, as compared to leukocytes from TNFRdbKO controls (**Figure 3.11A, left panel**), thus indicating that TNFRdbKO chimeras had neutrophils deficient in both TNFRs. In contrast, leukocytes from WT mice reconstituted with cells from other WT mice showed an increase in fluorescence intensity for the TNFRs, p55 and p75, as compared to TNFRdbKO controls (**Figure 3.11A, right panel**), thus indicating that these WT chimeras possessed neutrophils with expression of both TNFRs. The percentage of circulating neutrophils was also looked at and this proved to be about the same (~25%) for both chimeras at the peak of inflammation (16 h) (**Figure 3.11B**).

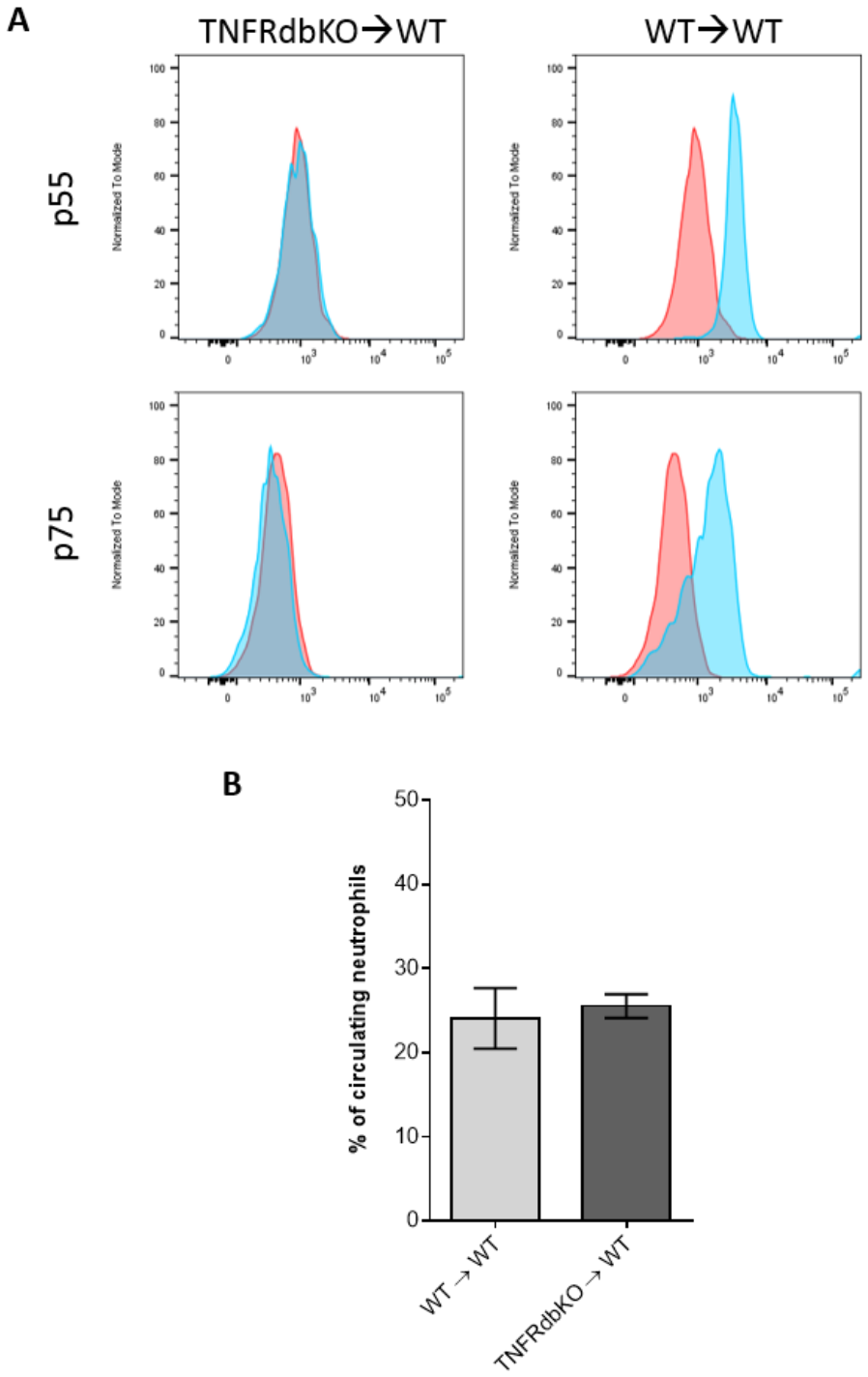

Figure 3.11: Phenotypic analysis of blood neutrophils from TNFRs chimeric mice. Blood leukocytes from TNFRdbKO or chimeric animals were immunostained for neutrophil specific markers (CD45+ Ly6G+) and their surface expression of TNFRs p55 and p75 were analysed by flow cytometry. (A) Representative histograms of the fluorescence intensity for p55 (top panel) and p75 (bottom panel) of blood neutrophils from lethally irradiated WT mice and reconstituted with TNFRdbKO (TNFRdbKO→WT) or WT (WT→WT) bone marrow hematopoietic cells (blue) and compared to the intensity of staining from neutrophils of TNFRdbKO animals (as control, red). (B) Percentage of circulating neutrophils in WT→WT and TNFRdbKO→WT chimeric mice. Data are expressed as mean±SEM of N = 6-8 animals per group from at least 4 independent experiments. Statistical significance was determined using Student's T-test.

Following this, neutrophil migration responses in these mice were investigated. Similarly to full TNFRdbKO mice, the neutrophil migration response into the lymphatic system was impaired in chimeric animals exhibiting WT vasculature and tissue-resident cells along with neutrophils deficient in TNFRs, with a decrease of 77.6% and ~85% in the number of neutrophils present within lymphatic vessels and dLNs, respectively, as compared to the control group (**Figure 3.12A and B**). Neutrophil transmigration across PCVs was significantly higher in TNFRdbKO chimeric mice as compared to WT chimeric mice (**Figure 3.12C**).

Overall, these results demonstrate for the first time the direct involvement of TNF in triggering the migration of neutrophils into tissue-associated lymphatic vessels upon antigen challenge *in vivo*.

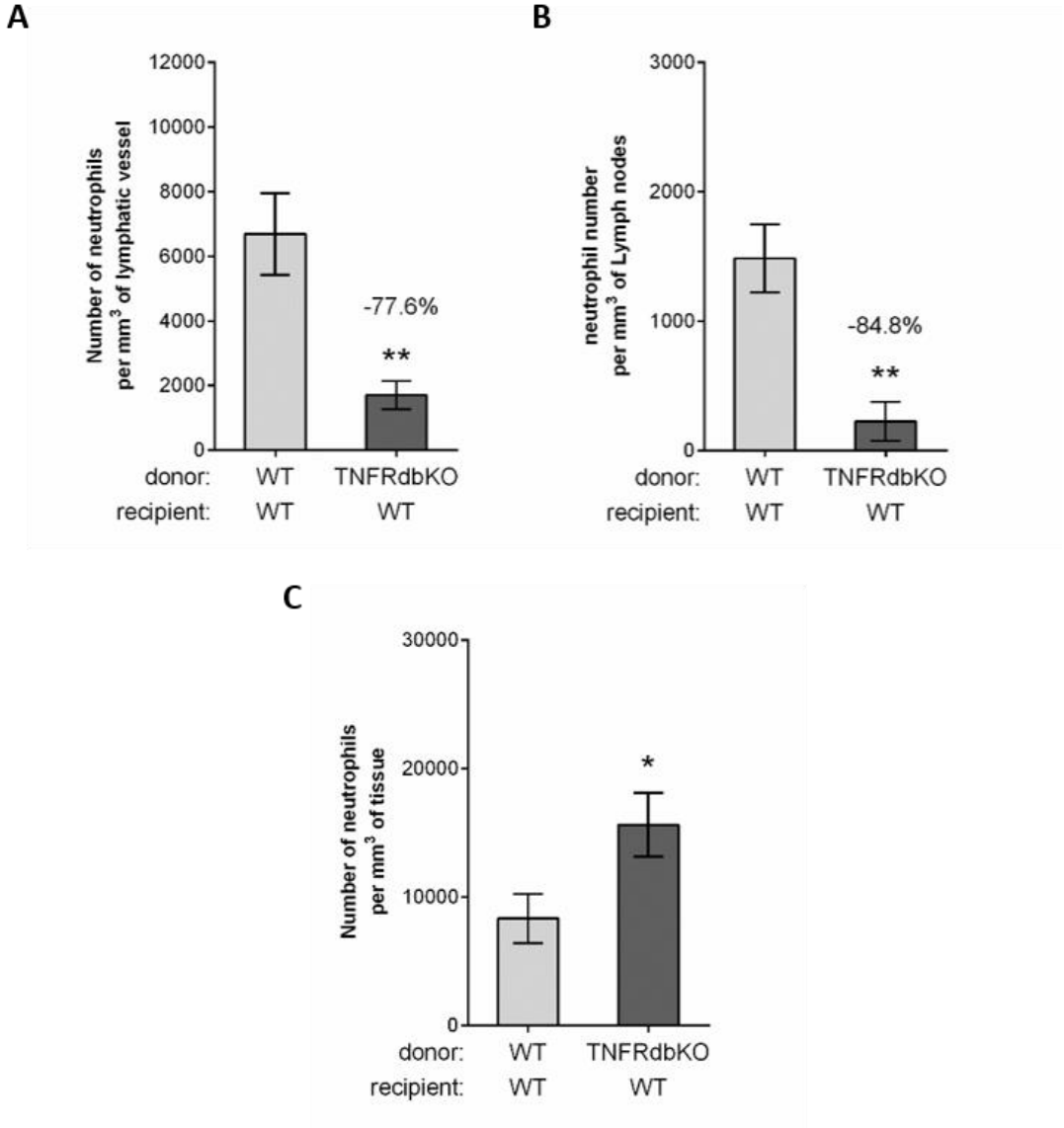

Figure 3.12: Neutrophil migration responses of WT and TNFRdbKO chimeric mice following CFA+Ag-induced inflammation in the cremaster muscle. Neutrophil migration into the lymphatic system of the cremaster muscle following antigen sensitisation with complete Freund's adjuvant (CFA+Ag) was induced in chimeric animals exhibiting neutrophils deficient in both TNFRs. Neutrophil migration responses were visualised by confocal microscopy and analysed by IMARIS Software. (A) Number of neutrophils within cremaster lymphatic vessels at 16 h post-CFA+Ag-stimulation from chimeric animals receiving bone marrow transplant of WT or TNFRdbKO donor mice and as quantified by confocal microscopy. (B) Number of neutrophils found in the dLNs of chimeric animals receiving bone marrow transplant of WT or TNFRdbKO donor mice as quantified by confocal microscopy 16 h post-CFA+Ag-stimulation. (C) Number of extravasated neutrophils in cremaster muscles at 16 h post-CFA+Ag-stimulation from chimeric animals receiving bone marrow transplant of WT or TNFRdbKO donor mice and as quantified by confocal microscopy. Data are expressed as mean±SEM of N = 6-7 animals (~10-12 images per pair of cremaster/dLNs for confocal microscopy) images per cremasters for confocal microscopy) per group from at least 5-10 experiments. Statistically significant differences between WT and TNFRdbKO mice are indicated by asterisks: *, $P < 0.05$; **, $P < 0.01$. Statistical significance between groups was determined using Student's T-test.

3.4 Discussion

In this chapter, the structure of lymphatic vessels in the murine cremaster muscle was lymphatic system during inflammation was also investigated. The link between TNF and CFA+Ag was then established by inducing inflammation in cremaster muscles using these inflammatory triggers.

The recirculation of fluid (lymph) and cells within interstitial tissues through the lymphatic system is an important process that occurs in normal tissue homeostasis, inflammatory diseases, and cancer. However, cellular features responsible for the entry of lymph and leukocytes, specifically neutrophils, into lymphatic vessels is still poorly understood. Reports have shown the presence of discontinuous button-like junctions between endothelial cells (ECs) of initial lymphatics at likely sites of fluid entry, with continuous zipper-like junctions found on collecting vessels in the mouse trachea and several other organs, including the diaphragm, urinary bladder, and skin of ear and tails (Baluk et al., 2007; Dejana et al., 2009). The reports also showed initial lymphatics had distinctive oak-leaf shaped LECs and immunostaining for the lymphatic endothelial cell marker, LYVE-1, was concentrated at the top of scalloped edges (flaps) of oak leaf-shaped cells. In the opening results chapter, investigations into the structure of initial lymphatic vessels found in the chosen inflammatory model were carried out, where the cremaster muscle was used. Whole-mount cremaster muscles immunostained for the lymphatic endothelial cell marker, LYVE-1, and the endothelial cell markers, PECAM-1/VE-Cadherin showed the presence of a fully developed unidirectional network of lymphatic vessels with blind-ended lymphatic capillaries and initial vessels with button-like junctions and oak-leaf shaped cells in accordance with what was found in initial lymphatics in Baluk et al.'s report. Despite previous findings indicating that LYVE-1 was mainly concentrated at flaps of initial lymphatics (Baluk et al., 2007; Dejana et al., 2009), this molecule was found to be expressed all over these vessels in the present study. These differences could be due to differences in the staining protocol and confocal settings. Collectively, these findings suggest that in the cremaster model for this study, majority of the lymphatic vessels that were looked at are initial lymphatics.

Next, the dynamics of leukocyte migration from the circulation into the lymphatic system was investigated. The dynamics of leukocyte, specifically neutrophil, transmigration, through venular walls (Proebstl et al., 2012; Woodfin et al., 2009) and their downstream entry into LNs (Abadie et al., 2005; Maletto et al., 2006; Rigby et al., 2015) in response

to inflammatory stimuli in mice has been previously looked at in separate *in vivo* and *in vitro* studies. However, the overall dynamics of these events occurring successively has not been studied. Innate immunity comes into play when tissues become inflamed due to tissue injury or infection. Chemokines produced by resident patrolling macrophages then cause neutrophils from the circulation to transmigrate across PCVs to the site of inflammation (Ley et al., 2007).

Studies have shown that neutrophils are detected in the interstitial tissue at the site of inflammation from as early as 45 min up to a period of 48 h (Frasch et al., 2013; Woodfin et al., 2009; Yadav et al., 2003). Neutrophil transmigration responses from the circulation across PCVs was investigated by carrying out a time-course experiment. Local injection of either TNF or an emulsion of CFA+Ag elicited neutrophil migration in a time-dependent manner. Following TNF-stimulation, neutrophils are still present in the inflamed tissue at 48 h but at low numbers, close to basal levels, which is in accordance with a previous study using another inflammatory mediator, zymosan (Frasch et al., 2013). The longest time-point looked at post CFA+Ag-stimulation was 24 h, and although neutrophils numbers are not quite back to basal levels, a decreasing trend can be seen. In accordance with the present study, an earlier study using CFA+Ag to induce peritonitis demonstrated that neutrophil migration recruitment into the peritoneal cavity also occurred in a time-dependent manner peaking at 6 h, and although neutrophil numbers were low at the 24 h time-point, numbers only fully returned to basal levels at the 48 h time-point (Klein et al., 1995). Additionally, in another model of intraperitoneal antigen (methylated BSA) challenge, neutrophil recruitment to the peritoneal cavity was also demonstrated to occur in a time-dependent manner with neutrophils being detected at the site of inflammation from 2 h, and neutrophil numbers peaking at 6 h before returning close to basal levels at 24 h post-i.s. injection (Vieira et al., 2009). Albeit the different peaks seen in the current model of antigen sensitisation, this is still in accordance with the time-course results.

Following elicitation of the innate immune response, the induction of an adaptive immune response depends on the effective transport of antigens through afferent lymphatic vessels. These antigens are transported to lymphoid tissue by either being taken up by antigen-presenting cells (APCs), which then carry them to dLNs, or they get drained to the nodes as a soluble component of lymph fluid. To date, most studies have focused on the ability of peripheral dendritic cells (DCs) to exert this function and studies looking at the ability of neutrophils to do this has been neglected. However, recent reports have

shown that these extravasated neutrophils play more than just a minor role in innate immunity. Once activated by an inflammatory stimulus, both mice and human neutrophils have been shown to express MHC-II and the co-stimulatory molecules CD80 and CD86, thus enabling them to function as APCs (Abi Abdallah et al., 2011; Culshaw et al., 2008; Lei et al., 2001). Rather than dying locally in the interstitial tissue, a sub-population of neutrophils can remain viable and migrate from tissues to dLNs via lymph where they then act as APCs. In particular, neutrophils bearing phagocytosed *M.bovis* BCG and *Toxoplasma gondii* have been found within the sinuses of draining lymph nodes in several models (Abadie et al., 2005; Chtanova et al., 2008; Maletto et al., 2006). This chapter sought to look at neutrophil migration into lymphatic vessels and their downstream entry into dLNs following TNF- or CFA+Ag-stimulation. As with neutrophil transmigration into interstitial tissues, this was both also found to occur in a time-dependent manner. The dynamics of neutrophil entry into lymphatic vessels has not been well characterised in the literature, but confocal IVM in the present study showed that neutrophils take ~4.5 minutes to breach the lymphatic endothelium in a TNF-stimulated cremaster muscle, which is similar to the time it takes (~2–5 minutes) for leukocytes to migrate through the vascular EC barrier (Ley et al., 2007). *In vitro*, Rigby et al. showed that TNF stimulation causes neutrophils to transmigrate across a monolayer of primary human dermal lymphatic endothelial cells (HDLECs) in a time-dependent manner starting at ~18 mins and peaking at ~90 mins before plateauing and decreasing in number (Rigby et al., 2015). Direct comparisons of these results cannot be made to the current *in vivo* study but similarities can be inferred as a time-dependent response was seen in the current study. Rigby et al. also showed that TNF stimulation triggers the secretion of neutrophil specific chemokines, CXCL2, CXCL5 and CXCL8, with the latter being particularly important in directing neutrophil transmigration across the lymphatic endothelium (Rigby et al., 2015). Other molecules involved in neutrophil migration through initial lymphatic vessels along with other cellular aspects that could account for the striking kinetics of this process, are only now starting to be elucidated but these will be further discussed in chapter 4 and 6 of this thesis. In particular, the roles of chemokines in this process will be investigated and discussed in further detail in chapter 4 of this thesis. Studies looking at the ability of neutrophils to migrate across the lymphatic endothelium following antigen sensitisation *in vivo* have been neglected.

Following this, the dynamics of neutrophil migration into dLNs following TNF- or CFA+Ag-induced inflammation was investigated. As mentioned before, such studies to

date have mainly involved looking at DC migration. DC migration from the interstitial tissue to dLNs is a slow process that typically peaks a couple of days after elicitation of the inflammatory response (Kissenpfennig et al., 2005; Shklovskaya et al., 2008). Rigby et al. demonstrated that DCs displayed a characteristic lag of 4–6 h before migrating across the lymphatic endothelium *in vitro*, whereas neutrophils initiated transmigration almost immediately (Rigby et al., 2015). Interestingly, there have been several recent studies that have shown neutrophils to be the first lymph-borne cell type transporting antigen to dLNs in different models of infection (Abadie et al., 2005; Beauvillain et al., 2011; Hampton et al., 2015).

These investigations not only demonstrated that neutrophil infiltration in dLNs was detected as early as 4–6 h after administration of inflammatory stimuli (Beauvillain et al., 2011; Hampton et al., 2015), but emerging data suggests that this early influx of neutrophils may perhaps impact the developing immune response (Hampton et al., 2015; Mocsai, 2013). Several other studies reported similar observations in vaccinal (using antigens and CFA) and parasitic infection models (Chtanova et al., 2008; Maletto et al., 2006; Yang et al., 2010). In these works, migration of neutrophils into dLNs was observed from as early as 15–30 min, with neutrophils still being detected at 24–48 h post immunisation/infection. Comparing this to the results from the present study, neutrophils were detected within dLNs of mice from as early as 2 h after stimulation with both TNF and CFA+Ag, with neutrophil infiltration continuing to increase until reaching a peak at 24 h and 8 h, respectively. Moreover, neutrophils were still detected after 24 h and 48 h of CFA+Ag- or TNF-stimulation, respectively, all of which is in accordance to previous observations. Furthermore, examination of the localisation of neutrophils within dLNs of the cremaster muscle showed that at 8 h post-CFA+Ag inflammation, a much higher number of neutrophils were found within lymphatic vessels in the dLNs at 16 h post-stimulation with CFA+Ag as compared to the 8 h timepoint. Additionally, majority of neutrophils were found in the stroma at this time point with only a minority found within HEVs. This all suggests that the early and rapid migration of neutrophils into dLNs may occur via afferent lymphatics and further strengthens previous findings from other models that neutrophils play a role in adaptive immune responses. It is worth mentioning that neutrophils can also enter LNs through an alternative route by migrating from the circulation across HEVs, as has been observed following intradermal injection of *S. aureus* and CFA (Gorlino et al., 2014; Kamenyeva et al., 2015). Thus, some of the

neutrophils present within dLNs at the early time-points could potentially have migrated via this route.

In the present study, either TNF or an emulsion of CFA+Ag were used as inflammatory mediators. Having observed both the efficacy of CFA+Ag and exogenous TNF in inducing neutrophil migration into lymphatic vessels, the potential role of endogenous TNF in this response in a model of antigen sensitisation was next investigated. Interestingly, CFA+Ag-stimulation of cremaster muscles induced a rapid release of TNF in the tissues. Owing to the fact that TNF can prime neutrophils and trigger their mobilisation to sites of infection or inflammation (Hallett and Lloyds, 1995), the functional role of endogenous TNF during CFA+Ag-induced inflammation at the 16 h time-point was investigated. TNF signalling was blocked using TNFRdbKO mice deficient in both TNF receptors, p55 and p75. Results showed that neutrophil migration into lymphatic vessels was impaired in these mice. Strikingly, TNF did not appear to have any effect on neutrophil transmigration across venular endothelial cells into interstitial tissues, signifying a distinct role for TNF in driving neutrophil migration into lymphatic vessels but not through blood vessels. This was also found to be the case at an earlier time point of 8 h (**Appendix 1**), thus confirming that the lower number of neutrophils seen at the 16 h timepoint is not due to faster efflux of neutrophils from lymphatic vessels. Furthermore, the use of chimeric animals showed that TNF is able to directly act on leukocytes to induce this neutrophil migration response as neutrophils deficient in both TNFRs showed impaired neutrophil migration into lymphatic vessels.

In contrast with pure TNFRdbKO mice, a significant increase was seen in extravasation of TNFRdbKO chimeric mice as compared to WT chimeric mice. Other studies have showed results similar to this study regarding neutrophil recruitment to sites of inflammation in the absence of TNF signalling (Peschon et al., 1998; Woodfin et al., 2009). In accordance with the results found in TNFRdbKO mice used in this study, Woodfin *et al*. showed *in vivo* in a model of cremaster inflammation that at 4 h post-stimulation with IL-1β, no differences in neutrophil extravasation were seen between WT and TNFRdbKO mice (Woodfin et al., 2009). Peschon *et al*. also demonstrated in an *in vivo* model of LPS-induced peritonitis that neutrophil recruitment to the peritoneum is the same in both WT and TNFRdbKO mice. This suggests an accumulation of neutrophils is occurring within the inflamed tissue of TNFRdbKO chimeric mice for unidentified reasons. The percentage of circulating neutrophils between both WT and TNFRdbKO chimeras was the same, therefore this could be disregarded as an explanation as to why a

higher number of neutrophils were seen in the inflamed tissue. Another explanation could be the presence of higher concentrations of neutrophil chemoattractants in the inflamed tissue of TNFRdbKO chimeric mice. In order to generate these chimeric mice, WT mice had to be subjected to two low doses (5 Gy) of irradiation before reconstitution of either WT or TNFRdbKO bone marrow hematopoietic cells. A study looking at the effect of low-dose irradiation (8 Gy) on chemokine expression in mice liver demonstrated an upregulation of gene expression of several chemokines in the parenchyma, including the chemoattractants implicated in neutrophil recruitment - CXCL1, CXCL2 and CXCL8 (Malik et al., 2010). However, this study only looked at several timepoints up to 48 h after irradiation. Another study in humans showed that TNF induces a stop signal that promotes firm neutrophil adhesion and inhibits polarisation and chemotaxis of neutrophils to chemoattractants including IL-8 and C5a, thus promoting the retention of neutrophils within blood vessels (Lokuta and Huttenlocher, 2005). Although these findings were found in a different tissue to the cremaster muscle and in humans, an upregulation in the expression of these chemokines in the interstitial tissues along with dysfunctional leukocyte TNF signalling, could be an explanation as to why TNFRdbKO chimeric mice exhibit higher neutrophil numbers within the interstitial tissue. There have been few reports of the direct effect of blocking TNF signalling on neutrophils with the use of anti-TNF agents (den Broeder et al., 2003; Taylor et al., 2000). However, these drugs have been shown to significantly reduce migration of neutrophils from peripheral blood into chronically inflamed joints, in the case of rheumatoid arthritis (den Broeder et al., 2003; Taylor et al., 2000). Its effect on neutrophil migration into lymphatic vessels is still unknown, although findings in the present study have implicated a role for TNF in this process.

Collectively, the findings in this chapter indicate that lymphatic vessels of the cremaster muscle analysed via confocal microscopy are mainly initial lymphatics and also highlight the dynamic responses of neutrophil migration from blood vasculatures into the lymphatic system during TNF and CFA+Ag-induced inflammation. Furthermore, findings here demonstrate for the first time the involvement of TNF in triggering the migration of neutrophils into tissue-associated lymphatic vessels upon antigen challenge *in vivo*. This work has recently been published in Nature Scientific Reports (Arokiasamy et al., 2017).

Limitations of the study

As with most studies, there are certain limitations to the model used in this study. The obvious being the use of mice in the *in vivo* inflammatory models, which renders it less relevant to humans. However, due to ethical reasons, the mouse model is the best alternative as it allows the visualisation of neutrophil migration responses at any chosen time-point of the inflammation at the cellular and molecular level in structures (blood and lymphatic vessels, LNs etc.) that are not easily accessible in humans. Furthermore, it also allows the visualisation of these responses within lymphatic vessels in real-time using confocal IVM, a technique that is not currently applicable to human studies. Another caveat is the fact that the model of inflammation used in this study makes use of the mouse cremaster muscle, which might not be relevant to the female population as it has been shown that there are sex differences in immune responses (Klein and Flanagan, 2016). To overcome this, another vascular bed such as the ear or mesentery can be used to confirm these results in female mice. Finally, the use of CFA is not relevant to humans as the use of this adjuvant is prohibited due to its toxicity. However, it is widely used in animal models to mimic the classical immunisation protocols used in humans, which makes it appropriate for this study.

4 : Investigating the chemokine:chemokine receptor axes responsible for TNF-dependent migration of neutrophils into lymphatic vessels *in vivo*

4.1 Introduction

Neutrophil migration into the lymphatic system has been described in models of infections and immunisation sensitisation (Abadie et al., 2005; Beauvillain et al., 2011; Chtanova et al., 2009; Maletto et al., 2006), but the mechanisms associated with this response are not fully understood. As supported by the literature, Chapter 3 presented results indicating initial lymphatics form blind-ended structures, with the presence of discontinuous endothelial junctions with distinctive PECAM-1-rich flaps and VE-Cadherin-rich buttons. These flaps have been shown to serve as entry portals for leukocytes, such as DCs, which are reported to migrate at steady-state into initial lymphatics via integrin-independent mechanisms that are largely controlled by CCL21/CCR7-mediated chemotaxis (Pflicke and Sixt, 2009).

To date, there is controversy surrounding the involvement of chemotactic stimuli in neutrophil migration into draining lymph nodes via lymphatic vessels. The first study reported that CCR7 is key for this process (Beauvillain et al., 2011), whereas a following study provided evidence to show that CCR7 is entirely dispensable (Hampton et al., 2015). Additionally, the chemokine axis, CXCR4:CXCL12, and Sphingosine-1-Phosphate (Gorlino et al., 2014; Hampton et al., 2015) have recently been implicated in neutrophil trafficking into LNs. Additionally, the chemokine CXCL8, a ligand of chemokine receptors CXCR1 and CXCR2, has been found to be expressed by human LECs and identified as the main chemotactic driver in the transmigration of neutrophils across a monolayer of LECs *in vitro* (Rigby et al., 2015). Conversely, CXCR2 has been shown to not have a role in neutrophil trafficking to draining lymph nodes (Gorlino et al., 2014). In light of this, it has to be mentioned that all these studies made use of very different inflammatory models, ranging from inflammation induced by injection of inactivated pathogens, immune complexes in CFA to live bacilli, with some of these chemokine axes being implicated in neutrophil trafficking to LNs via HEVs as opposed to via lymphatic vessels (Beauvillain et al., 2011; Gorlino et al., 2014; Hampton et al.,

2015). The involvement of chemokine:chemokine receptor axes may possibly vary with the type of inflammatory model used, especially since the up-regulation of chemokines in LECs has been widely shown to be highly stimulus specific (Aebischer et al., 2014). With relevance to this, it has been demonstrated that TNF is likely to be a master regulator of the signals responsible for directing cells to the site of infection, with TNF influencing appropriate chemokine expression by infected macrophages to orchestrate neutrophil recruitment to sites of inflammation (Algood et al., 2005; Vieira et al., 2009). The chemokines IL-8 (CXCL8), MIP-2 (CXCL2) and KC (CXCL1) have been shown to be the most critical for neutrophil recruitment to these sites (De Filippo et al., 2008; Shen et al., 2004). A study by Ihenetu *et al*. showed *in vitro* in an epithelial cell line that IL-8 release was time-dependent following stimulation with TNF (Ihenetu et al., 2003). Another study by Lo *et al*. demonstrated *in vitro* using HUVECs that TNF stimulation induces the release of CXCL1 and its mRNA expression in a time-dependent manner (Lo et al., 2014). In the context of LECs, TNF stimulation has been demonstrated to induce a dramatic increase in CX_3CL_1, which has been implicated in DC cell migration across the lymphatic endothelium both *in vivo* and *in vitro* (Johnson and Jackson, 2013). TNF has also been shown to upregulate CCL21 expression by lymphatic vessels, which leads to DC migration across LECs via a β2-integrin-mediated mechanism *in vitro* (Johnson and Jackson, 2010).

As the specific mechanisms by which neutrophils migrate into lymphatic vessels remains largely unknown, the present study set out to decipher further molecular mechanisms involved in neutrophil migration into lymphatic vessels, and more specifically, which chemokine:chemokine receptor axes are associated with this response under inflammatory conditions.

4.2 Aims

Neutrophils are the first immune cells to be recruited from the circulating blood to sites of infection or diseased tissues. CXC chemokines including IL-8 (CXCL8 – human equivalent of murine CXCL1/2), MIP-2 (CXCL2) and KC (CXCL1) have been widely demonstrated to be the most critical for such recruitment (Kobayashi, 2008). In the context of leukocyte migration across the lymphatic endothelium, the CCL21:CCR7, CXCL12:CXCR4, and CX_3CL1:CX_3CR1 chemokine axes have all been implicated in DC migration into the lymphatic system. In contrast, the chemokine:chemokine receptor axes involved in neutrophil trafficking into lymphatic vessels are still relatively unknown. Having previously identified a role for endogenous TNF in controlling the entry of neutrophils into lymphatic vessels in the previous chapter, this chapter aimed to elucidate chemokine:chemokine receptor axes responsible for promoting this response. The specific aims of this chapter were to:

- Investigate the role of the CXCL1:CXCR1/2 and CXCL12:CXCR4 chemokine axes in neutrophil migration into lymphatic vessels of WT mice using anti-CXCL1 blocking mAbs and AMD3100 (CXCR4 inhibitor) following CFA+Ag-stimulation. *Ex vivo* immunofluorescence staining and confocal microscopy analysis will be carried out.
- Investigate neutrophil expression of CCR7 following TNF- or CFA+Ag-stimulation both *in vivo* and *in vitro* through the use of flow cytometric analysis.
- Investigate the role of the CCL21:CCR7 chemokine axis in neutrophil migration into lymphatic vessels by confocal microscopy following TNF- or CFA+Ag-stimulation through the use of CCR7KO mice as a means of abolishing CCR7 signalling.
- Investigate the importance of CXCR4 in neutrophil recruitment into the lymphatic system via confocal microscopy, in the absence of the CCR7 signalling with the use of CCR7KO mice.
- Further investigate the role of CCR7 on neutrophils in a WT environment by generating chimeric mice exhibiting CCR7KO-deficient neutrophils and examining the migration responses in these mice by confocal microscopy following CFA+Ag-stimulation.

4.3 Results

4.3.1 Effects of the CXCL1:CXCR1/2 chemokine axis on neutrophil migration during CFA+Ag-induced inflammation of the cremaster muscle

The role of the CXCL1:CXCR1/2 chemokine axis was first investigated in neutrophil trafficking into the lymphatic system during antigen sensitisation *in vivo*, as the human equivalent of murine CXCL1, CXCL8, has recently been shown to promote neutrophil migration through a monolayer of LECs *in vitro* (Rigby et al., 2015). Furthermore, CXCL1 has been demonstrated to be upregulated in lymphatic vessels of mice ears following CHS-induced inflammation *in vivo* (Vigl et al., 2011).

For this purpose, neutrophil migration responses were looked at following 8 h (peak of neutrophil migration into lymphatic vessels) CFA+Ag-induced inflammation of the cremaster muscle of WT mice. Briefly, WT mice were given i.s injections of an emulsion of CFA+Ag (200 µg of each in 300 µl total volume) and were i.s injected with 30 µg of anti-CXCL1 blocking/isotope control antibody 4 h post-i.s. injection. This dosage was chosen as it has been demonstrated to inhibit neutrophil migration across blood vessels by other members of the group (unpublished data). Unstimulated control mice were given i.s injections of PBS. Eight hours post-i.s. injection, mice cremaster muscles and dLNs were dissected away, fixed and whole-mounted for immunofluorescence staining and confocal analysis. Cremaster muscles were immunostained with anti-PECAM-1, anti-LYVE-1 and anti-MRP14 mAbs to label blood vasculatures, lymphatic vasculatures and neutrophils, respectively. Draining LNs were immunostained with anti-MECA-79, anti-LYVE-1 and anti-mRP14 mAbs to label HEVs, lymphatic vasculatures and neutrophils, respectively. Images obtained from confocal microscopy were analysed using IMARIS software.

No significant differences were seen via confocal microscopy in the interstitial tissue surrounding postcapillary venules at 8 h post-i.s. injection in mice treated with anti-CXCL1 blocking antibody (**Figure 4.1A, right panels**) as compared to isotype controls (**Figure 4.1A**, **left panels**). Quantification of confocal images showed that a delayed local delivery of anti-CXCL1 blocking antibody did not affect the migration of neutrophils across postcapillary venules (**Figure 4.1B**). Additionally, 3D-reconstructed images from

confocal microscopy showed no differences in neutrophil numbers within lymphatic vessels of mice treated with anti-CXCL1 blocking antibody (**Figure 4.2A, right panels**) as compared to isotope controls (**Figure 4.2A, left panels**). Quantification of these images showed that treatment with anti-CXCL1 blocking antibody had no significant effect on neutrophil migration into lymphatic vessels (**Figure 4.2B**). Finally, 3D-reconstructed images from confocal microscopy showed no differences in number of neutrophils seen within dLNs of mice treated with anti-CXCL1 blocking antibody (**Figure 4.3A, right panels**) as compared to those that received i.s. injections of isotype control antibody (**Figure 4.3A, left panels**). Quantification of confocal images showed that treatment with anti-CXCL1 blocking antibody demonstrated no significant effect on neutrophil infiltration in dLNs (**Figure 4.3B**).

Collectively, the results in this section suggests that the CXCL1:CXCR1/2 chemokine axis does not play any significant role in neutrophil recruitment into lymphatic vessels during antigen sensitisation, as induced by CFA+Ag *in vivo*.

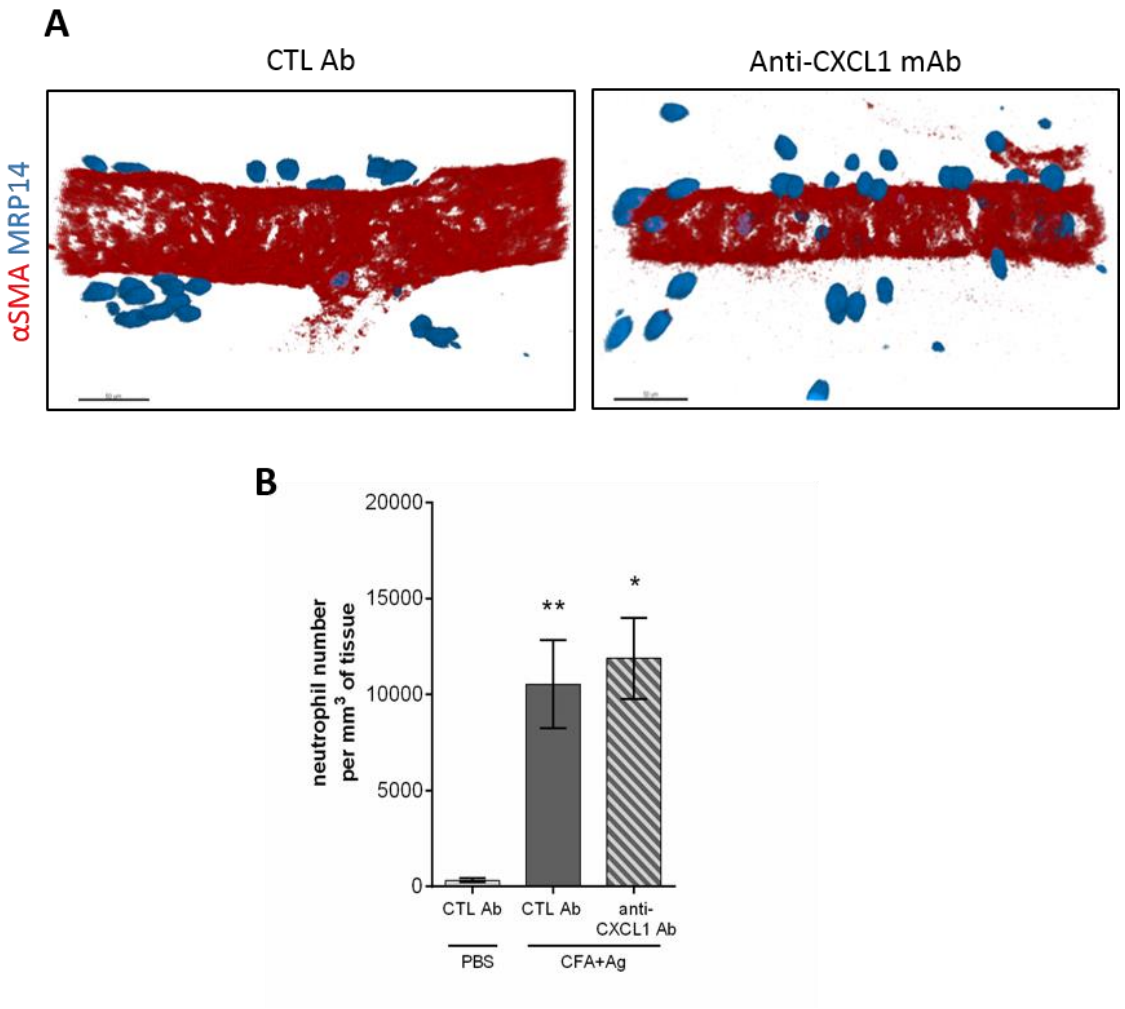

Figure 4.1: Neutrophil transmigration responses across postcapillary venules of WT mice following *in vivo* blockade of the chemokine CXCL1 in unstimulated and CFA+Ag-stimulated cremasters. WT C57BL/6 mice were subjected to CFA+Ag-induced cremaster inflammation. Four hours later, an anti-CXCL1 blocking mAb (30µg/mouse) or and an isotype control mAb was given i.s. to all mice. This dose was selected for its capacity to block neutrophil extravasation following cytokine-induced inflammation (data not shown). Eight hours post-stimulation, cremaster muscles were dissected away, fixed and immunostained for αSMA (red) and MRP14 (blue) to visualise the blood vasculatures and neutrophils, respectively. Neutrophil migration responses were visualised by confocal microscopy and analysed by IMARIS Software. (A) Representative 3D-confocal images of neutrophil extravasation from postcapillary venules in the cremaster muscles of CFA+Ag-stimulated WT mice treated with isotype control Ab (left) or anti-CXCL1 blocking mAb (right). (B) Number of extravasated neutrophils in inflamed cremaster muscles. Data are expressed as mean ± SEM of n=5-7 animals per group (~10-12 images per pair of dLNs for confocal microscopy). Statistically significant differences between stimulated and unstimulated treatment groups are indicated by asterisks: *, $P < 0.05$; **, $P < 0.01$. Statistical significance was determined using one-way ANOVA.

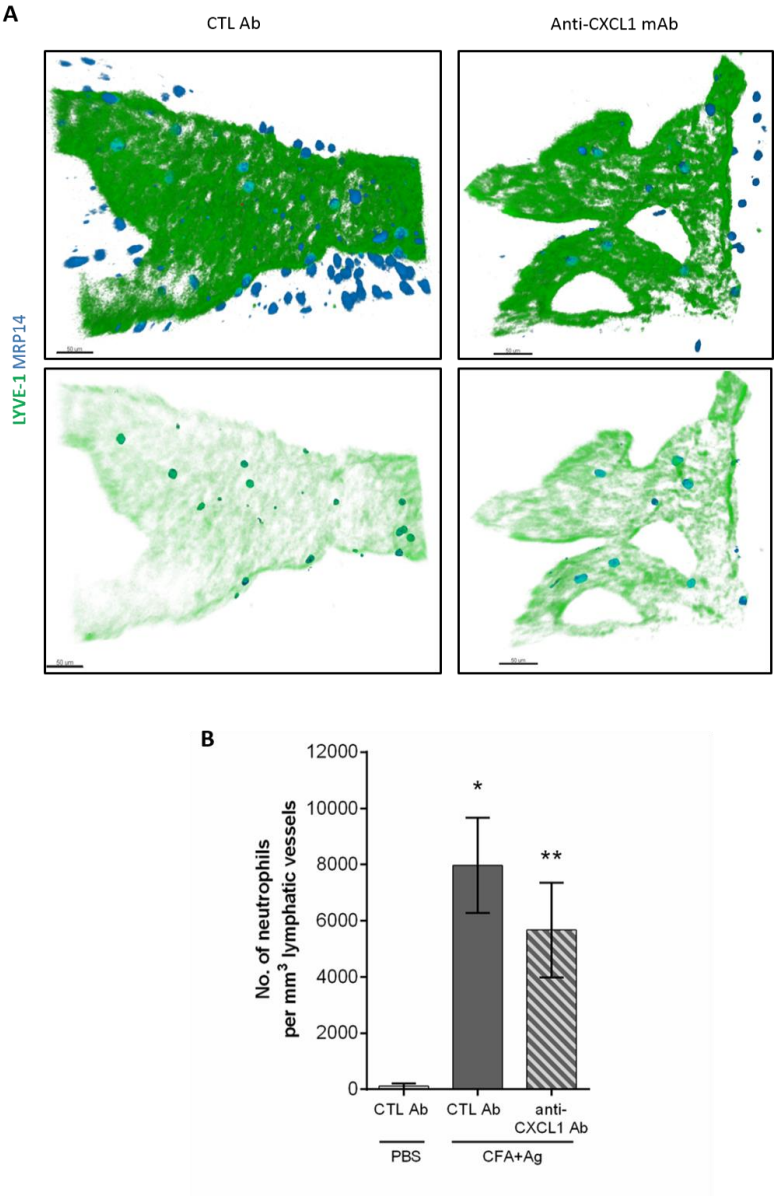

Figure 4.2: Neutrophil migration responses into lymphatic vessels of WT mice following *in vivo* blockade of the chemokine CXCL1 in unstimulated and CFA+Ag-stimulated cremasters. WT C57BL/6 mice were subjected to CFA+Ag-induced cremaster inflammation. Four hours later, an anti-CXCL1 blocking mAb (30µg/mouse) or and an isotype control mAb was given i.s. to all mice. This dose was selected for its capacity to block neutrophil extravasation following cytokine-induced inflammation (data not shown). Eight hours post-stimulation, cremaster muscles were dissected away, fixed and immunostained for LYVE-1 (green) and MRP14 (blue) to visualise the lymphatic vasculatures and neutrophils, respectively. Neutrophil migration responses were visualised by confocal microscopy and analysed by IMARIS Software. (A) Representative 3D-confocal images of neutrophils within lymphatic vessels in the cremaster muscles of CFA+Ag-stimulated WT mice treated with isotype control Ab (left) or anti-CXCL1 blocking mAb (right). The top panels show all neutrophils present in the field of view. The bottom panels show neutrophils present only within the lymphatic vessels. Bars: 50 µm. (B) Number of neutrophils within the cremaster lymphatic vessels. Data are expressed as mean ± SEM of n=5-7 animals per group (~10-12 images per pair of dLNs for confocal microscopy). Statistically significant differences between stimulated and unstimulated treatment groups are indicated by asterisks: *, $P < 0.05$; **, $P < 0.01$. Statistical significance was determined using one-way ANOVA.

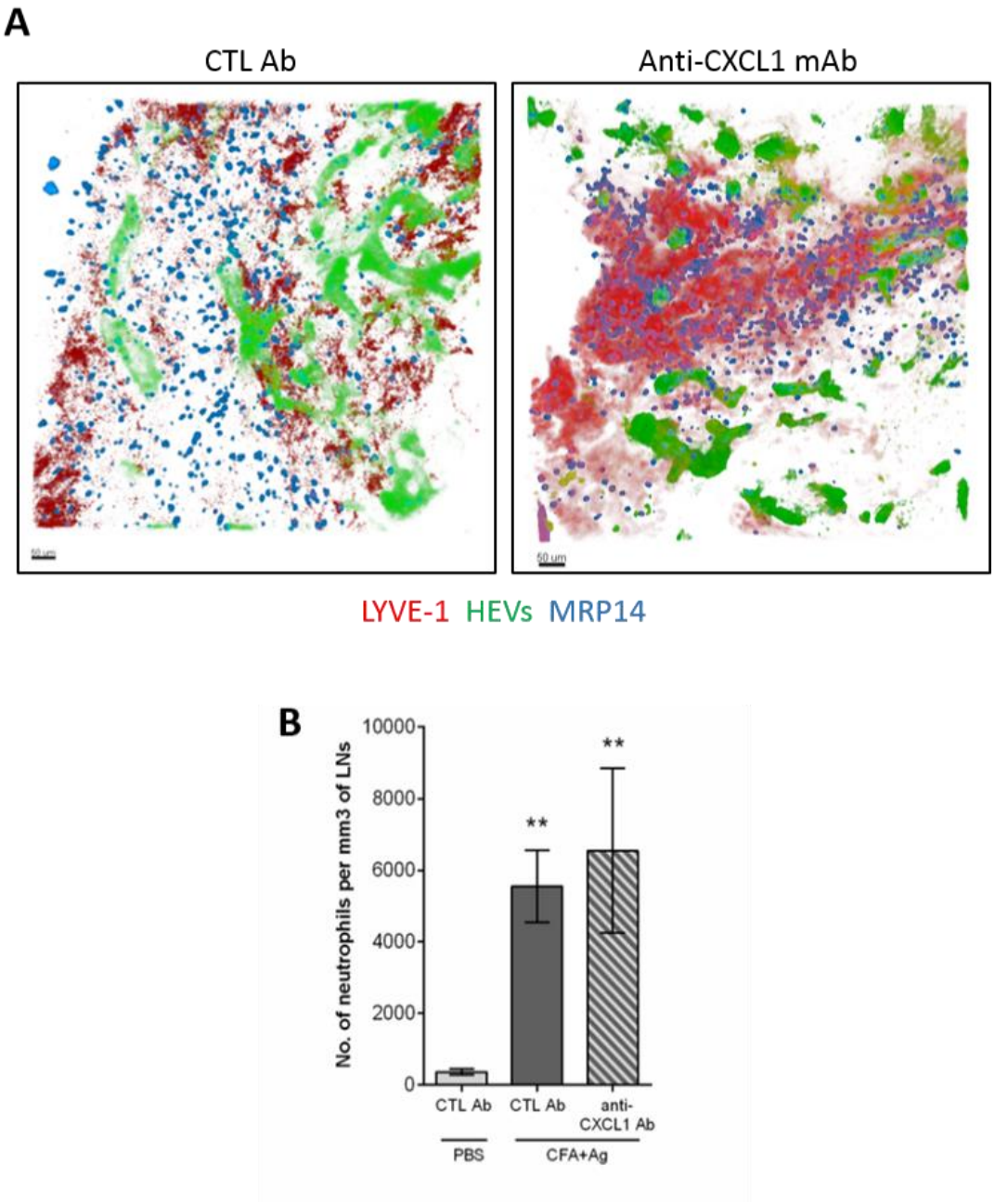

Figure 4.3: Neutrophil migration responses into dLNs of WT mice following *in vivo* blockade of the chemokine CXCL1 in unstimulated and CFA+Ag-stimulated cremasters. WT C57BL/6 mice were subjected to CFA+Ag-induced cremaster inflammation. Four hours later, an anti-CXCL1 blocking mAb (30µg/mouse) or an isotype control mAb was given i.s. to all mice. This dose was selected for its capacity to block neutrophil extravasation following cytokine-induced inflammation (data not shown). Eight hours post-stimulation, dLNs (inguinal) were dissected away, fixed and halved before being immunostained for LYVE-1 (red), HEVs (green) and MRP14 (blue) before being analysed by confocal microscopy and IMARIS software. (A) The figure shows representative 3D-confocal images of neutrophil infiltration into the dLNs of mice that received i.s injection of isotope control Ab (left) or treatment of anti-CXCL1 blocking mAb (right) Bars: 50 µm. (B) Number of neutrophils found in the dLNs. Data are expressed as mean ± SEM of n=5-7 animals per group (~10-12 images per pair of dLNs for confocal microscopy). Statistically significant differences between stimulated and unstimulated treatment groups are indicated by asterisks: *, $P < 0.05$; **, $P < 0.01$. Statistical significance was determined using one-way ANOVA.

4.3.2 Effects of the CXCL12:CXCR4 chemokine axis on neutrophil migration during CFA+Ag-induced inflammation of the cremaster muscle

The role of the CXCL12:CXCR4 chemokine axis was next investigated on neutrophil trafficking into the lymphatic system during antigen sensitisation. For this purpose, a CXCR4 specific inhibitor, AMD3100, was used. As before, neutrophil migration responses were looked at following 16 h (peak of neutrophil migration into lymphatic vessels) of CFA+Ag-induced inflammation in the cremaster muscle of WT mice. Briefly, WT mice were given i.s injections of 200 μg of an emulsion of CFA+Ag (200 μg of each in 300 μl total volume) and were i.s injected with AMD3100/vehicle control (PBS) 4 h post-i.s. injection. Unstimulated control mice were given i.s injections of PBS. Sixteen hours post-i.s. injection, cremaster muscles and dLNs were dissected away, fixed and whole-mounted for immunofluorescence staining and confocal analysis. Cremaster muscles were immunostained with anti-PECAM-1, anti-LYVE-1 and anti-MRP14 mAbs to label blood vasculatures, lymphatic vasculatures and neutrophils, respectively. Draining LNs were immunostained with anti-MECA-79, anti-LYVE-1 and anti-MRP14 mAbs to label HEVs, lymphatic vasculatures and neutrophils, respectively. Images obtained from confocal microscopy were analysed using IMARIS software.

Similarly to CXCL1-blockade, quantification of 3D-reconstructed confocal images showed that local delivery of AMD3100 did not significantly affect the migration of neutrophils across postcapillary venules at 16 h post-i.s. injection although there was an increased tendency towards there being more neutrophils in the interstitial tissue of AMD3100 treated mice as compared to vehicle controls (**Figure 4.4A**). Furthermore, quantification of confocal images showed that treatment with AMD3100 had no significant effect on neutrophil migration into lymphatic vessels (**Figure 4.4B**). Finally, quantification of confocal images showed that treatment with AMD3100 demonstrated no significant effect on neutrophil infiltration in dLNs (**Figure 4.4C**).

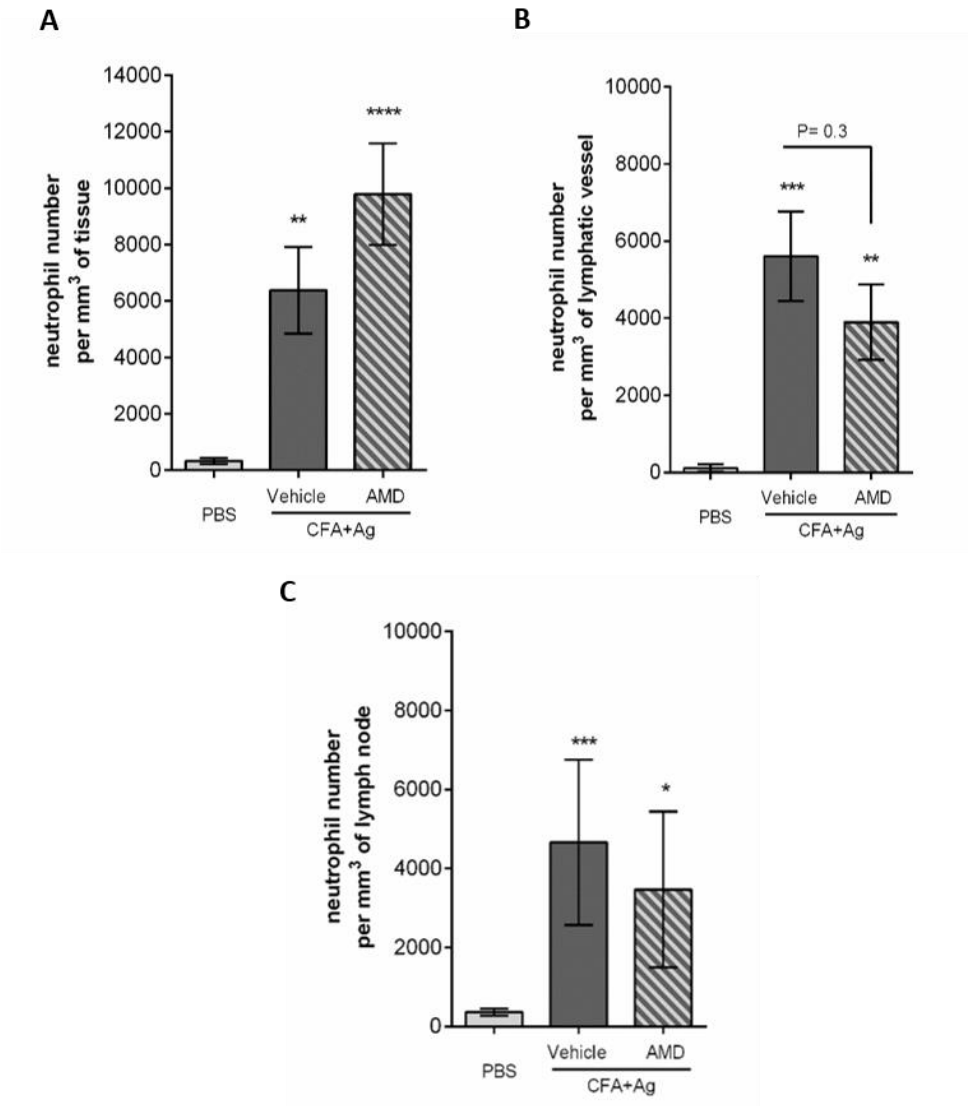

Figure 4.4: Neutrophil migration responses of WT mice following *in vivo* blockade of the chemokine receptor CXCR4 in unstimulated and CFA+Ag-stimulated cremasters. WT C57BL/6 mice were subjected to CFA+Ag-induced inflammation of the cremaster muscles. Four hours later, mice received an i.s. injection of the CXCR4 specific inhibitor AMD3100 (10mg/kg) or PBS vehicle as control. Sixteen hours post-stimulation, cremaster muscles were dissected away, fixed and immunostained for αSMA/MECA-79, LYVE-1 and MRP14 to visualise the blood vasculatures, lymphatics and neutrophils, respectively. Neutrophil migration responses were visualised by confocal microscopy and analysed by IMARIS Software. (A) Number of extravasated neutrophils in unstimulated and CFA+Ag-stimulated mice treated with AMD3100 or vehicle control. (B) Number of neutrophils within the cremaster lymphatic vessels of unstimulated and CFA+Ag-stimulated mice treated with AMD3100 or vehicle control. (C) Number of neutrophils found in the dLNs of unstimulated and CFA+Ag-stimulated mice treated with AMD3100 or vehicle control. Data are expressed as mean±SEM of n = 5-12 animals (~10-12 images per pair of cremaster/dLNs for confocal microscopy) per group from at least 5 independent experiments. Statistically significant differences between unstimulated and stimulated groups are indicated by asterisks: *, $P < 0.05$; **, $P < 0.01$; ***, $P < 0.001$; ****, $P < 0.0001$.

The blockade of CXCR4 by AMD3100 has been previously been reported to result in a rapid increase in circulating neutrophils as a result of egress from the BM (Liu et al., 2014; Ma et al., 1999; Martin et al., 2003). To ensure AMD3100 treatment was not affecting other aspects of neutrophil migration such as causing an increase in neutrophil numbers within the circulation, the percentage of circulating neutrophils within AMD3100/vehicle control treated mice were assessed by flow cytometry. The expression of the chemokine receptor, CXCR4, was also investigated in these mice. For this purpose, whole blood was taken from mice via cardiac puncture. Red blood cells were lysed in preparation for immunostaining. Blood leukocytes were immunostained for neutrophil specific markers (CD45+ Ly6G+) before the percentage of circulating neutrophils and their surface expression of CXCR4 were analysed by flow cytometry.

Although a significant increase was found in the percentage of circulating neutrophils between unstimulated and CFA+Ag stimulated mice, no significant difference was established between CFA+Ag-stimulated mice treated with either AMD3100 or vehicle control (**Figure 4.5A**). Similarly, no difference in the surface expression of CXCR4 was established between CFA+Ag-stimulated mice treated with either AMD3100 or vehicle control (**Figure 4.5B**). Interestingly, a down-regulation of CXCR4 expression was found between unstimulated and CFA+Ag-stimulated mice (**Figure 4.5B**).

Collectively, the results in this section suggests that the CXCL12:CXCR4 chemokine axis does not play any significant role in neutrophil recruitment into lymphatic vessels during antigen sensitisation, as induced by CFA+Ag *in vivo*.

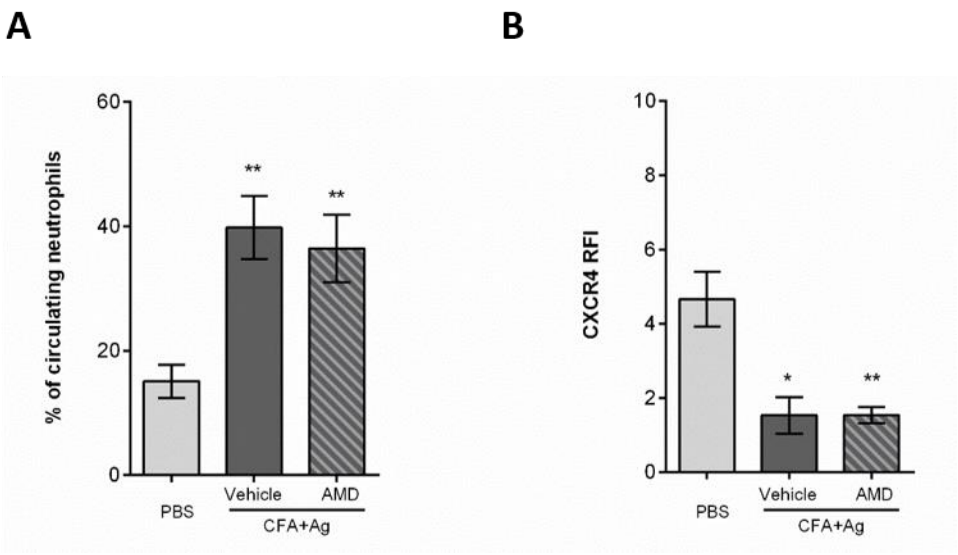

Figure 4.5: Percentage of circulating neutrophils and their CXCR4 expression in CFA+Ag-stimulated and AMD3100-treated mice compared to unstimulated/vehicle controls. WT C57BL/6 mice were subjected to CFA+Ag-induced inflammation of the cremaster muscles. Four hours later, mice received an i.s. injection of the CXCR4 specific inhibitor AMD3100 (or PBS vehicle as control). After 16 hours, whole blood was taken from each mouse via cardiac puncture and cells were immunostained for CD45.2, Ly6G, CD3ε and CXCR4 for flow cytometry analysis. (A) Percentage of neutrophils into the blood circulation as assessed by flow cytometry. (B) Surface expression of CXCR4 (RFI) on blood circulating neutrophils as assessed by flow cytometry. Data are expressed as mean ± SEM of n=5-7 animals per group. Statistically significant differences between stimulated and unstimulated treatment groups are indicated by asterisks: *, $P < 0.05$; **, $P < 0.01$. Statistical significance was determined using one-way ANOVA.

4.3.3 Expression profile of CCR7 by circulating neutrophils

Before investigating the potential involvement of the CCL21/CCR7 axis that has been widely linked with DC/T-cell migration into the lymphatic system (Johnson and Jackson, 2008), the expression of CCR7 on blood-borne, cremaster tissue-infiltrating and dLN-infiltrating neutrophils were first examined by flow cytometry post CFA+Ag-induced inflammation (**Figure 4.6**). Experiments investigating CCR7 expression on different tissues were carried out by Dr. Mathieu-Benoit Voisin. For this purpose, WT and CCR7KO mice were used, with the latter used as negative controls. 16 h post CFA+Ag-stimulation, cremaster and dLNs tissues were dissected away and digested in preparation for immunostaining. Whole blood was also taken from these mice via cardiac puncture before red blood cells were lysed in preparation for immunostaining. Leukocytes were fixed in some cases to examine intracellular expression of CCR7. Leukocytes were immunostained for neutrophil specific markers (CD45+ Ly6G+) and their surface expression of CCR7 was analysed by flow cytometry (**Figure 4.6**). Whilst WT blood neutrophils did not express CCR7 on their surface, intracellular stores of the molecule were detected. Interestingly, neutrophils isolated from CFA+Ag-stimulated cremaster muscles showed a small but significant expression of CCR7 on their cell surface suggesting neutrophils were being primed post-i.s. injection.

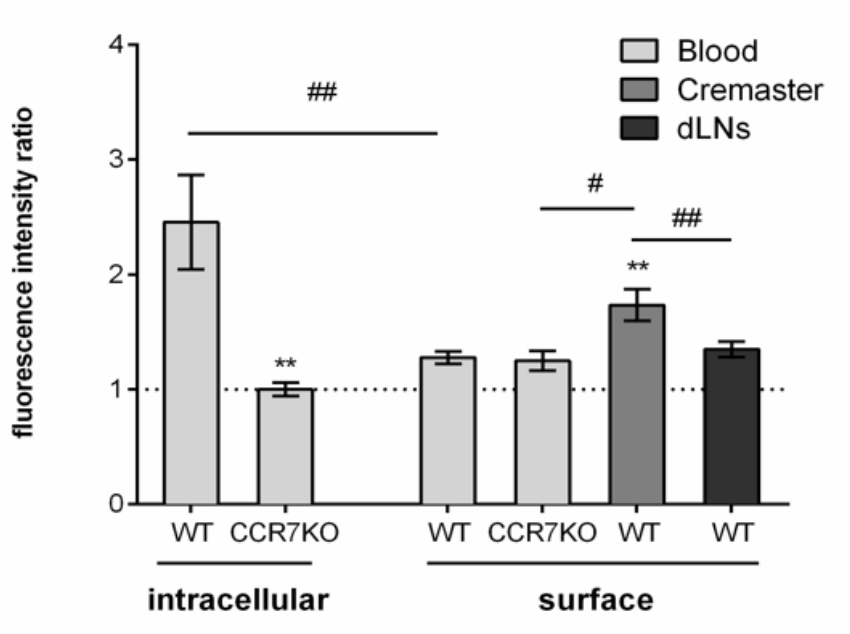

Figure 4.6: Neutrophil migration responses following 16 h CFA+Ag-induced inflammation. WT and CCR7KO mice were stimulated with CFA+Ag for 16 h before leukocytes from blood circulation, cremaster muscle and dLNs were isolated. Blood leukocytes from WT or CCR7KO animals were immunostained with an anti-CCR7 mAb or an isotype control mAb before being analysed by flow cytometry. Data are expressed as mean ± SEM of n=7-12 animals per group. Statistically significant differences between stimulated and unstimulated treatment groups are indicated by asterisks: **, $P < 0.01$. Significant differences between responses in WT vs. CCR7KO animals (or between different tissues) are indicated by hash signs: #, $P < 0.05$; ##, $P < 0.01$. Statistical significance was determined using one-way ANOVA. Data was acquired with Jessica Dilliway and Dr Mathieu-Benoit Voisin.

Next, CCR7 up-regulation following TNF stimulation was investigated. Due to the previous experiment demonstrating that WT blood neutrophils do not express CCR7 on the surface after CFA+Ag-induced inflammation (**Figure 4.6**), and a previous study also reporting that both murine and human neutrophils contain intracellular stores of CCR7, which are rapidly mobilised to the cell surface following activation (Beauvillain et al., 2011), it was hypothesised that CCR7 was being rapidly internalised and recycled through endocytosis. Therefore, the possibility of this occurrence was next examined with the use of a caveolae-dependent endocytosis inhibitor, nystatin, during stimulation with different doses of TNF (**Figure 4.7**). For this purpose, blood leukocytes were stimulated *in vitro*. Briefly, whole blood was taken from WT mice via cardiac puncture and blood cells were lysed. Blood leukocytes were then stimulated with TNF for 4 h in dose-response experiments along with simultaneous treatments of nystatin. TNF was used as the inflammatory stimuli in this case as *in vitro* stimulation of cells with an emulsion of

CFA+Ag is not possible, and TNF was previously shown in Chapter 3 to be released in response to CFA+Ag-stimulation. Leukocytes were immunostained for neutrophil specific markers (CD45+ Ly6G+) and their surface expression of CCR7 was analysed by flow cytometry. Blood neutrophils' surface expression of CCR7 was demonstrated to decrease in a TNF dose-dependent manner. The lowest dose of TNF (1 ng/ml) resulted in a small but significant expression of cell surface CCR7. This surface expression of CCR7 decreased with increasing doses of TNF, with 10 ng/ml TNF still resulting in a smaller but still significant surface expression and 100 ng/ml TNF resulting in insignificant surface expression.

Overall, the results from this section suggests that neutrophils are primed post-stimulation in order to induce cell surface expression of CCR7. CCR7 on neutrophils also seems to be internalised via caveolae-dependent endocytic pathways and this expression is inversely correlated to increasing doses of TNF (i.e. low doses of TNF can induce the surface expression of CCR7 on neutrophils).

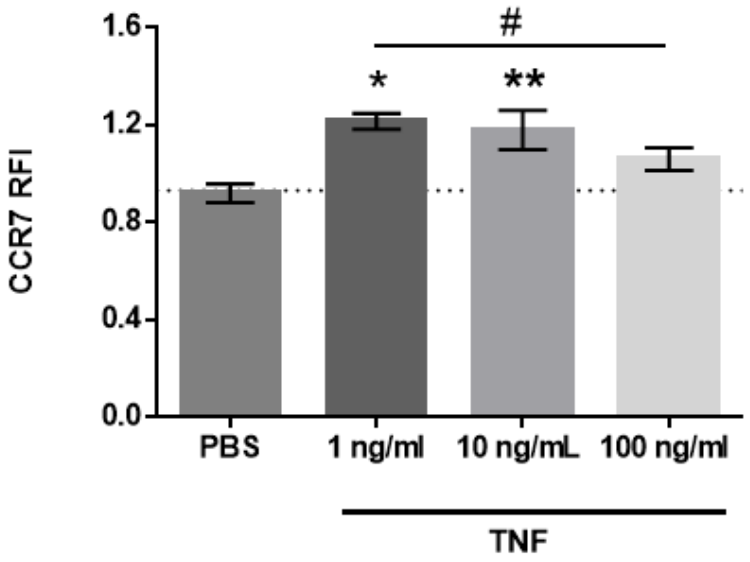

Figure 4.7: CCR7 expression on surface of TNF-stimulated neutrophils following treatment with caveolae-dependent endocytosis inhibitor, nystatin. Whole blood was taken from WT mice via cardiac puncture, the red blood cells were lysed, and the leukocytes were cultured with various doses of TNF for 4 h. Leukocytes were then immunostained for neutrophil specific markers (CD45+ Ly6G+) and the expression of CCR7 on blood neutrophils was analysed by flow cytometry. Data are from n = 6-17 mice from 16 independent experiments. Statistically significant differences between stimulated and unstimulated treatment groups are indicated by asterisks: *, $P < 0.05$; **, $P < 0.01$. Significant differences between stimulated groups are indicated by hash signs: #, $P < 0.05$. Statistical significance was determined using one-way ANOVA.

4.3.4 Effects of the CCL21:CCR7 chemokine axis on neutrophil migration during TNF- or CFA+Ag-induced inflammation of the cremaster muscle

Having discovered that tissue-infiltrated neutrophils up-regulate CCR7 on their cell surface, it was hypothesised that this chemokine receptor may mediate the migration of neutrophils through lymphatic vessels of the cremaster muscles. To address the potential involvement of the CCL21:CCR7 axis, neutrophil migration responses at 16 h-post inflammation in WT and CCR7KO mice were examined and compared by confocal microscopy analysis following TNF- or CFA+Ag-stimulation. The other CCR7 ligand, CCL19, will not be looked at in this study as it has been shown to not be constitutively expressed at steady-state or in inflamed tissue-associated LECs (Russo et al., 2013; Vigl et al., 2011). For this purpose, WT and CCR7KO mice were given i.s injections of TNF or an emulsion of CFA+Ag as before. Control mice received i.s injections of PBS. Sixteen hours later, cremaster muscles were dissected away, fixed and immunostained with anti-PECAM-1, anti-LYVE-1 and anti-MRP14 mAbs to label blood vasculatures, lymphatic vasculatures and neutrophils, respectively. DLNs were immunostained with anti-MECA-79, anti-LYVE-1 and anti-MRP14 mAbs to label HEVs, lymphatic vasculatures and neutrophils, respectively. Images obtained from confocal microscopy were analysed on IMARIS software.

Following TNF-stimulation, 3D-reconstructed confocal images showed no difference in the neutrophil numbers within the interstitial surrounding postcapillary venules at 16 h post-i.s. injection in CCR7KO mice (**Figure 4.8A, right**) as compared to WT mice (**Figure 4.8A, left**). Quantification of these confocal microscopy images demonstrated that neutrophil transmigration across postcapillary venules was unaffected in CCR7KO mice 16 h post-i.s. injection (**Figure 4.8B**). Strikingly, 3D-reconstructed confocal images showed neutrophil migration into the lymphatic vessels of CCR7KO mice was almost completely absent (**Figure 4.9A, right**) as compared to WT mice (**Figure 4.9A, left**). Quantification of these confocal images showed that trafficking of neutrophils into cremaster lymphatic vessels was completely inhibited (~97% suppression) in CCR7KO animals as compared to WT animals (**Figure 4.9B**). Furthermore, and in contrast to WT animals, the level of dLN-infiltrated neutrophils was not increased in CCR7KO mice after stimulation with TNF, as observed by confocal microscopy (**Figure 4.10A, bottom**). Quantification of 3D-reconstructed confocal images showed that TNF induced an

increase of neutrophils in WT mice as compared to WT control group (**Figure 4.10B**). However, neutrophil numbers within dLNs of TNF-stimulated CCR7KO mice was comparable to neutrophil infiltration exhibited by the unstimulated control group (**Figure 4.10B**).

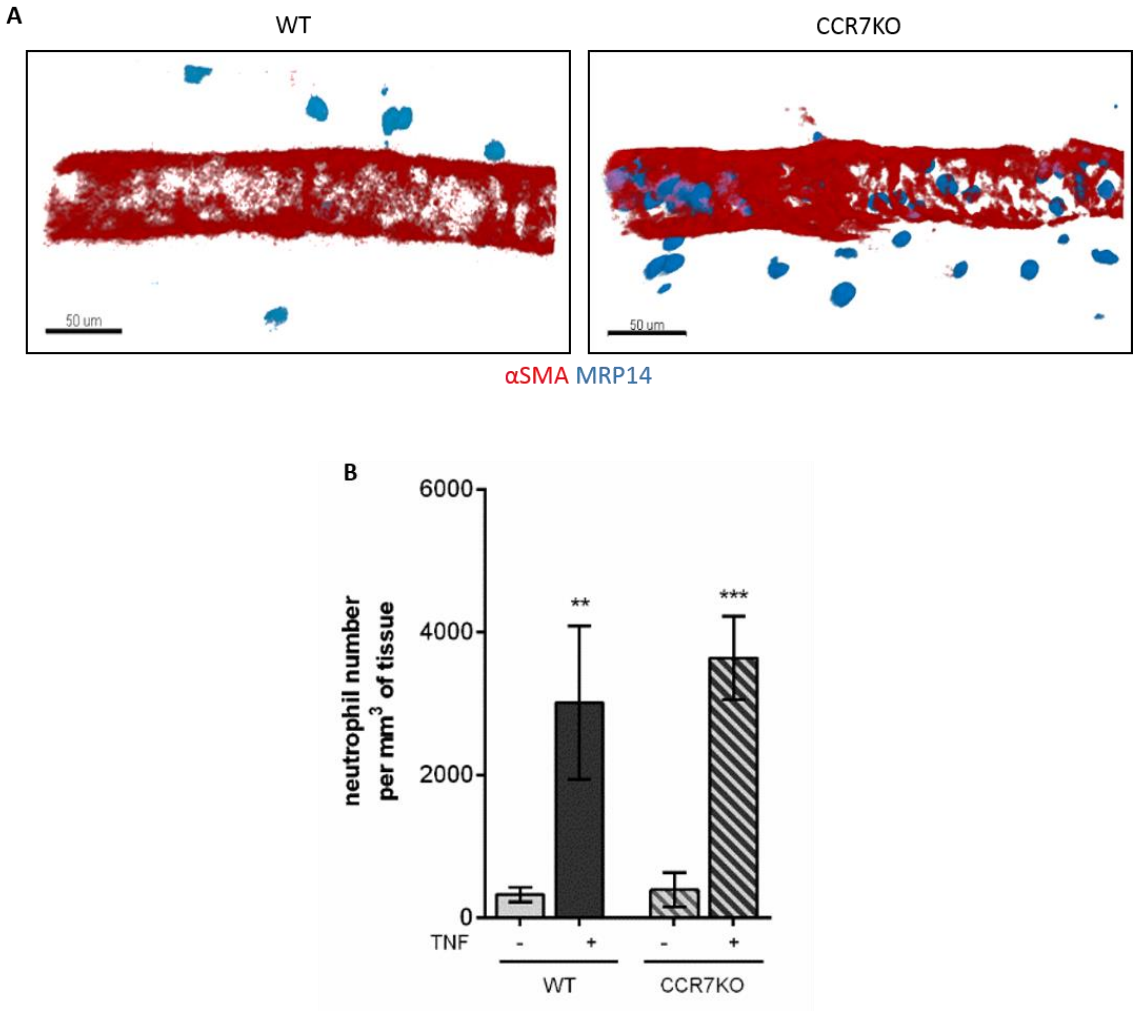

Figure 4.8: Neutrophil migration responses across postcapillary venules of WT and CCR7KO mice in unstimulated and TNF-stimulated cremaster muscles. WT C57BL/6 and CCR7KO mice were subjected to TNF-induced inflammation of the cremaster muscles. Control mice received i.s injection of PBS. Sixteen hours later, cremaster muscles were dissected away, fixed and immunostained for αSMA (red) and MRP14 (blue) to label blood vasculatures and neutrophils, respectively, before being analysed by confocal microscopy and IMARIS. (A) Representative 3D-confocal images of neutrophil extravasation from postcapillary venules following TNF-stimulation of the cremaster muscles of WT (left) and CCR7KO (right) mice. Bar: 50 μm. (B) Number of extravasated neutrophils in inflamed cremaster muscles of unstimulated and TNF-stimulated WT and CCR7KO mice. Data are expressed as mean ± SEM from at least 4 independent experiments with n = 5-12 animals per group (~10-12 images per pair of cremasters for confocal microscopy). Statistically significant difference between stimulated and unstimulated animals are indicated by asterisks: *, P< 0.05; **, P< 0.01; ***, P < 0.001; ****, P < 0.0001. Statistical significance was determined using one-way ANOVA. Statistical significance was determined using one-way ANOVA.

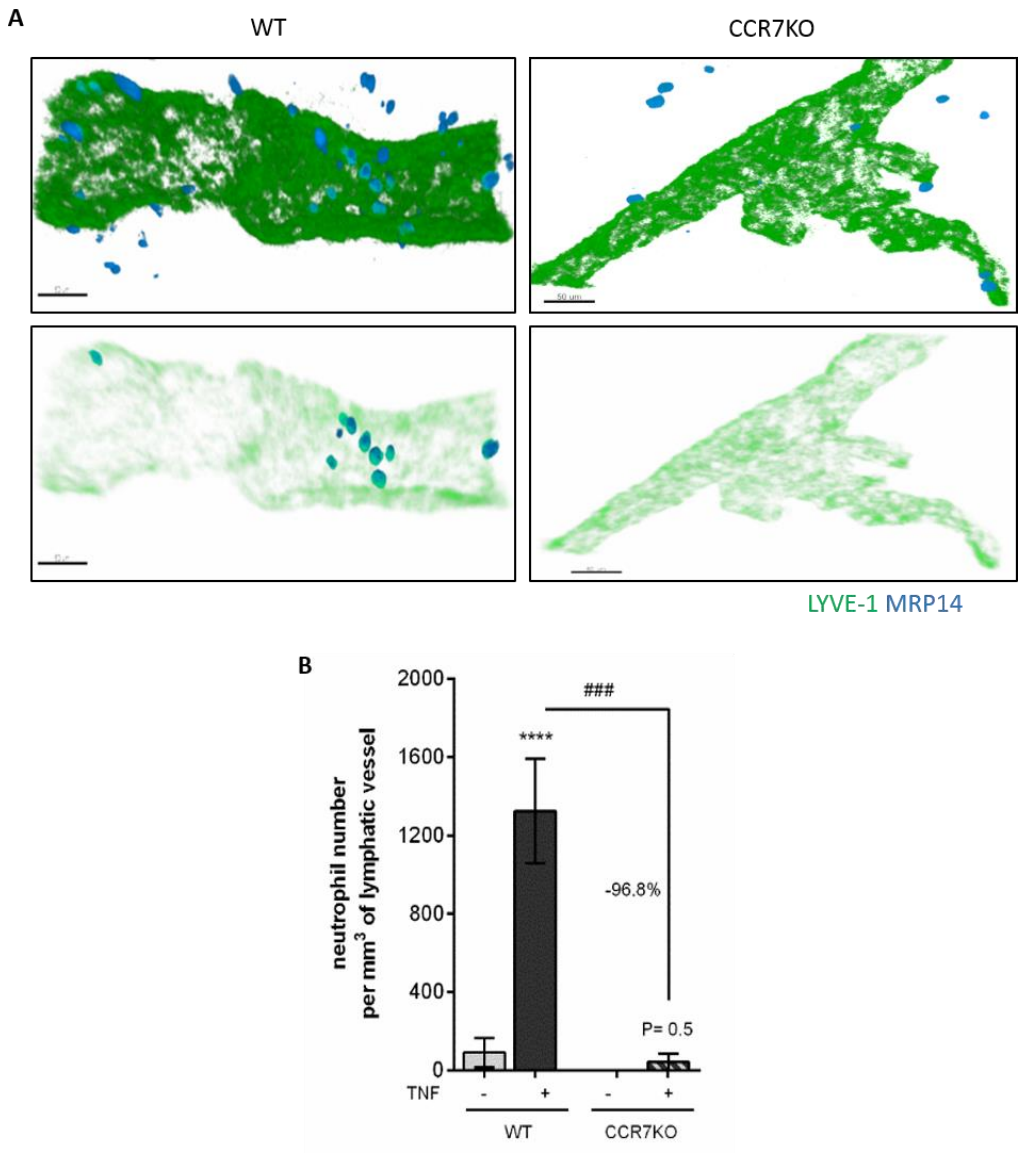

Figure 4.9: Neutrophil migration responses into lymphatic vessels of WT and CCR7KO mice in unstimulated and TNF-stimulated cremaster muscles. WT C57BL/6 and CCR7KO mice were subjected to TNF-induced inflammation of the cremaster muscles. Control mice received i.s injection of PBS. Sixteen hours later, cremaster muscles were dissected away, fixed and immunostained for LYVE-1 (green) and MRP14 (blue) to visualise the lymphatic vasculatures and neutrophils, respectively, before being analysed by confocal microscopy and IMARIS. Neutrophil migration responses were visualised by confocal microscopy and analysed by IMARIS Software. (A) Representative 3D-confocal images of neutrophils within lymphatic vessels following TNF-stimulation of the cremaster muscles of WT (left panels) and CCR7KO (right panels) mice. The top panels show all neutrophils present in the field of view. The bottom panels show neutrophils present only within the lymphatic vessels. Bars: 50 µm. (B) Number of neutrophils within the cremaster lymphatic vessels of unstimulated and TNF-stimulated WT and CCR7KO mice. Data are expressed as mean ± SEM from at least 4 independent experiments with n = 5-12 animals per group (~10-12 images per pair of cremasters for confocal microscopy). Statistically significant differences between stimulated and unstimulated animals are indicated by asterisks: ****, $P < 0.0001$. Statistically significant differences between WT and CCR7KO mice are indicated by hash signs: ###. $P < 0.001$. Statistically significant differences between WT and CCR7KO mice are indicated by hash signs: ###. $P < 0.001$. Statistical significance was determined using one-way ANOVA.

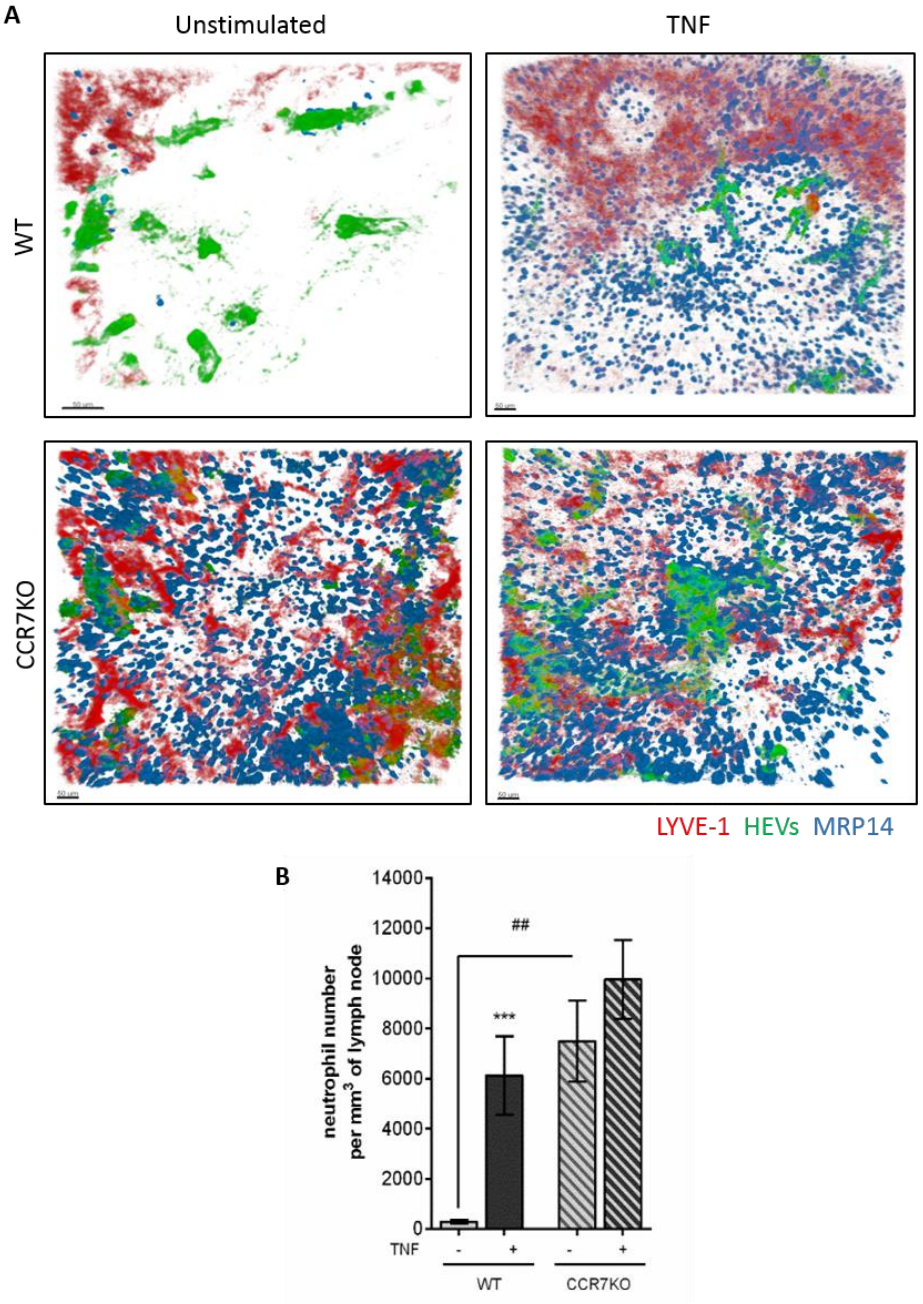

Figure 4.10: Neutrophil migration responses into dLNs of WT and CCR7KO mice in unstimulated and TNF-stimulated cremaster muscles. WT C57BL/6 and CCR7KO mice were subjected to TNF-induced inflammation of the cremaster muscles. Control mice received i.s injection of PBS. Sixteen hours later, cremaster dLNs were dissected away and immunostained for LYVE-1, HEVs and MRP14. Neutrophil migration responses were visualised by confocal microscopy and analysed by IMARIS Software. (A) The figure shows representative 3D-confocal images of neutrophil infiltration into the dLNs of unstimulated (left panel) and TNF-stimulated (right panel) of WT (top panel) and CCR7KO (bottom panel) mice. Bars: 50 µm. (B) Number of neutrophils within the cremaster dLNs of unstimulated and TNF-stimulated WT and CCR7KO mice. Data are expressed as mean ± SEM from at least 4 independent experiments with n = 5-12 animals per group (~10-12 images per pair of dLNs for confocal microscopy). Statistically significant difference between stimulated and unstimulated animals are indicated by asterisks: ***, $P < 0.001$. Statistically significant differences between WT and CCR7KO mice are indicated by hash signs: ##. $P < 0.01$. Statistical significance was determined using one-way ANOVA. Statistical significance was determined using one-way ANOVA.

Similarly, quantification of 3D-reconstructed confocal images showed that CFA+Ag-stimulation of both WT and CCR7KO mice resulted in no differences in neutrophil extravasation between both groups (**Figure 4.11A**). However, unlike TNF-stimulation, quantification of confocal images showed that neutrophil migration into lymphatic vessels was suppressed by ~75% in CCR7KO mice as compared to WT mice in response to CFA+Ag-induced inflammation (**Figure 4.11B**). Furthermore, comparable to TNF-stimulation, quantification of confocal images proved that neutrophil infiltration into dLNs following CFA+Ag stimulation was not increased in CCR7KO mice (**Figure 4.11C**). In particular, CCR7KO animals exhibited ~25 times more LN-infiltrated neutrophils than WT mice in unstimulated conditions.

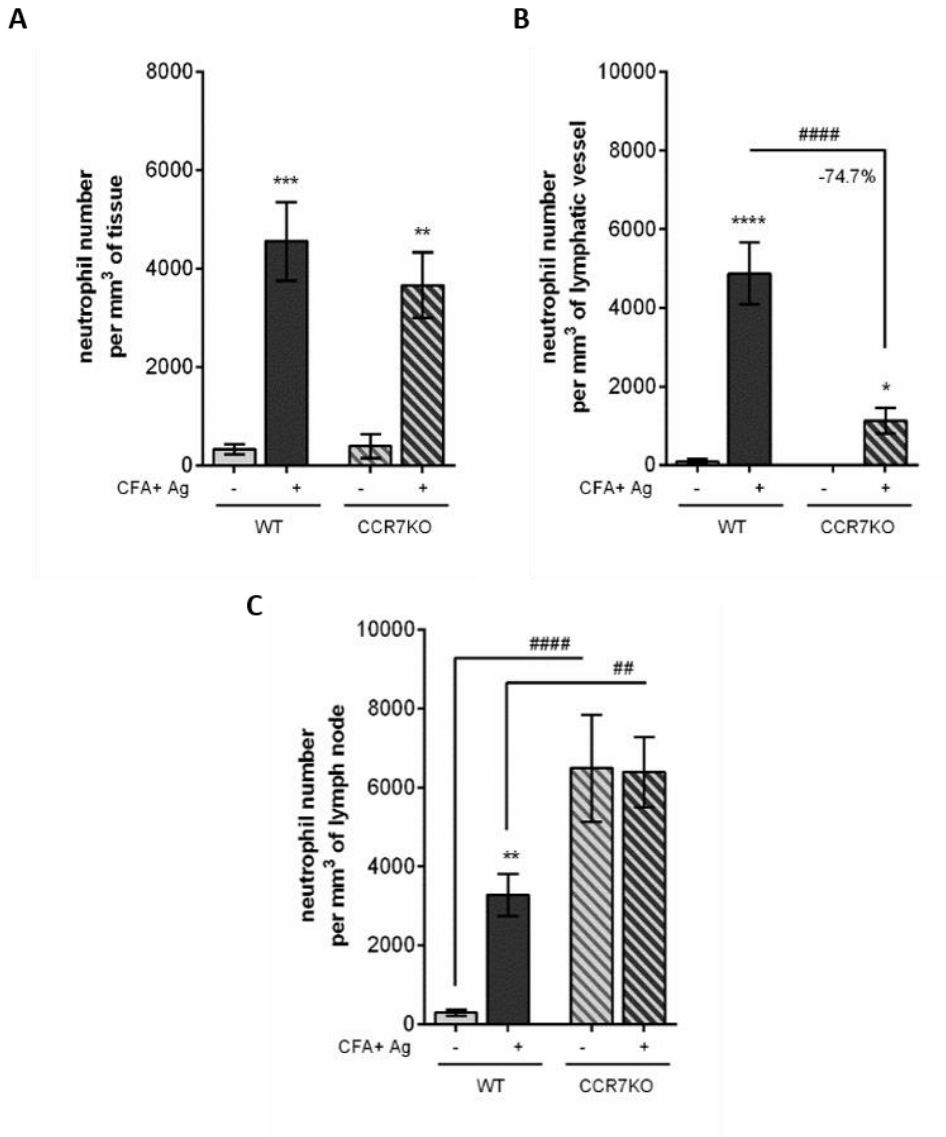

Figure 4.11: Neutrophil migration responses of WT and CCR7KO mice in unstimulated and CFA+Ag-stimulated cremaster muscles. WT C57BL/6 and CCR7KO mice were subjected to CFA+Ag-induced inflammation of the cremaster muscles. Control mice received i.s injection of PBS. Sixteen hours later, cremaster muscles and dLNs were dissected away, fixed and immunostained for αSMA/MECA-79, LYVE-1 and MRP14 to visualise the blood vasculatures, lymphatics and neutrophils, respectively. Neutrophil migration responses were visualised by confocal microscopy and analysed by IMARIS Software. (A) Number of extravasated neutrophils in unstimulated and CFA+Ag-stimulated WT and CCR7KO mice. (B) Number of neutrophils within the cremaster lymphatic vessels of unstimulated and CFA+Ag-stimulated WT and CCR7KO mice. (C) Number of neutrophils found in the dLNs of unstimulated and CFA+Ag-stimulated WT and CCR7KO mice. Data are expressed as mean±SEM of n = 5-12 animals (~10-12 images per pair of cremaster/dLNs for confocal microscopy) per group from at least 4 independent experiments. Statistically significant difference between stimulated and unstimulated animals are indicated by asterisks: **, $P < 0.01$; ***, $P < 0.001$; ****, $P < 0.0001$. Statistically significant differences between WT and CCR7KO mice are indicated by hash signs: ##, $P < 0.01$; #### < 0.0001. Statistical significance was determined using one-way ANOVA. Statistical significance was determined using one-way ANOVA.

CCR7KO chimeric mice

To overcome the abnormal architecture of dLNs in CCR7KO mice, chimeric animals were generated by injecting lethally irradiated WT mice with bone marrow hematopoietic cells from either WT or LysM-eGFP-CCR7KO animals. These mice were then subjected to 16 h CFA+Ag-stimulation.

Chimerism of reconstituted mice were also checked alongside each experiment. Briefly, whole blood was taken from LysM-eGFP mice (used as positive controls) or chimeric mice via cardiac puncture before being lysed in preparation for immunostaining. Blood leukocytes were immunostained for neutrophil specific markers (CD45+ Ly6G+) and their expression of GFP was analysed by flow cytometry. Since bone marrow cells from CCR7KO animals exhibiting GFP+ neutrophils were used for reconstitution of chimeras, GFP+ neutrophils would indicate the level of chimerism. Comparisons in the percentage of circulating neutrophils in WT and CCCR7KO chimeras proved to be the same (~30%) (**Figure 4.12A**). Phenotypic analysis also confirmed all CCR7KO chimeras were fully reconstituted with the intended bone marrow hematopoetic cells as shown by the presence of ~98% of GFP+ neutrophils within the circulation (**Figure 4.12B**).

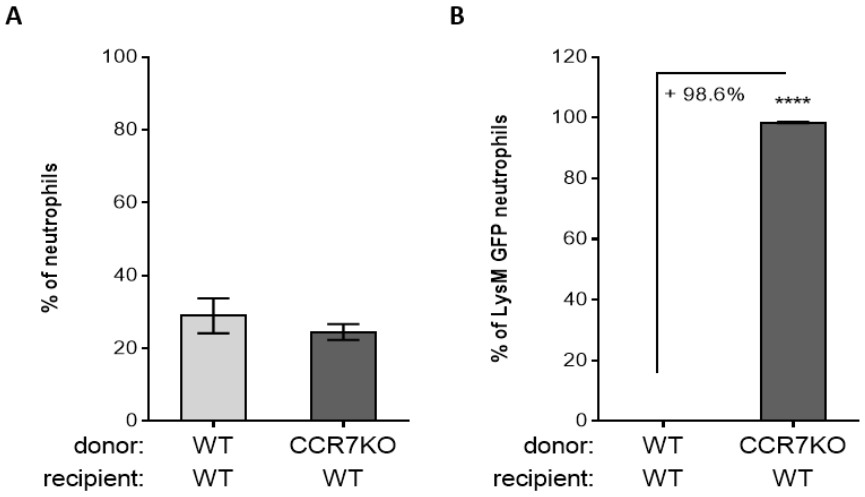

Figure 4.12: Phenotypic analysis of blood neutrophils from WT and CCR7KO chimeric mice. Blood leukocytes from LysM-eGFP or chimeric animals were immunostained for neutrophils specific markers (CD45+ Ly6G+) and their expression of GFP was analysed by flow cytometry. (A) Percentage of circulating neutrophils in WT→WT and CCR7KO→WT chimeric mice. (B) Percentage of GFP+ neutrophils in WT→WT and CCR7KO→WT chimeric mice. CCR7KO-LysM-eGFP Data are expressed as mean±SEM of N = 4-6 animals per group from at least 4 independent experiments. Statistically significant difference between stimulated and unstimulated animals are indicated by asterisks: ****, $P < 0.0001$. Statistical significance was determined using Student's t-test.

Following this, neutrophil migration responses in these chimeras were investigated 16 h post-antigen sensitisation. Similar to a full KO, chimeric mice exhibiting CCR7KO neutrophils showed no difference in neutrophil extravasation across blood vasculatures post-i.s. injection, although there was an increased tendency towards there being more neutrophils in the interstitial tissue of CCR7KO chimeras as compared to WT chimeras (**Figure 4.13A**). Also reminiscent to full CCR7KO mice, CCR7KO chimeric mice showed a reduced migration of these leukocytes (~76% less) into lymphatic vessels as compared to WT chimeric mice (**Figure 4.13B**). Interestingly, unlike full KO mice, CCR7KO chimeras showed a reduced number of neutrophils infiltrating the dLNs (~62% less) as compared to control littermates (**Figure 4.13C**). This suggests that neutrophils from CCR7KO donor cells are not able to migrate efficiently into the dLNs of the WT recipient mice.

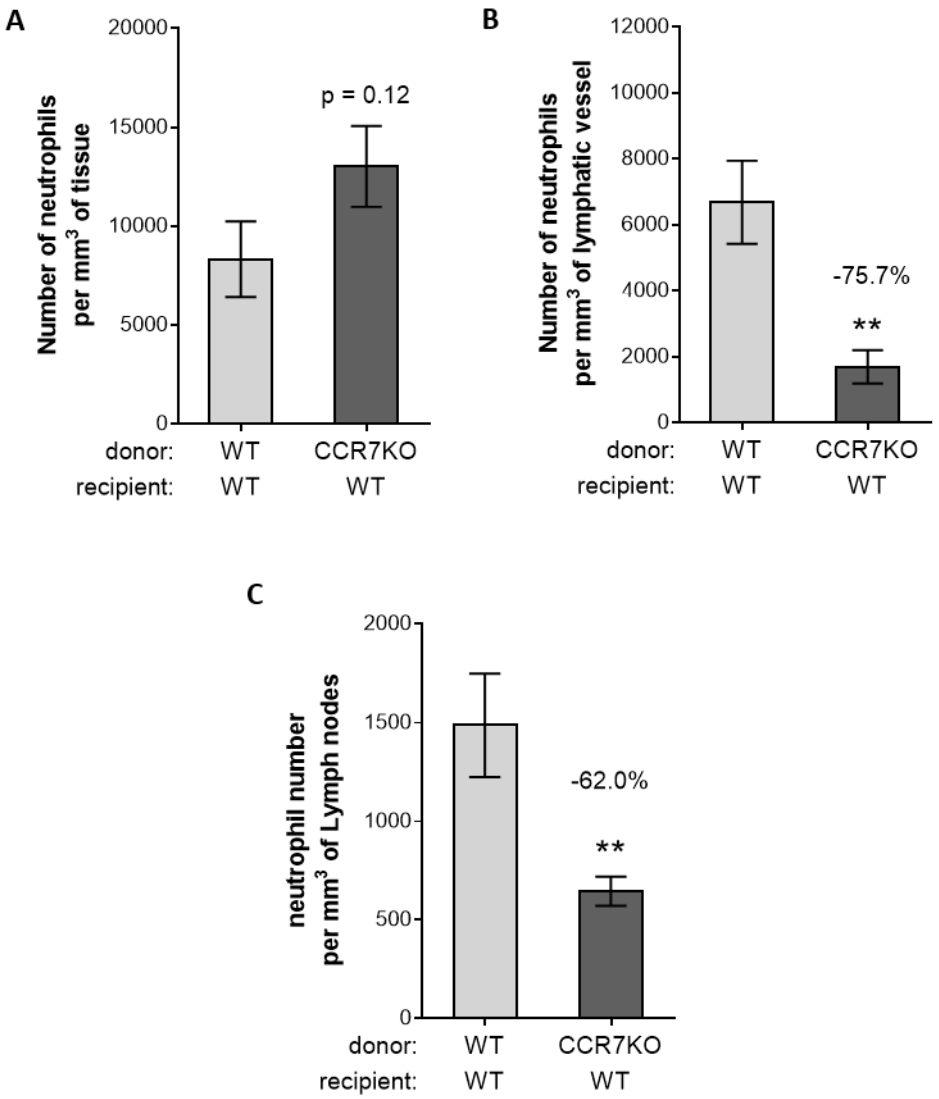

Figure 4.13: Neutrophil migration responses of WT and CCR7KO chimeric mice following CFA+Ag-induced inflammation in the cremaster muscle. Neutrophil migration into the lymphatic system of the cremaster muscle following antigen sensitisation with complete Freund's adjuvant (CFA+Ag) was induced in chimeric animals exhibiting neutrophils deficient in CCR7. Neutrophil migration responses were visualised by confocal microscopy and analysed by IMARIS Software. (A) Number of extravasated neutrophils in cremaster muscles at 16 h post-CFA+Ag-stimulation from chimeric animals receiving bone marrow transplant of WT or CCR7KO donor mice and as quantified by confocal microscopy. (B) Number of neutrophils within cremaster lymphatic vessels at 16 h post-CFA+Ag-stimulation from chimeric animals receiving bone marrow transplant of WT or CCR7KO donor mice and as quantified by confocal microscopy. (C) Number of neutrophils found in the dLNs of chimeric animals receiving bone marrow transplant of WT or CCR7KO donor mice as quantified by confocal microscopy 16 h post-CFA+Ag-stimulation. Data are expressed as mean±SEM of N = 6-7 animals (~10-12 images per pair of cremaster/dLNs for confocal microscopy) images per cremaster for confocal microscopy) per group from at least 5-10 experiments. Statistically significant differences between WT and CCR7KO chimeric mice are indicated by asterisks: **, $P < 0.01$. Statistical significance between groups was determined using Student's t-test.

4.3.4.1 Investigating the cause of abnormal neutrophil trafficking into dLNs of CCR7KO mice

Due to the previous observation that CCR7KO mice had an increase in neutrophil numbers within dLNs in steady state conditions (**Figure 4.10** & **Figure 4.11**), the possible cause of this abnormal trafficking of neutrophils in these mice was explored. As CXCR4 has previously been shown to be a key regulator of neutrophil release from the bone marrow (Eash et al., 2010), the potential role of the CXCL12:CXCR4 chemokine axis in abnormal trafficking of neutrophils into dLNs of full CCR7KO mice was investigated. For this purpose, neutrophil migration responses at 16 h-post inflammation in CCR7KO mice were examined by confocal microscopy analysis following CFA+Ag-stimulation. Briefly, CCR7KO mice were given i.s injections of TNF or an emulsion of CFA+Ag as before. Unstimulated control mice received i.s injections of PBS. Four hours post-i.s. injection, i.s. of the CXCR4-specific inhibitor, AMD3100, or vehicle control (PBS) was carried out. Sixteen hours post-i.s. injection, cremaster muscles were dissected away, fixed and immunostained as described in the previous sections. Images obtained from confocal microscopy were analysed on IMARIS software.

Following CFA+Ag-stimulation, 3D-reconstructed confocal images showed much higher neutrophil numbers within the interstitial surrounding postcapillary venules at 16 h post-i.s. injection in AMD3100-treated CCR7KO mice (**Figure 4.14A, right**) as compared to vehicle controls (**Figure 4.14A, left**). Quantification of confocal microscopy images demonstrated that neutrophil transmigration across postcapillary venules was significantly increased (~100% more) in AMD3100-treated CCR7KO mice at 16 h post-i.s. injection as compared to vehicle controls (**Figure 4.14B**). Interestingly, 3D-reconstructed confocal images showed similar numbers of neutrophils within lymphatic vessels of AMD3100-treated CCR7KO mice (**Figure 4.15A, right**) as compared to the vehicle control-treated mice (**Figure 4.15A, left**). Quantification of these confocal images demonstrated that trafficking of neutrophils into cremaster lymphatic vessels remained unchanged in AMD3100-treated CCR7KO animals as compared to the vehicle control-treated mice (**Figure 4.15B**). Strikingly, 3D-reconstructed confocal images showed that neutrophil migration into the dLNs of AMD3100-treated CCR7KO mice (**Figure 4.16A, right**) was lower as compared to vehicle control-treated mice (**Figure 4.16A, left**). Quantification of these confocal images proved that treatment with the CXCR4 antagonist resulted in a significant reduction (~63% less) in the number of neutrophils infiltrating CCR7KO dLNs (**Figure 4.16B**).

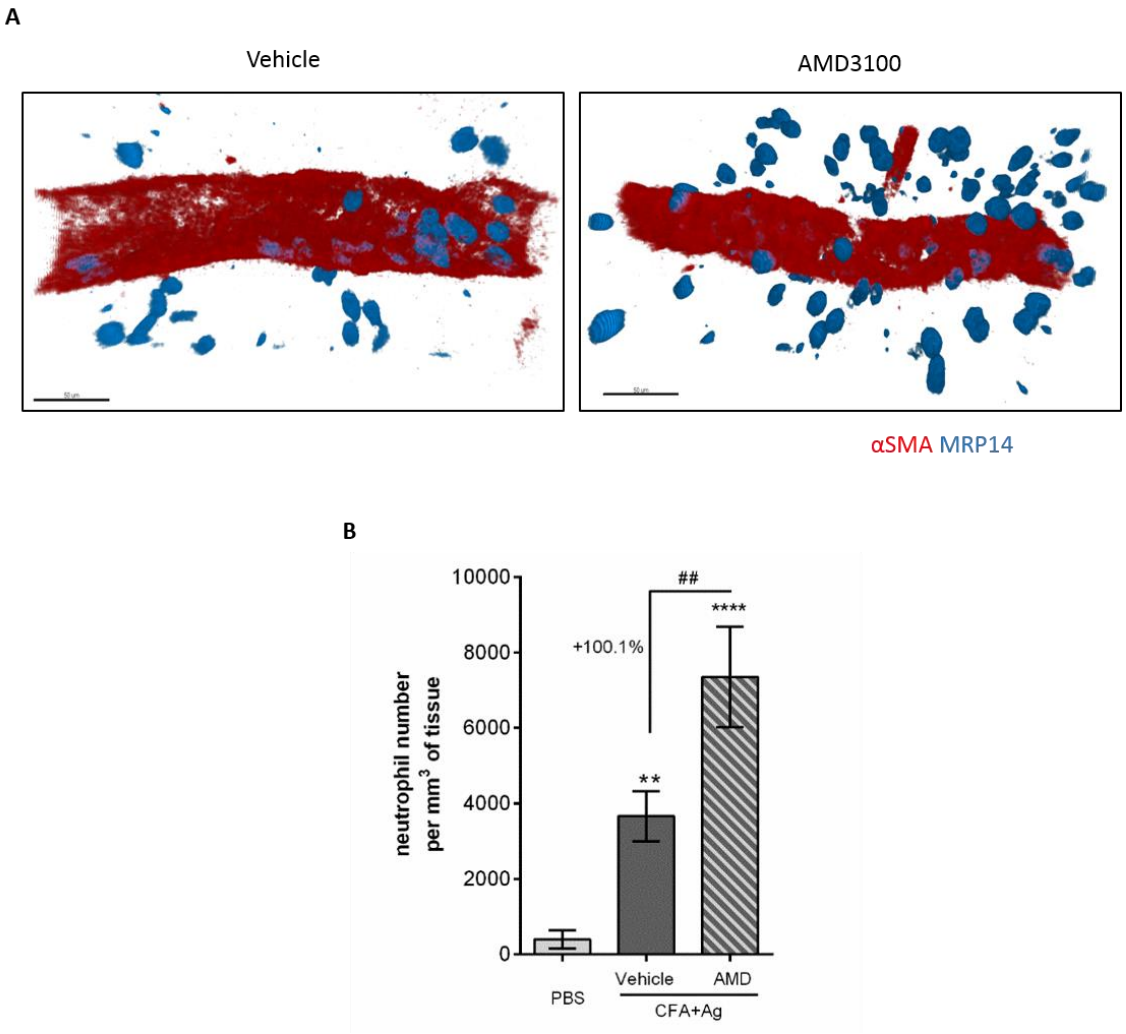

Figure 4.14: Neutrophil migration responses across postcapillary venules of CCR7KO mice following *in vivo* blockade of the chemokine receptor CXCR4 in CFA+Ag-stimulated cremasters. CCR7KO mice were subjected to CFA+Ag-induced inflammation of the cremaster muscles. Four hours later, mice received an i.s. injection of the CXCR4 specific inhibitor AMD3100 (10mg/kg) or PBS vehicle as control. Sixteen hours post-stimulation, cremaster muscles were dissected away, fixed and immunostained for αSMA (red) and MRP14 (blue) to visualise the blood vasculatures and neutrophils, respectively. Neutrophil migration responses were visualised by confocal microscopy and analysed by IMARIS Software. (A) Representative 3D-confocal images of neutrophil extravasation from postcapillary venules in the cremaster muscles of CFA+Ag-stimulated CCR7KO mice injected i.s with vehicle control (left) or treated with AMD3100 (right). Bars: 50 µm. (B) Number of extravasated neutrophils in inflamed cremaster muscles. Data are expressed as mean ± SEM from at least 4 independent experiments with n = 5-12 animals per group (~10-12 images per pair of cremasters for confocal microscopy). Statistically significant differences between stimulated and unstimulated animals are indicated by asterisks: **, P< 0.01; ****, P < 0.0001. Statistically significant differences between vehicle control and AMD3100 treated groups are indicated by hash signs: ##, P < 0.01. Statistical significance was determined using one-way ANOVA.

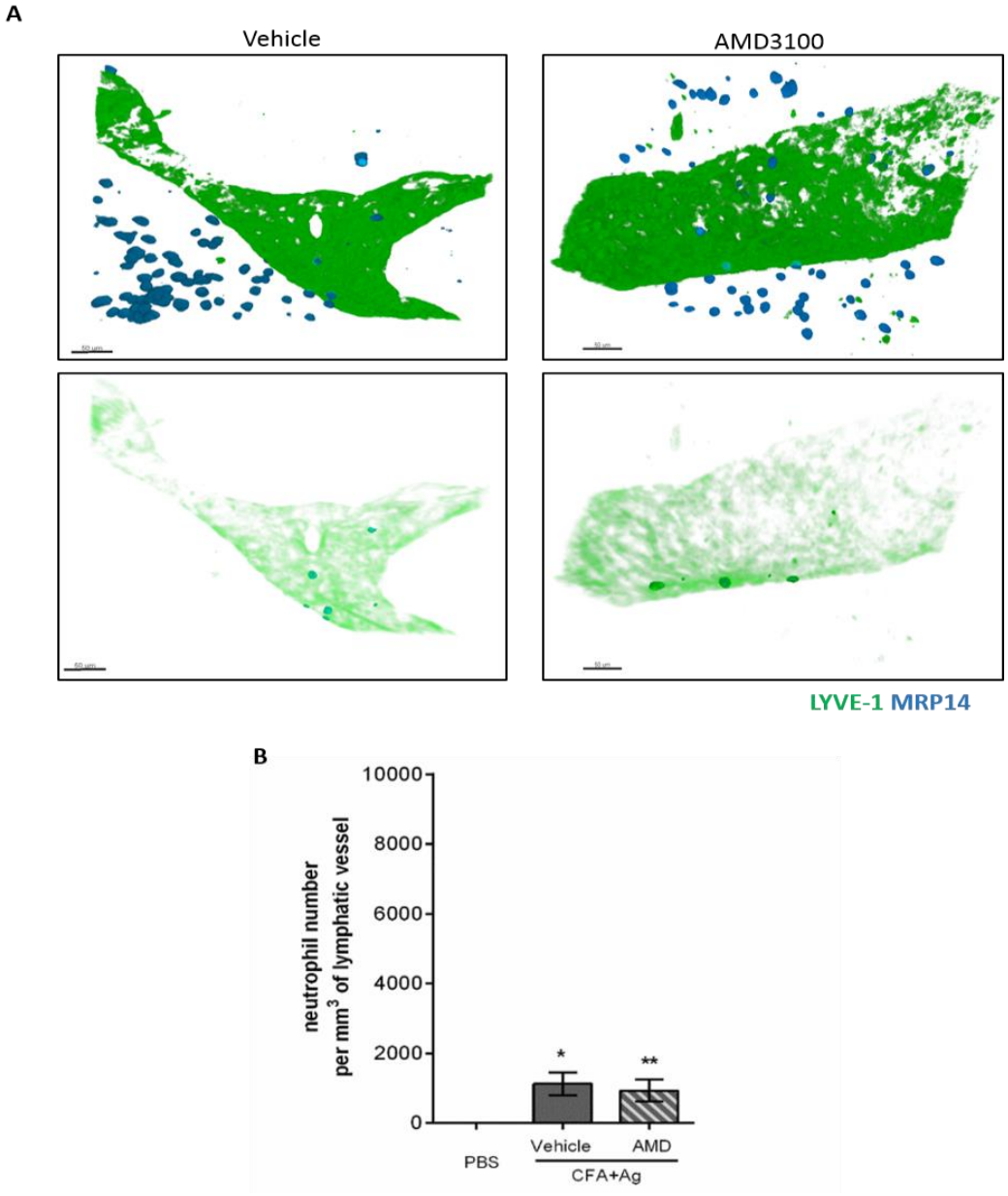

Figure 4.15: Neutrophil migration responses into lymphatic vessels of CCR7KO mice following *in vivo* blockade of the chemokine receptor CXCR4 in CFA+Ag-stimulated cremasters. WT C57BL/6 mice were subjected to CFA+Ag-induced inflammation of the cremaster muscles. Four hours later, mice received an i.s. injection of the CXCR4 specific inhibitor AMD3100 (10mg/kg) or PBS vehicle as control. Sixteen hours post-i.s. injection, cremaster muscles were dissected away, fixed and immunostained for LYVE-1 (green) and MRP14 (blue) before being analysed by confocal microscopy and IMARIS. (A) Representative 3D-confocal images of neutrophils within lymphatic vessels in the cremaster muscles of CFA+Ag-stimulated CCR7KO mice injected i.s with vehicle control (left) or treated with AMD3100 (right). The top panels show all neutrophils present in the field of view. The bottom panels show neutrophils present only within the lymphatic vessels. Bars: 50 µm. (B) Number of neutrophils within the cremaster lymphatic vessels of unstimulated and CFA+Ag-stimulated mice treated with AMD3100 or vehicle control. Data are expressed as mean ± SEM from at least 4 independent experiments with n = 5-12 animals per group (~10-12 images per pair of cremasters for confocal microscopy). Statistically significant differences between stimulated and unstimulated animals are indicated by asterisks: *, $P< 0.05$; **, $P< 0.01$. Statistical significance was determined using one-way ANOVA.

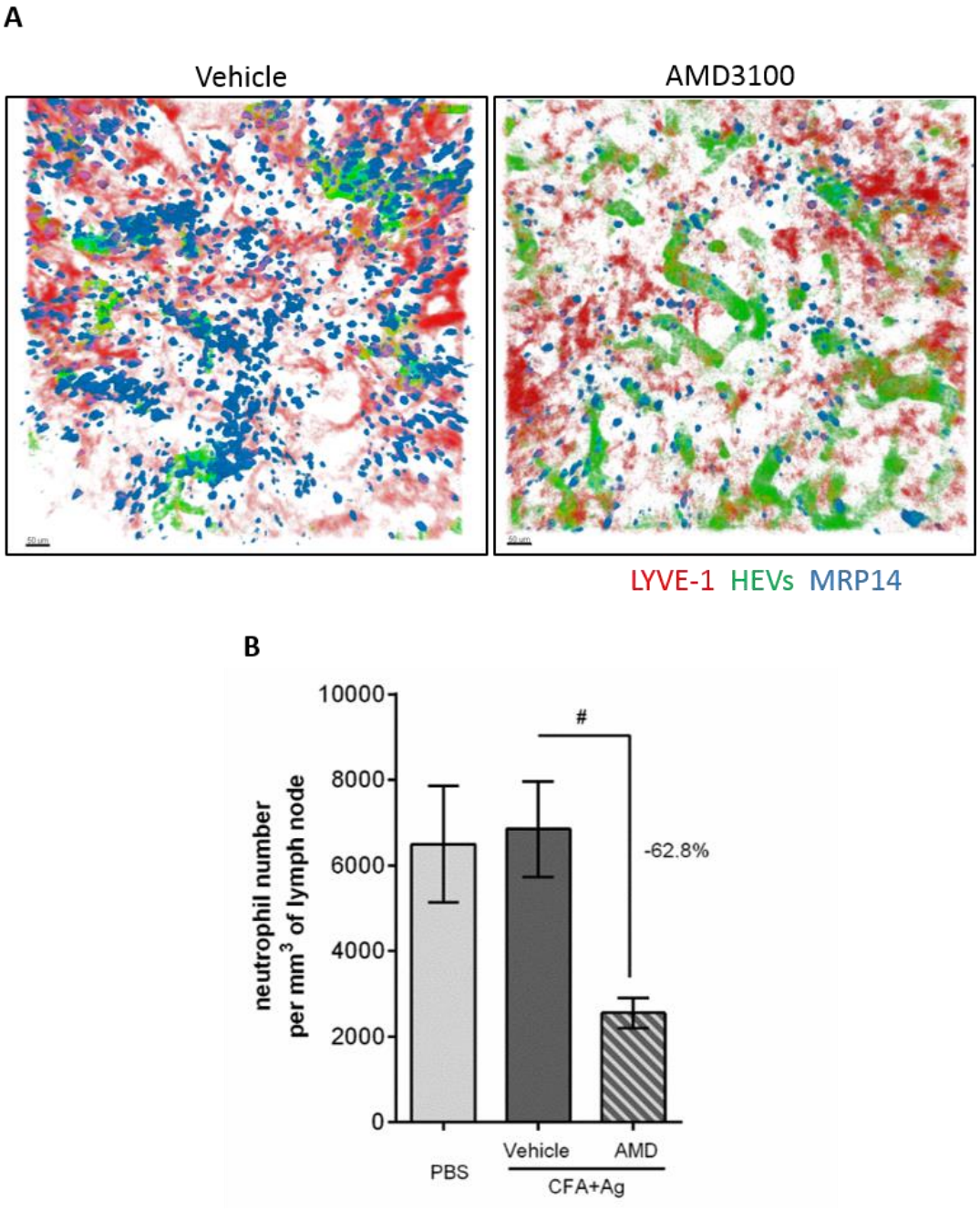

Figure 4.16: Neutrophil migration responses into dLNs of CCR7KO mice following *in vivo* blockade of the chemokine receptor CXCR4 in CFA+Ag-stimulated cremasters. CCR7KO mice were subjected to CFA+Ag-induced inflammation of the cremaster muscles. Four hours later, mice received an i.s. injection of the CXCR4 specific inhibitor AMD3100 (10mg/kg) or PBS vehicle as control. Sixteen hours post-stimulation, dLNs (inguinal) were dissected away, fixed and halved before being immunostained for LYVE-1 (red), HEVs (green) and MRP14 (blue) before being analysed by confocal microscopy and IMARIS software. (A) The figure shows representative 3D-confocal images of neutrophil infiltration into the dLNs of CCR7KO mice that received i.s injection of vehicle control Ab (left) or treatment of AMD3100 (right) Bars: 50 μm. (B) Number of neutrophils found in the dLNs. Data are expressed as mean±SEM from at least 4 independent experiments with n = 5-12 animals per group (~10-12 images per pair of dLNs for confocal microscopy). Statistically significant differences between vehicle control and AMD3100 treated groups are indicated by hash signs: #, $P < 0.05$. Statistical significance was determined using one-way ANOVA.

Subsequently, investigations were carried out to determine differences in the phenotype of neutrophils relating to CXCR4 between WT and CCR7KO animals under basal conditions. For this purpose, whole blood was taken from mice via cardiac puncture and lysed. Blood leukocytes were immunostained for neutrophil specific markers (CD45+ Ly6G+) and their surface expression of CXCR4 was analysed by flow cytometry. Draining LNs of WT and CCR7KO mice were also dissected away, snap-frozen and homogenised for analysis of CXCL12 expression levels by ELISAs. Flow cytometry analysis showed no differences in the percentage of circulating neutrophils (**Figure 4.17A**) and expression levels of CXCR4 (**Figure 4.17B**) between WT and CCR7KO mice. Interestingly, CXCL12 generation at basal levels was significantly increased in dLNs of CCR7KO mice as compared to dLNs of WT mice (**Figure 4.17C**). This response could be related to ~25 times more neutrophil infiltration seen in dLNs of CCR7KO mice as compared to WT mice in unstimulated conditions, discovered previously (**Figure 4.10B**). This supports the hypothesis that CXCR4 signalling contributes to neutrophil homing to LNs through HEVs (Gorlino et al., 2014).

Overall, these results implicate the CCL21:CCR7 chemokine axis in promoting neutrophil migration into lymphatic vessels. TNF was also shown to be particularly important in promoting neutrophil migration into lymphatic vessels in a CCR7-dependent manner as complete inhibition of this process occurred following TNF-stimulation, with only partial inhibition seen following antigen sensitisation. Additionally, the CXCL12:CXCR4 chemokine axis was shown to be responsible for the high number of neutrophils found within dLNs of CCR7KO mice under steady state conditions.

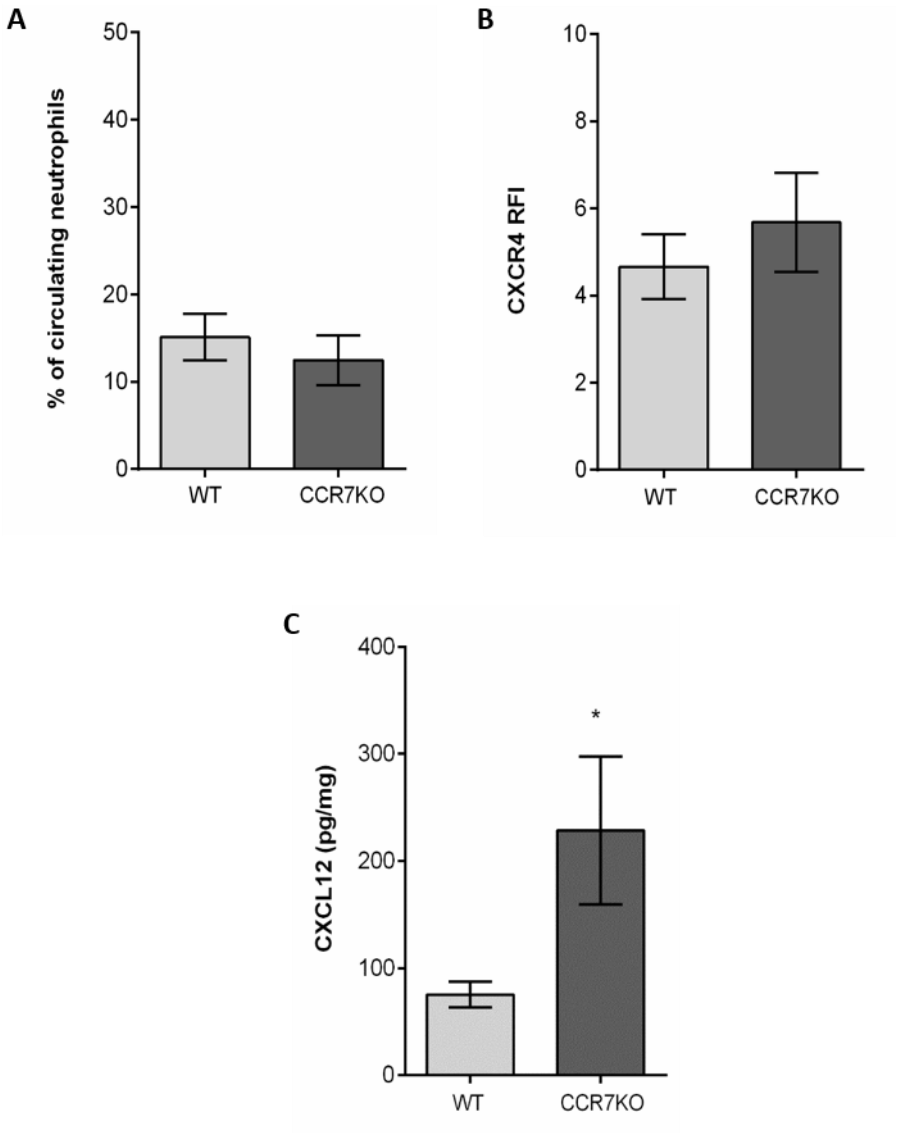

Figure 4.17: CXCR4 expression on neutrophils and CXCL12 generation in dLNs of naïve WT and CCR7KO mice. Blood leukocytes from WT or CCR7KO animals were immunostained for neutrophils specific markers (CD45+ Ly6G+) and their expression of CXCR4 on blood neutrophils was analysed by flow cytometry. Draining LNs were dissected away from naïve WT and CCR7KO mice, snap-frozen and homogenised for quantification of CXCL12 generation by ELISA. (**A**) Percentage of circulating neutrophils in naive WT and CCR7KO mice. (**B**) Relative fluorescence intensity (RFI) of CXCR4 expression on blood circulating neutrophils. (**C**) CXCL12 release as quantified by ELISA. Data are expressed as mean ± SEM of N = 4-6 animals per group from at least 4 independent experiments. Statistically significant difference between WT and CC7KO animals are indicated by asterisks: *, $P < 0.05$. Statistical significance was determined using Student's T-test.

4.4 Discussion

It is now well established that neutrophils contribute to the shaping of the adaptive immune response against a huge repertoire of foreign antigens or infectious agents following their rapid migration into the lymphatic system (Gorlino et al., 2014; Hampton et al., 2015; Lynskey et al., 2015). However, unlike neutrophil transmigration across blood vessel walls, the mechanisms of this migratory response is massively understudied. The results from this chapter demonstrated that neither CXCL1:CXCR1/2 nor CXCL12:CXCR4 chemokine axes were found to play significant roles in neutrophil migration across the lymphatic endothelium during antigen sensitisation at the time-points analysed (8 and 16 h). However, the CCL21:CCR7 chemokine axis was implicated in promoting neutrophil migration into lymphatic vessels. Additionally, neutrophils were shown to be primed to upregulate CCR7 surface expression post-stimulation with CFA+Ag *in vivo* and this response was associated with an inverse relationship to increasing doses of TNF-stimulation *in vitro*. Finally, the CXCL12:CXCR4 chemokine axis was shown to be responsible for the high number of neutrophils found within dLNs of CCR7KO mice under steady state conditions. In general, the main finding within this chapter is the discovery of a previously unknown role for endogenous TNF in orchestrating neutrophil trafficking into lymphatic vessels of inflamed tissues in a strictly CCR7-dependent manner *in vivo*.

It was demonstrated earlier on in Chapter 3 of this thesis that TNF could induce the rapid migration of neutrophils from inflamed tissues into lymphatic vessels. These studies were then extended to a model of antigen sensitisation characterised by the generation of endogenous TNF. CFA+Ag-stimulation was also associated with rapid neutrophil migration into lymphatic vessels, a response that was impaired in mice deficient in both TNF receptors, p55 and p75. Furthermore, the use of chimeric animals demonstrated that TNF acts directly on leukocytes to induce this neutrophil migration response.

In the present study, TNF was demonstrated to trigger migration of neutrophils into lymphatic vessels in a strictly CCR7-dependent, with complete inhibition of neutrophil migration into lymphatic vessels seen following TNF-induced inflammation in CCR7KO mice. The role of CCR7 in neutrophil recruitment into the lymphatic system was first demonstrated by Beauvillain *et al*. in a model of intradermal immunisation (Beauvillain et al., 2011). In accordance with their study, intracellular stores of CCR7 were detected in murine blood neutrophils. However, in the present study, a significant up-regulation of

CCR7 on the cell surface was found on neutrophils recruited into inflamed tissues following antigen sensitisation as compared to blood neutrophils within the circulation. Since Eruslanov *et al*. recently showed a similar up-regulation of CCR7 on human neutrophils in a tumour model (Eruslanov et al., 2014), data from the present study suggests that neutrophils are being primed for enhanced chemokine receptor expression. Two of the key activators of neutrophils, GM-CSF and IL-17, have both been shown to prime neutrophils for potent migration towards CCL21 and CCL19 *in vitro* (Beauvillain et al., 2011). However, unlike the release of TNF demonstrated in Chapter 3, the generation of these cytokines in inflamed cremaster muscles could not be detected at any of the time-points analysed *in vivo* (**Appendix 2**), thus suggesting the predominant role of TNF in this response *in vivo*. An up-regulation found in CCR7 expression on the surface of neutrophils following TNF-stimulation *in vitro* provides further evidence of neutrophil priming by TNF. Differences in the extent of CCR7 up-regulation on primed neutrophils were seen between *in vitro* and *in vivo* experimental setups. Although similar levels of CCR7 was found on the surface of blood neutrophils for both setups, CCR7 upregulation was found on the surface of neutrophils isolated from cremaster muscles in the *in vivo* setup. This could be due to differences in the techniques used, where leukocytes were primed within the animals (i.s. injection of CFA+Ag) before being isolated for CCR7 staining in the *in vivo* setup, whilst leukocytes were isolated from blood and stimulated in culture before staining in the *in vitro* setup. This suggests that the microenvironment is important for the appropriate priming of neutrophils. Additionally, the inflammatory stimulus (and timepoints) used in both setups were different. CFA+Ag (16 h) was used in the *in vivo* setup whilst TNF (4 h) was used for the *in vitro* setup. The use of CFA+Ag *in vivo* results in a multifactorial response, where pro-inflammatory cytokines such as Tyrode's salt solution was used to constantly superfuse cremaster muscles during all experiments.

IL-1β, IFNγ and TNF are produced (Awate et al., 2013). Additionally, other cells within the microenvironment could also be activated leading to the production of other factors leading to more efficient priming of neutrophils. The use of only TNF in the *in vitro* setup may not be as potent as CFA+Ag at priming neutrophils thus could be a reason for why CCR7 is up-regulated more in the *in vivo* setup. To confirm this, further experiments using neutrophils isolated from the cremaster muscles could be stimulated with TNF *in vitro*.

Interestingly, high basal levels of neutrophils within dLNs of naïve CCR7O mice was observed as compared to naïve WT mice, with inflammation of the cremaster muscles with TNF or CFA+Ag not further increasing the number of neutrophils found in the LNs. This abnormal trafficking was seen despite there being no difference in the percentage of circulating neutrophils between WT and CCR7KO mice. An explanation for this could be due to the 2.5-fold increase in generation of CXCL12 in the dLNs of naïve CCR7KO mice as compared to WT mice, thus causing more neutrophil homing to occur in the former. Spontaneous autoimmunity in CCR7KO mice could also be driving this phenotype although this will have to be further investigated. This study has demonstrated for the first time that high levels of CXCL12 within dLNs contributes to neutrophil migration via HEVs in steady-state.

Whilst the expression of the chemokine receptor for CXCL12, CXCR4, was similar in both WT and CCR7KO mice, treatment with the CXCR4 antagonist, AMD3100, resulted in a significant reduction in the number of neutrophils infiltrating the dLNs of CCR7KO mice; this was not found to be the case for neutrophil migration into lymphatic vessels upon CFA+Ag inflammation. This is in accordance with previous studies that demonstrated the importance of CXCR4 in the homing of neutrophils from inflamed skin to LNs via HEVs (Gorlino et al., 2014; Hampton et al., 2015). Chimeric mice generated to overcome this abnormal trafficking of neutrophils into dLNs further confirmed that CCR7KO neutrophils were unable to migrate into lymphatic vessels in a WT environment, although further experiments will have to be carried out to determine if CXCL12 levels are normal in these mice.

Since the role of CCR7 in neutrophil trafficking into the lymphatic system has proven to be controversial, other chemokine:chemokine receptor axes were investigated. The CXCL12:CXCR4 chemokine axis was recently demonstrated to be involved in neutrophil trafficking to the lymphatic system in a model of bacterial infection with *S. aureus* (Hampton et al., 2015). The current study provided evidence that CXCR4 blockade did not significantly inhibit neutrophil migration into cremaster lymphatic vessels and dLNs upon CFA+Ag-stimulation, thus highlighting potential differences between models. Regarding the higher numbers of neutrophils seen within the inflamed tissues of AMD3100-treated mice, evidence has shown that humans and mice treated with this CXCR4 antagonist or CXCR4-blocking antibodies exhibit a rapid mobilisation of neutrophils into the blood (Broxmeyer et al., 2005; Liles et al., 2003), which in turn potentially leads to more neutrophil transmigration across venular walls.

The potent neutrophil-chemoattractant, CXCL8, has recently been shown to be up-regulated in TNF-stimulated human dermal endothelial cells *in vitro*; and promote human neutrophil migration through a monolayer of LECs (Rigby et al., 2015). In mice, LECs isolated from mouse skin showed an up-regulation of CXCL1 gene expression upon inflammation induced by contact hypersensitivity (Vigl et al., 2011). However, the *in vivo* model in the current study provided clear evidence of the predominant role of CCR7 in neutrophil trafficking into lymphatic vessels following TNF-stimulation. Moreover, local treatment with an anti-CXCL1 blocking mAb did not affect the capacity of neutrophils to enter the lymphatic system upon inflammation *in vivo*. Data from previproteous studies along with the current one highlights differences between *in vivo* and *in vitro* models.

This chapter has shown that chemokine:chemokine receptor axis, CCL21:CCR7, is important for neutrophil migration into lymphatic vessels in both CFA+Ag- or TNF-induced inflammation; the latter signalling of which is crucial for this phenomenon. It is also worth mentioning that at 8 h post-i.s. injection with CFA+Ag, the same partial impairment in neutrophil migration into lymphatic vessels was seen in CCR7KO mice, thus indicating that the decreased number of neutrophils seen within lymphatic vessels at 16 h post-i.s. injection was not due to a time-dependent efflux of neutrophils out of lymphatic vessels to dLNs (**Appendix 1**). This chapter has also shown that the chemokine:chemokine receptor axes, CXCL1:CXCR1/2 and CXCL12:CXCR4, are not involved in neutrophil migration into lymphatic vessels following CFA+Ag-induced inflammation. Collectively, the results in this chapter provide evidence that TNF signalling triggers neutrophil migration into lymphatic vessels in a strictly CCR7-dependent manner. This work has recently been published in Nature Scientific Reports (Arokiasamy et al., 2017).

Limitations of the study

In addition to the other limitations discussed at the end of Chapter 3, the fluorescently conjugated CCR7 antibodies used to analyse this chemokine receptor expression on neutrophils both *in vivo* and *in vitro* did not work under normal staining conditions of either room temperature or 4 °C. This is in accordance with the data sheet and published literature (Ohl, 2004). Due to this, cells had to be incubated with the antibody at 37 °C before the fluorescence was able to successfully be detected by flow cytometry at low levels. Staining at this high temperature could have resulted in the modulation and internalisation of these surface receptors, leading to a loss of fluorescence intensity. Thus,

this may be why such low fluorescence intensities were detected in these experiments. The generation of more efficient CCR7 antibodies or the use of labelled chemokines could have been carried out. However, these were not able to be done due to time constraints.

5 : Glycocalyx and chemokine regulation on lymphatic vessels during inflammation *in vivo*

5.1 Introduction

The glycocalyx is a carbohydrate-enriched layer, which coats all healthy mammalian cells. *In vivo* studies have revealed the glycocalyx of blood capillaries to be a layer of about 0.5 μm thick (Vink and Duling, 1996), with this thickness increasing with vascular diameter, ranging from 2 to 3 μm in small arteries and 4.5 μm in carotid arteries (Megens et al., 2007; van Haaren et al., 2003). The glycocalyx is composed of sugar residues from cell surface membrane glycoproteins, sulphated proteoglycans, alongside their associated GAG side chains. Sugar residues can be specifically characterised by their binding to carbohydrate-binding proteins called lectins. Glycoproteins are also a component of the glycocalyx and include adhesion molecules, selectins and integrins (Reitsma et al., 2007). Proteoglycans are considered to be the "backbone" molecules of the glycocalyx, and consist of a core protein (Reitsma et al., 2007). The core protein is either anchored to the cell membrane (syndecans, glypicans) or secreted into the glycocalyx structure (mimecans, perlecans and biglycans). GAG side chains are bound to these proteoglycans and are comprised of heparan sulfate (HS), chondroitin sulfate (CS), and hyaluronan (HA), with HS being the most abundant in the endothelial glycocalyx (Oohira et al., 1983). GAGs play significant roles by interacting with a variety of proteins within the lumen of blood vessels and are involved in the mediation of numerous physiological and pathological functions, including inflammation. The blood vascular EC (BEC) glycocalyx forms an integral part of the vascular barrier between flowing blood and the EC wall of blood vessels, and is involved in the regulation of leukocyte transmigration following inflammatory stimuli. In particular, HS is involved in the initial adhesion of leukocytes to the endothelium following inflammation by interacting with leukocyte-expressed L-selectin during neutrophil rolling (Wang et al., 2005). Additionally, HS has been shown to be a key controller of chemokine presentation during the recruitment process of lymphocytes and DCs to lymph nodes (Bao et al., 2010). Bao *et al.* demonstrated *in vivo* that CCL21 chemokine presentation in ECs of lymph node HEVs was diminished in transgenic mice exhibiting impairments in HS synthesis, thus reducing immune cell trafficking into dLNs (Bao et al., 2010).

The BEC glycocalyx plays a critical role in many physiological processes, including regulation of vascular permeability, regulation of leukocyte adhesion during TEM, as well as the modulation of inflammatory processes (Kolarova et al., 2014; Reitsma et al., 2007; Tarbell et al., 2005; Wang, 2007). In contrast, the presence of a glycocalyx on lymphatic vasculatures has not really been investigated, thus the role it plays in the context of the lymphatics is poorly understood. Nevertheless, recent emerging evidence has demonstrated that the LEC glycocalyx is present within the luminal side of rat mesenteric collecting lymphatic vessels and is an important element of lymphatic transport (Zolla et al., 2015). Components of the LEC glycocalyx in collecting lymphatic vessels has also been demonstrated to be similar to that of the BEC glycocalyx, thus one would expect the functions of both to be comparable (Zolla et al., 2015). In the context of lymphatic vasculatures, the LEC glycocalyx is thought to maintain permeability, aid lymphocyte rolling, generate a cytokine/chemokine gradient, as well as balance exchanges between lymphatic vessels and the surrounding interstitium (Levick and Michel, 2010; Reitsma et al., 2007; Zolla et al., 2015). It has been reported that collecting lymphatic vessels of aged rats (24 months old) exhibits reduced glycocalyx thickness as compared to those of adult rats (9 months old) (Zolla et al., 2015). This is associated with an increase in the permeability of aged lymphatic vessels, which results in increased extravasation of bacteria and fungi, and a reduced ability to maintain fluid transport (Zolla et al., 2015). This increased capacity of pathogens to escape aged lymphatic vessels could potentially contribute to the decreased ability of the immune system to control infections in aging. This is likely due to pathogens causing more infection and inflammation within the interstitium, as well as not being transported to dLNs, thus resulting in the host being unable to elicit an efficient adaptive immune response.

Owing to a considerable lack of literature available regarding the composition of the glycocalyx on lymphatic vessels, especially in tissue-capillary lymphatics, this chapter aims to contribute to this sparsely studied field by characterising components of the LEC glycocalyx and investigating changes in their expression following inflammation.

5.2 Aims

The LEC glycocalyx is vastly under-studied as compared to the BEC glycocalyx. Whether or not initial lymphatic vessels possess a glycocalyx is, as yet, unknown. This chapter therefore aimed to characterise the LEC glycocalyx by probing for the presence of several endothelial glycocalyx components and if successful, investigate the effects of inflammation on their expression. As HS is the most abundant GAG within the endothelial glycocalyx, its expression will be examined in lymphatic vessels. To tie in with investigations in the previous chapter looking at roles of chemokine:chemokine receptor axes in neutrophil migration into lymphatic vasculatures, particular due to CCR7 being shown to have a key role in TNF-dependent neutrophil migration into lymphatic vessels, CCL21 expression on lymphatic vessels will also be examined. Therefore, the specific aims were to:

- Characterise the composition and distribution of sugar residues on the LEC glycocalyx and compare this with the BEC glycocalyx. This was looked at in naïve mouse cremaster muscles.
- Visualise and investigate the expression of HS and several sugar residues (with the use of the selected lectins) within the LEC glycocalyx following inflammation (i.e. TNF or CFA+Ag) *in vivo*. This was done through the use of several different fluorescent staining methods and confocal microscopy analysis.
- Investigate the expression of the prototypical lymphatic chemokine, CCL21, on lymphatic vessels in relation to the LEC glycocalyx following TNF- or CFA+Ag-induced inflammation *in vivo*, through the use of immunostaining and confocal microscopy analysis.

5.3 Results

5.3.1 Assessment of lectin staining on lymphatic vessels under naïve conditions and comparison with blood vessels

To visualise components of the glycocalyx present on the surface of and within lymphatic vessels in WT cremaster muscles, 2 different methods of staining were tested for specific sugar chains with the use of different lectins: *ex vivo*-fixed and *in vivo*-live staining (as detailed in sections 2.5.2 & 2.5.3, respectively). Briefly, *ex vivo*-fixed staining involved staining with lectins and other antibodies at 4 °C overnight after fixation and permeabilisation of tissues. *In vivo*-live staining involved i.s. injection of lectins and other antibodies for 2 h before harvesting tissues for immediate confocal analysis. Four different lectins were originally tested (**Table 5.1**) but only IB4 (specific to α-D-Galactosyl moieties) and MAL-1 (specific for α2,3-sialylated glycans) positively stained lymphatic vessels. LEL and SNA failed to stain lymphatic vessels (**Appendix 3**), thus were dropped from any further analyses. Binding specificity of lectins were confirmed using competitive sugar binding assays with the use of their inhibitory sugars (**Table 5.1**) to show their staining on lymphatic vessels was specific (**Appendix 4**).

Lectins	Preferred Sugar Specificity	Inhibitory Sugars	Reference
Griffonia simplicifolia Lectin I – isolectin B4 (IB4)	α-D-galactosyl moieties	Galactose	(Goldstein and Winter, 1999)
Maackia amurensis Lectin 1 (MAL-1)	α-2,3 sialic acids moieties on N-linked glycans	Lactose	(Khatua et al., 2013; Wang and Cummings, 1988)
Lycopersicon esculentum (Tomato) Lectin (LEL)	N-Acetylglucosamine$_{2-4}$	Chitin hydrolysate	(Robertson et al., 2015)
Sambucus nigra Agglutinin (SNA)	α-2,6 sialic acids N-Acetylneuraminic$_{2-6}$	Lactose	(Khatua et al., 2013; Shibuya et al., 1987)

Table 5.1: Plant lectins used to assess sugar expression of the glycocalyx present on the lymphatic endothelium, their sugar binding preferences, and their inhibiting sugars. Lectins were chosen for their ability to bind to specific sugar residues on BECs.

Under naïve conditions, 3D-reconstructed confocal images of lymphatic vessels stained with IB4 using both methods showed that different expression patterns occurred, with *in vivo*-live staining (**Figure 5.1A**) resulting in a more diffused staining pattern than *ex vivo*-fixed staining (**Figure 5.1B**). However, quantification of confocal images showed no differences in IB4 staining (α-D-Galactosyl moiety expression) between both methods (**Figure 5.2**). Interestingly, *ex vivo*-fixed staining of IB4 seemed to result in punctuate (dotted) staining, indicating the presence of intracellular stores (**Figure 5.1B**).

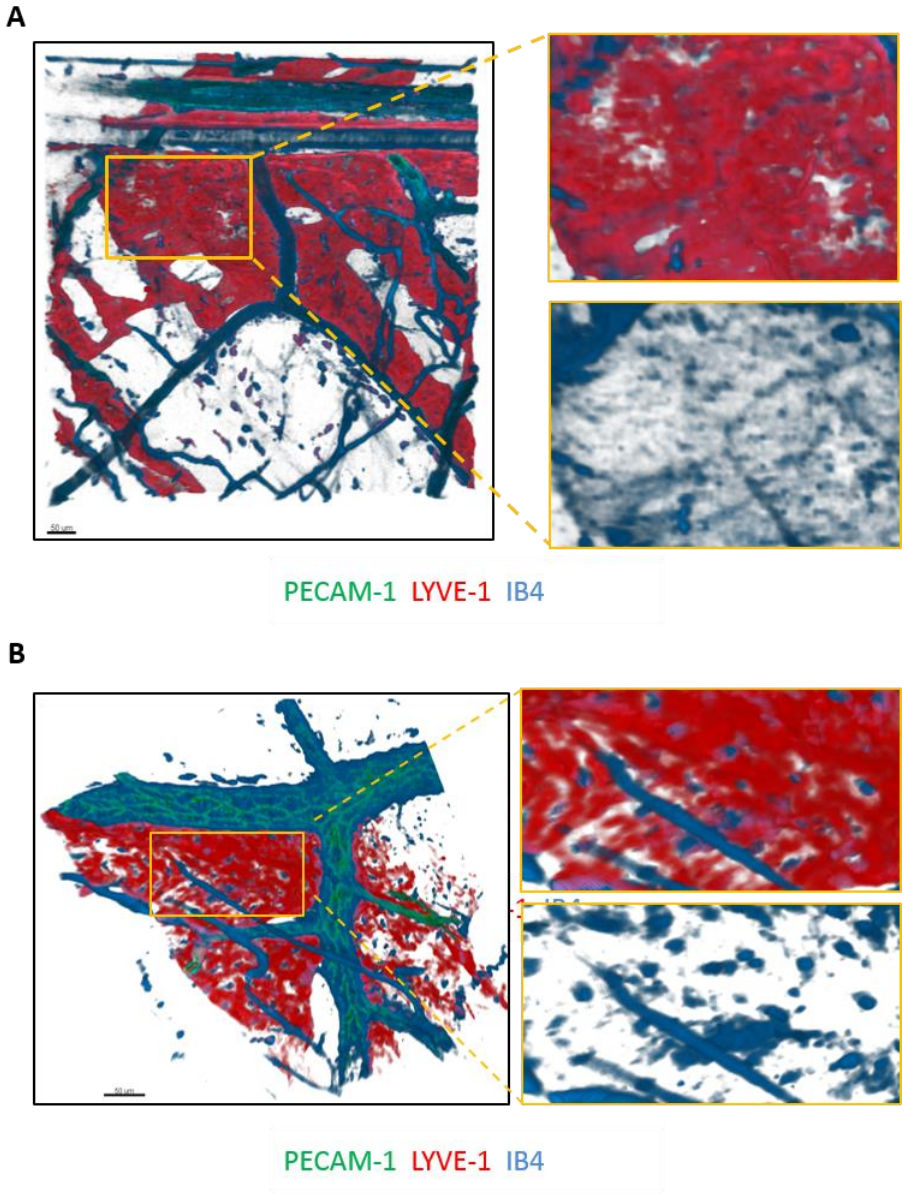

Figure 5.1: Representative binding of IB4 to LECs of mouse cremaster muscles. Cremaster muscles from naïve C57BL/6 WT mice were labelled with anti-PECAM-1 (green), anti-LYVE-1 (red) and IB4 lectin (blue) via both methods. Tissues were analysed on a confocal microscope and IMARIS software. (A-B) Orange boxes on images (left) indicate the region of vessel which is depicted on the zoomed-in images (right). Top right images show LYVE-1 and IB4 staining, and bottom right boxes show just IB4 staining. (A) *In vivo*-live staining via intrascrotal injection (live i.s. route) of IB4. (B) *Ex vivo*-fixed staining (Post-fixation/perm-block) of IB4. Bars: 50 µm.

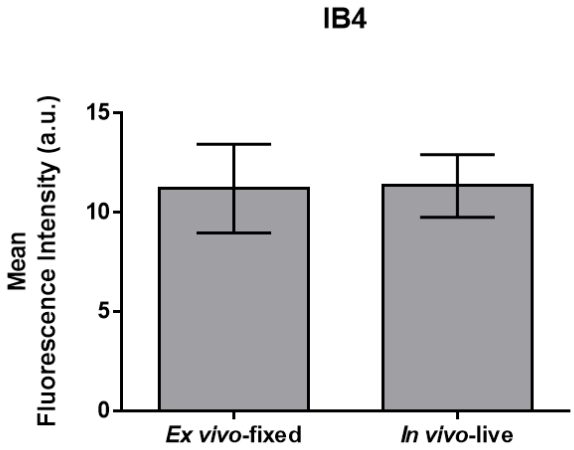

Figure 5.2: MFI of IB4 binding to glycocalyx present on lymphatic vessels under naïve conditions. Quantification of the MFI of IB4 (specific for α D-Galactosyl moieties) binding to the surface of lymphatic vessels using 2 different staining methods – *ex vivo*-fixed and *in vivo*-live. This also represents expression of α D-Galactosyl moieties on the surface of lymphatic vessels. For ex *vivo*-fixed staining, cremaster muscles from naïve WT C57BL/6 mice were dissected away before being labelled post-fixation/permeabilisation with IB4 and LYVE-1 overnight for confocal analysis, respectively. For *in vivo*-live staining, i.s. injections of IB4 and anti-LYVE-mAb were given to naïve WT C57BL/6 mice before cremaster muscles were dissected away and fixed for confocal analysis. IB4 binding was quantified by creating isosurfaces on lymphatic vessels to determine the MFI of lectin binding on vessels. Data are expressed as mean ± SEM from at least 8-10 vessels/animals, with at least 3 animals per group from 4 independent experiments. Statistical significance was determined using one-way ANOVA.

3D-reconstructed confocal images of lymphatic vessels stained with MAL-1 using both methods showed that *ex vivo-fixed* staining (**Figure 5.3A**) and *in vivo*-live staining (**Figure 5.3B**) resulted in similar distribution of these lectins under naïve conditions. Quantification of these confocal images confirmed that staining of MAL-1 (N-linked α2,3-sialylated glycans expression) using *ex vivo*-fixed and *in vivo*-live staining methods were both at similar levels (**Figure 5.4**).

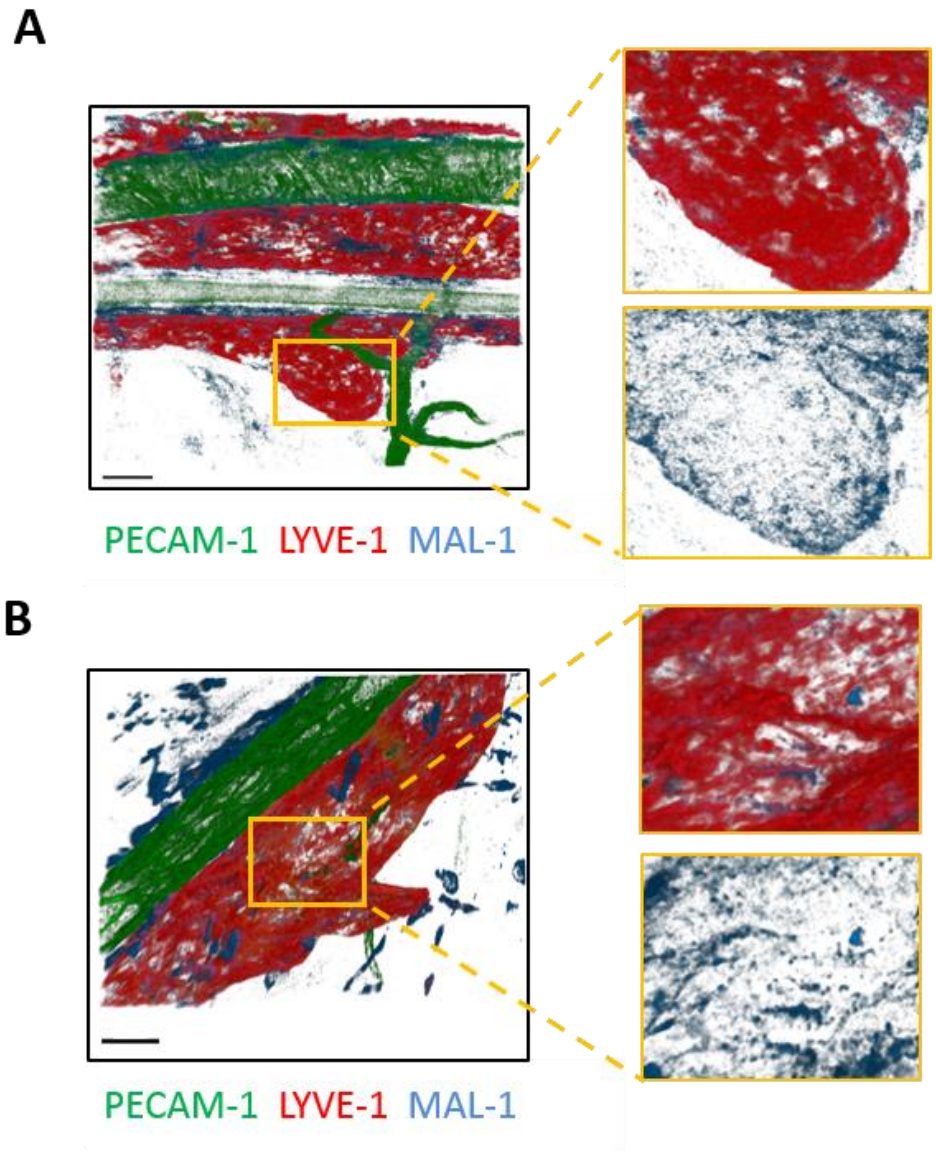

Figure 5.3: Representative binding of MAL-1 to LECs of mouse cremaster muscles. Cremaster muscles from naïve C57BL/6 WT mice were labelled with anti-PECAM-1 (green), anti-LYVE-1 (red) and MAL-1 lectin (blue) via 3 different methods. Tissues were analysed on a confocal microscope and IMARIS software. (A-B) Orange boxes on images (left) indicate the region of vessel which is depicted on the zoomed-in images (right). Top right images show LYVE-1 and MAL-1 staining, and bottom right boxes show just MAL-1 staining. (A) *Ex vivo*-fixed staining (Post-fixation/perm-block) of MAL-1. (B) *In vivo*-live staining via intrascrotal injection (live i.s. route) of IB4. Bars: 50 μm.

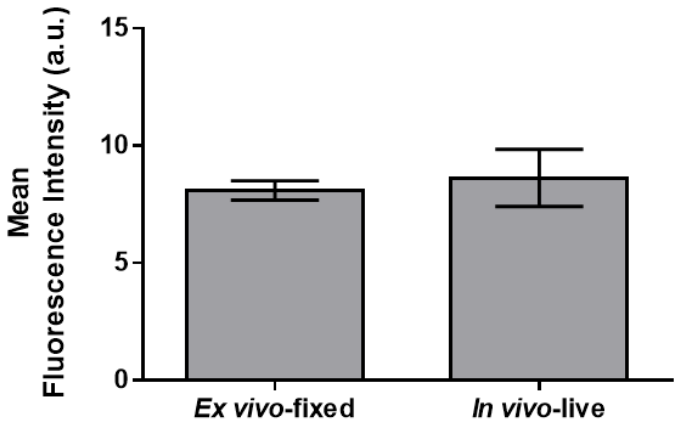

Figure 5.4: MFI of MAL-1 binding to glycocalyx present on lymphatic vessels under naïve conditions. Quantification of the MFI of MAL-1 (specific for α2,3-sialylated glycans) binding to the surface of lymphatic vessels using 2 different staining methods – *ex vivo*-fixed and *in vivo*-live. This also represents expression of α2,3-sialylated glycans on the surface of lymphatic vessels. For ex *vivo*-fixed staining, cremaster muscles from naïve WT C57BL/6 mice were dissected away before being labelled post-fixation/permeabilisation with MAL-1 and LYVE-1 overnight for confocal analysis, respectively. For *in vivo*-live staining, i.s. injections of MAL-1 and anti-LYVE-mAb were given to naïve WT C57BL/6 mice for 2 h before cremaster muscles were dissected away and fixed for confocal analysis. MAL-1 binding was quantified by creating isosurfaces on lymphatic vessels to determine the MFI of lectin binding on vessels. Data are expressed as mean ± SEM from at least 8-10 vessels/animals, with 3 animals per group from 3 independent experiments. Significant differences groups are indicated by asterisks: **, $P < 0.01$; ****. Statistical significance was determined using one-way ANOVA.

Finally, 3D-reconstructed images of IB4 staining on blood vessels using the *ex vivo*-fixed staining method showed that α D-Galactosyl moieties were distributed homogeneously on blood vessels (**Figure 5.5A**). 3D-reconstructed images also showed that MAL-1 staining (α2,3-sialylated glycans expression) on blood vessels was more patchy and heterogeneous as compared to IB4 (**Figure 5.5B**). Quantification of these images using IMARIS software, and comparisons with the previous results of lectin staining on lymphatic vessels revealed that IB4 staining on blood vessels was significantly higher (~3 fold) than on lymphatic vessels. In contrast, MAL-1 staining was significantly higher (~1.5 fold) on lymphatic vessels, as compared to blood vessels (**Figure 5.6**).

Overall, this section has demonstrated the presence of 2 types of sugars in the glycocalyx present on/within the lymphatic endothelium, namely α-D-Galactosyl moieties and sialylated N-linked glycans, by fluorescent staining with lectins *in vivo* and *ex vivo*. Furthermore, it has provided evidence of differences in the distribution and localisation

of different sugar chains on lymphatic vessels; MAL-1 staining of the N-linked α2,3-sialylated glycans was shown to be more homogenous on/within LECs as compared to IB4 staining of α-D-Galactosyl moieties. Finally, it has also highlighted differences in the specific organisation of sugars on both blood and lymphatic vasculatures.

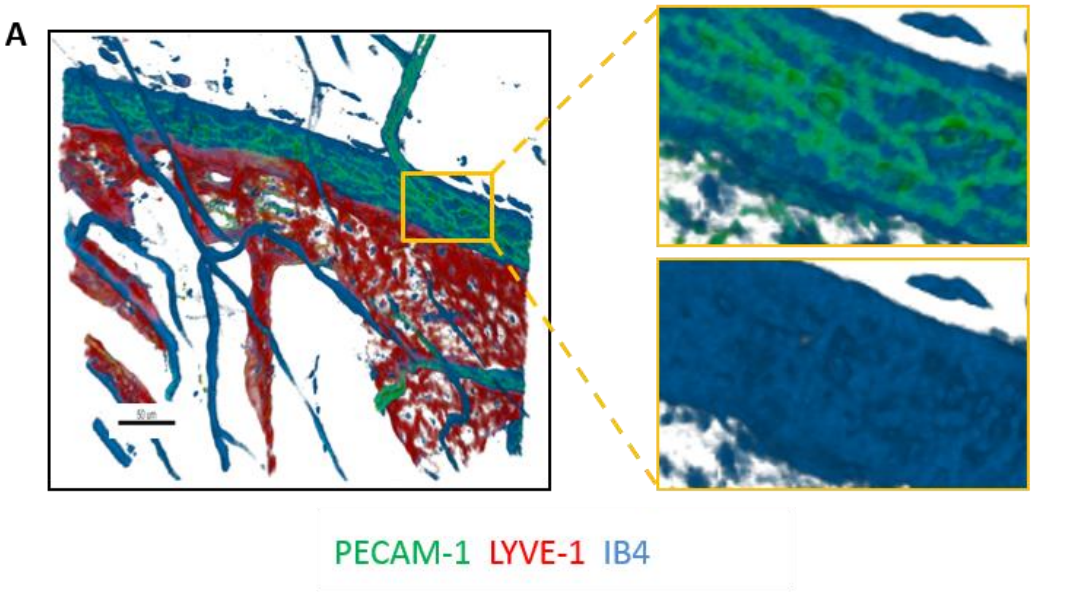

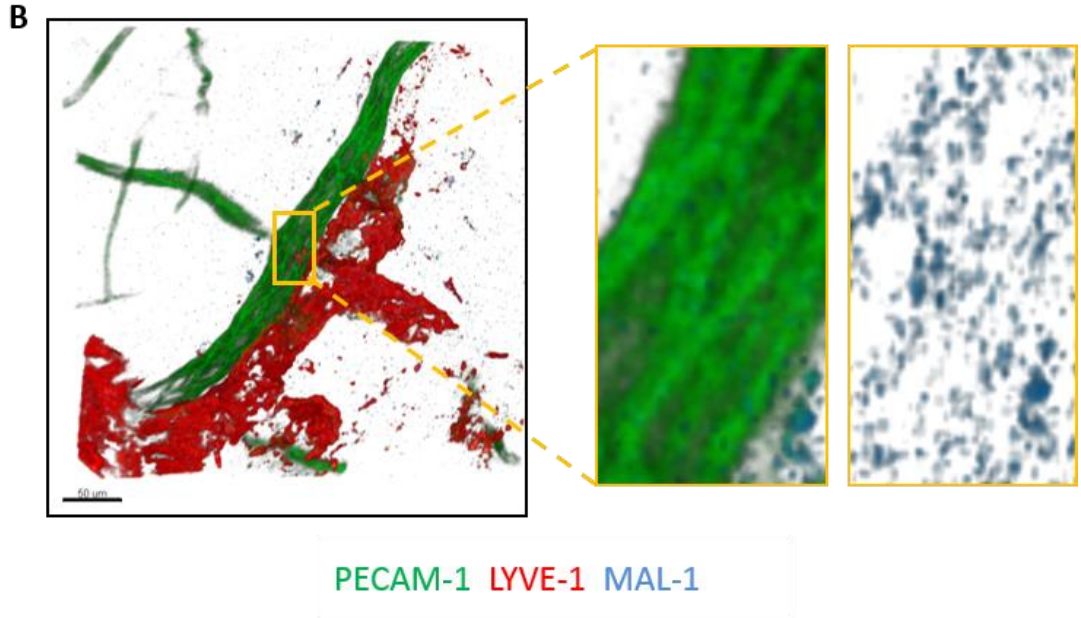

Figure 5.5: Representative confocal images of IB4 and MAL-1 binding to glycocalyx present on blood vessels under naïve conditions. Representative 3D-reconstructed confocal images of (A) IB4 (specific for α-D-Galactosyl moieties) and (B) MAL-1 (specific for α2,3-sialylated glycans) binding to the surface of blood vessels using *ex vivo*-fixed staining. For ex *vivo*-fixed staining, cremaster muscles from naïve WT C57BL/6 mice were dissected away before being labelled post-fixation/permeabilisation with IB4/MAL-1, and for PECAM-1and LYVE-1 overnight for confocal analysis, respectively.

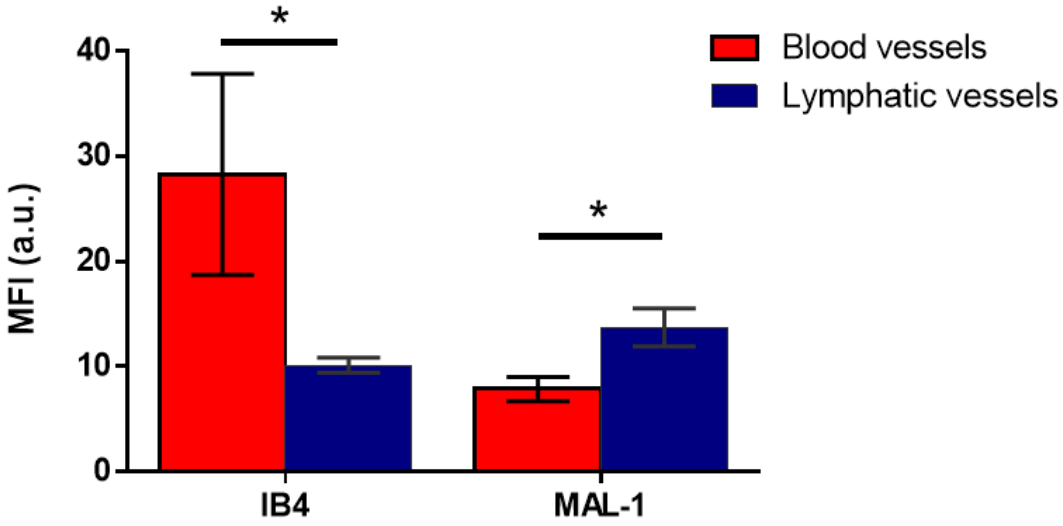

Figure 5.6: MFI of IB4 and MAL-1 binding to glycocalyx present on blood vessels under naïve conditions. Quantification of the MFI of IB4 (specific for α-D-Galactosyl moieties) and MAL-1 (specific for α2,3-sialylated glycans) binding to the surface of blood vessels using *ex vivo*-fixed staining. IB4/MAL-1 binding was quantified by creating isosurfaces on blood vessels to determine the MFI of lectin binding on vessels. Data are expressed as mean ± SEM from at least 8-10 vessels/animals, with 3 animals per group from 3 independent experiments. Significant differences groups are indicated by asterisks: *, $P < 0.05$. Statistical significance was determined using one-way ANOVA.

5.3.2 Effects of TNF- or CFA+Ag-induced inflammation on sugar residues and HS expression levels on lymphatic vessels in the cremaster muscle

To characterise the effects of TNF or CFA+Ag in the cremaster muscle in terms of glycocalyx regulation, lectin binding and HS expression on/within the lymphatic endothelium under basal and inflamed conditions were investigated via *ex vivo*-fixed and *in vivo*-live staining methods. For this purpose, WT mice were given i.s injections of 300 ng TNF (in 400 µl PBS) or 200 µg of an emulsion of CFA+Ag (200 µg of each in 300 µl total volume) and the inflammation allowed to develop for 16 h. Unstimulated control mice were given i.s injections of PBS. Tissues were subjected to either *ex vivo*-fixed or *in vivo*-live staining of lectins (IB4/MAL-1) and anti-LYVE-1 to label sugars and lymphatic vasculatures, respectively, for confocal analysis. In some experiments, an anti-MRP14 mAb was used to label neutrophils. Images obtained from confocal microscopy were analysed using IMARIS software.

Following TNF- or CFA+Ag-induced stimulation of mice cremaster muscles, 3D-reconstructed confocal images from both *in vivo*-live staining (not shown) and *ex vivo*-fixed staining (**Figure 5.7**) showed that IB4 staining (α-D-Galactosyl residue expression) on lymphatic vessels seemed to be lower in both TNF (**Figure 5.7, middle panel**) and CFA+Ag (**Figure 5.7, bottom panel**) stimulated tissues, as compared to unstimulated controls (**Figure 5.7, top panel**). Quantification of these confocal images confirmed that *ex vivo*-fixed staining resulted in significantly lower (~ 3 fold decrease) IB4 staining (α-D-Galactosyl residue expression) in TNF- or CFA+Ag-stimulated tissues; levels of expression were similar with both inflammatory mediators (**Figure 5.8A**). Although not significant, a similar decreasing trend was seen with *in vivo*-live staining (**Figure 5.8B**). These results suggest that α-D-Galactosyl moieties are being cleaved on lymphatic vessels following inflammation, thus resulting in a decrease of IB4 binding. Interestingly, when the relationship between the number of neutrophils found within lymphatic vessels and staining of IB4 was investigated in inflamed cremaster muscles, a negative correlation between IB4 staining and number of neutrophils present within lymphatic vessels was found, suggesting a possible contribution of α-D-Galactosyl cleavage in mediating neutrophil migration into lymphatic vessels (**Figure 5.9**).

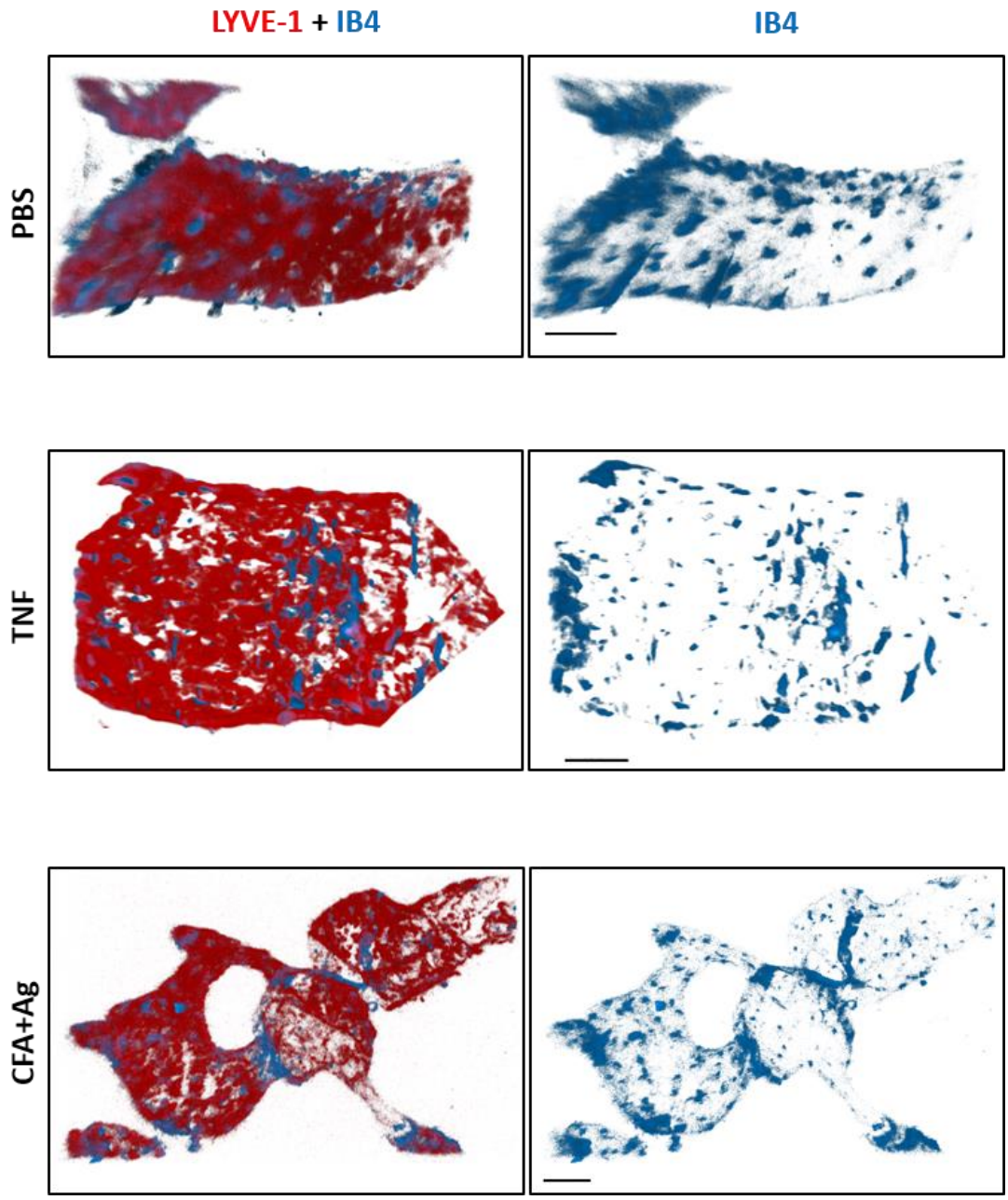

Figure 5.7: IB4 staining (α D-Galactose expression) on lymphatic vessels following TNF and CFA+Ag-induced inflammation of the cremaster muscle. WT C57BL/6 mice were given i.s injections of PBS (400 µl), TNF (300 ng in 400 µl PBS) or CFA+Ag (200 µg of each in 300 µl total volume) and inflammation was allowed to be induced for 16 h before the mice were sacrificed by cervical dislocation and their cremaster muscles dissected away, fixed, permeabilised and stained (IB4 [blue] and LYVE-1 [red] staining) for confocal analysis. The left panels shows IB4 binding (or α D-Galactose expression, blue) on lymphatic vessels (red) following i.s injection of PBS, TNF and CFA+Ag, from top to bottom, respectively. The right panels show only IB4 binding. Bars: 50 µm.

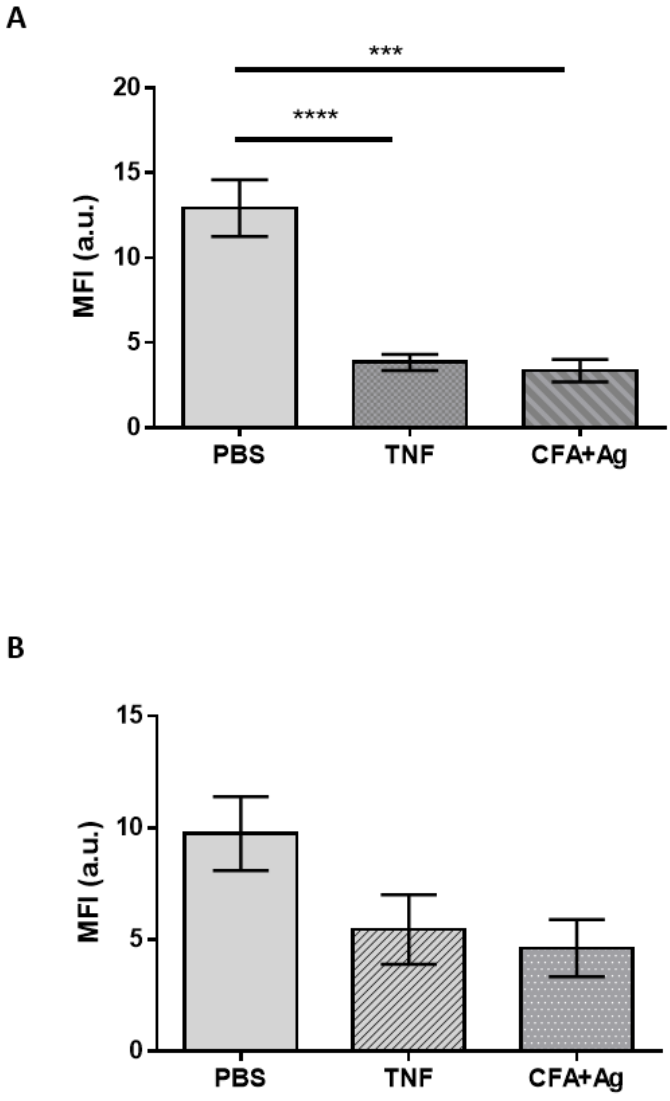

Figure 5.8: MFI of IB4 staining on lymphatic vessels following (A) *ex vivo*-fixed and (B) *in vivo*-live staining of cremaster muscles from unstimulated, TNF and CFA+Ag stimulated WT C57BL/6 mice. WT C57BL/6 mice were intrascrotally stimulated with TNF or CFA+Ag for 16 h before they were sacrificed via cervical dislocation and their cremaster muscles dissected away and either directly stained (*in vivo*-live) or fixed and permeabilised before being stained (*ex vivo*-fixed) with IB4 (binds to α D-Galactose) and labelled for LYVE-1. Control mice received i.s. injection of PBS. IB4 binding was quantified by creating isosurfaces on lymphatic vessels to determine the MFI of lectin binding on vessels. (A) MFI of IB4 staining following *ex vivo*-fixed staining. (B) MFI of IB4 staining following *in vivo*-live staining. Results are from n = 8-12 vessels per mouse with 3-6 animals per group from 14 independent experiments. Statistically significant differences between stimulated and unstimulated treatment groups are indicated by asterisks: ***, $P < 0.001$; ****, $P < 0.0001$. As the imaging techniques are different, it is not possible to compare A) with B). Statistical significance was determined using one-way ANOVA.

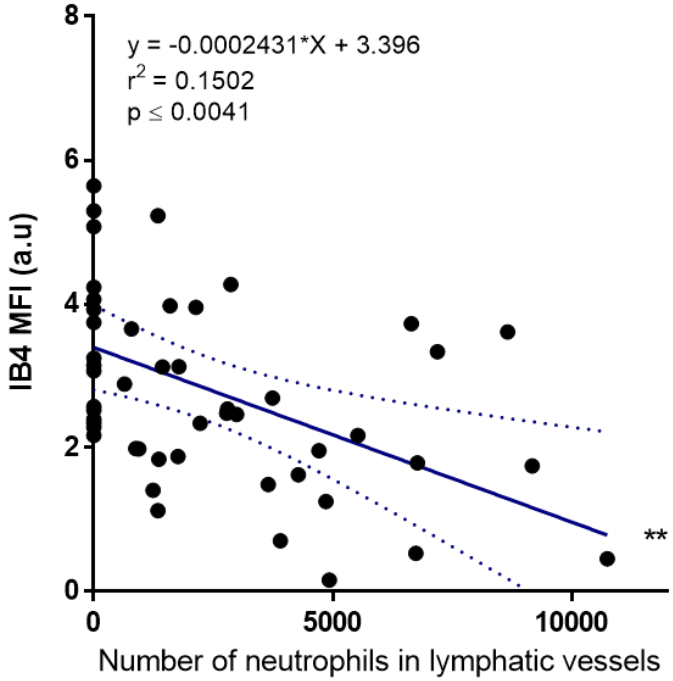

Figure 5.9: Correlation between IB4 (α-D-galactose expression) and neutrophil migration into lymphatic vessels of inflamed cremaster tissues of WT mice. Graph showing correlation between MFI of ICAM-1 expression (y-axis) and number of neutrophils within combined lymphatic vessels (x-axis) of TNF- or CFA+Ag-stimulated WT mice as analysed by IMARIS software. Data are expressed as mean±SEM of n = 53 vessels (8-12 vessels/animals from 6 animals, 6 independent experiments). Statistical significance was determined using linear regression analysis: **, $P < 0.01$.

Due to *in vivo*-live staining resulting in similar binding of IB4 to lymphatic vessels as compared with *ex vivo*-fixed staining, changes in MAL-1 staining was examined with the latter technique. 3D-reconstructed images of MAL-1 staining with *ex vivo*-fixed staining (**Figure 5.10**) showed little difference in MAL-1 binding (α2,3-sialylated glycans expression) to lymphatic vessels following TNF (**Figure 5.10**, **middle panel**) and CFA+Ag (**Figure 5.10, bottom panel**), as compared to unstimulated controls (**Figure 5.10, top panel**). MAL-1 binding (α2,3-sialylated glycans expression) to lymphatic vessels remained heterogeneous following stimulation with both inflammatory mediators. Quantification of these images showed no change in MAL-1 binding (α2,3-sialylated glycans expression) to lymphatic vessels following TNF- or CFA+Ag- stimulation, as compared to unstimulated controls (**Figure 5.11**).

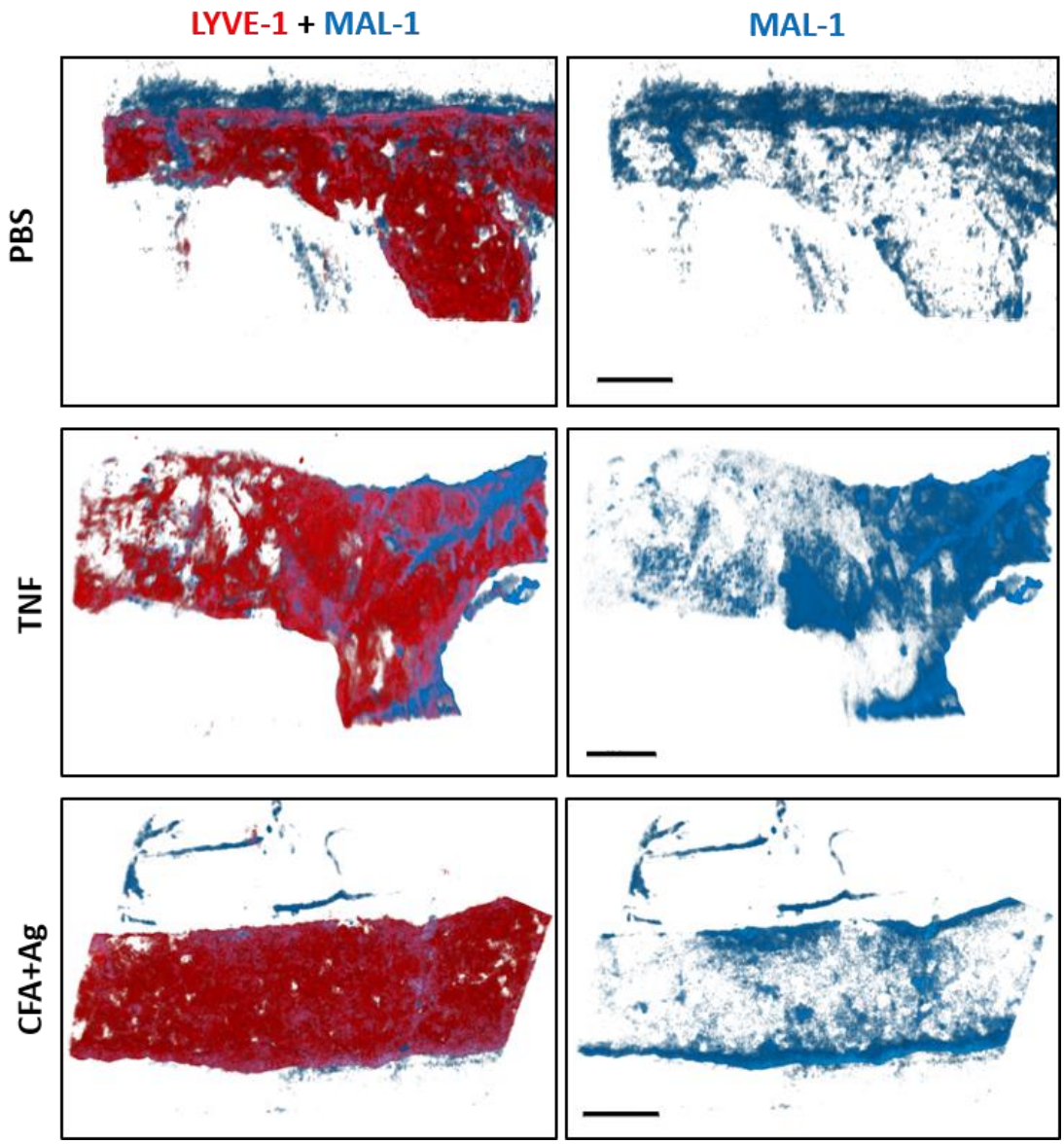

Figure 5.10: α2,3-sialylated glycans expression on lymphatic vessels following TNF and CFA+Ag-induced inflammation of the cremaster muscle. WT C57BL/6 mice were given i.s injections of PBS (400 µl), TNF (300 ng in 400 µl PBS) or CFA+Ag (200 µg of each in 300 µl total volume) and inflammatory response was allowed to develop for 16 h before the mice were sacrificed by cervical dislocation and their cremaster muscles dissected away, fixed, permeabilised and stained for MAL-1 (blue) and immunostained with anti-LYVE-1 mAb (red) for confocal analysis. The left panels show MAL-1 binding (or α2,3-sialylated glycans expression, blue) on lymphatic vessels (red) following i.s injection of PBS, TNF and CFA+Ag, from top to bottom, respectively. The right panels show only MAL-1 binding. Bars: 50 µm.

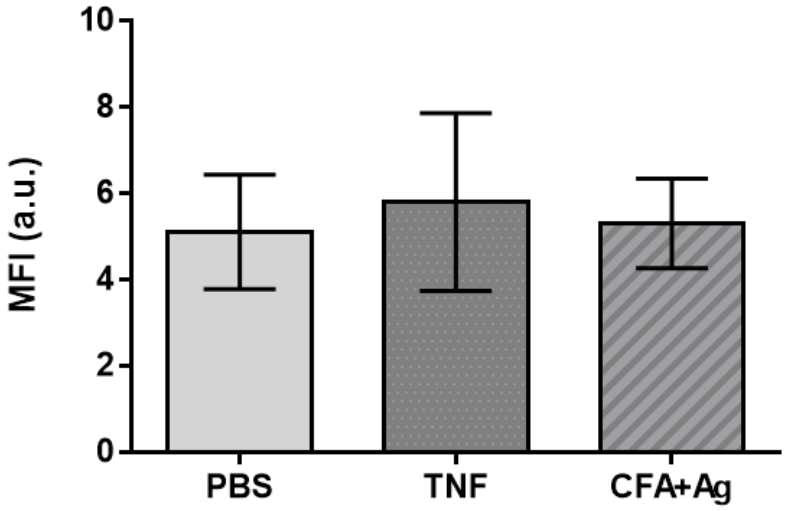

Figure 5.11: MFI of MAL-1 staining on lymphatic vessels following *ex vivo*-fixed staining of cremaster muscles from unstimulated, TNF and CFA+Ag-stimulated WT C57BL/6 mice. WT C57BL/6 mice were i.s. stimulated with TNF or CFA+Ag for 16 h before they were sacrificed via cervical dislocation and their cremaster muscles dissected away, fixed and permeabilised before being stained with MAL-1 (α2,3-sialylated glycans) and labelled for LYVE-1. Control mice received i.s. injection of PBS. MAL-1 binding was quantified by creating isosurfaces on lymphatic vessels to determine the MFI of lectin binding on vessels. Results are from n = 8-12 vessels per mouse with 3-10 animals per group from 6 independent experiments. Statistical significance was determined using one-way ANOVA.

Next, changes in the expression of one of the major GAGs in the glycocalyx, HS, were investigated following inflammation. HS was investigated as it has been demonstrated to be critically required for chemokine immobilisation and functional presentation on the cell surface of both HEV cells and LECs, during the process of lymphocyte and DC homing to dLNs (Bao et al., 2010). For this purpose, WT mice were given i.s injections of 300 ng TNF (in 400 µl PBS) and the inflammation allowed to develop for 16 h. Due to CFA+Ag-stimulation resulting in similar changes to glycocalyx sugar chains as demonstrated in the previous section, and in the interest of time, this inflammatory mediator was not used. Unstimulated control mice were given i.s injections of PBS. At the end of the inflammation period, tissues were fixed, permeabilised and immunostained with an anti-HS/isotype control Ab and anti-LYVE-1 mAb to label HS and lymphatic vasculatures, respectively, for confocal analysis. Images obtained from confocal microscopy were analysed on IMARIS software. 3D-reconstructed confocal images showed that a change in the distribution of HS on lymphatic vessels seemed to occur following TNF-stimulation, with this expression being more diffused and homogeneous on vessels as compared to patchy and heterogeneous expression seen in unstimulated

tissues (**Figure 5.12**). Quantification of confocal images showed that although redistribution of HS was seen following inflammation, there were no changes in total HS expression on lymphatic vessels in both unstimulated and TNF-stimulated tissues (**Figure 5.13**).

Overall, this section has demonstrated that IB4 binding (specific to α-D-Galactosyl moieties) to lymphatic vessels significantly decreases following TNF- or CFA+Ag-stimulation, whilst MAL-1 binding (specific for α2,3-sialylated glycans) remains unchanged. This suggests that cleaving of α-D-Galactosyl moieties on lymphatic vessels is occurring following inflammation. Furthermore, no changes in expression of heparan sulfate was found on lymphatic vessels following TNF-stimulation, suggesting that redistribution of this GAG on lymphatic vessels could be instrumental in the formation of chemokine gradients on the lymphatic endothelium during inflammation.

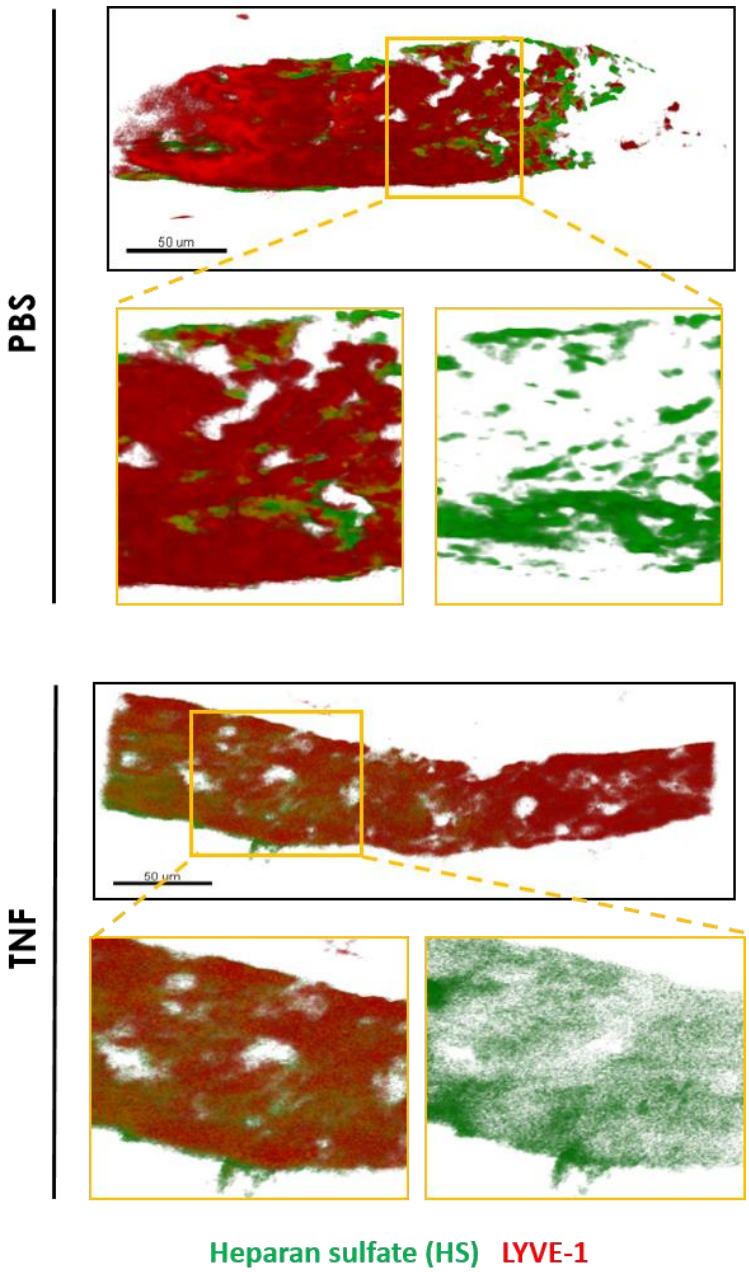

Figure 5.12: Representative HS expression in unstimulated and TNF-stimulated murine cremaster muscles. C57BL/6 WT mice were given i.s injections of TNF (300 ng in 400 µl PBS) and the inflammatory response was allowed to develop for 16 h before the mice were sacrificed by cervical dislocation and their cremaster muscles dissected away, fixed, permeabilised and immunostained for HS (green) and LYVE-1 (red) to label the lymphatic vasculatures. Unstimulated controls received i.s injection of PBS. The images show representative 3D-reconstructed confocal images of HS and LYVE-1 seen with the *ex vivo*-fixed (post-fixation/perm-block) staining method. The orange box in the top images of unstimulated and TNF-tissues shows the selected region of lymphatic vessel depicted in the magnified images below, where heparan sulfate expression on the lymphatic vessel (left) and HS expression alone (right) is shown. Bar: 50 µm.

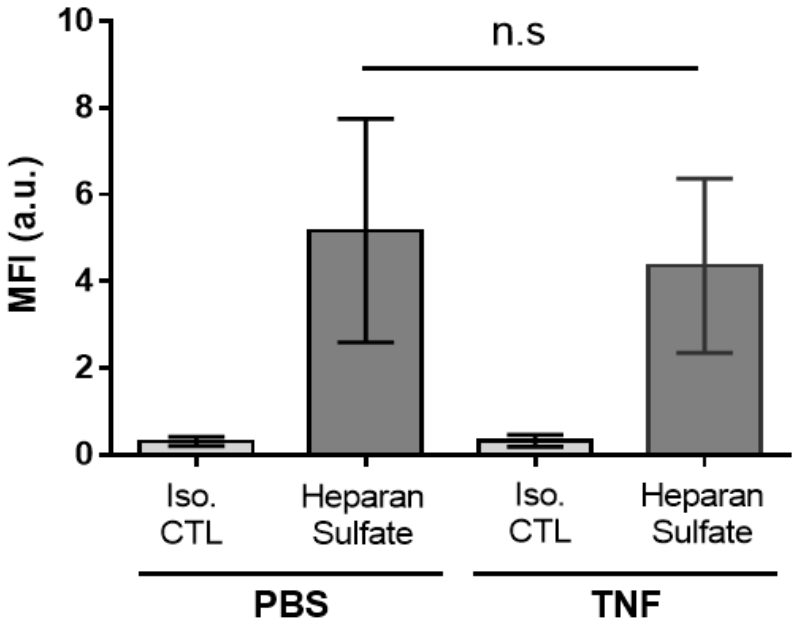

Figure 5.13: MFI of HS expression by lymphatic vessels following ex vivo-fixed staining of cremaster muscles from unstimulated and TNF-stimulated WT C57BL/6 mice. WT C57BL/6 mice were i.s. stimulated with TNF for 16 h before they were sacrificed via cervical dislocation and their cremaster muscles dissected away, fixed and permeabilised before being immunostained for isotype control/HS and LYVE-1. Control mice received i.s. injection of PBS. HS expression was quantified by creating isosurfaces on lymphatic vessels to determine the MFI of HS staining on vessels. Results are from n = 8-12 vessels per mouse with 2-4 animals per group from 3 independent experiments. Statistical significance between groups was determined using one-way ANOVA.

5.3.3 Expression of chemokine CCL21 on lymphatic vessels in TNF- or CFA+Ag-stimulated cremaster muscles

Changes in the expression of the chemokine, CCL21, by lymphatic vessels during inflammation were next investigated. Both CCL19 and CCL21 are prototypical lymphoid chemokines that are ligands for the chemokine receptor CCR7. However, constitutive expression of only CCL21 by the lymphatic endothelium has been found (Gunn et al., 1998; Vigl et al., 2011). Personal communication with my supervisor, Dr Mathieu-Benoit Voisin, has also indicated the lack of CCL19 detection via ELISAs. Furthermore, as the previous chapter has shown that CCR7 is important for neutrophil trafficking into lymphatic vessels in a TNF-dependent manner, presumably through its interactions with CCL21, the expression of this chemokine by initial lymphatic vessels was explored. First *ex vivo*-fixed staining of CCL21 was carried out. For this purpose, WT mice were i.s. injected with 300 ng TNF (in 400 µl PBS) or an emulsion of CFA+Ag (200 µg of each in 300 µl total volume) and the inflammation allowed to develop for 16 h. Unstimulated control mice were given i.s injections of PBS. At the end of the inflammatory period, cremaster muscles were dissected away and immunostained for CCL21 and LYVE-1 and labelled with IB4 for confocal analysis. Images obtained from confocal microscopy were analysed using IMARIS software.

Interestingly, when *ex vivo*-fixed immunostaining of CCL21 was carried out, the characteristic punctuate staining observed with IB4 staining previously (**Figure 5.7**), was also detected (**Figure 5.14**). Co-immunostaining of IB4 and CCL21 was therefore carried out following 16 h TNF-stimulation of WT mice cremaster muscles to investigate their co-localisation. 3D-reconstructed confocal images showed that IB4 and CCL21 punctuate staining exhibited co-localisation in the middle of single LECs (**Figure 5.14, bottom panel**). As *ex vivo*-fixed staining requires tissues to be permeabilised, this suggests that these punctuate staining could be intracellular stores of CCL21 and α-D-Galactosyl moieties being held within LECs.

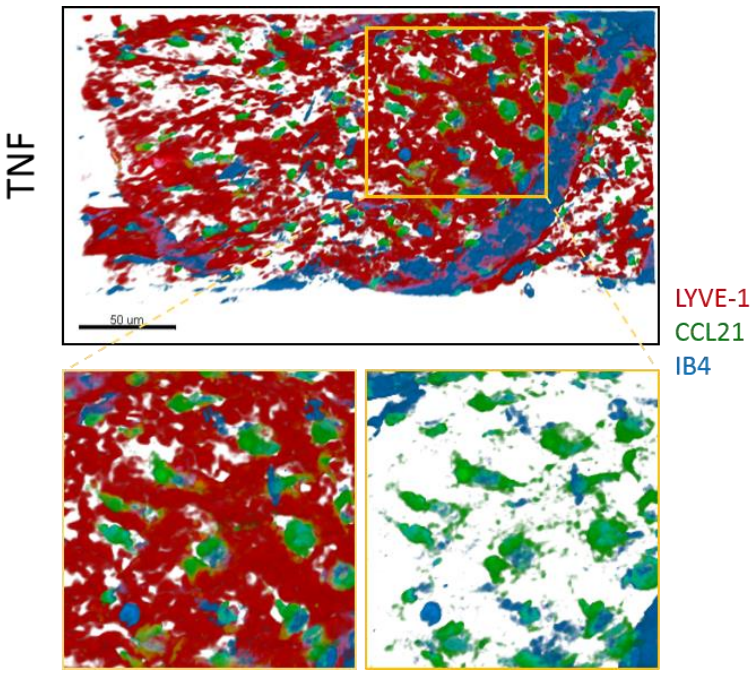

Figure 5.14: Co-localisation of IB4 and CCL21 on the surface of lymphatic vessels with *ex vivo*-fixed staining following TNF-induced inflammation. C57BL/6 WT mice were given i.s injections of TNF (300 ng in 400 µl PBS). Sixteen hours post-i.s. injection, mice were sacrificed by cervical dislocation and their cremaster muscles dissected away, fixed and permeabilised, then stained with IB4 (blue) and immunostained with anti-LYVE-1mAb (red) and anti-CCL21 mAb (green). Tissues were then washed and analysed via confocal microscopy and IMARIS software. The figure shows representative 3D-reconstructed confocal images of co-localisation between CCL21 and IB4 dotted staining seen with the *ex vivo*-fixed (Post-fixation/perm-block) staining protocol. The orange box in the top panel shows the selected region of lymphatic vessel depicted in the magnified images on the bottom panel. The bottom left image shows LYVE-1, CCL21 and IB4 staining. The bottom right image shows just CCL21 and IB4 staining. Bar: 50 µm.

Due to the potential detection of signal from intracellular stores, *in vivo*-live staining of CCL21 was carried out. For this purpose, WT mice were given i.s injections of 300 ng TNF (in 400 µl PBS) or an emulsion of CFA+Ag (200 µg of each in 300 µl total volume) and the inflammation allowed to develop for 16 h. Unstimulated control mice were given i.s injections of PBS. Two hours before the end of the inflammation period, mice received i.s. injections (*in vivo*-live immunostaining) of anti-LYVE-1 mAb and anti-CCL21/isotype control mAb to label lymphatic vasculatures and CCL21, respectively, for confocal analysis. Images obtained from confocal microscopy were analysed using IMARIS software. Following TNF- or CFA+Ag-stimulation, a down-regulation and redistribution of CCL21 expression on lymphatic vessels was observed; expression of CCL21 was patchy and heterogeneous as compared to the more diffused and homogeneous expression observed in unstimulated tissue (**Figure 5.15**). Quantification

of confocal images provided evidence that expression of CCL21 by lymphatic vessels was significantly reduced (~0.5 fold lower) in TNF-stimulated tissues, whilst CFA+Ag-stimulation resulted in an even more significant reduction (~3 fold lower) of CCL21 expression (**Figure 5.16A**). Additionally, to ensure that lymphatic vessel size was not giving rise to differences in MFI, the volume of vessels in PBS, TNF or CFA+Ag-stimulated tissues were quantified (**Figure 5.16B**). This showed no significant changes in lymphatic vessel size in TNF and CFA+Ag-stimulated tissues as compared to unstimulated tissues. This indicates that the differences in MFI of CCL21 staining on lymphatics following inflammation are not due to changes in vessel size. In order to determine whether CCL21 was being released into the interstitium, the concentration gradient of CCL21 from the abluminal side of the lymphatic endothelium up to 10 μm away from the lymphatic vessel was quantified. The results from CFA+Ag-stimulated cremaster muscles showed that there was a higher expression (~2.5 fold higher) of CCL21 on lymphatic vessels, as compared to the interstitial tissue (**Figure 5.17A**). Additionally, the results from unstimulated and CFA+Ag-stimulated cremaster muscles demonstrated that CCL21 expression was generally highest closest to the abluminal side of the lymphatic endothelium, and exhibited a decreasing trend as quantification moved away from the lymphatic vessel, thus establishing a CCL21 gradient (**Figure 5.17B**). Additionally, CFA+Ag-stimulated cremaster muscles resulted in the formation of a steeper gradient, as compared to unstimulated controls.

Overall, this section has demonstrated that the expression of CCL21 on lymphatic vessels is not only reduced in response to TNF- or CFA+Ag-stimulation, but a redistribution of this chemokine is also seen on the surface of LECs. Furthermore, a steeper gradient of CCL21 is also formed within the interstitium following inflammation.

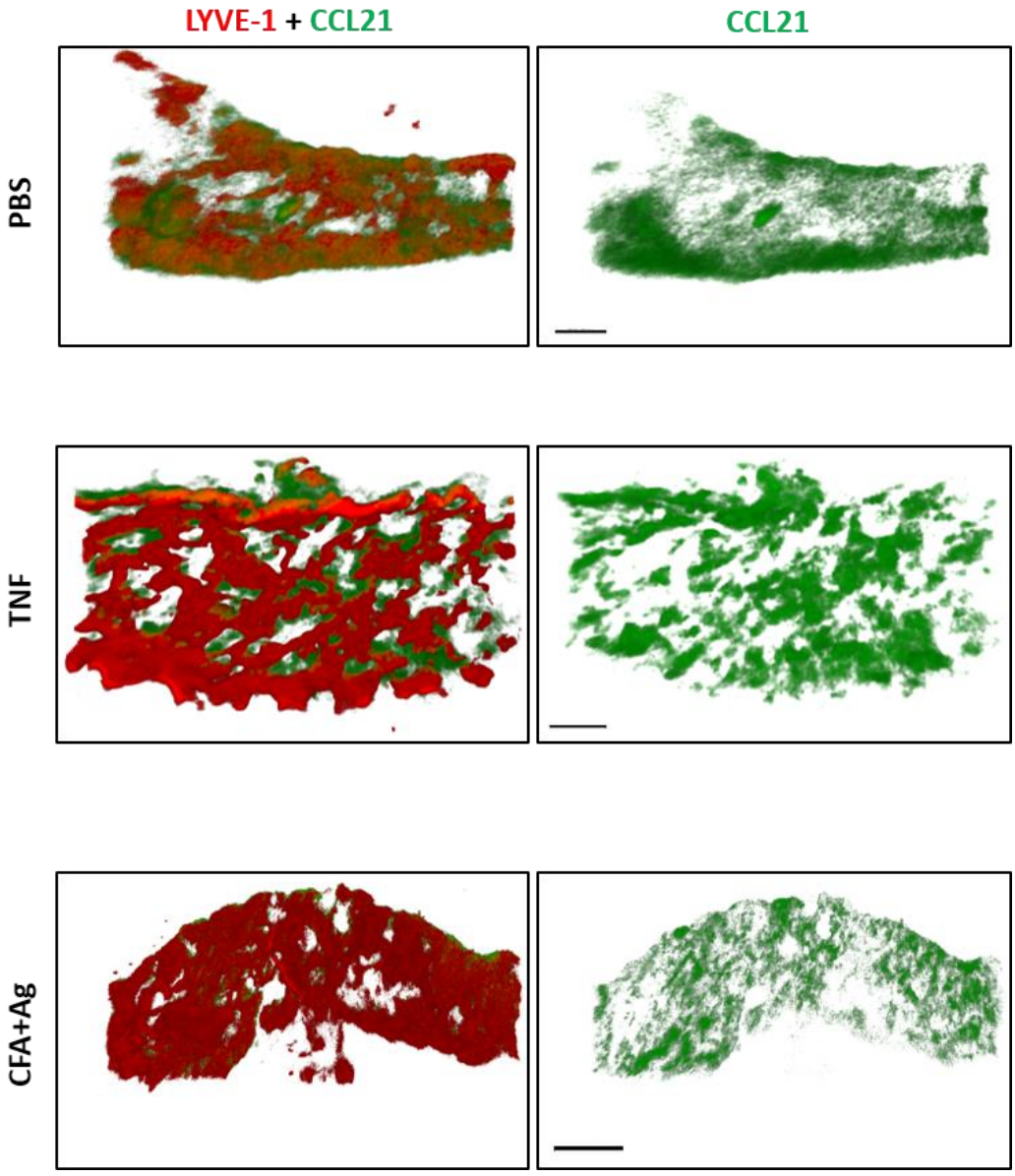

Figure 5.15: CCL21 staining on lymphatic vessels in unstimulated, TNF- or CFA+Ag-stimulated conditions. WT C57BL/6 mice were given i.s injections of PBS (400 µl), TNF (300 ng in 400 µl PBS) or CFA+Ag (200 µg of each in 300 µl total volume) for 16 h and the inflammatory response allowed to develop for 16 h. Two hours before the end of the inflammation period, mice received an i.s. injection of anti-LYVE-1 mAb (red) and anti-CCL21 mAb/rabbit IgG isotype control (green) Ab. At the end of the inflammation period, cremaster muscles were dissected away and immediately analysed via confocal microscopy and IMARIS software. The images show representative 3D-reconstructed confocal images of CCL21 expression on lymphatic vessels following *in vivo-live* staining (no fixation/no permeabilisation) in unstimulated (top panel), TNF (middle panel) or CFA+Ag (bottom panel) stimulated tissues. Bar: 40 µm.

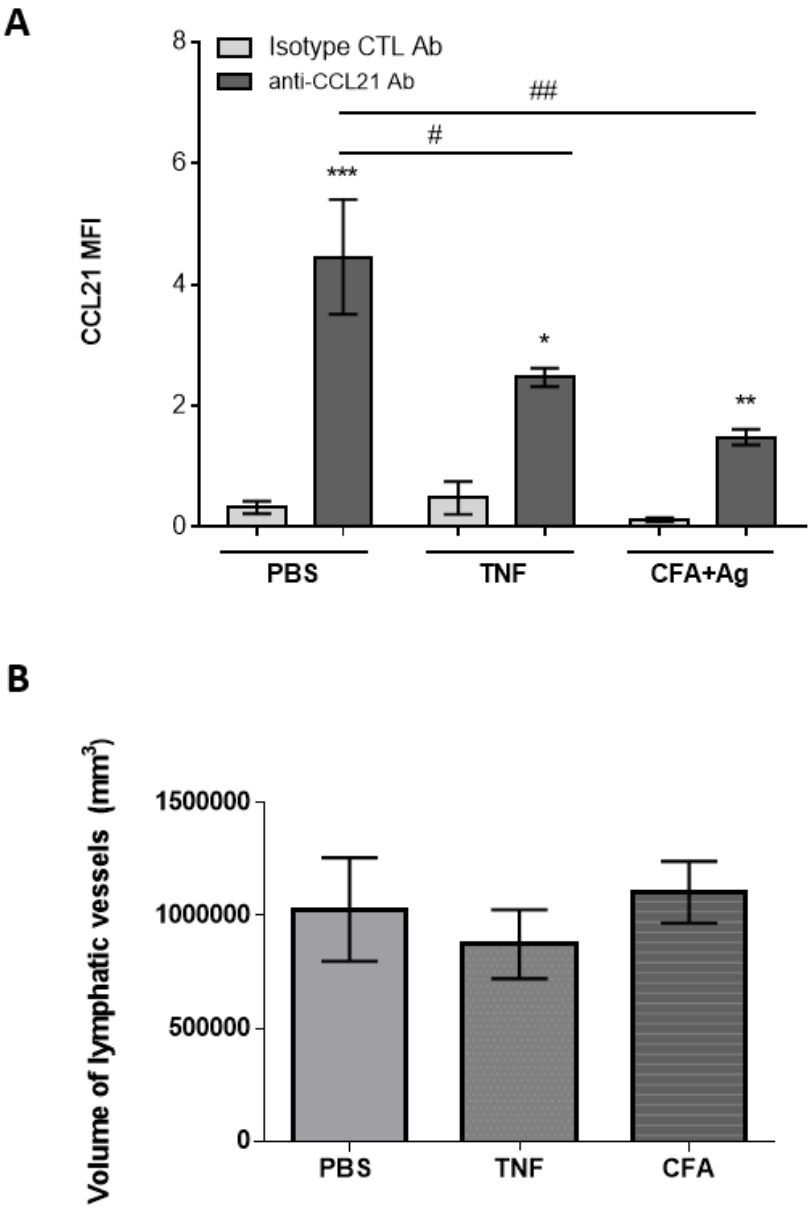

Figure 5.16: MFI of CCL21 expression and lymphatic vessel volume of unstimulated, TNF and CFA+Ag-stimulated cremaster muscles. C57BL/6 WT mice were given i.s injections of TNF (300 ng in 400 µl PBS) or CFA+Ag (200 µg of each in 300 µl total volume) and the inflammatory response allowed to develop for 16 h. Two hours before the end of the inflammation period, mice received an i.s. injection of anti-LYVE-1 mAb and anti-CCL21 mAb/rabbit IgG isotype control Ab. (A) CCL21 expression was quantified by creating isosurfaces on lymphatic vessels to determine the MFI of CCL21 staining on vessels. Results are from n = 8-12 vessels per mouse with 3-5 animals per group from 3 independent experiments. (B) Volume of lymphatic vessels were quantified by creating isosurfaces on lymphatic vessels. Statistically significant differences between isotype control Ab and CCL21 Ab groups are indicated by asterisks: *, $P < 0.05$; **, $P < 0.01$; ***, $P < 0.001$. Statistically significant differences between stimulated and unstimulated treatment groups are indicated by hash signs: #, $P < 0.05$; ##, $P < 0.01$. Statistical significance was determined using one-way ANOVA.

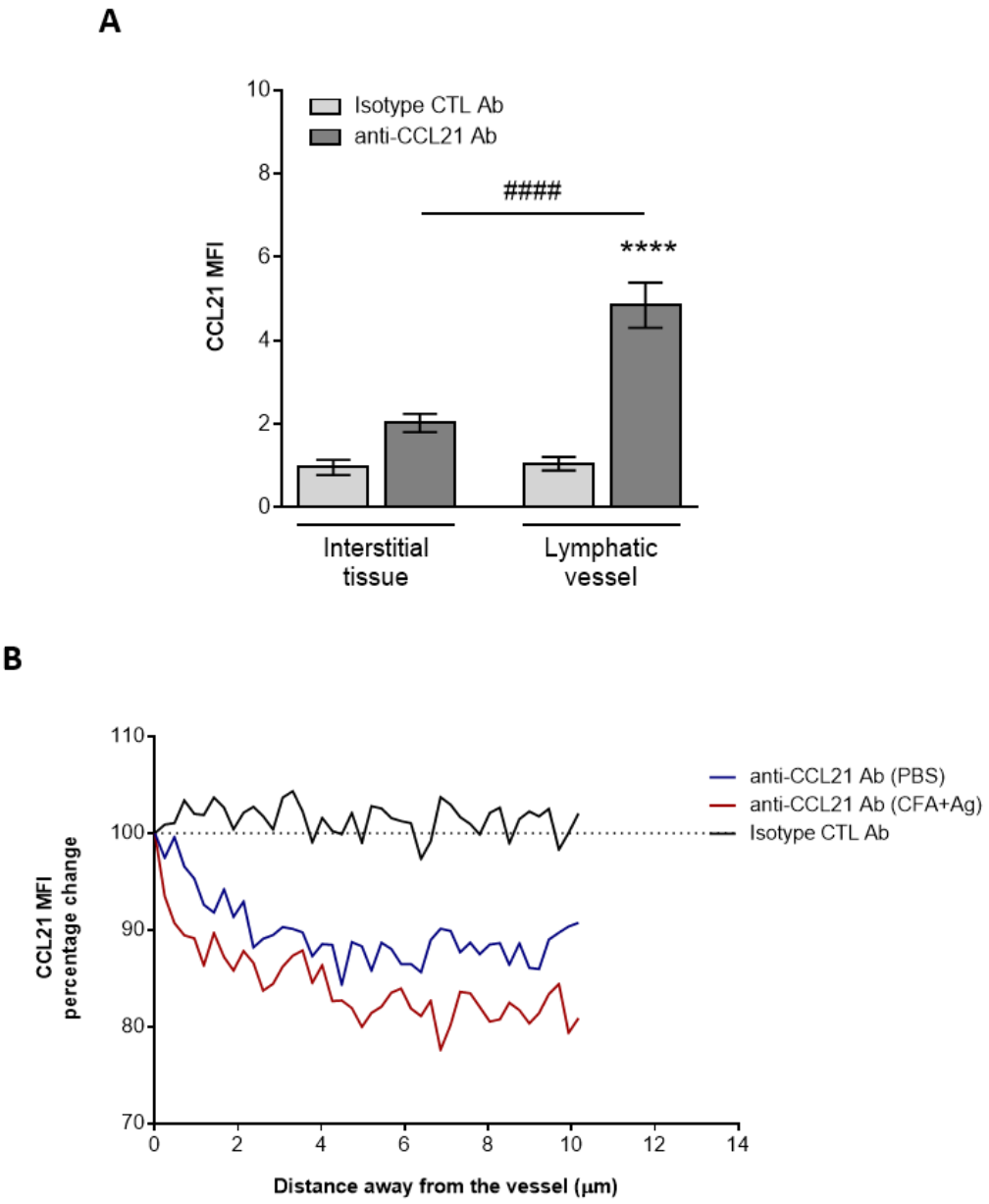

Figure 5.17: CCL21 gradient in unstimulated (PBS) or CFA+Ag-stimulated cremaster muscles. C57BL/6 WT mice were given i.s injections of CFA+Ag (200 µg of each in 300 µl total volume) and the inflammatory response allowed to develop for 16 h. Two hours before the end of the inflammation period, mice received an i.s. injection of anti-LYVE-1 mAb and anti-CCL21 mAb/rabbit IgG isotype control Ab. (A) IMARIS quantification showing levels of CCL21 expression in the interstitial tissue vs. lymphatic vessels of CFA+Ag stimulated WT mice. (B) A line intensity profile was generated perpendicular to the direction of the vessel (10 lines/vessel) from the abluminal surface into the tissue (10 µm length) using ImageJ to look at the potential gradient of CCL21 guiding leukocytes toward lymphatic vessels. Data are presented as percentage change from the first pixel of the line. Results are from n = 8-12 vessels per mouse with 2-3 animals per group from 3 independent experiments. Statistically significant differences between isotype control Ab and anti-CCL21 Ab groups are indicated by asterisks: **, $P < 0.01$; ****, $P < 0.0001$. Statistically significant differences between the interstitial tissue vs. the lymphatic vessels are indicated by hash signs: ####, $P < 0.0001$. Statistical significance was determined using one-way ANOVA.

5.4 Discussion

In contrast to the BEC glycocalyx, the LEC glycocalyx is not very well studied. Thus, this chapter aimed to characterise the LEC glycocalyx with the use of several lectins and antibodies targeted to the most abundant proteoglycan, HS, and the prototypical lymphatic chemokine, CCL21, which is thought to be associated with HS (Weber et al., 2013). The potential regulation and redistribution of these components of the LEC glycocalyx following TNF- or CFA+Ag-induced inflammation was also investigated.

Initially, in an effort to characterise the glycocalyx present on lymphatic vessels, a panel of 4 lectins were utilised: IB4, MAL-1, SNA, and LEL. However, only IB4 and MAL-1 successfully bound to lymphatic vessels. LEL binds to N-acetylglucosamine and has been used effectively to label the blood vascular endothelium in rodents (Robertson et al., 2015), however this does not seem to be the case for the lymphatic endothelium. SNA binds to α2,6 SAs and has been shown to interact with the LEC marker, LYVE-1, but this was demonstrated in LYVE-1 transfected HEK 293T cells, and is therefore not a good indicator of the true binding capabilities of this lectin to lymphatic vessels (Nightingale et al., 2009). It is possible that there is competition of binding between SNA and the anti-LYVE-1 Ab, thus preventing proper binding of this lectin to lymphatic vessels. It is perhaps also possible that α2,6 SAs are not present within the LEC glycocalyx, as the current study has shown this to be the case in lymphatic vessels.

Using different staining methods, α-D-galactosyl moieties (bound by IB4) and N-linked α2,3-sialylated glycans (bound by MAL-1), were found to be present both intracellularly and on the surface of LECs. It was also found that the BEC glycocalyx had a far higher expression of α-D-galactosyl moieties, with this expression being more homogeneous than that of the LEC glycocalyx. Additionally, N-linked α2,3-sialylated glycans were found to be expressed more highly within the LEC glycocalyx, as compared to the BEC glycocalyx. IB4 has never been reported to bind to lymphatic vessels, but it has been demonstrated to specifically bind to terminal α-D-galactosyl residues expressed by various cell types, including BECs in mouse, rabbit, rat and human tissues (Brabec et al., 1980; Goldstein and Winter, 1999; Laitinen, 1987; Peters and Goldstein, 1979). Consequently, it is now recognised as a blood vasculature marker that has been widely used in a variety of angiogenesis studies (Bryson et al., 2011; Ernst and Christie, 2006; Walchli et al., 2015). This is in accordance with results from the present study where a higher and more homogeneous staining of IB4 was observed on blood vessels. This study

has, however, shown for the first time, the presence of α-D-Galactosyl moieties as a component of the LEC glycocalyx. MAL-1 has been utilised in many studies to detect N-linked α2,3-sialylated glycans (Khatua et al., 2013; Knibbs et al., 1991; Nicholls et al., 2007; Wang and Cummings, 1988). The detection of sialic acids (SAs) on lymphatic vessels is particularly relevant as SAs are known to play important roles in several human viral infections. Pathogens such as influenza viruses, rotaviruses, polyoma viruses and adenoviruses, have been shown to use host-sialylated structures for binding to their target host cell (Cashman et al., 2004; Dugan et al., 2008; Isa et al., 2006; Skehel and Wiley, 2000). SAs are thought to be a good target for these viruses as they are highly conserved and are found in abundance in all mammalian cells. Viral infections of LECs have been shown to induce increased LEC permeability (Gavrilovskaya et al., 2012, 2013), thus the binding of viruses to SAs on lymphatic vessels could potentially result in increased viral entry into the lymphatic system and their recirculation into the bloodstream, consequently leading to systemic viral infections. Alternatively, as previously observed with bacteria escaping aged lymphatic vessels exhibiting decreased glycocalyx coverage and increased permeability, this increased permeability caused by viral LEC infection could result in other pathogens being released back into the interstitium, thus disrupting host immune responses in controlling infections (Zolla et al., 2015). Furthermore, bacteria use host SAs in order to colonise, persist and cause disease in humans (Severi et al., 2007). The most abundant and best-studied SA in these studies in N-acetylneuraminic acid (Neu5Ac) (Severi et al., 2007). MAL-1 has been shown to react with greatest affinity with Neu5Ac (Knibbs et al., 1991), thus making the current study relevant to this field as MAL-1 staining is abundantly present on lymphatic vessels. These results therefore implicate lymphatic vessels as having potentially causative roles in immune evasion by such microbes.

This chapter next sought to characterise the effects of inflammation on LEC glycocalyx regulation and redistribution. TNF- or CFA+Ag-induced inflammation of the cremaster muscle resulted in a reduction of α-D-Galactosyl residues (IB4 staining) present in the LEC glycocalyx on lymphatic vessels. A reduction in α-D-Galactosyl residue expression by lymphatic vessels was associated with an increased number of neutrophils found within the lumen of these vessels, providing evidence that neutrophil migration across the lymphatic endothelium is associated with cleavage of α-D-Galactosyl residues. Under inflammatory conditions, activated immune cells, such as neutrophils, macrophages and mast cells degranulate enzymes, which can contribute to the degradation of the glycocalyx

(Henry and Duling, 2000; VanTeeffelen et al., 2007). In particular, activated neutrophils can induce glycocalyx damage through the production of ROS and proteases from their storage granules (van Golen et al., 2012), all of which supports the result observed in the present study. It has also been reported that the vascular glycocalyx is rapidly shed in response to inflammatory mediators, such as cytokines and chemokines, under various experimental models of inflammation (Becker et al., 2010; Chappell et al., 2009a). Glycocalyx shedding induced by TNF is particularly relevant to the current study (Chappell et al., 2009a). As adhesion molecules are harboured within the glycocalyx (Chappell et al., 2008), the release of inflammatory mediators, such as TNF, could increase the accessibility of leukocytes to adhesion molecules through the degradation of the enveloping glycocalyx (Chappell et al., 2009a). All of these factors could be an explanation as to why a reduction in α-D-Galactosyl residues results in a higher number of neutrophils being able to migrate into lymphatic vessels.

In contrast, TNF- or CFA+Ag-induced inflammation did not result in a down-regulation of α2,3-sialylated glycans (MAL-1 staining). Despite the expression levels of both components remaining the same under both basal and inflamed conditions, a redistribution of their expression within the LEC glycocalyx occurred. Although this has not been demonstrated in the context of inflammation, SA redistribution has been shown to occur within the BEC glycocalyx during shear flow *in vitro* (Bai and Wang, 2014). It has been reported that shear stress results in the redistribution and relocalisation of SAs to the cell-cell junctions of human umbilican vein endothelial cells (HUVECs) (Bai and Wang, 2014). As discontinuities of tight junctions in intercellular clefts between adjacent ECs has been demonstrated to provide a leakage route for macromolecules (Adamson et al., 1993), this redistribution of the glycocalyx is important for permeability control. Therefore, the redistribution of SAs observed in the current study could potentially also play similar roles in the regulation of lymphatic vessel permeability and barrier function during inflammation.

In the present study, HS expression remained unchanged following TNF stimulation. HS has been shown to be cleaved and shed in response to TNF, as well as in surgical diseases states (I/R injury) (Chappell et al., 2009a; Chappell et al., 2009b). Under physiological conditions, heparan sulfate proteoglycans (HSPGs) have been shown to inhibit neutrophil adhesion (Schmidt et al., 2012). However, in an experimental sepsis model of acute lung injury, the production of endogenous TNF was shown to activate ECs to produce the enzyme, heparanase, which catalyses the partial degradation of HS constituents of the

glycocalyx; this loss of HS resulted in a significant increase in neutrophil binding to vascular walls and inflammation (Schmidt et al., 2012). HS degradation not only exposes underlying adhesion molecules but could also release pro-inflammatory mediators (e.g. IL-8), which are typically sequestered within the BEC layer, thus facilitating neutrophil adhesion and their extravasation (Reitsma et al., 2007). In the current experimental model, a redistribution of HS on lymphatic vessels was observed, despite no changes in total expression levels being found. An explanation for this could be due to the fact that the present study has shown differences in the distribution of sugars on the BEC and LEC glycocalyx, thus what is observed on blood vessels does not necessarily translate to the same observation on lymphatic vessels. Additionally, it could be due to a matter of differences in time-points investigated. Previous studies looking at changes in the BEC glycocalyx looked at shedding after just 0-90 mins of TNF stimulation (Chappell et al., 2009a; Schmidt et al., 2012), and 20 mins of I/R injury (Chappell et al., 2009b). These inflammatory time-points are far more acute than the timepoint investigated in the present study, where changes in the LEC glycocalyx were only looked at 16 h post-i.s. injection (appropriate time for neutrophil-LECs interactions). Furthermore, it has recently been demonstrated that whilst short-term (30 min) shear stress results in shedding of the BEC glycocalyx, long-term (24 h) exposure to shear stress results in glycocalyx components, such as HS expression, being increased on the cell surface, close to static levels (Zeng and Tarbell, 2014). As only 16 h post-i.s. injection was looked at in the present study, this could very well be happening at earlier time-points, but further experiments will have to be carried out to determine this. It is worth mentioning that the shear stress in lymphatic vessels is very low, therefore what occurs in blood vessels may not necessarily be mirrored in lymphatic vessels. All of these differences could contribute to the explanation as to why no changes in HS expression were observed.

Besides having regulatory roles in cell adhesion as a component of the vascular EC glycocalyx, HS also promotes cell signalling by providing binding sites for growth factors and chemokines, which leads to the formation of ternary complexes with their receptors (Handel et al., 2005; Schlessinger et al., 2000). It has been reported that a chemotactic gradient of CXCL2 (MIP-2) sequestered on HS in the vascular EC glycocalyx induces the directional intraluminal crawling of neutrophils within blood vessels (Massena et al., 2010). Additionally, the constitutively expressed LEC chemokine, CCL21, has also been shown to bind to HS within the vascular EC glycocalyx, which leads to its immobilisation and the formation of a chemotactic gradient that guides DCs within the interstitium

towards lymphatic vessels (Weber et al., 2013). A similar interaction is thought to occur in LNs, where HS expression by HEVs is thought to control CCL21 chemokine presentation to facilitate lymphocyte homing into peripheral lymphoid organs (Bao et al., 2010; Tsuboi et al., 2013). Thus, the expression of CCL21 on lymphatic vessels following TNF- or CFA+Ag-induced inflammation was investigated in the present study. Interestingly, despite the expression levels of HS remaining the same following inflammation, a decrease in the expression levels of CCL21 was found on lymphatic vessels. Despite this difference in expression, a redistribution of CCL21 was observed via confocal microscopy, as was observed with HS, although further experiments have to be carried out to check if they do indeed co-localise. Furthermore, the characteristic punctuate staining of CCL21 observed in lymphatic vessels is in line with previous observations of intracellular stores of this chemokine within LECs (Johnson and Jackson, 2010; Weber et al., 2013). Since a down-regulation in CCL21 expression by lymphatic vessels was observed, the possibility of CCL21 release into the interstitium was next investigated. Although this did not turn out to be the case, preliminary results showed that CFA+Ag-induced inflammation resulted in a higher concentration gradient forming within the interstitium as compared to unstimulated conditions, with the highest expression of CCL21 being found nearest to the abluminal side of the lymphatic vessel. The expression of CCL21 decreased along a line up to 10 μm away from the abluminal side of the lymphatic endothelium, appearing to form a concentration gradient, which may potentially guide neutrophils towards lymphatic vessels, as is presumed to be the case for DCs (Haessler et al., 2011). This is also akin to the 'source and sink' hypothesis as proposed for morphogen gradients, where the establishment of a chemoattractant gradient in principle would require a stable production of the molecule (source) and its subsequent diffusion and elimination (sink) (Crick, 1970). The 'source' of CCL21 in this case would be the LECs, and the 'sink' would be the interstitial tissue and CCR7 expressed by neutrophils, thus leading to the formation of a CCL21 gradient. This could in turn lead to the polarisation of migrating neutrophils and their chemotaxis towards LECs.

As results from the present study indicate CCL21 is not being released into the interstitium, it is likely CCL21 is being drained away via the initial lymphatics, as is indicated by recent quantifications by Dr Voisin, showing the presence of a CCL21 gradient within initial lymphatic vessels (**Appendix 5A**). Furthermore, the total CCL21 expression within the tissue is also not altered (**Appendix 5B)**. Interestingly, in support

of this hypothesis, a recent report provided *in vitro* evidence that an intraluminal CCL21 gradient is induced by lymph flow, thus guiding DCs migrating within capillaries in the downstream direction of collecting lymphatic vessels (Russo et al., 2016).

Collectively, the results in this chapter have demonstrated for the first time the presence of α-D-Galactosyl moieties as a component of the LEC glycocalyx, in addition to N-linked α2,3-sialylated glycans (SAs). These sugar residues are either down-regulated (α-D-Galactosyl moieties) or redistributed (sialylated N-linked glycans) within the LEC glycocalyx following TNF- or CFA+Ag-induced inflammation. The down-regulation of α-D-Galactosyl moieties is associated with increased neutrophil numbers found within lymphatic vessels. Furthermore, HS and CCL21 are also redistributed within the LEC glycocalyx following inflammation. Finally, down-regulation of CCL21 expression by lymphatic vessels was found following TNF- or CFA+Ag-induced inflammation, and this is associated with the formation of a steeper chemokine gradient within the interstitium, presumably to provide chemotactic cues to guide leukocytes within the tissue towards lymphatic vessels. This down-regulation in CCL21 is also associated with the formation of a gradient within initial lymphatic vessels in the direction of flow, thus guiding neutrophils in the right direction. Clearly, the LEC glycocalyx and its molecular constituents are potential targets of glycan-centered therapeutic approaches for the prevention of pathogen dissemination through the lymphatic vessels. However, further studies have to be carried out in order to determine the exact constituents that mediate neutrophil migration into the lymphatic system.

Limitations of the study

In addition to the limitations discussed at the end of Chapter 3 in this thesis, another caveat is that confocal microscopy does not give a high enough resolution for distinguishing the different structures of the LEC glycocalyx. Furthermore, degradation of the sugar chains could have also occurred due to sample manipulation. To achieve higher resolution, the gold standard method for the visualisation of the glycocalyx – electron microscopy – could be used to further characterise its structure (e.g. thickness). Intravital confocal microcopy could also be used to identify the exact locations of the sugar chains within the LEC glycocalyx. However, labelling of glycocalyx structures with lectins are an accepted protocol as exemplified with numerous articles using this technique both *in vivo* (labelling of blood vasculature) and *ex vivo* (tissue sections) (Wang, 2007; Reitsma, 2017).

6 : Investigating the roles of TNF and ICAM-1 in driving neutrophil intraluminal crawling following their migration into lymphatic vessels *in vivo*

6.1 Introduction

Akin to the process of neutrophil migration into lymphatic vessels being massively understudied, investigations into subsequent neutrophil-lymphatic vessel interactions following their transmigration across the lymphatic endothelium is of greater paucity. To date, only one seminal study observing neutrophil crawling within lymphatic vessels exists (Hampton et al., 2015). The study mainly investigated the mechanisms of neutrophil migration from inflamed tissue into lymphoid organs following *S. aureus* infection. Therefore, migration of neutrophils into lymphatic vessels and their crawling parameters following inflammation were not studied in detail. LysM-eGFP mice were used to examine neutrophil interactions with lymphatic vessels following bacterial infection (Hampton et al., 2015). However, their data do not clearly show whether this is intraluminal crawling.

Due to the scarcity of studies investigating neutrophil crawling within lymphatic vessels, the mechanisms of this phenomena has yet to be dissected. In light of this, possible mechanisms of this process could be inferred from current findings of intraluminal crawling of other leukocytes within lymphatic vessels. Up till now, majority of studies have focused on leukocyte (DCs in particular) crawling along the lymphatic endothelium towards lymph nodes (Nitschke et al., 2012; Sen et al., 2010; Tal et al., 2011); initiation of adaptive immune responses require DCs to carry antigens into lymph nodes. To do this, intravital microscopy (IVM) has been used as the main tool for observing leukocyte crawling behaviour. These studies showed that once within the lumen of initial lymphatic vessels, DCs actively crawl along the luminal side of the lymphatic endothelium guided by the directional flow of lymph. Interestingly, once reaching collecting lymphatics, DCs switch to passive drifting to exploit the faster lymph flow so as to rapidly reach draining lymph nodes (Tal et al., 2011). It has also recently been observed that integrin ligands of the adhesion molecules, ICAM-1 and VCAM-1, contribute to DC crawling over LECs (Barreiro et al., 2002; Carman et al., 2003; Teijeira et al., 2013). DC crawling within

lymphatic vessels resembles the inflammation-mediated integrin crawling of leukocytes within the lumen of blood postcapillary venules before transendothelial migration into the interstitial tissues occurs (Phillipson et al., 2006). Phillipson et al. demonstrated using time-lapse video-microscopy within blood vessels in WT mice that immediately upon neutrophil adhesion to the venular walls, a significant intraluminal crawling of all neutrophils to distant sites of inflammation was observed (Phillipson et al., 2006). However, mice deficient in the ICAM-1 integrin ligand, MAC-1, exhibited crawling impairments; this crawling was found to be mediated by ICAM-1 as when a blocking antibody against this adhesion molecule was used, neutrophils could no longer crawl in response to the chemoattractant, MIP-2 (Phillipson et al., 2006).

Owing to the current lack of understanding regarding the specific mechanisms by which neutrophils crawl within the lumen of lymphatic vessels, this study set out to look at the dynamics of this crawling behaviour and reveal potential mechanisms by which this process occurs during inflammation *in vivo*.

6.2 Aims

Neutrophil intraluminal crawling within lymphatic vessels has rarely been studied, thus leaving a plethora of neutrophil-LECs interactions to be unravelled. Hence, this chapter aims to investigate crawling behaviours of neutrophils within lymphatic vessels during TNF- or CFA+Ag-stimulation *in vivo*. This thesis has already shown TNF and CFA+Ag-stimulation induces the migration of neutrophils into lymphatic vessels. Specifically, Chapter 4 of this thesis demonstrated the role of the CCL21:CCR7 chemokine axis in TNF-driven neutrophil migration into lymphatic vessels *in vivo*. Consequently, this chapter aimed to investigate the involvement of TNF signalling in driving neutrophil intraluminal crawling within lymphatic vessels. It also aimed to elucidate the mechanisms of neutrophil crawling within the luminal side of the lymphatic endothelium; in particular, the role of the adhesion molecule, ICAM-1, was considered as it has previously been implicated in neutrophil crawling within the lumen of blood vessels (Phillipson et al., 2006).

Therefore, the specific aims of this chapter were to:

- Use neutrophil reporter LysM-eGFP mice to track GFP^{high} neutrophils using confocal IVM to observe the dynamics of TNF-induced intraluminal crawling within lymphatic vessels *in vivo*.
- Use confocal IVM to investigate the role of TNF in driving neutrophil intraluminal crawling within lymphatic vessels of LysM-eGFP mice by using anti-TNF blocking mAbs as a means of abolishing TNF signalling.
- Visualise and investigate the expression of ICAM-1 on lymphatic vessels following TNF- or CFA+Ag-induced inflammation *in vivo* through the use of immunostaining and confocal microscopy analysis.
- Investigate the relationship between TNF and ICAM-1 in driving neutrophil intraluminal crawling within lymphatic vessels.

6.3 Results

6.3.1 Confocal intravital microscopy to observe TNF-induced crawling of neutrophils within lymphatic vessels in real-time and in 4D *in vivo*

Neutrophil interactions with lymphatic vessels *in vivo*, particularly post-migration across the lymphatic endothelium, upon TNF- or CFA+Ag-stimulation was first investigated in real-time. For this purpose, LysM-eGFP mice were given i.s injections of either 300 ng TNF (in 400 µl PBS) or an emulsion of CFA+Ag (200 µg of each in 300 µl total volume) for 4 h and 6 h, respectively. Following this, *in vivo* fluorescent-immunostaining with a non-inhibitory dose of anti-LYVE-1 mAbs was applied to the tissues to visualise lymphatic vessels to allow the tracking of GFP^{high} neutrophils migrating into and within the lymphatic vasculature by confocal IVM. Mice were anaesthetised and cremaster muscles were exteriorised and pinned out flat over the optical window of a heated microscope stage. Z-stack images of a lymphatic vessel were captured every minute for 90 min in order to capture neutrophil interactions with the luminal side of the lymphatic endothelium in 4D between the time frames of 4 – 5.5 h (for TNF stimulation) and 6 – 7.5 h (for CFA+Ag-stimulation). These time frames were chosen to record events around the peak of neutrophil migration into lymphatic vessels as found in time-course

experiments, to allow neutrophil interactions with vessels to be observed. Tyrode's salt solution was used to constantly superfuse cremaster muscles during all experiments.

Following stimulation with TNF, neutrophils were observed crawling along the luminal side of the lymphatic (**Figure 6.1** & **Video 2**). An example of confocal IVM analysis of a single neutrophil demonstrated that over the course of an hour, the neutrophil remained attached to the luminal side of the endothelium and continuously crawled along the vessel wall (**Figure 6.1**). Analysis of neutrophil crawling parameters within lymphatic vessels provided evidence that majority of these leukocytes moved in the direction towards collecting lymphatic vessels/lymph flow (63.5 ± 5.7 %) (**Figure 6.2A**), at a speed of 4.3 ± 0.2 μm/min (**Figure 6.2C**), and with a straightness index of 0.5 ± 3 (**Figure 6.2D**); whilst in contrast, cells going against lymph flow exhibited reduced displacement length, speed and straightness (**Figure 6.2A-D)**.

The results in this section demonstrated that TNF can not only trigger the migration of neutrophils into lymphatic vessels, but can also induce their intraluminal crawling along the luminal side of the lymphatic endothelium towards lymph flow in the direction of collecting lymphatic vessels.

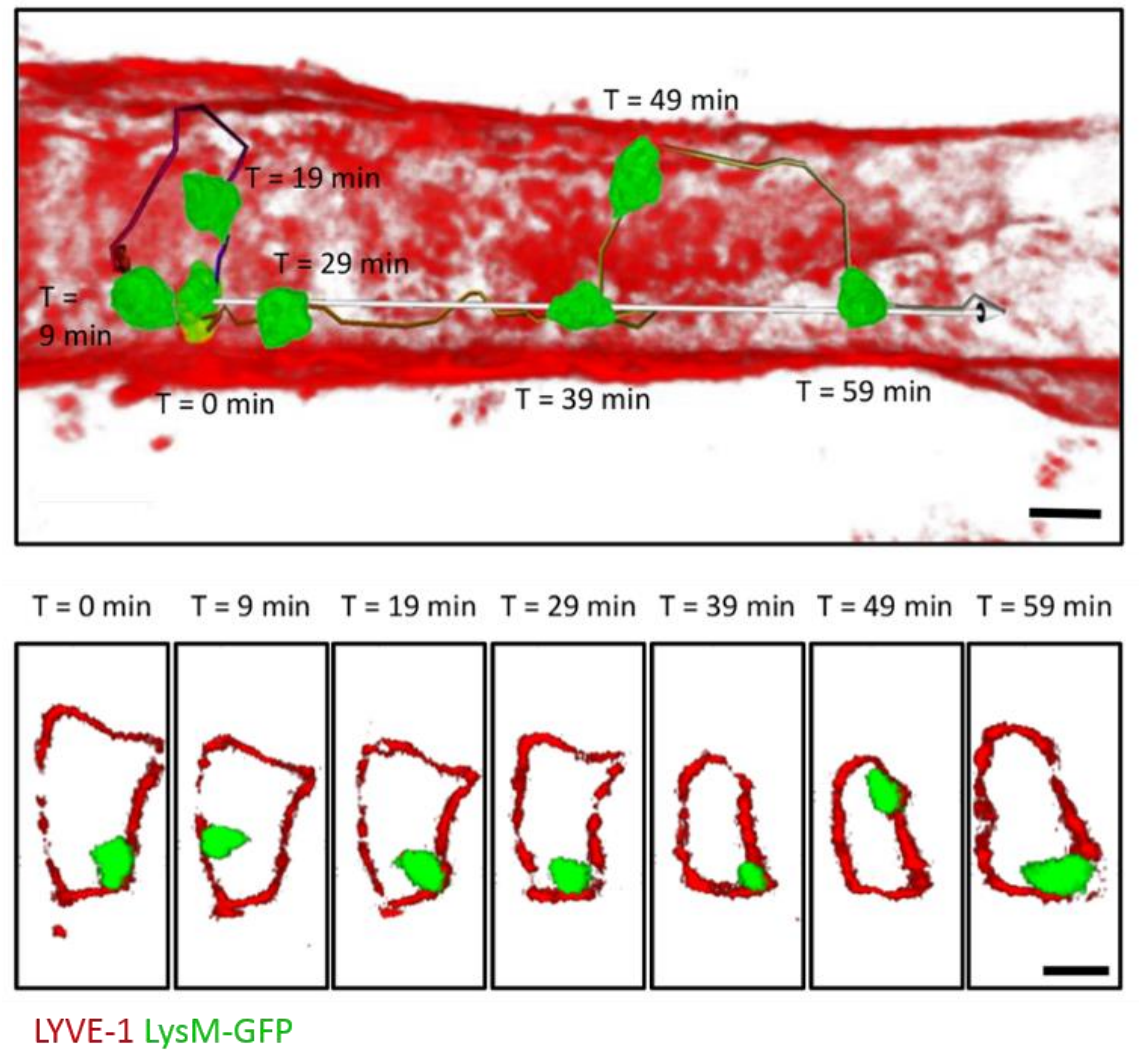

Figure 6.1: Dynamics of neutrophil crawling within lymphatic vessels of TNF-stimulated cremaster muscles in real-time *in vivo*. These are representative 3D-reconstructed still images of a live recording of a TNF-stimulated cremaster tissue from a LysM-eGFP mouse and immunostained with a non-blocking low dose of anti-LYVE-1 mAb (red) *in vivo*. The dynamics of neutrophil crawling within lymphatic vessels was then analysed by intravital confocal microscopy and IMARIS software. The top image illustrates the crawling of a neutrophil along the lumen of the lymphatic vessel endothelium at different time-points. The crawling path (colour-coded line) and directionality (white arrow) of the neutrophil is shown on the image. The bottom panel images are a series of high magnification cross-sections of the main image at indicated time-points illustrating the continuous attachment of the neutrophil to the lymphatic endothelium. Bars: 10 μm. T, time.

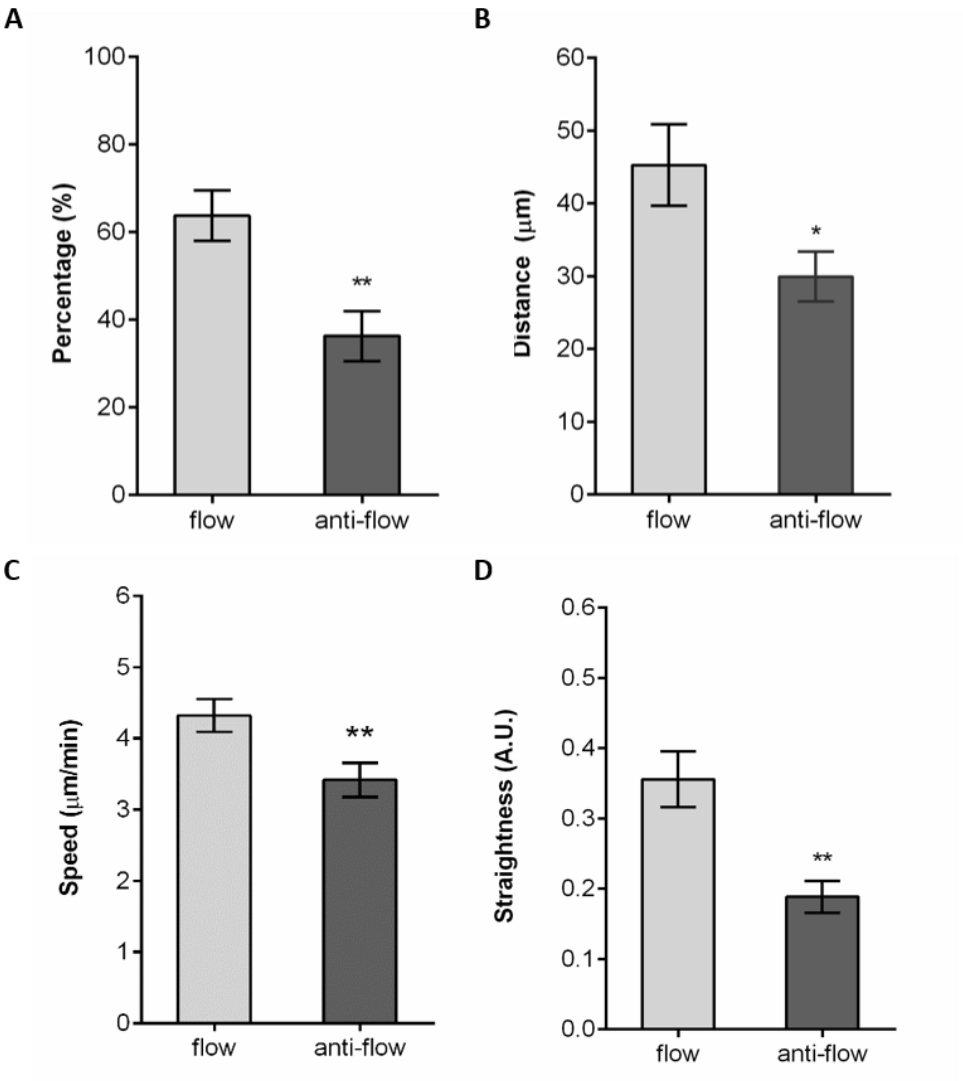

Figure 6.2: Crawling parameters within lymphatic vessels of TNF-stimulated cremaster muscles in real time *in vivo*. Mice were subjected to TNF-induced inflammation of the cremaster muscle and the dynamics of neutrophil crawling within lymphatic vessels were analysed by intravital confocal microscopy. The resulting video was analysed using IMARIS software. (A) Percentage of neutrophils crawling in the direction of lymph flow (flow) or in the opposite direction (anti-flow). Directionality (B), speed (C), and straightness (D) of neutrophils crawling in the direction of lymph flow (flow) or opposite direction (anti-flow) of the cremaster lymphatic vessels. Data are expressed as mean ± SEM from 8 independent experiments. For the crawling parameter analysis, a total of 63 cells were quantified from 8 mice. Statistically significant differences between flow and anti-flow groups of crawling cells are indicated by asterisks: *, $P < 0.05$; **, $P < 0.01$.Bar = 10 μm. Statistical significance was determined using one-way ANOVA.

6.3.2 Effects of TNF signalling on intraluminal crawling of neutrophils within lymphatic vessels following CFA+Ag-stimulation as observed by confocal intravital microscopy

In order to look at the impact of TNF signalling on neutrophil migration into lymphatic vasculatures, mice were subjected to CFA+Ag-induced inflammation in the cremaster muscle as before; an anti-TNF blocking Ab or isotope control Ab was then injected 4 h post-i.s. injection and mice were prepared for confocal IVM as described at the start of this section. Neutrophil crawling behaviours within the lumen of lymphatic vessels were observed and compared between anti-TNF/isotype control-treated mice. Movements of neutrophils within lymphatic vessels were tracked and analyses showed that cells in mice stimulated with CFA+Ag and treated with the isotype control Ab were able to crawl freely along the luminal side of the lymphatic endothelium in the direction of lymph flow (**Figure 6.3A** & **Video 3**). In contrast, mice treated with anti-TNF blocking Ab exhibited neutrophils with crawling impairments; most, if not all, lost all sense of directionality, exhibited meandering crawling paths and were mostly rendered immobile once crossing over to the luminal side of the lymphatic endothelium (**Figure 6.3B** & **Video 4**).

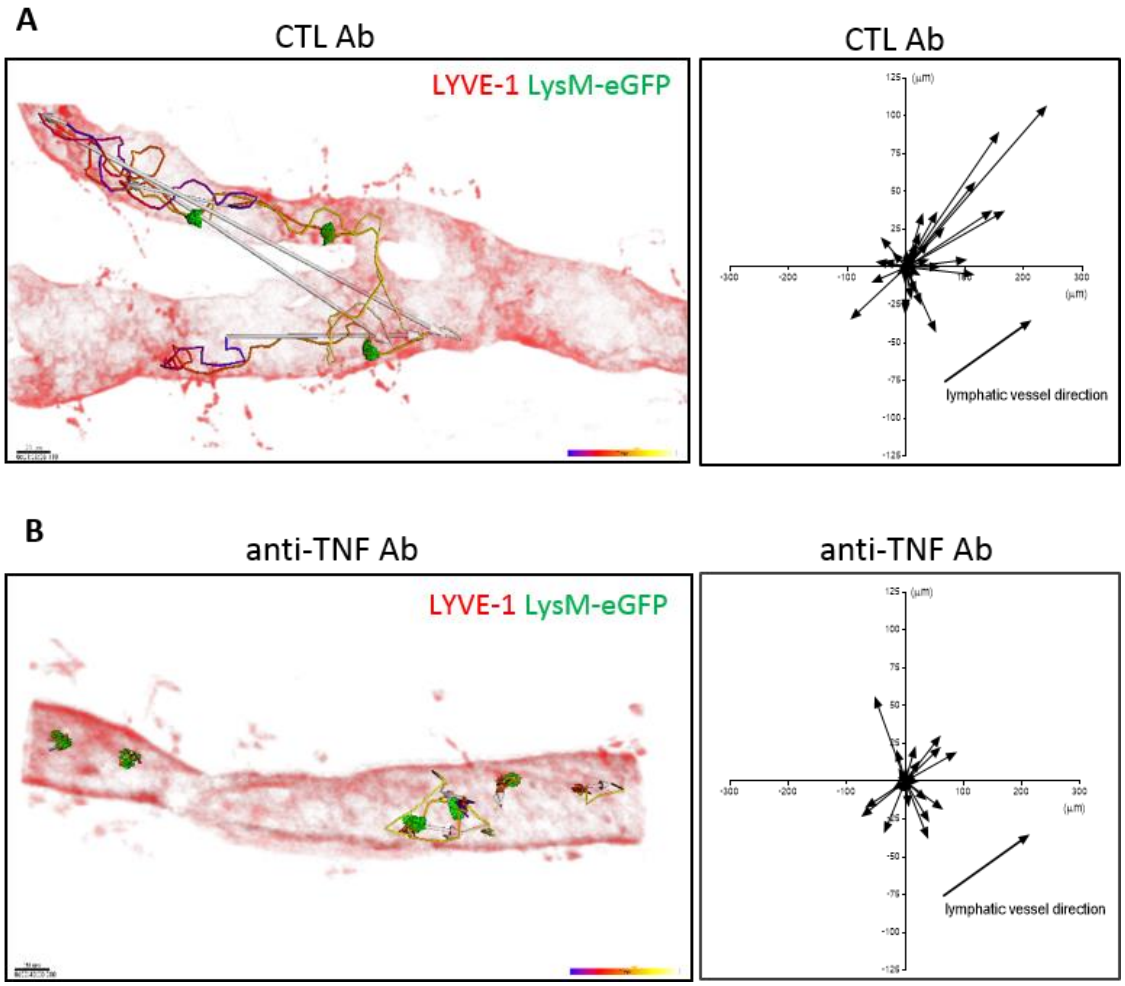

Figure 6.3: The effect of TNF signalling on neutrophil intraluminal crawling within lymphatic vessels. LysM-eGFP mice were subjected to CFA+Ag-induced cremaster inflammation and immunostained *in vivo* i.s with non-blocking dose of anti-LYVE-1 mAb (red). Isotype control or anti-TNF blocking mAbs were i.s injected 4 h post-i.s. injection. (A) The 3D-reconstructed image (left) is a representative still image at one time point of the IVM recording showing lymphatic-infiltrated neutrophils (green) and their associated crawling path (time-coloured mapped line) and/or directionality (white arrow) in mice treated with isotype CTL Ab, as analysed by IMARIS software. The directionality plot (right) shows the crawling paths of lymphatic-infiltrated neutrophils in the X & Y planes of the lymphatic vessels from CTL Ab-treated mice. Bar: 30 µm. (B) Representative still image (left) at one time point of the IVM recording showing lymphatic-infiltrated neutrophils (green) and their associated crawling path and/or directionality in mice treated with anti-TNF mAb, as analysed by IMARIS software. The directionality plot (right) shows the crawling paths of lymphatic-infiltrated neutrophils in the X & Y planes of the lymphatic vessels from anti-TNF mAb -treated mice. Bars: 30 µm. A total of 76 cells were analysed from 10 independent experiments.

Analysis of neutrophil crawling parameters within lymphatic vessels provided evidence that in isotype control Ab-treated mice, majority of these leukocytes moved in the direction towards collecting lymphatic vessels/lymph flow (67.8 ± 3.8 %) (**Figure 6.4A**), at a further displacement length of 90.9 ± 10.6 um (**Figure 6.4B**), at a speed of 5.8 ± 0.3 um/min (**Figure 6.4C**), and with a straightness index of 0.4 ± 0.04 (**Figure 6.4D**); whilst cells going against lymph flow had significantly reduced speed, directionality of movement and straightness (**Figure 6.4A-D**). Interestingly, analysis of neutrophil crawling parameters within lymphatic vessels of mice treated with the anti-TNF blocking Ab confirmed that they exhibited neutrophils that had lost all sense of directionality with significantly reduced speed, and straightness as compared to isotype control Ab-treated mice (**Figure 6.4A-D**).

The results in this section suggest that during the acute phase of the inflammatory response to CFA+Ag, TNF controls the directional crawling of neutrophils within the lymphatic vessels.

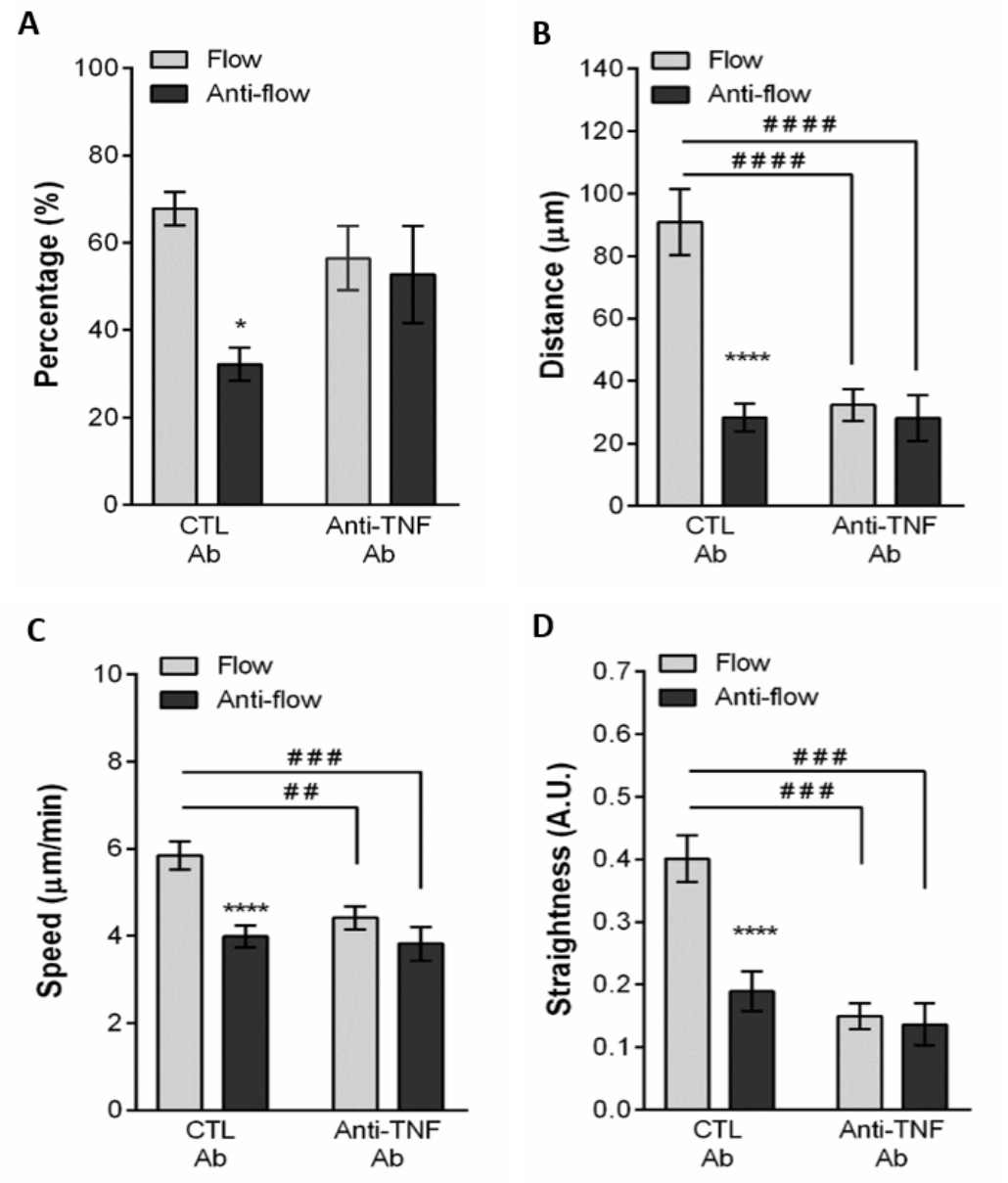

Figure 6.4: Crawling parameters of intraluminal crawling within lymphatic vessels of CFA+Ag-stimulated cremaster muscles in real time *in vivo* with TNF signalling-blockade. The effect of anti-TNF blocking mAb on neutrophil crawling along the luminal side of the lymphatic endothelium was analysed by intravital confocal microscopy (IVM) using LysM-eGFP mice subjected to CFA+Ag-induced cremaster inflammation. Isotype control or anti-TNF blocking mAbs were injected i.s. 4 h post-i.s. injection. (A) Quantification (in percentage) of neutrophils crawling in the direction of lymph flow (flow) or opposite direction (anti-flow) of the lymphatic vessel. Directionality (B), mean speed (C), and straightness (D) of neutrophils crawling in CTL mAb and anti-TNF treated groups. A total of 280 cells were analysed. Results are expressed as mean ± SEM of N = 4–9 mice (1-2 vessels analysed/mouse each mice representing one independent experiment). Significant differences between flow and anti-flow crawling cells are indicated by *, $P < 0.05$; ****, $P < 0.0001$. Significant differences between the CTL and anti–TNF mAb treated groups are indicated by hash symbols: ##, $P < 0.01$; ###, $P < 0.001$; ####, $P < 0.0001$. Statistical significance was determined using one-way ANOVA.

6.3.3 Role of ICAM-1 in mediating TNF-induced neutrophil intraluminal crawling within lymphatic vessels

To investigate the molecular mechanisms of TNF-dependent neutrophil intraluminal crawling within lymphatic vessels, the role of ICAM-1, an adhesion molecule known to support neutrophil crawling along both the luminal and abluminal surfaces of blood vessels was studied (Phillipson et al., 2006; Proebstl et al., 2012). ICAM-1 expression on cremaster lymphatic vessels under basal and inflamed conditions were first analysed by immunostaining methods. For this purpose, WT mice were stimulated with i.s injections of either 300 ng TNF (in 400 µl PBS) or an emulsion of CFA+Ag (200 µg of each in 300 µl total volume) for 6 h and 8 h, respectively. Unstimulated control mice received i.s. injections of PBS (400 µl). At the end of the inflammation period, cremaster muscles were dissected away, fixed, permeabilised and immunostained with anti-LYVE-1 and anti-ICAM-1 (or isotype control) mAbs to label the lymphatic vasculatures and ICAM-1, respectively, for analysis by confocal microscopy and IMARIS software. 3D-reconstructed images showed that ICAM-1 expression was up-regulated on lymphatic vessels in TNF- or CFA+Ag-stimulated tissues as compared to unstimulated tissues (**Figure 6.5**). These images also showed that TNF-stimulated tissues seemed to generally exhibit a higher and more heterogeneous expression of ICAM-1. Quantification of confocal images provided evidence of this up-regulation of ICAM-1 on stimulated tissues, with CFA+Ag resulting in an ~2-fold increase in expression, and TNF resulting in an even bigger (~3-fold) increase in ICAM-1 expression on lymphatic vessels, as compared to unstimulated controls (**Figure 6.6**). Staining with ICAM-1 isotype control Ab confirmed that the possibility of non-specific binding and autofluorescence was negligible (**Appendix 6**).

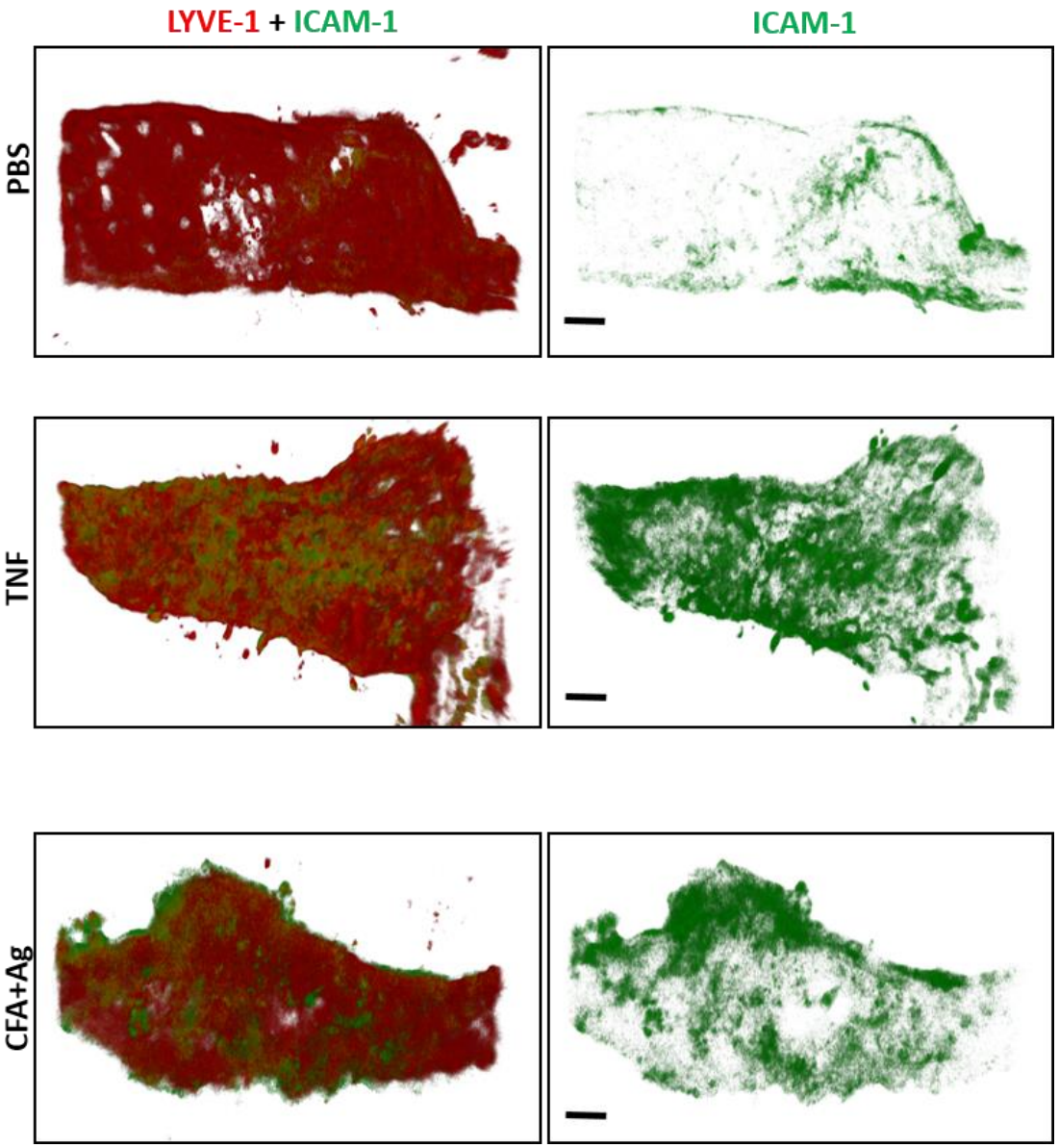

Figure 6.5: ICAM-1 expression on lymphatic endothelial cells in unstimulated, TNF and CFA+Ag-stimulated conditions *in vivo*. Cremaster muscles of C57BL/6 WT mice were stimulated with TNF or CFA+Ag (6 and 8 h, respectively) and immunostained with anti-LYVE-1 (red) and anti-ICAM-1/isotype control mAbs (green) to label the lymphatic vasculature and ICAM-1, respectively. The pictures are representative 3D-reconstructed confocal images of cremaster lymphatic vessels showing the expression of ICAM-1 on selected lymphatic vessels from a PBS-treated control (top panels), TNF-stimulated (middle panels) and CFA+Ag-stimulated (bottom panels) animals. The left panels show both LYVE-1 and ICAM-1/isotype control staining, and the right panels shows only ICAM-1. Bars: 30 µm.

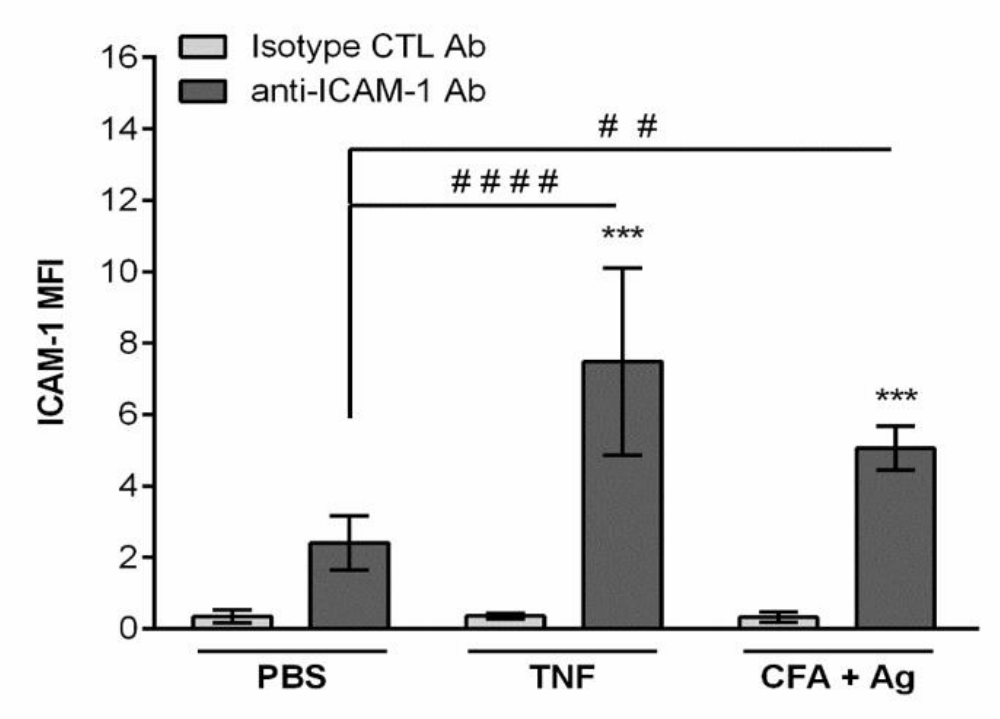

Figure 6.6: ICAM-1 expression on lymphatic vessels in unstimulated, TNF- or CFA+Ag-stimulated cremaster muscles *in vivo*. The graph shows ICAM-1 expression (mean fluorescent intensity or MFI) on vessels from PBS-treated control, TNF-stimulated and CFA+Ag-stimulated cremaster muscles as quantified by IMARIS software. Data are expressed as mean ± SEM of N = 8-12 vessels/animals from 4-11 animals per group (7 independent experiments). Statistically significant differences between the staining of isotype control and anti-ICAM-1 Abs treated groups are indicated by asterisks: *, $P < 0.05$; ****, $P < 0.0001$. Significant differences between unstimulated and inflamed groups are indicated by hash signs: ##, $P < 0.01$; ####, $P < 0.0001$. Statistical significance was determined by one-way ANOVA.

Having discovered that TNF resulted in the biggest up-regulation of ICAM-1 on lymphatic vessels, TNF signalling upon CFA+Ag challenge was blocked using an anti-TNF blocking mAb to see the effects of this on ICAM-1 expression. For this purpose, WT mice were stimulated with CFA+Ag as before and an anti-TNF blocking mAb or isotype control mAb was i.s injected 4 h post-i.s. injection. Eight hours post-i.s. injection, cremaster muscles were dissected away, fixed, permeabilised and immmunostained with anti-LYVE-1, anti-ICAM-1/isotype control mAb and MRP14 for confocal microscopy and IMARIS software analysis. Interestingly, 3D-reconstructed images showed a decrease in ICAM-1 expression in mice treated with the anti-TNF blocking mAb (**Figure 6.7A**). Quantification of these images further confirmed these findings of a reduction (~2.5 fold less) in ICAM-1 expression on lymphatic vessels of mice treated with the anti-TNF blocking mAb (**Figure 6.7B**). Intriguingly, when the relationship between ICAM-1 expression and the number of neutrophils found within lymphatic vessels was investigated, a positive correlation between ICAM-1 expression and number of neutrophils present within lymphatic vessels was found, suggesting a role for ICAM-1 in mediating neutrophil interactions with lymphatic vessels (**Figure 6.8**).

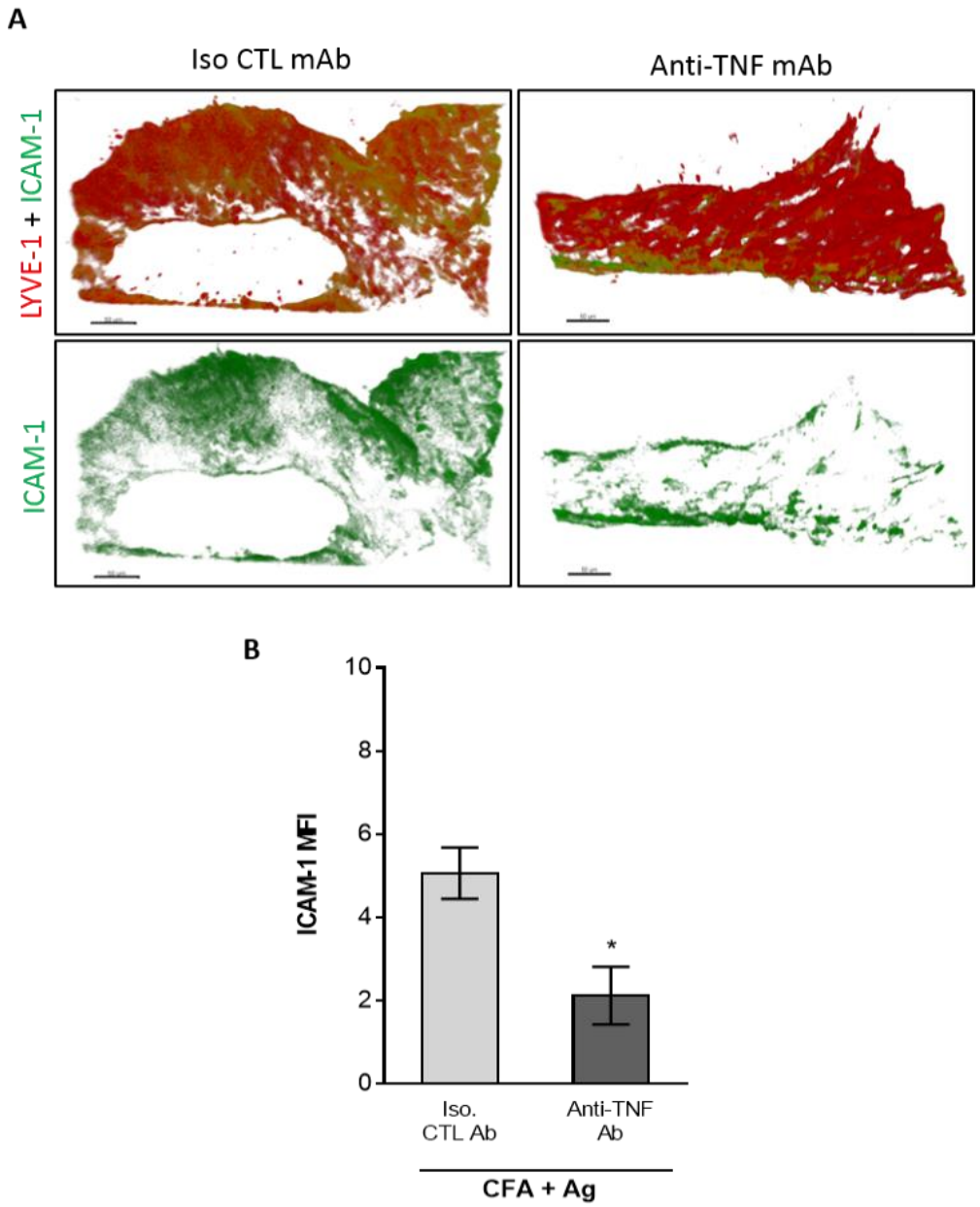

Figure 6.7: TNF controls ICAM-1 expression on lymphatic endothelial cells *in vivo*. C57BL/6 WT mice were stimulated with CFA+Ag and i.s injected with an anti-TNF blocking mAb/isotype CTL mAb was injected 4 h later. Eight hours post-i.s. injection, cremaster muscles were dissected away, fixed, permeabilised and immunostained with anti-LYVE-1 (red) and anti-ICAM-1/isotype control mAbs (green) to label the lymphatic vasculature and ICAM-1, respectively. (A) Representative 3D-reconstructed confocal images of cremaster lymphatic vessels showing the expression of ICAM-1 on selected lymphatic vessels from isotype CTL mAb-treated mice (top panels) and anti-TNF mAb--treated mice (bottom panels) animals. The right panels show both LYVE-1 and ICAM-1/isotype control staining, and the left panels shows only ICAM-1/Isotype control staining. Bar: 30 µm. (B) ICAM-1 expression on lymphatic vessels of CFA+Ag-stimulated cremaster muscles from animals pre-treated with an anti-TNF blocking mAb or isotype CTL mAb injected 4 h post-i.s. injection. Data are expressed as mean ± SEM from at least 8-10 vessels/animals, with 3-11 animals per group (at least 5 independent experiments). Statistically significant differences between the staining of isotype control- and anti-TNF Abs-treated groups are indicated by asterisks: *, $P < 0.05$. Statistical difference was determined using one-way ANOVA.

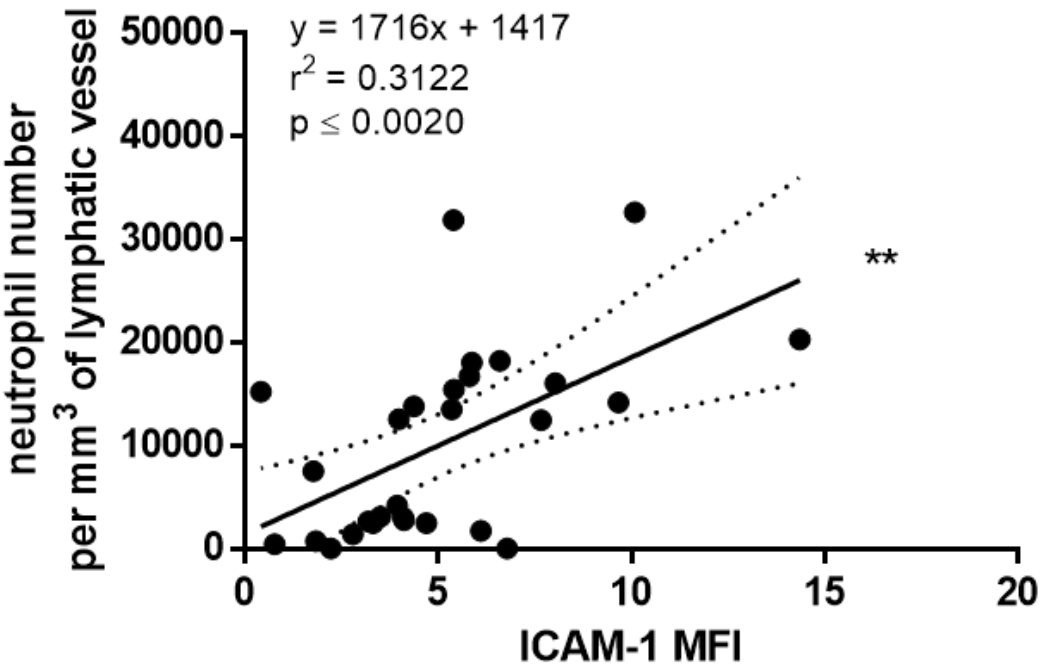

Figure 6.8: Correlation between ICAM-1 expression and neutrophil migration into lymphatic vessels of TNF-stimulated WT mice. Graph showing correlation between MFI of ICAM-1 expression (y) and number of neutrophils within lymphatic vessels (×) in TNF-stimulated WT mice as analysed by IMARIS software. Data are expressed as mean±SEM of n = 28 (8-12 vessels/animals from 3 animals, 2 independent experiments). Statistical significance was determined using linear regression analysis: **, $P < 0.01$.

These results are corroborated by previous findings from Dr Mathieu-Benoit Voisin, which provided evidence of the role of ICAM-1 in neutrophil crawling behaviour within lymphatic vessels (**Appendix 7 & Videos 5/6/7**). Functional assays were performed using local administration (4.5 h post-i.s. injection) of functional blocking antibodies against ICAM-1 or its leukocyte binding ligand, the integrin MAC-1, in CFA+Ag-stimulated cremaster muscles of LysM-eGFP mice. Confocal IVM was then carried out to observe neutrophil crawling parameters. Of significance to the ICAM-1 data in the current study, Dr Voisin found that blocking either ICAM-1 or MAC-1 resulted in a significant reduction (~50%) in the speed of crawling, displacement length, and straightness, on the luminal side of the lymphatic endothelium (**Figure 6.9**). These results are reminiscent of current findings following blockade of TNF-signalling (**Figure 6.4**).

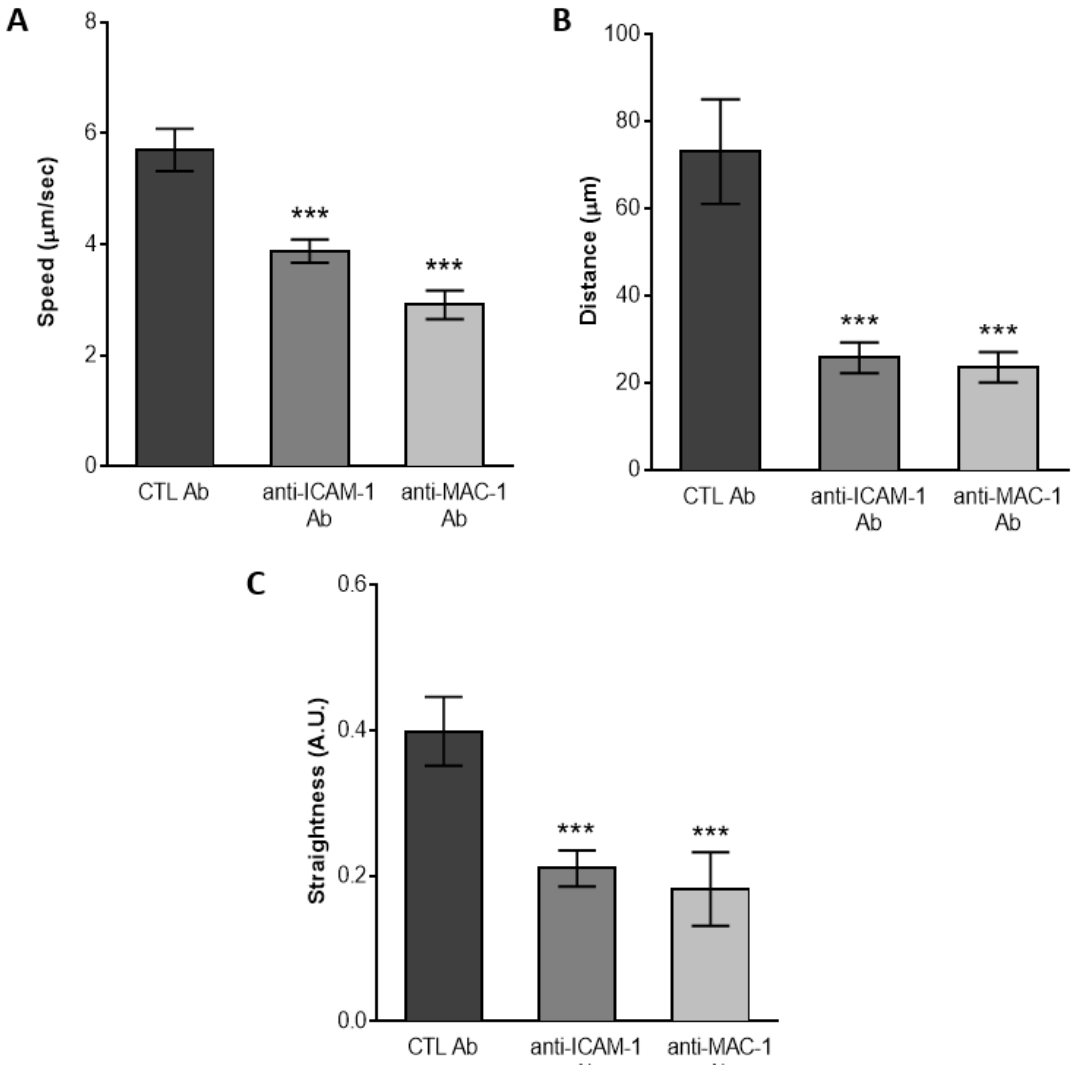

Figure 6.9: The effect of anti–ICAM-1 and anti-MAC-1 blocking antibodies on neutrophil intraluminal crawling parameters. LysM-eGFP mice were subjected to CFA+Ag-induced cremaster inflammation for 6 h. Mice also received at 4.5hrs post inflammation an i.s. injection of non-blocking dose of anti-LYVE-1 (red) and anti-PECAM-1 mAbs (not shown on the image) for the visualisation of both the lymphatic and blood vasculatures. Ninety minutes later, tissues were exteriorised to perform time-lapse recordings of the neutrophil responses for 2 h by intravital confocal microscopy. The effect of blocking antibodies against ICAM-1 and MAC-1 (injected locally 90min before recordings) on neutrophil migration paths in the interstitium and lymphatic vessels was investigated and analysed using IMARIS software. (A-C) Neutrophil intraluminal crawling in blocking Ab-treated mice was quantified and compared to the responses obtained with an isotype CTL mAb. The three graphs show the mean speed (A), directionality (B) and straightness (C) of neutrophils crawling. A total of 280 cells were analysed. Results are expressed as mean ± SEM of N = 4–9 mice (1-2 vessels analysed/mouse for intravital confocal microscopy, each mice is a single experiment). Significant differences between blocking antibodies treated and control groups are indicated by *, $P < 0.05$; ***, $P < 0.001$; ****, $P < 0.0001$. Significant differences between other groups are indicated by # ($P < 0.05$). Experiments and quantifications were carried out by Dr. Mathieu-Benoit Voisin.

Overall, the results in this section, along with previous findings from Dr Voisin, identify ICAM-1 as an adhesion molecule that is up-regulated on lymphatic vessels following TNF- or CFA+Ag-stimulation; thus mediating neutrophil crawling along the luminal side of the lymphatic endothelium following inflammation. Additionally, the results here identify TNF as a key regulator of neutrophil directional motility within lymphatic vessels *in vivo*.

6.4 Discussion

In order for leukocytes, such as antigen-bearing DCs, to travel to lymph nodes for the initiation of adaptive immune responses, they have to first migrate into tissue associated lymphatic vessels and crawl along the luminal side of the lymphatic endothelium of initial lymphatics, passively drift through the lumen of collecting lymphatics before finally reaching draining lymph nodes (Tal et al., 2011). Though the mechanisms of this phenomenon have only been characterised for DCs to a certain extent, studies investigating intraluminal crawling of neutrophils within lymphatic vessels preceding entry into draining lymph nodes have been thoroughly neglected. Chapter 4 of this thesis investigated the role of chemokine:chemokine receptor axes in neutrophil migration across the lymphatic endothelium into the lumen of lymphatic vessels; providing clear evidence that TNF signalling triggers this migration process in a strictly CCR7-dependent manner. Despite this, it is important to unravel the processes that occur after neutrophil entry into the lumen of lymphatic vessels and before their arrival in draining lymph nodes. Along with this, elucidating the mechanisms that drive these processes is also imperative as neutrophils have been shown to play roles in shaping adaptive immunity. The results from this chapter demonstrated that TNF could not only drive neutrophil migration into initial lymphatic vessels, but it could also induce their intraluminal crawling within lymphatic vessels. They have also demonstrated that during the acute phase of inflammatory response to CFA+Ag, TNF signalling is critical in controlling the directional crawling of neutrophils within lymphatic vessels. Collectively, corroborating data from previous findings by Dr Voisin with those from the current study, ICAM-1 was identified as a key mediator of neutrophil intraluminal crawling within lymphatic vessels.

This chapter first sought to characterise neutrophil crawling behaviours within lymphatic vessels during inflammation with the use of confocal IVM. Observation of neutrophil intraluminal crawling events following TNF- or CFA+Ag-stimulation showed that they exhibited a characteristic crawling behaviour on the luminal side of the lymphatic endothelium, with their general movement going towards lymph flow in the direction of collecting lymphatic vessels. In line with this, Hampton et al. also observed neutrophil interactions with lymphatic vessels in a different model using *S. aureus* infection, although it is not clear from their data if the neutrophils are truly within the lumen of lymphatic vessels (Hampton et al., 2015). Additionally, they found that neutrophils frequently exhibited reverse direction of crawling although overall crawling paths were

not assessed in detail. In the current study, neutrophils were also observed reversing in direction during intraluminal crawling; however, examination of their overall crawling paths indicated they crawled in the general direction of lymph flow (**white arrow**, **Figure 6.1** & **Video 2**, **Figure 6.3A** & **Video 3**). An explanation for this random behaviour could be due to reduced lymph flow induced by the ketamine/xylazine anaesthesia used during the confocal IVM experiments. Alternatively, it could be attributable to the exteriorisation process of the tissue or just be a natural phenomenon. Indeed, more directional crawling of DCs within lymphatic vessels was observed when mice were anaesthetised with 1.5 % isoflurane, which had a lesser effect on lymphatic contraction (Tal et al., 2011). As no other studies looking at neutrophil intraluminal crawling behaviours within lymphatic vessels exist, the present study provides the first comprehensive characterisation of these crawling parameters within initial lymphatics.

This chapter next investigated the effects of TNF signalling on intraluminal crawling of neutrophils within lymphatic vessels of CFA+Ag-stimulated mice as findings from previous chapters of this thesis demonstrated a critical role of TNF in driving neutrophil migration into lymphatic vessels. The use of anti-TNF blocking Abs resulted in crawling impairments of neutrophils; loss of directionality and meandering crawling paths were observed, with most neutrophils rendered immobile on the luminal side of the lymphatic endothelium. Subsequently, the molecular mechanisms of intraluminal crawling within lymphatic vessels were explored. The role of the adhesion molecule, ICAM-1, was examined due to previous findings of its importance in mediating neutrophil crawling along both the luminal and abluminal surfaces of postcapillary venules during the process of leukocyte recruitment to sites of inflammation (Phillipson et al., 2006). ICAM-1 has also been demonstrated to be key in DC migration from the skin to dLNs, suggesting the involvement of LEC-expressed ICAM-1 in this process (Xu et al., 2001). In the present study, ICAM-1 expression was up-regulated on lymphatic vessels of murine cremaster muscles following TNF- or CFA+Ag-stimulation; blocking TNF signalling with the use of functional blocking Abs resulted in its down-regulation. TNF has been shown to up-regulate ICAM-1 expression on vascular ECs both *in vivo* and *in vitro* (Fingar et al., 1997; Yang et al., 2005). LECs express very low levels of ICAM-1 in uninflamed conditions, but can up-regulate this molecule upon TNF-stimulation in both human ECs *in vitro* (Johnson et al., 2006; Sawa et al., 2007) and mice (**Figure 6.5**). As CFA+Ag-stimulation was previously shown in Chapter 3 to result in the production of endogenous TNF within cremaster muscles, this could be an explanation as to why a lower level of ICAM-1

upregulation was seen on lymphatic vessels as compared to TNF-stimulation. The exact role of ICAM-1 in leukocyte migration into the lymphatic system is still unclear, although *in vitro* antibody blockade has been shown to inhibit both adhesion and transmigration responses of DCs through cultured human LECs (Johnson et al., 2006); *in vivo*, ICAM-1 has been reported to mediate crawling of DCs along the lymphatic endothelium (Nitschke et al., 2012). Interestingly, a positive correlation was found in the present study between ICAM-1 expression and neutrophil migration into lymphatic vessels of mice during inflammation, which corroborates previous *in vivo* data involving DC migration across the lymphatic endothelium (Miteva et al., 2010)

In conclusion, this chapter has shown that neutrophils crawl along the endothelium within initial lymphatics following a local inflammatory stimulus; a response that was TNF-dependent. Confocal IVM by Dr Voisin showed that anti-ICAM-1 and anti-MAC-1 mAbs impaired neutrophil intraluminal crawling within lymphatic vessels as compared to the isotype control Abs (**Appendix 7 & Videos 5/6/7**). Thus, local blockade of ICAM-1 or its integrin ligand, MAC-1, inhibited this crawling response whilst their capacity to cross the lymphatic endothelium to gain entry into the lumen of lymphatic vessels were unaffected (**Appendix 8**). Interestingly, ICAM-1 blockade also resulted in a reduction of neutrophils numbers within dLNs as compared to when an isotype control Ab is used (**Appendix 8**); an explanation for this could be due to the inability of neutrophils to migrate towards dLNs due to their crawling response within initial lymphatics being inhibited. The results seen with local blockade of ICAM-1/MAC-1 is interesting as this mirrors findings from another study investigating neutrophil crawling within blood vessels; neutrophils were rendered immobile on the vascular endothelium following administration of anti-ICAM blocking Abs (Phillipson et al., 2006).

Overall, this chapter has provided new insights into the processes that occur following neutrophil migration into lymphatic vessels, as well as the mechanisms underlying neutrophil crawling within these vessels during inflammation. This highlights potential and effective targets to manipulate the role of neutrophils in adaptive immune responses *in vivo*.

Limitations of the study

The limitations here are the same as those discussed at the end of Chapter 3 with an additional potential caveat. In summary, the use of mouse cremasters in the *in vivo* inflammatory models may not be as relevant to humans, albeit being a gold standard

method. The model also does not address possible sex differences in immune responses, however this can be remedied through the use of other vascular beds (e.g. ear or mesentery) in female mice. Furthermore, the use of CFA is not approved for use in humans but it mimics the classical immunisation protocols used in humans, which makes it appropriate for this study. Finally, the blocking antibodies against MAC-1 and ICAM-1 used in this study could potentially alter the behaviour of neutrophils due to the fact they can bind to Fc receptors on these cells. To overcome this potential issue, the use of small molecule antagonists or conditional KO mice could be used instead. However, the use of an isotype control antibody in the current study provides evidence that the Fc receptor does not contribute to the response as tissues treated with the specific blocking antibody show clear differences when compared to tissues treated with the isotype control antibody.

7 : General Discussion

7.1 Project Overview

During inflammatory responses, the recruitment of neutrophils from the circulation to sites of inflammation is crucial in providing a critical first line of defence in the immune response against invading pathogens. However, recent accumulating evidence has shown that the role of neutrophils spans beyond the basic but fundamental immunological processes of innate immunity (Mocsai, 2013). Specifically, neutrophils have been implicated in the regulation of adaptive immunity following exposure to pathogens and antigen sensitisation (Abadie et al., 2005; Maletto et al., 2006; Mocsai, 2013; Yang et al., 2010), through their ability to act as APCs (Iking-Konert et al., 2001), or through cytokine release for the activation of T and B lymphocytes (Abi Abdallah et al., 2011; Beauvillain et al., 2007; Cerutti et al., 2013), and DCs (Bennouna et al., 2003).

Whilst the role of neutrophils in regulating adaptive immunity is now well-documented, the precise mechanisms underlying neutrophil migration into LNs via the initial lymphatics are still very poorly understood. Several studies have indicated that neutrophils within dLNs originate from tissue-associated lymphatic capillaries via the afferent lymphatic vessels (Abadie et al., 2005; Chtanova et al., 2008; Gorlino et al., 2014; Hampton et al., 2015), but the mechanisms associated with neutrophil migration into the lymphatic vasculature remained unclear. This study therefore aimed to elucidate some of the mechanisms by which neutrophils act to cross the initial lymphatic endothelium barrier and migrate into associated LNs. This work has shown that components of the LEC glycocalyx present on lymphatic vessels are regulated and redistributed during inflammation; this is particularly relevant as the glycocalyx has previously been implicated in the regulation of leukocyte adhesion during their recruitment to sites of inflammation (Reitsma et al., 2007). This work also provides evidence for the involvement of endogenous TNF and the molecular mechanisms associated with trafficking of neutrophils into, as well as within the lymphatic vasculature *in vivo*. Specifically, using a mouse model of antigen sensitisation and cytokine-induced inflammation of the cremaster muscle, this study has shown that TNF orchestrates the migration of neutrophils into lymphatic vessels in a CCR7-dependent manner, as well as their subsequent crawling along the luminal side of the lymphatic endothelium in an

ICAM-1/MAC-1 dependent manner. Collectively, the findings of this work provide evidence for a previously unknown role for TNF in orchestrating the sequential interactions of neutrophils with tissue-associated lymphatic vessels during the acute inflammatory response of antigen sensitisation. TNF as a potential target for the development of future therapeutic interventions to manipulate adaptive immune responses through the context of neutrophil trafficking into the lymphatic system is also highlighted. The following discussion gives an overview of our findings and discusses the potential role of components of the LEC glycocalyx, chemokine:chemokine receptor axes, and TNF in inducing neutrophil migration into initial lymphatic vessels and their subsequent intraluminal crawling along the lymphatic endothelium (Arokiasamy et al., 2017).

7.1.1 Structure of murine cremaster muscle lymphatic vessels and neutrophil migration responses during TNF- or CFA+Ag-induced inflammation *in vivo*.

Previous studies have reported the structure of lymphatic vessels in various murine tissues (Baluk et al., 2007), but not in the cremaster muscle. Initial studies investigated the structure of lymphatic vessels through immunostaining of whole-mounted cremaster tissues from naïve WT C57BL/6 mice. These experiments showed that lymphatic vessels in murine cremaster muscles exhibited characteristic blind-ended lymphatic capillaries and the heterogeneous distribution of adhesion molecules made up of button-like junctions (VE-Cadherin) and flaps (PECAM-1). Additionally, lymphatic vessels in this tissue were shown to be made up of oak-leaf shaped cells. All of these results are in accordance with previous findings of the composition of initial lymphatics in other murine tissues (Baluk et al., 2007). Therefore, this indicates that majority of the lymphatic vessels looked at in the present study are initial capillary lymphatics. This is the first description of lymphatic vessels within murine cremaster muscles.

Neutrophils undergo transmigration through blood vessel walls into the interstitium during leukocyte recruitment to sites of inflammation (Proebstl et al., 2012; Woodfin et al., 2009). Following this, neutrophils have been shown to migrate to dLNs via afferent lymphatics (Abadie et al., 2005; Gorlino et al., 2014; Hampton et al., 2015; Rigby et al., 2015). However, the overall dynamics of these events occurring successively has not been

investigated, thus neutrophil migration responses were investigated following TNF and CFA+Ag-induced inflammation of the cremaster muscle.

The results revealed that local injections of both these inflammatory mediators not only induced the migration of neutrophils across blood vessels, but also into lymphatic vessels and their associated dLNs in a time-dependent manner. In particular, tissue infiltrated neutrophils were found to rapidly migrate into lymphatic vessels within the first 16 h post-i.s. injection, which provided us with an indication of suitable time-points to look at in subsequent studies. Although no other *in vivo* studies of the dynamics of neutrophil migration into lymphatic vessels currently exists, these results agree with an *in vitro* study, which showed that neutrophil migration across a monolayer of primary HDLECs also occurs in a time-dependent manner (Rigby et al., 2015). Interestingly, the rapid migration of neutrophils into lymphatic vessels was transient (peaking at 8 h post-i.s. injection) as compared to their extravasation from blood vessels, which continued to increase at 16 h post-i.s. injection. This suggests that not all neutrophils are capable of migrating through initial lymphatics and might indicate that only a sub-population of neutrophils that are amongst the first to be recruited to the tissue have the capacity to continue their journey to the lymphatics. This hypothesis is supported by a previous study by Beauvillain *et al*. that showed only a sub-population of blood neutrophils express CCR7 on their surface post-purification (Beauvillain et al., 2011). To support this hypothesis, our *in vitro* work demonstrated that only low doses of TNF resulted in significant CCR7 upregulation on the surface of neutrophils. Similarly, the generation of TNF in inflamed tissues *in vivo* was significantly detected in modest amount at 8 h, whilst the higher concentrations were found at 16 h post CFA+Ag stimulation. Altogether, our data could be an indication that neutrophils lose their capacity to migrate into lymphatic vessels if the release of TNF is too high through a modulation of their expression for CCR7 expression on the surface of neutrophils. However, further analyses are needed to confirm this hypothesis.

Additionally, by combining confocal IVM and computer-assisted image processing with the use of IMARIS software, GFP^{high} neutrophils could be directly visualised undergoing transmigration across the lymphatic endothelium *in situ* in the cremaster muscle, providing a platform to study in great detail interactions made between individual neutrophils and LECs. Such analyses were conducted on live cremaster tissue in anaesthetised LysM-eGFP mice (confocal IVM). This enabled the tracking of neutrophils in lymphatic vasculatures in real-time and in 4D, which provided valuable insight into the dynamics and mechanisms of neutrophil migration into lymphatic vessels *in vivo*. These

results showed that neutrophils in mice subjected to TNF-stimulation could be seen breaching the lymphatic endothelium at time-points analysed (4–5.5 h) before the peak of neutrophil migration into lymphatic vasculatures, and that this breaching process only took approximately 4.5 min, which is similar to the time taken for leukocytes to migrate through the vascular endothelium (Ley et al., 2007). Neutrophil migration across the lymphatic endothelium was not able to be observed at the time-points analysed (6–7.5 h) following CFA+Ag-stimulation, despite still being before the peak of neutrophil migration into lymphatic vessels. This could simply be due to the fact that most neutrophils had already undergone transmigration into lymphatic vessels by these time-points. Moreover, as we are visually limited to one vessel segment per video from each confocal IVM experiment, we may be missing cells which are migrating across the lymphatic endothelium in other vessels of the cremaster muscle.

7.1.2 Endogenous TNF controls the entry of neutrophils into initial lymphatic vessels following antigen sensitisation *in vivo*.

Findings from the studies above proved that both exogenous TNF and antigen sensitisation with an emulsion of CFA+Ag could induce a rapid but transient migration of neutrophils into the lymphatic vessels of murine cremaster muscles. Mouse cremaster muscles stimulated with an i.s. injection of an emulsion of CFA+Ag resulted in the rapid generation of endogenous TNF. Thus, the potential role of endogenous TNF in this response was investigated through the use of TNFRdbKO mice as a means of abolishing TNF signaling. The results showed that at 16 h post-i.s. injection with CFA+Ag, neutrophil migration into lymphatic vessels was impaired. This impaired response was also observed at the earlier time point of 8 h, thus eliminating the possibility that the reduction in neutrophil numbers observed at 16 h post-i.s. injection was due to the faster efflux of neutrophils from lymphatic vessels of the TNFRdbKO animals. Interestingly, TNF did not appear to mediate neutrophil extravasation from blood vessels into interstitial tissues, indicating a specific role for TNF in driving neutrophil migration into lymphatic vessels but not through blood vasculature at these time points. Furthermore, the use of chimeric mice exhibiting neutrophils deficient in both TNFRs in a WT microenvironment showed that TNF directly acts on leukocytes to induce this neutrophil migration response. These results demonstrate for the first time the direct involvement of TNF in triggering

the migration of neutrophils into tissue-associated lymphatic vessels upon antigen challenge *in vivo* (**Figure 7.1**).

It is interesting to note that neutrophil extravasation across the blood vessels of TNFRdbKO mice is not affected despite the fact that TNF inhibitors have been successfully used to treat many chronic inflammatory diseases (e.g. RA, vasculitis and Crohn's disease) by preventing leukocyte recruitment from the circulation (Taylor et al., 2000; Little et al., 2006; Ghosh et al., 2003). An explanation for this could be that the present study makes use of an acute inflammatory model wherein TNF does not seem to contribute to the recruitment of neutrophils *in vivo*. Therapeutically, TNF inhibitors are mainly used to treat chronic inflammatory diseases in which these drugs have to be maintained systemically and requires time to take effect (Combe, 2010).

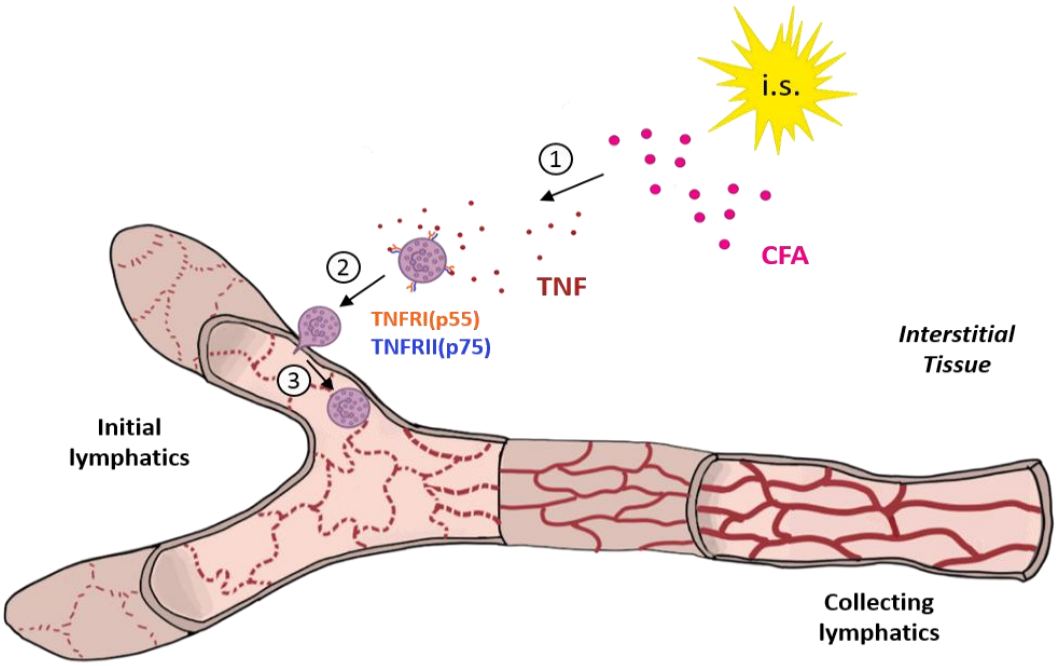

Figure 7.1: Schematic illustration of TNF triggering the migration of neutrophils into initial lymphatic vessels upon antigen sensitisation. (1) I.s. injection of CFA+Ag leads to TNF release within the interstitium. (2) TNF binds to neutrophil-expressed TNFRI/II and directly triggers their migration into initial lymphatic vessels (3).

7.1.3 The LEC glycocalyx is regulated and undergoes redistribution following TNF-induced inflammation of the cremaster muscle

The BEC glycocalyx has been widely studied and described (Reitsma et al., 2007), in contrast to the LEC glycocalyx. Apart from a recent study demonstrating the presence of a glycocalyx, similar to that of the BEC glycocalyx, on the luminal side of rat mesenteric collecting lymphatic vessels (Zolla et al., 2015), no other studies on the LEC glycocalyx exists. Thus, the present study investigated the regulation of the LEC glycocalyx of initial lymphatic vessels during inflammation by first probing for the presence of several known EC glycocalyx components. Initial studies investigated sugar residues expressed by lymphatic vessels with the use of carbohydrate-binding proteins called lectins. Staining of tissues with fluorescent lectins (IB4 and MAL-1, respectively) followed by confocal microscopy analysis, both of which are techniques used to visualise the BEC glycocalyx (Bai and Wang, 2014), revealed the presence of α-D-Galactosyl moieties and N-linked 2,3 sialylated glycans (α2,3 SAs), respectively, within the glycocalyx of lymphatic vessels. Additionally, the results showed that α-D-Galactosyl moieties were cleaved on lymphatic vessels following TNF and CFA+Ag-induced inflammation of cremaster muscles. This response was associated with an increased number of neutrophils observed within lymphatic vessels; this suggests that cleavage of α-D-Galactosyl residues on lymphatic vessels may either potentially contribute to the mediation of neutrophil trafficking into lymphatics or that neutrophil interactions with the lymphatic endothelium during their migration across this barrier triggers this cleavage (**Figure 7.2**). In support of the former hypothesis, glycocalyx shedding induced as a conquence of TNF stimulation could be a potential explanation, as has been shown to be the case in the BEC glycocalyx, although the mechanisms of this remained unknown (Henry and Duling, 2000; Chappell et al., 2009a). Chemokine receptors and adhesion molecules harboured within the glycocalyx could be exposed following TNF stimulation due to degradation of the enveloping glycocalyx (Chappell et al., 2008), thus could increase the accessibility of neutrophils to these molecules enabling the migration of more neutrophils. In support of the latter hypothesis, activated neutrophils have been shown to induce BEC glycocalyx damage through the production of ROS and proteases from their storage granules (van Golen et al., 2012). Further experiments will have to be done to see if neutrophil migration is affected by this cleavage, or if neutrophil migration across the lymphatic endothelium triggers this response (see section 7.2.4.2 for potential experimental setups).

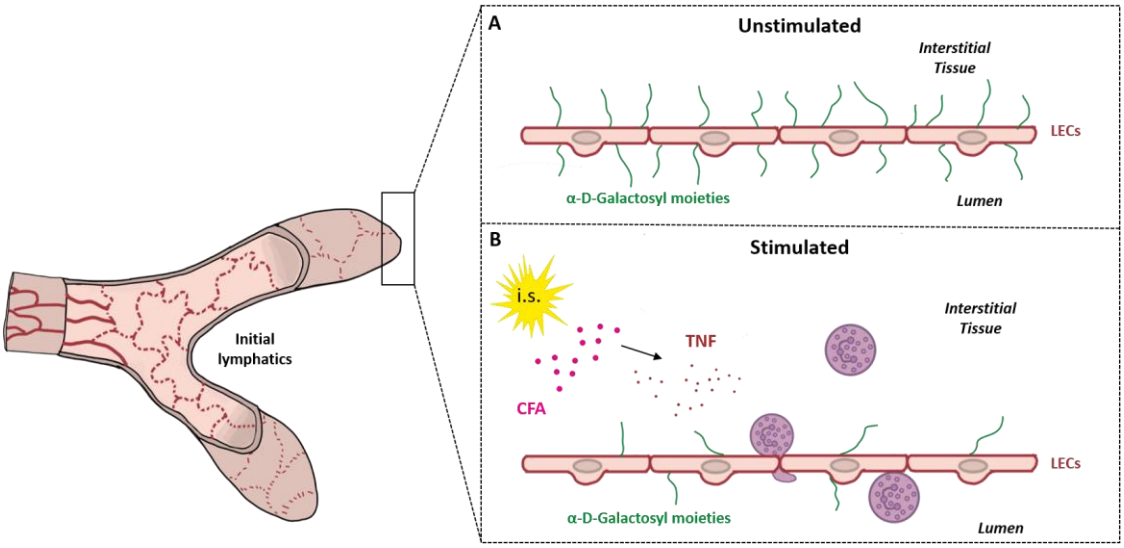

Figure 7.2: Hypothetical scenario in which cleavage of α-D-Galactosyl moieties mediates neutrophil migration across the lymphatic endothelium. (A) Under unstimulated conditions, α-D-Galactosyl moieties are present either in the lumen or abluminal side of the lymphatic endothelium as part of the LEC glycocalyx. (B) Following i.s. injection of CFA+Ag (which induces TNF release) or exogenous TNF, α-D-Galactosyl moieties are cleaved either as a direct consequence of TNF acting on the lymphatic endothelium or due to ROS/protease release by activated neutrophils as they migrate across the lymphatic endothelium.

IB4 is widely used as a blood vasculature marker (Ernst and Christie, 2006), but in the context of lymphatics, our results have shown for the first time that α-D-Galactosyl residues of the LEC glycocalyx are cleaved with inflammation. In contrast, confocal microscopy analysis of MAL-1 staining showed no changes in overall expression of N-linked α2,3 SAs on lymphatic vessels following inflammation, although it seems that redistribution of these SAs on lymphatic vessels occurred. α2,3 SAs expression was found near the edges of lymphatic vessels in TNF stimulated tissue, whereas this was not present in CFA+Ag stimulated tissues. In the BEC glycocalyx, SA redistribution has been shown to play key roles in permeability control during shear stress *in vitro* (Bai and Wang, 2014), thus redistribution of SAs observed in the LEC glycocalyx could potentially play similar roles in the regulation of lymphatic vessel permeability and function in the context of inflammation. Further studies will have to be carried out to determine the consequence of this redistribution on neutrophil trafficking into lymphatic vessels (see section 7.2.4 for potential experimental setups). Nevertheless, the presence of N-linked sialylated glycans on lymphatics implicates these vessels as potential targets for increased viral entry and their systemic dissemination. Certain viruses (influenza viruses, rotaviruses, adenoviruses) have been shown to use host-sialylated structures for binding to their target

host cell (Cashman et al., 2004; Dugan et al., 2008; Isa et al., 2006; Skehel and Wiley, 2000). Furthermore, viral infections of LECs induces permeability (Gavrilovskaya et al., 2012, 2013), thus binding of viruses to SAs on lymphatic vessels could potentially lead to increased viral entry. Alternatively, this increased permeability could also lead to the disruption of host pathogen clearance by potentially allowing other pathogens being transported within lymphatic vessels back into the interstitium. In support of this, pathogen release into the interstitium has previously been observed in senescent vessels exhibiting decreased glycocalyx coverage and increased permeability (Zolla et al., 2015). Additionally, numerous bacteria have also been demonstrated to make use of host-sialylated acids to evade host immune responses through a strategy of 'molecular mimicry', and inhibition of opsonisation and their phagocytosis *in vivo* (Harvey et al., 2001; Telang et al., 2001; Vogel and Frosch, 1999). The results from the present study thus implicate lymphatic vessels as having potential roles in immune evasion by such microbes and highlights the potential of these vessels as being therapeutic targets for the prevention of viral entry and their subsequent dissemination.

The regulation of HS on lymphatic vessels was next investigated following TNF-stimulation. HS is the most abundant GAG on ECs, and has been reported to be critical for chemokine mobilisation and functional presentation on both HEVs and the lymphatic endothelium during lymphocyte and DC homing to dLNs (Bao et al., 2010). Immunostaining and confocal microscopy analysis demonstrated that although there were no changes in total HS expression on lymphatic vessels in response to TNF, redistribution of this GAG on lymphatic vessels was observed. HS distribution on lymphatic vessels was far more homogenous and diffused, as compared to the patchy expression on vessels of unstimulated tissues. In the context of blood vessels, HS has been shown to be down-regulated in an *in vivo* sepsis model of acute lung injury due to the production of heparanase by blood vascular endothelium activated by endogenous TNF; this was associated with increased neutrophil binding to blood vascular walls (Schmidt et al., 2012). As no changes were seen in HS expression, further studies will have to be carried out to determine the exact function of its redistribution on lymphatic vessels in the context of neutrophil trafficking (see section 7.2.4.3 for potential experimental setups). An explanation for why we see no differences could simply be due to the fact that the present study has already shown variations in the distribution of sugars on the BEC and LEC glycocalyx, thus what is observed on blood vessels does not necessarily translate to the same observation on lymphatic vessels. Differences in the time-points looked at could

also be a factor; previous studies investigating changes in the BEC glycocalyx looked at far more acute time-points ranging from 0-90 minutes post-i.s. injection (Chappell et al., 2009a; Chappell et al., 2009b; Schmidt et al., 2012), as compared to the present study (16 h post-i.s. injection).

HS binding of the lymphatic chemokine, CCL21, leads to its immobilisation and the formation of a chemotactic gradient that guides DCs within interstitial tissues towards lymphatic vessels (Weber et al., 2013). In addition, HS expression by HEVs controls CCL21 chemokine presentation to facilitate the homing of lymphocytes into lymphoid organs (Bao et al., 2010; Tsuboi et al., 2013). Investigations into CCL21 expression by lymphatic vessels show that expression levels decrease in response to TNF and CFA+Ag stimulation, despite no changes in total HS expression. Our results show the formation of a higher CCL21 chemokine concentration gradient during inflammation. As has been shown to be the case for DC migration within the interstitium (Weber et al., 2013), this CCL21 gradient formation presumable provides chemotactic cues to guide neutrophils within the tissue towards lymphatic vessels. Further studies will have to be carried out to determine if HS expressed by lymphatic vessels does indeed bind CCL21 for presentation to neutrophils (see section 7.2.4.3 for potential experimental setups). Overall, these results demonstrate the glycan-centred therapeutic potential of the LEC glycocalyx for the prevention of pathogen dissemination through the lymphatic vessels. However, further studies have to be carried out to elucidate the interplay between the redistribution/regulation of HS and CCL21 in mediating neutrophil trafficking into lymphatic vessels (see section 7.2.4.3 for potential experimental setups).

7.1.4 TNF promotes the migration of neutrophils into lymphatic vessels in a strictly CCR7-dependent manner *in vivo*.

7.1.4.1 The CXCL1:CXCR1/2 and CXCL12/CXCR4 chemokine axes play no significant roles in neutrophil migration across the lymphatic endothelium during the acute phase of antigen sensitisation.

To elucidate the mechanisms of neutrophil migration into lymphatic vessels, several chemokine:chemokine receptor axes were initially investigated. The CXCL1:CXCR1/2 chemokine axis was investigated as another study demonstrated that the human neutrophil chemoattractant, CXCL8, is up-regulated in TNF stimulated HDLECs *in vitro*, and promotes neutrophil migration across a monolayer of human LECs (Rigby et al., 2015). In the mouse system, LECs isolated from mouse skin showed an up-regulation of the CXCL1 gene following 24 h of CFA-induced inflammation *in vivo* (Vigl et al., 2011). However, the present *in vivo* model of CFA+Ag-induced neutrophil trafficking into lymphatic vessels proved that this chemokine axis did not play any significant role in this process; CXCL1 blockade with the use of an anti-CXCL1 blocking mAb did not affect the capacity of neutrophils to migrate into lymphatic vessels. These data highlight differences between *in vivo* and *in vitro* models. Indeed, several studies have pointed to the importance of the microenvironment for LECs to retain their specific lymphatic characteristics that are lost in culture, such as the capacity to generate CCL21 (Amatschek et al., 2007; Wick et al., 2007).

Additionally, the role of the CXCL12:CXCR4 axis was investigated since it was recently shown to be involved neutrophil trafficking into the lymphatic system following *S. aureus* infection. The results from the present study demonstrated that CXCR4 blockade with the CXCR4-specific inhibitor, AMD3100, did not significantly inhibit neutrophil migration into lymphatic vessels of CFA+Ag-stimulated cremaster muscles. An explanation for this conflicting data could be due to differences in the model and inflammatory pathway involved. *S. aureus* infection preferentially activates the TLR2 pathway *in vivo* (Kielian et al., 2005; Stenzel et al., 2008; Yimin et al., 2013), whereas CFA-stimulation activates the TLR4 pathway to induce an immune response (Kleinnijenhuis et al., 2011). In addition to this, activation of TNF and TLR4 signalling pathways have been shown to result in the down-regulation of CXCR4 on neutrophils, thus rendering them less responsive to CXCL12 stimulation (Bruhl et al., 2003; Kim et al., 2007). This supports

results from the present study where a down-regulation of CXCR4 expression on neutrophils was found in a model of CFA+Ag-induced inflammation. Taken together, these studies indicate that the pathway of activation may influence the molecular axis used for neutrophil migration into the lymphatic system.

7.1.4.2 The CCL21:CCR7 chemokine axis mediates neutrophil trafficking into the lymphatic system in vivo.

The above findings highlighted the possibility that other chemokine:chemokine receptor axes may play regulatory roles in facilitating neutrophil migration across the lymphatic endothelium following the acute inflammatory response as induced by CFA+Ag *in vivo*. Thus, the potential involvement of the CCL21:CCR7 chemokine axis was investigated as it has been widely implicated in mediating DC/T cell migration into the lymphatic system (Johnson and Jackson, 2008). The role of CCR7 in neutrophil recruitment into the lymphatic system was first demonstrated in a mouse model of intradermal immunisation and in human neutrophils by Beauvillain *et al*. (Beauvillain et al., 2011). In accordance with their study, intracellular stores of CCR7 were detected in murine blood neutrophils. Beauvillain *et al*. also demonstrated that activation of these neutrophils through purification of BM-derived cells lead to the detection of CCR7 expression on the cell surface (Beauvillain et al., 2011). Similarly, the results in the present study showed that neutrophils recruited into inflamed tissues (i.e. inflamed cremaster muscles) had an up-regulation of CCR7 expression on their cell surface as compared to blood neutrophils. Interestingly, TNF stimulation of murine blood neutrophils *in vitro* promoted the surface expression of CCR7; low concentrations of TNF were enough to initiate this response. This is further supported by a previous study showing a similar up-regulation of CCR7 on human neutrophils in a tumour model (Eruslanov et al., 2014), although the mechanism and physiological consequences of this response in humans is still unclear. These results suggest that the priming of neutrophils for enhanced chemokine receptor expression was occurring post-i.s. injection. Thus, the potential involvement of GM-CSF and IL-17 in this priming process was investigated, having been previously shown to prime human neutrophils to migrate towards the chemokines, CCL19 and CCL21, *in vitro* (Beauvillain et al., 2011). However, we did not detect the generation of these cytokines in the cremaster muscle at any of the time-points analysed (0 h, 4 h, 8 h, 16 h and 24 h). Overall, these data suggests a predominant role of TNF in this response and may highlight

the importance of the origin of the cells analysed (e.g. BM vs. blood, tissue-infiltrated vs. naïve cells, murine vs. human leukocytes).

CCR7KO mice were used to address the potential involvement of the CCL21:CCR7 chemokine axis following both CFA+Ag and TNF stimulation; migration responses in these mice were compared with those of WT mice. The results showed that neutrophil migration across blood vasculatures was unaffected in CCR7KO mice as compared to WT mice at both 8 h and 16 h post-TNF/CFA+Ag stimulation. However, in comparison to WT mice, whilst neutrophil migration into lymphatic vessels of CCR7KO mice was partially inhibited (~75% reduction) following CFA+Ag stimulation, neutrophil migration into lymphatic vessels of these mice was strikingly completely suppressed (~97% reduction) in response to TNF stimulation. Whilst we appreciate that CCR7KO mice are constitutive knock-outs, deficient for CCR7 in all of their cells, the generation of chimeric mice exhibiting CCR7KO neutrophils further confirmed that in a WT microenvironment, CCR7KO neutrophils are unable to migrate into the lymphatic system. These results thus indicate the importance of TNF in promoting neutrophil migration into lymphatic vessels in a strictly CCR7-dependent manner (**Figure 7.3**).

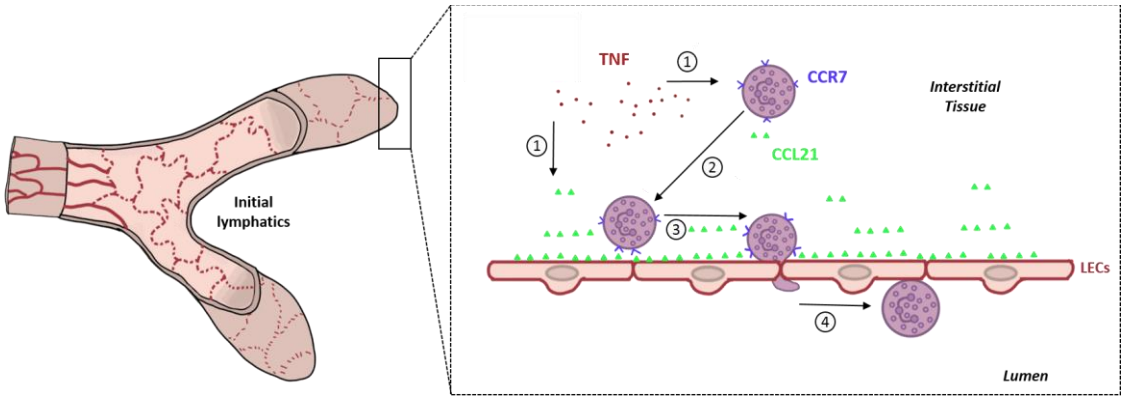

Figure 7.3: TNF triggers the migration of neutrophils into initial lymphatics in a strictly CCR7-dependent manner. (1) TNF stimulation induces surface expression of CCR7 on neutrophils *in vitro* and the formation of a CCL21 concentration gradient from the abluminal surface of the lymphatic endothelium into the interstitial tissue *in vivo*. (2) CCR7-expressing cells migrate along the CCL21 gradient. (3) Interactions between CCR7 and CCL21 on lymphatic endothelium results in the migration of neutrophils across the lymphatic endothelium into the lumen of lymphatic vessels (4).

7.1.4.3 Increased levels of CXCL12 are responsible for neutrophil trafficking into dLNs of CCR7KO mice

An interesting observation was made in the dLNs of CCR7KO mice under basal conditions. In comparison to WT mice, unstimulated CCR7KO mice exhibited approximately 25 times more neutrophils within their dLNs; inflammation of the cremaster muscles with TNF or following antigen sensitisation with an emulsion of CFA+Ag did not further increase the number of neutrophils found in the dLNs. As flow cytometry analysis showed no difference in the percentage of circulating neutrophils between WT and CCR7KO mice, this abnormal trafficking of neutrophils into the dLNs of CCRKO mice could be related to higher levels of CXCL12 expression found in the dLNs of these unstimulated mice as compared to WT dLNs. Additionally, whilst neutrophil expression levels of the CXCL12 receptor, CXCR4, were found to be similar in both genotypes, treatment with the CXCR4 antagonist AMD3100 significantly reduced the number of these leukocytes infiltrating CCR7KO dLNs, whereas neutrophil migration into initial lymphatics was not affected. The generation of chimeric mice exhibiting CCR7KO neutrophils in a WT microenvironment was able to address this abnormal trafficking of neutrophils into LNs. Taken together, these data not only supports the hypothesis that CXCR4 signalling contributes to neutrophil homing to LNs via HEVs (Gorlino et al., 2014), but also demonstrates for the first time that in steady-state, increased CXCL12 levels within LNs contribute to neutrophil migration via this route.

7.1.5 TNF is a key regulator of neutrophil crawling within initial lymphatic vessels through the induction of ICAM-1 up-regulation *in vivo*.

Having identified TNF as a key signal for promoting neutrophil trafficking into lymphatic vessels, its potential involvement in mediating other neutrophil-lymphatic vessel interactions was investigated. Studies looking at neutrophil responses following TNF stimulation (and CFA+Ag stimulation) were carried out in real-time using confocal IVM and LysM-eGFP mice through the tracking of GFP^{high} neutrophils. Following TNF stimulation (and CFA+Ag stimulation), neutrophils were observed crawling along the luminal side of the lymphatic endothelium. Analysis of crawling parameters showed that majority of neutrophils crawled towards the directional flow of lymph. In contrast, neutrophils going against lymph flow exhibited reduced displacement length, speed and

straightness. In support of these data, a previous study also observed the crawling of neutrophils within lymphatic vessels, although there was no clear evidence as to whether this was intraluminal or abluminal crawling (Hampton et al., 2015). The results from the present study thus indicate that TNF is not only able to trigger the migration of neutrophils into lymphatics (as discussed above in section 7.1.4.2), but also shows for the first time that local inflammatory stimuli are able to induce the intraluminal crawling of neutrophils within initial lymphatic vessels in the direction of collecting lymphatics. The present study also provides the first comprehensive characterisation of neutrophil intraluminal crawling parameters within initial lymphatic vessels following inflammation.

TNF is a prototypical pro-inflammatory cytokine that plays a key role in many immune responses, including cell recruitment and leukocyte activation (Cross et al., 2008; Dewas et al., 2003; Fujishima et al., 1993; Ginis and Tauber, 1990). It has also been implicated in the pathogenesis of numerous inflammatory conditions and autoimmune disorders, such as RA, lupus, psoriasis and atherosclerosis (Aringer and Smolen, 2008; Matsuno et al., 2002; Popa et al., 2007). TNF is not usually expressed under healthy conditions, but increased levels in serum and tissue are detected during inflammation and infectious conditions. Despite there being considerable evidence for the successful usage of TNF blockers in the treatment of certain chronic inflammatory conditions, anti-TNF therapy is associated with a heightened risk of opportunistic infections and poor vaccination responses in patients (Murdaca et al., 2015). Furthermore, their precise mechanism of action remains unclear, although the suppression of leukocyte recruitment and activation is considered to be a principle mode of action (Tracey et al., 2008). TNF is able to activate blood vascular EC (BECs), leading to the expression of both chemoattractants and adhesion molecules on the vascular endothelium (Pober, 2002). In particular, ICAM-1, an adhesion molecule demonstrated to be essential for neutrophil directional crawling during their recruitment through blood vessels (Phillipson et al., 2006; Proebstl et al., 2012), has been shown to be up-regulated by BECs in response to TNF stimulation both *in vivo* and *in vitro* (Fingar et al., 1997; Leeuwenberg et al., 1992; Yang et al., 2005). At resting state, LECs express ICAM-1 at very low levels, but this is up-regulated following TNF stimulation in humans (Johnson and Jackson, 2010; Sawa et al., 2007). This up-regulation was also observed in primary murine LECs from previous experiments (data not shown). ICAM-1 also plays a key role in DC adhesion and transmigration through HDLECs *in vitro* (Johnson et al., 2006), and has been shown to mediate crawling of DCs along the lymphatic endothelium *in vivo* (Nitschke et al., 2012). However, its role in

neutrophil trafficking within lymphatic vessels *in vivo* has yet to be determined. Thus, this formed the basis of subsequent investigations in the present study.

Immunostaining for ICAM-1 on lymphatic vessels followed by confocal analysis showed that ICAM-1 was constitutively expressed in unstimulated tissues, but this expression was up-regulated in response to TNF and antigen sensitisation with an emulsion of CFA+Ag. This response was associated with increased neutrophil numbers found within initial lymphatics during inflammation, which is in accordance with a previous study involving DC migration across the lymphatic endothelium (Miteva et al., 2010). Interestingly, TNF blockade through the administration of anti-TNF mAbs *in vivo* inhibited this up-regulation of ICAM-1 on initial lymphatic vessels. Furthermore, confocal IVM using LysM-eGFP mice demonstrated that TNF blockade *in vivo* following CFA+Ag stimulation resulted in neutrophil intraluminal crawling impairments, with majority of neutrophils being rendered immobile on the luminal side of the lymphatic endothelium due to losing all sense of directionality. Finally, previous results from my supervisor, Dr Voisin, demonstrated that ICAM-1 and MAC-1 blockade with blocking antibodies also resulted in impaired neutrophil intraluminal crawling within lymphatic vessels, whilst neutrophils' capacity to cross the lymphatic endothelium from the interstitium remained unaffected. This response was also associated with a reduction of neutrophil numbers infiltrating the LNs. DCs migration from inflamed tissues to dLNs is well recognised as an important step in the initiation of adaptive immune responses (Randolph et al., 2008). However, it has been found that neutrophils are in fact the first immune cell type to reach LNs from sites of bacterial infection (Abadie et al., 2005). Thus, these results highlight potential and effective targets to manipulate the role of neutrophils in adaptive immune responses *in vivo*.

Overall, these findings demonstrate for the first time that TNF and CFA+Ag stimulation induces the up-regulation of ICAM-1 expression by lymphatic vessels, thus enabling their intraluminal crawling on the luminal side of the lymphatic endothelium; a response that was shown to be TNF-dependent (**Figure 7.4**).

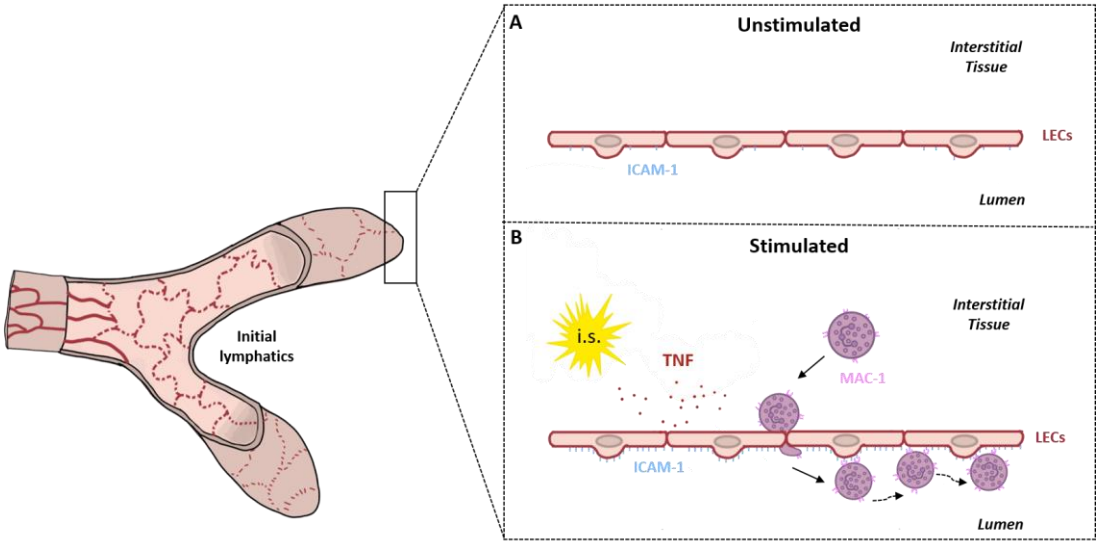

Figure 7.4: TNF induces ICAM-1/MAC-1 dependent intraluminal crawling through the upregulation of ICAM expression by initial lymphatic vessels. (A) Under unstimulated conditions, ICAM is constitutively expressed by the lymphatic endothelium. (B) Following i.s. injection of TNF, leading to up-regulation of ICAM-1 expression by the lymphatic endothelium. Neutrophil migration across the lymphatic endothelium occurs and mediates neutrophil crawling on the luminal side of the endothelium in an ICAM-1/MAC-1 dependent manner; this response is TNF-dependent.

7.2 Open questions and future perspectives

7.2.1 What is the source of endogenous TNF following antigen sensitisation?

The present study demonstrated that antigen sensitisation of the cremaster muscle with an emulsion of CFA+Ag induced the rapid release of TNF in these tissues. Naturally, the next step would be to investigate the source of this TNF release. Indeed, recent studies conducted by Dr Voisin, has shown that mice depleted of tissue macrophages following the local delivery of clodronate liposomes (van Rooijen and Hendrikx, 2010) exhibited a significant reduction in TNF release as compared to control liposome-treated animals. Though significant, TNF release was not fully suppressed. This could be due to release from other cells or even activated neutrophils themselves. Although activated macrophages are thought to be the primary source of TNF (Arango Duque and Descoteaux, 2014; Parameswaran and Patial, 2010), neutrophils have been shown to be able to release TNF in different models of inflammation as induced by chemoattractants (Chou et al., 2010; Gaudreault and Gosselin, 2009; Finsterbusch et al., 2014), or other inflammatory mediators such as LPS (Dubravec et al., 1990), or upon exposure to Candida albicans (Bazzoni et al., 1991; Djeu et al., 1990). Furthermore, in an immunisation model using CFA+Ag, neutrophils recruited to LNs were shown to secrete TNF within these tissues (Maletto et al., 2006). Thus, further studies are needed to clarify whether they indeed secrete TNF in our model, or whether this pro-inflammatory cytokine is secreted by other cell types previously shown to do so, including ECs (Imaizumi et al., 2000), smooth muscle actin cells (Newman et al., 1996), fibroblasts (Fahey et al., 1995) and mast cells (Woolley and Tetlow, 2000). Specifically, to investigate the involvement of neutrophils in TNF release, ELISA and/or western blot analysis of tissue lysates from neutrophil-depleted tissues following the use of anti-GR-1 mAbs (Daley et al., 2008) could be compared to control-depleted tissues. Alternatively, mice exhibiting neutrophil-specific deficiencies in both TNFRs could be used for these experiments. LECs have never been shown to secrete TNF, thus future work could involve investigating this *in vitro* by either using flow cytometry analysis of stimulated and permeabilised cells or ELISA and/or Western Blot analysis of cell culture supernatants.

7.2.2 Which TNF receptor is involved in CCR7 up-regulation on neutrophils and in mediating their migration into lymphatic vessels?

The results from the present study have shown that TNF induces the up-regulation of CCR7 on neutrophils, and directly acts on leukocytes to trigger their migration across the lymphatic endothelium into the lumen of initial lymphatic vessels. However, the specific signalling mechanisms leading to this response remain unclear. Thus, it would be interesting to further investigate this and determine which of the two TNFRs (p55 or p75), or if both, are required for this response. Work that has been done during the course of this study has shown that neutrophils have surface expression of both TNFRs (**Appendix 9**). Thus, future experiments could include the use of TNFR single KO mice instead of TNFRdbKO mice. Alternatively, confocal microscopy analysis of fixed tissues from stimulated WT mice receiving i.s. injections of TNFRI/II specific blockers or blocking Abs (Richter et al., 2013; Dong et al., 2016) to observe if neutrophil migration is suppressed with inhibition of either TNRI or TNFRII signalling. Alternatively, transgenic mice with targeted deletion of either the TNFRI or TNFRII gene could be used. Furthermore, *in vitro* studies involving pre-treatment of isolated neutrophils with TNFRI/II specific blockers or blocking Abs before TNF stimulation could be carried out to observe if inhibition of either TNFR signalling pathways results in a lack of CCR7 up-regulation on the cell surface. Nystatin would have to be used in these experiments, as in the present study, to prevent endocytosis of CCR7. Finally, as a sub-population of neutrophils were found to express CCR7 following activation (Beauvillain et al., 2011), it would be interesting to extend these studies to an *ex vitro/in vitro* human model. Primary human LECs and human neutrophils could be isolated from tissues (e.g. skin) and blood, and transwell assays could be carried out with the use of TNFRI/II specific blockers or blocking Abs. Primary HDLECs could be grown on the underside of transwell filters before the addition of primed exogenous neutrophils (with GS-CSF and IL-17 [Beauvillain et al., 2011]) pre-treated with TNFRI/II specific blockers or blocking Abs to the top chamber, followed by the addition of exogenous TNF. Alternatively, neutrophils isolated from cantharidin-induced skin blisters could be used in these experiments and they would already be primed (Phong et al., 2011). Neutrophil migration responses across HDLECs could then be monitored to see if migration is suppressed with inhibition of either TNFRs, as compared to control treated cells. Flow cytometry analysis of isolated human neutrophils pre-treated with TNFRI/II specific

blockers or blocking Abs before TNF stimulation could also be carried out to observe if inhibition of either TNFR signalling pathways results in a lack of CCR7 up-regulation on the cell surface.

7.2.3 Does TNF-induced CCR7-dependent neutrophil migration into lymphatic vessels occur with other stimuli and during chronic inflammatory conditions?

In the present study, the role of TNF in neutrophil migration into lymphatic vessels was demonstrated following antigen challenge. However, the effects of other inflammatory stimuli on the CCL21:CCR7 chemokine axis-dependent neutrophil migration should also be investigated in more detail, such as with the use of other inflammatory mediators (e.g. LPS or LTB_4). Live bacteria or other pathogens (e.g. fungi) could also be tested although a previous study involving S. aureus challenge has demonstrated that the CCR7 chemokine pathway is not involved in neutrophil migration to dLNs via afferent lymphatics (Gorlino et al., 2014). Similar studies like the ones used in the present study involving CCR7KO mice could be carried out to determine if other inflammatory stimuli also produce the same response. ELISAs could also be carried out to determine if TNF is produced within tissues following the use of these inflammatory stimuli.

Additionally, as all investigated reactions to date have been acute inflammatory responses, it would be interesting to compare responses occurring during chronic inflammation. Neutrophil migration responses into lymphatic vessels could be studied in experimental mouse models of chronic inflammatory conditions, such as inflammatory bowel disease or autoimmune diseases (e.g. mouse model of collagen II induced arthritis), with the use of anti-CCR7 mAbs at specific time-points (i.e. after extravasation has occurred) to see if this pathway could be exploited for future therapeutic developments.

7.2.4 What is the functional consequence of the regulation and redistribution of the LEC glycocalyx?

7.2.4.1 Is the LEC glycocalyx present on the luminal or abluminal (or both) sides of LECs?

The vascular EC glycocalyx is present on the luminal side of ECs and plays a role in leukocyte extravasation from the blood into inflamed interstitial tissues (Reitsma et al., 2007). Is the LEC glycocalyx therefore present mainly on the abluminal surface to mediate leukocyte migration into the lumen of lymphatic vessels? Our studies have shown using *in vivo*-live staining (non-permeabilised) and *ex vivo*-fixed staining (permeabilised) of tissues that both intracellular and surface expression is present, but whether this is mainly luminal or abluminal expression remains unclear from the data. This is due to the lack of natural lymph flow in harvested tissues, which results in lymphatic vessels collapsing and thus making it extremely difficult to determine if staining is abluminal or luminal. To elucidate this, further confocal IVM experiments could be carried out to visualise the LEC glycocalyx in real-time *in vivo* with a higher magnification. With this experimental set-up, natural lymph flow occurs and the structural integrity of lymphatic vessels are not compromised, which will enable us to have a clearer indication of abluminal or luminal expression of the LEC glycocalyx. To do this, LYVE-1 and the lectins would have to be i.s. administered to stain lymphatic vessels and the LEC glycocalyx. Furthermore, as only 2 lectins representing 2 sugar residues successfully stained lymphatic vessels in the present model, a wider panel of lectins could be tested out. This includes but is not limited to: succinylated wheat germ agglutinin (sWGA, specific for N-acetylglucosamine), helix pomatia (HP, specific for α-D sialic acid), peanut agglutinin (PNA, specific for gal β1, 3, N-acetylgalactosamine); all of these have been used to characterise the EC glycocalyx (Brouland et al., 1999; Nakanuma et al., 1993). In addition, HS could also be i.s. injected in these experiments to observe the localisation of this GAG in relation to the sugar residues. Studies could include the pre-treatment of TNF and CFA+Ag to observe changes in these components during inflammation, and a ×63 objective could be used for higher magnification in order to determine if the glycocalyx is situated on the abluminal or luminal side of the lymphatic endothelium. Neutrophil interactions with the LEC glycocalyx following TNF- or CFA+Ag-induced inflammation could also be investigated in real-time using confocal

IVM and LysM-eGFP mice in the above experiments to observe if GFP^{high} neutrophils exhibit any preferential migration into lymphatic vessels at sites with high/low expression of sugar residues or HS. Confocal IVM could also be used to measure the changes in the thickness of the glycocalyx during inflammation, as compared to basal conditions. Finally, electron microscopy techniques could be used to visualise the LEC glycocalyx under both basal and inflamed conditions. This has previously been done in collecting lymphatics, with the results showing a glycocalyx spanning the luminal side of the lymphatic endothelium (Zolla et al., 2015). However, this has yet to be done in the initial lymphatics thus could be an interesting avenue to pursue.

7.2.4.2 Does the cleavage of α-D-Galactosyl residues on lymphatic vessels mediate neutrophil migration across the lymphatic endothelium?

This study showed that a reduction in α-D-Galactosyl moieties on lymphatic vessels was correlated with an increased number of neutrophils found within the lumen of these vessels, thus suggesting that two possible scenarios were occurring: 1) cleavage of these sugars (presumably by indirect TNF signalling) could be mediating neutrophil migration across the lymphatic endothelium, or 2) neutrophil interactions with the lymphatic endothelium during their migration across may be causing this cleavage. Future experiments to test this out could include the use of *in vivo* (i.s.) administration of the enzyme, α-D-Galactosidase, followed by confocal analysis to look at neutrophil migration into lymphatic vessels of stimulated tissues, as compared to the responses in non-treated tissues. In addition, confocal IVM and LysM-eGFP mice could be used to look at these responses in real-time to observe if cleavage of these sugars results in an increased capacity of GFP^{high} neutrophils to adhere to the surface of lymphatic vessels and migrate into the lumen of these vessels. Additionally, local depletion of neutrophils in the cremaster muscle could be carried out through i.s. injections of anti-GR-1 mAbs to see if the glycocalyx is cleaved following inflammation in the absence of neutrophils. The role of TNF in cleaving these sugar residues could be examined through the use of TNFRdbKO mice and neutrophil-depletion of the tissues before stimulation. Confocal analysis of lectin staining would allow us to observe if sugar residues are cleaved in the absence of TNF signalling, as compared to similarly treated WT animals. Finally, *in vitro* experiments could be carried out, starting with a monolayer of primary LECs. Stimulated exogenous neutrophils could then be added on the top of these LECs and removed/washed off before subsequently staining the LECs with IB4 and analysis by confocal microscopy.

Comparisons of IB4 staining could be made between LECs encountering exogenous neutrophils and LECs that are only subjected to the washing step to determine whether changes in α-D-Galactosyl residue expression occurs due to neutrophil interactions with the lymphatic endothelium.

7.2.4.3 Are CCL21 chemokine gradients formed within lymphatic vessels? Does this induce directional intraluminal crawling of neutrophils?

This study showed that following TNF and CFA+Ag stimulation, most neutrophils crawled on the luminal side of the lymphatic endothelium in the general direction of lymph flow. Whilst it could be assumed that neutrophils were being directed towards collecting lymphatics by the natural flow of lymph, other factors may also affect the directionality of neutrophil crawling within lymphatic vessels. However, whether neutrophil crawling is a random process or follows a characteristic pattern remains unclear (Phillipson et al., 2006; Ryschich et al., 2006; Wojciechowski and Sarelius, 2005). Perhaps mechanotaxis (driven by mechanical force of shear flow), or the formation of chemokine gradients leading to chemotaxis, chemokinesis and haptotaxis (attraction to chemokines attached to ECM) play roles in neutrophil intraluminal crawling. Other studies of neutrophil intraluminal crawling in blood vessels have shown that the crawling of neutrophils does not appear to be biased in the direction of blood flow, suggesting that crawling is not simply a result of the dragging motion due to hydrodynamic force displacement (Phillipson et al., 2006; Ryschich et al., 2006; Wojciechowski and Sarelius, 2005). It is now known that chemotactic gradients along the endothelium provide directional cues for leukocyte crawling, and ultimately TEM - the final step in the adhesion cascade (Massena et al., 2010; Zimmerman et al., 1992). Specifically, HS has been shown to sequester the neutrophil chemoattractant, MIP-2, and present these chemokines on the luminal side of the blood vascular endothelium for chemotaxis-driven neutrophil crawling (Massena et al., 2010). Therefore, since HS was detected on lymphatic vessels in the present study, does it bind CCL21 for its presentation on the lymphatic endothelium?

Recent quantifications by Dr Voisin of confocal images from this study showed that inflamed initial lymphatic vessels exhibited a gradient of CCL21 within the vessel in the direction of lymph flow. This gradient could explain why the majority of neutrophils crawl along the luminal side of the lymphatic endothelium in the direction of lymphatic

flow. Thus, further studies would have to be carried out to determine if this is due to HS-dependent presentation of CCL21. Experiments could include the use of confocal IVM and i.s. injections of both an anti-HS Ab and anti-CCL21 Ab to provide further insights into the interactions of CCL21 and HS in real-time *in vivo*. Additionally, inflammation could be induced in the cremaster muscle before these confocal IVM experiments to address if the redistribution of HS observed on lymphatic vessels in the present study mimics the redistribution of CCL21 presentation in real-time *in vivo*. *In vivo* administration (i.s.) of the sugar degrading enzyme, heparanase, could also be used to remove HS on lymphatic vessels; tissues could then be collected and followed up with *ex vivo*-fixed staining of both HS and CCL21, followed by the use of confocal microscopy analysis to look at changes in their expression on lymphatic vessels as compared to non-treated mice. A heparanase inhibitor could also be used in similar experiments for comparison. Further functional studies could also be carried out by using LysM-eGFP mice and confocal IVM to track GFP^{high} neutrophil interactions with lymphatic vessels following the i.s. administration of heparanase in the cremaster muscle in real-time. Alternatively, transgenic mice exhibiting impairments in HS synthesis could be used to look at neutrophil migration responses *in vivo* (Bao et al., 2010). *In vitro* studies could also be carried out to determine the functional importance of HS. Primary murine LECs could be grown on the underside of transwell filters, and either pre-treated with heparanase or transfected with siRNA targeting HS biosynthetic enzymes, before the addition of exogenous CCL21 to the bottom chamber and primed exogenous neutrophils (with GS-CSF and IL-17 [Beauvillain et al., 2011]) to the top chamber. Neutrophil migration responses across LECs could then be monitored to see if migration is inhibited as compared to control treated LECs.

Finally, as ICAM-1 was found to play a key role in neutrophil intraluminal crawling within initial lymphatics in the present study, it would be interesting to see if a gradient of these adhesion molecule forms within the lumen of lymphatic vessels. Confocal IVM experiments could be carried out to visualise the expression of ICAM-1 on the luminal side of the lymphatic endothelium in real-time *in vivo*. A fluorescently conjugated anti-ICAM-1 mAb would have to be intrascrotally injected into WT mice, and comparisons could be made between stimulated and unstimulated mice. This would give an indication as to whether the formation of an ICAM-1 gradient potentially guides neutrophil intraluminal crawling towards collecting lymphatics and dLNs.

7.2.5 Are ICAM-1/MAC-1 the only molecules involved in intraluminal neutrophil crawling on the luminal side of the lymphatic endothelium? What other molecules could be involved?

This study demonstrated that TNF-dependent neutrophil crawling on the luminal side of the lymphatic endothelium following administration of a local inflammatory stimulus occurs through the upregulation of ICAM-1 on initial lymphatics, leading to ICAM-1/MAC-1-dependent crawling. In blood vessels, the interaction of both these molecules has been shown to be critical for neutrophil crawling in response to CXCL2 (MIP-2) and TNF (Phillipson et al., 2006), ultimately leading to their successful transmigration across the vascular endothelium. However, before neutrophil crawling can occur, their firm adhesion and stabilisation to the luminal surface of the vascular endothelium is required. This has been shown to be dependent on the interaction of LFA-1 with ICAM-1 *in vivo* (Phillipson et al., 2006). Since the present study demonstrates that neutrophil intraluminal crawling within lymphatic vessels involves the same molecules as those involved in crawling within blood vessels, it would be interesting to see if the LFA-1/ICAM-1 interactions also play roles within lymphatics. Thus, confocal IVM experiments involving the stimulation of LysM-eGFP mice and inhibition of LFA-1 with the use of blocking antibodies, or LFA-1 KO crossed with LysM-eGFP mice, could be carried out to analyse if LFA-1 mediated adhesion to the luminal side of the lymphatic endothelium is required for subsequent neutrophil intraluminal crawling within lymphatic vessels. Additionally, the role of ICAM-2, an adhesion molecule that binds both LFA-1 and MAC-1 (Li et al., 1993; Xie et al., 1995), could also be explored. ICAM-2 is constitutively expressed on ECs and has been shown to have a key role in the regulation of neutrophil crawling dynamics within the lumen of blood vessels (Halai et al., 2014). Functional or genetic blockade of ICAM-2 *in vivo* resulted in aberrant and reduced neutrophil crawling velocity (Halai et al., 2014), which is similar to what we observed within initial lymphatics following ICAM-1 blockade. Thus, experiments involving ICAM-2 blockade through the use of blocking Abs or ICAM-2 KO mice crossed with LysM-eGFP mice could be carried out, and neutrophil crawling on the luminal side of the lymphatic endothelium could be observed in real-time using confocal IVM. It would also be interesting to investigate the potential formation of an ICAM-2 gradient within initial lymphatics following stimulation with the use of confocal IVM (as described for ICAM-1 at the end of section 7.2.4.3), to determine if this plays a potential role in guiding neutrophils towards the direction of collecting lymphatics and LNs.

Finally, it has been recently demonstrated that HS-dependent haptotactic gradients of CCL21 mediate DC migration to dLNs *in vivo* (Weber et al., 2013), and that murine LECs generate a gradient of CCL21 when exposed to low shear stress, which is responsible for the directional crawling of DCs *in vitro* (Russo et al., 2016). Thus, HS and CCL21 could also potentially affect neutrophil interactions with the luminal side of the lymphatic endothelium in our model *in vivo*. This could be investigated via confocal IVM using stimulated LysM-eGFP mice crossed with those that have impaired HS biosynthesis, in addition to i.s. injection of a fluorescently-conjugated anti-CCL21 Ab to visualise this chemokine. This would allow us to observe GFP^{high} neutrophils' intraluminal crawling along the lymphatic endothelium in real-time *in vivo* in order to determine if HS-dependent CCL21 presentation within the lumen occurs, and if HS-deficiency results in aberrant intraluminal crawling.

7.2.6 Concluding remarks

A greater understanding of the distinctive molecular mechanisms that control neutrophil recruitment to LNs via initial lymphatics would provide insight into the possible therapeutic avenues based on regulating neutrophil migration. In light of this, the present study has provided evidence for some of the mechanisms underlying neutrophil trafficking into and within initial lymphatic vessels of inflamed tissues. This study has shown that components of the LEC glycocalyx are regulated and redistributed during inflammation. The consequences of this on neutrophil migration into initial lymphatics are still unclear although it is tempting to speculate that modulation of the glycocalyx is key for this process, as this has been shown to be the case in neutrophil extravasation from blood vessels (Kolarova et al., 2014). More importantly, this study has demonstrated for the first time a predominant role for endogenous TNF in orchestrating both CCR7-dependent migration of neutrophils into initial lymphatics and ICAM-1 dependent crawling on the luminal surface of the lymphatic endothelium during the acute phase of the inflammatory response, as induced by antigen sensitisation (**Figure 7.5**). Taken together, the findings of the present study identify TNF as a new molecular regulator of neutrophil migration into the lymphatic system *in vivo* and has also shed significant light onto a new potential mechanism of action – and limitations – for anti-TNF therapy. The findings also highlight potential and effective targets, which could very well be exploited for the optimisation of neutrophil-based vaccination strategies or for reshaping protective immune responses *in vivo*. Finally, potential therapeutic targets have been revealed, which may prove useful in preventing further dissemination of pathogens through the recirculation of antigen-bearing neutrophils via the lymphatic system, thus preventing the establishment of systemic infections that could lead to severe clinical conditions, such as sepsis and septic shock.

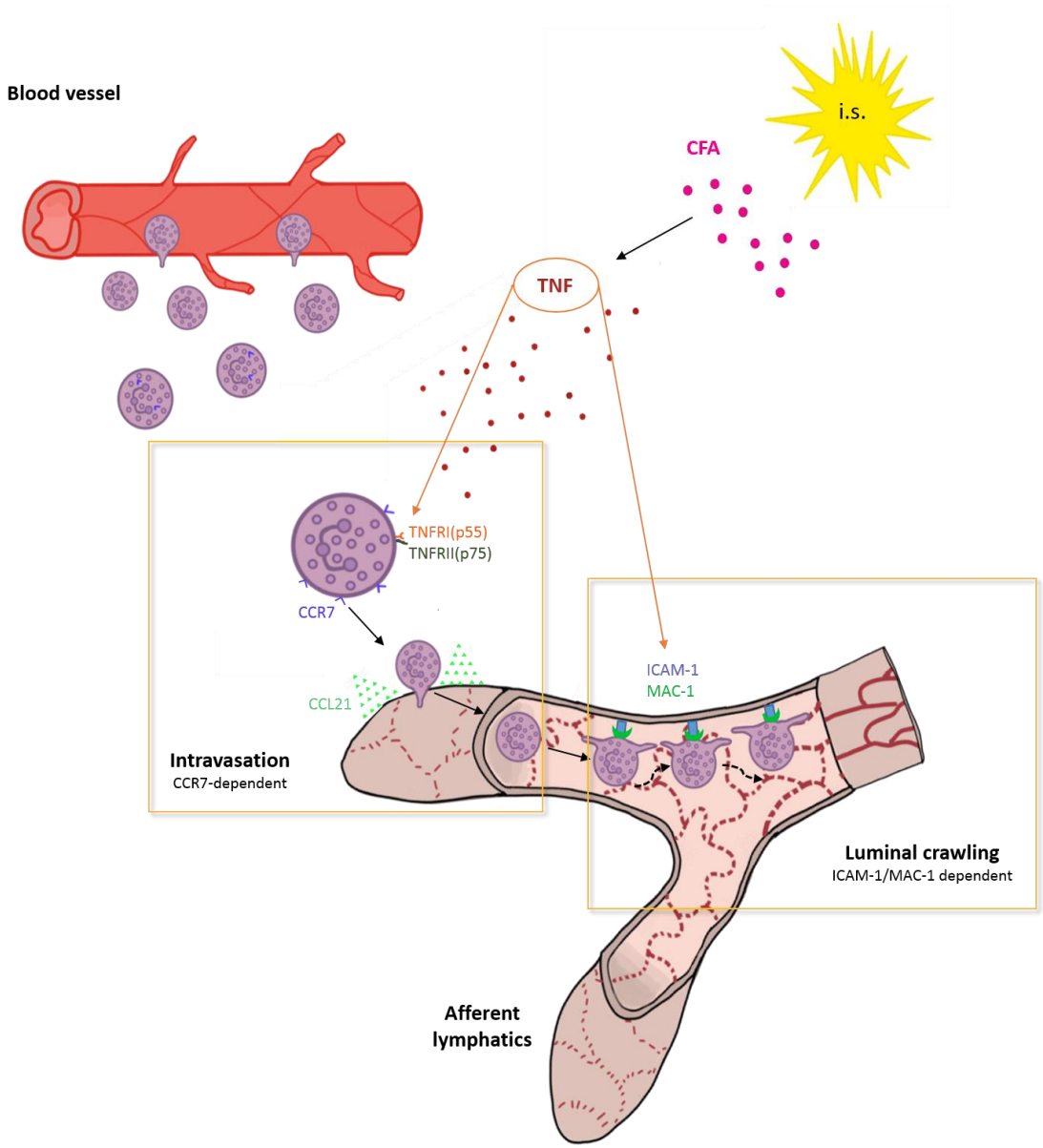

Figure 7.5: Schematic diagram illustrating the dual mechanisms of action of TNF leading to trafficking of neutrophils into initial lymphatic vessels, and their subsequent intraluminal crawling upon acute inflammation *in vivo*. During the acute inflammatory response of the tissue following antigen sensitisation with an emulsion of CFA+Ag, endogenous TNF is released leading to the direct priming of freshly recruited neutrophils. CFA+Ag also leads to the formation of a gradient of CCL21 forming within the interstitial tissues. TNF allows neutrophils to be attracted to the lymphatic vessels, presumably through the CCL21 gradient formed within the interstitium, and triggers the migration of neutrophils into initial lymphatics in a CCR7-dependent manner (intravasation). Furthermore, endogenous TNF activates the lymphatic endothelium leading to an up-regulation of ICAM-1 expression, thus allowing neutrophils present within lymphatic vessels to adhere and crawl along the luminal side of the lymphatic endothelium in the direction of the lymph flow.

References

Abadie, V., Badell, E., Douillard, P., Ensergueix, D., Leenen, P.J., Tanguy, M., Fiette, L., Saeland, S., Gicquel, B., and Winter, N. (2005). Neutrophils rapidly migrate via lymphatics after Mycobacterium bovis BCG intradermal vaccination and shuttle live bacilli to the draining lymph nodes. Blood *106*, 1843-1850.

Abadie, V., Bonduelle, O., Duffy, D., Parizot, C., Verrier, B., and Combadiere, B. (2009). Original Encounter with Antigen Determines Antigen-Presenting Cell Imprinting of the Quality of the Immune Response in Mice. PloS one *4*.

Abi Abdallah, D.S., Egan, C.E., Butcher, B.A., and Denkers, E.Y. (2011). Mouse neutrophils are professional antigen-presenting cells programmed to instruct Th1 and Th17 T-cell differentiation. International immunology *23*, 317-326.

Abram, C.L., and Lowell, C.A. (2009). The ins and outs of leukocyte integrin signaling. Annual review of immunology *27*, 339-362.

Adamson, R.H., Michel, C.C., Parker, K.H., Phillips, C.G., and Wang, W. (1993). Pathways through the Intercellular Clefts of Frog Mesenteric Capillaries. J Physiol-London *466*, 303-327.

Aebischer, D., Iolyeva, M., and Halin, C. (2014). The inflammatory response of lymphatic endothelium. Angiogenesis *17*, 383-393.

Ahn, S.M., and Simpson, R.J. (2007). Body fluid proteomics: Prospects for biomarker discovery. Proteom Clin Appl *1*, 1004-1015.

Akahoshi, T., Namai, R., Sekiyama, N., Tanaka, S., Hosaka, S., and Kondo, H. (1997). Rapid induction of neutrophil apoptosis by sulfasalazine: implications of reactive oxygen species in the apoptotic process. J Leukoc Biol *62*, 817-826.

Akl, T.J., Nagai, T., Cote, G.L., and Gashev, A.A. (2011). Mesenteric lymph flow in adult and aged rats. Am J Physiol-Heart C *301*, H1828-H1840.

Alberts, B. (2002). Lymphocytes and the Cellular Basis of Adaptive Immunity. In Mol Biol Cell (New York: Garland Science), pp. xxxiv, 1548 p.

Algood, H.M., Lin, P.L., and Flynn, J.L. (2005). Tumor necrosis factor and chemokine interactions in the formation and maintenance of granulomas in tuberculosis. Clin Infect Dis *41 Suppl 3*, S189-193.

Alitalo, K., and Carmeliet, P. (2002). Molecular mechanisms of lymphangiogenesis in health and disease. Cancer Cell *1*, 219-227.

Alvarez, D., Vollmann, E.H., and von Andrian, U.H. (2008). Mechanisms and consequences of dendritic cell migration. Immunity *29*, 325-342.

Amatschek, S., Kriehuber, E., Bauer, W., Reininger, B., Meraner, P., Wolpl, A., Schweifer, N., Haslinger, C., Stingl, G., and Maurer, D. (2007). Blood and lymphatic endothelial cell-specific differentiation programs are stringently controlled by the tissue environment. Blood *109*, 4777-4785.

Amulic, B., Cazalet, C., Hayes, G.L., Metzler, K.D., and Zychlinsky, A. (2012). Neutrophil function: from mechanisms to disease. Annual review of immunology *30*, 459-489.

Angus, D.C., and van der Poll, T. (2013). Severe Sepsis and Septic Shock REPLY. New Engl J Med *369*, 2063-2063.

Ardeshna, K.M., Pizzey, A.R., Walker, S.J., Devereux, S., and Khwaja, A. (2002). The upregulation of CC chemokine receptor 7 and the increased migration of maturing dendritic cells to macrophage inflammatory protein 3beta and secondary lymphoid chemokine is mediated by the p38 stress-activated protein kinase pathway. Br J Haematol *119*, 826-829.

Aringer, M., and Smolen, J.S. (2008). The role of tumor necrosis factor-alpha in systemic lupus erythematosus. Arthritis research & therapy *10*, 202.

Arokiasamy, S., Zakian, C., Dilliway, J., Wang, W., Nourshargh, S, and Voisin, M-B. (2017). Endogenous TNFα orchestrates the trafficking of neutrophils into and within lymphatic vessels during acute inflammation. Sci Rep. *7*, 44189.

Athens, J.W., Haab, O.P., Raab, S.O., Mauer, A.M., Ashenbrucker, H., Cartwright, G.E., and Wintrobe, M.M. (1961). Leukokinetic studies. IV. The total blood, circulating and marginal granulocyte pools and the granulocyte turnover rate in normal subjects. J Clin Invest *40*, 989-995.

Austyn, J.M. (1989). Migration Patterns of Dendritic Leukocytes. Res Immunol *140*, 898-902.

Awate, S., Babiuk, L.A., and Mutwiri, G. (2013). Mechanisms of action of adjuvants. Frontiers in immunology 4, 114.

Baggiolini, M., Walz, A., and Kunkel, S.L. (1989). Neutrophil-Activating Peptide-1 Interleukin-8, a Novel Cytokine That Activates Neutrophils. J Clin Invest *84*, 1045-1049.

Bai, K., and Wang, W. (2014). Shear stress-induced redistribution of the glycocalyx on endothelial cells in vitro. Biomechanics and modeling in mechanobiology *13*, 303-311.

Baluk, P., Fuxe, J., Hashizume, H., Romano, T., Lashnits, E., Butz, S., Vestweber, D., Corada, M., Molendini, C., Dejana, E., *et al.* (2007). Functionally specialized junctions between endothelial cells of lymphatic vessels. J Exp Med *204*, 2349-2362.

Baluk, P., Yao, L.C., Feng, J., Romano, T., Jung, S.S., Schreiter, J.L., Yan, L., Shealy, D.J., and McDonald, D.M. (2009). TNF-alpha drives remodeling of blood vessels and lymphatics in sustained airway inflammation in mice. J Clin Invest *119*, 2954-2964.

Banerji, S., Ni, J., Wang, S.X., Clasper, S., Su, J., Tammi, R., Jones, M., and Jackson, D.G. (1999). LYVE-1, a new homologue of the CD44 glycoprotein, is a lymph-specific receptor for hyaluronan. Journal of Cell Biology *144*, 789-801.

Bao, X.F., Moseman, E.A., Saito, H., Petryanik, B., Thiriot, A., Hatakeyama, S., Ito, Y., Kawashima, H., Yamaguchi, Y., Lowe, J.B., *et al.* (2010). Endothelial Heparan Sulfate Controls Chemokine Presentation in Recruitment of Lymphocytes and Dendritic Cells to Lymph Nodes. Immunity *33*, 817-829.

Barondes, S.H., Castronovo, V., Cooper, D.N.W., Cummings, R.D., Drickamer, K., Feizi, T., Gitt, M.A., Hirabayashi, J., Hughes, C., Kasai, K., *et al.* (1994). Galectins - a Family of Animal Beta-Galactoside-Binding Lectins. Cell *76*, 597-598.

Barreiro, O., Yanez-Mo, M., Serrador, J.M., Montoya, M.C., Vicente-Manzanares, M., Tejedor, R., Furthmayr, H., and Sanchez-Madrid, F. (2002). Dynamic interaction of VCAM-1 and ICAM-1 with moesin and ezrin in a novel endothelial docking structure for adherent leukocytes. The Journal of cell biology *157*, 1233-1245.

Bazan, J.F., Bacon, K.B., Hardiman, G., Wang, W., Soo, K., Rossi, D., Greaves, D.R., Zlotnik, A., and Schall, T.J. (1997). A new class of membrane-bound chemokine with a CX3C motif. Nature *385*, 640-644.

Bazigou, E., Wilson, J.T., and Moore, J.E., Jr. (2014). Primary and secondary lymphatic valve development: molecular, functional and mechanical insights. Microvasc Res *96*, 38-45.

Beauvillain, C., Cunin, P., Doni, A., Scotet, M., Jaillon, S., Loiry, M.L., Magistrelli, G., Masternak, K., Chevailler, A., Delneste, Y., *et al.* (2011). CCR7 is involved in the migration of neutrophils to lymph nodes. Blood *117*, 1196-1204.

Beauvillain, C., Delneste, Y., Scotet, M., Peres, A., Gascan, H., Guermonprez, P., Barnaba, V., and Jeannin, P. (2007). Neutrophils efficiently cross-prime naive T cells in vivo. Blood *110*, 2965-2973.

Becker, B.F., Chappell, D., and Jacob, M. (2010). Endothelial glycocalyx and coronary vascular permeability: the fringe benefit. Basic Res Cardiol *105*, 687-701.

Benjamim, C.F., Ferreira, S.H., and Cunha, F.D. (2000). Role of nitric oxide in the failure of neutrophil migration in sepsis. Journal of Infectious Diseases *182*, 214-223.

Bennouna, S., Bliss, S.K., Curiel, T.J., and Denkers, E.Y. (2003). Cross-talk in the innate immune system: neutrophils instruct recruitment and activation of dendritic cells during microbial infection. J Immunol *171*, 6052-6058.

Bisno, A., and Stevens, D. (1996). Current concepts - Streptococcal infections of skin and soft tissues. New Engl J Med *334*, 240-245.

Bixel, M.G., Petri, B., Khandoga, A.G., Khandoga, A., Wolburg-Buchholz, K., Wolburg, H., Marz, S., Krombach, F., and Vestweber, D. (2007). A CD99-related antigen on endothelial cells mediates neutrophil but not lymphocyte extravasation in vivo. Blood *109*, 5327-5336.

Blum, J.S., Wearsch, P.A., and Cresswell, P. (2013). Pathways of antigen processing. Annual review of immunology *31*, 443-473.

Boehm, T. (2012). Evolution of Vertebrate Immunity. Current Biology *22*, R722-R732.

Bonecchi, R., and Graham, G.J. (2016). Atypical Chemokine Receptors and Their Roles in the Resolution of the inflammatory Response. Frontiers in immunology *7*.

Bonilla, F.A., and Oettgen, H.C. (2010). Adaptive immunity. J Allergy Clin Immunol *125*, S33-40.

Borregaard, N. (2010). Neutrophils, from marrow to microbes. Immunity *33*, 657-670.

Bozic, C.R., Kolakowski, L.F., Gerard, N.P., Garciarodriguez, C., Vonuexkullguldenband, C., Conklyn, M.J., Breslow, R., Showell, H.J., and Gerard, C. (1995). Expression and Biologic Characterization of the Murine Chemokine Kc. J Immunol *154*, 6048-6057.

Brabec, R.K., Peters, B.P., Bernstein, I.A., Gray, R.H., and Goldstein, I.J. (1980). Differential lectin binding to cellular membranes in the epidermis of the newborn rat. Proc Natl Acad Sci U S A *77*, 477-479.

Brinkmann, V., Reichard, U., Goosmann, C., Fauler, B., Uhlemann, Y., Weiss, D.S., Weinrauch, Y., and Zychlinsky, A. (2004). Neutrophil extracellular traps kill bacteria. Science *303*, 1532-1535.

Britschgi, M.R., Favre, S., and Luther, S.A. (2010). CCL21 is sufficient to mediate DC migration, maturation and function in the absence of CCL19. Eur J Immunol *40*, 1266-1271.

Bromley, S.K., Thomas, S.Y., and Luster, A.D. (2005). Chemokine receptor CCR7 guides T cell exit from peripheral tissues and entry into afferent lymphatics. Nature Immunology *6*, 895-901.

Brouland, J.P., Gilbert, M.A., Bonneau, M., Pignaud, G., Bal Dit Solier, C., and Drouet, L. (1999). Macro and microheterogeneity in normal endothelial cells: differential composition of luminal glycocalyx and functional implications. Endothelium : journal of endothelial cell research *6*, 251-262.

Broxmeyer, H.E., Orschell, C.M., Clapp, D.W., Hangoc, G., Cooper, S., Plett, P.A., Liles, W.C., Li, X., Graham-Evans, B., Campbell, T.B., *et al.* (2005). Rapid mobilization of murine and human hematopoietic stem and progenitor cells with AMD3100, a CXCR4 antagonist. J Exp Med *201*, 1307-1318.

Bruhl, H., Cohen, C.D., Linder, S., Kretzler, M., Schlondoff, D., and Mack, M. (2003). Post-translational and cell type-specific regulation of CXCR4 expression by cytokines. Eur J Immunol *33*, 3028-3037.

Bruns, S., Kniemeyer, O., Hasenberg, M., Aimanianda, V., Nietzsche, S., Thywissen, A., Jeron, A., Latge, J.P., Brakhage, A.A., and Gunzer, M. (2010). Production of Extracellular Traps against Aspergillus fumigatus In Vitro and in Infected Lung Tissue Is Dependent on Invading Neutrophils and Influenced by Hydrophobin RodA. Plos Pathogens *6*.

Bryson, J., Coles, M., and Manley, N. (2011). A Method for Labeling Vasculature in Embryonic Mice. Jove-Journal of Visualized Experiments.

Burns, A.R., Bowden, R.A., MacDonell, S.D., Walker, D.C., Odebunmi, T.O., Donnachie, E.M., Simon, S.I., Entman, M.L., and Smith, C.W. (2000). Analysis of tight junctions during neutrophil transendothelial migration. Journal of cell science *113 (Pt 1)*, 45-57.

Burroughs, N.J., Ferreira, M., Oliveira, B.M.P.M., and Pinto, A.A. (2011). Autoimmunity arising from bystander proliferation of T cells in an immune response model. Math Comput Model *53*, 1389-1393.

Carman, C.V., Jun, C.D., Salas, A., and Springer, T.A. (2003). Endothelial cells proactively form microvilli-like membrane projections upon intercellular adhesion molecule 1 engagement of leukocyte LFA-1. J Immunol *171*, 6135-6144.

Casale, T.B., Abbas, M.K., and Carolan, E.J. (1992). Degree of Neutrophil Chemotaxis Is Dependent Upon the Chemoattractant and Barrier. American journal of respiratory cell and molecular biology *7*, 112-117.

Cashman, S.M., Morris, D.J., and Kumar-Singh, R. (2004). Adenovirus type 5 pseudotyped with adenovirus type 37 fiber uses sialic acid as a cellular receptor. Virology *324*, 129-139.

Cera, M.R., Del Prete, A., Vecchi, A., Corada, M., Martin-Padura, I., Motoike, T., Tonetti, P., Bazzoni, G., Vermi, W., Gentili, F., *et al.* (2004). Increased DC trafficking to lymph nodes and contact hypersensitivity in junctional adhesion molecule-A-deficient mice. J Clin Invest *114*, 729-738.

Cerutti, A., Puga, I., and Magri, G. (2013). The B cell helper side of neutrophils. J Leukoc Biol *94*, 677-682.

Chaitanya, G.V., Franks, S.E., Cromer, W., Wells, S.R., Bienkowska, M., Jennings, M.H., Ruddell, A., Ando, T., Wang, Y., Gu, Y., *et al.* (2010). Differential cytokine responses in human and mouse lymphatic endothelial cells to cytokines in vitro. Lymphatic research and biology *8*, 155-164.

Chappell, D., Hofmann-Kiefer, K., Jacob, M., Rehm, M., Briegel, J., Welsch, U., Conzen, P., and Becker, B.F. (2009a). TNF-alpha induced shedding of the endothelial glycocalyx is prevented by hydrocortisone and antithrombin. Basic Res Cardiol *104*, 78-89.

Chappell, D., Jacob, M., Hofmann-Kiefer, K., Rehm, M., Welsch, U., Conzen, P., and Becker, B.F. (2009b). Antithrombin reduces shedding of the endothelial glycocalyx following ischaemia/reperfusion. Cardiovasc Res *83*, 388-396.

Chappell, D., Jacob, M., Becker, B.F., Hofmann-Kiefer, K., Conzen, P., and Rehm, M. (2008). Expedition glycocalyx. A newly discovered "Great Barrier Reef". Der Anaesthesist *57*, 959-969.

Charo, I.F., and Ransohoff, R.M. (2006). Mechanisms of disease - The many roles of chemokines and chemokine receptors in inflammation. New Engl J Med *354*, 610-621.

Cheminay, U., Chakravortty, D., and Hensel, M. (2004). Role of neutrophils in murine salmonellosis. Infection and immunity *72*, 468-477.

Choi, I., Lee, S., and Hong, Y.K. (2012). The New Era of the Lymphatic System: No Longer Secondary to the Blood Vascular System. Csh Perspect Med *2*.

Chtanova, T., Schaeffer, M., Han, S.J., van Dooren, G.G., Nollmann, M., Herzmark, P., Chan, S.W., Satija, H., Camfield, K., Aaron, H., *et al.* (2008). Dynamics of neutrophil migration in lymph nodes during infection. Immunity *29*, 487-496.

Clark, S.R., Ma, A.C., Tavener, S.A., McDonald, B., Goodarzi, Z., Kelly, M.M., Patel, K.D., Chakrabarti, S., McAvoy, E., Sinclair, G.D., *et al.* (2007). Platelet TLR4 activates neutrophil extracellular traps to ensnare bacteria in septic blood. Nature medicine *13*, 463-469.

Clement, C.C., Rotzschke, O., and Santambrogio, L. (2011). The lymph as a pool of self-antigens. Trends in immunology *32*, 6-11.

Coffman, R.L., Sher, A., and Seder, R.A. (2010). Vaccine adjuvants: putting innate immunity to work. Immunity *33*, 492-503.

Cohen, J. (2002). The immunopathogenesis of sepsis. Nature *420*, 885-891.

Colotta, F., Re, F., Polentarutti, N., Sozzani, S., and Mantovani, A. (1992). Modulation of Granulocyte Survival and Programmed Cell-Death by Cytokines and Bacterial Products. Blood *80*, 2012-2020.

Combe, B. (2010). Impact of dosing on treatment with TNF inhibitors: managing dose adjustment. Clinical and Experimental Rheumatology 28, S13-S17.

Constantinescu, A.A., Vink, H., and Spaan, J.A. (2003). Endothelial cell glycocalyx modulates immobilization of leukocytes at the endothelial surface. Arteriosclerosis, thrombosis, and vascular biology *23*, 1541-1547.

Crick, F. (1970). Diffusion in embryogenesis. Nature 225, 420-422.

Cross, A., Moots, R.J., and Edwards, S.W. (2008). The dual effects of TNFalpha on neutrophil apoptosis are mediated via differential effects on expression of Mcl-1 and Bfl-1. Blood *111*, 878-884.

Cueni, L.N., and Detmar, M. (2008). The lymphatic system in health and disease. Lymphatic research and biology *6*, 109-122.

Culshaw, S., Millington, O.R., Brewer, J.M., and McInnes, I.B. (2008). Murine neutrophils present Class II restricted antigen. Immunol Lett *118*, 49-54.

Cursiefen, C., Chen, L., Borges, L.P., Jackson, D., Cao, J., Radziejewski, C., D'Amore, P.A., Dana, M.R., Wiegand, S.J., and Streilein, J.W. (2004). VEGF-A stimulates lymphangiogenesis and hemangiogenesis in inflammatory neovascularization via macrophage recruitment. J Clin Invest *113*, 1040-1050.

Daley, J.M., Thomay, A.A., Connolly, M.D., Reichner, J.S., and Albina, J.E. (2008). Use of Ly6G-specific monoclonal antibody to deplete neutrophils in mice. J Leukocyte Biol *83*, 64-70.

De Filippo, K., Henderson, R.B., Laschinger, M., and Hogg, N. (2008). Neutrophil chemokines KC and macrophage-inflammatory protein-2 are newly synthesized by tissue macrophages using distinct TLR signaling pathways. J Immunol *180*, 4308-4315.

Dean, R.A., Cox, J.H., Bellac, C.L., Doucet, A., Starr, A.E., and Overall, C.M. (2008). Macrophage-specific metalloelastase (MMP-12) truncates and inactivates ELR+CXC chemokines and generates CCL2,-7,-8, and-13 antagonists: potential role of the macrophage in terminating polymorphonuclear leukocyte influx. Blood *112*, 3455-3464.

Debes, G.F., Arnold, C.N., Young, A.J., Krautwald, S., Lipp, M., Hay, J.B., and Butcher, E.C. (2005). Chemokine receptor CCR7 required for T lymphocyte exit from peripheral tissues. Nat Immunol *6*, 889-894.

Dejana, E., Orsenigo, F., Molendini, C., Baluk, P., and McDonald, D.M. (2009). Organization and signaling of endothelial cell-to-cell junctions in various regions of the blood and lymphatic vascular trees. Cell Tissue Res *335*, 17-25.

Del Maschio, A., De Luigi, A., Martin-Padura, I., Brockhaus, M., Bartfai, T., Fruscella, P., Adorini, L., Martino, G.V., Furlan, R., De Simoni, M.G., *et al.* (1999). Leukocyte

recruitment in the cerebrospinal fluid of mice with experimental meningitis is inhibited by an antibody to junctional adhesion molecule (JAM). J Exp Med *190*, 1351-1356.

DeLeo, F.R. (2004). Modulation of phagocyte apoptosis by bacterial pathogens. Apoptosis *9*, 399-413.

den Broeder, A.A., Wanten, G.J., Oyen, W.J., Naber, T., van Riel, P.L., and Barrera, P. (2003). Neutrophil migration and production of reactive oxygen species during treatment with a fully human anti-tumor necrosis factor-alpha monoclonal antibody in patients with rheumatoid arthritis. J Rheumatol *30*, 232-237.

Detmar, M., and Hirakawa, S. (2002). The formation of lymphatic vessels and its importance in the setting of malignancy. J Exp Med 196, 713-718.

Dewas, C., Dang, P.M.C., Gougerot-Pocidalo, M.A., and El-Benna, J. (2003). TNF-alpha induces phosphorylation of p47(phox) in human neutrophils: Partial phosphorylation of p47(phox) is a common event of priming of human neutrophils by TNF-alpha and granulocyte-macrophage colony-stimulating factor. J Immunol *171*, 4392-4398.

Diazflores, L., Gutierrez, R., Varela, H., Rancel, N., and Valladares, F. (1991). Microvascular Pericytes - a Review of Their Morphological and Functional-Characteristics. Histology and Histopathology *6*, 269-286.

Dixon, J.B., Greiner, S.T., Gashev, A.A., Cote, G.L., Moore, J.E., and Zawieja, D.C. (2006). Lymph flow, shear stress, and lymphocyte velocity in rat mesenteric prenodal lymphatics. Microcirculation *13*, 597-610.

Dixon, J.B., Zawieja, D.C., Gashev, A.A., and Cote, G.L. (2005). Measuring microlymphatic flow using fast video microscopy. Journal of biomedical optics *10*.

Dong, Y., Fischer, R., Naude, P.J.W., Maier, O., Nyakas, C., Duffey, M., Van der Zee, E.A., Dekens, D., Douwenga, W., Herrmann, A., et al. (2016). Essential protective role of tumor necrosis factor receptor 2 in neurodegeneration. P Natl Acad Sci USA 113, 12304-12309.

Dransfield, I., Buckle, A.M., Savill, J.S., Mcdowall, A., Haslett, C., and Hogg, N. (1994). Neutrophil Apoptosis Is Associated with a Reduction in Cd16 (Fc-Gamma-Riii) Expression. J Immunol *153*, 1254-1263.

Du, L.C., Chen, X.C., Wang, D., Wen, Y.J., Wang, C.T., Wang, X.M., Kan, B., Wei, Y.Q., and Zhao, X. (2014). VEGF-D-induced draining lymphatic enlargement and tumor lymphangiogenesis promote lymph node metastasis in a xenograft model of ovarian carcinoma. Reproductive biology and endocrinology : RB&E *12*, 14.

Dubey, A.K., Handu, S.S., Dubey, S., Sharma, P., Sharma, K.K., and Ahmed, Q.M. (2011). Belimumab: First targeted biological treatment for systemic lupus erythematosus. Journal of pharmacology & pharmacotherapeutics *2*, 317-319.

Dugan, A.S., Gasparovic, M.L., and Atwood, W.J. (2008). Direct correlation between sialic acid binding and infection of cells by two human polyomaviruses (JC virus and BK virus). Journal of virology *82*, 2560-2564.

Dunworth, W.P., Fritz-Six, K.L., and Caron, K.M. (2008). Adrenomedullin stabilizes the lymphatic endothelial barrier in vitro and in vivo. Peptides *29*, 2243-2249.

Eash, K.J., Greenbaum, A.M., Gopalan, P., Diaz, G.A., and Link, D.C. (2009). CXCR2 Signals Act in Concert with CXCR4 to Regulate Neutrophil Release From the Bone Marrow. Blood *114*, 101-102.

Eash, K.J., Greenbaum, A.M., Gopalan, P.K., and Link, D.C. (2010). CXCR2 and CXCR4 antagonistically regulate neutrophil trafficking from murine bone marrow. J Clin Invest *120*, 2423-2431.

Elferink, J.G., Daha, M.R., and de Koster, B.M. (1997). A cyclic GMP- and G-kinase-dependent effect of azathioprine on migration by human neutrophils. Cellular and molecular life sciences : CMLS *53*, 593-599.

Eltzschig, H.K., and Eckle, T. (2011). Ischemia and reperfusion-from mechanism to translation. Nature medicine *17*, 1391-1401.

Ernst, C., and Christie, B. (2006). Isolectin-IB4 as a vascular stain for the study of adult neurogenesis. Journal of Neuroscience Methods *150*, 138-142.

Eruslanov, E.B., Bhojnagarwala, P.S., Quatromoni, J.G., Stephen, T.L., Ranganathan, A., Deshpande, C., Akimova, T., Vachani, A., Litzky, L., Hancock, W.W., *et al.* (2014). Tumor-associated neutrophils stimulate T cell responses in early-stage human lung cancer. J Clin Invest *124*, 5466-5480.

Evans, A.L., Bell, R., Brice, G., Comeglio, P., Lipede, C., Jeffery, S., Mortimer, P., Sarfarazi, M., and Child, A.H. (2003). Identification of eight novel VEGFR-3 mutations in families with primary congenital lymphoedema. J Med Genet *40*, 697-703.

Fahey, T.J., 3rd, Turbeville, T., and McIntyre, K. (1995). Differential TNF secretion by wound fibroblasts compared to normal fibroblasts in response to LPS. The Journal of surgical research *58*, 759-764.

Farrera, C., and Fadeel, B. (2013). Macrophage Clearance of Neutrophil Extracellular Traps Is a Silent Process. J Immunol *191*, 2647-2656.

Faurschou, M., and Borregaard, N. (2003). Neutrophil granules and secretory vesicles in inflammation. Microbes and infection *5*, 1317-1327.

Faust, N., Varas, F., Kelly, L.M., Heck, S., and Graf, T. (2000). Insertion of enhanced green fluorescent protein into the lysozyme gene creates mice with green fluorescent granulocytes and macrophages. Blood *96*, 719-726.

Feldmann, M., Williams, R.O., and Paleolog, E. (2010). What have we learnt from targeted anti-TNF therapy? Annals of the Rheumatic Diseases *69*, 97-99.

Ferrell, R.E., Levinson, K.L., Esman, J.H., Kimak, M.A., Lawrence, E.C., Barmada, M.M., and Finegold, D.N. (1998). Hereditary lymphedema: evidence for linkage and genetic heterogeneity. Hum Mol Genet *7*, 2073-2078.

Fialkow, L., Wang, Y.C., and Downey, G.P. (2007). Reactive oxygen and nitrogen species as signaling molecules regulating neutrophil function. Free Radical Bio Med *42*, 153-164.

Fingar, V.H., Taber, S.W., Buschemeyer, W.C., ten Tije, A., Cerrito, P.B., Tseng, M., Guo, H., Johnston, M.N., and Wieman, T.J. (1997). Constitutive and stimulated expression of ICAM-1 protein on pulmonary endothelial cells in vivo. Microvasc Res *54*, 135-144.

Finsterbusch, M., Voisin, M.B., Beyrau, M., Williams, T.J., and Nourshargh, S. (2014). Neutrophils recruited by chemoattractants in vivo induce microvascular plasma protein leakage through secretion of TNF. J Exp Med *211*, 1306-1313.

Fleming, T.J., Fleming, M.L., and Malek, T.R. (1993). Selective expression of Ly-6G on myeloid lineage cells in mouse bone marrow. RB6-8C5 mAb to granulocyte-differentiation antigen (Gr-1) detects members of the Ly-6 family. J Immunol *151*, 2399-2408.

Forster, R., Schubel, A., Breitfeld, D., Kremmer, E., Renner-Muller, I., Wolf, E., and Lipp, M. (1999). CCR7 coordinates the primary immune response by establishing functional microenvironments in secondary lymphoid organs. Cell *99*, 23-33.

Foti, M., Granucci, F., Aggujaro, D., Liboi, E., Luini, W., Minardi, S., Mantovani, A., Sozzani, S., and Ricciardi-Castagnoli, P. (1999). Upon dendritic cell (DC) activation chemokines and chemokine receptor expression are rapidly regulated for recruitment and maintenance of DC at the inflammatory site. International immunology *11*, 979-986.

Fra, A.M., Locati, M., Otero, K., Sironi, M., Signorelli, P., Massardi, M.L., Gobbi, M., Vecchi, A., Sozzani, S., and Mantovani, A. (2003). Cutting edge: Scavenging of inflammatory CC chemokines by the promiscuous putatively silent chemokine receptor D6(1). J Immunol *170*, 2279-2282.

Frasch, S.C., Fernandez-Boyanapalli, R.F., Berry, K.A., Murphy, R.C., Leslie, C.C., Nick, J.A., Henson, P.M., and Bratton, D.L. (2013). Neutrophils regulate tissue Neutrophilia in inflammation via the oxidant-modified lipid lysophosphatidylserine. The Journal of biological chemistry *288*, 4583-4593.

Freitas, A., Alves-Filho, J.C., Secco, D.D., Neto, A.F., Ferreira, S.H., Barja-Fidalgo, C., and Cunha, F.Q. (2006). Heme oxygenase/carbon monoxide-biliverdin pathway down regulates neutrophil rolling, adhesion and migration in acute inflammation. Brit J Pharmacol *149*, 345-354.

Fuchs, T.A., Abed, U., Goosmann, C., Hurwitz, R., Schulze, I., Wahn, V., Weinrauch, Y., Brinkmann, V., and Zychlinsky, A. (2007). Novel cell death program leads to neutrophil extracellular traps. The Journal of cell biology *176*, 231-241.

Fujishima, S., Hoffman, A.R., Vu, T., Kim, K.J., Zheng, H., Daniel, D., Kim, Y., Wallace, E.F., Larrick, J.W., and Raffin, T.A. (1993). Regulation of Neutrophil Interleukin-8 Gene-Expression and Protein Secretion by Lps, Tnf-Alpha, and Il-1-Beta. Journal of cellular physiology *154*, 478-485.

Fulcher, J.A., Chang, M.H., Wang, S., Almazan, T., Hashimi, S.T., Eriksson, A.U., Wen, X.S., Pang, M., Baum, L.G., Singh, R.R., *et al.* (2009). Galectin-1 Co-clusters CD43/CD45 on Dendritic Cells and Induces Cell Activation and Migration through Syk and Protein Kinase C Signaling. Journal of Biological Chemistry *284*, 26860-26870.

Fulcher, J.A., Hashimi, S.T., Levroney, E.L., Pang, M., Gurney, K.B., Baum, L.G., and Lee, B. (2006). Galectin-1-matured human monocyte-derived dendritic cells have enhanced migration through extracellular matrix. J Immunol *177*, 216-226.

Furze, R.C., and Rankin, S.M. (2008). Neutrophil mobilization and clearance in the bone marrow. Immunology *125*, 281-288.

Galanzha, E.I., Tuchin, V.V., and Zharov, V.P. (2005). In vivo integrated flow image cytometry and lymph/blood vessels dynamic microscopy. Journal of biomedical optics *10*.

Gale, N.W., Thurston, G., Hackett, S.F., Renard, R., Wang, Q., McClain, J., Martin, C., Witte, C., Witte, M.H., Jackson, D., *et al.* (2002). Angiopoietin-2 is required for postnatal angiogenesis and lymphatic patterning, and only the latter role is rescued by angiopoietin-1. Developmental Cell *3*, 411-423.

Garcia-Romo, G.S., Caielli, S., Vega, B., Connolly, J., Allantaz, F., Xu, Z.H., Punaro, M., Baisch, J., Guiducci, C., Coffman, R.L., *et al.* (2011). Netting Neutrophils Are Major Inducers of Type I IFN Production in Pediatric Systemic Lupus Erythematosus. Science translational medicine *3*.

Gavrilovskaya, I.N., Gorbunova, E.E., and Mackow, E.R. (2012). Andes virus infection of lymphatic endothelial cells causes giant cell and enhanced permeability responses that are rapamycin and vascular endothelial growth factor C sensitive. Journal of virology *86*, 8765-8772.

Gavrilovskaya, I.N., Gorbunova, E.E., and Mackow, E.R. (2013). Hypoxia induces permeability and giant cell responses of Andes virus-infected pulmonary endothelial cells by activating the mTOR-S6K signaling pathway. Journal of virology *87*, 12999-13008.

Gerli, R., Ibba, L., and Fruschelli, C. (1990). A fibrillar elastic apparatus around human lymph capillaries. Anatomy and embryology *181*, 281-286.

Ghosh, S., Goldin, E., Gordon, F.H., Malchow, H.A., Rask-Madsen, J., Rutgeerts, P., Vyhnalek, P., Zadorova, Z., Palmer, T., Donoghue, S., et al. (2003). Natalizumab for active Crohn's disease. New Engl J Med 348, 24-32.

Ginis, I., and Tauber, A.I. (1990). Activation Mechanisms of Adherent Human Neutrophils. Blood *76*, 1233-1239.

Goldstein, I.J., and Winter, H.G. (1999). The Griffonia simplicifolia I-B4 isolectin. A probe for alpha-D-galactosyl end groups. Subcell Biochem *32*, 127-141.

Gorlino, C.V., Ranocchia, R.P., Harman, M.F., Garcia, I.A., Crespo, M.I., Moron, G., Maletto, B.A., and Pistoresi-Palencia, M.C. (2014). Neutrophils exhibit differential requirements for homing molecules in their lymphatic and blood trafficking into draining lymph nodes. J Immunol *193*, 1966-1974.

Griffith, J.W., Sokol, C.L., and Luster, A.D. (2014). Chemokines and chemokine receptors: positioning cells for host defense and immunity. Annual review of immunology 32, 659-702.

Gunn, M.D., Kyuwa, S., Tam, C., Kakiuchi, T., Matsuzawa, A., Williams, L.T., and Nakano, H. (1999). Mice lacking expression of secondary lymphoid organ chemokine have defects in lymphocyte homing and dendritic cell localization. J Exp Med *189*, 451-460.

Gunn, M.D., Tangemann, K., Tam, C., Cyster, J.G., Rosen, S.D., and Williams, L.T. (1998). A chemokine expressed in lymphoid high endothelial venules promotes the adhesion and chemotaxis of naive T lymphocytes. Proc Natl Acad Sci U S A *95*, 258-263.

Haessler, U., Pisano, M., Wu, M., and Swartz, M.A. (2011). Dendritic cell chemotaxis in 3D under defined chemokine gradients reveals differential response to ligands CCL21 and CCL19. Proc Natl Acad Sci U S A *108*, 5614-5619.

Hager, M., Cowland, J.B., and Borregaard, N. (2010). Neutrophil granules in health and disease. Journal of internal medicine *268*, 25-34.

Hakkim, A., Furnrohr, B.G., Amann, K., Laube, B., Abu Abed, U., Brinkmann, V., Herrmann, M., Voll, R.E., and Zychlinsky, A. (2010). Impairment of neutrophil extracellular trap degradation is associated with lupus nephritis. P Natl Acad Sci USA *107*, 9813-9818.

Halai, K., Whiteford, J., Ma, B., Nourshargh, S., and Woodfin, A. (2014). ICAM-2 facilitates luminal interactions between neutrophils and endothelial cells in vivo. Journal of cell science *127*, 620-629.

Haldenby, K.A., Chappell, D.C., Winlove, C.P., Parker, K.H., and Firth, J.A. (1994). Focal and regional variations in the composition of the glycocalyx of large vessel endothelium. Journal of vascular research *31*, 2-9.

Hallett, M.B., and Lloyds, D. (1995). Neutrophil priming: the cellular signals that say 'amber' but not 'green'. Immunology today *16*, 264-268.

Halpern, W.G., Lappin, P., Zanardi, T., Cai, W., Corcoran, M., Zhong, J., and Baker, K.P. (2006). Chronic administration of belimumab, a BLyS antagonist, decreases tissue and peripheral blood B-lymphocyte populations in cynomolgus monkeys: pharmacokinetic, pharmacodynamic, and toxicologic effects. Toxicological sciences : an official journal of the Society of Toxicology *91*, 586-599.

Hampton, H.R., Bailey, J., Tomura, M., Brink, R., and Chtanova, T. (2015). Microbe-dependent lymphatic migration of neutrophils modulates lymphocyte proliferation in lymph nodes. Nat Commun *6*, 7139.

Hampton, H.R., and Chtanova, T. (2016). The lymph node neutrophil. Seminars in immunology *28*, 129-136.

Handel, T.M., Johnson, Z., Crown, S.E., Lau, E.K., Sweeney, M., and Proudfoot, A.E. (2005). Regulation of protein function by glycosaminoglycans - as exemplified by chemokines. Annual Review of Biochemistry *74*, 385-410.

Hargreaves, D.C., Hyman, P.L., Lu, T.T., Ngo, V.N., Bidgol, A., Suzuki, G., Zou, Y.R., Littman, D.R., and Cyster, J.G. (2001). A coordinated change in chemokine responsiveness guides plasma cell movements. J Exp Med 194, 45-56.

Haribabu, B., Verghese, M.W., Steeber, D.A., Sellars, D.D., Bock, C.B., and Snyderman, R. (2000). Targeted disruption of the leukotriene B-4 receptor in mice reveals its role in inflammation and platelet-activating factor-induced anaphylaxis. J Exp Med *192*, 433-438.

Harmsen, A.G., Muggenburg, B.A., Snipes, M.B., and Bice, D.E. (1985). The role of macrophages in particle translocation from lungs to lymph nodes. Science *230*, 1277-1280.

Harvey, H.A., Swords, W.E., and Apicella, M.A. (2001). The mimicry of human glycolipids and glycosphingolipids by the lipooligosaccharides of pathogenic neisseria and haemophilus. Journal of autoimmunity *16*, 257-262.

Harvey, N.L., Srinivasan, R.S., Dillard, M.E., Johnson, N.C., Witte, M.H., Boyd, K., Sleeman, M.W., and Oliver, G. (2005). Lymphatic vascular defects promoted by Prox1 haploinsufficiency cause adult-onset obesity. Nature Genetics *37*, 1072-1081.

Haubitz, M. (2010). New and emerging treatment approaches to lupus. Biologics : targets & therapy *4*, 263-271.

Hellberg, L., Fuchs, S., Gericke, C., Behnen, M., Solbach, W., and Laskay, T. (2011). Proinflammatory stimuli enhance clearance of apoptotic cells by neutrophil granulocytes. European journal of clinical investigation *41*, 43-43.

Henry, C.B.S., and Duling, B.R. (2000). TNF-alpha increases entry of macromolecules into luminal endothelial cell glycocalyx. Am J Physiol-Heart C *279*, H2815-H2823.

Hetland, G., Johnson, E., and Aasebo, U. (1986). Human alveolar macrophages synthesize the functional alternative pathway of complement and active C5 and C9 in vitro. Scandinavian journal of immunology *24*, 603-608.

Hobbs, J.A., May, R., Tanousis, K., McNeill, E., Mathies, M., Gebhardt, C., Henderson, R., Robinson, M.J., and Hogg, N. (2003). Myeloid cell function in MRP-14 (S100A9) null mice. Mol Cell Biol *23*, 2564-2576.

Hoenderdos, K., Lodge, K.M., Hirst, R.A., Chen, C., Palazzo, S.G., Emerenciana, A., Summers, C., Angyal, A., Porter, L., Juss, J.K., *et al.* (2016). Hypoxia upregulates neutrophil degranulation and potential for tissue injury. Thorax *71*, 1030-1038.

Hong, Y.K., Harvey, N., Noh, Y.H., Schacht, V., Hirakawa, S., Detmar, M., and Oliver, G. (2002). Prox1 is a master control gene in the program specifying lymphatic endothelial cell fate. Dev Dynam *225*, 351-357.

Hsu, D.K., Chernyavsky, A.I., Chen, H.Y., Yu, L., Grando, S.A., and Liu, F.T. (2009). Endogenous Galectin-3 Is Localized in Membrane Lipid Rafts and Regulates Migration of Dendritic Cells. Journal of Investigative Dermatology *129*, 573-583.

Huang, F.P., Platt, N., Wykes, M., Major, J.R., Powell, T.J., Jenkins, C.D., and MacPherson, G.G. (2000). A discrete subpopulation of dendritic cells transports apoptotic intestinal epithelial cells to T cell areas of mesenteric lymph nodes. J Exp Med *191*, 435-444.

Huang, M.T., Larbi, K.Y., Scheiermann, C., Woodfin, A., Gerwin, N., Haskard, D.O., and Nourshargh, S. (2006). ICAM-2 mediates neutrophil transmigration in vivo: evidence for stimulus specificity and a role in PECAM-1-independent transmigration. Blood *107*, 4721-4727.

Huggenberger, R., Siddiqui, S.S., Brander, D., Ullmann, S., Zimmermann, K., Antsiferova, M., Werner, S., Alitalo, K., and Detmar, M. (2011). An important role of lymphatic vessel activation in limiting acute inflammation. Blood *117*, 4667-4678.

Huggenberger, R., Ullmann, S., Proulx, S.T., Pytowski, B., Alitalo, K., and Detmar, M. (2010). Stimulation of lymphangiogenesis via VEGFR-3 inhibits chronic skin inflammation. J Exp Med *207*, 2255-2269.

Hughes, R.C. (2001). Galectins as modulators of cell adhesion. Biochimie *83*, 667-676.

Huntington, G.S., and McClure, C.F.W. (1910). The anatomy and development of the jugular lymph sacs in the domestic cat (Felis domestica). American Journal of Anatomy *10*, 177-312.

Hyun, Y.M., Sumagin, R., Sarangi, P.P., Lomakina, E., Overstreet, M.G., Baker, C.M., Fowell, D.J., Waugh, R.E., Sarelius, I.H., and Kim, M. (2012). Uropod elongation is a common final step in leukocyte extravasation through inflamed vessels. J Exp Med *209*, 1349-1362.

Ingulli, E., Mondino, A., Khoruts, A., and Jenkins, M.K. (1997). In vivo detection of dendritic cell antigen presentation to CD4(+) T cells. J Exp Med *185*, 2133-2141.

Ihenetu, K., Molleman, A., Parsons, M.E., and Whelan, C.J. (2003). Inhibition of interleukin-8 release in the human colonic epithelial cell line HT-29 by cannabinoids. European journal of pharmacology *458*, 207-215.

Iking-Konert, C., Cseko, C., Wagner, C., Stegmaier, S., Andrassy, K., and Hansch, G.M. (2001). Transdifferentiation of polymorphonuclear neutrophils: acquisition of CD83 and other functional characteristics of dendritic cells. Journal of molecular medicine *79*, 464-474.

Isa, P., Arias, C.F., and López, S. (2006). Role of sialic acids in rotavirus infection. Glycoconj J *23*, 27-37.

Issa, A., Le, T.X., Shoushtari, A.N., Shields, J.D., and Swartz, M.A. (2009). Vascular endothelial growth factor-C and C-C chemokine receptor 7 in tumor cell-lymphatic cross-talk promote invasive phenotype. Cancer Res *69*, 349-357.

Jaeschke, H., Farhood, A., and Smith, C.W. (1990). Neutrophils contribute to ischemia/reperfusion injury in rat liver in vivo. Faseb J *4*, 3355-3359.

Janeway, C. (1999). Immunobiology : the immune system in health and disease, 4th edn (London, New York, NY, US: Current Biology Publications; Garland Pub).

Janeway, C. (2005). Macrophage activation by armed CD4 TH1 cells. In Immunobiology : the immune system in health and disease (New York: Garland Science), pp. xxiii, 823 p.

Jeon, B.H., Jang, C., Han, J., Kataru, R.P., Piao, L., Jung, K., Cha, H.J., Schwendener, R.A., Jang, K.Y., Kim, K.S., *et al.* (2008). Profound but dysfunctional lymphangiogenesis via vascular endothelial growth factor ligands from CD11b+ macrophages in advanced ovarian cancer. Cancer Res *68*, 1100-1109.

Johnson, L.A., Clasper, S., Holt, A.P., Lalor, P.F., Baban, D., and Jackson, D.G. (2006). An inflammation-induced mechanism for leukocyte transmigration across lymphatic vessel endothelium. J Exp Med *203*, 2763-2777.

Johnson, L.A., and Jackson, D.G. (2008). Cell traffic and the lymphatic endothelium. Annals of the New York Academy of Sciences *1131*, 119-133.

Johnson, L.A., and Jackson, D.G. (2010). Inflammation-induced secretion of CCL21 in lymphatic endothelium is a key regulator of integrin-mediated dendritic cell transmigration. International immunology *22*, 839-849.

Johnson, L.A., and Jackson, D.G. (2010). Inflammation-induced secretion of CCL21 in lymphatic endothelium is a key regulator of integrin-mediated dendritic cell transmigration. International immunology *22*, 839-849.

Johnson, L.A., and Jackson, D.G. (2013). The chemokine CX3CL1 promotes trafficking of dendritic cells through inflamed lymphatics. Journal of cell science *126*, 5259-5270.

Johnson, L.A., and Jackson, D.G. (2014). Control of dendritic cell trafficking in lymphatics by chemokines. Angiogenesis *17*, 335-345.

Jones, D., and Min, W. (2011). An overview of lymphatic vessels and their emerging role in cardiovascular disease. Journal of cardiovascular disease research *2*, 141-152.

Kabashima, K., Shiraishi, N., Sugita, K., Mori, T., Onoue, A., Kobayashi, M., Sakabe, J.I., Yoshiki, R., Tamamura, H., Fujii, N., *et al.* (2007). CXCL12-CXCR4 engagement is required for migration of cutaneous dendritic cells. Am J Pathol *171*, 1249-1257.

Kaipainen, A., Korhonen, J., Mustonen, T., Vanhinsbergh, V.W.M., Fang, G.H., Dumont, D., Breitman, M., and Alitalo, K. (1995). Expression of the Fms-Like Tyrosine Kinase-4 Gene Becomes Restricted to Lymphatic Endothelium during Development. P Natl Acad Sci USA *92*, 3566-3570.

Kamenyeva, O., Boularan, C., Kabat, J., Cheung, G.Y.C., Cicala, C., Yeh, A.J., Chan, J.L., Periasamy, S., Otto, M., and Kehrl, J.H. (2015). Neutrophil Recruitment to Lymph Nodes Limits Local Humoral Response to Staphylococcus aureus. Plos Pathogens *11*.

Kansas, G.S. (1996). Selectins and their ligands: Current concepts and controversies. Blood *88*, 3259-3287.

Karaman, S., and Detmar, M. (2014). Mechanisms of lymphatic metastasis. J Clin Invest *124*, 922-928.

Kastenmuller, W., Torabi-Parizi, P., Subramanian, N., Lammermann, T., and Germain, R.N. (2012). A Spatially-Organized Multicellular Innate Immune Response in Lymph Nodes Limits Systemic Pathogen Spread. Cell *150*, 1235-1248.

Kessenbrock, K., Krumbholz, M., Schonermarck, U., Back, W., Gross, W.L., Werb, Z., Grone, H.J., Brinkmann, V., and Jenne, D.E. (2009). Netting neutrophils in autoimmune small-vessel vasculitis. Nature medicine *15*, 623-625.

Khatua, B., Roy, S., and Mandal, C. (2013). Sialic acids siglec interaction: A unique strategy to circumvent innate immune response by pathogens. Indian Journal of Medical Research *138*, 648-662.

Kielian, T., Esen, N., and Bearden, E.D. (2005). Toll-like receptor 2 (TLR2) is pivotal for recognition of S. aureus peptidoglycan but not intact bacteria by microglia. Glia *49*, 567-576.

Kim, H., Kataru, R.P., and Koh, G.Y. (2012). Regulation and implications of inflammatory lymphangiogenesis. Trends in immunology *33*, 350-356.

Kim, H., Nguyen, V.P.K.H., Petrova, T.V., Cruz, M., Alitalo, K., and Dumont, D.J. (2010). Embryonic vascular endothelial cells are malleable to reprogramming via Prox1 to a lymphatic gene signature. Bmc Dev Biol *10*.

Kim, H.K., Kim, J.E., Chung, J., Han, K.S., and Cho, H.I. (2007). Surface expression of neutrophil CXCR4 is down-modulated by bacterial endotoxin. Int J Hematol *85*, 390-396.

Kissenpfennig, A., Henri, S., Dubois, B., Laplace-Builhe, C., Perrin, P., Romani, N., Tripp, C.H., Douillard, P., Leserman, L., Kaiserlian, D., *et al.* (2005). Dynamics and function of Langerhans cells in vivo: dermal dendritic cells colonize lymph node areas distinct from slower migrating Langerhans cells. Immunity *22*, 643-654.

Klausner, J.M., Paterson, I.S., Goldman, G., Kobzik, L., Rodzen, C., Lawrence, R., Valeri, C.R., Shepro, D., and Hechtman, H.B. (1989). Postischemic Renal Injury Is Mediated by Neutrophils and Leukotrienes. Am J Physiol *256*, F794-F802.

Klein, A., Cunha, F.Q., and Ferreira, S.H. (1995). The role of lymphocytes in the neutrophil migration induced by ovalbumin in immunized rats. Immunology *84*, 577-584.

Klein, S.L., and Flanagan, K.L. (2016). Sex differences in immune responses. Nat Rev Immunol 16, 626-638.

Kleinnijenhuis, J., Oosting, M., Joosten, L.A., Netea, M.G., and Van Crevel, R. (2011). Innate immune recognition of Mycobacterium tuberculosis. Clin Dev Immunol *2011*, 405310.

Knibbs, R.N., Goldstein, I.J., Ratcliffe, R.M., and Shibuya, N. (1991). Characterization of the carbohydrate binding specificity of the leukoagglutinating lectin from Maackia amurensis. Comparison with other sialic acid-specific lectins. The Journal of biological chemistry *266*, 83-88.

Kobayashi, Y. (2008). The role of chemokines in neutrophil biology. Front Biosci *13*, 2400-2407.

Kohtani, T., Abe, Y., Sato, M., Miyauchi, K., and Kawachi, K. (2002). Protective effects of anti-neutrophil antibody against myocardial ischemia/reperfusion injury in rats. European surgical research Europaische chirurgische Forschung Recherches chirurgicales europeennes *34*, 313-320.

Kolaczkowska, E., and Kubes, P. (2013). Neutrophil recruitment and function in health and inflammation. Nat Rev Immunol *13*, 159-175.

Kolarova, H., Ambruzova, B., Svihalkova Sindlerova, L., Klinke, A., and Kubala, L. (2014). Modulation of endothelial glycocalyx structure under inflammatory conditions. Mediators of inflammation *2014*, 694312.

Kowanko, I.C., Ferrante, A., Clemente, G., and Kumaratilake, L.M. (1996). Tumor necrosis factor primes neutrophils to kill Staphylococcus aureus by an oxygen-dependent mechanism and Plasmodium falciparum by an oxygen-independent mechanism. Infection and immunity *64*, 3435-3437.

Kraan, M.C., de Koster, B.M., Elferink, J.G., Post, W.J., Breedveld, F.C., and Tak, P.P. (2000). Inhibition of neutrophil migration soon after initiation of treatment with leflunomide or methotrexate in patients with rheumatoid arthritis: findings in a prospective, randomized, double-blind clinical trial in fifteen patients. Arthritis Rheum *43*, 1488-1495.

Krammer, P.H., Arnold, R., and Lavrik, I.N. (2007). Life and death in peripheral T cells. Nat Rev Immunol *7*, 532-542.

Kriehuber, E., Breiteneder-Geleff, S., Groeger, M., Soleiman, A., Schoppmann, S.F., Stingl, G., Kerjaschki, D., and Maurer, D. (2001). Isolation and characterization of dermal lymphatic and blood endothelial cells reveal stable and functionally specialized cell lineages. J Exp Med *194*, 797-808.

Laitinen, L. (1987). Griffonia simplicifolia lectins bind specifically to endothelial cells and some epithelial cells in mouse tissues. Histochem J *19*, 225-234.

Lammermann, T., Afonso, P.V., Angermann, B.R., Wang, J.M., Kastenmuller, W., Parent, C.A., and Germain, R.N. (2013). Neutrophil swarms require LTB4 and integrins at sites of cell death in vivo. Nature *498*, 371-+.

Lande, R., Ganguly, D., Facchinetti, V., Frasca, L., Conrad, C., Gregorio, J., Meller, S., Chamilos, G., Sebasigari, R., Riccieri, V., *et al.* (2011). Neutrophils Activate Plasmacytoid Dendritic Cells by Releasing Self-DNA-Peptide Complexes in Systemic Lupus Erythematosus. Science translational medicine *3*.

Leak, L.V., and Burke, J.F. (1966). Fine structure of the lymphatic capillary and the adjoining connective tissue area. The American journal of anatomy *118*, 785-809.

Lee, K.M., McKimmie, C.S., Gilchrist, D.S., Pallas, K.J., Nibbs, R.J., Garside, P., McDonald, V., Jenkins, C., Ransohoff, R., Liu, L., *et al.* (2011). D6 facilitates cellular migration and fluid flow to lymph nodes by suppressing lymphatic congestion. Blood *118*, 6220-6229.

Leeuwenberg, J.F., Smeets, E.F., Neefjes, J.J., Shaffer, M.A., Cinek, T., Jeunhomme, T.M., Ahern, T.J., and Buurman, W.A. (1992). E-selectin and intercellular adhesion molecule-1 are released by activated human endothelial cells in vitro. Immunology *77*, 543-549.

Lei, L., Altstaedt, J., von der Ohe, M., Proft, T., Gross, U., and Rink, L. (2001). Induction of interleukin-8 in human neutrophils after MHC class II cross-linking with superantigens. J Leukoc Biol *70*, 80-86.

Leliefeld, P.H.C., Koenderman, L., and Pillay, J. (2015). How Neutrophils Shape Adaptive Immune Responses. Frontiers in immunology *6*.

Levick, J., and Michel, C. (2010). Microvascular fluid exchange and the revised Starling principle. Cardiovasc Res *87*, 198-210.

Ley, K., Laudanna, C., Cybulsky, M.I., and Nourshargh, S. (2007). Getting to the site of inflammation: the leukocyte adhesion cascade updated. Nat Rev Immunol *7*, 678-689.

Li, R., Nortamo, P., Valmu, L., Tolvanen, M., Huuskonen, J., Kantor, C., and Gahmberg, C.G. (1993). A peptide from ICAM-2 binds to the leukocyte integrin CD11a/CD18 and inhibits endothelial cell adhesion. The Journal of biological chemistry *268*, 17513-17518.

Liles, W.C., Broxmeyer, H.E., Rodger, E., Wood, B., Hubel, K., Cooper, S., Hangoc, G., Bridger, G.J., Henson, G.W., Calandra, G., *et al.* (2003). Mobilization of hematopoietic progenitor cells in healthy volunteers by AMD3100, a CXCR4 antagonist. Blood *102*, 2728-2730.

Little, M.A., Bhangal, G., Smyth, C.L., Nakada, M.T., Cook, H.T., Nourshargh, S., and Pusey, C.D. (2006). Therapeutic effect of anti-TNF-alpha antibodies in an experimental model of anti-neutrophil cytoplasm antibody-associated systemic vasculitis. J Am Soc Nephrol 17, 160-169.

Liu, F.T. (2005). Regulatory roles of galectins in the immune response. Int Arch Allergy Imm *136*, 385-400.

Liu, Q., Li, Z.Z., Gao, J.L., Wan, W.Z., McDermott, D., and Murphy, P. (2014). CXCR4 antagonist AMD3100 mobilizes leukocytes from bone marrow and thymus to blood in mice. J Immunol *192*.

Lo, H.M., Lai, T.H., Li, C.H., and Wu, W.B. (2014). TNF-alpha induces CXCL1 chemokine expression and release in human vascular endothelial cells in vitro via two distinct signaling pathways. Acta Pharmacol Sin *35*, 339-350.

Lokuta, M.A., and Huttenlocher, A. (2005). TNF-alpha promotes a stop signal that inhibits neutrophil polarization and migration via a p38 MAPK pathway. J Leukoc Biol *78*, 210-219.

Luster, A.D. (1998). Chemokines - Chemotactic cytokines that mediate inflammation. New Engl J Med *338*, 436-445.

Luther, S.A., Tang, H.L., Hyman, P.L., Farr, A.G., and Cyster, J.G. (2000). Coexpression of the chemokines ELC and SLC by T zone stromal cells and deletion of the ELC gene in the plt/plt mouse. P Natl Acad Sci USA *97*, 12694-12699.

Lynskey, N.N., Banerji, S., Johnson, L.A., Holder, K.A., Reglinski, M., Wing, P.A., Rigby, D., Jackson, D.G., and Sriskandan, S. (2015). Rapid Lymphatic Dissemination of

Encapsulated Group A Streptococci via Lymphatic Vessel Endothelial Receptor-1 Interaction. PLoS Pathog *11*, e1005137.

Ma, J., Wang, J.H., Guo, Y.J., Sy, M.S., and Bigby, M. (1994). In-Vivo Treatment with Anti-Icam-1 and Anti-Lfa-1 Antibodies Inhibits Contact Sensitization-Induced Migration of Epidermal Langerhans Cells to Regional Lymph-Nodes. Cellular immunology *158*, 389-399.

Ma, Q., Jones, D., and Springer, T.A. (1999). The chemokine receptor CXCR4 is required for the retention of B lineage and granulocytic precursors within the bone marrow microenvironment. Immunity *10*, 463-471.

Mackay, C.R., Marston, W.L., and Dudler, L. (1990). Naive and Memory T-Cells Show Distinct Pathways of Lymphocyte Recirculation. J Exp Med *171*, 801-817.

Maddaluno, L., Verbrugge, S.E., Martinoli, C., Matteoli, G., Chiavelli, A., Zeng, Y.P., Williams, E.D., Rescigno, M., and Cavallaro, U. (2009). The adhesion molecule L1 regulates transendothelial migration and trafficking of dendritic cells. J Exp Med *206*, 623-635.

Maletto, B.A., Ropolo, A.S., Alignani, D.O., Liscovsky, M.V., Ranocchia, R.P., Moron, V.G., and Pistoresi-Palencia, M.C. (2006). Presence of neutrophil-bearing antigen in lymphoid organs of immune mice. Blood *108*, 3094-3102.

Malik, I.A., Moriconi, F., Sheikh, N., Naz, N., Khan, S., Dudas, J., Mansuroglu, T., Hess, C.F., Rave-Frank, M., Christiansen, H., *et al.* (2010). Single-dose gamma-irradiation induces up-regulation of chemokine gene expression and recruitment of granulocytes into the portal area but not into other regions of rat hepatic tissue. Am J Pathol *176*, 1801-1815.

Mancardi, S., Vecile, E., Dusetti, N., Calvo, E., Stanta, G., Burrone, O.R., and Dobrina, A. (2003). Evidence of CXC, CC and C chemokine production by lymphatic endothelial cells. Immunology *108*, 523-530.

Mantovani, A., Bonecchi, R., and Locati, M. (2006). Tuning inflammation and immunity by chemokine sequestration: decoys and more. Nat Rev Immunol *6*, 907-918.

Marasco, W.A., Phan, S.H., Krutzsch, H., Showell, H.J., Feltner, D.E., Nairn, R., Becker, E.L., and Ward, P.A. (1984). Purification and Identification of Formyl-Methionyl-Leucyl-Phenylalanine as the Major Peptide Neutrophil Chemotactic Factor Produced by Escherichia-Coli. Journal of Biological Chemistry *259*, 5430-5439.

Martin-Fontecha, A., Sebastiani, S., Hopken, U.E., Uguccioni, M., Lipp, M., Lanzavecchia, A., and Sallusto, F. (2003). Regulation of dendritic cell migration to the draining lymph node: Impact on T lymphocyte traffic and priming. J Exp Med *198*, 615-621.

Martin, C., Burdon, P.C., Bridger, G., Gutierrez-Ramos, J.C., Williams, T.J., and Rankin, S.M. (2003). Chemokines acting via CXCR2 and CXCR4 control the release of neutrophils from the bone marrow and their return following senescence. Immunity *19*, 583-593.

Massena, S., Christoffersson, G., Hjertstrom, E., Zcharia, E., Vlodavsky, I., Ausmees, N., Rolny, C., Li, J.P., and Phillipson, M. (2010). A chemotactic gradient sequestered on endothelial heparan sulfate induces directional intraluminal crawling of neutrophils. Blood *116*, 1924-1931.

Matsuno, H., Yudoh, K., Katayama, R., Nakazawa, F., Uzuki, M., Sawai, T., Yonezawa, T., Saeki, Y., Panayi, G.S., Pitzalis, C., *et al.* (2002). The role of TNF-alpha in the pathogenesis of inflammation and joint destruction in rheumatoid arthritis (RA): a study using a human RA/SCID mouse chimera. Rheumatology *41*, 329-337.

Matsuo, Y., Kihara, T., Ikeda, M., Ninomiya, M., Onodera, H., and Kogure, K. (1995). Role of neutrophils in radical production during ischemia and reperfusion of the rat brain: effect of neutrophil depletion on extracellular ascorbyl radical formation. Journal of cerebral blood flow and metabolism : official journal of the International Society of Cerebral Blood Flow and Metabolism *15*, 941-947.

McEver, R.P., and Cummings, R.D. (1997). Role of PSGL-1 binding to selectins in leukocyte recruitment. J Clin Invest *100*, S97-S103.

McGill, J., and Legge, K.L. (2009). Cutting edge: contribution of lung-resident T cell proliferation to the overall magnitude of the antigen-specific CD8 T cell response in the lungs following murine influenza virus infection. J Immunol *183*, 4177-4181.

McKimmie, C.S., Singh, M.D., Hewit, K., Lopez-Franco, O., Le Brocq, M., Rose-John, S., Lee, K.M., Baker, A.H., Wheat, R., Blackbourn, D.J., *et al.* (2013). An analysis of the function and expression of D6 on lymphatic endothelial cells. Blood *121*, 3768-3777.

Megens, R.T.A., Reitsma, S., Schiffers, P.H.M., Hilgers, R.H.P., De Mey, J.G.R., Slaaf, D.W., Egbrink, M.G.A.O., and van Zandvoort, M.A.M.J. (2007). Two-photon microscopy of vital murine elastic and muscular arteries - Combined structural and functional imaging with subcellular resolution. Journal of vascular research *44*, 87-98.

Merad, M., and Manz, M.G. (2009). Dendritic cell homeostasis. Blood 113, 3418-3427.

Mercier, F.E., Ragu, C., and Scadden, D.T. (2012). The bone marrow at the crossroads of blood and immunity. Nat Rev Immunol *12*, 49-60.

Mestas, J., and Hughes, C.C. (2004). Of mice and not men: differences between mouse and human immunology. J Immunol *172*, 2731-2738.

Miteva, D.O., Rutkowski, J.M., Dixon, J.B., Kilarski, W., Shields, J.D., and Swartz, M.A. (2010). Transmural Flow Modulates Cell and Fluid Transport Functions of Lymphatic Endothelium. Circ Res *106*, 920-U181.

Mocsai, A. (2013). Diverse novel functions of neutrophils in immunity, inflammation, and beyond. J Exp Med *210*, 1283-1299.

Mohr, W. (2003). Polymorphonuclear granulocytes in rheumatic tissue destruction VIII. Considerations on the inflammatory cartilage destruction in chronic arthritides in comparison with liver injuries by PMN's. Z Rheumatol *62*, 539-546.

Molloy, E.S., and Langford, C.A. (2006). Advances in the treatment of small vessel vasculitis. Rheum Dis Clin N Am *32*, 157-+.

Monari, C., Kozel, T.R., Bistoni, F., and Vecchiarelli, A. (2002). Modulation of C5aR expression on human neutrophils by encapsulated and acapsular Cryptococcus neoformans. Infection and immunity *70*, 3363-3370.

Muller, W.A. (2003). Leukocyte-endothelial-cell interactions in leukocyte transmigration and the inflammatory response. Trends in immunology *24*, 327-334.

Muller, W.A. (2009). Mechanisms of transendothelial migration of leukocytes. Circ Res *105*, 223-230.

Murdaca, G., Spano, F., Contatore, M., Guastalla, A., Penza, E., Magnani, O., and Puppo, F. (2015). Infection risk associated with anti-TNF-alpha agents: a review. Expert opinion on drug safety *14*, 571-582.

Nakahara, S., Oka, N., and Raz, A. (2005). On the role of galectin-3 in cancer apoptosis. Apoptosis *10*, 267-275.

Nakano, H., and Gunn, M.D. (2001). Gene duplications at the chemokine locus on mouse chromosome 4: Multiple strain-specific haplotypes and the deletion of secondary lymphoid-organ chemokine and EBI-1 ligand chemokine genes in the plt mutation. J Immunol *166*, 361-369.

Nakanuma, Y., Sasaki, M., and Kono, N. (1993). Succinylated wheat germ agglutinin lectin binding in intrahepatic vessels. A new histochemical tool. Archives of pathology & laboratory medicine *117*, 809-811.

Ni, K., and ONeill, H.C. (1997). The role of dendritic cells in T cell activation. Immunology and cell biology *75*, 223-230.

Nibbs, R.J.B., Kriehuber, E., Ponath, P.D., Parent, D., Qin, S.X., Campbell, J.D.M., Henderson, A., Kerjaschki, D., Maurer, D., Graham, G.J., *et al.* (2001). The beta-chemokine receptor D6 is expressed by lymphatic endothelium and a subset of vascular tumors. Am J Pathol *158*, 867-877.

Nicholls, J.M., Bourne, A.J., Chen, H., Guan, Y., and Peiris, J.S. (2007). Sialic acid receptor detection in the human respiratory tract: evidence for widespread distribution of potential binding sites for human and avian influenza viruses. Respir Res *8*, 73.

Nieuwdorp, M., Holleman, F., de Groot, E., Vink, H., Gort, J., Kontush, A., Chapman, M.J., Hutten, B.A., Brouwer, C.B., Hoekstra, J.B., *et al.* (2007). Perturbation of hyaluronan metabolism predisposes patients with type 1 diabetes mellitus to atherosclerosis. Diabetologia *50*, 1288-1293.

Nightingale, T.D., Frayne, M.E.F., Clasper, S., Banerji, S., and Jackson, D.G. (2009). A Mechanism of Sialylation Functionally Silences the Hyaluronan Receptor LYVE-1 in Lymphatic Endothelium. Journal of Biological Chemistry *284*, 3935-3945.

Nitschke, M., Aebischer, D., Abadier, M., Haener, S., Lucic, M., Vigl, B., Luche, H., Fehling, H.J., Biehlmaier, O., Lyck, R., *et al.* (2012). Differential requirement for ROCK in dendritic cell migration within lymphatic capillaries in steady-state and inflammation. Blood *120*, 2249-2258.

Nourshargh, S., Hordijk, P.L., and Sixt, M. (2010). Breaching multiple barriers: leukocyte motility through venular walls and the interstitium. Nat Rev Mol Cell Biol *11*, 366-378.

Ohl, L., Mohaupt, M., Czeloth, N., Hintzen, G., Kiafard, Z., Zwirner, J., Blankenstein, T., Henning, G., and Forster, R. (2004). CCR7 governs skin dendritic cell migration under inflammatory and steady-state conditions. Immunity *21*, 279-288.

Oliver, G., and Alitalo, K. (2005). The lymphatic vasculature: recent progress and paradigms. Annual review of cell and developmental biology *21*, 457-483.

Oliver, G., and Detmar, M. (2002). The rediscovery of the lymphatic system: old and new insights into the development and biological function of the lymphatic vasculature. Gene Dev *16*, 773-783.

Oohira, A., Wight, T.N., and Bornstein, P. (1983). Sulfated proteoglycans synthesized by vascular endothelial cells in culture. The Journal of biological chemistry *258*, 2014-2021.

Ooi, Y.M., Harris, D.E., Edelson, P.J., and Colten, H.R. (1980). Post-Translational Control of Complement (C5) Production by Resident and Stimulated Mouse Macrophages. J Immunol *124*, 2077-2081.

Pepper, M.S., and Skobe, M. (2003). Lymphatic endothelium: morphological, molecular and functional properties. The Journal of cell biology *163*, 209-213.

Peschon, J.J., Torrance, D.S., Stocking, K.L., Glaccum, M.B., Otten, C., Willis, C.R., Charrier, K., Morrissey, P.J., Ware, C.B., and Mohler, K.M. (1998). TNF receptor-deficient mice reveal divergent roles for p55 and p75 in several models of inflammation. J Immunol *160*, 943-952.

Peters, B.P., and Goldstein, I.J. (1979). The use of fluorescein-conjugated Bandeiraea simplicifolia B4-isolectin as a histochemical reagent for the detection of alpha-D-galactopyranosyl groups. Their occurrence in basement membranes. Exp Cell Res *120*, 321-334.

Pflicke, H., and Sixt, M. (2009). Preformed portals facilitate dendritic cell entry into afferent lymphatic vessels. J Exp Med *206*, 2925-2935.

Phillipson, M., Heit, B., Colarusso, P., Liu, L., Ballantyne, C.M., and Kubes, P. (2006). Intraluminal crawling of neutrophils to emigration sites: a molecularly distinct process from adhesion in the recruitment cascade. J Exp Med *203*, 2569-2575.

Phillipson, M., and Kubes, P. (2011). The neutrophil in vascular inflammation. Nature medicine *17*, 1381-1390.

Phong, H.D.D., Corraza, F., Mestdagh, K., Kassengera, Z., Doyen, V., and Michel, O. (2011). Validation of the cantharidin-induced skin blister as an in vivo model of inflammation. Brit J Clin Pharmaco 72, 912-920.

Pierro, A., and Eaton, S. (2004). Intestinal ischemia reperfusion injury and multisystem organ failure. Seminars in pediatric surgery *13*, 11-17.

Pillay, J., den Braber, I., Vrisekoop, N., Kwast, L.M., de Boer, R.J., Borghans, J.A., Tesselaar, K., and Koenderman, L. (2010). In vivo labeling with 2H2O reveals a human neutrophil lifespan of 5.4 days. Blood *116*, 625-627.

Pober, J.S. (2002). Endothelial activation: intracellular signaling pathways. Arthritis research *4 Suppl 3*, S109-116.

Podolnikova, N.P., Podolnikov, A.V., Haas, T.A., Lishko, V.K., and Ugarova, T.P. (2015). Ligand Recognition Specificity of Leukocyte Integrin alpha(M)beta(2) (Mac-1, CD11b/CD18) and Its Functional Consequences. Biochemistry *54*, 1408-1420.

Popa, C., Netea, M.G., van Riel, P.L., van der Meer, J.W., and Stalenhoef, A.F. (2007). The role of TNF-alpha in chronic inflammatory conditions, intermediary metabolism, and cardiovascular risk. Journal of lipid research *48*, 751-762.

Pratesi, F., Dioni, I., Tommasi, C., Alcaro, M.C., Paolini, I., Barbetti, F., Boscaro, F., Panza, F., Puxeddu, I., Rovero, P., *et al.* (2014). Antibodies from patients with rheumatoid arthritis target citrullinated histone 4 contained in neutrophils extracellular traps. Ann Rheum Dis *73*, 1414-1422.

Pries, A.R., Secomb, T.W., and Gaehtgens, P. (2000). The endothelial surface layer. Pflugers Archiv : European journal of physiology *440*, 653-666.

Proebstl, D., Voisin, M.B., Woodfin, A., Whiteford, J., D'Acquisto, F., Jones, G.E., Rowe, D., and Nourshargh, S. (2012). Pericytes support neutrophil subendothelial cell crawling and breaching of venular walls in vivo. J Exp Med *209*, 1219-1234.

Pruenster, M., Mudde, L., Bombosi, P., Dimitrova, S., Zsak, M., Middleton, J., Richmond, A., Graham, G.J., Segerer, S., Nibbs, R.J.B., *et al.* (2009). The Duffy antigen receptor for chemokines transports chemokines and supports their promigratory activity (vol 10, pg 101, 2008). Nature Immunology *10*, 223-223.

Puga, I., Cols, M., Barra, C.M., He, B., Cassis, L., Gentile, M., Comerma, L., Chorny, A., Shan, M.M., Xu, W.F., *et al.* (2014). B cell-helper neutrophils stimulate the diversification and production of immunoglobulin in the marginal zone of the spleen (vol 13, pg 170, 2012). Nature Immunology *15*, 205-205.

Qu, C.F., Edwards, E.W., Tacke, F., Angeli, V., Llodra, J., Sanchez-Schmitz, G., Garin, A., Haque, N.S., Peters, W., van Rooijen, N., *et al.* (2004). Role of CCR8 and other chemokine pathways in the migration of monocyte-derived dendritic cells to lymph nodes. J Exp Med *200*, 1231-1241.

Rabinovich, G.A., Liu, F.T., Hirashima, M., and Anderson, A. (2007). An emerging role for galectins in tuning the immune response: Lessons from experimental models of inflammatory disease, autoimmunity and cancer. Scandinavian journal of immunology *66*, 143-158.

Radsak, M., Iking-Konert, C., Stegmaier, S., Andrassy, K., and Hansch, G.M. (2000). Polymorphonuclear neutrophils as accessory cells for T-cell activation: major histocompatibility complex class II restricted antigen-dependent induction of T-cell proliferation. Immunology *101*, 521-530.

Rae, C., and MacEwan, D.J. (2004). Granulocyte macrophage-colony stimulating factor and interleukin-3 increase expression of type II tumour necrosis factor receptor, increasing susceptibility to tumour necrosis factor-induced apoptosis. Control of leukaemia cell life/death switching. Cell death and differentiation *11 Suppl 2*, S162-171.

Randolph, G.J. (2001). Dendritic cell migration to lymph nodes: cytokines, chemokines, and lipid mediators. Seminars in immunology *13*, 267-274.

Randolph, G.J., Angeli, V., and Swartz, M.A. (2005). Dendritic-cell trafficking to lymph nodes through lymphatic vessels. Nat Rev Immunol *5*, 617-628.

Randolph, G.J., Ochando, J., and Partida-Sanchez, S. (2008). Migration of dendritic cell subsets and their precursors. Annual review of immunology *26*, 293-316.

Reitsma, S., Slaaf, D.W., Vink, H., van Zandvoort, M.A., and oude Egbrink, M.G. (2007). The endothelial glycocalyx: composition, functions, and visualization. Pflugers Archiv : European journal of physiology *454*, 345-359.

Renshaw, S.A., Timmons, S.J., Eaton, V., Usher, L.R., Akil, M., Bingle, C.D., and Whyte, M.K. (2000). Inflammatory neutrophils retain susceptibility to apoptosis mediated via the Fas death receptor. J Leukoc Biol *67*, 662-668.

Richter, F., Liebig, T., Guenzi, E., Herrmann, A., Scheurich, P., Pfizenmaier, K., and Kontermann, R.E. (2013). Antagonistic TNF Receptor One-Specific Antibody (ATROSAB): Receptor Binding and In Vitro Bioactivity. PloS one 8.

Rigby, D.A., Ferguson, D.J., Johnson, L.A., and Jackson, D.G. (2015). Neutrophils rapidly transit inflamed lymphatic vessel endothelium via integrin-dependent proteolysis and lipoxin-induced junctional retraction. J Leukoc Biol *98*, 897-912.

Robertson, R., Levine, S., Haynes, S., Gutierrez, P., Baratta, J., Tan, Z., and Longmuir, K. (2015). Use of labeled tomato lectin for imaging vasculature structures. Histochemistry and cell biology *143*, 225-234.

Roche, J.K., Keepers, T.R., Gross, L.K., Seaner, R.M., and Obrig, T.G. (2007). CXCL1/KC and CXCL2/MIP-2 are critical effectors and potential targets for therapy of Escherichia coli O157 : H7-associated renal inflammation. Am J Pathol *170*, 526-537.

Rockson, S.G. (2016). Lymphedema. Vasc Med *21*, 77-81.

Romero, V., Fert-Bober, J., Nigrovic, P.A., Darrah, E., Haque, U.J., Lee, D.M., van Eyk, J., Rosen, A., and Andrade, F. (2013). Immune-mediated pore-forming pathways induce cellular hypercitrullination and generate citrullinated autoantigens in rheumatoid arthritis. Science translational medicine *5*, 209ra150.

Ronnblom, L., and Pascual, V. (2008). The innate immune system in SLE: type I interferons and dendritic cells. Lupus *17*, 394-399.

Russo, E., Nitschke, M., and Halin, C. (2013). Dendritic cell interactions with lymphatic endothelium. Lymphatic research and biology *11*, 172-182.

Russo, E., Teijeira, A., Vaahtomeri, K., Willrodt, A.H., Bloch, J.S., Nitschke, M., Santambrogio, L., Kerjaschki, D., Sixt, M., and Halin, C. (2016). Intralymphatic CCL21 Promotes Tissue Egress of Dendritic Cells through Afferent Lymphatic Vessels. Cell Reports 14, 1723-1734.

Ryschich, E., Kerkadze, V., Lizdenis, P., Paskauskas, S., Knaebel, H.P., Gross, W., Gebhard, M.M., Buchler, M.W., and Schmidt, J. (2006). Active leukocyte crawling in microvessels assessed by digital time-lapse intravital microscopy. The Journal of surgical research *135*, 291-296.

Saaristo, A., Veikkola, T., Enholm, B., Hytonen, M., Arola, J., Pajusola, K., Turunen, P., Jeltsch, M., Karkkainen, M.J., Kerjaschki, D., *et al.* (2002). Adenoviral VEGF-C overexpression induces blood vessel enlargement, tortuosity, and leakiness but no sprouting angiogenesis in the skin or mucous membranes. Faseb J *16*, 1041-1049.

Sabin, F.R. (1902). On the origin of the lymphatic system from the veins and the development of the lymph hearts and thoracic duct in the pig. American Journal of Anatomy *1*, 367-389.

Sabin, F.R. (1904). On the development of the superficial lymphatics in the skin of the pig. American Journal of Anatomy *3*, 183-195.

Sadik, C.D., Kim, N.D., and Luster, A.D. (2011). Neutrophils cascading their way to inflammation. Trends in immunology *32*, 452-460.

Saeki, H., Moore, A.M., Brown, M.J., and Hwang, S.T. (1999). Cutting edge: Secondary lymphoid-tissue chemokine (SLC) and CC chemokine receptor 7 (CCR7) participate in the emigration pathway of mature dendritic cells from the skin to regional lymph nodes. J Immunol *162*, 2472-2475.

Sagoo, P., Garcia, Z., Breart, B., LemaOtre, F., Michonneau, D., Albert, M.L., Levy, Y., and Bousso, P. (2016). In vivo imaging of inflammasome activation reveals a subcapsular macrophage burst response that mobilizes innate and adaptive immunity. Nature medicine *22*, 64-+.

Sallusto, F., Lenig, D., Forster, R., Lipp, M., and Lanzavecchia, A. (1999). Two subsets of memory T lymphocytes with distinct homing potentials and effector functions. Nature *401*, 708-712.

Sanchez-Sanchez, N., Riol-Blanco, L., and Rodriguez-Fernandez, J.L. (2006). The multiple personalities of the chemokine receptor CCR7 in dendritic cells. J Immunol 176, 5153-5159.

Sawa, Y., Sugimoto, Y., Ueki, T., Ishikawa, H., Sato, A., Nagato, T., and Yoshida, S. (2007). Effects of TNF-alpha on leukocyte adhesion molecule expressions in cultured human lymphatic endothelium. The journal of histochemistry and cytochemistry : official journal of the Histochemistry Society *55*, 721-733.

Schenk, B.I., Petersen, F., Flad, H.D., and Brandt, E. (2002). Platelet-derived chemokines CXC chemokine ligand (CXCL)7, connective tissue-activating peptide III, and CXCL4 differentially affect and cross-regulate neutrophil adhesion and transendothelial migration. J Immunol *169*, 2602-2610.

Schlessinger, J., Plotnikov, A.N., Ibrahimi, O.A., Eliseenkova, A.V., Yeh, B.K., Yayon, A., Linhardt, R.J., and Mohammadi, M. (2000). Crystal structure of a ternary FGF-FGFR-heparin complex reveals a dual role for heparin in FGFR binding and dimerization. Molecular Cell *6*, 743-750.

Schmidt, E.P., Yang, Y., Janssen, W.J., Gandjeva, A., Perez, M.J., Barthel, L., Zemans, R.L., Bowman, J.C., Koyanagi, D.E., Yunt, Z.X., *et al.* (2012). The pulmonary endothelial glycocalyx regulates neutrophil adhesion and lung injury during experimental sepsis. Nature medicine *18*, 1217-1223.

Schneider, M.A., Meingassner, J.G., Lipp, M., Moore, H.D., and Rot, A. (2007). CCR7 is required for the in vivo function of CD4(+) CD25(+) regulatory T cells. J Exp Med 204, 735-745.

Schoppmann, S.F., Birner, P., Stockl, J., Kalt, R., Ullrich, R., Caucig, C., Kriehuber, E., Nagy, K., Alitalo, K., and Kerjaschki, D. (2002). Tumor-associated macrophages express lymphatic endothelial growth factors and are related to peritumoral lymphangiogenesis. Am J Pathol *161*, 947-956.

Schulte, D., Kuppers, V., Dartsch, N., Broermann, A., Li, H., Zarbock, A., Kamenyeva, O., Kiefer, F., Khandoga, A., Massberg, S., *et al.* (2011). Stabilizing the VE-cadherin-catenin complex blocks leukocyte extravasation and vascular permeability. Embo Journal *30*, 4157-4170.

Schuster, S., Hurrell, B., and Tacchini-Cottier, F. (2013). Crosstalk between neutrophils and dendritic cells: a context-dependent process. J Leukocyte Biol *94*, 671-675.

Semerad, C.L., Liu, F.L., Gregory, A.D., Stumpf, K., and Link, D.C. (2002). G-CSF is an essential regulator of neutrophil trafficking from the bone marrow to the blood. Immunity *17*, 413-423.

Sen, D., Forrest, L., Kepler, T.B., Parker, I., and Cahalan, M.D. (2010). Selective and site-specific mobilization of dermal dendritic cells and Langerhans cells by Th1- and Th2-polarizing adjuvants. Proc Natl Acad Sci U S A *107*, 8334-8339.

Severi, E., Hood, D.W., and Thomas, G.H. (2007). Sialic acid utilization by bacterial pathogens. Microbiology *153*, 2817-2822.

She, Z.W., Wewers, M.D., Herzyk, D.J., Sagone, A.L., and Davis, W.B. (1989). Tumor necrosis factor primes neutrophils for hypochlorous acid production. Am J Physiol *257*, L338-345.

Shen, L., Fahey, J.V., Hussey, S.B., Asin, S.N., Wira, C.R., and Fanger, M.W. (2004). Synergy between IL-8 and GM-CSF in reproductive tract epithelial cell secretions promotes enhanced neutrophil chemotaxis. Cellular immunology *230*, 23-32.

Shibuya, N., Goldstein, I. J., Broekaert, W. F., Nsimba-Lubaki, M., Peeters, B., and Peumans, W. J. (1987). The elderberry (Sambucus nigra L.) bark lectin recognizes the Neu5Ac(alpha 2-6)Gal/GalNAc sequence. J Biol Chem *262*, 1596-1601.

Shimada, T., Kitamura, H., and Nakamura, M. (1992). 3-Dimensional Architecture of Pericytes with Special Reference to Their Topographical Relationship to Microvascular Beds. Arch Histol Cytol *55*, 77-85.

Shklovskaya, E., Roediger, B., and Fazekas de St Groth, B. (2008). Epidermal and dermal dendritic cells display differential activation and migratory behavior while sharing the ability to stimulate CD4+ T cell proliferation in vivo. J Immunol *181*, 418-430.

Sierra, M.D.L.L., Gasperini, P., McCormick, P.J., Zhu, J.F., and Tosato, G. (2007). Transcription factor Gfi-1 induced by G-CSF is a negative regulator of CXCR4 in myeloid cells. Blood *110*, 2276-2285.

Skehel, J.J., and Wiley, D.C. (2000). Receptor binding and membrane fusion in virus entry: the influenza hemagglutinin. Annu Rev Biochem *69*, 531-569.

Skobe, M., Hamberg, L.M., Hawighorst, T., Schirner, M., Wolf, G.L., Alitalo, K., and Detmar, M. (2001). Concurrent induction of lymphangiogenesis, angiogenesis, and

macrophage recruitment by vascular endothelial growth factor-C in melanoma. Am J Pathol *159*, 893-903.

Sleeman, J.P., Krishnan, J., Kirkin, V., and Baumann, P. (2001). Markers for the lymphatic endothelium: in search of the holy grail? Microscopy research and technique *55*, 61-69.

Sligh, J.E., Ballantyne, C.M., Rich, S.S., Hawkins, H.K., Smith, C.W., Bradley, A., and Beaudet, A.L. (1993). Inflammatory and Immune-Responses Are Impaired in Mice Deficient in Intercellular-Adhesion Molecule-1. P Natl Acad Sci USA *90*, 8529-8533.

Smith, A., Bracke, M., Leitinger, B., Porter, J.C., and Hogg, N. (2003). LFA-1-induced T cell migration on ICAM-1 involves regulation of MLCK-mediated attachment and ROCK-dependent detachment. Journal of cell science *116*, 3123-3133.

Soehnlein, O., and Lindbom, L. (2010). Phagocyte partnership during the onset and resolution of inflammation. Nat Rev Immunol *10*, 427-439.

St John, A.L., Ang, W.X.G., Huang, M.N., Kunder, C.A., Chan, E.W., Gunn, M.D., and Abraham, S.N. (2014). S1P-Dependent Trafficking of Intracellular Yersinia pestis through Lymph Nodes Establishes Buboes and Systemic Infection. Immunity *41*, 440-450.

Steinman, R.M., Hawiger, D., and Nussenzweig, M.C. (2003). Tolerogenic dendritic cells. Annual review of immunology *21*, 685-711.

Stenzel, W., Soltek, S., Sanchez-Ruiz, M., Akira, S., Miletic, H., Schluter, D., and Deckert, M. (2008). Both TLR2 and TLR4 are required for the effective immune response in Staphylococcus aureus-induced experimental murine brain abscess. Am J Pathol *172*, 132-145.

Summers, C., Rankin, S.M., Condliffe, A.M., Singh, N., Peters, A.M., and Chilvers, E.R. (2010). Neutrophil kinetics in health and disease. Trends in immunology *31*, 318-324.

Tacchini-Cottier, F., Zweifel, C., Belkaid, Y., Mukankundiye, C., Vasei, M., Launois, P., Milon, G., and Louis, J.A. (2000). An immunomodulatory function for neutrophils during the induction of a CD4(+) Th2 response in BALB/c mice infected with Leishmania major. J Immunol *165*, 2628-2636.

Takashima, A., and Yao, Y. (2015). Neutrophil plasticity: acquisition of phenotype and functionality of antigen-presenting cell. J Leukocyte Biol *98*, 489-496.

Tal, O., Lim, H.Y., Gurevich, I., Milo, I., Shipony, Z., Ng, L.G., Angeli, V., and Shakhar, G. (2011). DC mobilization from the skin requires docking to immobilized CCL21 on lymphatic endothelium and intralymphatic crawling. J Exp Med *208*, 2141-2153.

Tarbell, J.M., Weinbaum, S., and Kamm, R.D. (2005). Cellular fluid mechanics and mechanotransduction. Annals of biomedical engineering *33*, 1719-1723.

Taylor, P.C., Peters, A.M., Paleolog, E., Chapman, P.T., Elliott, M.J., McCloskey, R., Feldmann, M., and Maini, R.N. (2000). Reduction of chemokine levels and leukocyte traffic to joints by tumor necrosis factor alpha blockade in patients with rheumatoid arthritis. Arthritis Rheum *43*, 38-47.

Teijeira, A., Garasa, S., Pelaez, R., Azpilikueta, A., Ochoa, C., Marre, D., Rodrigues, M., Alfaro, C., Auba, C., Valitutti, S., *et al.* (2013). Lymphatic Endothelium Forms Integrin-Engaging 3D Structures during DC Transit across Inflamed Lymphatic Vessels. Journal of Investigative Dermatology *133*, 2276-2285.

Teijeira, A., Palazon, A., Garasa, S., Marre, D., Auba, C., Rogel, A., Murillo, O., Martinez-Forero, I., Lang, F., Melero, I., *et al.* (2012). CD137 on inflamed lymphatic endothelial cells enhances CCL21-guided migration of dendritic cells. Faseb J *26*, 3380-3392.

Teijeira, A., Rouzaut, A., and Melero, I. (2013). Initial Afferent Lymphatic Vessels Controlling Outbound Leukocyte Traffic from Skin to Lymph Nodes. Frontiers in immunology *4*, 433.

Teijeira, A., Russo, E., and Halin, C. (2014). Taking the lymphatic route: dendritic cell migration to draining lymph nodes. Seminars in immunopathology *36*, 261-274.

Telang, S., Vimr, E., Mahoney, J., Law, I., Lundqvist-Gustafsson, H., Qian, M., and Eaton, J. (2001). Strain-specific iron-dependent virulence in Escherichia coli. Journal of Infectious Diseases *184*, 159-165.

Thannickal, V.J., and Fanburg, B.L. (2000). Reactive oxygen species in cell signaling. Am J Physiol-Lung C *279*, L1005-L1028.

Thijssen, V.L., HuIsmans, S., and Griffioen, A.W. (2008). The galectin profile of the endothelium - Altered expression and localization in activated and tumor endothelial cells. Am J Pathol *172*, 545-553.

Thompson, R.D., Noble, K.E., Larbi, K.Y., Dewar, A., Duncan, G.S., Mak, T.W., and Nourshargh, S. (2001). Platelet-endothelial cell adhesion molecule-1 (PECAM-1)-deficient mice demonstrate a transient and cytokine-specific role for PECAM-1 in leukocyte migration through the perivascular basement membrane. Blood *97*, 1854-1860.

Tobler, N.E., and Detmar, M. (2006). Tumor and lymph node lymphangiogenesis - impact on cancer metastasis. J Leukocyte Biol *80*, 691-696.

Torzicky (2012). Platelet Endothelial Cell Adhesion Molecule-1 (PECAM-1/CD31) and CD99 Are Critical in Lymphatic Transmigration of Human Dendritic Cells (vol 132, pg 1149, 2011). Journal of Investigative Dermatology *132*, 1938-1938.

Tough, D.F., Borrow, P., and Sprent, J. (1996). Induction of bystander T cell proliferation by viruses and type I interferon in vivo. Science *272*, 1947-1950.

Tracey, D., Klareskog, L., Sasso, E.H., Salfeld, J.G., and Tak, P.P. (2008). Tumor necrosis factor antagonist mechanisms of action: a comprehensive review. Pharmacol Ther *117*, 244-279.

Tsuboi, K., Hirakawa, J., Seki, E., Imai, Y., Yamaguchi, Y., Fukuda, M., and Kawashima, H. (2013). Role of High Endothelial Venule-Expressed Heparan Sulfate in Chemokine Presentation and Lymphocyte Homing. J Immunol *191*, 448-455.

van den Berg, B.M., Spaan, J.A., Rolf, T.M., and Vink, H. (2006). Atherogenic region and diet diminish glycocalyx dimension and increase intima-to-media ratios at murine carotid artery bifurcation. American journal of physiology Heart and circulatory physiology *290*, H915-920.

van Golen, R.F., van Gulik, T.M., and Heger, M. (2012). Mechanistic overview of reactive species-induced degradation of the endothelial glycocalyx during hepatic ischemia/reperfusion injury. Free Radical Bio Med *52*, 1382-1402.

van Haaren, P.M.A., VanBavel, E., Vink, H., and Spaan, J.A.E. (2003). Localization of the permeability barrier to solutes in isolated arteries by confocal microscopy. Am J Physiol-Heart C *285*, H2848-H2856.

Van Teeffelen, J.W., Brands, J., Stroes, E.S., and Vink, H. (2007). Endothelial glycocalyx: sweet shield of blood vessels. Trends in cardiovascular medicine *17*, 101-105.

Varki, N.M., and Varki, A. (2007). Diversity in cell surface sialic acid presentations: implications for biology and disease. Laboratory investigation; a journal of technical methods and pathology *87*, 851-857.

Vassileva, G., Soto, H., Zlotnik, A., Nakano, H., Kakiuchi, T., Hedrick, J.A., and Lira, S.A. (1999). The reduced expression of 6Ckine in the plt mouse results from the deletion of one of two 6Ckine genes. J Exp Med *190*, 1183-1188.

Vicente-Manzanares, M., Ma, X.F., Adelstein, R.S., and Horwitz, A.R. (2009). Non-muscle myosin II takes centre stage in cell adhesion and migration. Nat Rev Mol Cell Bio *10*, 778-790.

Vieira, S.M., Lemos, H.P., Grespan, R., Napimoga, M.H., Dal-Secco, D., Freitas, A., Cunha, T.M., Verri, W.A., Jr., Souza-Junior, D.A., Jamur, M.C., *et al.* (2009). A crucial role for TNF-alpha in mediating neutrophil influx induced by endogenously generated or exogenous chemokines, KC/CXCL1 and LIX/CXCL5. Br J Pharmacol *158*, 779-789.

Vigl, B., Aebischer, D., Nitschke, M., Iolyeva, M., Rothlin, T., Antsiferova, O., and Halin, C. (2011). Tissue inflammation modulates gene expression of lymphatic endothelial cells and dendritic cell migration in a stimulus-dependent manner. Blood *118*, 205-215.

Vindenes, T., and McQuillen, D. (2015). Images in clinical medicine. Acute lymphangitis. N Engl J Med *372*, 649.

Vink, H., Constantinescu, A.A., and Spaan, J.A. (2000). Oxidized lipoproteins degrade the endothelial surface layer : implications for platelet-endothelial cell adhesion. Circulation *101*, 1500-1502.

Vink, H., and Duling, B.R. (1996). Identification of distinct luminal domains for macromolecules, erythrocytes, and leukocytes within mammalian capillaries. Circ Res *79*, 581-589.

Vinten-Johansen, J. (2004). Involvement of neutrophils in the pathogenesis of lethal myocardial reperfusion injury. Cardiovasc Res *61*, 481-497.

Visuri, M.T., Honkonen, K.M., Hartiala, P., Tervala, T.V., Halonen, P.J., Junkkari, H., Knuutinen, N., Yla-Herttuala, S., Alitalo, K.K., and Saarikko, A.M. (2015). VEGF-C and VEGF-C156S in the pro-lymphangiogenic growth factor therapy of lymphedema: a large animal study. Angiogenesis *18*, 313-326.

Vogel, U., and Frosch, M. (1999). Mechanisms of neisserial serum resistance. Molecular Microbiology *32*, 1133-1139.

Voisin, M.B., and Nourshargh, S. (2013). Neutrophil transmigration: emergence of an adhesive cascade within venular walls. J Innate Immun *5*, 336-347.

Voisin, M.B., Probstl, D., and Nourshargh, S. (2010). Venular Basement Membranes Ubiquitously Express Matrix Protein Low-Expression Regions Characterization in Multiple Tissues and Remodeling during Inflammation. Am J Pathol *176*, 482-495.

von der Weid, P.Y., Rehal, S., and Ferraz, J.G. (2011). Role of the lymphatic system in the pathogenesis of Crohn's disease. Current opinion in gastroenterology *27*, 335-341.

Walchli, T., Mateos, J., Weinman, O., Babic, D., Regli, L., Hoerstrup, S., Gerhardt, H., Schwab, M., and Vogel, J. (2015). Quantitative assessment of angiogenesis, perfused blood vessels and endothelial tip cells in the postnatal mouse brain. Nat Protoc *10*, 53-74.

Wandall, J.H. (1991). Effects of sulphasalazine and its metabolites on neutrophil chemotaxis, superoxide production, degranulation and translocation of cytochrome b-245. Aliment Pharmacol Ther *5*, 609-619.

Wang, L., Fuster, M., Sriramarao, P., and Esko, J.D. (2005). Endothelial heparan sulfate deficiency impairs L-selectin- and chemokine-mediated neutrophil trafficking during inflammatory responses. Nat Immunol *6*, 902-910.

Wang, S., Dangerfield, J.P., Young, R.E., and Nourshargh, S. (2005). PECAM-1, alpha6 integrins and neutrophil elastase cooperate in mediating neutrophil transmigration. Journal of cell science *118*, 2067-2076.

Wang, W. (2007). Change in properties of the glycocalyx affects the shear rate and stress distribution on endothelial cells. J Biomech Eng-T Asme *129*, 324-329.

Wang, W.C., and Cummings, R.D. (1988). The immobilized leukoagglutinin from the seeds of Maackia amurensis binds with high affinity to complex-type Asn-linked oligosaccharides containing terminal sialic acid-linked alpha-2,3 to penultimate galactose residues. The Journal of biological chemistry *263*, 4576-4585.

Wardlaw, A.J., Moqbel, R., Cromwell, O., and Kay, A.B. (1986). Platelet-Activating-Factor - a Potent Chemotactic and Chemokinetic Factor for Human Eosinophils. J Clin Invest *78*, 1701-1706.

Warrington, R., Watson, W., Kim, H.L., and Antonetti, F.R. (2011). An introduction to immunology and immunopathology. Allergy, asthma, and clinical immunology : official journal of the Canadian Society of Allergy and Clinical Immunology *7 Suppl 1*, S1.

Watt, S.M., Salanewby, G., Hoang, T., Gilmore, D.J., Grunert, F., Nagel, G., Murdoch, S.J., Tchilian, E., Lennox, E.S., and Waldmann, H. (1991). Cd66 Identifies a Neutrophil-Specific Epitope within the Hematopoietic System That Is Expressed by Members of the Carcinoembryonic Antigen Family of Adhesion Molecules. Blood *78*, 63-74.

Weber, M., Blair, E., Simpson, C.V., O'Hara, M., Blackburn, P.E., Rot, A., Graham, G.J., and Nibbs, R.J.B. (2004). The chemokine receptor D6 constitutively traffics to and from the cell surface to internalize and degrade chemokine. Mol Biol Cell *15*, 2492-2508.

Weber, M., Hauschild, R., Schwarz, J., Moussion, C., de Vries, I., Legler, D.F., Luther, S.A., Bollenbach, T., and Sixt, M. (2013). Interstitial dendritic cell guidance by haptotactic chemokine gradients. Science *339*, 328-332.

Wegmann, F., Petri, B., Khandoga, A.G., Moser, C., Khandoga, A., Volkery, S., Li, H., Nasdala, I., Brandau, O., Fassler, R., *et al.* (2006). ESAM supports neutrophil extravasation, activation of Rho, and VEGF-induced vascular permeability. J Exp Med *203*, 1671-1677.

Weinbaum, S., Tarbell, J.M., and Damiano, E.R. (2007). The structure and function of the endothelial glycocalyx layer. Annual review of biomedical engineering *9*, 121-167.

Wengner, A.M., Pitchford, S.C., Furze, R.C., and Rankin, S.M. (2008). The coordinated action of G-CSF and ELR plus CXC chemokines in neutrophil mobilization during acute inflammation. Blood *111*, 42-49.

Wick, N., Saharinen, P., Saharinen, J., Gurnhofer, E., Steiner, C.W., Raab, I., Stokic, D., Giovanoli, P., Buchsbaum, S., Burchard, A., *et al.* (2007). Transcriptomal comparison of human dermal lymphatic endothelial cells ex vivo and in vitro. Physiol Genomics *28*, 179-192.

Wigle, J.T., Harvey, N., Detmar, M., Lagutina, I., Grosveld, G., Gunn, M.D., Jackson, D.G., and Oliver, G. (2002). An essential role for Prox1 in the induction of the lymphatic endothelial cell phenotype. EMBO J *21*, 1505-1513.

Wigle, J.T., and Oliver, G. (1999). Prox1 function is required for the development of the murine lymphatic system. Cell *98*, 769-778.

Wigle, T., Sosa-Pineda, B., and Oliver, G. (1999). Prox1 function is required for the development of the murine lymphatic vasculature. Developmental Biology *210*, 195-195.

Wojciechowski, J.C., and Sarelius, I.H. (2005). Preferential binding of leukocytes to the endothelial junction region in venules in situ. Microcirculation *12*, 349-359.

Woodfin, A., Reichel, C.A., Khandoga, A., Corada, M., Voisin, M.B., Scheiermann, C., Haskard, D.O., Dejana, E., Krombach, F., and Nourshargh, S. (2007). JAM-A mediates neutrophil transmigration in a stimulus-specific manner in vivo: evidence for sequential roles for JAM-A and PECAM-1 in neutrophil transmigration. Blood *110*, 1848-1856.

Woodfin, A., Voisin, M.B., Beyrau, M., Colom, B., Caille, D., Diapouli, F.M., Nash, G.B., Chavakis, T., Albelda, S.M., Rainger, G.E., *et al.* (2011). The junctional adhesion molecule JAM-C regulates polarized transendothelial migration of neutrophils in vivo. Nat Immunol *12*, 761-769.

Woodfin, A., Voisin, M.B., Imhof, B.A., Dejana, E., Engelhardt, B., and Nourshargh, S. (2009). Endothelial cell activation leads to neutrophil transmigration as supported by the sequential roles of ICAM-2, JAM-A, and PECAM-1. Blood *113*, 6246-6257.

Woolley, D.E., and Tetlow, L.C. (2000). Mast cell activation and its relation to proinflammatory cytokine production in the rheumatoid lesion. Arthritis research *2*, 65-74.

Worbs, T., Mempel, T.R., Bolter, J., von Andrian, U.H., and Forster, R. (2007). CCR7 ligands stimulate the intranodal motility of T lymphocytes in vivo. J Exp Med *204*, 489-495.

Wright, H.L., Chikura, B., Bucknall, R.C., Moots, R.J., and Edwards, S.W. (2011). Changes in expression of membrane TNF, NF-κB activation and neutrophil apoptosis during active and resolved inflammation. Annals of the Rheumatic Diseases *70*, 537-543.

Wright, H.L., Moots, R.J., Bucknall, R.C., and Edwards, S.W. (2010). Neutrophil function in inflammation and inflammatory diseases. Rheumatology *49*, 1618-1631.

Wright, H.L., Moots, R.J., and Edwards, S.W. (2014). The multifactorial role of neutrophils in rheumatoid arthritis. Nature Reviews Rheumatology *10*, 593-601.

Wu, T.F., Carati, C.J., MacNaughton, W.K., and von der Weid, P.Y. (2006). Contractile activity of lymphatic vessels is altered in the TNBS model of guinea pig ileitis. Am J Physiol-Gastr L *291*, G566-G574.

Wuyts, A., Proost, P., Lenaerts, J.P., Ben-Baruch, A., Van Damme, J., and Wang, J.M. (1998). Differential usage of the CXC chemokine receptors 1 and 2 by interleukin-8, granulocyte chemotactic protein-2 and epithelial-cell-derived neutrophil attractant-78. Eur J Biochem *255*, 67-73.

Xie, J.L., Li, R., Kotovuori, P., Vermotdesroches, C., Wijdenes, J., Arnaout, M.A., Nortamo, P., and Gahmberg, C.G. (1995). Intercellular-Adhesion Molecule-2 (Cd102) Binds to the Leukocyte Integrin Cd11b/Cd18 through the a-Domain. J Immunol *155*, 3619-3628.

Xu, H., Guan, H., Zu, G., Bullard, D., Hanson, J., Slater, M., and Elmets, C.A. (2001). The role of ICAM-1 molecule in the migration of Langerhans cells in the skin and regional lymph node. Eur J Immunol *31*, 3085-3093.

Yadav, R., Larbi, K.Y., Young, R.E., and Nourshargh, S. (2003). Migration of leukocytes through the vessel wall and beyond. Thrombosis and haemostasis *90*, 598-606.

Yang, C.W., Strong, B.S.I., Miller, M.J., and Unanue, E.R. (2010). Neutrophils Influence the Level of Antigen Presentation during the Immune Response to Protein Antigens in Adjuvants. J Immunol *185*, 2927-2934.

Yang, C.W., and Unanue, E.R. (2013). Neutrophils control the magnitude and spread of the immune response in a thromboxane A2-mediated process. J Exp Med *210*, 375-387.

Yang, L., Froio, R.M., Sciuto, T.E., Dvorak, A.M., Alon, R., and Luscinskas, F.W. (2005). ICAM-1 regulates neutrophil adhesion and transcellular migration of TNF-alpha-activated vascular endothelium under flow. Blood *106*, 584-592.

Yimin, Kohanawa, M., Zhao, S., Ozaki, M., Haga, S., Nan, G., Kuge, Y., and Tamaki, N. (2013). Contribution of toll-like receptor 2 to the innate response against Staphylococcus aureus infection in mice. PloS one *8*, e74287.

Yoshida, K., Kondo, R., Wang, Q., and Doerschuk, C.M. (2006). Neutrophil cytoskeletal rearrangements during capillary sequestration in bacterial pneumonia in rats. Am J Resp Crit Care *174*, 689-698.

Zeng, Y., and Tarbell, J.M. (2014). The adaptive remodeling of endothelial glycocalyx in response to fluid shear stress. PloS one *9*, e86249.

Zimmerman, G.A., Prescott, S.M., and McIntyre, T.M. (1992). Endothelial cell interactions with granulocytes: tethering and signaling molecules. Immunology today *13*, 93-100.

Zolla, V., Nizamutdinova, I.T., Scharf, B., Clement, C.C., Maejima, D., Akl, T., Nagai, T., Luciani, P., Leroux, J.C., Halin, C., *et al.* (2015). Aging-related anatomical and biochemical changes in lymphatic collectors impair lymph transport, fluid homeostasis, and pathogen clearance. Aging cell *14*, 582-594.

Appendices

Appendix 1

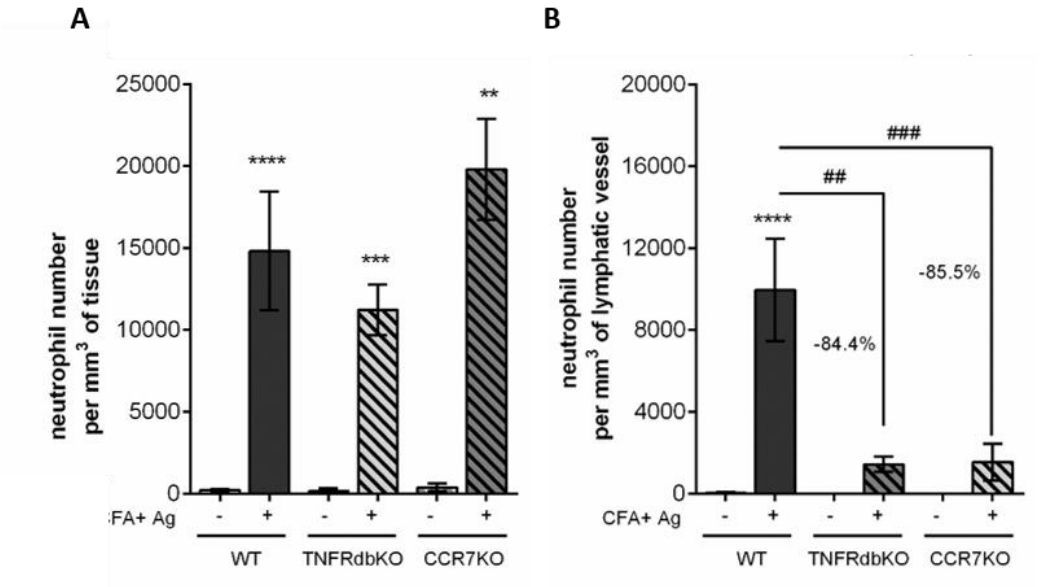

Appendix 1: Neutrophil migration response in the cremaster muscle following stimulation with CFA+Ag (CFA+Ag) for 8 h in WT, TNRdbKO and CCR7KO mice. WT, TNFRdbKO and CCR7KO mice were subjected to CFA+Ag-induced inflammation of the cremaster muscles. Controlled mice were injected with PBS. Eight hours later, the cremaster muscles were dissected away, fixed and immunostained for LYVE-1, PECAM-1 and MRP14 to visualise the lymphatic vasculatures the endothelial cells junctions and neutrophils, respectively before analysis of the neutrophil migration responses by confocal microscopy. (A) Number of extravasated neutrophils in the cremaster muscles. (B) Number of neutrophils within the cremaster lymphatic vessels. Data are expressed as mean ± SEM from n = at least 4 animals per group. Statistically significant difference between stimulated and unstimulated animals are indicated by asterisks: **, P< 0.01; ***, P < 0.001; ****, P < 0.0001. Statistically significant difference between WT and KO animals are indicated by dashes: ##, P < 0.01; ###, P < 0.001.

Appendix 2

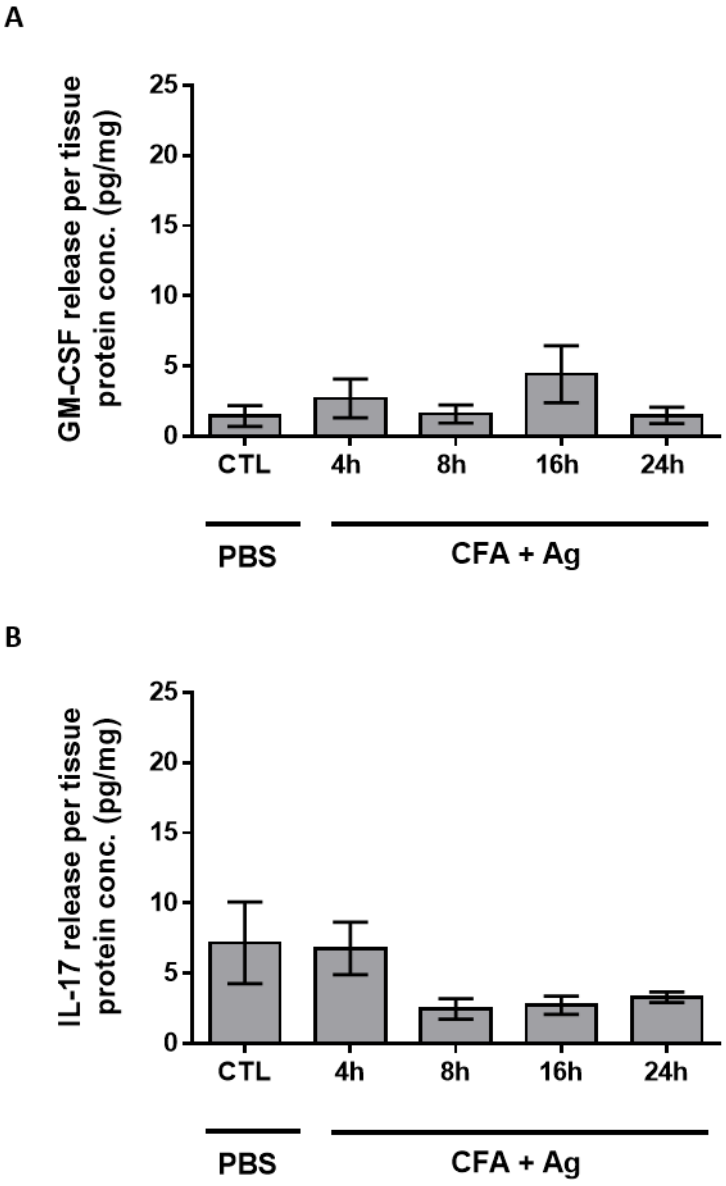

Appendix 2: GM-CSF and IL-17 release in the cremaster muscle following CFA+Ag (CFA+Ag)-induced inflammation *in vivo*. Time-course of TNF release in the cremaster muscles of WT C57BL/6 mice following i.s injection of CFA+Ag and as quantified by ELISA. Mice were stimulated intrascrotally with CFA+Ag for different *in vivo* test periods before being sacrificed by cervical dislocation and their cremaster muscles isolated, snap-frozen and homogenised for use in ELISAs. (A) Time-course of GM-CSF release in the cremaster muscles of WT C57BL/6 mice. (B) Time-course of IL-17 release in the cremaster muscles of WT C57BL/6 mice. Data are expressed as mean ± SEM of N = 6-10 animals per group from 2 independent experiments. Statistical significance was determined using one-way ANOVA.

Appendix 3

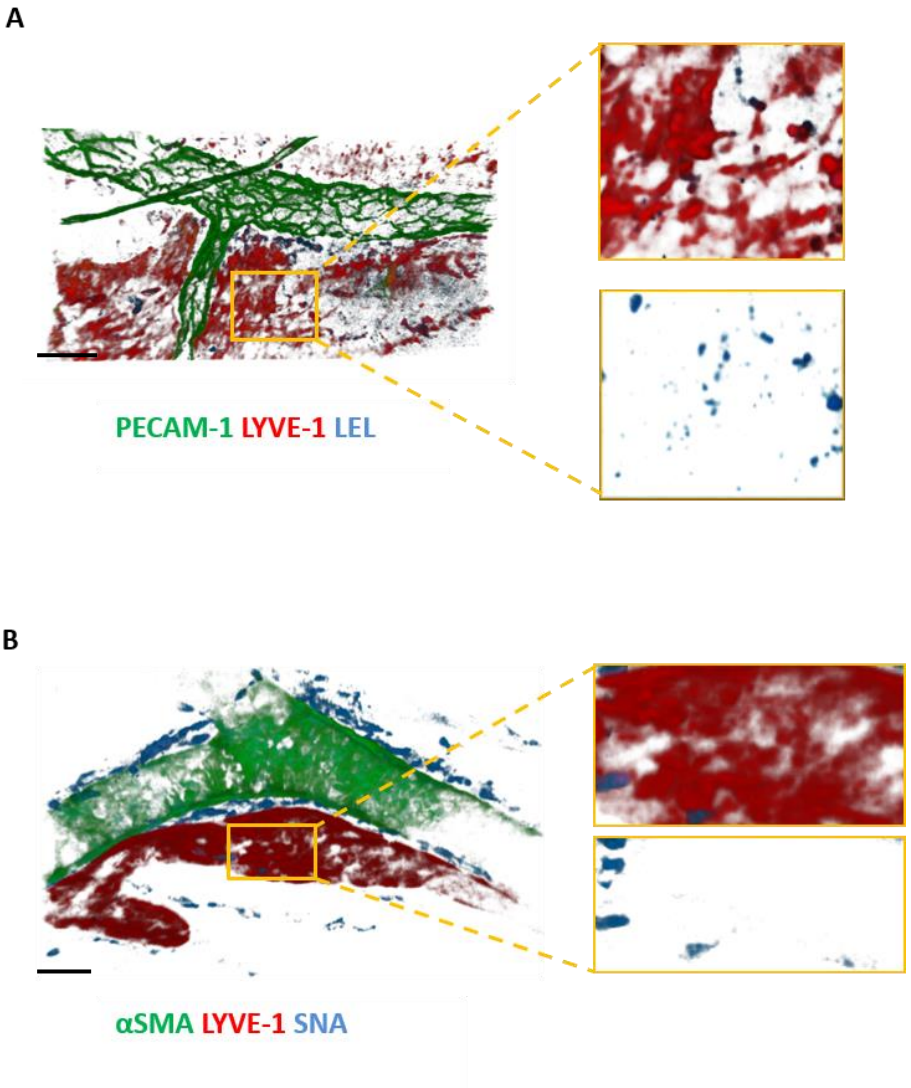

Appendix 3: Representative binding of LEL (top) and SNA (bottom) to LECs of mice cremaster muscles. WT mice were subjected to BECs/LECs/lectin labelling using directly conjugated Alexa Fluor 488/555/647 non-blocking mAb to PECAM-1/LYVE-1/lectin via cold staining. Tissues were analysed on a confocal microscope (Leica, Switzerland). Black boxes on images (left) indicate the region of vessel which is depicted on the zoomed-in images (right). (A) *Ex vivo*-live staining (Pre-fixation/perm-block) of LEL. (B) *Ex vivo*-live staining (Pre-fixation/perm-block) of SNA. Bars = 50 µm. N = 4 mice from 4 independent experiments.

Appendix 4

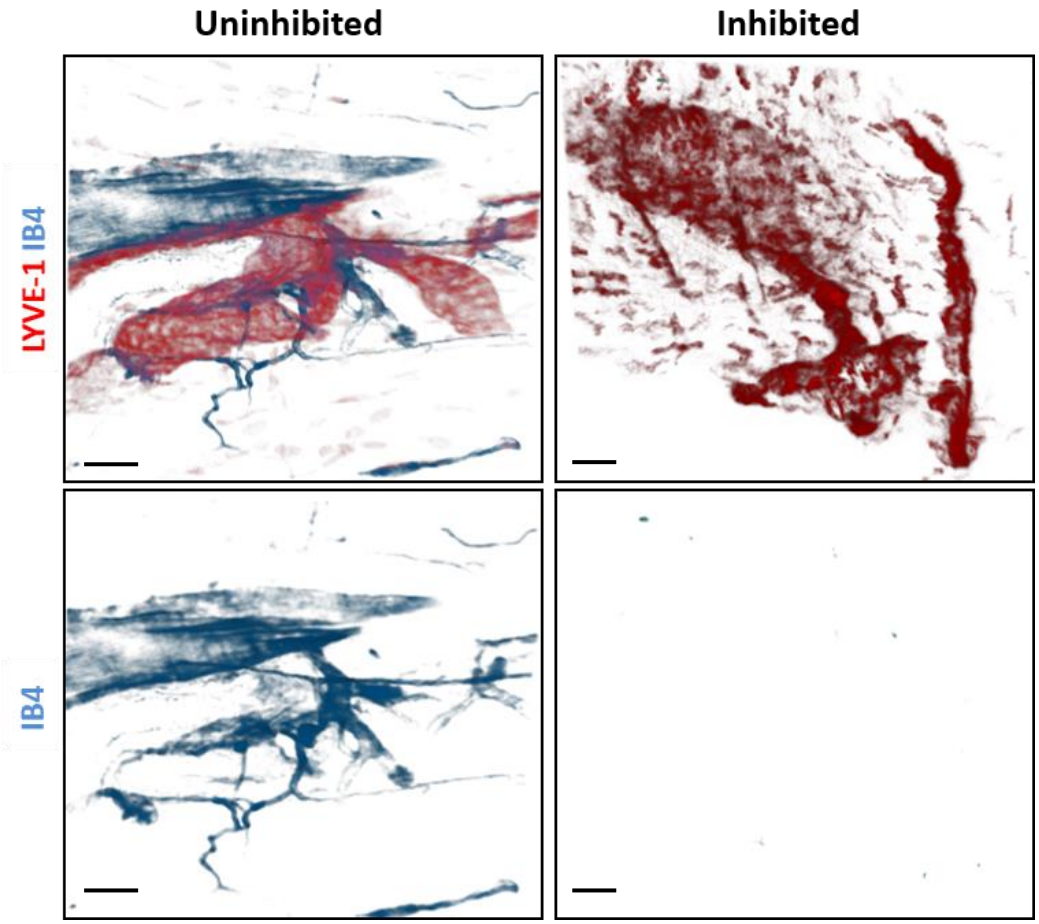

Appendix 4: Confirmation of lectin specificity. WT C57BL/6 mice were given i.s injections of PBS (400 µl) for 16 h before they were sacrificed by cervical dislocation and their cremaster muscles dissected away, fixed, permeabilised and placed in either PBS or 50 mM galactose solution to block competitively block IB4 lectin binding for 2 hours. Tissues were then stained for IB4 (blue) and immunostained for LYVE-1 (red). Representative 3D reconstructed confocal images on the left show tissues that have not been treated with blocking doses of galactose. Images on the right show tissues that have been treated with blocking doses of galactose. Bars = 50 µm. N = 3 mice from 3 independent experiments.

Appendix 5

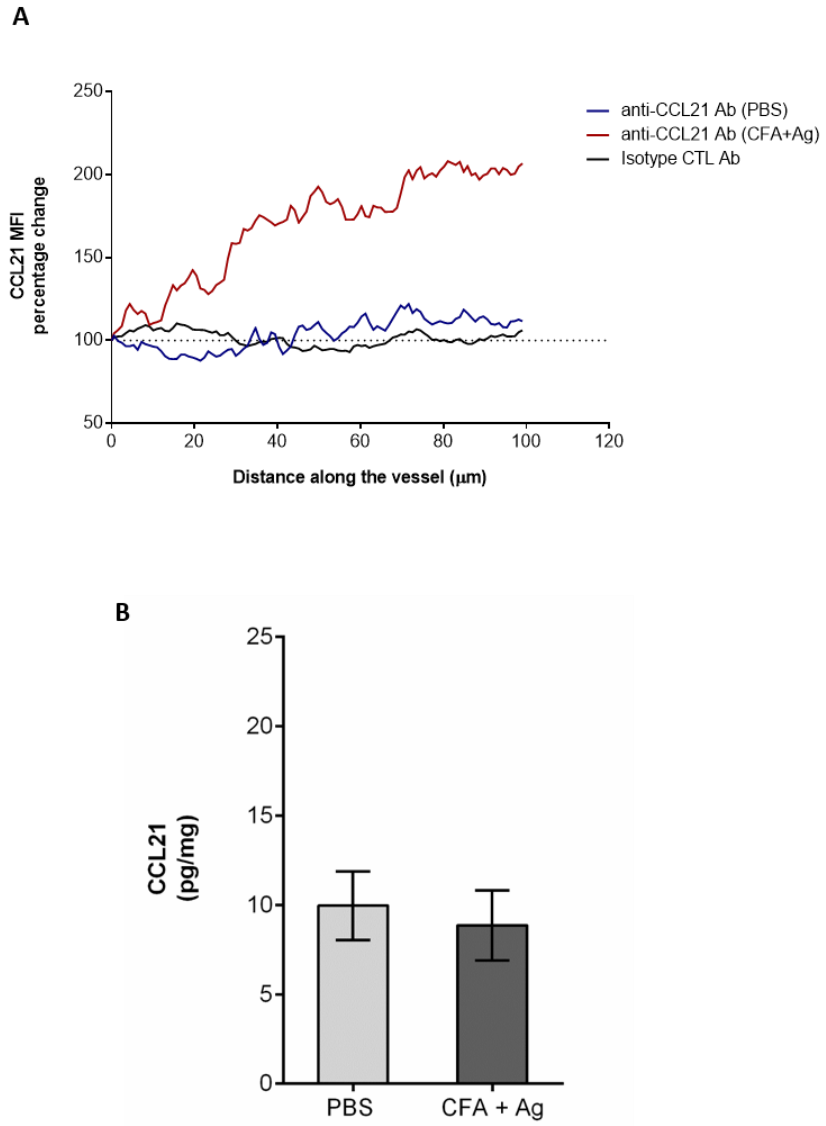

Appendix 5: CCL21 expression in cremaster tissues

C57BL/6 WT mice were given i.s injections of CFA+Ag (CFA+Ag) (200 µg in 300 µl IFA/OVA/PBS) and the inflammatory response allowed to develop for 16 h. Two hours before the end of the inflammation period, mice received an i.s. injection of anti-LYVE-1 mAb and anti-CCL21 mAb/rabbit IgG isotype control Ab. CCL21 expression within lymphatic vessels was quantified using ImageJ. For ELISAs, cremaster muscles were dissected away at the end of the inflammatory period and snap-frozen before being homogenised. (A) CCL21 gradient within afferent lymphatic vessels. A surface intensity profile within the lymphatic vessels was generated in the direction of flow (100 µm length). Data are expressed as percentage change from the first measure pixel of the surface. (B) CCL21 expression within cremaster tissues of PBS and CFA+Ag stimulated mice as quantified by ELISAs. Results are from n = at least 4 animals per group from 3 independent experiments (with 8-12 vessels per mouse for confocal images). (B) Statistical significance was determined using unpaired Student's T-test.

Appendix 6

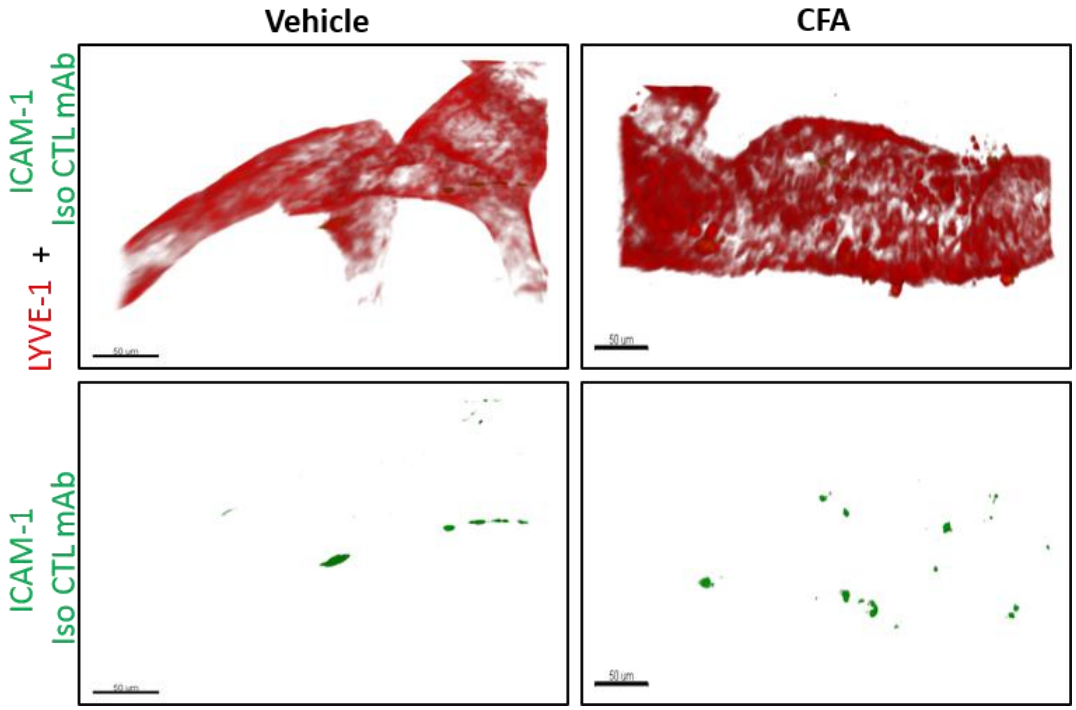

Appendix 6: ICAM-1 isotype control staining. Representative 3D confocal images of LVs (red) from whole mount ICAM-1 isotype control (green) immunostained tissues from WT mice administered with vehicle (left panel) and upon CFA+Ag stimulation (right panel) of the cremaster muscles. Bars = 50 µm. N = 4-6 mice from 4 independent experiments.

Appendix 7

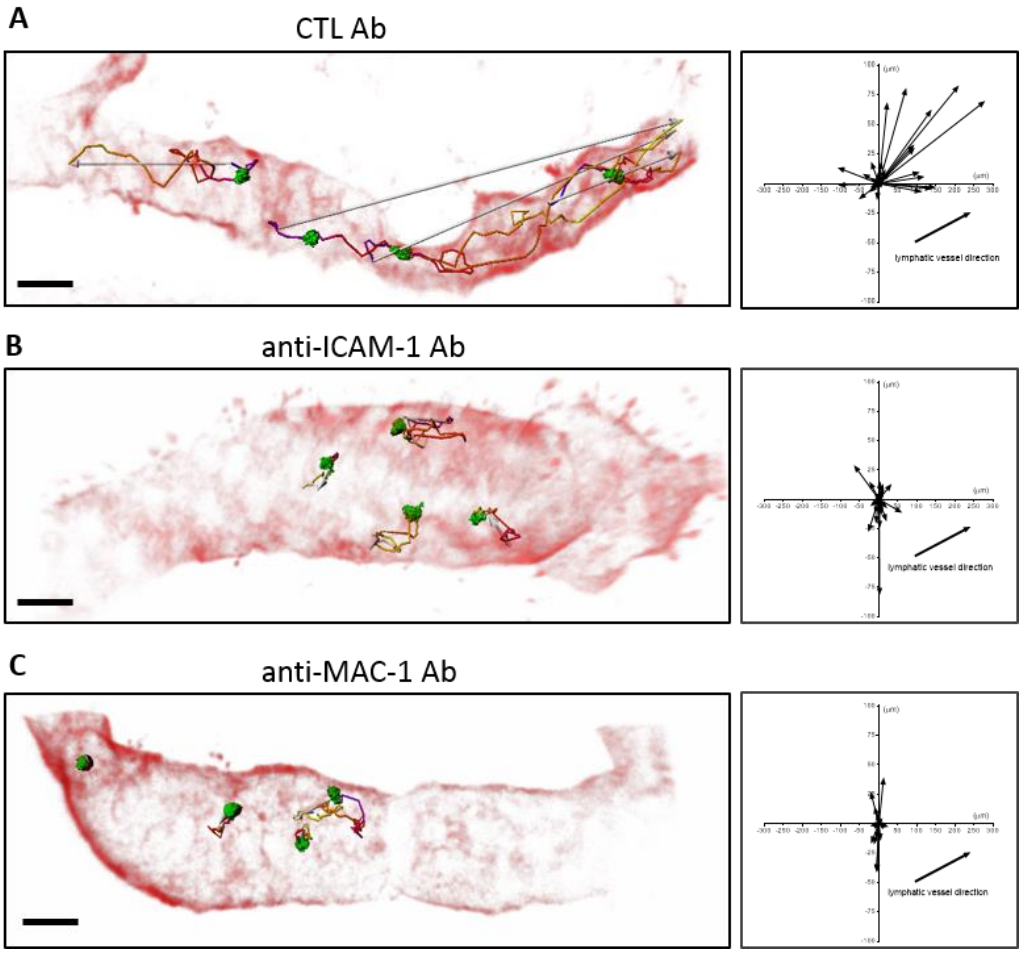

Appendix 7: The effect of ICAM-1/MAC-1 blockade on neutrophil intraluminal crawling within lymphatic vessels. LysM-eGFP mice were subjected to CFA+Ag-induced cremaster inflammation for 6hrs. At 4.5 h post inflammation, mice received an i.s. injection of non-blocking dose of anti-LYVE-1 (red) and anti-PECAM-1 mAbs (not shown on the image) for the visualisation of both the lymphatic and blood vasculatures. Ninety minutes later, tissues were exteriorised to perform time-lapse recordings of the neutrophil responses for 2 h by intravital confocal microscopy. The effect of blocking antibodies against ICAM-1 and MAC-1 (injected locally 90min before recordings) on neutrophil migration paths in lymphatic vessels was investigated and analysed using IMARIS software. The pictures (left panels) are representative 3D still images showing neutrophils (green) within the lymphatic vessels (red) and their respective crawling path (time-coloured mapped line) and/or directionality (white arrow) from mice pre-treated with an isotype control (A), anti-ICAM-1 (B) or anti-MAC-1 (C) mAbs. The directionality plot (right) shows the crawling paths of lymphatic-infiltrated neutrophils in the X & Y planes of the lymphatic vessels from CTL Ab-treated mice. Bar: 30 µm. The graphs (right panels) show the crawling paths of neutrophils in the X & Y planes of the lymphatic vessels from CTL Ab, anti-ICAM-1 and anti-MAC-1 mAbs treated groups. A total of 76 cells were analysed from 10 independent experiments. Bar: 30 µm. Experiments and quantifications were carried out by Dr. Mathieu-Benoit Voisin.

Appendix 8

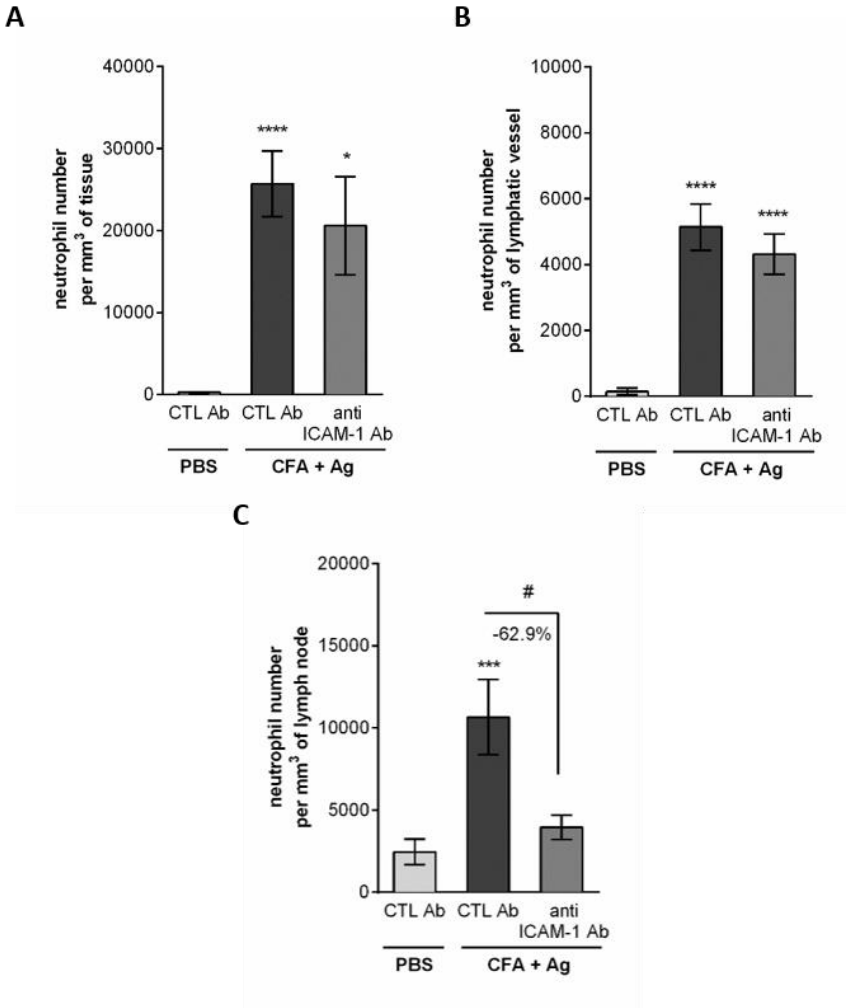

Appendix 8: The effect of anti–ICAM-1 and anti-MAC-1 blocking antibodies on neutrophil extravasation, and migration into lymphatic vessels and their associated dLNs. LysM-eGFP mice were subjected to CFA+Ag-induced cremaster inflammation for 6 h. Mice also received at 4.5hrs post inflammation an i.s. injection of non-blocking dose of anti-LYVE-1 (red) and anti-PECAM-1 mAbs for the visualisation of both the lymphatic and blood vasculatures. Cremaster muscles were dissected way at the end of the inflammatory period, fixed, permeabilised and labelled with anti-MRP14 mAbs to visualise neutrophils. dLNs were dissected way at the end of the inflammatory period, fixed, permeabilised and labelled with anti-HEV, anti LYVE-1 and anti-MRP14 mAbs. Neutrophil migration responses was analysed using IMARIS software. The numbers of neutrophils in the interstitial tissue (A) and inside the lymphatic vessels (B) were quantified by confocal microscopy. (C) Neutrophil infiltration of cremaster dLNs was also quantified at the end of the experiment. Results are expressed as mean ± SEM of N = 4–9 mice (1-2 vessels analysed/mouse for intravital confocal microscopy, each mice is a single experiment). Significant differences between blocking antibodies treated and control groups are indicated by *, $P < 0.05$; ***, $P < 0.001$; ****, $P < 0.0001$. Significant differences between other groups are indicated by # ($P < 0.05$). Experiments and quantifications were carried out by Dr. Mathieu-Benoit Voisin.

Appendix 9

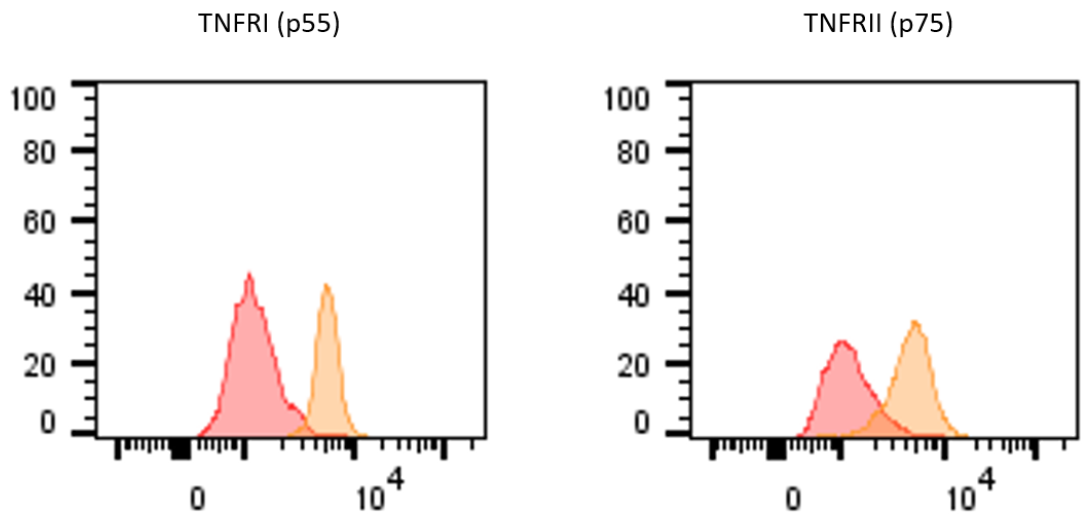

Appendix 9: Neutrophil expression of TNFRI (p55) and TNFRII (p75). Blood leukocytes from WT C57BL/6 mice were immunostained for neutrophils specific markers (CD45+ Ly6G+) and their surface expression of TNFRs p55 and p75 were analysed by flow cytometry. The figure shows representative histograms of the fluorescence intensity for p55 (left, orange) and p75 (right, orange) of blood neutrophils as compared to the intensity of staining of isotype control mAb (red). N = 6-8 animals per group from at least 4 independent experiments.

Video appendices

(N.B. videos are stored on accompanying memory card)

Video 1: Neutrophil breaching of the lymphatic endothelium following TNF stimulation. The video captures the breaching of the lymphatic endothelium by a neutrophil in a TNF-stimulated (300 ng/mouse i.s.) cremaster lymphatic vessel of a LysM-eGFP mouse (exhibiting GFP-labelled leukocytes (green). Cremaster muscles were immunostained *in vivo* for LECs with non-blocking dose of an Alexa555-labelled anti-LYVE-1 mAb (red). The video shows the migration of a neutrophil (in green and isolated from the rest of the inflammatory response by creating an isosurface on it using IMARIS software for clarity of the image) into the lumen of the lymphatic vessel (recorded from 2 h after injection of the cytokine). Images were captured every minute for 90 min.

Video 2: TNF-induced intraluminal neutrophil crawling along the lumen of the lymphatic endothelium. The video captures the intraluminal crawling of neutrophils (in green) along the lymphatic endothelial cell wall in a TNF-stimulated (300 ng/mouse i.s.) cremaster of a LysM-eGFP mouse (exhibiting GFP-labelled leukocytes (green). Lymphatic vessels were immunostained *in vivo* with Alexa555-labelled anti–LYVE-1 mAb (red) and Alexa647-labelled anti-PECAM-1 mAb (blue). Images were captured from 4 h post-i.s. injection at one stack per minute for a duration of 90 min. Still images of this video are shown in Figure 6.1.

Video 3: Intraluminal neutrophil crawling with isotype control (IgG1, κ) mAb. The video captures the intraluminal crawling of several neutrophils (in green and isolated from the rest of the inflammatory response by creating an isosurface on them using IMARIS software for clarity of the image) along the LEC wall in a CFA+Ag-stimulated (200 μg/mouse i.s.) cremaster of a LysM-eGFP mouse (exhibiting GFP-labelled leukocytes (green) immunostained *in vivo* with Alexa555–labelled anti–LYVE-1 mAb (red) and Alexa647-labelled anti-PECAM-1 mAb (blue), in the presence of an IgG1, κ isotype control (50 μg/mouse). The IgG1, κ isotype control mAb was injected i.s. 4 h post-i.s.

injection before exteriorisation of the cremaster muscles to perform intravital confocal microscopy 2 h later. At the end of the sequence, the track followed by the neutrophils during their crawling on the luminal side of the lymphatic endothelium is shown, alongside the displacement (arrow). Images were captured at one stack per minute for a duration of 90 min. A still image of this is shown in Figure 6.3A.

Video 4: Intraluminal neutrophil crawling with anti-TNF blocking mAb. The video captures the intraluminal crawling of several neutrophils (in green and isolated from the rest of the inflammatory response by creating an isosurface on them using IMARIS software for clarity of the image) along the lymphatic endothelial cell wall in a CFA+Ag-stimulated cremaster of a LysM-eGFP mouse (exhibiting GFP-labelled leukocytes (green) and immunostained *in vivo* with Alexa555–labelled anti–LYVE-1 mAb (red) and Alexa647-labelled anti-PECAM-1 mAb (blue), in the presence of an anti-TNF blocking Ab (50 μg/mouse). The anti-TNF blocking Ab was injected i.s. 4 h post-i.s. injection before exteriorisation of the cremaster muscles to perform intravital confocal microscopy 2 h later. At the end of the sequence, the track followed by the neutrophils during their crawling on the luminal side of the lymphatic endothelium is shown, alongside the displacement (arrow). Images were captured at one stack per minute for a duration of 90 min. A still image of this is shown in Figure 6.3B.

Video 5: Intraluminal neutrophil crawling with isotype control (IgG2b, κ) mAb. The video captures the intraluminal crawling of several neutrophils (in green and isolated from the rest of the inflammatory response by creating an isosurface on them using IMARIS software for clarity of the image) along the lymphatic endothelial cell wall in a CFA+Ag-stimulated cremaster of a LysM-eGFP mouse (exhibiting GFP-labelled leukocytes (green) immunostained *in vivo* with Alexa555–labelled anti–LYVE-1 mAb (red) and Alexa647-labelled anti-PECAM-1 mAb (blue), in the presence of an IgG2b, κ isotype control (10 μg/mouse). Antibodies were injected i.s. 90min before exteriorisation of the cremaster muscles and visualisation by intravital confocal microscopy from 6hrs post inflammation. At the end of the sequence, the track followed by the neutrophils during their crawling on the luminal side of the lymphatic endothelium is shown, alongside the displacement (arrow). Images were captured at one stack per minute for a duration of 90min. A still image of this is shown in Appendix 7A.

Video 6: Intraluminal neutrophil crawling with anti-ICAM-1 blocking mAb. The video captures the intraluminal crawling of several neutrophils (in green and isolated from the rest of the inflammatory response by creating an isosurface on them using IMARIS software for clarity of the image) along the lymphatic endothelial cell wall in a CFA+Ag-stimulated cremaster of a LysM-eGFP mouse (exhibiting GFP-labelled leukocytes (green) immunostained *in vivo* with Alexa555–labelled anti–LYVE-1 mAb (red) and Alexa647-labelled anti-PECAM-1 mAb (blue), in the presence of an anti-ICAM-1 blocking mAb (10 μg/mouse). Antibodies were injected i.s. 90 min before exteriorisation of the cremaster muscles and visualisation by intravital confocal microscopy. At the end of the sequence, the track followed by the neutrophils during their crawling on the luminal side of the lymphatic endothelium is shown, alongside the displacement (arrow). Images were captured at one stack per minute for a duration of 90min. A still image of this is shown in Appendix 7B.

Video 7: Intraluminal neutrophil crawling with anti-MAC-1 blocking mAb. The video captures the intraluminal crawling of several neutrophils (in green and isolated from the rest of the inflammatory response by creating an isosurface on them using IMARIS software for clarity of the image) along the lymphatic endothelial cell wall in a CFA+Ag-stimulated cremaster of a LysM-eGFP mouse (exhibiting GFP-labelled leukocytes (green) immunostained *in vivo* with Alexa555–labelled anti–LYVE-1 mAb (red) and Alexa647-labelled anti-PECAM-1 mAb (blue), in the presence of an anti-MAC-1 blocking mAb (10 μg/mouse). Antibodies were injected i.s. 90 min before exteriorisation of the cremaster muscles and visualisation by intravital confocal microscopy. At the end of the sequence, the track followed by the neutrophils during their crawling on the luminal side of the lymphatic endothelium is shown, alongside the displacement (arrow). Images were captured at one stack per minute for a duration of 90 min. A still image of this is shown in Appendix 7C.

SCIENTIFIC REPORTS

OPEN

Endogenous TNFα orchestrates the trafficking of neutrophils into and within lymphatic vessels during acute inflammation

Received: 28 October 2016
Accepted: 06 February 2017
Published: 13 March 2017

Samantha Arokiasamy[1,2], Christian Zakian[1], Jessica Dilliway[1], Wen Wang[2,*], Sussan Nourshargh[1,*] & Mathieu-Benoit Voisin[1]

Neutrophils are recognised to play a pivotal role at the interface between innate and acquired immunities following their recruitment to inflamed tissues and lymphoid organs. While neutrophil trafficking through blood vessels has been extensively studied, the molecular mechanisms regulating their migration into the lymphatic system are still poorly understood. Here, we have analysed neutrophil-lymphatic vessel interactions in real time and *in vivo* using intravital confocal microscopy applied to inflamed cremaster muscles. We show that antigen sensitisation of the tissues induces a rapid but transient entry of tissue-infiltrated neutrophils into lymphatic vessels and subsequent crawling along the luminal side of the lymphatic endothelium. Interestingly, using mice deficient in both TNF receptors p55 and p75, chimeric animals and anti-TNFα antibody blockade we demonstrate that tissue-release of TNFα governs both neutrophil migration through the lymphatic endothelium and luminal crawling. Mechanistically, we show that TNFα primes directly the neutrophils to enter the lymphatic vessels in a strictly CCR7-dependent manner; and induces ICAM-1 up-regulation on lymphatic vessels, allowing neutrophils to crawl along the lumen of the lymphatic endothelium in an ICAM-1/MAC-1-dependent manner. Collectively, our findings demonstrate a new role for TNFα as a key regulator of neutrophil trafficking into and within lymphatic system *in vivo*.

Neutrophils have classically been considered to be prototypical short-lived and terminally differentiated phagocytes involved in innate immune responses following their rapid recruitment at site of infections and acute inflammation[1–3]. Compared to other leukocytes, their life span does not exceed 1–5 days in the circulation[4] though several cytokines such as GM-CSF[5,6], bacteria-derived products[7], hypoxia[8] or their migration through the blood vessel walls[9,10] can significantly expand their life expectancy both *in vivo* and *in vitro*. Until recently, neutrophils were thought to end their life in inflamed tissues by apoptosis before being engulfed by other phagocytic cells to limit and resolve inflammation[11,12]. However, 45 years ago, neutrophils were detected within the lymphatic system[13]. It was suggested that this response represented a way for neutrophils to recirculate back into the blood vasculature; and their role in the lymphatic system was thus largely neglected. Recently, however, accumulating evidence has shown that the role of neutrophils spans beyond the basic but fundamental immunological processes of innate immunity[14]. Specifically, neutrophils can actively participate in the regulation of adaptive immunity following exposure to pathogens and antigens sensitisation[14–17] by means of antigen presentation or cytokine release for stimulating T- and B-lymphocytes[18–22] as well as DCs[23].

While their role in regulating adaptive immunity is now well documented, few studies have investigated the mechanisms associated with neutrophil migration into the lymphatic vasculature. A clue to this phenomenon was first suggested through neutrophil localisation in the draining lymph nodes (dLNs) within the capsula and carrying fluorescently-labelled antigens or pathogens from the sites of antigen-sensitisation or infection[15,16,24]. These results indicated their provenance from tissue-associated lymphatic capillaries via afferent lymphatic vessels. Furthermore, antigen-bearing neutrophils trafficking to dLNs preceded the influx of other professional antigen-presenting cells such as DCs and macrophages[25]; and blocking their entry or depleting mice in circulating

[1]William Harvey Research Institute, Barts and the London School of Medicine and Dentistry, London, UK. [2]School of Engineering and Materials Science; Queen Mary University of London, London, UK. *These authors contributed equally to this work. Correspondence and requests for materials should be addressed to M.-B.V. (email: m.b.voisin@qmul.ac.uk)

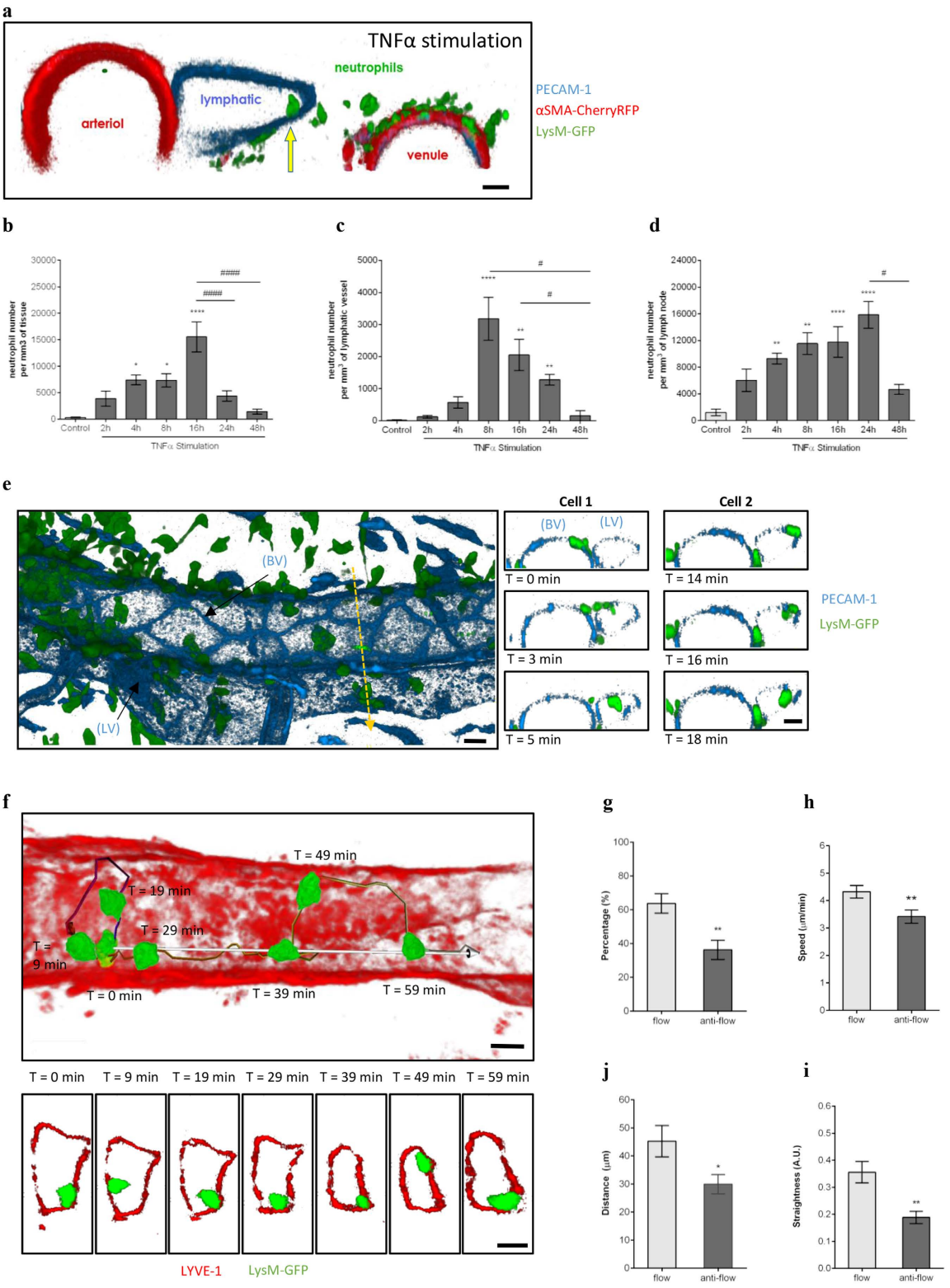

Figure 1. Dynamics of neutrophil migration into cremaster muscle lymphatics upon TNFα-stimulation. The dynamics of neutrophil migration into the tissue and lymphatic vessels was analysed by intravital confocal microscopy in TNFα-stimulated mouse cremaster muscles. (**a**) Representative 3D-reconstructed still image (2 μm cross-section) from a LysM-GFP × αSMA-CherryRFP mouse [exhibiting both endogenous GFP-fluorescent neutrophils (green) and RFP-fluorescent pericytes/smooth muscle cells (red) and immunostained with a non-blocking anti-PECAM-1 mAb (blue)] cremaster tissue showing a neutrophil within the lymphatic vessel (yellow arrow) post TNFα-stimulation. (**b**) Time-course of neutrophil extravasation in TNFα-stimulated cremaster muscles. (**c**) Time-course of neutrophil migration into lymphatic vessels upon TNFα-stimulation. (**d**) Total neutrophil-infiltrate in dLNs upon TNFα-stimulation. (**e**) Representative 3D-reconstructed still image of a post-capillary venule and an adjacent lymphatic vessel from a LysM-GFP mouse (immunostained with

non-blocking anti-PECAM-1 mAb (blue)]. The right panel images illustrate a time-lapse series of 2 μm-thick cross-sections along the z-plane (dotted-yellow arrow) showing the migration of two neutrophils (Cell-1 & Cell-2) into the lymphatic vessel. (**f**) Representative 3D-reconstructed still image of a lymphatic vessel from a TNFα-stimulated cremaster tissue of a LysM-GFP mouse and immunostained with an anti-LYVE-1 mAb (red) *in vivo*. Neutrophil crawling path (colour-coded line) and directionality (white arrow) is shown on the image. The bottom panel images are a series of high magnification cross-sections of the main image at indicated time-points illustrating the continuous attachment of the neutrophil to the lymphatic endothelium. (**g**) Percentage of neutrophils crawling in the afferent direction (flow) or in the opposite direction (anti-flow). Speed (**h**), directionality (**i**) and straightness (**j**) of neutrophils crawling in the afferent (flow) or opposite direction (anti-flow) of the cremaster lymphatic vessels. Data are expressed as mean ± SEM from 5–12 animals per group (at least 5 independent experiments). For the crawling parameter analysis, a total of 63 cells were quantified from 8 mice. Statistically significant differences between stimulated and unstimulated treatment groups are indicated by asterisks: $^{*}P < 0.05$; $^{**}P < 0.01$; $^{***}P < 0.001$; $^{****}P < 0.0001$. Significant differences between responses at different time points are indicated by hash symbols: $^{\#}P < 0.05$; $^{\#\#\#\#}P < 0.0001$. Bar = 10 μm.

neutrophils reduced T-cell proliferation *in vivo*[26], confirming a critical role for these leukocyte in the development of adequate adaptive immune responses. Recently, neutrophils have also been shown to migrate directly into the LNs from the blood circulation via high endothelial venules (HEVs). The molecular signature of these migratory responses is however unclear; and there are currently conflicting data in the literature regarding the chemotaxis pathway involved in this phenomenon. A role for CCR7 in neutrophil migration into the LNs of immunised animals was first demonstrated[27], while other studies have implicated the CXCR4:CXCL12 axis and Sphingosine-1-Phosphate[26,28]. Leukocyte integrins and selectins have also been implicated in neutrophil trafficking to LNs[28], though their exact contribution to cell migration through afferent lymphatic vessels near sites of inflammation *in vivo* is still unclear.

Despite these seminal but conflicting reports, further investigations are required to fully understand the mechanisms associated with this response. Here we provide evidence for the involvement of TNFα in the trafficking of neutrophils into but also within the lymphatic vasculature *in vivo*. Specifically, using a mouse model of antigen sensitisation and cytokine-induced inflammation of the cremaster muscle, we demonstrate that TNFα orchestrates both neutrophil migration into lymphatic vessels in a CCR7-dependent manner and their subsequent crawling along the lymphatic endothelium in an ICAM-1/MAC-1-dependent manner. Collectively, the present findings identify a previously unknown role for TNFα in orchestrating sequential interactions of neutrophils with tissue-associated lymphatic vessels during the acute inflammatory response of antigen sensitisation; and highlight TNFα as a potential target for the manipulation of neutrophil regulation of adaptive immune responses within the lymphatic system.

Results

TNFα promotes neutrophil migration into lymphatic vessels of murine cremaster muscles.

Neutrophil migration into the lymphatic system has been described in models of infections and immunisation sensitisation[15,16,24,27], but the mechanisms associated with this response are not fully understood and somewhat controversial. For this purpose, we studied neutrophil-lymphatic vessel interactions *in vivo* using a mouse model of cremaster muscle inflammation, allowing the direct visualisation in 3- and 4- dimensions of cell-cell interactions by high-resolution confocal microscopy. Whole-mount cremaster tissues of mice immunostained for LYVE-1 and PECAM-1/VE-Cadherin, showed the presence of a unidirectional network of lymphatic vessels with characteristic blind-ended lymphatic capillaries and collecting afferent vessels made up of oak-leaf shaped lymphatic endothelial cells (LEC) (Supplementary Fig. S1) as previously described in other tissues[29,30]. Following tissue-stimulation with exogenous TNFα, neutrophils were rapidly detected in the lumen of lymphatic vessels (Fig. 1a). Detailed analysis of TNFα-stimulated tissues demonstrated a time-dependent migration of neutrophils out of blood vessels post TNFα-administration (Fig. 1b). This response was associated with a rapid and transient migration of neutrophils into lymphatic vessels at 8 hrs post-inflammation (Fig. 1c), as well as into the cremaster muscle draining lymph nodes (dLNs) (Fig. 1d). We then went on to analyse *in vivo* and in real time the dynamics of neutrophil-lymphatic vessel interactions in the cremaster muscle of the neutrophil reporter LysM-GFP mice upon TNFα-stimulation. For this purpose, *in vivo* fluorescent-immunostaining with non-blocking anti-PECAM-1 and/or a non-inhibitory dose of anti-LYVE-1 mAbs was applied to the tissues to visualise endothelial cells and lymphatic vessels, respectively, to allow the tracking of GFP^{high} neutrophils responses into the lymphatic vasculature by intravital confocal microscopy. With this technique, neutrophils were seen to migrate rapidly (4.5 ± 0.6 min) through LECs (Fig. 1e and Videos 1 and 2). Furthermore, we observed that following their entry into the lymphatic vessels, intravasated neutrophils were firmly attached to the LECs and were crawling along the luminal surface of the lymphatic endothelium. (Fig. 1f and Video 3). Analysis of neutrophil crawling dynamics showed that 63.7 ± 5.7% of the neutrophils crawl along the luminal surface of the LECs in the direction of the lymphatic flow at a speed of 4.3 ± 0.2 μm/min; while the few neutrophils venturing against the natural direction of lymphatic flow showed a reduced crawling speed, displacement length and straightness (Fig. 1g–j).

Collectively, these results demonstrate that the cytokine TNFα induces the migration of neutrophils into lymphatic vessels and promotes their crawling along the luminal aspect of LECs *in vivo.*

TNFα controls the entry of neutrophils into lymphatic vessels following antigen sensitisation.

Having observed the efficacy of exogenous TNFα in inducing neutrophil migration into lymphatic vessels, we next investigated the potential role of endogenous TNFα in this response in a model of antigen sensitisation.

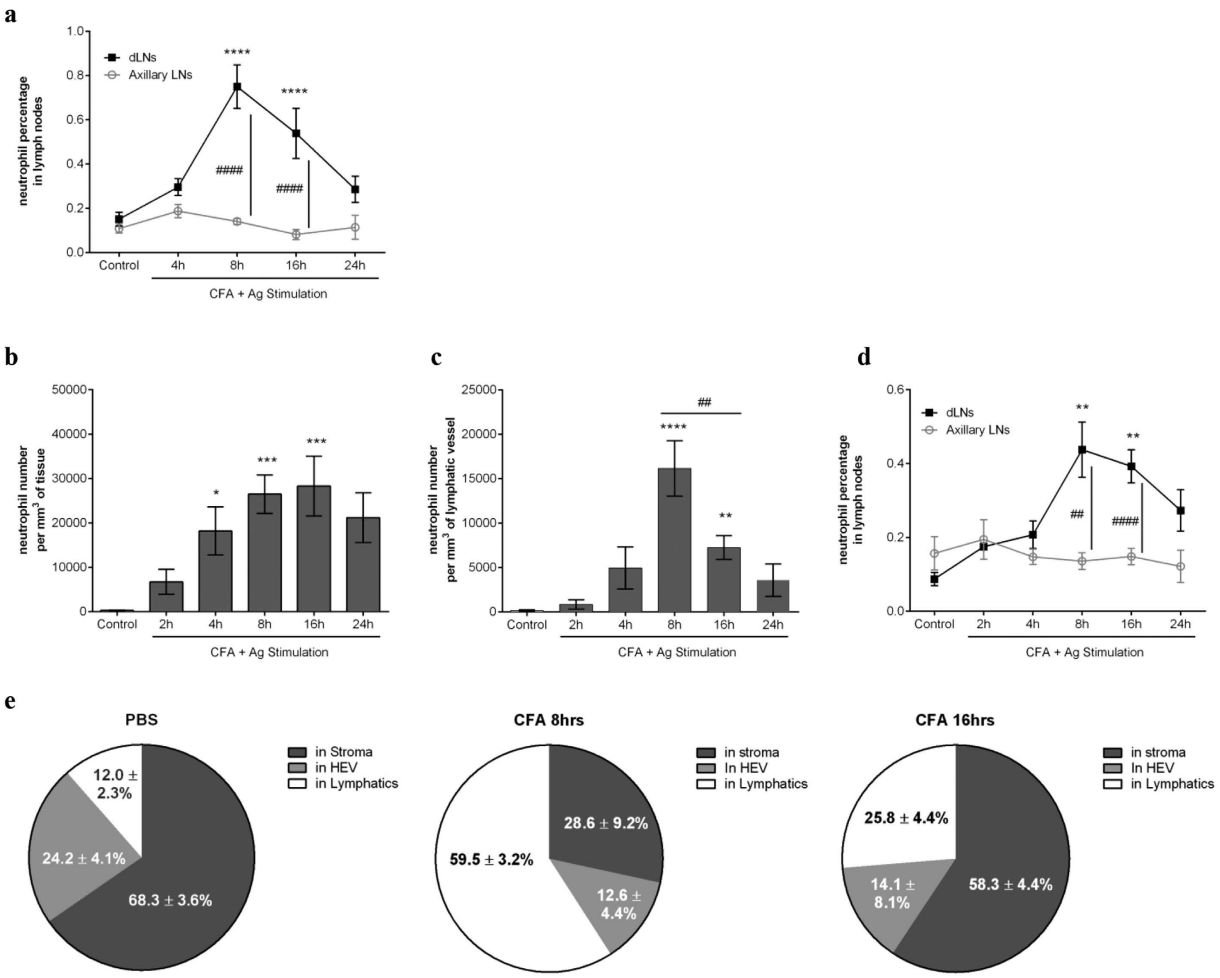

Figure 2. Neutrophil rapidly migrates into lymphatic system of the cremaster muscle during antigen sensitisation *in vivo*. Neutrophil migration into the lymphatic system was induced in WT animals following antigen sensitisation with complete Freund's adjuvant (CFA+Ag). (**a**) Time course of neutrophil migration into draining LNs (inguinal) or non-draining LNs (axillary) of mice injected intradermally with CFA+Ag and as analysed by flow cytometry. (**b**) Time course of CFA+Ag-induced neutrophil extravasation in mice injected intra-scrotally with CFA+Ag as visualised by confocal microscopy. (**c**) Time course of CFA+Ag-induced neutrophil intravasation into the cremaster lymphatic vessels of WT mice as visualised by confocal microscopy. (**d**) Time course of neutrophil migration into draining and non-draining LNs in mice as analysed by flow cytometry. (**e**) Quantification of neutrophil localisation in the dLNs of mice stimulated intra-scrotally with CFA (8 or 16 hrs) or with PBS (control), and as analysed by confocal microscopy. Data are represented as percentages of neutrophils present in the HEV, LYVE-1+ vessels and in the stroma of the LNs. Data are expressed as mean ± SEM of N = 5–12 animals (~10 images per cremasters for confocal microscopy) per group from at least 5–10 experiments. Statistically significant differences between stimulated and control groups or between WT and TNFRdbKO mice are indicated by asterisks: $^{*}P < 0.05$; $^{**}P < 0.01$; $^{***}P < 0.001$; $^{****}P < 0.0001$. Significant differences between other groups are indicated by hash symbols: $^{\#\#}P < 0.01$; $^{\#\#\#\#}P < 0.0001$.

For this purpose, we first analysed the migration response of neutrophils into the dLNs of mice subjected to skin inflammation with an emulsion of an antigen in Complete Freund's Adjuvant (CFA+Ag), reproducing the classical immunisation procedure. Injection of CFA+Ag induced a time-dependent increase in the number of neutrophils in the dLNs (namely inguinal and lumbar LNs) as compared to non-dLN (i.e. axillary LNs) (Fig. 2a). This model was then extended to the cremaster muscle to look at neutrophil-lymphatic vessel interactions *in vivo*. Quantification of neutrophil migration responses through blood and into lymphatic vasculatures showed a time-dependent increase in the number of neutrophils (Fig. 2b,c), both peaking at 8 hrs post-inflammation. This response was associated with an increase in neutrophil infiltration of the dLNs of the cremaster muscles but not of non-dLNs (Fig. 2d). Because of the low incidence of cells (less than 1% of total LN-infiltrated leukocytes as observed by flow cytometry) and to exclude from the analysis the increase of circulating neutrophils due to CFA+Ag-induced neutrophilia (Fig. S2), we performed detailed analysis of whole-mount dLNs immunostained for HEVs (blood vasculature), LYVE-1 (lymphatic vasculature) and MRP14 (neutrophils) by confocal microscopy. We showed that ~60% of neutrophils (Fig. 2e) at 8 hrs post-inflammation were within LYVE-1+ vessels. At 16 hrs

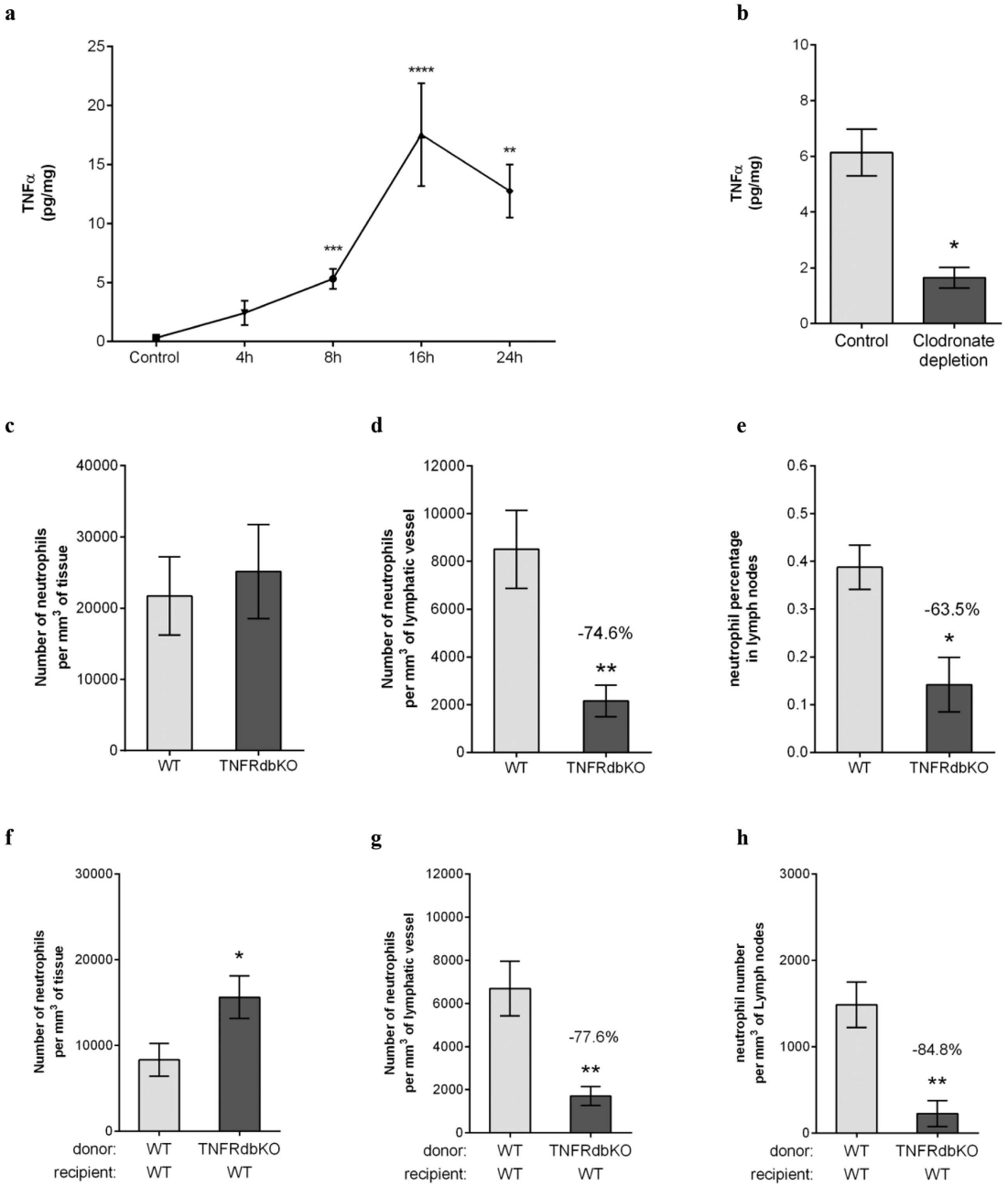

Figure 3. TNFα instruct the neutrophils to migrate into the lymphatic system upon antigen sensitisation. Neutrophil migration into the lymphatic system of the cremaster muscle following antigen sensitisation with complete Freund's adjuvant (CFA+Ag) was induced in WT and TNFRdbKO animals as well as in chimeric animals exhibiting neutrophils deficient in TNFRs. (**a**) Time course of TNFα release in the cremaster muscles of WT mice following intra-scrotal injection of CFA+Ag and as quantified by ELISA. (**b**) TNFα release in mice subjected to clodronate liposome-induced macrophage depletion. (**c**) Number of extravasated neutrophils in cremaster muscles of WT and TNFRdbKO mice at 16 hrs post-CFA+Ag-stimulation as quantified by confocal microscopy. (**d**) Number of neutrophils within cremaster lymphatic vessels of WT and TNFRdbKO mice at 16 hrs post-CFA+Ag-stimulation as quantified by confocal microscopy. (**e**) Percentage of neutrophils in dLNs of WT and TNFRdbKO mice at 16 hrs post-CFA+Ag-stimulation as quantified by flow cytometry. (**f**) Number of extravasated neutrophils in cremaster muscles at 16 hrs post-CFA+Ag-stimulation from chimeric animals receiving bone marrow transplant from WT or TNFRdbKO donor mice and as quantified by confocal microscopy. (**g**) Number of neutrophils within cremaster lymphatic vessels at 16 hrs post-CFA+Ag-stimulation from chimeric animals receiving bone marrow transplant from WT or TNFRdbKO donor mice and as quantified by confocal microscopy. (**h**) Number of neutrophils found in the dLNs of chimeric animals receiving bone marrow transplant from WT or TNFRdbKO donor mice as quantified by confocal microscopy 16 hrs post-CFA+Ag-stimulation. Data are expressed as mean ± SEM of N = 5–12 animals per group from at least 5–10 experiments. Statistically significant differences between stimulated and control groups or between WT and TNFRdbKO mice are indicated by asterisks: *$P < 0.05$; **$P < 0.01$; ****$P < 0.0001$.

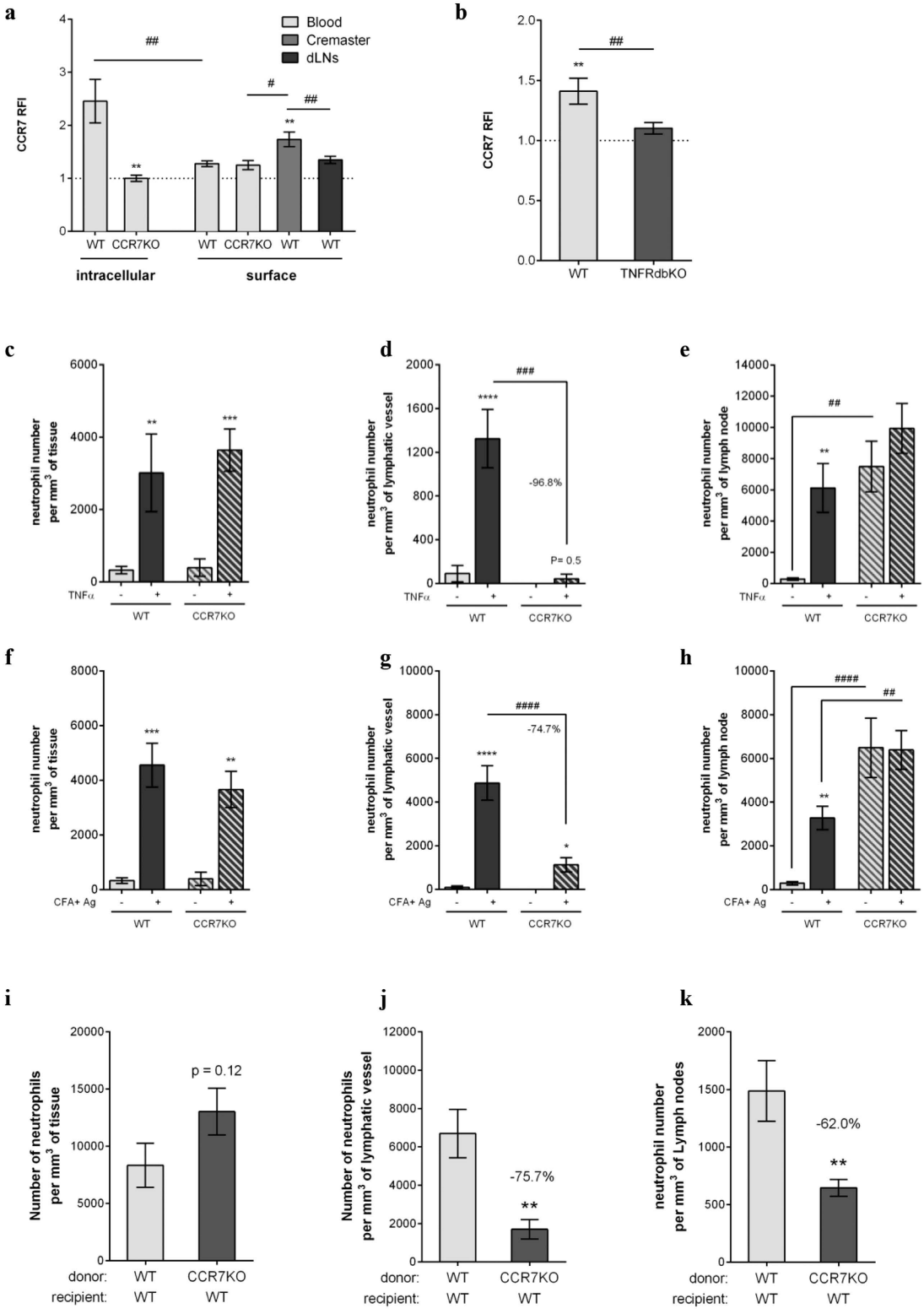

Figure 4. TNFα promotes CCR7-dependent migration of neutrophils into lymphatic vessels *in vivo*. (**a**) Analysis by flow cytometry of CCR7 expression (intracellular and cell-surface) on neutrophils isolated from the blood circulation, CFA+Ag-stimulated-cremaster muscles and dLNs of WT and CCR7KO animals. (**b**) CCR7 surface expression on tissue-infiltrated neutrophils from WT and TNFRdbKO mice subjected to CFA+Ag-induced inflammation. (**c–e**) WT and CCR7KO mice were subjected to TNFα-induced cremaster muscle inflammation and neutrophil responses in the tissue and dLNs was assessed by confocal microscopy 16 hrs post-inflammation. (**c**) Number of extravasated neutrophils in of WT and CCR7KO mice. (**d**) Number of intravasated neutrophils in lymphatic vessels of cremaster muscles from WT and CCR7KO mice. (**e**) Neutrophil number in the cremaster dLNs of WT and CCR7KO animals. (**f–k**) WT, CCR7KO mice or CCR7KO-neutrophil chimeric animals were subjected to antigen sensitisation (CFA+Ag) and neutrophil responses in the cremaster

muscle and dLNs (16 hrs post-inflammation) was assessed by confocal microscopy. (**f**) Number of extravasated neutrophils in inflamed cremaster muscles of WT and CCR7KO mice. (**g**) Number of intravasated neutrophils in cremaster lymphatic vessels of WT and CCR7KO mice. (**h**) Neutrophil number in the cremaster dLNs of WT and CCR7KO mice. (**i**) Number of neutrophils recruited to the cremaster muscles from lethally irradiated WT animals receiving bone marrow transplant from either WT or CCR7KO donor mice. (**j**) Number of neutrophils within cremaster lymphatic vessels post-CFA+Ag-stimulation from lethally irradiated WT animals receiving bone marrow transplant from either WT or CCR7KO donor mice. (**k**) Neutrophil number in the cremaster dLNs from lethally irradiated WT animals receiving bone marrow transplant from either WT or CCR7KO donor mice. Data are expressed as mean ± SEM of N = 7–12 animals per group (from at least 5 independent experiments). Statistically significant differences between stimulated/specific mAb and unstimulated treatment/isotype control groups are indicated by asterisks: $^{*}P < 0.05$; $^{**}P < 0.01$; $^{***}P < 0.001$; $^{****}P < 0.0001$. Significant differences between responses in WT vs. CCR7KO animals (or between different tissues) are indicated by hash symbols: $^{\#}P < 0.05$; $^{\#\#}P < 0.01$; $^{\#\#\#}P < 0.001$; $^{\#\#\#\#}P < 0.0001$.

post-inflammation, only ~25% of the neutrophils were found in this location while ~58% of the cells were found in the LN stroma. Overall, only a minority of the neutrophils were found within the HEVs at these time-points. These data suggest that the early and rapid migration of neutrophils into dLNs may occur via afferent lymphatics.

Interestingly, CFA+Ag-stimulation of cremaster muscles induced a rapid release of TNFα in tissues from 8 hrs onward and reaching the maximum response at 16 hrs post-inflammation (Fig. 3a). Furthermore, mice depleted in resident phagocytes (i.e. macrophages) following the local delivery of clodronate liposomes exhibited a reduction in TNFα release as compared to control liposome-treated animals (Fig. 3b). To investigate the functional role of endogenous TNFα during CFA+Ag-inflammation, neutrophil migration responses were quantified in mice deficient in both TNFR p55 and P75 receptors (TNFRdKO mice). These studies showed that while neutrophil extravasation into tissues was similar between WT and TNFRdbKO mice (Supplementary Figs S3a and Fig. 3c), neutrophil migration into cremaster lymphatic vessels was reduced by 84% and 75% in KO animals at 8 hrs and 16 hrs post-inflammation, respectively (Supplementary Fig. S3b and Fig. 3d). This response was associated with a reduced (~64%) neutrophil-infiltration of the dLNs (Fig. 3e). In order to address the origin of cell type responding to the endogenous release of TNFα during inflammation and promoting neutrophil migration into the lymphatic vessels, we generated chimeric animals. For this purpose, lethally irradiated WT mice were reconstituted with bone marrow hematopoietic cells from either WT or TNFRdbKO animals before being subjected to antigen sensitisation (Supplementary Fig. S4). Similarly to full TNRFdbKO mice, the neutrophil migration response into the lymphatic system was impaired in chimeric animals exhibiting WT vasculature and tissue-resident cells but neutrophils deficient in TNFRs, as compared to the control group; while extravasation through blood vessels was not affected (Fig. 3f–h).

Together these data demonstrate that endogenous TNFα directly primes the leukocytes to trigger the migration of neutrophils into tissue-associated lymphatic vessels post-antigen sensitisation *in vivo*.

TNFα promotes CCR7-dependent migration of neutrophils into lymphatic vessels *in vivo*. Having identified a role for endogenous TNFα in controlling the entry of neutrophils into lymphatic vessels, we then went on to decipher the molecular mechanism involved and more specifically which chemokine/chemokine axis was associated with this response. We first investigated the role of CXCL1 on neutrophil trafficking into the lymphatic vasculature *in vivo*, as the human equivalent of this chemokine has been shown recently to promote neutrophil migration through a monolayer of lymphatic endothelial cells *in vitro*[31]. However, local delivery of anti-CXCL1 blocking antibody did not affect the migration of neutrophil into the lymphatic vasculature of inflamed cremaster muscles *in vivo* (Supplementary Fig. S5a–c). We then went on to analyse the role of CXCR4:CXCL12 axis shown previously to promote the entry of neutrophils into the lymphatic system in different inflammatory models[26,28]. Similarly to CXCL1-blockade, local injection the CXCR4 specific inhibitor AMD3100 did not significantly influenced the capacity of neutrophils to migrate into the lymphatic vessels upon antigen sensitisation (Supplementary Fig. S5d–f). In fact, analysis of blood circulating leukocytes by flow cytometry showed that while CFA+Ag-inflammation induced neutrophilia in both AMD3100- and vehicle-treated mice as compared to unstimulated animals (Fig. S5g), CXCR4 surface expression was down-regulated with the inflammation (Fig. S5h). Collectively, these results suggest that the chemotactic axes CXCL12:CXCR4 and CXCL1:CXCR1/2 do not play a significant role in neutrophil recruitment into the lymphatic vessels during the acute inflammatory response as induced by CFA+Ag *in vivo*.

Finally, the potential involvement of the CCL21/CCR7 axis, widely linked with DC/T-cell migration into the lymphatic system[32] was then explored in our model despite conflicting studies regarding the role of CCR7 in neutrophils[26,27]. The expression of CCR7 on blood-born, cremaster tissue-infiltrated and dLN-infiltrated neutrophils, was first examined by flow cytometry post CFA+Ag-induced inflammation (Fig. 4a). WT blood neutrophils did not express CCR7 on their surface, we could detect intracellular stores of the molecule. Interestingly, neutrophils isolated from CFA+Ag-inflamed cremaster muscles showed a small but significant expression of CCR7 on their cell surface. Interestingly, this upregulation of CCR7 on tissue-infiltrated neutrophils was absent in TNFRdbKO as compared to WT littermates (Fig. 4b). Furthermore, stimulation of mouse blood neutrophils with low concentrations of TNFα *in vitro* induced the surface expression of CCR7 (Supplementary Fig. S6). Having found that tissue-infiltrated neutrophils up-regulate CCR7 on their cell surface, we hypothesised that this chemokine receptor may mediate the migration of neutrophils through lymphatic vessels of the cremaster muscles. To address this, we initially looked at neutrophil migration responses in both WT and CCR7KO animals following TNFα stimulation. Interestingly, while neutrophil extravasation into tissues was not affected (Fig. 4c), trafficking of neutrophils

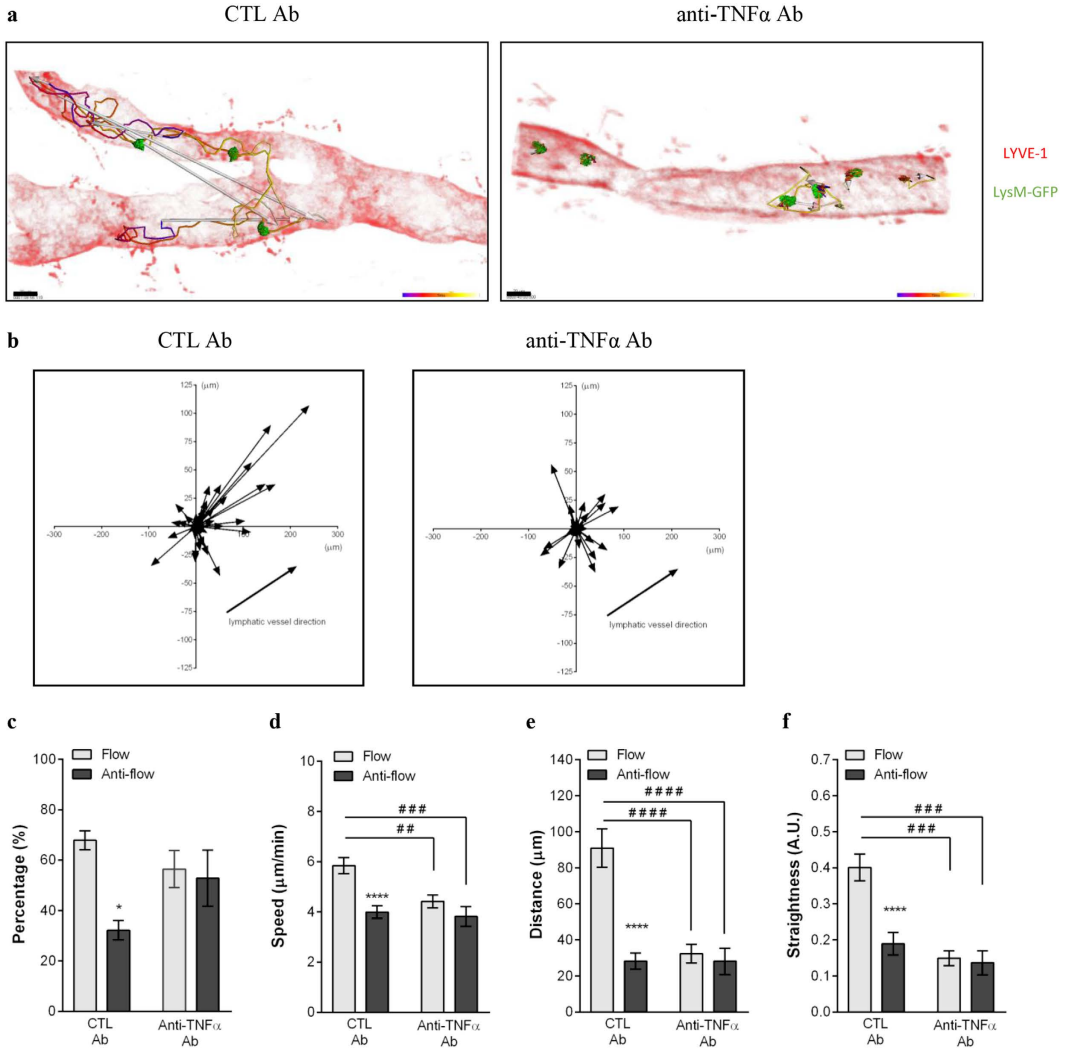

Figure 5. TNFα controls the crawling of neutrophils into the lymphatic vessels *in vivo*. The effect of anti-TNFα blocking mAb on neutrophil crawling along the luminal side of the lymphatic endothelium was analysed by intravital confocal microscopy (IVM) using LysM-GFP mice subjected to CFA+Ag-induced cremaster inflammation and immunostained *in vivo* with a non-blocking dose of Alexa555-conjugated anti-LYVE-1 mAb. Isotype control or anti- TNFα blocking mAbs were injected i.s. 4 hrs post-inflammation. (**a**) The pictures are representative still images at one time point of the IVM recording showing lymphatic-infiltrated neutrophils (green) and their associated crawling path (time-coloured mapped line) and/or directionality (arrow) as analysed by IMARIS software (LYVE-1 with an opacity filter of 5% to see the intravasated leukocytes) from CTL (left panel) or anti- TNFα (right panel) mAb-treated groups. (**b**) The graphs show the crawling paths of lymphatic-infiltrated neutrophils in the X & Y planes of the lymphatic vessels from CTL mAb (left panel) and anti- TNFα mAb (right panel) treated groups. (**c**) Quantification (in percentage) of neutrophils crawling in the afferent (flow) or opposite direction (anti-flow) of the lymphatic vessel. Mean speed (**d**), directionality (**e**) and straightness (**f**) of neutrophils crawling in CTL mAb and anti- TNFα treated groups. A total of 280 cells were analysed. Results are expressed as mean ± SEM of N = 4–9 mice (each mouse representing one independent experiment). Significant differences between flow and anti-flow crawling cells are indicated by $^{*}P < 0.05$; $^{****}P < 0.0001$. Significant differences between the CTL and anti– TNFα mAb treated groups are indicated by hash symbols: $^{\#\#}P < 0.01$; $^{\#\#\#}P < 0.001$; $^{\#\#\#\#}P < 0.0001$. Bar = 20 µm.

into cremaster muscle lymphatic vessels was completely inhibited in CCR7KO animals as compared to WT animals (~97% suppression) (Fig. 4d). With regard to their infiltration into cremaster dLNs, TNFα induced an increase of neutrophils compared to control group (Fig. 4e). However, in TNFα-stimulated CCR7KO mice, the number of neutrophils into the dLNs was comparable to the levels found in unstimulated animals. Similarly, while neutrophil extravasation in response to CFA+Ag was unaffected in CCR7KO mice (Supplementary Fig. S3a and Fig. 4f), neutrophil migration into lymphatic vessels was suppressed by ~86% and 75% in CCR7KO animals as compared to WT mice in this model at 8 and 16 hrs post-inflammation, respectively (Supplementary Fig. S3b and Fig. 4g). Furthermore, and in contrast to WT animals, the level of dLN-infiltrated neutrophils was not increased in CCR7KO mice after stimulation with CFA+Ag (Fig. 4h). Of note, CCR7KO animals exhibited ~25 times more

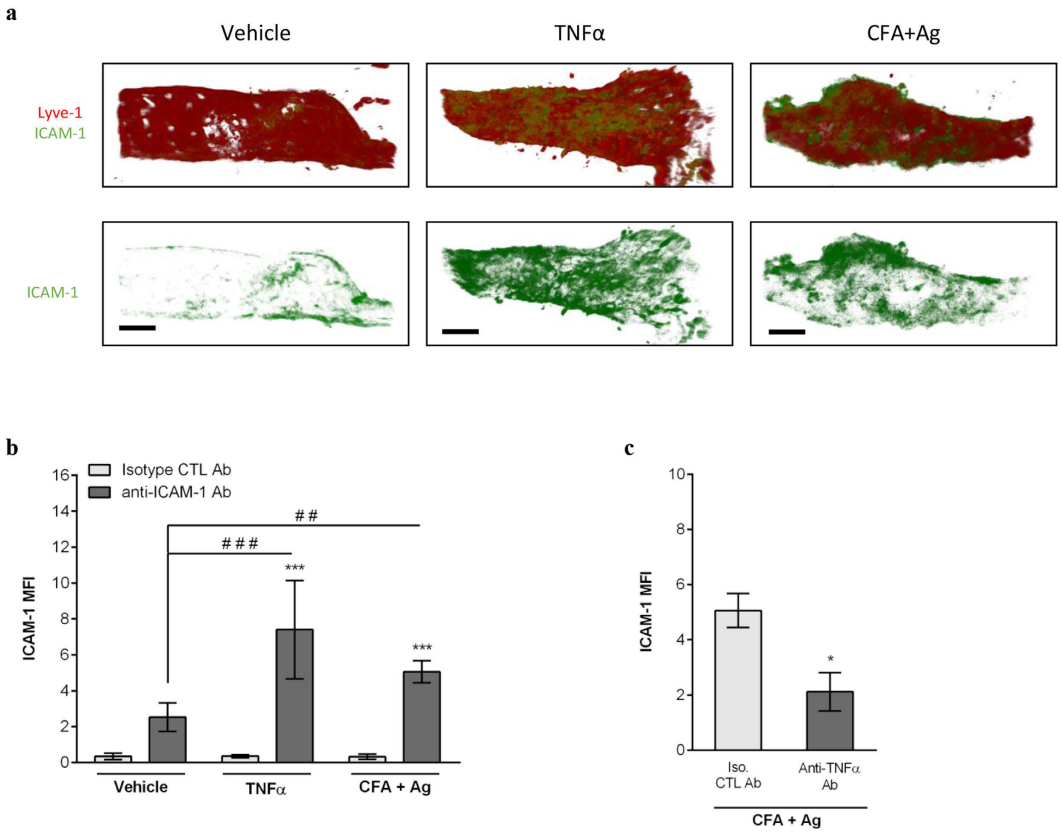

Figure 6. TNFα controls ICAM-1 expression on lymphatic endothelial cells *in vivo*. Cremaster muscles of WT mice were stimulated with TNFα or CFA+Ag (6–8 hrs) and immunostained with Alexa555-conjugated anti-LYVE-1 and Alexa488-conjugated anti-ICAM-1 (or an isotype control) mAbs to label the lymphatic vasculature and ICAM-1, respectively. (**a**) The pictures are representative confocal images of cremaster lymphatic vessels showing the expression of ICAM-1 on selected lymphatic vessels from a PBS-treated control (left panels), TNFα-stimulated (middle panels) and CFA+Ag-stimulated (right panels) animals. (**b**) ICAM-1 expression (mean fluorescent intensity or MFI) on vessels from PBS-treated control, TNFα-stimulated and CFA+Ag-stimulated cremaster muscles as quantified by IMARIS software. (**c**) ICAM-1 expression on lymphatic vessels of CFA+Ag-stimulated cremaster muscles from animals pre-treated with an anti- TNFα blocking mAb or isotype CTL mAb injected 4 hrs post-inflammation. Data are expressed as mean ± SEM of N = 8–12 vessels/animals from 4 animals per group (3 independent experiments). Statistically significant differences between the staining of isotype control and anti-ICAM-1 Abs treated groups are indicated by asterisks: $^{*}P < 0.05$; $^{****}P < 0.0001$. Significant differences between unstimulated and inflamed groups are indicated by hash symbols: $^{\#\#}P < 0.01$; $^{\#\#\#\#}P < 0.0001$. Bar = 50 μm.Results are expressed as mean ± SEM of N = 4–9 mice (1–2 vessels analysed/mouse for intravital confocal microscopy, each mice is a single experiment). Significant differences between blocking antibodies treated and control groups are indicated by $^{*}P < 0.05$; $^{***}P < 0.001$; $^{****}P < 0.0001$. Significant differences between other groups are indicated by $^{\#}(P < 0.05)$. Bar = 30 μm.

LN-infiltrated neutrophils than WT mice in unstimulated conditions, a response related to a higher expression of CXCL12 in the LNs of CCR7KO animals as compared to WT mice (Supplementary Fig. S7), suggesting a compensatory mechanism during the development of these GM mice. Furthermore, using the specific inhibitor of CXCR4 (receptor for CXCL12), AMD3100, we could reduce the number of neutrophils present in the LNs of CCR7KO animals (Supplementary Fig. S7). To overcome the abnormal trafficking of neutrophils into the LNs in CCR7KO animals, we generated chimeric animals by injecting lethally irradiated WT mice with bone marrow cells from CCR7KO animals (or WT bone marrow cells as control). This resulted in the generation of animals exhibiting CCR7KO circulating neutrophils in a WT environment. Similarly to a full KO, chimeric exhibiting CCR7KO neutrophils showed a reduced migration of these leukocytes (~76% reduction) into the lymphatic vasculature of the cremaster muscle upon antigen challenge while neutrophil recruitment from the blood into the tissue was similar to the control chimeric group (Fig. 4i–j). Interestingly, CCR7KO-neutrophil chimeric animals also showed a reduced number of neutrophils infiltrating the dLNs (~62%) as compared to control littermate (Fig. 4k); suggesting that neutrophils from CCR7KO donor cells are not able to migrate efficiently into the LNs of the WT recipient mice.

Collectively, these data demonstrate that TNFα mediates CCR7-dependent migration of neutrophils into afferent lymphatic vessels.

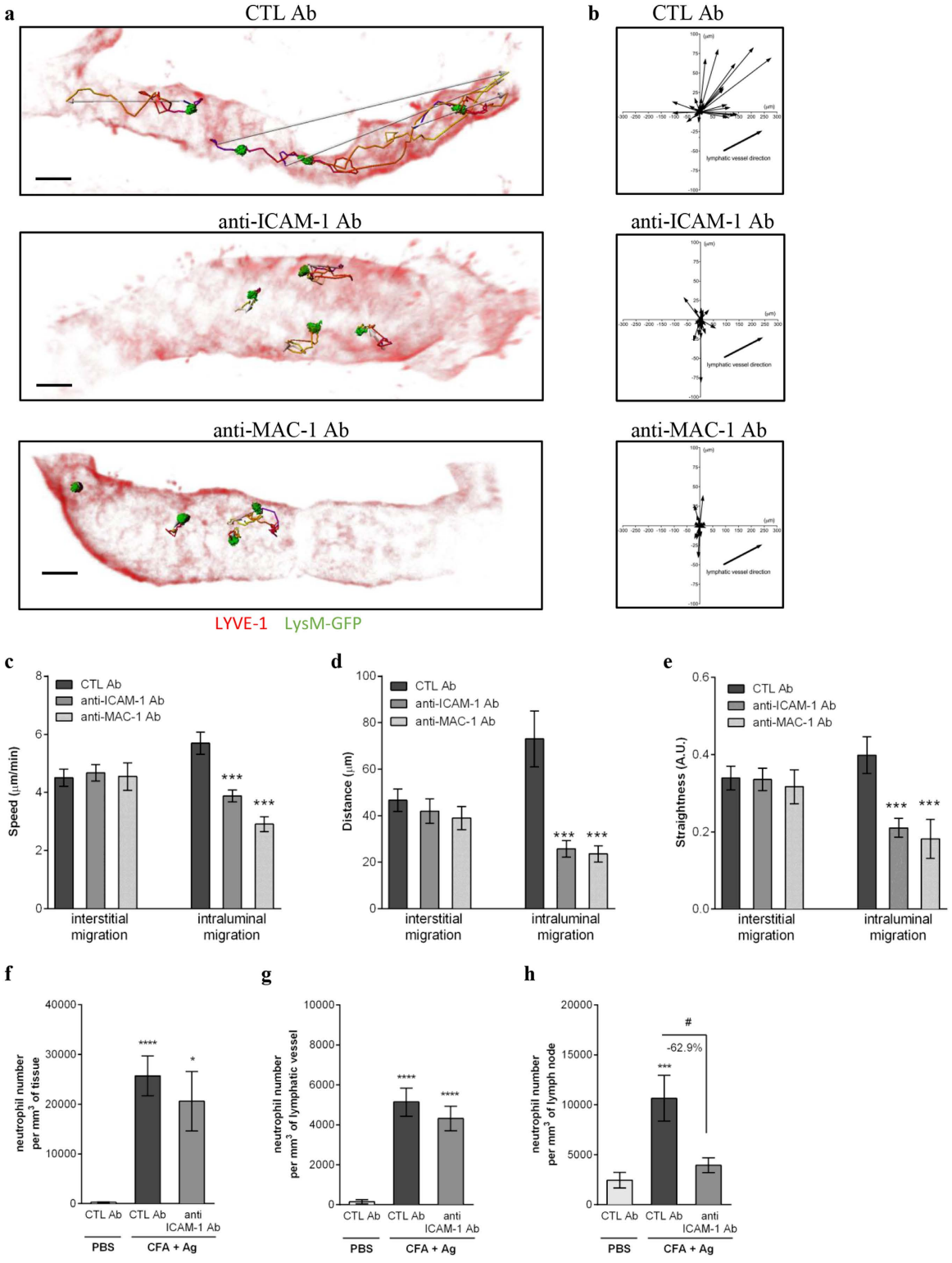

Figure 7. Neutrophil crawling along the lymphatic endothelium is ICAM-1/MAC-1 dependent. LysM-GFP mice were subjected to CFA+Ag-induced cremaster inflammation for 6 hrs. Mice also received at 4.5 hrs post inflammation an i.s. injection of non-blocking dose of Alexa555-conjugated anti-LYVE-1 (red) and Alexa647-conjugated anti-PECAM-1 mAbs (not shown on the image) for the visualisation of both the lymphatic and blood vasculatures. Ninety minutes later, tissues were exteriorised to perform time-lapse recordings of the neutrophil responses for 2 hrs by intravital confocal microscopy. The effect of blocking antibodies against ICAM-1 and MAC-1 (injected locally 90 min before recordings) on neutrophil migration paths in the interstitium and lymphatic vessels was investigated and analysed using IMARIS software. (**a**) The pictures are representative 3D still images showing neutrophils (green) within the lymphatic vessels (red) and their respective crawling path (time-coloured mapped line) and directionality (arrow) from mice pre-treated with an

isotypic control (CTL, top panel), anti-ICAM-1 (middle panel) or anti-MAC-1 (bottom panel) mAbs. (**b**) The graphs show the crawling paths of neutrophils in the X & Y planes of the lymphatic vessels from CTL Ab, anti-ICAM-1 and anti-MAC-1 mAbs treated groups. (**c**-**e**) The effect of anti–ICAM-1 and anti-MAC-1 blocking antibodies on neutrophil migration parameters (i.e. interstitial and intraluminal crawling) was quantified and compared to the responses obtained with an isotype CTL mAb. The three graphs show the mean speed (**c**), directionality (**d**) and straightness (**e**) of neutrophils crawling. A total of 280 cells were analysed. The numbers of neutrophils in the interstitial tissue (**f**) and inside the lymphatic vessels (**g**) were quantify by confocal microscopy. (**h**) Neutrophil infiltration of cremaster dLNs was also quantified at the end of the experiment.Results are expressed as mean ± SEM of N = 4–9 mice (1–2 vessels analysed/mouse for intravital confocal microscopy, each mice is a single experiment). Significant differences between blocking antibodies treated and control groups are indicated by $^{*}P < 0.05$; $^{***}P < 0.001$; $^{****}P < 0.0001$. Significant differences between other groups are indicated by $^{\#}(P < 0.05)$. Bar = 30 μm.

TNFα also controls the crawling of neutrophils along the luminal side of afferent lymphatic endothelium. Using intravital confocal microscopy we observed that TNFα-induced inflammation results in neutrophils crawling along the lymphatic endothelium (Fig. 1f and Video 3). Similarly to TNFα-stimulation, CFA+Ag led to neutrophil crawling along the lumen of LECs (Video 4). The majority of these leukocytes moved in the direction towards collecting lymphatic vessels/lymph flow (67.8 ± 3.8%) at a speed of 5.8 ± 0.2 μm/min and with a straightness index of 0.40 ± 0.04; while cells going against lymph flow direction had reduced speed and directionality of movement (Fig. 5 and Video 5). Interestingly, the favoured directionality of neutrophils was associated with the establishment of a gradient of CCL21 within the lymphatic vessel in the direction of the lymph flow during inflammation (Supplementary Fig. S8). Furthermore, when an anti-TNFα blocking antibody was injected 4 hrs post-CFA + Ag-stimulation, the few neutrophils present within the lymphatic lumen completely lost their directional motility. Cells did not show any preferential direction of migration but exhibited instead a meandering crawling path associated with reduced speed and directionality as compared to isotype control treated animals.

These data suggest that, during the acute phase of the inflammatory response to CFA+Ag, TNFα controls the directional crawling of neutrophils within the lymphatic vessels.

ICAM-1 mediates TNFα-induced neutrophil crawling within lymphatic vessels. To investigate the molecular mechanisms of neutrophil intraluminal crawling in lymphatics, we studied the role of ICAM-1, an adhesion molecule known to support neutrophil crawling along both the luminal[33] and abluminal[34] surfaces of blood vessels. In initial studies we analysed ICAM-1 expression on cremaster lymphatics under basal and inflamed conditions by immunostaining. Both TNFα and CFA+Ag induced an up-regulation of ICAM-1 expression *in vivo* as compared to vehicle-treated animals (Fig. 6a,b). Interestingly, when CFA+Ag-stimulated cremaster muscles were pre-treated with an anti- TNFα blocking antibody, the expression of ICAM-1 on lymphatics was reduced as compared to the control antibody-treated group (Fig. 6c). To further assess the role of ICAM-1 in neutrophil crawling behaviour within the lymphatic vessels, we performed functional assays using local administration (injected 4.5 hrs post-inflammation) of functional blocking antibodies against ICAM-1 or its leukocyte binding partner, the integrin MAC-1 in CFA+Ag-stimulated cremaster muscles of LysM-GFP mice. Both anti–ICAM-1 and anti–MAC-1 mAbs impaired neutrophil intraluminal crawling within lymphatics as compared to an isotype control Ab (Fig. 7a,b and Video 6/7/8). Specifically, blocking ICAM-1 or MAC-1 resulted in a ~50% reduction in the speed of crawling, displacement length and straightness within the luminal side of lymphatic endothelium (Fig. 7c–e). In contrast, interstitial migration was not affected by these treatments. Overall, while the time and route of delivery of the blocking antibodies had no effect on leukocyte extravasation from blood vessels and migration into lymphatic vessels, respectively (Fig. 7f,g), blocking the intraluminal crawling of neutrophils within lymphatic vessels resulted in a reduction in the number of neutrophils infiltrating the dLNs (Fig. 7h).

Collectively, the present findings identify ICAM-1 as an adhesion molecule that mediates neutrophil crawling along the lymphatic endothelium and identify TNFα as a key regulator of neutrophil directional motility within lymphatic vessels *in vivo*.

Discussion

It is now well established that neutrophils contribute to the shaping of the adaptive immunity against many foreign antigens or infectious agents following their rapid migration into the lymphatic system[15,19,35]. However, the mechanisms of his migratory behaviour are poorly understood. In the present study we have identified a previously unknown role for endogenous TNFα in orchestrating neutrophil trafficking into and within the lymphatic vasculature of inflamed tissues *in vivo.* Specifically, we demonstrate that in a mouse model of antigen sensitisation, endogenous TNFα directly instructs the neutrophils to migrate into the lymphatic vessels in a strictly CCR7-dependent manner and also induces their subsequent directional crawling along the lumen of the lymphatic endothelium as mediated by ICAM-1 up-regulation on lymphatic endothelial cells. The new mechanisms of TNFα action on neutrophil-lymphatic interactions are summarised in Fig. 8.

In initial studies aimed at investigating TNFα-induced neutrophil trafficking into extravascular tissues, we noted that tissue infiltrated neutrophils could rapidly migrate into lymphatic vessels. These studies were then extended to a model of antigen sensitisation characterised by the generation of endogenous TNFα. This reaction was also associated with rapid neutrophil migration into lymphatic vessels, a response that was impaired in mice deficient in both TNF receptors p55 and p75. Interestingly, TNFα did not appear to mediate neutrophil extravasation from blood vessels into tissues, indicating a specific role for TNFα in driving neutrophil motility

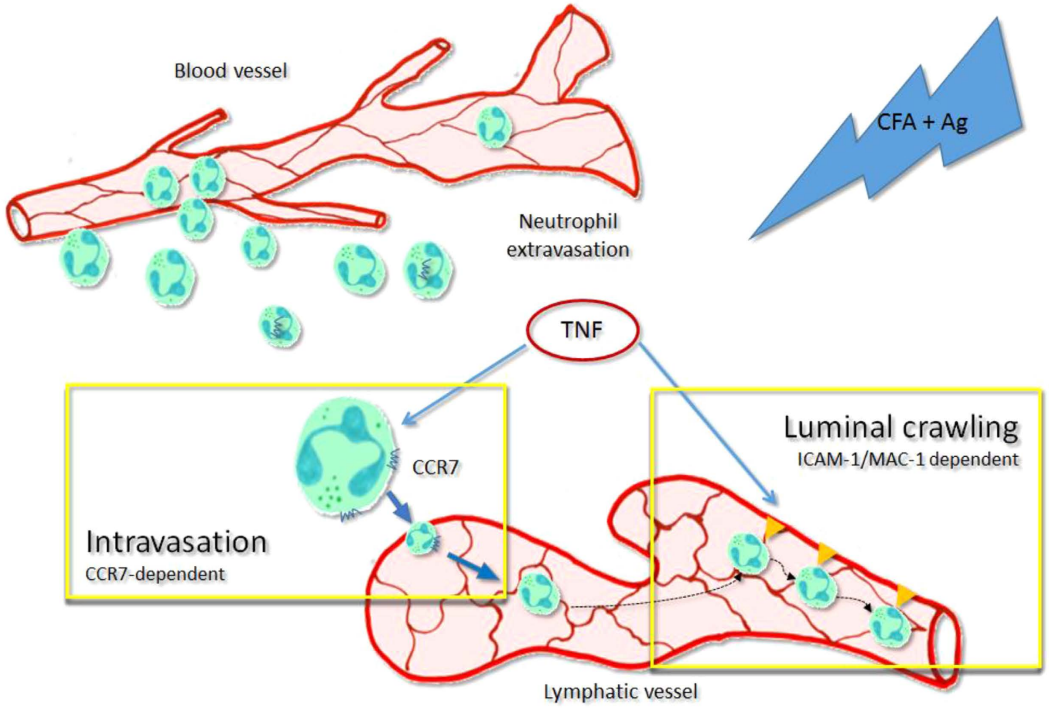

Figure 8. Schematic diagram illustrating the dual mechanisms of action of TNFα leading to the trafficking of neutrophils into and within the lymphatic vasculature upon acute inflammation *in vivo*. During the acute inflammatory response of the tissue following antigen sensitisation, endogenous TNFα release primed the freshly recruited neutrophils. This cytokine allow these leukocytes to be attracted to the lymphatic vessels in a CCR7 dependent manner (intravasation). Furthermore, endogenous TNFα also stimulate the lymphatic endothelium to express ICAM-1 on their surface, allowing the neutrophils present in the lymphatic vessels to adhere and crawl along the luminal side in the correct direction toward the flow of the vessel.

into lymphatic vessels but not through blood vasculature. Furthermore, using chimeric animals we showed that TNFα acts directly of the leukocytes to induce this neutrophil migration response.

In the present study, we clearly demonstrated that the TNFα-driven migration of neutrophils into lymphatic vessels is strictly CCR7-dependent. The role of CCR7 in neutrophil recruitment to the lymphatic system was demonstrated both in a mouse model of intradermal immunisation and in human neutrophils by Beauvillain *et al.*[27]. In accordance with their study, we only detected intracellular stores of CCR7 in murine blood neutrophils, but not on their cell surface. However our results shows that neutrophils recruited into inflamed tissues up-regulated CCR7 on their surface as compared to blood circulating cells. A study by Eruslanov *et al.* have shown similar up-regulation of CCR7 on human neutrophils in a tumour model[36], though the mechanism and physiological consequences of this response in human is still unclear. Our current data suggests priming of neutrophils for enhanced chemokine receptor expression. While GM-CSF and IL-17 have been shown to prime human neutrophils to migrate toward the chemokines CCL21 and CCL19 *in vitro*[27], we did not detect the generation of these cytokines in the inflamed cremaster muscles at any time-point analysed (Supplementary Fig. S9). However, TNFRdbKO tissue-infiltrated neutrophils did not show an increase in CCR7 expression on neutrophils *in vivo*; while low concentrations of TNFα promoted the surface expression of CCR7 on murine blood neutrophils *in vitro*. Altogether these data suggest a predominant role of TNFα in this response and may highlight the importance of the origin of the cells analysed (e.g. bone marrow vs blood, tissue-infiltrated vs naïve cells, murine vs. human leukocytes). Interestingly, we observed that CCR7KO animals exhibited a high basal level of neutrophils within the LNs of naïve animals as compared to WT mice; and inflammation of the cremaster muscles with TNFα or following antigen sensitisation did not increase further the number of neutrophils found in the LNs. This abnormal trafficking of neutrophils into the LNs of these mice could be related to a higher expression of CXCL12 in naïve CCR7KO dLNs as compared to WT dLNs. CXCR4 expression was similar in both genotypes, however, CXCR4 antagonist treatment reduced significantly the number of these leukocytes infiltrating CCR7KO dLNs, while their migration into the afferent lymphatics was not affected (Supplementary Fig. S7). These data support the hypothesis that CXCR4 signalling contributes to neutrophil homing in LN through HEV[28].

Since the role for CCR7 in neutrophils trafficking has been contentious to date, we have also investigated other chemokine/chemokine receptor axes in this phenomenon, such as the CXCL12/CXCR4 axis. This axis was shown recently to be involved in neutrophil trafficking to the lymphatic system in a model of bacterial infection with *S. aureus*[26]. However, our data demonstrate that CXCR4 blockade did not significantly inhibit neutrophil migration into cremaster lymphatic vessels upon CFA+Ag-stimulation (Supplementary Fig. S5). Such differences between their study and ours could be related to the model and inflammatory pathway involved: *S. aureus* infection may

preferentially activates the toll-like receptor 2 (TLR2) pathway *in vivo*[37–40]. Recently, TLR2 was shown to be associated with CXCR4 in lipid rafts of monocytes to induce signalling[41], a response not yet investigated for neutrophils. In contrast, the TLR4 pathway is involved in *M. tuberculosis* infections, *LPS or* CFA stimulation[42]; and TLR4 ligands can induce TNFα release more rapidly than TLR2 agonists *in vitro*[43]. Finally, both TNFα[44] and TLR4 activation[45] have been shown to down-regulate the expression of CXCR4 on neutrophils, rendering them less responsive to CXCL12 stimulation. This supports our observation of a similar down-regulation of CXCR4 expression by neutrophils in our inflammatory model (Supplementary Fig. S5). Furthermore, CXCR4 is highly expressed on a subclass of ageing neutrophils rather than healthy mature cells[46]. Altogether, these observations may indicate that different sub-populations of neutrophils or their pathway of activation might be important for the molecular axis used for their migration into the lymphatic system.

Another study has shown that the potent neutrophil-chemoattractant CXCL8 was up-regulated in TNFα-stimulated human dermal endothelial cells *in vitro*; and promotes neutrophil migration through a monolayer of human LECs[31]. In the mouse system, LECs isolated from mouse skin showed an upregulation of CXCL1 gene upon inflammation[47]. However, our *in vivo* model of TNFα-induced neutrophil trafficking into lymphatic vessels, clearly indicated the predominant role of CCR7 in this phenomenon. Furthermore local treatment with an anti-CXCL1 blocking mAb did not affect the capacity of neutrophils to enter the lymphatic system upon inflammation *in vivo*. These data highlight differences between *in vivo* and *in vitro* models. Indeed, several studies pointed to the importance of the microenvironment for the LECs to retain their specific lymphatic characteristic that are lost in culture such as the capacity to generate CCL21[48,49]. Similarly to a mouse model of contact hypersensitivity[47], we did not observed a change in total CCL21 expression between naïve and inflamed animals (Supplementary Fig. S8). We however noticed that lymphatic vessels exhibited higher expression of CCL21 as compared to the interstitial tissue with the establishment of a gradient that could direct the neutrophils toward the vessels *in vivo*. The formation of a gradient of CCL21 driving the migration of DCs within the LNs has been recently reported in the literature[50].

Having identified TNFα as a key signal for promoting neutrophil trafficking to the lymphatic vessels, the potential involvement of this cytokine in mediating other neutrophil-lymphatic vessel interactions was investigated. TNFα is the prototypical pro-inflammatory cytokine playing a key role in many immune responses such as cell recruitment and leukocyte activation. It is also involved in numerous pathological conditions and autoimmune disorders such as rheumatoid arthritis, lupus, psoriasis and atherosclerosis and there is now considerable evidence for successful use of TNFα blockers for the treatment of certain chronic inflammatory conditions. However, anti- TNFα therapy is associated with a heightened risk of serious infections and poor vaccination responses in patients[51]. Furthermore, the mechanism through which these drugs work is not fully known; though suppressing leukocyte recruitment and activation is considered to be a principle mode of action[52]. In our acute model of cremasteric inflammation however, we neither genetic deficiency for TNFα signalling nor antibody blockade inhibited neutrophil recruitment to the tissue, suggesting different roles for TNFα in acute vs chronic inflammation. During physiological conditions, TNFα can prime blood vascular endothelial cells (BECs) to present both adhesion molecules and chemoattractants in order to induce leukocyte migration. Specifically, TNFα has been shown to up-regulate ICAM-1 expression on BECs both *in vivo* and *in vitro*, an adhesion molecule essential for neutrophil directional crawling during their recruitment through blood vessels[33,34]. Lymphatic endothelial cells (LECs) express very low levels of ICAM-1 in uninflamed condition, but can up-regulate this molecule upon TNFα-stimulation in both humans[53,54] and mice (Fig. 6). The exact role of ICAM-1 in leukocyte migration into the lymphatic system is however controversial: *in vitro* antibody blockade inhibits both adhesion and transmigration responses of DCs through cultured human LECs[53], and *in vivo* ICAM-1 have been reported to mediate crawling of DCs along the lymphatic endothelium[55]. In contrast, DC interstitial migration was not affected in mice exhibiting leukocyte-specific deletion of ICAM-1-ligand integrins[56]. In the present study, we have observed that neutrophils crawl along the luminal surface of the lymphatic endothelium following a local inflammatory stimulus. This response was associated with a formation of a gradient of CCL21 within the vessel (Supplementary Fig. S8e). This gradient could explain why the majority of neutrophils crawl along in the direction of the lymphatic flow. Interestingly, Russo *et al.*, have recently demonstrated that *in vitro*, murine LECs generate a gradient of CCL21 when exposed to low sheer stress and that this gradient was responsible for the directionality of crawling of DCs[57]. In our model, the neutrophil crawling response (as well as ICAM-1 upregulation) was blocked when mice received an injection of an anti-TNFα blocking antibody. Furthermore, local blockade of ICAM-1 or MAC-1 inhibited this crawling response while interstitial migration of the leukocytes and their capacity to enter the lymphatic vessels were unaffected. Overall, the local injection of blocking antibodies inhibiting neutrophil-lymphatic endothelium luminal interactions resulted in a reduction of neutrophil numbers infiltrating the LNs, highlighting potential and effective targets to manipulate the role of neutrophils in adaptive immune responses *in vivo*.

In conclusion, the data presented here provide an insight into the mechanisms underlying neutrophil trafficking into and within lymphatic vessels of inflamed tissues. Specifically, we have unravelled a predominant role for endogenous TNFα in orchestrating both CCR7-dependent migration of neutrophils into afferent lymphatics and ICAM-1-dependent crawling on the luminal surface of lymphatic endothelium during the acute phase of the inflammatory response as induced by antigen sensitisation. Overall, our findings identify TNFα as a new molecular regulator of neutrophil migration into the lymphatic system that may provide the opportunity for the development of improved immunisation protocols but also highlight a new potential mechanism of action - and limitations - for anti- TNFα therapy.

Methods

Reagents. Recombinant murine TNFα purchased from R&D Systems, Complete Freund's Adjuvant from AMSbio, Ovalbumin and AMD3100 from Sigma; and chick Collagen II from MB Biosciences. The following

primary antibodies were used for immunofluorescence labelling for confocal imaging and confocal IVM: rat anti–mouse LYVE-1 mAb (clone ALY7; eBioscience); non-blocking rat anti–mouse PECAM-1 Ab (clone C390, eBioscience); rat anti–mouse ICAM-1 mAb (clone YN1/1.4.7; purified and Alexa 488-conjugated, eBioscience); rat anti–mouse MAC-1 mAb (clone M1/70, BioLegend); monoclonal rat anti–mouse MRP14 mAb (clone 2B10; a gift from N. Hogg, Cancer Research UK, London, UK); rat anti-mouse Ly6G mAb (clone 1A8, Alexa 647-conjugated, Biolegend); rat anti-mouse CXCR4 mAb (clone 2B11, PE-conjugated, eBioscience), rat anti-mouse/human High Endothelial Venule mAb (MECA-79, Alexa 488-conjugated eBioscience), rat anti-mouse CCR7 mAb (clone 4B12, Alexa 488- or biotin-conjugated, eBioscience); rat anti-mouse CD45.2 mAb (clone 104, PE/Cy7-conjugated, Biolegend), rat anti-mouse TNFα mAb (clone MP6-XT22, Biolegend), anti-mouse CCL21, anti-mouse CXCL1 and anti-mouse CXCL12 mAbs (R&D systems), polyclonal goat anti–mouse TNFR p55 and p75 Abs (R&D Systems). The following purified antibodies were used as isotype-matched control Abs: rat IgG1, IgG2a and IgG2b (Biolegend). Unlabelled antibodies were directly conjugated Alexa Fluor dyes using Molecular Probes Alexa Fluor Monoclonal Antibody Labeling kit (Invitrogen) for confocal microscopy analysis.

Animals. Male mice (8–12 weeks) wild-type (WT, Charles Rivers), *CCR7 knockout* (CCR7KO, JAXLab), *LysM-EGFP ki* (LysM-GFP), *LysM-EGFP ki* × *CCR7 ko* (LysM-GFP/CCR7KO) (all on a C57BL/6 background) and *TNFRdb knockout* (TNF receptors p55 and p75 double knockout mice, JAXLab) mice were used for these experiments. Only heterozygote LysM-GFP animals exhibiting fluorescent myeloid cells (neutrophils comprising the highest percentage of GFP high cells) were used for this study with the permission of T. Graf (Albert Einstein College of Medicine, Bronx, NY). These animals were provided by M. Sperandio (Ludwig Maximilians University, Munich, Germany) and bred in-house in individually ventilated cages; and facilities were regularly monitored for health status and infections. Chimeric mice deficient in leukocyte TNFR p55 and p75 or were generated by lethal irradiation of C57BL/6 WT mice (5.5 Gy twice, 4 h apart) and injection of bone marrow cells (1.5×10^6 cells/recipient i.v.) from TNFRdbKO mice. C57BL/6 WT littermates receiving WT bone marrow were used as controls. The phenotype of blood circulating neutrophils in chimeric animals was then assess by flow cytometry (Fig. S4). Similar protocol was used for the generation of chimeric animals exhibiting CCR7KO leukocytes following the injection of donor LysM-GFP/CCR7KO bone marrow cells into lethally irradiated WT recipient animals. Depletion of tissue-resident macrophages of the cremaster muscles was achieved by 3 consecutive i.s. injections of clodronate liposomes (Encapsula NanoSciences LLC; 250 μg/mouse, 20 hrs apart) prior to the induction of inflammation. With this protocol we achieved ~85.9% of depletion as quantified by flow cytometry (data not shown). All experiments were approved by the local biological service unit Ethical Committee at Queen Mary University of London and carried out under the Home Office Project Licenses (70/7884 & 70/8264) according to the guidelines of the United Kingdom Animals Scientific Procedures Act (1986). At the end of all *in vivo* experiments, animals were humanely killed by cervical dislocation in accordance with UK Home Office regulations.

Induction of cremaster inflammation. WT C57BL/6 male mice (8–12 weeks old) were sedated with 30 μl intramuscular (i.m.) injection of ketamine (100 mg/kg) and xylazine (10 mg/kg) in saline before their cremaster muscles were stimulated via intrascrotal (i.s.) injection of TNFα (300 ng/400 μl PBS) or an emulsion of CFA (200 μg/300 μl per mouse) and ovalbumin or chick collagen II (200 μg per mouse). Control mice received 300–400 μl of PBS via i.s. injection. In some experiments, mice were pre-treated locally with the CXCR4 inhibitor AMD3100 or vehicle (10 mg/kg, 250 μl, i.s. 4 hrs post-inflammation) prior to the visualisation of the inflammatory response. Several time points following TNFα/CFA+Ag stimulation were investigated over the course of 48 hrs.

Confocal Microscopy. *Intravital confocal microscopy*. LysM-GFP mice were stimulated with i.s. injection of either TNFα or CFA+Ag and the inflammatory response was allowed to develop for 4 (TNFα) to 6 hrs (CFA+Ag) before visualisation of the response by intravital confocal microscopy. In some experiments, CFA+Ag-stimulated animals were pre-treated with a local (i.s.) injection of the following blocking antibodies 90 to 120 min before surgery: anti- TNFα or rat IgG1κ isotype control mAbs (50 μg/mouse), anti-ICAM-1/anti-MAC-1 mAbs or rat IgG2b isotype control mAbs (10 μg/mouse) along with non-blocking dose of an anti-LYVE-1 mAb (2 μg/mouse, Alexa555 conjugated) and/or a non-blocking anti-PECAM-1 mAb (2 μg/mouse, Alexa647 conjugated) to label the lymphatic and blood vasculatures, respectively. Thirty minutes before surgery, mice were sedated with i.p. injection of ketamine (100 mg/kg) and xylazine (10 mg/kg). Following surgery, cremaster muscles were imaged with a Leica SP5 or SP8 confocal microscope[58] for another 90 min with a superfusion of warm Tyrode's solution. Images were acquired every minute with the use of a 20 × water-dipping objective (NA:1.0) with sequential scanning of different channels at a resolution of 1024 × 700 pixels in the x × y plane and 0.7 μm steps in z-direction. 4D confocal image sequences were then analysed offline using IMARIS software (Bitplane, Switzerland), enabling the dynamic interaction of neutrophils with lymphatic vessels be observed, tracked, and quantified as previously described[34].

Confocal microscopy on fixed tissue. Following immunostaining, the cremaster muscles were imaged with a Leica SP8 confocal microscope with the use of a 20 × water-dipping objective (NA:1.0). Images of post-capillary venules and lymphatic vessels (at least 6 vessels per tissue) were attained with the use of sequential scanning of different channels at every 0.52 μm of tissue depth at a resolution of 1024 × 470 and 1024 × 800 pixels in the x × y plane, respectively. This resolution of pixels correspond to a voxel size of 0.24 × 0.24 × 0.5 μm in x × y × z. Post-capillary venules and lymphatic vessels were imaged at a zoom factor of × 1.9 and × 1.2, respectively. Quantification of neutrophil transmigration and intravasation into lymphatic vessels were analysed with the 3D-reconstructing image processing software IMARIS. Transmigrated neutrophils were defined as the number of neutrophils present in the extravascular tissue across a 300 μm blood vessel segment and within 50 μm

from each side of the venule of interest. Data was expressed as the number of neutrophils per volume of tissue. Intravasated neutrophils were defined as the number of neutrophils present inside the lymphatic vessels and data were expressed as the number of neutrophils per given volume of lymphatic vessel quantified by IMARIS Software by creating an isosurface representing exclusively the LYVE-1 positive lymphatic endothelium. To assess ICAM-1 and CCL21 expression on lymphatic vessels, specific primary antibodies or control isotype-matched antibodies were injected i.s. 1 hr prior to the exteriorisation of the cremaster muscles; and following the analysis of tissues by confocal microscopy, the mean fluorescence intensity (MFI) of the staining for molecule of interest was determined using IMARIS software on the LYVE-1 isofurface as determined by IMARIS software. Intensity profiles for CCL21 expression along a certain distance (10 μm away from or 100 μm within the lymphatic vessel) was performed using Image J. For the LNs, halved samples were imaged with a Leica SP8 confocal microscope with the use of a 10 × water-dipping objective (NA:0.3). Images (12 images per pair of LNs per mouse) were obtained with the use of sequential scanning of different channels at every 5.8 μm of tissue depth at a resolution of 1024 × 1024 pixels in the x × y plane, corresponding to a voxel size of 0.91 × 0.91 × 5.8 μm in x × y × z. Quantification of neutrophil recruitment into the inguinal LNs were analysed with the 3D-reconstructing image processing software IMARIS. Recruited neutrophils were defined as the number of neutrophils per volume of tissue, excluding (unless specified) the blood circulating neutrophils present in HEVs.

Flow cytometry. Whole blood and single cell suspension from (collagenase + DNAse)-digested cremaster muscles and LNs of CFA+Ag-stimulated WT and CCR7KO animals, were fluorescently labelled with conjugated antibodies against CD45.2, Ly6G, CD11c, CD3ε, CCR7, CXCR4, TNFRp55, TNFRp75 or the appropriate isotype control antibodies (0.2–2 μg/ml, various fluorochromes) and DAPI (for viability) for at least 1 hr at 4 °C. Viable leukocytes were identified by FSC and SSC characteristics and CD45.2 positive and DAPI negative staining. Neutrophils were identified based on Ly6G high staining. In some experiments, blood leukocytes where incubated at 37 C in RPMI medium (supplemented with 10% FCS and 2 mM of L-Glutamin) with various concentration of TNFα (1, 10 or 100 ng/ml) for 4 hrs in the presence of 50 μM of Nystatin (Sigma, an endocytosis inhibitor) prior to immunofluorescence staining. Samples were analysed using a BD LSR-Fortessa (BD Biosciences) and FlowJo analysis software (Treestar). In some studies the intracellular expression of CCR7 was performed using the Cytofix/Cytoperm kit (BD) according to the manufacturer's recommendations.

ELISA. Snap frozen cremaster tissues from WT mice stimulated with CFA+Ag were transferred into screw-top tubes containing homogenising beads along with 500 μl homogenising buffer (1% Triton™ X-100, 1% protease inhibitor, PBS) prior to being placed in a high-throughput tissue homogeniser, Precellys® 24 (Precellys, Derbyshire, UK), for 3 cycles of 20 s homogenisation at 6500 r.p.m with 40 s rest between each cycle. Homogenised samples were then frozen at −80 °C for 1 h before being thawed and centrifuged for 5 min at 10,000 g using a tabletop centrifuge. The supernatant was taken and used to quantify the release of TNFα, GM-CSF, IL-17, CCL21, CCL19 and CXCL12 by ELISA (eBioscience, Hatfield, UK or R&D Systems, UK) according to the manufacturer's protocol.

Statistical analysis. Data are presented as mean ± S.E.M per mouse. Significant differences between multiple groups were identified by one-way analysis of variance (ANOVA), followed by Newman-Keuls Multiple Comparison Test or a two-way analysis of variance (ANOVA) followed by Holm-Sidak Multiple Comparison Test when at least 2 different independent variables are being compared. Whenever two groups were compared Student's t test was used. P-values < 0.05 were considered significant.

References

1. Nemeth, T. & Mocsai, A. Feedback Amplification of Neutrophil Function. *Trends Immunol* **37,** 412–424, doi: 10.1016/j.it.2016.04.002 (2016).
2. Mayadas, T. N., Cullere, X. & Lowell, C. A. The multifaceted functions of neutrophils. *Annu Rev Pathol* **9,** 181–218, doi: 10.1146/annurev-pathol-020712-164023 (2014).
3. Kolaczkowska, E. & Kubes, P. Neutrophil recruitment and function in health and inflammation. *Nat Rev Immunol* **13,** 159–175, doi: 10.1038/nri3399 (2013).
4. Pillay, J. *et al. In vivo* labeling with 2H2O reveals a human neutrophil lifespan of 5.4 days. *Blood* **116,** 625–627, doi: 10.1182/blood-2010-01-259028 (2010).
5. Kobayashi, S. D., Voyich, J. M., Whitney, A. R. & DeLeo, F. R. Spontaneous neutrophil apoptosis and regulation of cell survival by granulocyte macrophage-colony stimulating factor. *J Leukoc Biol* **78,** 1408–1418, doi: 10.1189/jlb.0605289 (2005).
6. Coxon, A., Tang, T. & Mayadas, T. N. Cytokine-activated endothelial cells delay neutrophil apoptosis *in vitro* and *in vivo*. A role for granulocyte/macrophage colony-stimulating factor. *J Exp Med* **190,** 923–934 (1999).
7. Hachiya, O. *et al.* Inhibition by bacterial lipopolysaccharide of spontaneous and TNF-alpha-induced human neutrophil apoptosis *in vitro*. *Microbiol Immunol* **39,** 715–723 (1995).
8. Walmsley, S. R. *et al.* Hypoxia-induced neutrophil survival is mediated by HIF-1alpha-dependent NF-kappaB activity. *J Exp Med* **201,** 105–115, doi: 10.1084/jem.20040624 (2005).
9. Seely, A. J., Swartz, D. E., Giannias, B. & Christou, N. V. Reduction in neutrophil cell surface expression of tumor necrosis factor receptors but not Fas after transmigration: implications for the regulation of neutrophil apoptosis. *Arch Surg* **133,** 1305–1310 (1998).
10. McGettrick, H. M. *et al.* Chemokine- and adhesion-dependent survival of neutrophils after transmigration through cytokine-stimulated endothelium. *J Leukoc Biol* **79,** 779–788, doi: 10.1189/jlb.0605350 (2006).
11. Haslett, C. Resolution of acute inflammation and the role of apoptosis in the tissue fate of granulocytes. *Clin Sci* (*Lond*) **83,** 639–648 (1992).
12. Cox, G., Crossley, J. & Xing, Z. Macrophage engulfment of apoptotic neutrophils contributes to the resolution of acute pulmonary inflammation *in vivo*. *Am J Respir Cell Mol Biol* **12,** 232–237, doi: 10.1165/ajrcmb.12.2.7865221 (1995).
13. Smith, J. B., McIntosh, G. H. & Morris, B. The traffic of cells through tissues: a study of peripheral lymph in sheep. *J Anat* **107,** 87–100 (1970).
14. Mocsai, A. Diverse novel functions of neutrophils in immunity, inflammation, and beyond. *J Exp Med* **210,** 1283–1299, doi: 10.1084/jem.20122220 (2013).

15. Abadie, V. *et al.* Neutrophils rapidly migrate via lymphatics after Mycobacterium bovis BCG intradermal vaccination and shuttle live bacilli to the draining lymph nodes. *Blood* **106,** 1843–1850, doi: 10.1182/blood-2005-03-1281 (2005).
16. Maletto, B. A. *et al.* Presence of neutrophil-bearing antigen in lymphoid organs of immune mice. *Blood* **108,** 3094–3102, doi: 10.1182/blood-2006-04-016659 (2006).
17. Yang, C. W., Strong, B. S., Miller, M. J. & Unanue, E. R. Neutrophils influence the level of antigen presentation during the immune response to protein antigens in adjuvants. *J Immunol* **185,** 2927–2934, doi: 10.4049/jimmunol.1001289 (2010).
18. Abi Abdallah, D. S., Egan, C. E., Butcher, B. A. & Denkers, E. Y. Mouse neutrophils are professional antigen-presenting cells programmed to instruct Th1 and Th17 T-cell differentiation. *Int Immunol* **23,** 317–326, doi: 10.1093/intimm/dxr007 (2011).
19. Beauvillain, C. *et al.* Neutrophils efficiently cross-prime naive T cells *in vivo*. *Blood* **110,** 2965–2973, doi: 10.1182/blood-2006-12-063826 (2007).
20. Iking-Konert, C. *et al.* Transdifferentiation of polymorphonuclear neutrophils to dendritic-like cells at the site of inflammation in rheumatoid arthritis: evidence for activation by T cells. *Ann Rheum Dis* **64,** 1436–1442, doi: 10.1136/ard.2004.034132 (2005).
21. Iking-Konert, C. *et al.* Up-regulation of the dendritic cell marker CD83 on polymorphonuclear neutrophils (PMN): divergent expression in acute bacterial infections and chronic inflammatory disease. *Clin Exp Immunol* **130,** 501–508 (2002).
22. Cerutti, A., Puga, I. & Magri, G. The B cell helper side of neutrophils. *J Leukoc Biol* **94,** 677–682, doi: 10.1189/jlb.1112596 (2013).
23. Bennouna, S., Bliss, S. K., Curiel, T. J. & Denkers, E. Y. Cross-talk in the innate immune system: neutrophils instruct recruitment and activation of dendritic cells during microbial infection. *J Immunol* **171,** 6052–6058 (2003).
24. Chtanova, T. *et al.* Dynamics of T cell, antigen-presenting cell, and pathogen interactions during recall responses in the lymph node. *Immunity* **31,** 342–355, doi: 10.1016/j.immuni.2009.06.023 (2009).
25. Calabro, S. *et al.* Vaccine adjuvants alum and MF59 induce rapid recruitment of neutrophils and monocytes that participate in antigen transport to draining lymph nodes. *Vaccine* **29,** 1812–1823, doi: 10.1016/j.vaccine.2010.12.090 (2011).
26. Hampton, H. R., Bailey, J., Tomura, M., Brink, R. & Chtanova, T. Microbe-dependent lymphatic migration of neutrophils modulates lymphocyte proliferation in lymph nodes. *Nat Commun* **6,** 7139, doi: 10.1038/ncomms8139 (2015).
27. Beauvillain, C. *et al.* CCR7 is involved in the migration of neutrophils to lymph nodes. *Blood* **117,** 1196–1204, doi: 10.1182/blood-2009-11-254490 (2011).
28. Gorlino, C. V. *et al.* Neutrophils exhibit differential requirements for homing molecules in their lymphatic and blood trafficking into draining lymph nodes. *J Immunol* **193,** 1966–1974, doi: 10.4049/jimmunol.1301791 (2014).
29. Baluk, P. *et al.* Functionally specialized junctions between endothelial cells of lymphatic vessels. *J Exp Med* **204,** 2349–2362, doi: 10.1084/jem.20062596 (2007).
30. Dejana, E., Orsenigo, F., Molendini, C., Baluk, P. & McDonald, D. M. Organization and signaling of endothelial cell-to-cell junctions in various regions of the blood and lymphatic vascular trees. *Cell Tissue Res* **335,** 17–25, doi: 10.1007/s00441-008-0694-5 (2009).
31. Rigby, D. A., Ferguson, D. J., Johnson, L. A. & Jackson, D. G. Neutrophils rapidly transit inflamed lymphatic vessel endothelium via integrin-dependent proteolysis and lipoxin-induced junctional retraction. *J Leukoc Biol* **98,** 897–912, doi: 10.1189/jlb.1HI0415-149R (2015).
32. Johnson, L. A. & Jackson, D. G. Cell traffic and the lymphatic endothelium. *Ann N Y Acad Sci* **1131,** 119–133, doi: 10.1196/annals.1413.011 (2008).
33. Phillipson, M. *et al.* Intraluminal crawling of neutrophils to emigration sites: a molecularly distinct process from adhesion in the recruitment cascade. *J Exp Med* **203,** 2569–2575, doi: 10.1084/jem.20060925 (2006).
34. Proebstl, D. *et al.* Pericytes support neutrophil subendothelial cell crawling and breaching of venular walls *in vivo*. *J Exp Med* **209,** 1219–1234, doi: 10.1084/jem.20111622 (2012).
35. de Veer, M. *et al.* Cell recruitment and antigen trafficking in afferent lymph after injection of antigen and poly(I:C) containing liposomes, in aqueous or oil-based formulations. *Vaccine* **31,** 1012–1018, doi: 10.1016/j.vaccine.2012.12.049 (2013).
36. Eruslanov, E. B. *et al.* Tumor-associated neutrophils stimulate T cell responses in early-stage human lung cancer. *J Clin Invest* **124,** 5466–5480, doi: 10.1172/JCI77053 (2014).
37. Kielian, T., Esen, N. & Bearden, E. D. Toll-like receptor 2 (TLR2) is pivotal for recognition of S. aureus peptidoglycan but not intact bacteria by microglia. *Glia* **49,** 567–576, doi: 10.1002/glia.20144 (2005).
38. Stenzel, W. *et al.* Both TLR2 and TLR4 are required for the effective immune response in Staphylococcus aureus-induced experimental murine brain abscess. *Am J Pathol* **172,** 132–145, doi: 10.2353/ajpath.2008.070567 (2008).
39. Yimin *et al.* Contribution of toll-like receptor 2 to the innate response against Staphylococcus aureus infection in mice. *PLoS One* **8,** e74287, doi: 10.1371/journal.pone.0074287 (2013).
40. Fournier, B. & Philpott, D. J. Recognition of Staphylococcus aureus by the innate immune system. *Clin Microbiol Rev* **18,** 521–540, doi: 10.1128/CMR.18.3.521-540.2005 (2005).
41. Hajishengallis, G., Wang, M., Liang, S., Triantafilou, M. & Triantafilou, K. Pathogen induction of CXCR4/TLR2 cross-talk impairs host defense function. *Proc Natl Acad Sci USA* **105,** 13532–13537, doi: 10.1073/pnas.0803852105 (2008).
42. Kleinnijenhuis, J., Oosting, M., Joosten, L. A., Netea, M. G. & Van Crevel, R. Innate immune recognition of Mycobacterium tuberculosis. *Clin Dev Immunol* **2011,** 405310, doi: 10.1155/2011/405310 (2011).
43. Cui, W., Morrison, D. C. & Silverstein, R. Differential tumor necrosis factor alpha expression and release from peritoneal mouse macrophages *in vitro* in response to proliferating gram-positive versus gram-negative bacteria. *Infect Immun* **68,** 4422–4429 (2000).
44. Bruhl, H. *et al.* Post-translational and cell type-specific regulation of CXCR4 expression by cytokines. *Eur J Immunol* **33,** 3028–3037, doi: 10.1002/eji.200324163 (2003).
45. Kim, H. K., Kim, J. E., Chung, J., Han, K. S. & Cho, H. I. Surface expression of neutrophil CXCR4 is down-modulated by bacterial endotoxin. *Int J Hematol* **85,** 390–396, doi: 10.1532/IJH97.A30613 (2007).
46. Martin, C. *et al.* Chemokines acting via CXCR2 and CXCR4 control the release of neutrophils from the bone marrow and their return following senescence. *Immunity* **19,** 583–593 (2003).
47. Vigl, B. *et al.* Tissue inflammation modulates gene expression of lymphatic endothelial cells and dendritic cell migration in a stimulus-dependent manner. *Blood* **118,** 205–215, doi: 10.1182/blood-2010-12-326447 (2011).
48. Amatschek, S. *et al.* Blood and lymphatic endothelial cell-specific differentiation programs are stringently controlled by the tissue environment. *Blood* **109,** 4777–4785, doi: 10.1182/blood-2006-10-053280 (2007).
49. Wick, N. *et al.* Transcriptomal comparison of human dermal lymphatic endothelial cells *ex vivo* and *in vitro*. *Physiol Genomics* **28,** 179–192, doi: 10.1152/physiolgenomics.00037.2006 (2007).
50. Ulvmar, M. H. *et al.* The atypical chemokine receptor CCRL1 shapes functional CCL21 gradients in lymph nodes. *Nat Immunol* **15,** 623–630, doi: 10.1038/ni.2889 (2014).
51. Murdaca, G. *et al.* Infection risk associated with anti-TNF-alpha agents: a review. *Expert Opinion on Drug Safety* **14,** 571–582, doi: 10.1517/14740338.2015.1009036 (2015).
52. Taylor, P. C. *et al.* Reduction of chemokine levels and leukocyte traffic to joints by tumor necrosis factor alpha blockade in patients with rheumatoid arthritis. *Arthritis Rheum* **43,** 38–47, doi: 10.1002/1529-0131(200001)43:1<38::AID-ANR6>3.0.CO;2-L (2000).
53. Johnson, L. A. *et al.* An inflammation-induced mechanism for leukocyte transmigration across lymphatic vessel endothelium. *J Exp Med* **203,** 2763–2777, doi: 10.1084/jem.20051759 (2006).
54. Sawa, Y. *et al.* Effects of TNF-alpha on leukocyte adhesion molecule expressions in cultured human lymphatic endothelium. *J Histochem Cytochem* **55,** 721–733, doi: 10.1369/jhc.6A7171.2007 (2007).

55. Nitschke, M. *et al.* Differential requirement for ROCK in dendritic cell migration within lymphatic capillaries in steady-state and inflammation. *Blood* **120,** 2249–2258, doi: 10.1182/blood-2012-03-417923 (2012).
56. Pflicke, H. & Sixt, M. Preformed portals facilitate dendritic cell entry into afferent lymphatic vessels. *J Exp Med* **206,** 2925–2935, doi: 10.1084/jem.20091739 (2009).
57. Russo, E. *et al.* Intralymphatic CCL21 Promotes Tissue Egress of Dendritic Cells through Afferent Lymphatic Vessels. *Cell Rep* **14,** 1723–1734, doi: 10.1016/j.celrep.2016.01.048 (2016).
58. Woodfin, A. *et al.* The junctional adhesion molecule JAM-C regulates polarized transendothelial migration of neutrophils *in vivo*. *Nat Immunol* **12,** 761–769, doi: 10.1038/ni.2062 (2011).

Acknowledgements

This work was supported by funds from Arthritis Research UK (19913 to M.-B.V.) and the Wellcome Trust (098291/Z/12/Z to S.N.). S. A. was supported by a QMUL Principal's Award PhD Studentship. We thank Prof N. Hogg for the gift of the anti-MRP14 mAb and Prof T. Williams and Dr T. Nightingale for their critical reading of the manuscript.

Author Contributions

S.A. performed most experiments, analysed data, and contributed to the writing of the manuscript. C.Z. performed and analysed some of the time-course and confocal microscopy experiments. J.D. assisted with flow cytometry acquisition and analysis. W.W. secured funding for S.A. and contributed to the supervision of the project. S.N. provided valuable tools, secured funding for S.A. and contributed to the supervision of the project and writing of the manuscript. M.-B.V. provided the overall project supervision by designing and performing experiments, analysing the data, and writing the manuscript.

Additional Information

Supplementary information accompanies this paper at http://www.nature.com/srep

Competing Interests: The authors declare no competing financial interests.

How to cite this article: Arokiasamy, S. *et al.* Endogenous TNFα orchestrates the trafficking of neutrophils into and within lymphatic vessels during acute inflammation. *Sci. Rep.* **7**, 44189; doi: 10.1038/srep44189 (2017).

Publisher's note: Springer Nature remains neutral with regard to jurisdictional claims in published maps and institutional affiliations.

SUPPLEMENTARY INFORMATION

Endogenous TNFα orchestrates the trafficking of neutrophils into and within lymphatic vessels during acute inflammation

Samantha Arokiasamy [1,2], Christian Zakian [1], Jessica Dilliway [1], Wen Wang [2#], Sussan Nourshargh [1#] & Mathieu-Benoit Voisin [1*].

VIDEO LEGENDS

Video 1

Neutrophil breaching of the lymphatic endothelium in a TNF-stimulated tissue (**Figure 1e**). The video shows a cremaster lymphatic vessel of a LysM-GFP mouse (exhibiting GFP-labelled leukocytes (green), immunostained *in vivo* for ECs with Alexa647-labelled anti-PECAM-1 mAb (blue) and stimulated with TNF (300ng/mouse i.s.). The video shows the migration of a neutrophil (recorded from 4hrs after injection of the cytokine) into the lumen of the lymphatic vessel. Images were captured every minute for 90min. Still images are shown in **Fig. 1e**.

Video 2

Neutrophil breaching of the lymphatic endothelium in a TNF-stimulated (300ng/mouse i.s.) cremaster lymphatic vessel of a LysM-GFP mouse (exhibiting GFP-labelled leukocytes (green), and immunostained *in vivo* for LECs with non-blocking dose of an Alexa555-labelled anti-LYVE-1 mAb (red). The video shows the migration of a neutrophil (in green and isolated from the rest of the inflammatory response by creating an isosurface on it using IMARIS software for clarity of the image) into the lumen of the lymphatic vessel (recorded from 2hrs after injection of the cytokine). Images were captured every minute for 90min.

Video 3

Intraluminal neutrophil crawling along the lumen of the lymphatic endothelium (**Figure 1f**). The video captures the intraluminal crawling of neutrophils (in green) along the lymphatic endothelial cell wall in a TNF-stimulated cremaster of a LysM-GFP mouse (exhibiting GFP-labelled leukocytes (green). Lymphatic vessels were immunostained *in vivo* with Alexa555-labelled anti–LYVE-1 mAb (red) and Alexa647-labelled anti-PECAM-1 mAb (blue). Images were captured from 4hrs post-inflammation at one stack per minute for a duration of 90 min. Still images of this video are shown in **Fig. 1f**.

Video 4

Intraluminal neutrophil crawling with isotype control (IgG1, κ) mAb (**Figure 5a**). The video captures the intraluminal crawling of several neutrophils (in green and isolated from the rest of the inflammatory response by creating an isosurface on them using IMARIS software for clarity of the image) along the lymphatic endothelial cell wall in a CFA+Ag-stimulated cremaster of a LysM-GFP mouse (exhibiting

GFP-labelled leukocytes (green) immunostained *in vivo* with Alexa555–labelled anti–LYVE-1 mAb (red) and Alexa647-labelled anti-PECAM-1 mAb (blue), in the presence of an IgG1, κ isotype control (50μg/mouse). The IgG1, κ isotype control mAb was injected i.s. 4hrs post inflammation before exteriorisation of the cremaster muscles to perform intravital confocal microscopy 2hrs later. At the end of the sequence, the track followed by the neutrophils during their crawling on the luminal side of the lymphatic endothelium is shown, alongside the displacement (arrow). Images were captured at one stack per minute for a duration of 90min. A still image of this is shown in **Fig. 5a**.

Video 5

Intraluminal neutrophil crawling with anti-TNF blocking mAb (**Figure 5a**). The video captures the intraluminal crawling of several neutrophils (in green and isolated from the rest of the inflammatory response by creating an isosurface on them using IMARIS software for clarity of the image) along the lymphatic endothelial cell wall in a CFA+Ag-stimulated cremaster of a LysM-GFP mouse (exhibiting GFP-labelled leukocytes (green) and immunostained *in vivo* with Alexa555–labelled anti–LYVE-1 mAb (red) and Alexa647-labelled anti-PECAM-1 mAb (blue), in the presence of an anti-TNF blocking Ab (50μg/mouse). The anti-TNF blocking Ab was injected i.s. 4hrs post-inflammation before exteriorisation of the cremaster muscles to perform intravital confocal microscopy 2hrs later. At the end of the sequence, the track followed by the neutrophils during their crawling on the luminal side of the lymphatic endothelium is shown, alongside the displacement (arrow). Images were captured at one stack per minute for a duration of 90min. A still image of this is shown in **Fig. 5a**.

Video 6

Intraluminal neutrophil crawling with isotype control (IgG2b, κ) mAb (**Figure 7a**). The video captures the intraluminal crawling of several neutrophils (in green and isolated from the rest of the inflammatory response by creating an isosurface on them using IMARIS software for clarity of the image) along the lymphatic endothelial cell wall in a CFA+Ag-stimulated cremaster of a LysM-GFP mouse (exhibiting GFP-labelled leukocytes (green) immunostained *in vivo* with Alexa555–labelled anti–LYVE-1 mAb (red) and Alexa647-labelled anti-PECAM-1 mAb (blue), in the presence of an IgG2b, κ isotype control (10μg/mouse). Antibodies were injected i.s. 90min before exteriorisation of the cremaster muscles and visualisation by intravital confocal microscopy from 6hrs post inflammation. At the end of the sequence, the track followed by the neutrophils during their crawling on the luminal side of the lymphatic endothelium is shown, alongside the displacement (arrow). Images were captured at one stack per minute for a duration of 90min. A still image of this is shown in **Fig. 7a**.

Video 7

Intraluminal neutrophil crawling with anti-ICAM-1 blocking mAb (**Figure 7a**). The video captures the intraluminal crawling of several neutrophils (in green and isolated from the rest of the inflammatory response by creating an isosurface on them using IMARIS software for clarity of the image) along the lymphatic endothelial cell wall in a CFA+Ag-stimulated cremaster of a LysM-GFP mouse (exhibiting GFP-labelled leukocytes (green) immunostained *in vivo* with Alexa555–labelled anti–LYVE-1 mAb (red) and Alexa647-labelled anti-PECAM-1 mAb (blue), in the presence of an anti-ICAM-1 blocking mAb (10μg/mouse). Antibodies were injected i.s. 90min before exteriorisation of the cremaster muscles and visualisation by intravital confocal microscopy. At the end of the sequence, the track followed by the neutrophils during their crawling on the luminal side of the lymphatic endothelium is shown, alongside the displacement (arrow). Images were captured at one stack per minute for a duration of 90min. A still image of this is shown in **Fig. 7a**.

Video 8

Intraluminal neutrophil crawling with anti-MAC-1 blocking mAb (**Figure 7a**). The video captures the intraluminal crawling of several neutrophils (in green and isolated from the rest of the inflammatory response by creating an isosurface on them using IMARIS software for clarity of the image) along the lymphatic endothelial cell wall in a CFA+Ag-stimulated cremaster of a LysM-GFP mouse (exhibiting GFP-labelled leukocytes (green) immunostained *in vivo* with Alexa555–labelled anti–LYVE-1 mAb (red) and Alexa647-labelled anti-PECAM-1 mAb (blue), in the presence of an anti-MAC-1 blocking mAb (10μg/mouse). Antibodies were injected i.s. 90min before exteriorisation of the cremaster muscles and visualisation by intravital confocal microscopy. At the end of the sequence, the track followed by the neutrophils during their crawling on the luminal side of the lymphatic endothelium is shown, alongside the displacement (arrow). Images were captured at one stack per minute for a duration of 90min. A still image of this is shown in **Fig. 7a**.

SUPPLEMENTARY FIGURES

Figure S1

a

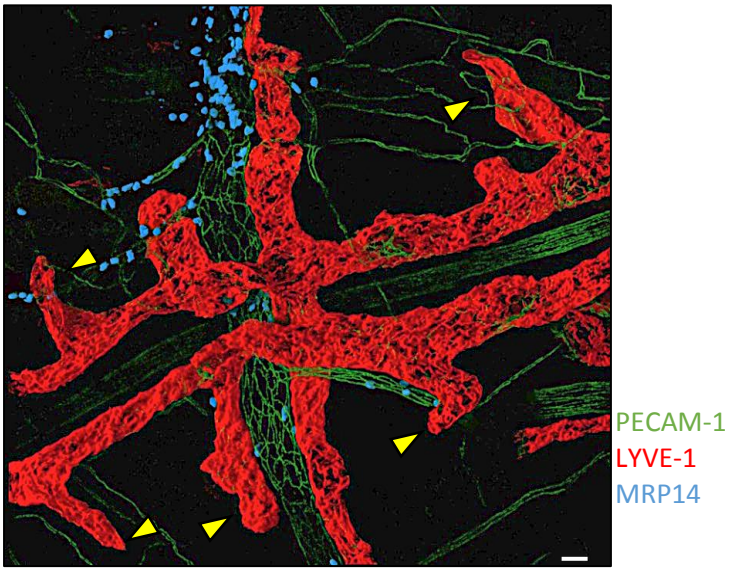

b

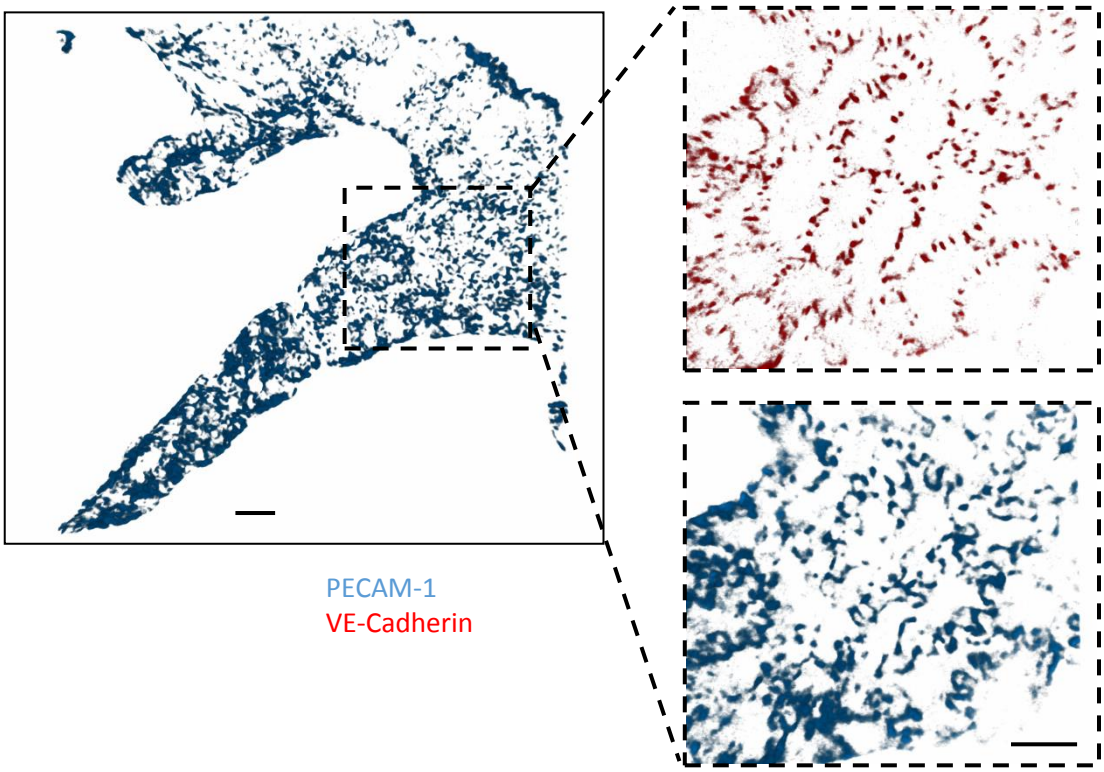

Figure S1: Lymphatic architecture of the cremasteric tissue

(**a**) Representative 3D-reconstructed confocal image of a whole-mount fixed cremaster muscle of a C57BL/6 WT animal and immunostained with antibodies against LYVE-1 (Alexa555-conjugated, red), PECAM-1 (Alexa488-conjugated, green) and MRP14 (Alexa647-conjugated, blue) to visualise the lymphatic vessels, the endothelial cell junctions and neutrophils, respectively, showing the presence of a fully developed lymphatic vasculature in this tissue with blind-ended lymphatic capillary vessels (arrow). (**b**) Representative confocal image of a fixed cremasteric lymphatic vessel immunostained for VE-Cadherin (Alexa555-conjugated, red) and PECAM-1 (Alexa647-conjugated, blue). The inserts on the right area show a magnified view of the heterogeneous distribution of the adhesion molecules (with VE-cadherin-rich buttons and PECAM-1-rich flaps) expressed by the endothelial cells of the cremasteric lymphatic vessels and exhibiting an oak-leaf shape morphology. Bar=20 µm.

Figure S2

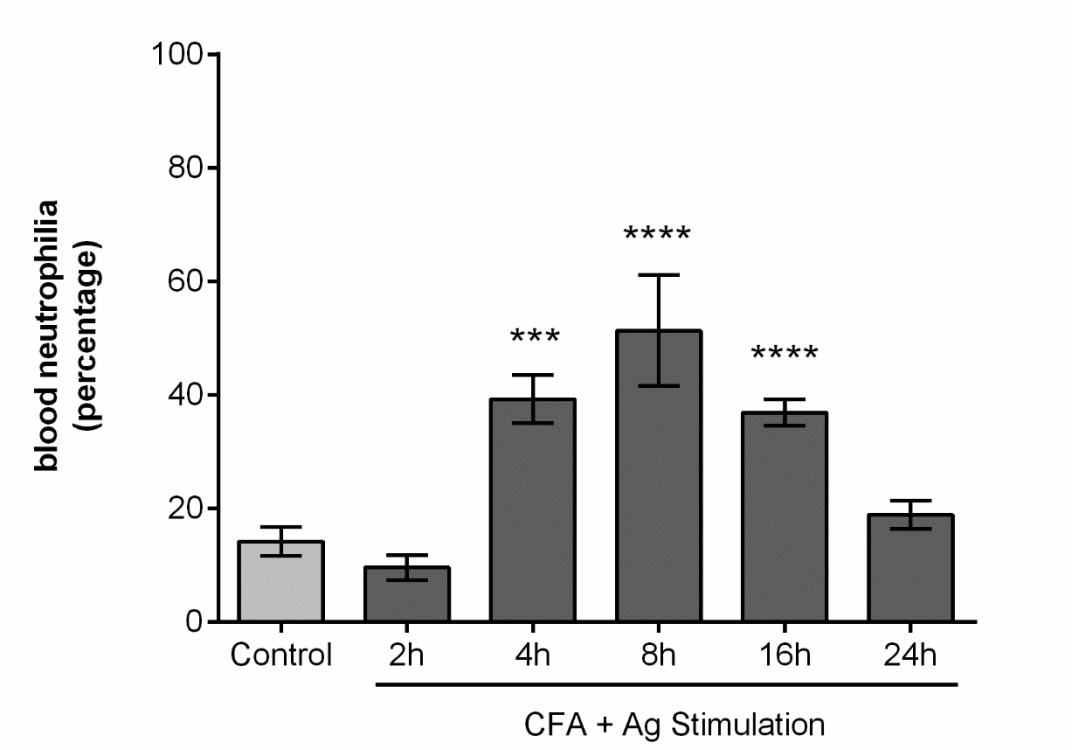

Figure S2: Blood neutrophilia following stimulation of the cremaster muscles with CFA+Ag.

Percentage of neutrophils with the blood circulation of WT mice subjected to cremaster muscle inflammation with CFA+Ag as analysed by flow cytometry. Data are expressed as mean±SEM from 4 independent experiments. Statistically significant differences between the stimulated and control groups are indicated by asterisks: ***, $P < 0.001$; ****, $P < 0.0001$.

Figure S3

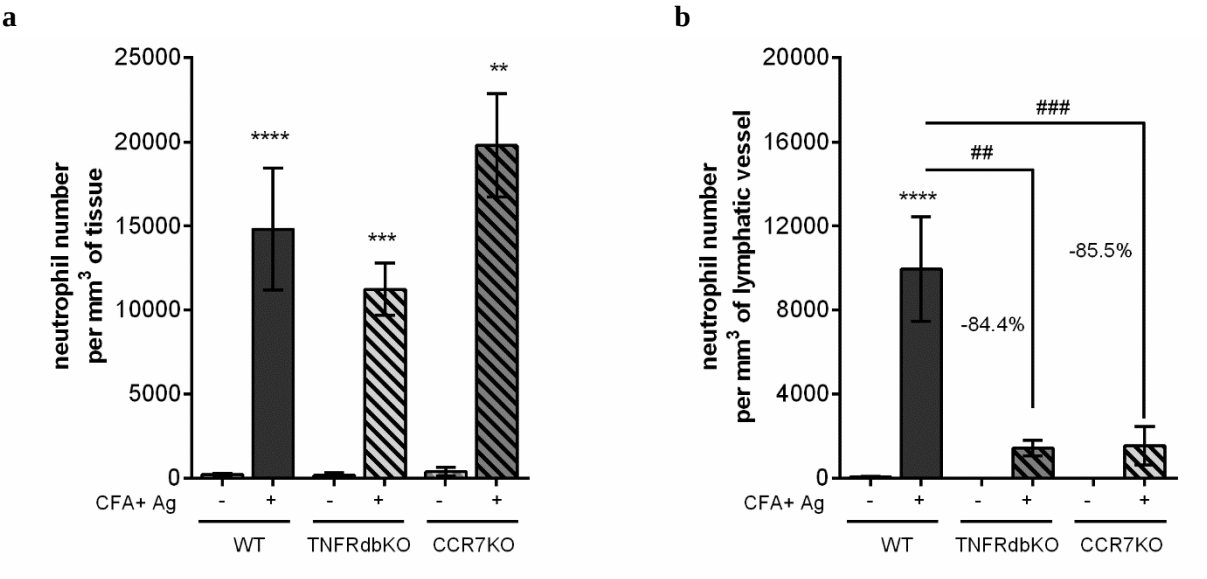

Figure S3: neutrophil migration response in the cremaster muscle following stimulation with CFA+Ag for 8hrs in WT, TNRdbKO and CCR7KO mice

WT, TNFRdbKO and CCR7KO mice were subjected to CFA+Ag-induced inflammation of the cremaster muscles. Controlled mice were injected with PBS. Eight hours later, the cremaster muscles were dissected away, fixed and immunostained for LYVE-1, PECAM-1 and MRP14 to visualise the lymphatic vasculatures the endothelial cells junctions and neutrophils, respectively before analysis of the neutrophil migration responses by confocal microscopy. (**a**) Number of extravasated neutrophils in the cremaster muscles. (**b**) Number of neutrophils within the cremaster lymphatic vessels. Data are expressed as mean±SEM from n = at least 4 animals per group. Statistically significant difference between stimulated and unstimulated animals are indicated by asterisks: **, P< 0.01; ***, P < 0.001; ****, P < 0.0001. Statistically significant difference between WT and KO animals are indicated by dashes: ##, P < 0.01; ###, P < 0.001.

Figure S4

a (p75)

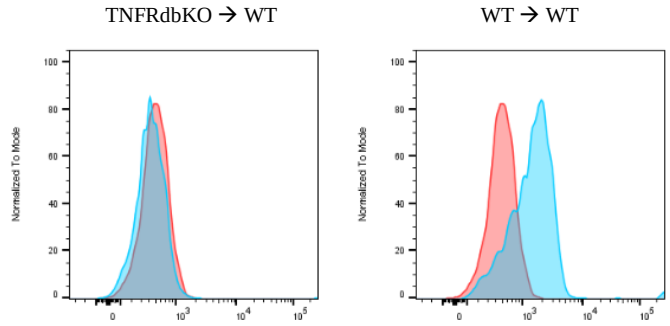

b (p55)

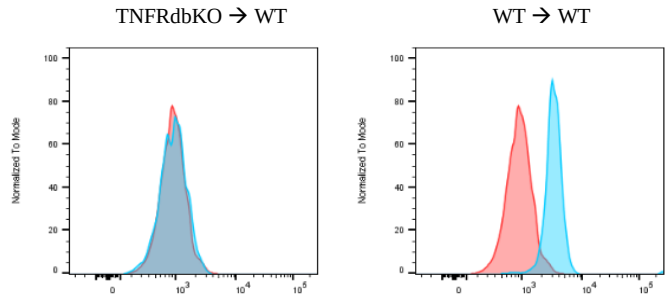

Figure S4: Phenotypic analysis of blood neutrophils from TNFRs chimeric animals

Blood leukocytes from TNFRdbKO or chimeric animals were immunostained for neutrophils specific markers (CD45+ Ly6G+) and their surface expression of TNFR p55 and p75 were analysed by flow cytometry. The figure shows representative histograms of the fluorescence intensity for P75 (**a**) and P55 (**b**) of blood neutrophils from lethally irradiated WT mice and reconstituted with TNFRdbKO (TNFRdbKO → WT) or WT (WT→WT) bone marrow hematopoietic cells (blue) and compared to the intensity of staining from neutrophils of TNFRdbKO animals (as control, red).

Figure S5

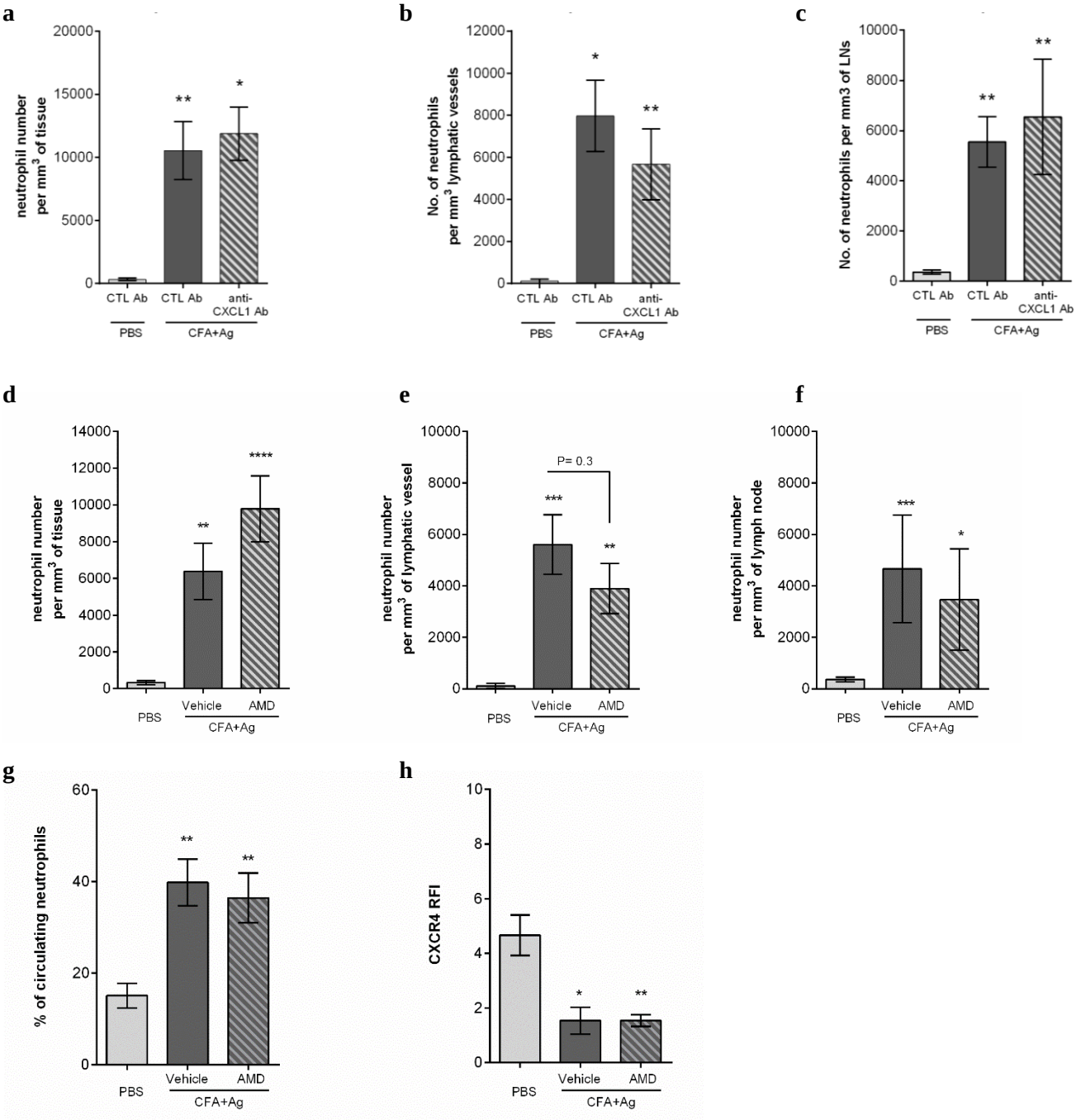

Figure S5:

Neither CXCL1:CXCR1/2 nor CXCL12:CXCR4 axes play a significant role in neutrophil migration across the lymphatic endothelium during antigen sensitisation.

WT mice were subjected to CFA+Ag-induced inflammation of the cremaster muscles. Four hours later, mice received an i.s. injection of an anti-CXCL1 blocking mAb (or an isotype control mAb) or the CXCR4 specific inhibitor AMD3100 (or vehicle as control). At the end of the inflammation period,

cremaster muscles were dissected away, fixed and immunostained for LYVE-1, PECAM-1 and MRP14 to visualise the lymphatic vasculatures the endothelial cells junctions and neutrophils, respectively before analysis of the neutrophil migration responses by confocal microscopy. (**a**) Number of extravasated neutrophils in the cremaster muscles of unstimulated and CFA+Ag-stimulated (8hrs) mice injected with anti-CXCL1 blocking antibody or isotype control. (**b**) Number of neutrophils within the cremaster lymphatic vessels of unstimulated and CFA+Ag-stimulated (8hrs) mice injected with anti-CXCL1 blocking antibody or isotype control. (**c**) Number of neutrophils found in the dLNs of the cremastermuscle of unstimulated and CFA+Ag-stimulated (8hrs) mice injected with anti-CXCL1 blocking antibody or isotype control. (**d**) Number of extravasated neutrophils in inflamed cremaster muscles of unstimulated and CFA+Ag-stimulated (16hrs) mice treated with AMD3100 or vehicle control. (**e**) Number of neutrophils within the cremaster lymphatic vessels of unstimulated and CFA+Ag-stimulated (16hrs) mice treated with AMD3100 or vehicle control. (**f**) Number of neutrophils found within the dLNs of unstimulated and CFA+Ag-stimulated (16hrs) mice treated with AMD3100 or vehicle control. (**g**) Percentage of neutrophils into the blood circulation as assessed by flow cytometry. (**h**) Surface expression of CXCR4 (RFI) on blood circulating neutrophils as assessed by flow cytometry. Data are expressed as mean±SEM from at least 4 independent experiments with n = 5-12 animals per group. Statistically significant difference between stimulated and unstimulated animals are indicated by asterisks: *, $P< 0.05$; **, $P< 0.01$; ***, $P < 0.001$; ****, $P < 0.0001$.

Figure S6

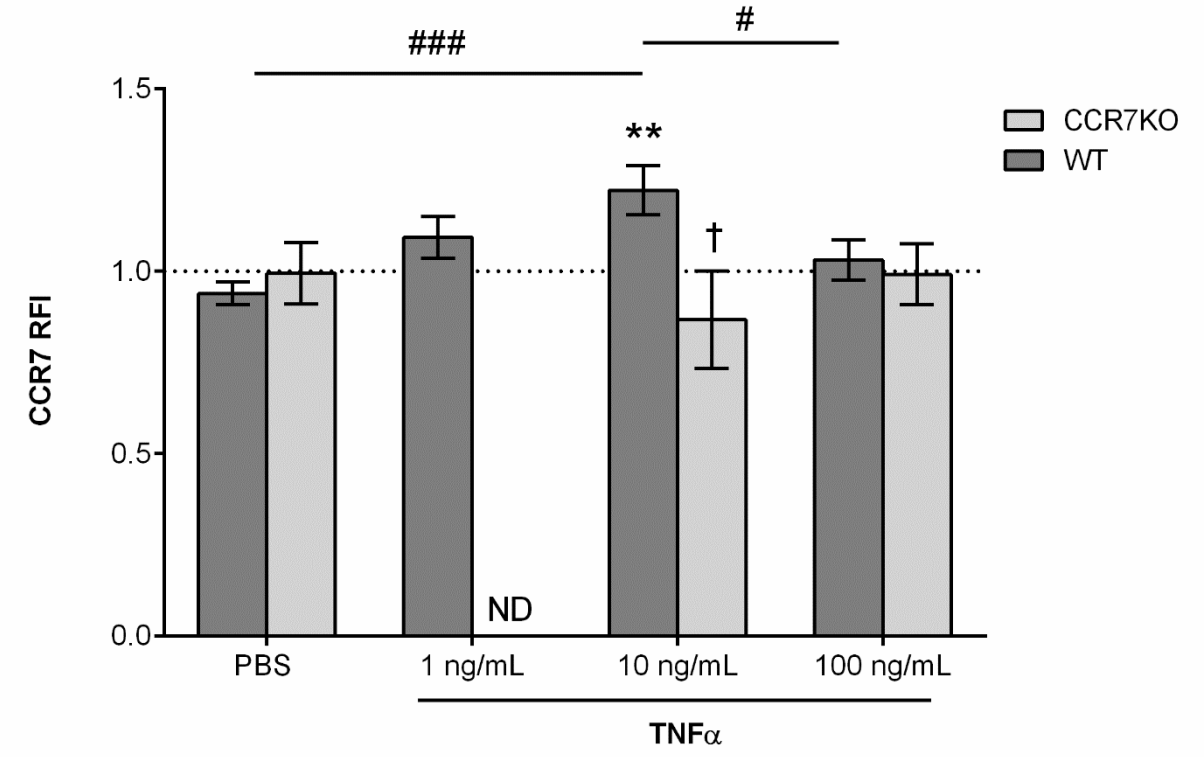

Figure S6: low dose of TNFα induces CCR7 expression on blood neutrophils *in vitro*.

Whole blood leukocytes from WT and CCR7KO animals were stimulated *in vitro* with different doses of TNFα for 4hrs in the presence of the endocytic inhibitor, nystatin (50 μM). Expression of CCR7 on the surface of neutrophils was then assessed by flow cytometry. Dotted line represent the RFI of the isotype control antibody. Data are expressed as mean±SEM from 7 independent experiments (at least 7 mice per condition). Statistically significant difference specific CCR7 staining and isotope control antibody are indicated by asterisks: **, P< 0.01. Data were analysed using a two-way analysis of variance (ANOVA), followed by Holm-Sidak's multiple comparisons test. Statistically significant difference TNFα-stimulated cells and PBS control group are indicated by dash symbols: #, P< 0.05, ### P < 0.001. Statistically significant difference TNFα-stimulated cells and PBS control group are indicated by dagger symbol; P < 0.0001. ND: not done.

Figure S7:

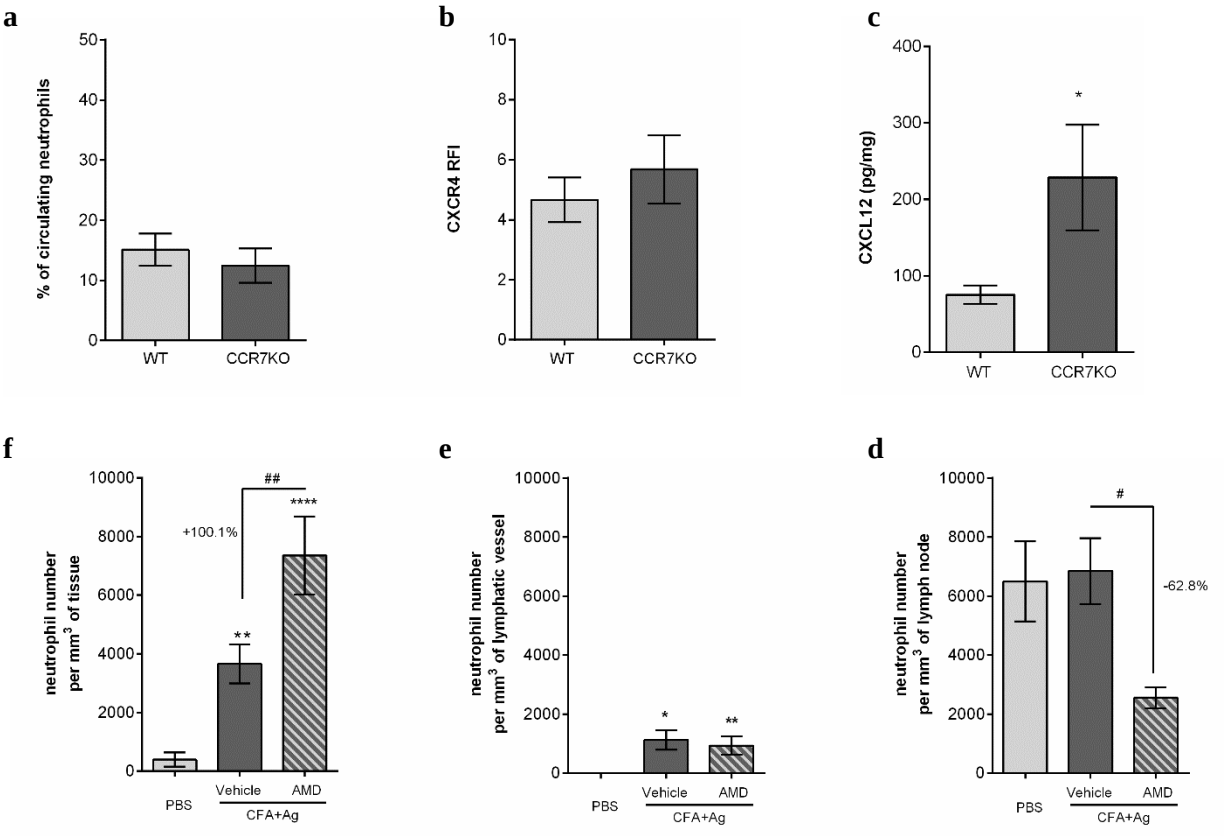

Figure S7: CXCL12:CXCR4 axis is responsible for the high number of neutrophils found into the lymph nodes of CCR7KO mice under steady state condition.

Neutrophil migration into the lymphatic system of the cremaster muscle following antigen sensitisation with complete Freund's adjuvant (CFA+Ag) was induced in WT and TNFRdbKO animals as well as in chimeric animals exhibiting neutrophils deficient for CCR7. (**a**) Percentage of circulating neutrophils in naïve WT and CCR7KO animals, as quantified by flow cytometry. (**b**) Surface expression of CXCR4 on circulating neutrophils from WT and CCR7KO animals, as quantified by flow cytometry. (**c**) CXCL12 expression in the LNs of naïve WT and CCR7KO mice, as quantified by ELISA. (**d**) Number of extravasated neutrophils in inflamed cremaster muscles of unstimulated and CFA+Ag-stimulated CCR7KO mice treated with AMD3100 or the vehicle. (**e**) Number of neutrophils within the cremaster lymphatic vessels of unstimulated and CFA+Ag-stimulated CCR7KO mice treated with AMD3100 or the vehicle. (**f**) Number of neutrophils found into the dLNs of unstimulated and CFA+Ag-stimulated CCR7KO mice treated with AMD3100 or the vehicle. Data are expressed as mean±SEM with 5-12 animals per group. Statistically significant differences between stimulated and unstimulated treatment groups are indicated by asterisks: *, $P < 0.05$; **, $P < 0.01$. Significant differences between responses PBS and AMD3100 treated groups are indicated by hash symbols: #, $P < 0.05$; ##, $P < 0.01$.

Figure S8

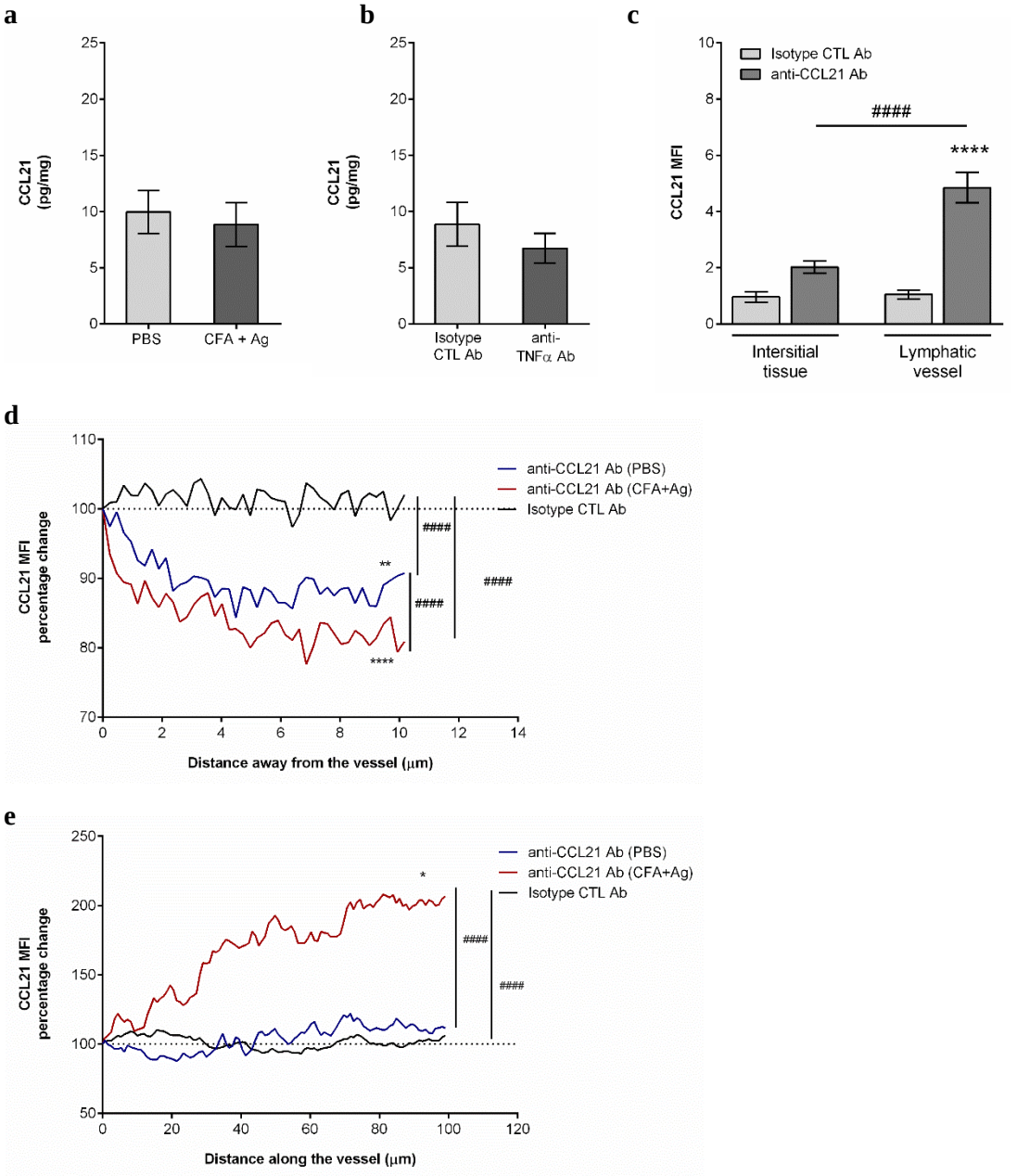

Figure S8: CCL21 expression in the tissue.

WT mice were subjected to CFA+Ag-induced inflammation of the cremaster muscles for 8hrs before harvesting the tissues for subsequent analysis for the expression of CCL21. (**a**) Quantification of CCL21 generation in the tissue of naïve and stimulated mice by ELISA. (**b**) WT mice subjected to CFA+Ag-induced inflammation also received a local (i.s.) injection of the anti-TNFα blocking antibody (or an isotype control antibody, 50μg/mouse) before quantifying the expression of CCL21 by ELISA. (**c**) In some experiments, at the end of the inflammatory period (8hrs), tissues were fixed and whole-mount immunostained for Lyve-1 and CCL21 (or isotype control antibody) before being analysed by confocal

microscopy. The intensity of staining for CCL21 was then quantified within both the lymphatic vessels and the interstitial tissue using IMARIS software. (**d**) A line intensity profile was generated perpendicular to the direction of the vessel (10 lines/vessel) from the abluminal surface into the tissue (10 µm length) to look at a potential gradient of CCL21 guiding the leukocytes toward lymphatic vessels. Data are presented as percentage change from the first pixel of the line. (**e**) Similarly, a surface intensity profile within the lymphatic vessels was generated in the direction of the flow (100 µm length). Data are presented as percentage change from the first measured pixels of the surface. Data are expressed as mean±SEM from at least with 4 animals per group (with at least 5 vessels per mouse fore confocal images). Statistically significant differences for CCL21 staining between the isotype control antibody vs. anti-CCL21 Ab (**c**) and for the intensity profiles from the first pixel to the last pixel measured (**d** & **e**) are indicated by asterisks: *, $P < 0.05$; **, $P < 0.01$; ****, $P < 0.0001$. Significant differences between the interstitial tissue vs. the lymphatic vessels and unstimulated vs. stimulated, are indicated by hash symbols: ####, $P < 0.0001$.

Figure S9

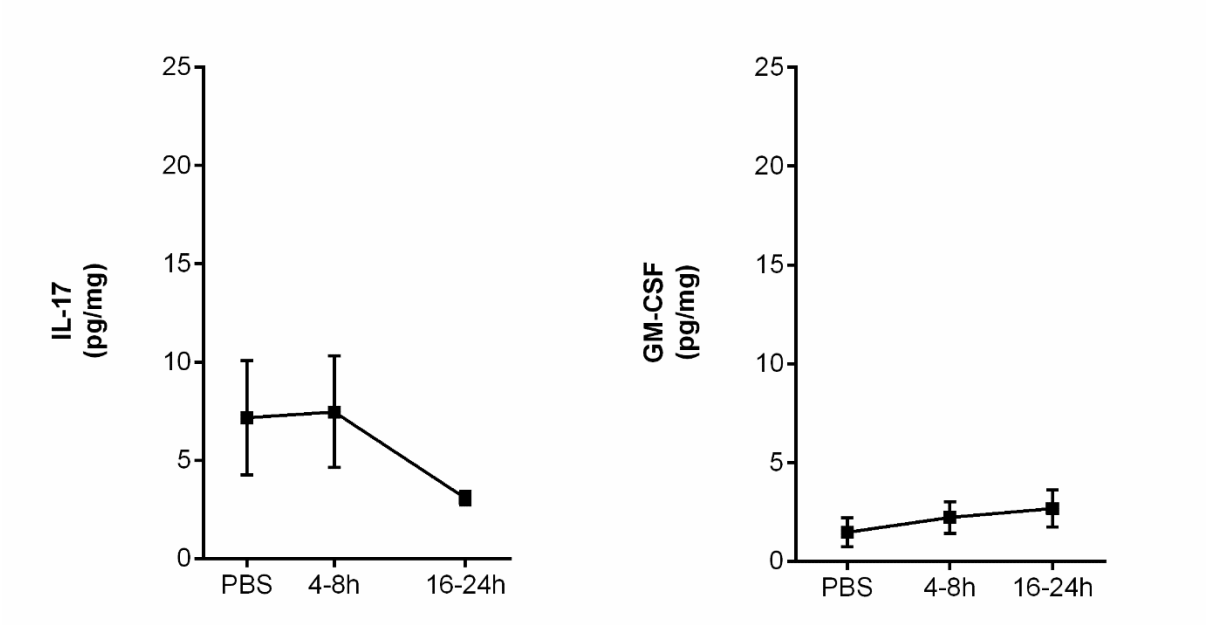

Figure S9: IL-17 and GM-CSF release upon antigen stimulation of the cremaster muscle.

Time course of IL17 (left panel) and GM-CSF (right panel) generated in the cremaster muscles of WT mice following intra-scrotal injection of CFA+Ag and as quantified by ELISA. Data are expressed as mean±SEM from 6-10 mice (from 4 independent experiments).